Directed melanocyte migration: the role of Stem cell factor, cytoskeleton and focal adhesions

Wehrle-Haller, Bernhard

Université de Genève, Faculté de Médecine

Directed melanocyte migration: The role of Stem cell factor, cytoskeleton and focal adhesions

Bernhard Wehrle-Haller

Département de Pathologie
Centre Médical Universitaire
Faculté de Médecine
Université de Genève
1211 Genève 4
Suisse

Thèse d'habilitation au titre de Privat-Docent
à la Faculté de Médecine de Genève: 2002

Pour Monique, Noëlle et Cédric

Content : Page: 3

1. Introduction

1.1. *Cell Migration in Health and Disease*

The evolutionary step from unicellular to multicellular organisms, not only required the development of adhesive systems that allowed the formation of cell layers due to homotypic cell-cell interactions, but also the ability of cells to segregate from each other and to reversibly interact with their extracellular environment. This change in cell morphology and behavior has been named epithelial to mesenchymal transformation (EMT) and is key to the development of a third germinal layer (the mesenchyme) during the process called gastrulation (Fig. 1) (Duband et al., 1995; Hay, 1995). EMT is not only crucial for gastrulation, it is implicated in the development of all organs that form by inductive mechanisms between two epithelial or an epithelial and a mesenchymal tissue. While the changes in gene expression associated with these inductive events are in the process of being understood, the mechanisms that lead to changes of cell shape or remodeling of cell-cell or cell-substrate interactions remain elusive. Although EMT is the process that gives rise to migrating cells, continuous and efficient control of the segregated cells is paramount to the survival of the entire organism.

The immune system is another example where cell migration is of importance. Millions of cells that constantly patrol to fight possible intruder, depend on efficient adhesion mechanism that are regulated by soluble or cell surface bound signaling proteins of the chemokine family (Baggiolini, 2001). In addition, after tissue damage, cleaning of cellular debris and recruitment of new cells by proliferation and migration requires very efficient control over the motile apparatus of each cell (Fig. 1).

Since cell motility is paramount to immune surveillance, tissue regeneration and homeostasis, pathological conditions are frequently associated with the loss of regulated cell migration. While in some situations, like during the formation of metastasis, the molecular causes that lead to the dispersion of tumor cells are not well understood, there has been progress in the identification of genes, that if mutated, can cause the reduction of cell adhesion and migration of cells of the immune system. Such conditions are often reflected by the failure of the immune or the hematopoietic system to function properly and have resulted in significant progress in the understanding of cell migration. For example, the Wiskott Aldrich Symptome protein (WASP) has been identified as an important regulator of the actin cytoskeleton of migrating macrophages, while defects in platelet glycoprotein GPIIb/IIIa, a member of the integrin family of cell-substrate receptors, results in bleeding disorders

such as the Glanzmann disease (Badolato et al., 1998; Chen et al., 1992; Jones, 2000; Nurden and Nurden, 2001). In other cases, naturally occurring mutations of growth factors or their receptors, and the specific knockout of signaling molecules of the chemokine receptor family have demonstrated the strict requirement of specific subsets of migratory cells on these signals for survival and migration (Debard et al., 1999; Dietrich et al., 1999; Forster et al., 1996; Schuchardt et al., 1994).

Here in this thesis, I will concentrate on the neural crest derived melanocyte lineage and show, how genetic analysis has helped to identify key proteins and cellular components required for melanocyte migration. In addition, these genetic studies are complemented by an in vitro approach to quantitatively analyze the role of crucial structural proteins in directed melanocyte migration.

I will demonstrate here, that despite limited information about the mechanisms of cell migration, the development of new therapeutic strategies targeting the various cellular and extracellular components involved in the regulation of motility may have an impact on the treatment of melanoma, one of the most aggressive type of cancers, and other pathological situations involving insufficient or superfluous cell motility.

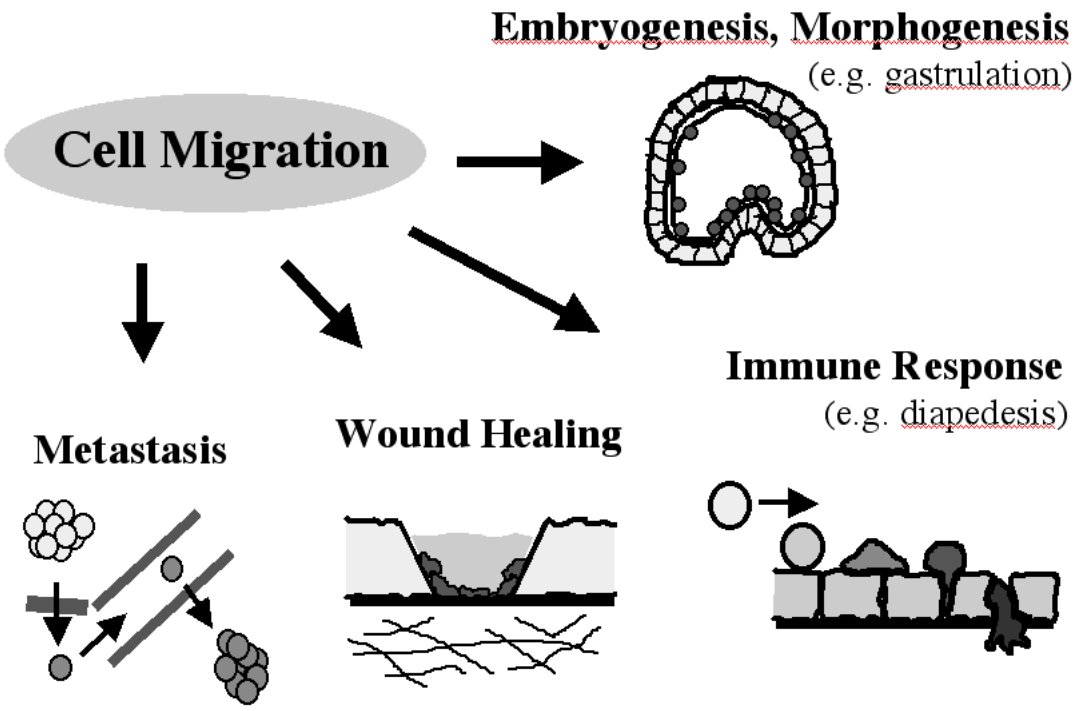

Fig. 1. Cell migration is implicated and plays a major role during development (e.g. gastrulation), tissue homeostasis, wound-healing, immune surveillance (represented by diapedesis) and pathological conditions such as metastasis formation.

1.2. *Mechanisms of Cell Migration*

Although cell migration is an extremely complex biological phenomenon, it requires three basic ingredients (Fig 2). First, attractive or repulsive signals stimulate migration and guide cells through the tissue. Growth factors, chemokines, or bacterial products mediate attractive or chemotactic signals. In contrast, repulsive behavior is induced by ligands of the Ephrin family (Krull et al., 1997; Wang and Anderson, 1997; Wilkinson, 2000). The second component is the cell, which captures these signals with specific cell surface receptors, that often belong to the family of receptor tyrosine kinase (RTK) or G-protein coupled receptors. Whether a signal is attractive or repulsive depends on the how the cell is able to transform this information into cell shape changes. Specifically, forward movement is generated by the polymerization of the actin cytoskeleton at specific sites in the cell called lamellipodia or filopodia (Ridley et al., 1992; Small et al., 2002). In contrast, repulsive signals induce the actin-myosin dependent contraction of the polymerized actin cytoskeleton leading to the retraction of cellular processes (Ridley and Hall, 1992; Wahl et al., 2000). However, without the third component, represented by the physical interaction with the extracellular environment, a cell will not be able to transform cytoskeletal changes into motility. In order to reversibly link the polymerized actin cytoskeleton to the extracellular matrix, the cell employs heterodimeric transmembrane receptors of the integrin family (Hynes, 1992). The coordinated interactions of these three components determine when, how and where a cell will migrate.

Here I will first analyze the individual role of these three different components during melanocyte migration and will subsequently link them to a comprehensive model of cell migration.

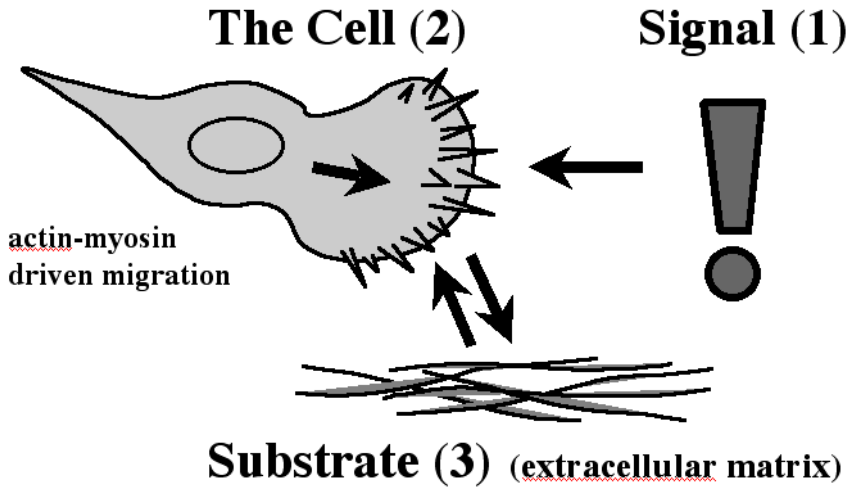

Fig. 2. *The process of cell migration can be reduced to three essential components*. A signal (1) stimulates and gives directional information for migration. The cell (2) provides receptors for these signals, which result in the specific reorganization of the cytoskeleton. The extracellular substrate (3) provides physical anchor points, in order to transform cell shape changes into motility.

1.3. *Choosing a Model System: Neural Crest Derived Melanocytes*

As mentioned above, migrating cells can be isolated from almost all organs and tissues. However, dependent on their origin and initial function, the manner in which cells migrate can vary extensively. For example, polymorphonuclear neutrophils (PMN) derived from the immune system migrate very fast towards a source of chemokine, maintaining a globular shape with a short protruding trail also called uropode (Niggli, 1999). While these cells hardly touch the substrate during migration, equally fast migrating fish keratinocytes exhibit large fan shaped flat lamella, which give the impression of an elegant gliding over the substrate (Lee and Jacobson, 1997; Lee et al., 1994). Due to their regular and flat lamellipodia these cells are ideally suited for histochemical analysis (Verkhovsky et al., 1999). On the other hand, slow moving fibroblasts can be genetically manipulated with ease, however advance by cycles of lamellipodia extension and retraction (Lauffenburger and Horwitz, 1996).

The ideal model system for the study of cell migration should combine all of the above features such as (i) directed migration in response to specific signaling molecules, (ii) flat and fast advancing lamellipodia that allow precise microscopic analysis and (iii) the accessibility to genetic and biochemical manipulations. Neural crest derived cells of the melanocyte lineage fulfill these requirements and are therefore ideally suited to analyze cell migration at the tissue as well as the single cell level.

The neural crest is specified by and forms between the neural plate and the ectoderm. During neural tube closure, cells from the dorsal neural tube are undergoing EMT and move into the extracellular matrix filled space bordered by the somites, ectoderm and neural tube, called the migration staging area (MSA) (Derby, 1978; Duband et al., 1995; Erickson et al., 1992; Loring and Erickson, 1987; Weston, 1991). The emigrated cells behave as stem cells migrating along stereotypic pathways to join their specific destinations where they are giving rise to peripheral neurons and glia, connective tissue and melanocytes (Le Douarin and Kalcheim, 1999; Selleck et al., 1993; Stemple and Anderson, 1993; Wehrle-Haller and Weston, 1997) (Fig. 3). Specifically, cells that will give rise to neural crest derived melanocytes migrate along the dorsolateral pathway that is bordered by the dermamyotome and the overlaying ectoderm. After a first phase of migration through the mesenchymal dermis, melanocyte precursors penetrate the basement membrane of the overlaying epidermis and continue to disperse over the entire surface of the embryo on the epidermal side of this basement membrane (Mackenzie et al., 1997; Nishikawa et al., 1991; Wehrle-Haller and Weston, 1995). After embryonic day 15 of mouse development, melanocyte precursors are beginning to migrate towards and into the forming hair bulbs (Jordan and Jackson, 2000b). Hair bulbs that fail to

get populated by the spreading melanocyte precursors will remain un-pigmented throughout live. Due to the precise timing and pattern of this migration, mouse mutations that affect coat pigmentation can give valuable information about the mechanism and the regulation of melanocyte migration (Jordan and Beermann, 2000). In chapter 2, I will discuss how the analysis of the *Steel* (Mgf^{Sl}) and *Dominant White Spotting* (Kit^{W}) mouse mutations that code for Stem Cell factor (also known as MGF, mast cell growth factor; KL, kit-ligand) and its respective receptor tyrosine kinase (RTK) c-kit, allowed to understand the regulation of melanocyte precursor migration by external signals in great detail.

In addition to the analysis of melanocyte migration *in vivo*, melanocyte precursors or transformed melanoma cells can be easily cultured and analyzed by live microscopy in vitro. While melanoma cells constitutively migrate by employing large flat lamellipodia, c-kit expressing melanocyte precursors (Sviderskaya et al., 1995) can be stimulated to migrate in response to added Stem Cell factor (Ballestrem et al., 2000). Since these cells can be transfected with wildtype or mutant forms of green fluorescent protein tagged proteins, the role of particular proteins in cell migration can be analyzed at a cellular or sub-cellular level. In chapter 3 and 4, experimental data is presented, that demonstrate the role of the actin and microtubule cytoskeleton in melanocyte migration and how migration dependent changes of the actin cytoskeleton are transmitted to the underlying extracellular matrix through heterodimeric receptors of the integrin family (Hynes, 1992).

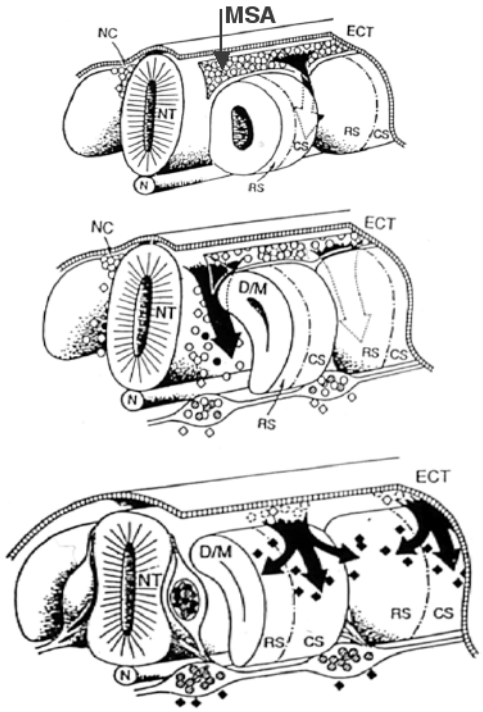

Fig. 3. *Graphic representation of the different stages of neural crest cell migration in the trunk.* Neural crest cells (NC) emigrate from the dorsal neural tube (NT) and transiently accumulate in the migration staging area (MSA). The "intersomitic pathway" (black arrow, upper graphic) is used prior to the segregation of the spherical somites into a medial sclerotome and dorsolateral dermamyotome (D/M). Neural crest cells subsequently invade the rostral portion of the sclerotome (RS) on the "medial pathway" (black arrow, middle graphic), reaching locations where sympathic and sensory ganglia will form. Neural crest cells will migrate along the dorso-lateral pathway (black arrow, lower graphic) that forms between the dermamyotome and the overlying ectoderm (ECT), almost a day later compared to the medial pathway. Neural crest cells migrating on this pathway will mainly develop into melanocytes, subsequently dispersing all over the surface of the embryo. Notochord (n), caudal somite (CS).

2. Directed Melanocyte Migration Induced by Growth Factor Signals

2.1. *Stem Cell factor and its receptor c-kit*

Pioneering work by Elisabeth Russell had led to the discovery of mouse mutants that specifically affected the fate and survival of neural crest derived melanocytes, but not melanocytes derived from the central nervous system (CNS), resulting in the characteristic black-eyed/white-coat phenotype of homozygous *Steel* and *Dominant White Spotting* mutants (Russell, 1979). This is in contrast to mutations of the tyrosinase gene which block the synthesis of melanin in neural crest and CNS derived melanocytes resulting in the *albino* phenotype (Silvers, 1979). In addition to the absence of melanocytes in the skin and hair, *Steel* and *Dominant White Spotting* mutant mice display also defects in their germ cells resulting in sterility, a reduction of hematopoietic stem cells in the bone marrow leading to anemia and a lack of peripheral mastocytes in the tissues (Morrison-Graham and Takahashi, 1993; Williams et al., 1992). While the genetic defect in the *Steel* mutation was traced to the tissue environment in which the affected cell populations were localized, the *Dominant White Spotting* mutation caused the loss of these cell populations even when transplanted into a normal environment (Russell, 1979). In 1990 several laboratories simultaneously identified the gene affected by the *Steel* mutation, encoding for a membrane-bound growth factor named Stem Cell factor (SCF) but also called (Mast cell growth factor, MGF or kit-ligand, KL) (Anderson et al., 1990; Copeland et al., 1990; Flanagan and Leder, 1990; Huang et al., 1990; Martin et al., 1990; Williams et al., 1990; Zsebo et al., 1990a; Zsebo et al., 1990b). In contrast, the receptor tyrosine kinase (RTK) c-Kit is encoded at the *Dominant White Spotting* locus and is structurally related to the RTK's c-fms, PDGF receptor alpha and beta, arranged pair wise on two related chromosomes (PDGFRα/c-kit and PDGFRβ/c-fms) (Kataoka et al., 1997; Qiu et al., 1988; Yarden et al., 1986; Yarden et al., 1987). The fact that c-Kit originates from a duplication of the PDGFR locus during the evolution of the vertebrates sheds some light on the evolutionary mechanisms involved, in order to create new cell populations with novel functions to increase the complexity and capacities of new organisms (see below). SCF is most homologous to the macrophage colony-stimulating factor (M-CSF or CSF-1), which binds to its receptor c-fms (Bazan, 1991). Similar to CSF-1, SCF is expressed as a dimeric membrane-bound precursor generated from two differentially spliced transcripts of which the longer one is readily cleaved by cell surface proteases to generate soluble SCF (Huang et al., 1992). The complex of SCF bound to c-Kit has recently been crystallized and reveals the common structure of a bundle of four α-helices linked by two intra-molecular disulfide bridges (Fig. 4) (Bazan, 1991; Jiang et al., 2000; Zhang et al., 2000). An interest in the differentially spliced forms of SCF and its

transmembrane and cytoplasmic domains has been generated due to the molecular characterization of a naturally occurring *Steel* allele (*Steel*-dickie) ($Mgf^{Sl\text{-}d}$) exhibiting a phenotype almost as severe as the null mutations (Brannan et al., 1991; Flanagan et al., 1991). The $Mgf^{Sl\text{-}d}$ allele represents a deletion of the transmembrane and cytoplasmic domain of SCF, resulting in the secretion of a fully functional form of SCF from cells transfected with the mutant SCF construct. Based on these data it was speculated that the membrane bound splice variant of SCF that lacks the major proteolytic cleavage site (Huang et al., 1992) is responsible for the survival of c-Kit expressing SCF-dependent cell populations in vivo (Brannan et al., 1991; Flanagan et al., 1991). Consequently, we (J.A. Weston and myself) began to speculate whether the soluble or proteolytically shed form of SCF may have a chemotactic function in attracting or guiding c-kit expressing cell populations such as melanocytes, that have been recognized to extensively migrate through the embryonic and adult tissue.

Particularly, it has been demonstrated in vitro, that PDGFRα, β, c-Kit and c-fms expressing motile cells show chemotactic responses towards concentration gradients of their ligands (Allen et al., 1997; Blume-Jensen et al., 1991; Kundra et al., 1995; Ueda et al., 2002). In addition, a c-Kit expressing small cell lung carcinoma cell line responds chemotactically to SCF *in vitro* (Sekido et al., 1993). Mast cells, which express high levels of c-Kit on their surface, respond to SCF stimulation by spreading on adhesive substrates. However, a 100-fold higher SCF concentration is required to obtain proliferation of these c-Kit expressing mast cells (Dastych and Metcalfe, 1994; Kinashi and Springer, 1994). These results suggest that both motogenic and mitogenic responses can be induced by SCF presentation towards responsive cells.

We conducted several experimental approaches to understand the role of SCF in melanocyte precursor migration in order to elucidate the role of the soluble and membrane bound forms of SCF (chapter 2.2). In addition, the presence of SCF proofed to be critical for melanocyte precursor migration and survival on the lateral pathway (chapter 2.3), which led us to hypothesize that growth factor dependent survival and chemotactic activities direct the migration and specific localization of other neural crest cell derivatives (chapter 2.4). In chapter 2.5 we provided the proof that SCF is the *only* chemotactic cue generated on the lateral neural crest migration pathway that is able to induce migration of melanocyte precursors *in vivo*. These data are complemented by studies on the role of the cytoplasmic tail of SCF for efficient presentation towards c-Kit expressing cells such as migrating melanocyte precursors (chapter 2.6 and 2.7). Furthermore, a short chapter discusses the potential role of pathological changes in SCF localization and production, and the respective changes in the behavior of c-kit expressing responsive cells of the mastocyte and melanocyte lineage (chapter 2.8). In addition, this chapter contains a paragraph suggesting, that SCF localization and expression may

provide a new therapeutic target to reduce hyperpigmented lesions in the skin and/or allergic reactions.

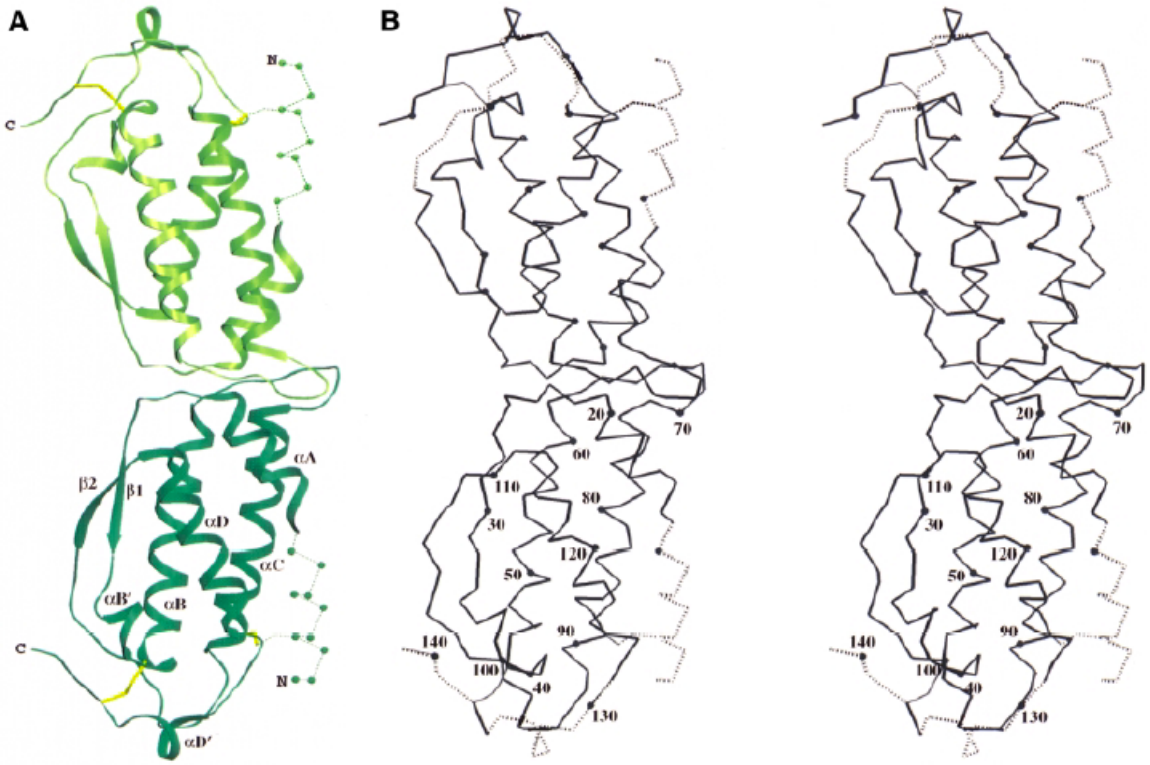

Fig. 4. *Crystal structure of head to head dimerized SCF.* Figure adapted from Jiang et al., 2001. (A) Ribbon diagram. (B) Cα stereodiagram of the AB dimer. Note that the bundle of four α-helices joined by two beta-strands and intra-molecularly cross-linked by two S-S bridges (yellow). The linker region and C-terminal sequences are not part of the crystal structure.

.

2.2. Distinct activities of soluble and membrane bound Stem Cell factor

Development 121, 731-742 (1995)
Printed in Great Britain © The Company of Biologists Limited 1995

Soluble and cell-bound forms of steel factor activity play distinct roles in melanocyte precursor dispersal and survival on the lateral neural crest migration pathway

Bernhard Wehrle-Haller and James A. Weston

Institute of Neuroscience, University of Oregon, Eugene, OR 97403, USA

Email: Weston@UONEURO.UOREGON.EDU

SUMMARY

Trunk neural crest cells segregate from the neuroepithelium and enter a 'migration staging area' lateral to the embryonic neural tube. After some crest cells in the migration staging area have begun to migrate on a medial pathway, a subpopulation of crest-derived cells remaining in the migration staging area expresses mRNAs for the receptor tyrosine kinase, c-kit, and tyrosinase-related protein-2, both of which are characteristic of melanocyte precursors. These putative melanocyte precursors are subsequently observed on the lateral crest migration pathway between the dermatome and overlying epithelium, and then dispersed in nascent dermal mesenchyme.

Melanocyte precursors transiently require the c-kit ligand, Steel factor for survival. Although Steel factor mRNA is transiently expressed in the dorsal dermatome before the onset of trunk neural crest cell dispersal on the lateral pathway, it is no longer produced by dermatomal cells when melanocyte precursors have dispersed in the dermal mesenchyme. To assess the role of Steel factor in migration of melanocyte precursors on the lateral pathway, we analyzed melanocyte precursor dispersal and fate on the lateral pathway of two different *Sl* mutants, *Sl*, a null allele, and Sl^d, which lacks cell surface-associated Steel factor but produces a soluble form. No melanocyte precursors were detected in the dermatome of embryos homozygous for the *Sl* allele or in *W* mutants that lack functional c-kit. In contrast, in embryos homozygous for the Sl^d allele, melanocyte precursors appeared on the lateral pathway, but subsequently disappear from the dermis. These results suggest that soluble Steel factor is required for melanocyte precursor dispersal on the lateral pathway, or for their initial survival in the migration staging area. In contrast, membrane-bound Steel factor appears to promote melanocyte precursor survival in the dermis.

Key words: Steel factor, melanocyte precursor, neural crest, c-kit, TRP-2

INTRODUCTION

In the trunk of vertebrate embryos, neural crest cells segregate from the neural epithelium and transiently reside in a 'migrating staging area' (MSA) delimited by the neural tube, the somite and the overlying epithelium. Crest cells immediately begin to disperse from the MSA on a ventromedial pathway along the myotome and into rostral sclerotomal mesenchyme (Erickson and Loring, 1987; Weston, 1991). Later, crest cells remaining in the MSA disperse on a dorsolateral pathway, migrating between the dermatome and the epidermis (Erickson et al., 1992). The crest cells on the lateral pathway subsequently become interspersed with dermal mesenchyme and cross the epithelial basement membrane to localize in the epidermis. In the mouse, these cells remain in the epithelium for many days before they undergo melanogenesis postnatally. Before early markers for pigment cell precursors were available, the timing of melanocyte precursor dispersal and localization in the skin was inferred by testing for the ability of cultured or grafted tissue to produce melanocytes (Rawles 1947; Derby 1978). Results of such studies revealed that the first melanocyte precursors are present on the lateral pathway of the embryonic trunk at about e11 and reach the limb buds by e12. At a lateral trunk level most of the melanocyte precursors enter the epidermis between e13 and e14 (Mayer, 1973). Recently, histochemical reagents that intensify pigment in melanosomes of otherwise undifferentiated melanocytes, or probes for melanocyte markers such as the tyrosine kinase receptor, c-kit, and tyrosinase-related protein-2 (TRP-2) confirmed these inferences, and revealed the presence of melanocyte precursors in the head as early as e10.5 (Manova and Bachvarova, 1991; Steel et al., 1992; Pavan and Tilghman, 1994).

Several mouse mutations affecting coat pigmentation have been described and their molecular defects characterized. Two of the best studied, *Steel* (*Sl*) and *Dominant spotting* (*W*), are embryonic lethals as homozygotes, due to failure of erythropoiesis, whereas heterozygous embryos are viable but eventually show a white spotting coat color pattern. The defective gene in *W* mutants codes for a receptor tyrosine kinase (c-kit;

Geissler et al., 1988) and its growth factor ligand, variously called Steel Factor (SlF), Stem cell factor (SCF), mast cell growth factor (MCF) or kit ligand (KL) (Anderson et al., 1990; Copeland et al., 1990; Huang et al., 1990; Nocka et al., 1990a; Williams et al., 1990; Flanagan and Leder, 1990) is encoded at the *Sl* locus. For both genes, less severe alleles have been described that are viable as homozygotes, but show a white coat, anaemia and sterility (see Morrison-Graham and Takahashi, 1993; Copeland et al., 1990; Flanagan et al., 1991; Brannan et al., 1991; Duttlinger et al., 1993).

A number of in vivo and in vitro approaches have been initiated to pinpoint the critical period when SlF or c-kit activity is required for survival of pigment precursors. For example, an early function for c-kit and SlF is suggested by expression of c-kit mRNA in cells found dorsal and lateral to the somites (Manova and Bachvarova, 1991) and the presence of SlF mRNA in the somitic dermatome at around e10.5 (Matsui et al., 1990). In utero injection of c-kit blocking antibody has revealed an early (e10.5), an intermediate (e14.5) and a late effect of c-kit function on melanogenesis (Nishikawa et al., 1991; Yoshida et al., 1993). Consistent with these inferences, analysis of melanogenesis in vitro has shown that SlF is transiently required for melanogenic precursor survival between day 2 and 6.5 in culture (equivalent to e11.5-16; Morrison-Graham and Weston, 1993).

SlF is normally expressed in two splice-variants, both of which are initially localized to the cell surface. The larger variant contains an extracellular proteolytic cleavage site, which permits release of SlF from the cell surface. The smaller splice-variant is usually not cleaved and normally remains associated with the cell surface (Flanagan et al., 1991; Huang et al., 1992; see also Williams et al., 1992). Although fragmentary distribution and mutational analysis of the influence of the c-kit/SlF system on melanocyte precursors exists (Steel et al., 1992), it is not yet clear whether the functions of alternatively spliced SlF are different, or even what such functions might be.

An opportunity to address this issue is provided by assessing the early morphogenetic behavior and fate of melanocyte precursors in embryos carrying various mutations at the *Steel* locus. For example, in the *Steel-dickie* (Sl^d) allele, the transmembrane and cytoplasmic domains of SlF are deleted so that only a secreted form of SlF is produced (Flanagan et al., 1991; Brannan et al., 1991). In spite of the presence of SlF activity (Brannan et al., 1991), mice heterozygous for Sl^d exhibit a distinct coat color phenotype. Embryos homozygous for this allele are viable but exhibit characteristic phenotypes including lack of coat pigmentation. In these mutants, melanocyte precursors are initially present in the head but fail to survive (Steel et al., 1992). It is not yet known, however, how these phenotypes arise, or if the migration behavior and growth factor requirements of trunk and head melanocyte precursors are different.

In the present study, we have examined the early dispersal and fate of melanocyte precursors in *Sl* (null) and Sl^d mutants to elucidate the function of SlF in determining the early pigment patterns, and to distinguish the role(s) of the soluble and cell-bound forms of SlF in regulating the early migration behavior of pigment cell precursors. Thus, we have characterized melanocyte precursor appearance in the MSA, and their dispersal and fate in relation to the time and location of SlF mRNA expression in normal embryos and embryos homozygous for two *Steel* alleles. Our results indicate that migrating melanocyte precursors respond to cues provided by diffusible (soluble) SlF, through activation of the c-kit receptor. We conclude that soluble SlF is sufficient for responsive melanoblast precursors to initiate their dispersal onto the lateral pathway in vivo, but that cell-bound SlF is necessary for subsequent survival of pigment cells in the newly formed dermal mesenchyme.

MATERIALS AND METHODS

Genotyping mouse embryos

Inbred colonies of B6, B6Sl^d, WBReSl and WBW were maintained in our laboratory. Dated matings were set up in the evening and plugs checked the following morning. The presence of a plug was considered as e0.5.

Since *Sl*, Sl^d and *W* homozygous are sterile, we mated heterozygous mice to obtain homozygous embryos. *Sl*, Sl^d or *W* homozygous embryos can only be recognized by morphological criteria after about e15.5, when their liver appears pale compared to wild-type or `heterozygous littermates. In order to identify the genotype of the *Sl* and Sl^d embryos earlier, we amplified a genomic sequence present in the *Steel* gene, which is deleted in the *Sl* (Copeland et al., 1990) and Sl^d (Flanagan et al., 1991) mutations. According to Steel et al. (1992) we used a set of primers from the 7th and 8th exon respectively to amplify a 700 bp fragment containing mainly intron sequences. Genomic DNA was isolated from excised limb buds by proteinase K and 0.5% SDS extraction and ethanol precipitation. Following an amplification with 35 cycles (45 seconds at 93°C, 1 minute at 56°C, 1 minute at 72°C) a 700 bp fragment was detected on a 1% agarose gel. Both *Sl/Sl* and Sl^d/Sl^d embryos could be identified by the absence of that amplified band. As a control for the quality of the genomic DNA as well as the amplification reaction (PCR), we used an alternative set of primers, amplifying a 500 bp genomic fragment from the gene coding for PDGFRα located on chromosome 5 (Orr-Urtreger et al., 1992). We performed separate amplifications with the same template DNA or included both sets of primers in one reaction. The following primers were used: *Sl* forward primer CCATGGCATTGCCGGCTCTC (bases 665 to 684; Huang et al., 1990) and *Sl* reverse primer CTGCCCTTGTAAGACTTGACTG (complement of bases 757 to 736). PDGFRα forward primer ACCTCCTTTCGGACGATGAC (bases 2417 to 2436; Wang et al., 1990, Acc# M57683) located within the interkinase region and a reversed genomic primer corresponding to a sequence located within an intron 500 bp apart ATCACTTCAGAATGGCTCCA (Peter Lonai; personal communication).

Embryos homozygous for the *W* gene, could not be identified using a PCR approach since the *W* (null) allele is a point mutation in a splice site (Hayashi et al., 1991), which generates a nonfunctional c-kit protein (Nocka et al., 1990b). Therefore, all embryos from a litter produced by mating heterozygotes were treated identically, and their mutant phenotype assessed by the localization of melanocyte precursors (see below). As expected, a quarter of all the embryos scored by PCR were homozygous for either *Sl* or Sl^d, or were identified as *W* homozygotes by their pigment pattern.

cDNA probes and antibodies

cDNAs for c-kit were kindly provided by Dr Robert J. Arceci (Boston), for Steel factor (KL-M1) by Dr John Flanagan (Boston) and TRP-2 by Dr Ian Jackson (London). Polyclonal anti-fibronectin and laminin were obtained from Collaborative Research. Rhodamine goat anti-rabbit was from Cappel.

Digoxigenin (DIG)-labeled sense and antisense riboprobes were

generated using a standard protocol (Boehringer Mannheim) from linearized plasmids and used for whole-mount in situ hybridization at concentrations of 1 μg/ml. RNA synthesis was checked by agarose gel electrophoresis.

Whole-mount in situ hybridization and antibody staining

Whole-mount in situ hybridization was performed according to Yamaguchi et al. (1992; Y. Takahashi, personal comm.). The hybridization of DIG-labeled single-stranded RNA probes was detected with anti-DIG antibodies coupled to alkaline phosphatase. Details of the protocol will be provided upon request.

As a control for the specificity of our in situ protocol, we hybridized with sense riboprobes for KL-M1 and c-kit under identical conditions. We were not able to generate a sense probe from our plasmid containing the TRP-2 probe. No staining could be detected in embryos hybridized with any of the sense probes. In experimental and control embryos, occasionally unspecific stain could be detected in the lumen of the spinal cord, otic vesicle and brain vesicles. Puncture of the hindbrain did reduce this unspecific trapping of stain. Embryos from e9.5 to e13.5 were treated identically with the exception of prolonging the proteinase K treatment for older embryos to enhance penetration of the probes. It must be emphasized that complete penetration could only be achieved with embryos of e9.5 to e10.5. In older embryos the detection of mRNAs was limited to the surface of the embryos. Fig. 3E roughly indicates the limit of penetration of the probes and antibodies. Sensitivity of the whole-mount in situ hybridization was comparable to in situs on sectioned material, since we were able to visualize every previously published source of SlF and c-kit mRNA in e9.5 to e10.5 embryos. However, compared to hybridization of tissue sections, the temporal and spatial resolution of the whole-mount in situ hybridizations is superior.

For immunohistochemistry, whole-mount in situ hybridized embryos were equilibrated in 20% sucrose and embedded in Tissue Tec, frozen and sectioned at 16 μm. Sections were dried on gelatin/alum-subbed slides and blocked with 0.5% BSA in PBT, incubated for 45 minutes with anti-fibronectin or anti-laminin rabbit antisera at 1/50 dilution in 0.5% BSA in PBT. After washing, secondary rhodamine-labeled goat anti-rabbit was added for 45 minutes diluted 1/100 in 0.5% BSA in PBT. Sections were washed and embedded in glycerol containing 1% n-propylgallate.

RESULTS

Cells expressing c-kit and TRP-2 mRNA (melanocyte precursors) in the migration staging area disperse on the dorsolateral pathway in a rostral-caudal sequence

As in previous reports (Keshet et al., 1991; Motro et al., 1991; Orr-Urtreger et al., 1990), cells expressing c-kit mRNA were observed in the head and trunk of e9.5 embryos (not shown). Although whole-mount in situ hybridization revealed c-kit mRNA in cells at various locations of e9.5 embryos, their neural crest origin could not be established. No hybridization signal was revealed by using the TRP-2 riboprobe (not shown), so melanocyte precursors could not be unequivocally identified.

By e10.5, cells located in sites usually occupied by migrating cranial crest cells can be seen to express the TRP-2 mRNA. These cells were detected between the forebrain-midbrain junction and the eye (Fig. 1B), at the level of the midbrain-hindbrain junction, and posterior to the otic vesicle. Cells expressing c-kit mRNA were also detected in these locations (Fig. 1A). Based on the time of appearance and their locations (compare with Steel et al., 1992), cells expressing both mRNAs seem likely to be the earliest crest-derived melanocyte precursors. It should be emphasized, however, that at this stage, c-kit mRNA-expressing cells were also detected in the olfactory pit, and the clefts of branchial arches I-IV, where TRP-2 mRNA expression was not detected (Fig. 1A,B). At this stage, only a few cells expressing TRP-2 or c-kit mRNA were detected at more posterior axial levels between the otic vesicle and the most rostral somites (Fig. 1A,B).

At e11, localization of TRP-2 and c-kit mRNA-expressing cells in the head is dramatically different. These cells were present in the head mesenchyme particularly in the region between the eye, forebrain and nose, and at the posterior regions of the branchial and hyoid arch. In addition, many TRP-2 as well as c-kit mRNA-expressing cells are localized in a stripe originating at the mid-to-hindbrain junction and extending towards the eye (Fig. 1E,F; arrowheads). In contrast, no TRP-2 mRNA-expressing cells could be detected in facial structures. Within the trunk, cells expressing TRP-2 mRNA were observed from the first somites to the level of the hind limb buds (Fig. 1D) in the same locations as cells expressing c-kit mRNA (Fig. 1C). These cells were variously localized in the migration staging area (MSA) just lateral to the neural tube at posterior axial levels, or further lateral over the somites at more anterior levels (Fig. 1C,D). Groups of TRP-2 or c-kit mRNA-expressing cells were present in a segmented pattern along the axis from very rostral to mid trunk levels. In addition, c-kit mRNA-positive cells were detected in the lateral mesenchyme, the dorsal neural tube (arrow in Fig. 1E), limb buds, and the posterior gut where no TRP-2 mRNA-expressing cells could be detected (Fig. 1D).

By e11.5, as previously reported (Steel et al., 1992), TRP-2 mRNA-expressing cells were detected at locations in the head mesenchyme anterior and posterior to the eye, over the hindbrain, around the otic vesicle and at the posterior aspect of the hyoid arch (Fig. 2B). In the trunk, all cells expressing TRP-2 mRNA were found distributed over the entire somite surface, but no cells were detected in the lateral mesenchyme and in the limb buds (Fig. 2A). In contrast, individual c-kit mRNA-expressing cells were found dispersed over the somite surface, but also more lateral within the lateral mesenchyme (Fig. 2C). This cell population never expressed TRP-2 mRNA. We do not yet know if these cells are crest-derived or represent a mesodermally derived population, which will require more specific probes to distinguish. Expression of c-kit mRNA in mesenchymal cells was similar to that seen at earlier stages (Fig. 1C). More caudally, at the base of the tail, cells expressing TRP-2 mRNA were localized in the MSA lateral to the neural tube, and just one or two somites more rostral cells were found over the somite lateral to the MSA (Fig. 2D). In progressively older (more rostral) somites, incrementally more cells were localized laterally, and fewer TRP-2 mRNA-expressing cells remained near the neural tube (Fig. 2E). In embryos of this age, TRP-2 mRNA-expressing cells were first observed at the base of the hind limb bud (Fig. 2E).

The temporal differences between developing segments are most distinct at the level of the hindlimb of e11.5 embryos. Accordingly, this axial region best displayed the various stages of the migration of crest cells on the lateral pathway. Therefore, embryos that had been stained as whole mounts

for TRP-2 mRNA were sectioned transversely and stained with antibodies against laminin and fibronectin to reveal the architecture of the somites (see Methods). Thus, Fig. 3A shows a bright-field view of a section at the base of the tail where two groups of TRP-2 mRNA-expressing cells can be seen (corresponding to A-B in Fig. 2D). One group of cells resides in the MSA lateral to the neural tube, and the other group was localized within the dermatome. The staining for laminin revealed the borders of the neural tube and the dermatomal epithelial tissue (Fig. 3B). A section of a different embryo at a slightly older (more rostral) axial level (corresponding to C-D in Fig. 2D) shows elongated TRP-2 mRNA-positive cells on the laminin-positive basement membrane (arrows in Fig. 3C,D). At an even more rostral level (corresponding to E-F in Fig. 2D), the epithelial dermatome has already transformed into the mesenchymal dermis, made obvious by the intense fibronectin staining (Fig. 3F). TRP-2 mRNA containing cells are evenly spread throughout the dermal mesenchyme at this axial level (see also Pavan and Tilghman, 1994, Fig. 2a).

By e12.5, cells expressing TRP-2 and c-kit mRNA were detected bordering the whisker fields and localized over the nose (Fig. 4C). The regions around the ear were also densely populated by TRP-2 mRNA-expressing cells (Fig. 4A-C). In the trunk at this stage, TRP-2 mRNA-expressing cells were present between the neural tube and the lateral midline, and some cells were seen as far ventrad as the base of the forelimb bud (Fig. 4A,B,D). No TRP-2 mRNA was detected on the ventral side of the body (Fig. 4D). Many TRP-2 mRNA-expressing cells were present on the posterior side of the hindlimb (Fig. 4C, arrow) as well as on the lateral sides of the tail.

Steel factor mRNA is expressed in a rostrocaudal sequence in the dorsal portion of the dermatome in e10.5-12.5 mouse embryos

At e9.5, whole-mount in situ hybridization reveals SlF mRNA expression in various places in the embryo: the head mesenchyme, branchial arches, the mesenchyme posterior to the last arch, part of the gut, the tail and the kidney primordium. At this stage, no SlF mRNA could be detected within the somitic tissue of the trunk (not shown).

In the head of e10.5 embryos, SlF mRNA was detected in the mesenchyme between the telencephalon and the olfactory pit, and in the mesenchyme surrounding the otic

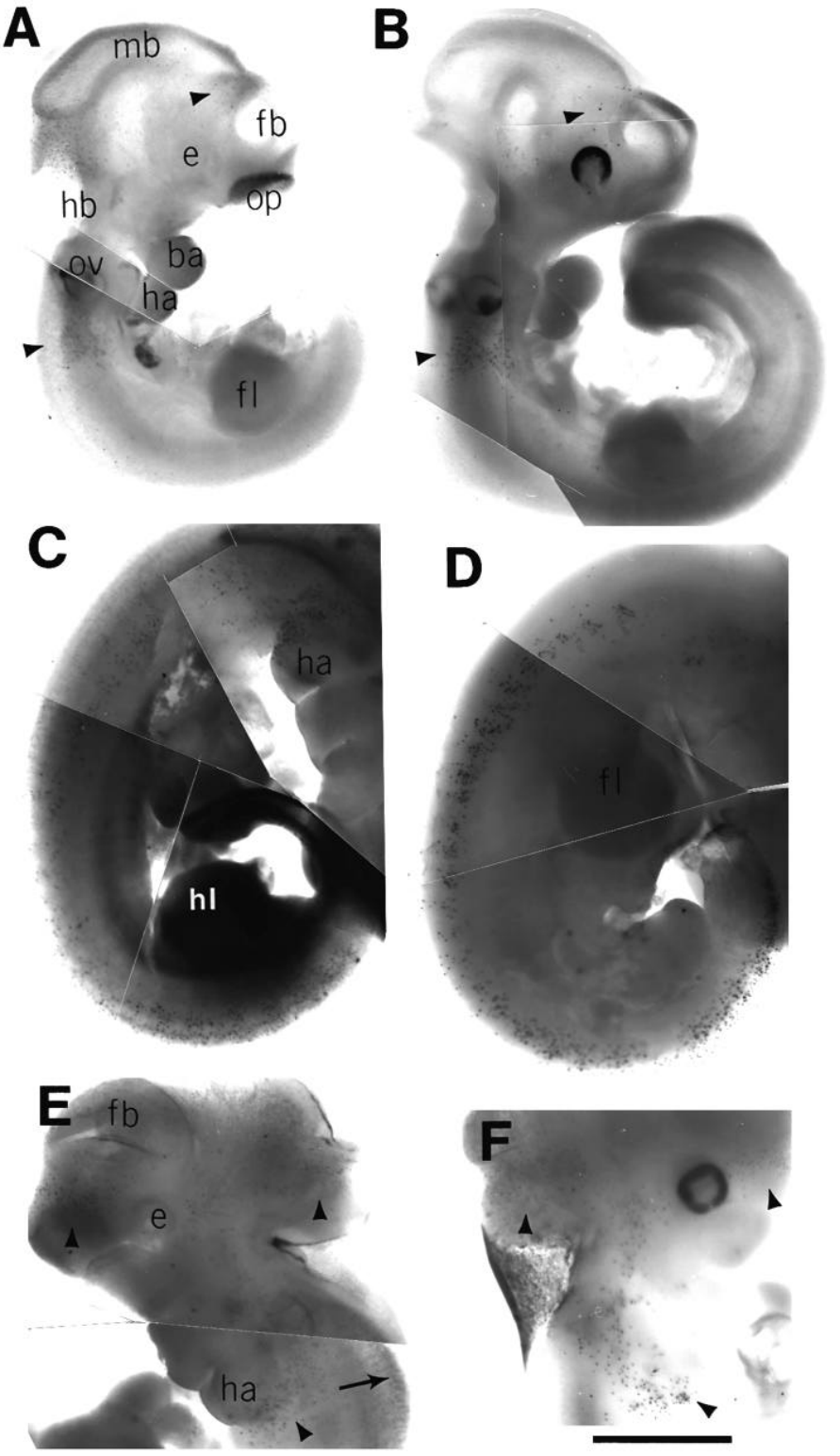

Fig. 1. c-kit and TRP-2 mRNA-expressing cells show a similar distribution pattern in e10.5 and e11 embryos. c-kit (left panel) and TRP-2 (right panel) antisense whole-mount in situ hybridization of e10.5 (A,B) and e11 (C,D) mouse embryos. (Note almost identical localization of punctate staining at arrowheads between c-kit and TRP-2 hybridized embryos, and the absence of forelimb and hindlimb in C and D, respectively.) The arrow in E points to c-kit mRNA expression in the spinal cord. ba, first branchial arch; e, eye; fb, forebrain; fl, forelimb; ha, hyoid arch; hb, hindbrain; hl, hindlimb; mb, midbrain; op, olfactory pit; ov, otic vesicle. Bar, 400 μm.

vesicle (see also Steel et al., 1992). SlF mRNA was also detected in the first and second branchial arches at their most posterior proximal edges (arrowheads in Fig. 5B). In the trunk of e10.5 embryos, the dermatomes express SlF mRNA in their dorsal portions. In slightly less-advanced embryos at that gestational stage, SlF mRNA was detected in dermatomes from the first somite to the midtrunk level (Fig. 5A), whereas in developmentally more advanced embryos, SlF mRNA expression was detected in dermatomes from the first somite back to somites at the hindlimb level. Transverse sections of whole-mount embryos counterstained with a polyclonal antiserum against laminin (Fig. 5K) or fibronectin (Fig. 5H) clearly localizes the SlF mRNA to the dorsal epithelial dermatome (Fig. 5G-K; see also Matsui et al., 1990). In progressively older dermatomal tissue, the location of SlF mRNA expression is shifted from the mediodorsal portion to a more dorsal location in the epithelial dermatome (Fig. 5G,I).

Embryos obtained half a gestational day later, at e11, revealed persistent SlF mRNA in the telencephalon, but expression in the cranial mesenchyme could no longer be detected. In the trunk, SlF mRNA expression is diminished in cervical somites, whereas the dorsal dermatome of all the posterior somites down to the base of the tail were strongly positive (Fig. 5C). No cells expressing SlF mRNA could be detected in the MSA (Fig. 5D).

At e11.5 SlF mRNA could no longer be detected in the head mesenchyme and the trunk somites. However the expression in the telencephalon and tail somites persisted (Fig. 5E). In addition, SlF mRNA expression was present in the posterior region of the hindlimb bud (Fig. 5F, arrow).

By e12.5, SlF mRNA expression in the telencephalon still persists, and new expression is detected in the interdigital mesenchyme of the limb buds. Expression in dorsal dermatome was detected only in the tail somites. At this stage, no hybridization signal for SlF mRNA could be detected in dermal mesenchyme associated with developing somites at more rostral axial levels (not shown).

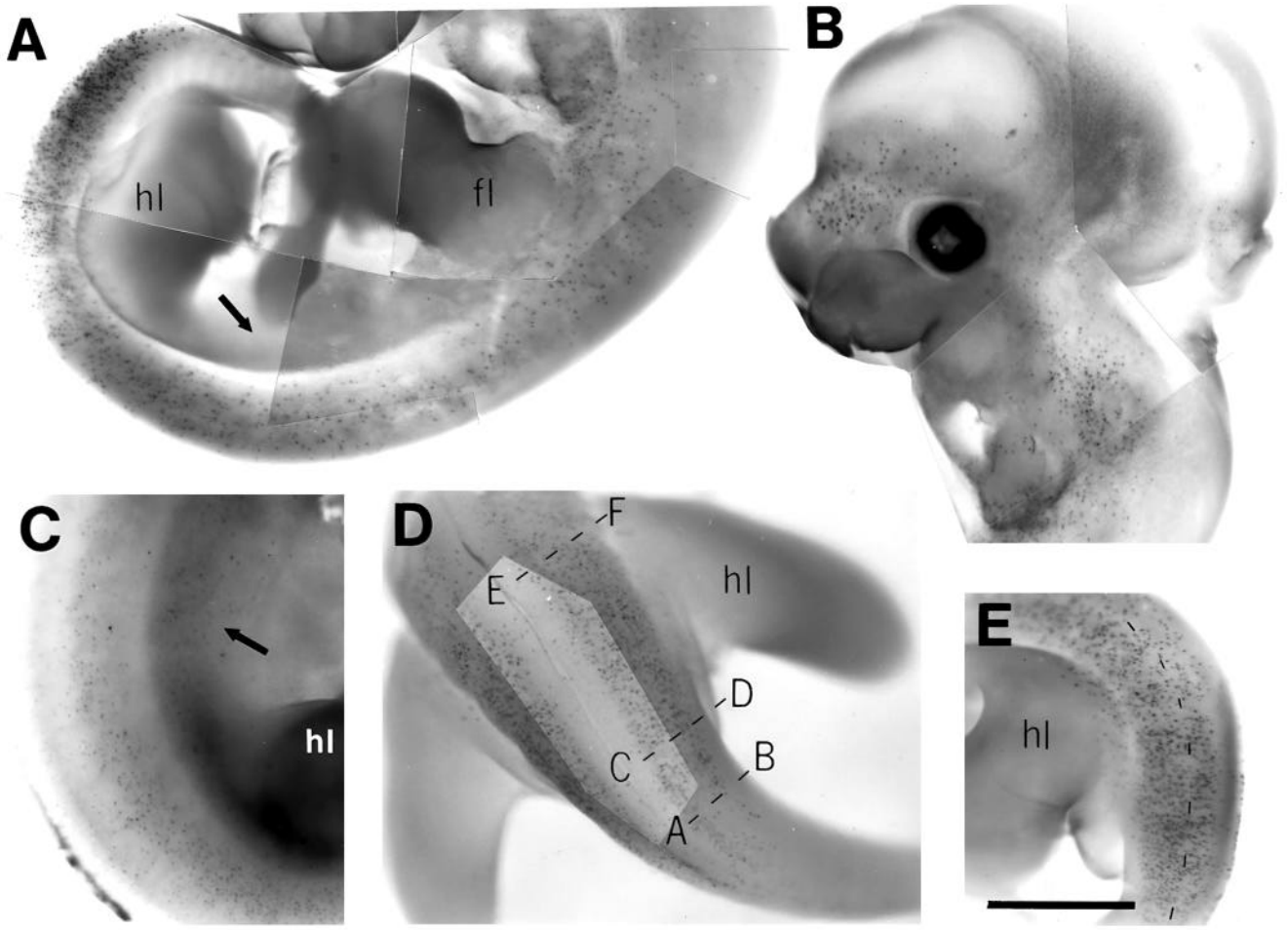

Fig. 2. Distribution of melanocyte precursors in e11.5 mouse embryos. TRP-2 and c-kit antisense whole-mount in situ hybridization of e11.5 embryos. (A,B) Lateral view of a TRP-2 antisense hybridization. (C) Lateral view of the mid trunk of an embryo hybridized with c-kit antisense probe. (D) Dorsal view of the tail and hindlimb buds of an embryo hybridized with TRP-2 antisense probe. The inset displays cells in the MSA that are at a higher focal level than the cells dispersing laterally on the dorsal migration pathway. (E) Lateral view of the hindlimb region of the embryo shown in A and B. The dashed line roughly indicates the lateral limit of the MSA. Note that many c-kit-positive cells can be detected in the lateral mesenchyme (arrow in C), which can not be detected with the TRP-2 probe (arrow in A). A-B, C-D and E-F approximately indicate the axial levels of transverse sections shown in Fig. 3. fl, forelimb; hl, hindlimb. Bar, 400 μm in A,B and E; 250 μm in C and 275 μm in D.

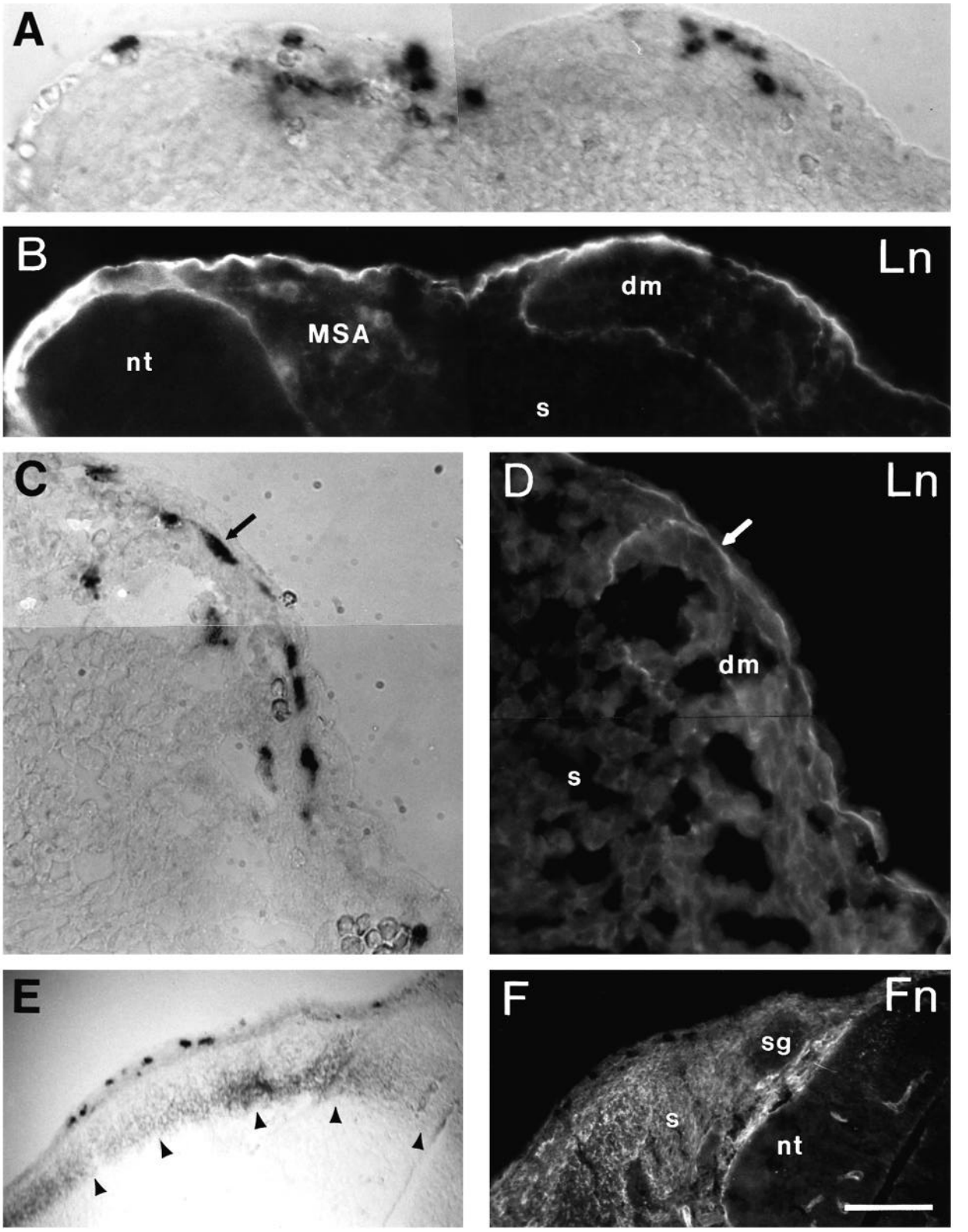

Fig. 3. Melanocyte precursor migration on the lateral pathway. Immunohistochemistry for laminin and fibronectin on transverse sections from an e11.5 TRP-2 antisense whole-mount in situ hybridization. Axial levels of each section are indicated in Fig. 2D. (A,C,E) Bright-field illuminations of sections corresponding to levels A-B, C-D and E-F, respectively. The sections are stained with either anti-laminin antiserum (B,D) or fibronectin antiserum (F). Note: TRP-2-positive cell elongated along a laminin-positive basement membrane (arrow in C and D). Arrowheads in E point to the penetration limit for the detection of mRNA in that particular embryo. Ln, laminin; Fn, fibronectin; nt, neural tube; dm, dermatome; s, sclerotome; MSA, migration staging area; sg, sensory ganglia. Bar, 25 μm in A-D and 100 μm in E,F.

Migration and localization of TRP-2 mRNA-expressing cells is different in embryos homozygous for Steel alleles compared to wild-type embryos

The *Sl* null mutation and the less severe Sl^d allele were used to reveal the function of SlF during melanocyte precursor migration on the lateral pathway. As above, the hindlimb level of e11.5 embryos was selected to compare melanocyte precursor migration and localization in normal and mutant embryos.

Fig. 6B shows the hindlimb level and the base of the tail of a *Sl/Sl* (null) embryo. Individual TRP-2 mRNA-expressing cells were detected in the MSA over a length of four to five segments (Fig. 6B, brackets). No cells were found more laterally on top of the dermatome. With the exception of a few cells localized to the mid-hindbrain border, no other TRP-2 mRNA-expressing cells were found in e11.5 embryos (not shown).

A Sl^d/Sl^d e11.5 embryo reveals a strikingly different distribution pattern of TRP-2 mRNA-expressing cells. In addition to cells localized in the MSA, many cells were found dispersed over the somites (Fig. 6C). However, no TRP-2 mRNA-expressing cells were detected anterior to the level of the hindlimb (Fig. 6C), with the exception of some cells at the mid-hindbrain border (not shown). In contrast, in wild-type embryos, a higher density of TRP-2 mRNA-expressing cells were localized over the dermatome compared to the Sl^d/Sl^d mutant embryos (Fig. 6A).

As a further test of the role of SlF function in promoting melanocyte precursor dispersal, embryos homozygous for the *W* mutation (phenotypically null for c-kit activity) were examined. Such embryos showed a pattern of TRP-2 mRNA-expressing cells in the tail region comparable to the pattern observed in *Sl/Sl* (null) embryos (Fig. 6D).

DISCUSSION

Melanocyte precursors arise in the migration staging area (MSA) prior to their dispersal on the lateral pathway

At e10.5, cells expressing TRP-2 and c-kit mRNA have been reported lateral to neural tube in the head (Steel et al., 1992). In the trunk c-kit-positive cells have been reported to be lateral to the neural tube between e10.5 and e11 (Manova and Bachvarova 1991). At later stages, we have observed c-kit and TRP-2 mRNA-positive cells at trunk levels posterior to the hindlimb buds (at the base of the tail). In addition to their presence in the MSA of the trunk, melanocyte precursors are known to be present initially in a few regions in the head, including the regions between brain vesicles and posterior to the otic vesicle. As has been suggested by Steel et al. (1992), it is very likely that these cells are melanocyte precursors and that they co-express both c-kit mRNA and TRP-2 mRNA. It is not yet known, but will be important to learn, what local environmental cues induce the expression of melanocyte specific genes, and when crest cells in the MSA respond to such cues.

Assuming that our marking studies do, in fact, reveal melanocyte precursors, it is of particular interest to note that

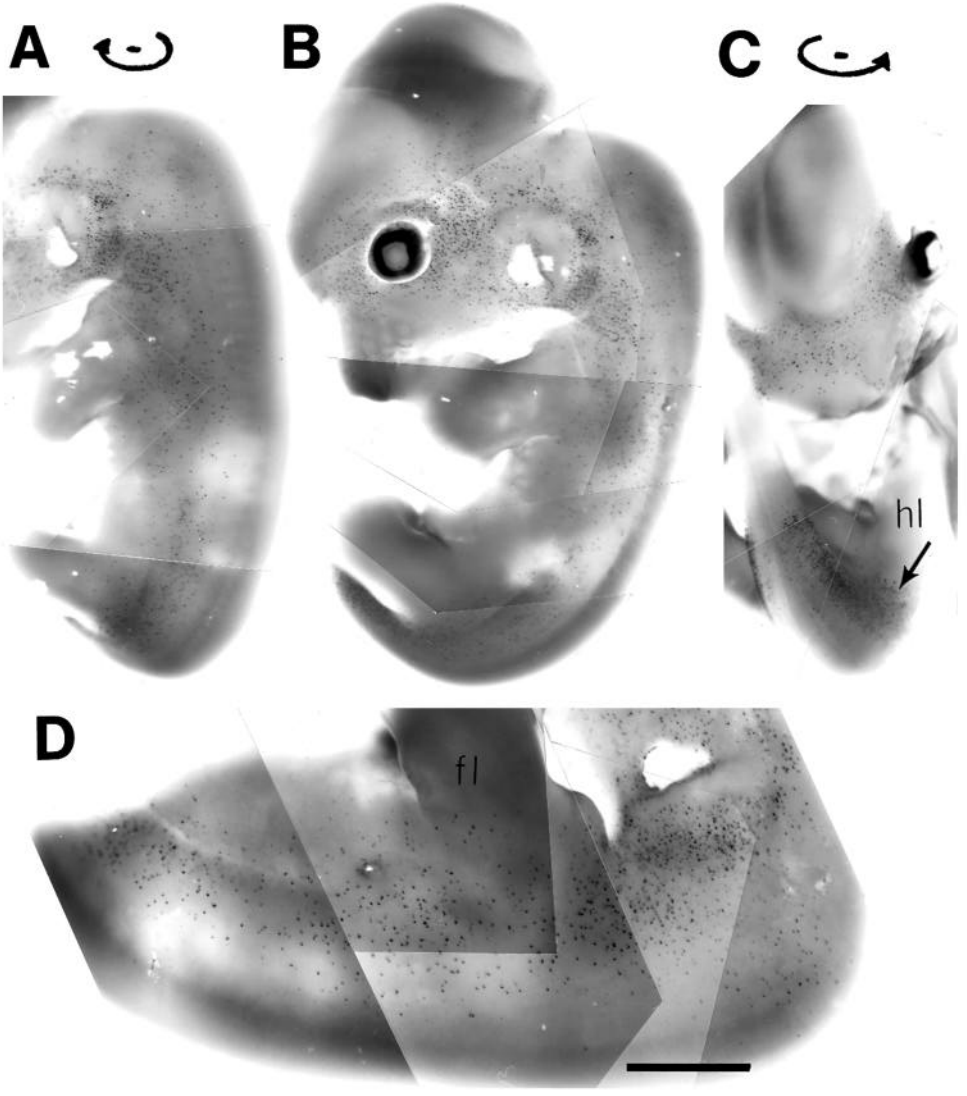

Fig. 4. Distribution of melanocyte precursors in e12.5 embryos. TRP-2 antisense whole-mount in situ hybridization of e12.5 mouse embryos. Alternative views are shown of one embryo in A-C. From B, the embryo is turned clockwise (A) or counter-clockwise (B) to reveal lateral and frontal views of the embryo. The lateral side of a different embryo is shown in D. Note: Arrow in C points to a population of TRP-2-positive cells entering the posterior aspect of the hindlimb. fl, forelimb; hl, hindlimb. Bar, 500 μm in A-C; 320 μm in D.

these cells appear belatedly as a subpopulation among crest-derived cells in the MSA. They seem to arise in the MSA after most of the neurogenic crest-derived cells have dispersed on the medial pathway (see Weston, 1991), but before dispersal has begun on the lateral crest migration pathway. In this regard, it is also of interest to note that Erickson and Goins (1995; personal communication) have also recently shown that older crest-derived cells that have become specified as melanocyte

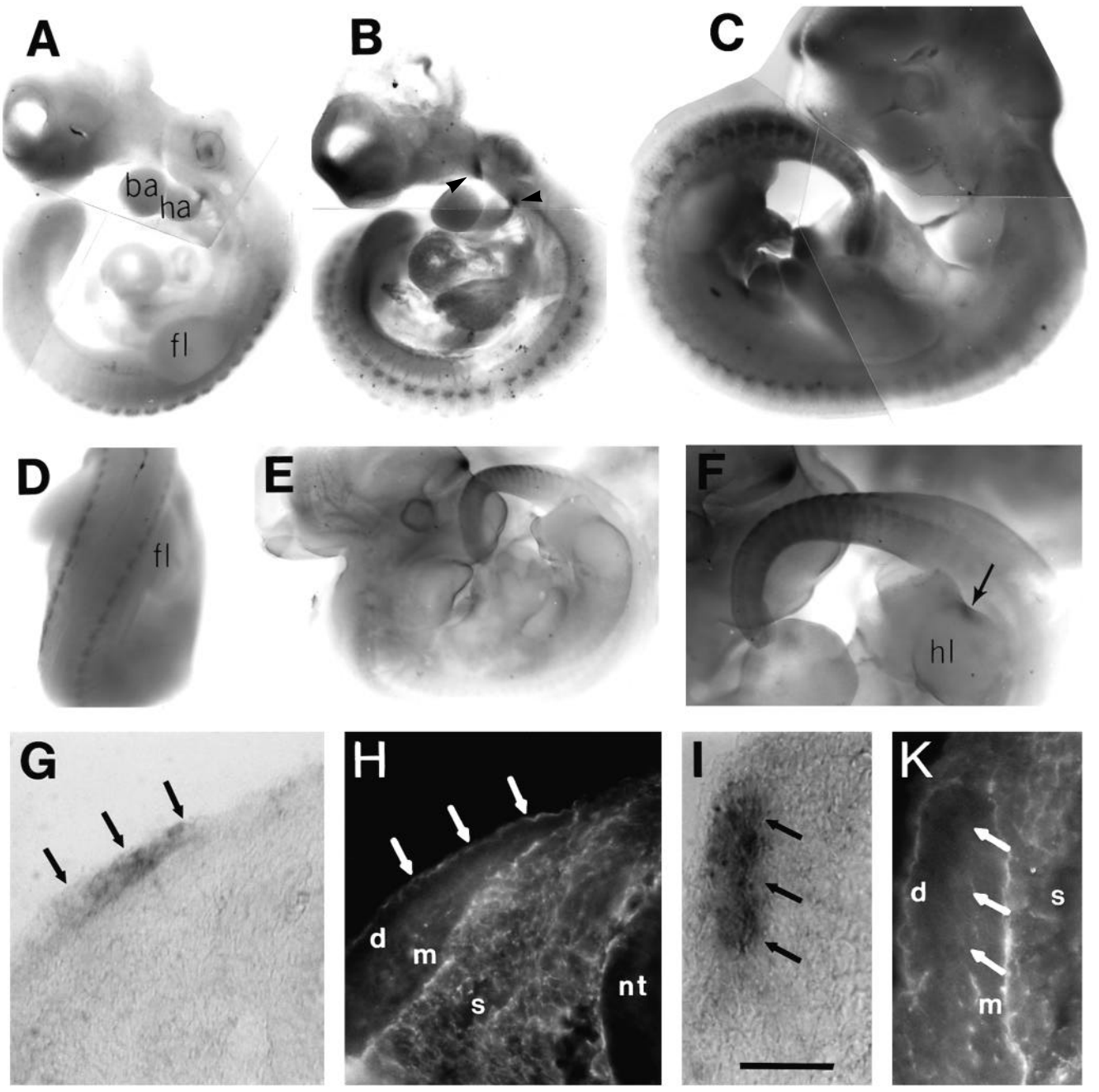

Fig. 5. Rostrocaudal sequence of SlF mRNA expression in the dorsal dermatome. SlF (KL-M1) antisense whole-mount in situ hybridization of e10.5, e11 and e11.5 mouse embryos and immunohistochemistry for laminin and fibronectin of e10.5 transverse sections. (A,B) Lateral view of two e10.5 embryos, A is slightly younger than B. Arrowheads point to mesenchymal SlF mRNA expression at the posterior border of the first and second branchial arches. (C) Lateral view of an e11 embryo. (D) Dorsal view of an e11 embryo. (E) Lateral view of an e11.5 embryo, a closeup of the tail region is shown in F. Note the expression of SlF mRNA in the posterior aspect of the hindlimb (arrow). Transverse sections of an e10.5 SlF whole-mount in situ hybridization from a midtrunk (G,H) and cervical (I,K) level. The dermatome shown in G,H is developmentally younger than that in I and K. Arrows mark the limits of the SlF mRNA expression. ba, first branchial arch; hyoid arch; fl, forelimb; hl, hindlimb; d, dermatome; m, myotome; s, sclerotome; nt, neural tube. Bar, 300 μm in A-C, E and F, 470 μm in D and 25 μm in G-K.

precursors can precociously invade the lateral migration pathway when they are grafted heterochronically into avian host embryos.

Transient expression of Steel Factor mRNA by dermatomal epithelial cells precedes dispersal of melanocyte precursors on the lateral pathway

Whole-mount in situ hybridization with a probe for SlF mRNA has confirmed earlier reports of its presence in the dorsal dermatome (Matsui et al., 1990). In addition, however, this method has revealed the precise expression pattern relative to the pattern of dispersal of putative melanocyte precursors. In particular, our results demonstrate, first, that SlF mRNA expression is transiently localized to the dorsal epithelial dermatome and, second, that this expression precedes the onset of melanocyte precursor dispersal on the migration path towards the dermatome. Finally, our results indicate that SlF mRNA is down regulated in the epithelial dermatome as it de-epithelializes to produce dermal mesenchyme. It is not known how long SlF protein persists in the dermal mesenchyme, or when SlF mRNA is re-expressed by these cells (Keshet et al., 1991; Motro et al., 1991; Orr-Urtreger et al., 1990). In utero injection of anti-c-kit antibodies (Nishikawa et al., 1991) has revealed a SlF-dependent period at around e14.5, corresponding to the time (e13-14) when melanocyte precursors localized in the dermal mesenchyme are known to enter the epidermis (Mayer, 1973). Since melanocyte precursors transiently depend on SlF for survival (see also Morrison-Graham and Weston, 1993), SlF protein must be retained and made accessible for the migrating melanocyte precursors in the newly formed dermis. No data are yet available on the presence and location of SlF protein after the transformation of the dermatome into dermal mesenchyme is completed.

Melanocyte precursors in the MSA initially disperse toward the site where SlF mRNA is transiently produced

In the head, at e11 c-kit/TRP-2 mRNA-positive cells localize to regions where SlF mRNA was detected at e10.5 (Steel et al., 1992). Likewise, melanocyte precursors disperse from the MSA

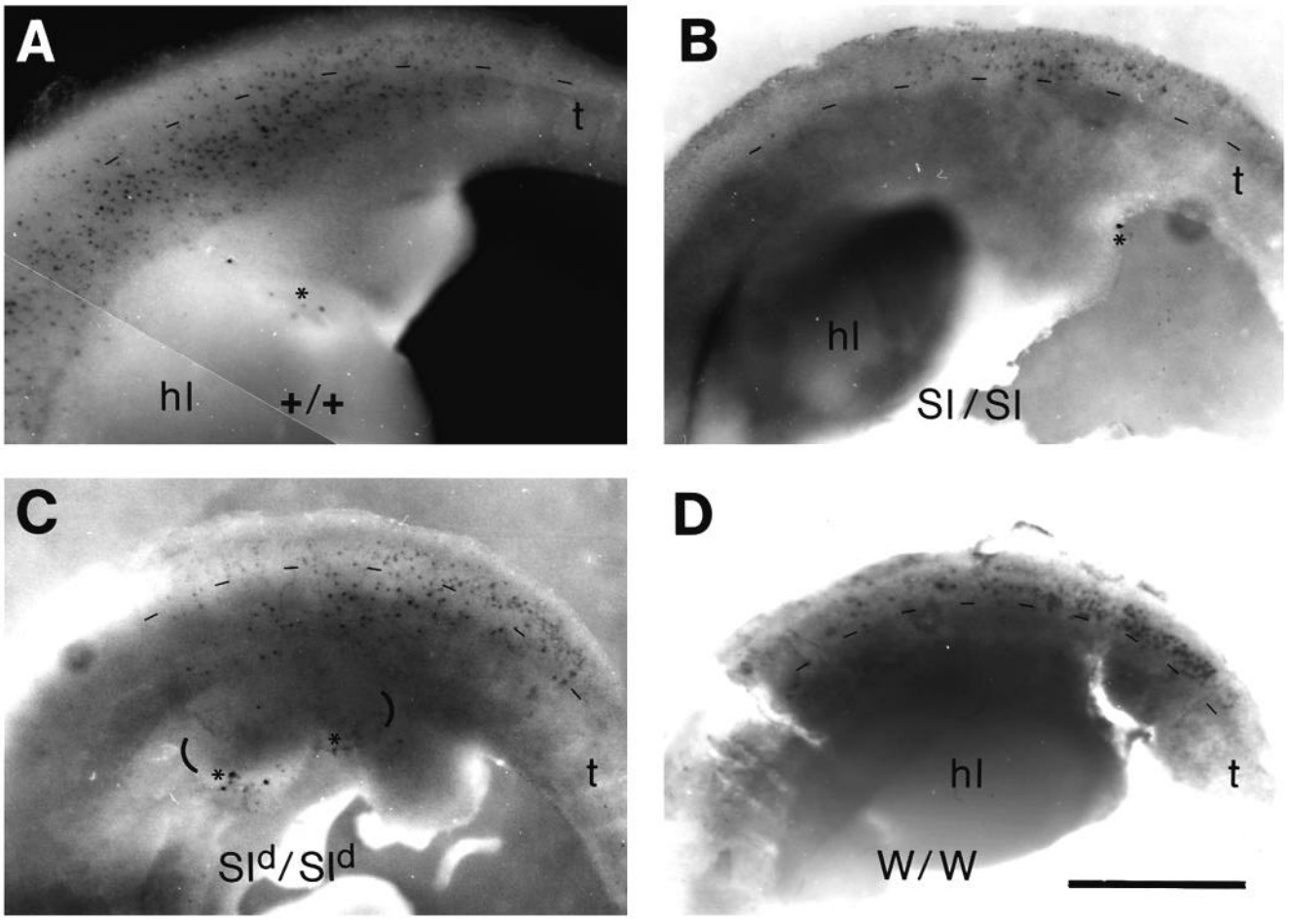

Fig. 6. Melanocyte precursors initially appear but behave differently in *Steel* mutant embryos. TRP-2 antisense whole-mount in situ hybridization of e11.5 mouse mutant embryos. The tail and hindlimb bud region is shown of embryos being wild type (A, +/+), homozygous for SlF null allele (B, *Sl*/*Sl*), homozygous for *Sl dickie* (C, Sl^d/Sl^d) or homozygous for c-kit functional null allele (D, *W/W*). The litter that contained embryo D was developmentally slightly younger than other 'e11.5' litters so that cells were seen over a wider area along the A-P axis compared to the developmentally older embryo seen in B. In addition, this embryo was stained longer than the other embryos, which affected the appearance of the stained cells. The dashed lines roughly indicate the lateral limits of the MSA. In C, the location of the limb bud, which was removed for genotyping (see Methods), is indicated with parentheses; dirt particles are marked with asterisk. hl, hindlimb; t, tail. Bar, 200 μm.

to sites where SlF mRNA had been transiently expressed about 6-12 hours previously, suggesting an influence of SlF protein on the migration and localization of melanocyte precursors. Interestingly, melanocyte precursors migrating on the lateral pathway seem to follow existing basement membranes, as do the medially migrating crest cells (Tosney et al., 1994). Two extreme models could explain the observed migration pattern. First, TRP-2/c-kit mRNA-expressing cells could migrate on both the medial and lateral pathways and survive only at locations expressing SlF. This model would imply a passive role of SlF on initial cell migration stressing only the survival effect of SlF on dependent cell populations. Alternatively, cells that express functional c-kit receptors, as implied by c-kit mRNA expression, could be selectively attracted onto the lateral pathway by SlF that is locally produced by dermatomal epithelium and diffuses from its site of expression. This notion is supported by the reports that c-kit-expressing carcinoma cells as well as c-kit transfected endothelial cells show chemotaxis towards SlF in vitro (Blume-Jensen et al., 1991; Sekido et al., 1993), and is consistent with the belated appearance of cells in the MSA that express c-kit and the corresponding delay in onset of migration on the lateral pathway. Although the initial onset of dispersal of melanocyte precursors on the lateral pathway is consistent with a chemotactic response to a source of SlF in the dermatome, the subsequent dispersal of melanocyte precursors that occurs after e11.5 in the dermal mesenchyme of the trunk, limb buds or ventral body wall, cannot be explained by a graded or localized source of SlF.

Melanocyte precursors fail to disperse or survive in Steel null mutant embryos

If SlF were required for initial dispersal of melanocyte precursors, then these cells would be predicted to remain in the MSA in mutants that do not produce this molecule. This prediction has been verified by our observations of the behavior of TRP-2 mRNA-expressing cells in Steel null embryos. Such cells appear in the MSA in a timely way, but never disperse, and ultimately disappear. The fate of these melanocyte precursors is not known. Alternatively, their apparent failure to disperse may be the result of failing to survive in the MSA long enough to do so. We know that melanocyte precursors in vitro require transient trophic support from SlF for about 5 days (Morrison-Graham and Weston, 1993). Since the time interval during which melanocyte precursors are generated in the MSA is not known, however, it is difficult to estimate how long individual TRP-2/c-kit mRNA-expressing cells can survive in the MSA in the absence of SlF. If this period were brief, however, SlF-dependent cells would probably not survive long enough to leave the MSA. In this regard, mast cells, which are also dependent on c-kit/SlF activity, begin to degenerate in vitro within 5 hours after SlF is removed from their culture medium (Iemura et al., 1994; Caceres-Cortes et al., 1994). Survival of individual melanocyte precursors in the MSA of SlF null mutants might be even shorter because these cells would never have received an SlF stimulus.

The conclusion that crest-derived melanocyte precursors require a timely SlF stimulus in the MSA is supported by our observations that TRP-2 mRNA-expressing melanocyte precursors are initially present in the MSA, but are never found on the lateral pathway of embryos that are homozygous for the *W* mutation. Thus, cells that lack functional c-kit receptors are unable to detect the presence of SlF, and therefore either fail to survive in the MSA or are unable to depart on the lateral pathway in response to a directional SlF signal.

Soluble SlF is sufficient to permit initial dispersal of melanocyte precursors from the MSA onto the lateral pathway, but not for eventual survival and/or differentiation

The *Steel dickie* (Sl^d) mutation results in a truncated but biologically active form of SlF that lacks a transmembrane domain (Brannan et al., 1991). The lack of a transmembrane anchor results in the secretion of SlF by cells from Sl^d homozygotes (Flanagan et al., 1991). Since Sl^d homozygotes exhibit an intermediate phenotype compared to *Sl* null mutants, the membrane-bound SlF appears to be required for normal development of these cells.

Paradoxically, neural crest cell cultures are able to give rise to melanocytes in vitro when cultured in the presence of exogenous soluble SlF (Morrison-Graham and Weston, 1993), or on detergent-extracted (cell-free) extracellular matrix (ECM) deposited by wild-type embryonic skin fibroblast in vitro (Morrison-Graham et al., 1990). ECM deposited by such cells seems to contain enough SlF to satisfy the SlF-dependent melanocyte precursors in vitro. In contrast, detergent-extracted ECM deposited by cultured fibroblasts from Sl^d homozygotes fail to support melanogenesis in vitro (Morrison-Graham et al., 1990), suggesting that the truncated SlF is not incorporated or retained in ECM secreted by these cells to permit survival and/or differentiation of melanocyte precursors.

Heterochronic grafting experiments (Erickson and Goins, 1995; personal communication) indicate that melanocyte precursors arise late and invade the dorsolateral migration pathway in response to some localized cue(s) in the avian embryo. It seems likely that the soluble form of SlF may be at least one such cue. Thus, in the present report, it is of particular interest that crest-derived melanocyte precursors do, in fact, leave the MSA on the lateral pathway in Sl^d homozygotes, suggesting that the truncated (soluble) SlF produced by the dorsal dermatome is sufficient for crest cells to initiate dispersal on the lateral pathway. However, since these dispersing melanocyte precursors fail to survive in the dermal mesenchyme, the truncated SlF appears not to provide an appropriate survival stimulus in the dermatomal ECM.

Taken together, the behavior and fate of melanocyte precursors in the null mutant compared to that in normal embryos or the Sl^d homozygotes suggests that cell-bound and soluble SlF have distinct functions. Although it is not known how much SlF is normally released by dermatomal cells and is present in interstitial crest migration spaces, it seems likely that soluble SlF might be required to promote dispersal of c-kit mRNA-expressing melanocyte precursors, or to attract them to its local source. Likewise, the behavior and fate of melanocyte precursors in Sl^d embryos suggests that an 'immobilized' form of SlF is required for survival of the responsive cell type. Three published reports support our inference that soluble and cell-bound SlF play distinct roles in cell dispersal and survival, respectively. First, in the head of Sl^d embryos, TRP-2 mRNA-expressing cells appear initially and disperse, but then disappear (Steel et al., 1992). Second, germ cells, which are known to require SlF and c-kit for survival can be found in small numbers at the genital ridges in Sl/Sl^d embryos

(McCoshen and McCallion, 1975), whereas in *Steel* null mutant embryos, germ cells do not proliferate and are retarded in their migration to the genital ridges (Mintz and Russell, 1957). Finally, on a fibronectin substratum in vitro, motility of mast cells, which are strictly dependent on c-kit for survival, is stimulated by an SlF dose which is 100-fold less than that required for survival (Kinashi and Springer, 1994; Dastych and Metcalf, 1994). Therefore different concentration of SlF in the cell environment may induce motogenic versus mitogenic responses (Blume-Jensen et al., 1993).

We are grateful to Drs Yoshiko Takahashi and Carol Erickson, who worked in our laboratory on preliminary experiments leading to this paper, and to Monique Wehrle-Haller, Drs Erickson, K. Morrison-Graham and Sherry Rogers, for their critical comments on the manuscript. We also thank Drs John Flanagan, Ian Jackson, Robert Arceci for generously providing cDNA plasmids and Dr Peter Lonai for sharing primer sequences. Special thanks to Rick Gosswiller, for his careful animal husbandry and Jerry Gleason for photographic assistance. Our work has been supported by grant DE-04316 from the USPHS. B. W-H is supported by an EMBO Postdoctoral Fellowship (169-1993). Dr Erickson's work in our laboratory was supported by grant DE-05620 from the USPHS.

REFERENCES

Anderson, D., Lyman, S., Baird, A., Wignall, J., Eisenman, J., Rauch, C., March, C. J., Boswell, H., Gimpel, S., Cosman, D. and Williams, D. (1990). Molecular cloning of mast cell growth factor a hematopoietin that is active in both membrane bound and soluble forms. *Cell* **63**, 235-243.

Blume-Jensen, P., Claesson-Welsh, L., Siegbahn, A., Zsebo, K., Westermark, B. and Heldin, C. (1991). Activation of the human c-*kit* product by ligand-induced dimerization mediates circular actin reorganization and chemotaxis. *EMBO J.* **10**, 4121-4128.

Blume-Jensen, P., Siegbahn, A., Stabel, S., Heldin, C. and Roennstrand, L. (1993). Increased kit/SCF receptor induced mitogenicity but abolished cell motility after inhibition of protein kinase C. *EMBO J.* **12**, 4199-4209.

Brannan, C., Lyman, S., Williams, D., Eisenman, J., Anderson, D., Cosman, D., Bedell, M., Jenkins, N. and Copeland, N. G. (1991). *Steel-dickie* mutation encodes a c-kit ligand lacking transmembrane and cytoplasmic domains. *Proc. Natl. Acad. Sci. USA* **88**, 4671-4674.

Caceres-Cortes, J., Rajotte, D., Dumouchel, J., Haddad, P. and Hoang, T. (1994). Product of the *Steel* locus suppresses apoptosis in hematopoietic cells. *J. Biol. Chem.* **269**, 12084-12091.

Copeland, N., Gilbert, D., Cho, B., Donovan, P., Jenkins, N., Cosman, D., Anderson, D., Lyman, S. and Williams, D. (1990). Mast cell growth factor maps near the *Steel* locus on mouse chromosome 10 and is deleted in a number of *Steel* alleles. *Cell* **63**, 175-183.

Dastych, J. and Metcalf, D. (1994). Stem cell factor induces mast cell adhesion to fibronectin. *J. Immunol.* **152**, 213-219.

Derby, M. (1978). Analysis of glysosaminoglycans within the extracellular environments encountered by migrating neural crest cells. *Dev. Biol.* **66**, 321-336.

Duttlinger, R., Manova, K., Chu, T., Gyssler, C., Zelenetz, A., Bachvarova, R. F. and Besmer, P. (1993). *W-sash* affects positive and negative elements controlling *c-kit* expression: ectopic *c-kit* expression at sites of kit-ligand expression affects melanogenesis. *Development* **118**, 705-717.

Erickson, C. and Loring, J. (1987). Neural crest cell migratory pathways in the trunk of the chick embryo. *Dev. Biol.* **121**, 220-236.

Erickson, C. and Goins, T. M. (1995). Neural crest cells can migrate in the dorsolateral path only if they are specified as pigment cells. *Development* (in press).

Erickson, C., Duong, T. and Tosney, K. (1992). Descriptive and experimental analysis of dispersion of neural crest cells along the dorsolateral path and their entry into ectoderm in the chick embryo. *Dev. Biol.* **151**, 251-271.

Flanagan, J. and Leder P. (1990). The *kit* ligand: a cell surface molecule altered in *Steel* mutant fibroblasts. *Cell* **63**, 185-194.

Flanagan, J., Chan, D. and Leder P. (1991). Transmembrane form of the kit ligand growth factor is determined by alternative splicing and is missing in the Sl^d mutant. *Cell* **64**, 1025-1035.

Geissler, E., Ryan, M. and Housman, D. E. (1988). The dominant-white spotting (W) locus of the mouse encodes the c-kit proto-oncogene. *Cell* **55**, 185-192.

Hayashi, S., Kunisade, T., Ogawa, M., Yamaguchi, K. and Nishikawa, S. (1991). Exon skipping by mutation of an authentic splice site of c-*kit* gene in *W/W* mouse. *Nuc. Acids. Res.* **19**, 1267-1271.

Huang, E., Nocka, K., Beier, D. R., Chu, T., Buck, J., Lahm, H., Wellner, D., Leder, P. and Besmer, P. (1990). The hematopoietic growth factor KL is encoded by the *Sl* locus and is the ligand of the *c-kit* receptor, the gene product of the *W* locus. *Cell* **63**, 225-233.

Huang, E., Nocka, K., Buck, J. and Besmer, P. (1992). Differential expression and processing of two cell associated forms of the kit-ligand: Kl-1 and Kl-2. *Mol. Biol. Cell* **3**, 349-362.

Iemura, A., Tsai, M., Ando, A., Wershil, B. and Galli, S. (1994). The c-*kit* ligand, stem cell factor, promotes mast cell survival by suppressing apoptosis. *Am. J. Pathol.* **144**, 321-328.

Keshet, E., Lyman, S., Williams, D., Anderson, D., Jenkins, N., Copeland, N. and Parada, L. (1991). Embryonic RNA expression patterns of the c-*kit* receptor and its cognate ligand suggest multiple functional roles in mouse development. *EMBO J.* **10**, 2425-2435.

Kinashi, T. and Springer, T. (1994). Steel factor and *c-kit* regulate cell-matrix adhesion. *Blood* **83**, 1033-1038.

Manova, K. and Bachvarova, R. (1991). Expression of c-*kit* encoded at the *W* locus of mice in developing embryonic germ cells and presumptive melanoblasts. *Dev. Biol.* **146**, 312-324.

Matsui, Y., Zsebo, K. and Hogan, B. (1990). Embryonic expression of a hematopoietic growth factor encoded by the *Sl* locus and the ligand for c-kit. *Nature* **347**, 667-669.

Mayer, T. C. (1973). The migratory pathway of neural crest cells into the skin of mouse embryos. *Dev. Biol.* **34**, 39-46.

McCoshen, J. and McCallion, J. (1975). A study of the primordial germ cells during their migratory phase in *Steel* mutant mice. *Experientia* **31**, 589-590.

Mintz, B. and Russell, E. S. (1957). Gene-induced embryological modifications of primordial germ cells in the mouse. *J. Exp. Zool.* **134**, 207-237.

Morrison-Graham, K., West-Johnsrud, L. and Weston, J. (1990). Extracellular matrix from normal but *Steel* mutant mice enhances melanogenesis in cultured mouse neural crest cells. *Dev. Biol.* **139**, 299-307.

Morrison-Graham, K. and Takahashi, Y. (1993). Steel factor and c-kit receptor: from mutants to a growth factor system. *BioEssays* **15**, 77-83.

Morrison-Graham, K. and Weston J. (1993). Transient Steel factor dependence by neural crest-derived melanocyte precursors. *Dev. Biol.* **159**, 346-352.

Motro, B., Van der Kooy, D., Rossant, J., Reith, A. and Bernstein, A. (1991). Contiguous patterns of c-*kit* and *Steel* expression: analysis of mutations at the *W* and *Sl* loci. *Development* **113**, 1207-1221.

Nishikawa, S., Kusakabe, M., Yoshinaga, K., Ogawa, M., Hayashi, S., Kunisade, T., Era, T., Sakakura, T. and Nishikawa, S. (1991). *In utero* manipulation of coat color formation by a monoclonal anti-*c-kit* antibody: two distinct waves of *c-kit* dependency during melanocyte development. *EMBO J.* **10**, 2111-2118.

Nocka, K., Buck, J., Levi, E. and Besmer, P. (1990a). Candidate ligand for the c-*kit* transmembrane kinase receptor: KL, a fibroblast derived growth factor stimulates mast cells and erythroid progenitors. *EMBO J.* **9**, 3287-3294.

Nocka, K., Tan, J., Chiu, E., Chu, T., Ray, P., Traktman, P. and Besmer, P. (1990b). Molecular bases of dominant negative and loss of function mutations at the murine c-kit/white spotting locus: W^{37}, W^{v}, W^{41}, and *W*. *EMBO J.* **9**, 1805-1813.

Orr-Urtreger, A., Avivi, A., Zimmer, Y., Givol, D., Yarden, Y. and Lonai, P. (1990). Developmental expression of c-kit, a proto-oncogene encoded by the *W* locus. *Development* **109**, 911-923.

Orr-Urtreger, A., Bedford, M., Do, M.-S., Eisenbach, L. and Lonai, P. (1992). Developmental expression of the a receptor for platelet-derived growth factor, which is deleted in the embryonic lethal *Patch* mutation. *Development* **115**, 289-303.

Pavan, W. and Tilghman, S. (1994). Piebald lethal (s^l) acts early to disrupt the development of neural crest-derived melanocytes. *Proc. Nat. Acad. Sci. USA* **91**, 7159-7163.

Rawles, M. E. (1947). Origin of pigment cells from the neural crest in the mouse embryo. *Physiol. Zool.* **20**, 248-265.

Sekido, Y., Takahashi, T., Ueda, R., Takahashi, M., Suzuki, H., Nishida, K., Tsukamoto, T., Hida, T., Shimokata, K., Zsebo, K. M. and

Takahashi, T. (1993). Recombinant human stem cell factor mediates chemotaxis of small-cell lung cancer cell lines aberrantly expressing the c-*kit* proto-oncogene. *Cancer Res.* **53**, 1709-1714.

Steel, K., Davidson, D. and Jackson, I. (1992). TRP-2/DT, a new early melanoblast marker, shows that Steel growth factor (c-kit ligand) is a survival factor. *Development* **115**, 111-1119.

Tosney, K., Dehnbostel, D. and Erickson, C. A. (1994). Neural crest cells prefer the myotome's basal lamina over the sclerotome as a substratum. *Dev. Biol.* **163**, 389-406.

Wang, C., Kelly, J., Bowen-Pope, D. and Stiles, C. (1990). Retinoic acid promotes transcription of the platelet-derived growth factor alpha receptor gene. *Mol. Cell Biol* **10**, 6781-6784.

Weston J. A. (1991). Sequential segregation and fate of developmentally restricted intermediate cell populations in the neural crest lineage. *Cur. Topics Dev. Biol.* **25**, 133-153.

Williams, D., Eisenman, J., Baird, A., Rauch, C., Van Ness, K., March, C., Park, L. S., Martin, U., Mochizuki, D., Boswell, H., Burgess, G., Cosman, D. and Lyman, S. D. (1990). Identification of a ligand for the c-*kit* proto-oncogene. *Cell* **63**, 167-174.

Williams, D., De Vries, P., Namen, A., Widmer, M. and Lyman, S. (1992). The *Steel* factor. *Dev. Biol.* **151**, 368-376.

Yamaguchi, T., Conlon, R. and Rossant, J. (1992). Expression of the fibroblast growth factor receptor FGFR-1/flg during gastrulation and segmentation in the mouse embryo. *Dev. Biol.* **152**, 75-78.

Yoshida, H., Nishikawa, S., Okamura, H., Sakakura, T. and Kusakabe, M. (1993). The role of c-*kit* proto-oncogene during melanocyte development in mouse. *in vivo* approach by the *in utero* microinjection of anti-c-kit antibody. *Dev. Growth Differ.* **35**, 209-220.

(Accepted 28 October 1994)

2.3. Limiting Stem Cell factor supply affects melanocyte migration and survival

In addition to the *Steel* (*Mgf*^{Sl}) and *Dominant White Spotting* (*Kit*^{W}) mutations, a number of other dominant "spotting" mouse mutants have been acquired and kept in the various mouse husbandries. The affected genes for some of these pigment pattern mutants have been identified as being crucial for the differentiation and proliferation of neural crest and melanocyte precursors. The genes that affect differentiation, survival and proliferation of melanocytes in their mutated forms include transcriptional activators such as the Sox 10 (Dominant megacolon) (Kapur, 1999; Southard-Smith et al., 1998) or Pax3 (Splotch) (Conway et al., 1997; Tassabehji et al., 1994) and the G-protein coupled receptor endothelin receptor B (Piebald spotting) (Hosoda et al., 1994) and its ligand endothelin3 (Lethal spotting) (Baynash et al., 1994). In addition to these genes that specifically affect melanocyte function, a number of dominant spotting mutations have been localized close to the c-Kit locus (Nagle et al., 1994; Stephenson et al., 1994). However, although pigment patterns were disturbed in a dominant fashion the c-kit expression in melanocyte precursors was not seemingly altered. The *Rumpwhite* and *Patch* mutation fall into this category. Although *Patch* mutant animals exhibit a very similar pigment pattern defect as one of the *Kit* alleles (*Kit*$^{W\text{-}sash}$), it was speculated that the PDGFRα gene (deleted in the *Patch* mutant (Stephenson et al., 1991)) plays a very important role in melanocyte survival or migration (Morrison-Graham et al., 1992). We have demonstrated however, that this large deletion of the PDGFRα locus induces the ectopic expression of the c-Kit receptor in dermal fibroblasts originating from the dermamyotome (see below). Interestingly, the ectopic expression of c-Kit mirrors precisely the normal endogenous expression pattern of the PDGFRα gene. A similar ectopic expression of c-Kit is observed in the *Kit*$^{W\text{-}sash}$ mutant (Duttlinger et al., 1995; Duttlinger et al., 1993), caused however by a genetic inversion with one of its breakpoints located in the c-Kit promoter (Nagle et al., 1995). It is therefore plausible, that the pigmentation defect in the *Patch* as well as the *Kit*$^{W\text{-}sash}$ mutation is caused by the deletion or separation of a silencer element that suppresses c-Kit expression in dermal fibroblasts or more generally in PDGFRα expressing cell populations.

Due to the collection of these rather peculiar pigment pattern mutants we can gain a glimpse of the mechanics of evolution and the development of the vertebrates in particular. In fact, the duplicated gene cluster consisting of three receptor tyrosine kinases (PDGFRα, c-Kit, Flk1;

PDGFRβ, c-fms, Flk2) have arisen by multiple gene- and one chromosomal-duplication (Kataoka et al., 1997). All six receptor tyrosine kinases (RTK) share a split tyrosine-kinase domain, while 4 of these RTK's exhibit 5 extracellular IgG-like domains (PDGFR's, c-Kit, c-fms) and 2 exhibit 7 IgG-like domains (Flk's). PDGFR's are expressed and required in mesenchymal cells of the connective tissue. Flk's are expressed and required for the proliferation of the hemangioblasts and endothelial cells and c-Kit and c-fms have important functions for the maintenance of the hematopoietic system (Kataoka et al., 1997).

Therefore we can hypothesis that during evolution, the birth of new mesenchymal cell types required not only gene duplications (promoter and coding region) but also adaptation to a new extracellular ligand (coding sequence) and new promoter elements allowing for cell type specific expression (promoter). In the case of c-kit, however, the acquisition of a silencer element that suppressed mesenchymal expression of the PDGFRα/c-Kit ancestral gene was pivotal for the usage of c-Kit in cell types that depend on mesenchymal expression of growth factors. The *Patch* deletion reveals the existence of such a mesenchymal silencer in the c-Kit promoter (Berrozpe et al., 1999). In its absence, ectopic expression of c-Kit in mesenchymal cells is consuming limited amounts of SCF produced by the same dermal mesenchyme leading to a change in the migration pattern and the subsequent loss of melanocyte precursors from the entire trunk region. However, due to the limitation of the ectopic c-Kit expression to the dermal mesenchyme, melanocyte precursors that succeeded to penetrate the epidermis in the head and tail regions proliferate in this SCF rich epidermal environment and move posterior and anterior to narrow the band of melanocyte free coat (Jordan and Jackson, 2000a).

DEVELOPMENTAL BIOLOGY 177, 463–474 (1996)
ARTICLE NO. 0178

Ectopic c-kit Expression Affects the Fate of Melanocyte Precursors in *Patch* Mutant Embryos

Bernhard Wehrle-Haller, Kathleen Morrison-Graham, and James A. Weston

Institute of Neuroscience, 1254 University of Oregon, Eugene, Oregon 97403-1254

The *Patch* (*Ph*) mutation in the mouse, a deletion that includes the gene for PDGFRα, is a recessive lethal that exhibits a dominant pigment phenotype in heterozygotes. To assess whether the *Ph* mutation acts cell-autonomously or non-autonomously on melanocyte development, we have examined the melanogenic potential of neural crest populations from normal and mutant crest cells *in vitro* and the pattern of dispersal and survival of melanocyte precursors (MPs) *in vivo*. We report that trunk neural crest cells from homozygous *Ph* embryos give rise to pigmented melanocytes *in vitro* in response to Steel factor (SlF). *In vivo,* homozygous *Ph* embryos contain a subpopulation of crest-derived cells that express c-kit and tyrosinase-related protein-2 characteristic of MPs. These cells begin to migrate normally on the lateral crest migration pathway, but then fail to disperse in the dermal mesenchyme and subsequently disappear. Although dermal mesenchyme is adversely affected in *Ph* homozygotes, SlF mRNA expression by the cells of the dermatome is normal in *Ph* embryos when neural crest-derived MPs start to migrate on the lateral pathway. In contrast, mRNA for the SlF receptor, c-kit, was observed to be ectopically expressed in somites and lateral mesenchyme in embryos carrying the *Ph* mutation. Based on this ectopic expression of c-kit in *Ph* mutant embryos, and the observed distribution of SlF protein in normal and mutant embryos, we suggest that competition for limited amounts of SlF localized on the lateral neural crest migration pathway alters melanocyte dispersal and survival.

INTRODUCTION

Several mouse pigment pattern mutants have been described and their defects analyzed at the molecular level. Two of the best characterized are the *Dominant spotting* (*W*) and the *Steel* (*Sl*) mutations, which encode the c-kit receptor tyrosine kinase (Geissler *et al.,* 1988) and its ligand, Steel factor (SlF, also known as stem cell factor, mast cell growth factor, or kit ligand), respectively. Both mutations affect development of pigment cells as well as hematopoietic and germ cells (Anderson *et al.,* 1990; Copeland *et al.,* 1990; Huang *et al.,* 1990; Williams *et al.,* 1990).

Another pigment pattern mutant, *Patch* (*Ph*), is a recessive lethal that shows a dominant pigment phenotype in heterozygotes. Homozygous *Ph* embryos die between e8-9 and e16-17 depending on the genetic background (Morrison-Graham *et al.,* 1992; Orr-Urtreger *et al.,* 1992). In *Ph* homozygotes, characteristic defects in mesenchymal tissues are accompanied by cleft palate, epidermal blisters, kinky neural tube, and failure of heart septation (Grüneberg and Truslove, 1960; Erickson and Weston, 1983; Morrison-Graham *et al.,* 1992; Orr-Urtreger *et al.,* 1992; Schatteman *et al.,* 1992). The *Ph* locus is located on chromosome five in the mouse, adjacent to the *W* locus that encodes c-kit, and has been shown to be a deletion of about 200 kb spanning the entire coding region of PDGFRα (Smith *et al.,* 1991; Stephenson *et al.,* 1991, 1994; Nagle *et al.,* 1994). Although much is known about the role of the c-kit gene for melanocyte development and survival (Nishikawa *et al.,* 1991; Steel *et al.,* 1992; Morrison-Graham and Weston, 1993; Wehrle-Haller and Weston, 1995; Reid *et al.,* 1995), it is not yet known how the lack of the PDGFRα gene results in the pigment pattern phenotype seen in *Patch* heterozygotes.

Since PDGFRα transcripts are normally expressed by cranial ectomesenchyme in branchial arches and the cardiac outflow tract, but not by neurons of the central nervous system or the crest-derived peripheral nervous system (Morrison-Graham *et al.,* 1992; Schatteman *et al.,* 1992), the defects in *Ph* homozygous embryos, like cleft palate and the absence of conotruncal septation, may be directly caused by the failure of nonneurogenic neural crest-derived cells to survive or proliferate in these locations. Similarly, since a

0012-1606/96 $18.00

subset of nonneurogenic crest-derived cells normally undergoes melanogenesis, the pigment phenotype observed in *Patch* heterozygotes might result cell-autonomously from a lack of PDGFRα expression in mutant melanocyte precursors (MPs). However, since melanocytes disperse and proliferate in the dermal mesenchyme (Wehrle-Haller and Weston, 1995), which is known to require PDGFRα activity (Morrison-Graham *et al.*, 1992; Schatteman *et al.*, 1992), the *Patch* mutation might alter the pigment pattern noncell-autonomously by adversely affecting the environment in which melanocytes develop.

Thus, various alternative hypotheses can explain the pigment phenotype in *Patch* mutants. First, as is the case for c-kit, PDGFRα might act cell-autonomously to promote MP survival and development. Second, loss of PDGFRα activity might indirectly affect the production or localization of SlF or other growth factors (Murphy *et al.*, 1994) required for MP migration, proliferation, and/or survival. Alternatively, the genomic deletion in *Patch* mentioned above might disrupt adjacent genes, such as c-kit (Nagle *et al.*, 1994; Duttlinger *et al.*, 1995; Bucan *et al.*, 1995), directly or indirectly causing the pigment phenotype.

In order to distinguish among these possibilities, we used a variety of techniques to examine melanogenesis *in vivo* and *in vitro*. We show that melanocyte precursors from *Patch* homozygotes can survive, express c-kit, and undergo melanogenesis in a supportive environment *in vitro*. We further demonstrate that the initial appearance of melanocyte precursors *in vivo* is normal, but their ultimate distribution and survival is altered in *Ph* mutant embryos. These results are not consistent with the hypothesis that PDGFRα acts cell-autonomously on crest-derived melanocyte precursors. We also show that expression of SlF mRNA and protein by the dermatome is not perturbed in *Patch* homozygotes. Finally, we show that c-kit is ectopically expressed in *Patch* embryos, which, taken together with our observations on the pattern of distribution of SlF protein in these embryos, suggests that melanocyte precursors might compete with mesenchyme cells that ectopically express c-kit for a limiting amount of ligand. We suggest that such a competition for SlF might explain the observed *Patch* pigment phenotype.

MATERIALS AND METHODS

Embryos

The *Patch* mutation has been carried on a C57Bl6 inbred background for many generations. In order to promote fecundity of the highly inbred strain we backcrossed it once with our C57Bl6 line and subsequently maintained it by brother sister mating. The *Patch* mutation within this background does not yield homozygous embryos older than e11.5. In order to obtain *Ph*/*Ph* homozygous embryos with a cleft palate phenotype (viable embryos older than e11.5), we mated F1 animals from a *Ph* $\times$ Balb/C cross (Morrison-Graham *et al.*, 1992). All embryos used for *in situ* hybridization and antibody staining were derived from such matings. E9.5 homozygous *Ph* embryos were identified by their kinky neural tube and occasional blisters in the trunk. Alternatively, a 500-bp band could be amplified as previously described (Wehrle-Haller and Weston, 1995) by PCR from genomic DNA of wildtype and heterozygous littermates, but not from homozygous embryos, using a forward primer ACCTCCTTTCGGACGATGAC from the interkinase domain of PDGFRα (bases 2417–2436; Wang *et al.*, 1990, Accession No. M57683) and a reverse primer from within the flanking intron ATCACTTCAGAATGGCTCCA (Dr. Peter Lonai; personal communication). A control PCR band, obtained in the same reaction with primers specific for the *Sl* gene (forward CCATGGCATTGCCGGCTCTC; bases 665–684; and reverse CTGCCCTTGTAAGACTTGACTG; complement of bases 757–736; Huang *et al.*, 1990; Steel *et al.*, 1992), verified the quality of the DNA (Wehrle-Haller and Weston, 1995). Homozygous embryos identified by PCR also exhibit kinky neural tube, blisters, and cleft palate when e11.5 or older. Heterozygous embryos were identified either by their melanocyte phenotype or by PCR analysis of genomic DNA obtained from a limb bud or tail by digestion in 50 μl of 10 m*M* Tris, pH 8, 2 m*M* EDTA, 0.2% Triton X-100, 200 mg/ml proteinase K for 3 hr at 55°C. Samples were boiled for 5 min and 10 μl was amplified with PCR using primer pairs for the *D5MIT135* locus (Research Genetics). This primer pair maps just outside of the *Ph* deletion and produces a 241-bp band from the *Ph* chromosome which originated in a C57Bl6 background and a 217-bp band from the Balb/C-derived chromosome (mouse genome database (MGD); Whitehead Institute/MIT Center for Genome Research (WI/MIT CGR); Dietrich *et al.*, 1994; Copeland *et al.*, 1993).

Neural Tube Cultures

C57Bl6 embryos were used to determine SlF-dependent survival of c-kit expressing neural crest cells. To determine the number of c-kit expressing cells in *Ph* neural tube cultures, we used homozygous *Patch* and heterozygous or wildtype littermates as controls from a F1 *Ph* $\times$ Balb/C mating (see above). All *Patch* crest cell cultures used to assess the ability to form pigment were derived from embryos produced by *Ph* $\times$ C57Bl6 mating. e9.5 embryos were dissected and cultured as described (Morrison-Graham and Weston, 1993). Recombinant SlF (obtained from Dr. D. Williams) was added at 100 ng/ml when indicated. c-kit expressing cells (putative melanocytes) were visualized as follows: Live cells were exposed to rat monoclonal antibody against mouse c-kit (ACK-2 conditioned medium; generously supplied by Dr. S. Nishikawa) for 45 min at 37°C, washed, and fixed in 4% paraformaldehyde. After blocking with 5% goat serum, biotinylated goat anti-rat antibody followed by avidin–Texas red was used to detect bound ACK-2 antibody. Neuronal cells were identified by staining with an anti-Hu monoclonal antibody (Marusich and Weston, 1992) as described (Morrison-Graham and Weston, 1993). In order to visualize melanocytes in culture prior to overt pigmentation, we fixed and stained cultures with D,L-DOPA (Sigma) as described (Morrison-Graham and Weston 1993).

RNA Probes and Whole Mount in Situ Hybridization

Digoxigenin-labeled riboprobes were synthesized according to standard protocols (Boehringer-Mannheim) from linearized cDNAs coding for mouse SlF (KL-M1; kindly provided by Dr. John Flanagan, Boston); mouse c-kit (bp 745–2380; obtained from Dr. Robert J.

Arceci, Boston), mouse PDGFRα (bp 952–1837; Wang *et al.,* 1990; obtained from Dr. Dan Bowen-Pope, Seattle) and mouse tyrosinase-related protein-2 (TRP-2; obtained from Dr. Ian Jackson, London, UK). Whole mount *in situ* hybridization was performed according to Conlon and Rossant (1992) with the following minor modifications: Proteinase K treatment was prolonged for older embryos, hybridization was performed at 68°C, and some embryos were developed in the presence of 5% polyvinyl alcohol (low molecular weight, Aldrich) to enhance color development. Detailed protocols will be provided upon request. Color photographs were taken on a Wild stereo microscope, scanned, and converted to grayscale in Photoshop 3.0 (Adobe). In all cases figures shown were representative of the typical appearance of at least three embryos per stage, genotype, and riboprobe.

Antibody Production and Immunostaining

Affinity-purified mouse SlF antiserum was prepared from rabbit immunized against a fusion protein of SlF with bacterial glutathione S-transferase (GST-SlF). Mouse SlF DNA was PCR amplified from KL-M1 plasmid (kindly provided by Dr. J. Flanagan; Flanagan *et al.,* 1991) using primers TATGGATCCAAGGAGATCTGCGGG and TATGGATCCTTATGCAACAGGGGGTAACAT. The obtained fragment was cleaved and inserted at the *Bam*HI site of pGEX-2T expression vector (Pharmacia). GST-SlF present in inclusion bodies was denatured with 8 *M* urea and 10 m*M* DTT, renatured in 50 m*M* Tris, pH 8, and 0.5 *M* NaCl, and purified with glutathione Sepharose 4B (Pharmacia). In order to enhance the specificity of the GST-SlF antiserum we affinity purified SlF-specific antibodies with double-tagged recombinant SlF lacking GST sequences. Two complementary oligonucleotides (GTCCCGAGCAGAAGCTTATCTCC-GAGGAGGACCTCG and GACCGAGGTCCTCCTCGGAGATAAGCTTCTGCTCGG) coding for an epitope recognized by the c-myc antibody (9E-10; Evans *et al.,* 1985) were annealed and cloned into the *Ppu*MI site in KL-M1 (Flanagan *et al.,* 1991) located in the extracellular domain of SlF (KL-M1/myc). From KL-M1/myc a PCR fragment was amplified with the same primers used to construct the GST-SlF fusion protein and cloned into pTrcHisA (Invitrogen) at the *Bam*HI site, which resulted in the addition of six N-terminal histidines and a linker to the myc-tagged SlF. His/myc-tagged SlF was affinity purified from bacterial lysates with Ni^{2+}-agarose (Quiagen) and coupled to Cn-activated Sepharose 4B (Pharmacia). Anti-SlF-specific antibodies were affinity purified from GST-SlF antiserum and eluted with 0.1 *M* glycine, pH 2.5, and immediately neutralized with 1 *M* Tris, pH 8.0. Specificity of the affinity-purified antiserum was tested on Western blots with crude bacterial extracts from induced bacteria transformed with His/myc-tagged SlF in pTrcHisA.

For whole mount immunostaining, embryos were fixed for 2–5 hr in 4% paraformaldehyde in phosphate-buffered saline (PBS) at 4°C, washed in PBS, and transferred and stored in methanol at −20°C. Embryos were rehydrated in Tris-buffered saline, 0.1% Tween 20 (TBST), heat inactivated for 30 min at 70°C, and then blocked in 10% heat-inactivated normal goat serum (hiNGS) in TBST, 0.5% Triton X-100 (TBSTT). Embryos were incubated in 1:200 affinity-purified anti-SlF antiserum in 5% hiNGS in TBSTT at 4°C overnight. Primary antibody was absorbed with embryo acetone powder from e15.5 *Sl*/*Sl* embryos, which lack SlF protein. Embryos were extensively washed in TBSTT and incubated at 4°C in affinity-purified goat anti-rabbit alkaline phosphatase (Bio-Rad) diluted 1:2000 in 5% hiNGS in TBSTT, previously absorbed with e13.5 mouse acetone powder. After washing in TBSTT embryos were equilibrated in 100 m*M* Tris, pH 9.5, 25 m*M* $MgCl_2$, 100 m*M* NaCl, 0.1% Tween 20, 0.5% Triton X-100, and 5% polyvinyl alcohol. Embryos were stained in the same buffer in the presence of NBT and BCIP, washed in TBST, dehydrated through methanol, rehydrated in TBST, and equilibrated in 30% sucrose in PBS or 80% glycerol in PBS. Embryos in sucrose were embedded in Tissue-Tek OCT (Miles) and cryosectioned at 16 μm. In order to enhance morphological structures, sections were counterstained with 1:200 rabbit anti-laminin serum (Collaborative Research) and 1:200 Texas red-conjugated goat anti-rabbit antiserum as described (Wehrle-Haller and Weston, 1995). Color photographs of whole mounts and sections were taken on a Wild stereo microscope and Zeiss Axioplan, respectively. Photographic transparencies were scanned and converted to grayscale in Photoshop 3.0 (Adobe). Contrast and brightness was adjusted to improve presentation of visual appearance of stained tissue. All changes were made identically in wild-type and mutant material so that no artifactual differences were introduced.

RESULTS

Cultures of Crest Cells from Ph Homozygotes Contain c-kit Expressing Cells, Which Undergo Melanogenesis in the Presence of SlF

The melanogenic subpopulation of neural crest cells transiently depends on SlF for its survival *in vivo* and *in vitro* (Morrison-Graham and Weston, 1993) and hence must express functional c-kit. To confirm that c-kit staining specifically marks melanocytes *in vitro,* we correlated c-kit antibody staining with SlF-dependent survival in cultures of normal mouse neural crest cells. Cells that express c-kit are first detected in a subpopulation of crest-derived cells by Day 2 of culture. Initially, neither the intensity of the staining nor the number of positive cells are affected by the addition of SlF. However, the persistence of c-kit expressing cells depended upon SlF (Fig. 1). In cultures containing exogenous SlF (100 ng/ml), the numbers of c-kit-positive cells increased over the next few days (Days 2–5). By Day 6, both c-kit expression (ACK-2 staining) and melanin granules could be detected in melanocytes. In contrast, following the initial appearance of ACK-2-immunoreactive cells at Day 2, the numbers of c-kit-positive cells in cultures deprived of SlF (for example, in the presence of antibody to SlF in the culture medium) decreased progressively between Days 2 and 5, and by Day 6, no positive cells were detectable (Fig. 1). Since no neurogenic (anti-Hu-immunoreactive) neural crest-derived cell ever expressed c-kit immunoreactivity (c-kit-IR) (Figs. 2A and 2B), we conclude that the c-kit expression reliably marks melanocyte precursors in our cultures and that the loss of c-kit immunoreactive cells in the absence of SlF represents a loss of melanocyte precursors (see Morrison-Graham and Weston, 1993; Reid *et al.,* 1995).

Using c-kit-IR as a marker for melanocytes and their precursors, we then cultured *Ph*/*Ph* neural tubes in the presence of exogenous SlF and examined them for c-kit expres-

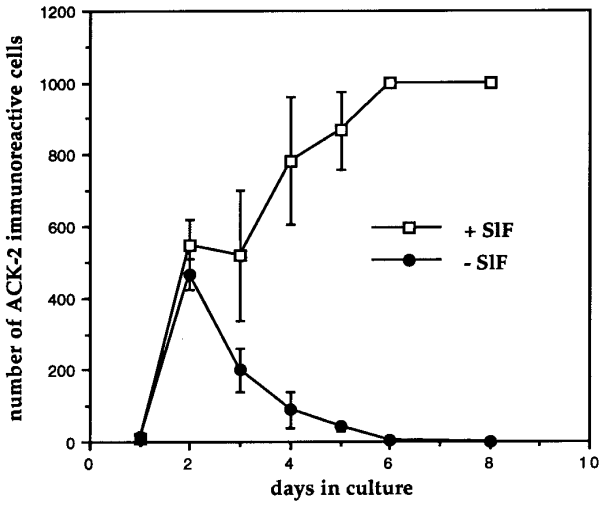

FIG. 1. The number of c-kit expressing cells decreases in the absence of SlF in mouse neural crest cultures. The number of ACK-2-immunoreactive cells (c-kit expressing cells) per neural tube culture was plotted against the time in culture in the presence of SlF (100 ng/ml) (squares) and in the absence of SlF (anti-SlF antibody) (filled circles). The standard deviation is given for Days 1 and 2 ($n = 2$); for all other data points the standard error is given ($n = 3$). In the presence of SlF at Days 6 and 8 the number of ACK-2-IR cells exceeded 1000 per culture and has not been determined accurately.

sion after 4–5 days. Although crest cell outgrowth from explanted neural tubes of *Ph* homozygotes was smaller than outgrowth from neural tubes of wildtype or heterozygous littermates, c-kit expressing cells were observed in all cultures. (*Ph*/*Ph:* 279 ± 192; $n = 3$; +/+ or heterozygotes: 754 ± 204; $n = 3$). Thus, the *Patch* mutation does not prevent expression of c-kit by a subset of crest-derived cells (presumed melanocyte precursors). To determine if such cells could undergo melanogenesis, some cultures were left for a 10-day culture period. Pigmentation in such cultures was diminished, but not absent. Pigmented cells were observed in approximately half of the cultures (5/12), suggesting that PDGFRα is not required for the initial differentiation of melanocytes.

The Patch Mutation Alters Dispersal of MPs in the Dermis, but Not Their Initial Migration on the Lateral Pathway

To follow the initial migration and subsequent dispersal of MPs *in vivo*, we used whole mount *in situ* hybridization to detect melanocyte-specific mRNA for TRP-2 (Steel *et al.*, 1992; Wehrle-Haller and Weston, 1995) in e11.5–e13.5 wildtype, *Ph*/+, and *Ph*/*Ph* embryos. At e11.5, MPs have already reached lateral positions in the head and anterior trunk but have just begun to migrate onto the lateral crest migration pathway in the posterior trunk. In the posterior trunk, TRP-2 mRNA expressing cells are initially distributed within the dorsal aspect of the lateral crest migration pathway extending from the migration staging area (MSA: Wehrle-Haller and Weston, 1995) to the dorsal aspect of the dermatome. In contrast to wildtype, MPs of *Ph*/*Ph* embryos did not reach the base of the hind limb bud (Fig. 3A; compare with Figs. 2A and 2E in Wehrle-Haller *et al.*, 1995). At developmentally more advanced (more rostral) axial levels, TRP-2 mRNA-positive cells were clustered in a segmental pattern dorsolaterally in mutant embryos (Fig. 3B, arrow), compared to the more uniform distribution of cells observed in wildtype embryos (Fig. 3C).

The patterns of MP distribution were qualitatively simi-

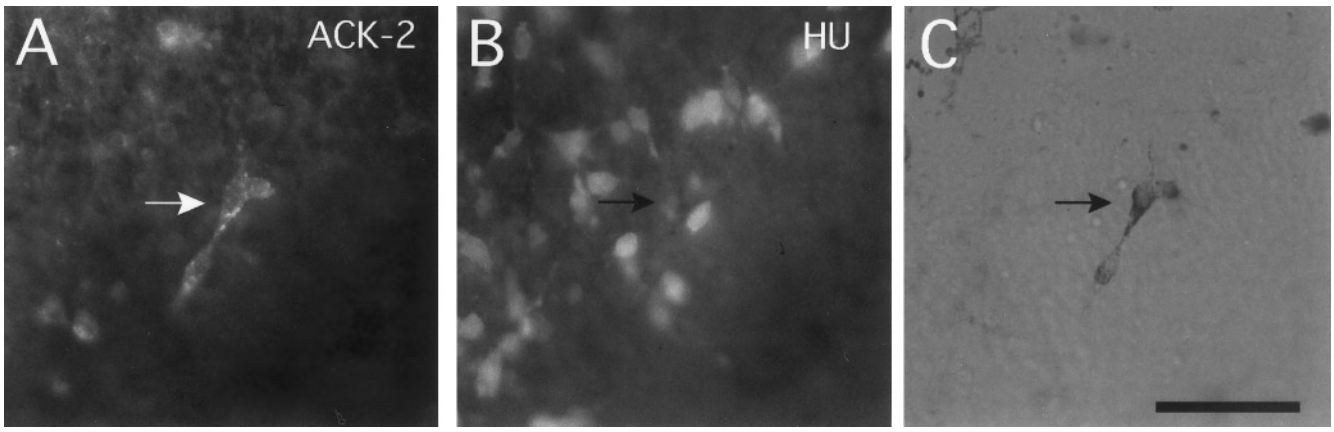

FIG. 2. Melanocyte precursors (c-kit$^+$) and neurogenic cells (Hu$^+$) represent distinct neural crest subpopulations. Neural tube explants cultured in the presence of SlF (100 ng/ml) were cultured for 8 days and stained with ACK-2 rat monoclonal antibody (A) and with anti-Hu mouse monoclonal antibody (B) as described under Materials and Methods. (C) Bright-field photo reveals pigmented melanocytes. Arrows point to the same ACK-2-reactive, Hu-negative, and pigmented melanocyte. Bar, 66 μm.

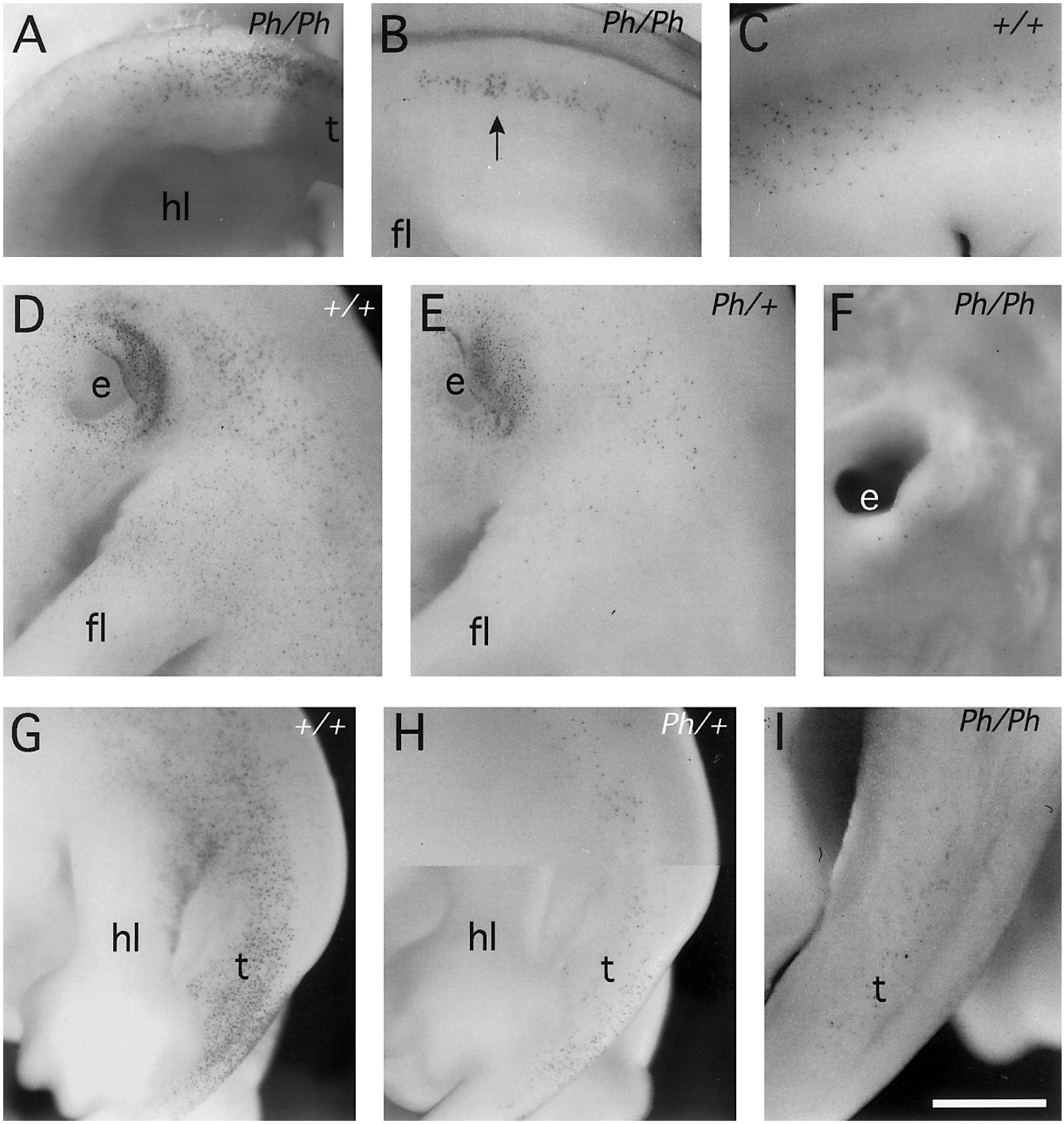

FIG. 3. Melanocyte phenotype of wildtype and Ph mutant embryos. TRP-2 mRNA *in situ* hybridization of e11.5 (A–C) and e13.5 (D–I) +/+ and *Ph* mutant embryos. (A) Lateral view of hind limb bud and tail of a *Ph*/*Ph* embryo. (B) Lateral view of the mid-trunk of a *Ph*/*Ph* embryo. (C) Lateral view of the mid-trunk region of a +/+ embryo. (D, E) Lateral view of the shoulder and ear of +/+ and *Ph*/+ embryos, respectively. (F) Magnified view of the ear from a *Ph*/*Ph* embryo. (G, H) Hind limb bud and tail region of a +/+ and *Ph*/+ embryo respectively. (I) Magnified view of the tail of a *Ph*/*Ph* embryo. Arrow points to clusters of MPs in e11.5 *Ph*/*Ph* embryos. Note the presence of only a few MPs in the ear (F) and tail (I) of e13.5 *Ph*/*Ph* embryos. In H, two pictures taken at different focal levels of the tail region are combined into a montage. e, ear; fl, fore limb bud; hl, hind limb bud; t, tail. Each photograph is representative of the reproducible staining pattern seen in multiple embryos, as follows: A, B, $n = 3$; C, $n = 6$; D, $n = 3$; E, F, $n = 4$; G, $n = 3$; H, I, $n = 4$. Bar corresponds to 0.6 mm in A, B, C, F; to 0.93 mm in D, E; to 1.08 mm in G, H; and to 0.46 mm in I.

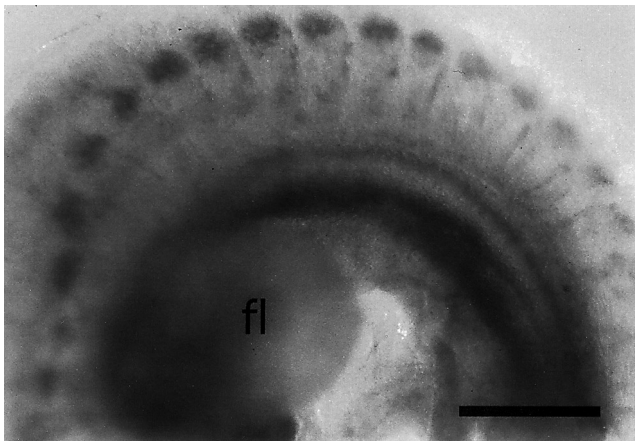

FIG. 4. SlF mRNA expression in *Ph*/*Ph* e10.5 embryo. Lateral view of the trunk of a whole mount *in situ* hybridization with the antisense SlF riboprobe. The photograph represents the reproducible staining pattern seen in three different mutant embryos. fl, fore limb bud. Bar, 360 μm.

lar in e12.5 and e13.5 embryos. Generally, the number of MPs was reduced in heterozygotes and was almost absent from homozygotes compared to wildtype (Figs. 3D–3I). In the trunk of heterozygotes, MPs were present at the shoulder, absent in the mid-trunk region, reduced at the base of the hind limb, and present in the tail (Fig. 3H; compare to wildtype, Fig. 3G). In *Patch* homozygotes, a few cells could be found at shoulder level at e12.5, but were no longer present at e13.5. MPs were not detected in the trunk of e12.5 and e13.5 embryos, but remain in small numbers in the ear (Fig. 3F) and in dorsolateral locations in the tail (Fig. 3I).

SlF mRNA Expression Pattern Is Not Affected in Ph/Ph Mutant Embryos

Melanocytes start to disappear in *Ph* embryos when SlF is known to be required for survival of melanocytes *in vivo* (Nishikawa *et al.*, 1991; Wehrle-Haller and Weston, 1995) and *in vitro* (Morrison-Graham and Weston, 1993). To determine whether expression patterns of SlF by somite-derived mesenchymal cells was affected in mutant embryos, we used whole mount *in situ* hybridization to examine the distribution of SlF mRNA in *Ph*/*Ph* embryos. At e10.5, when SlF mRNA is known to be expressed at sites which are later populated by melanocytes in wildtypes (Wehrle-Haller and Weston, 1995), the expression pattern of SlF mRNA in *Ph*/*Ph* was comparable to those of wildtype or heterozygous littermates (Fig. 4; compare with Figs. 5A and 5B in Wehrle-Haller and Weston, 1995).

SlF Protein, Initially Localized to the Epithelial Dermatome, Is Subsequently Found at Low Levels in the Dermal Mesenchyme

In order to test for possible changes in SlF protein distribution in *Patch* mutant tissue, we used immunohistochemistry to determine SlF protein distribution along the lateral crest migration pathway of mutant and wildtype embryos. At e10.5 (35–36 somites), SlF protein pattern in both mutant and wildtype embryos was similar to the localization of its mRNA. In the trunk, SlF protein was detected in the dorsal aspect of the epithelial dermatome (Figs. 5A and 5F).

At e11 (39–40 somites), in wildtype and *Patch* embryos, SlF protein is expressed in dorsal aspects of the dermatome at hind limb levels (not shown), whereas at more anterior axial levels, SlF immunoreactivity (SlF-IR) associated with the epithelial dermatome decreases as the epithelial dermatome transforms into mesenchymal dermis (Figs. 5B and 5G). When these whole mounts were sectioned and SlF-IR was compared between wildtype and *Ph*/*Ph* embryos, weak SlF-IR was consistently detected in the newly transformed dermal mesenchyme of wildtype embryos (Figs. 5C and 5E), whereas under identical staining conditions, SlF-IR could not be detected in corresponding dermal mesenchyme of *Patch* homozygotes (Figs. 5H and 5J).

c-kit mRNA Expression Is Altered in Ph/Ph and Ph/+ Embryos Compared to Wildtype

In the course of studying c-kit expression by MPs *in vivo*, we observed altered c-kit mRNA expression patterns in *Ph* mutant embryos. Specifically, at e10.5 in *Ph* mutant embryos, c-kit mRNA expression can be detected in MPs in the head similar to that of wildtype embryos (Steel *et al.*, 1992; Wehrle-Haller and Weston, 1995). However, in mutant embryos, c-kit mRNA expression was strongly enhanced in the dorsal aspect of the spinal cord compared to wildtype embryos (Figs. 6A and 6B). Likewise, mesenchymal c-kit expression in the first and second branchial arches (not shown), the lateral mesenchyme, and the limb buds was dramatically enhanced in *Ph* mutant embryos (compare Fig. 6A with 6B). In addition, in mutant embryos c-kit mRNA was expressed ectopically in the newly transformed dermis at mid-trunk levels (arrow in Fig. 6B) and the limb bud apical ectodermal ridge (AER) (Fig. 6B). Interestingly, the ectopic c-kit expression pattern in *Patch* mutant embryos was similar to the expression pattern of PDGFRα mRNA in wildtype embryos (Fig. 6C).

By e11.5, the c-kit mRNA staining initially detected in wildtype mesenchyme had disappeared, whereas it was still strongly expressed in *Ph* mutant embryos, especially within the developing ear pinna, the limb buds, and the lateral and dermal mesenchyme. The enhanced expression of c-kit in the neural tube as well as ectopic expression in the AER seen at e10.5 was still evident in e11.5 mutant embryos (Fig. 6D).

In e12.5 and e13.5 *Ph* mutant embryos, in contrast to wildtype, ectopic mesenchymal c-kit expression persisted in the ear pinna, the limb buds, the dermal mesenchyme, and the neural tube (Fig. 7). These results suggest that embryos carrying the *Ph* mutation express c-kit mRNA not only in MPs but also ectopically in tissues adjacent to the lateral neural crest migration pathway.

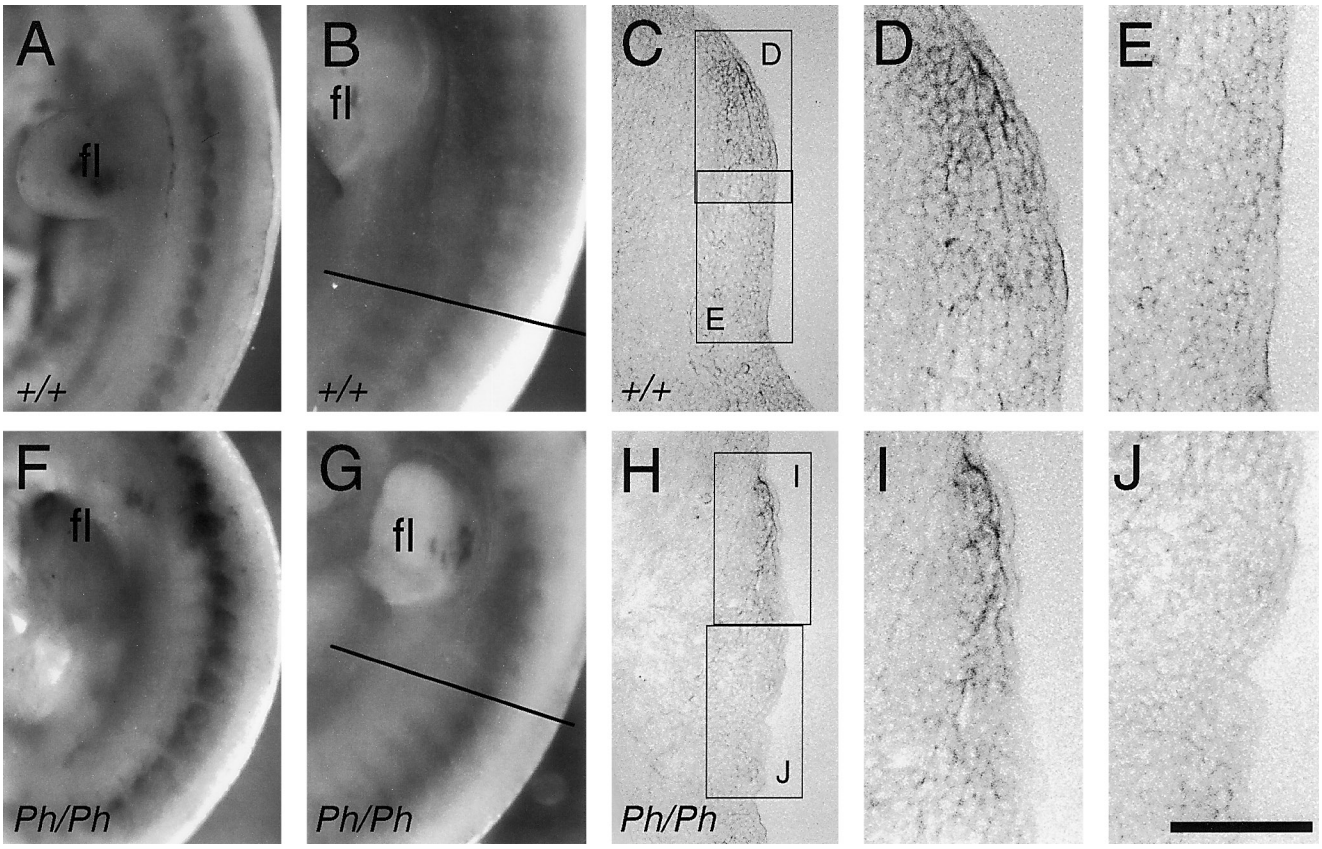

FIG. 5. SlF protein distribution in e10.5 and e11 wildtype and *Ph*/*Ph* mutant embryos. Lateral view of e10.5 +/+ (A) and *Ph*/*Ph* (F) embryos processed for whole mount immunohistochemistry with anti-SlF antiserum. Lateral view at the fore limb level of e11 +/+ (B) and *Ph*/*Ph* (G) embryos processed for anti-SlF antiserum whole mount immunohistochemistry. Control embryos treated with secondary antibodies, but not anti-SlF antiserum, were unstained (not shown). Cross section of whole mount immunostained e11 embryos. 16-μm cryostat sections of +/+ (C) and *Ph*/*Ph* (H). Boxed areas in C and H are magnified in D,E and I,J respectively. Boxed areas D, I correspond to the epithelial dorsal aspect of the dermatome. Boxed areas E, J correspond to the mesenchymal mediolateral aspect of the dermis. Approximate plane of sections shown in C and H are indicated in B and G, respectively. Each photograph is representative of the reproducible staining pattern seen in three different embryos. Bar corresponds to 0.8 mm in A, F; to 0.69 mm in B, C; to 0.16 mm in C, H; and to 0.06 mm in D, E, I, J.

DISCUSSION

We and others have shown that MPs transiently require SlF signaling via c-kit for survival *in vivo* and *in vitro* (Nishikawa *et al.*, 1991; Steel *et al.*, 1992; Morrison-Graham and Weston, 1993; Lahav *et al.*, 1994; Reid *et al.*, 1995). Although *Patch* homozygotes do not survive long enough to observe pigmentation, a function for PDGFRα in MP development has been suggested since altered pigment patterns are observed in *Patch* heterozygotes. As discussed below, we have now elucidated how the PDGFRα deletion in *Patch* mutants might affect pigment pattern in the trunk.

The Patch Mutation Acts Non-Cell-Autonomously with Respect to Melanogenesis

In order to understand whether the PDGFRα signal-transduction mechanism acts cell-autonomously in MPs, we determined the melanogenic ability of neural crest populations from mouse embryos homozygous for the *Ph* mutation. We have shown that c-kit-positive MPs disappear within 3 days when normal neural crest cells are cultured in the absence of the c-kit ligand SlF. In cultures of both *Ph*/*Ph* and wildtype neural crest cells, however, melanocytes survive in the presence of SlF well beyond this critical period and terminally differentiate. This suggests that PDGFRα, which is absent in *Ph* homozygotes, is not required for the initial expression and maintenance of c-kit in MPs, nor is it absolutely required for terminal differentiation. It is possible that PDGFRα activity is required for some aspect of early neural tube development or later in melanocyte differentiation or survival. However, since pigment cells do differentiate in cultures of *Ph*/*Ph* neural crest cells, it seems likely that the *Ph* pigment pattern results from an initially non-cell-autonomous defect. This conclu-

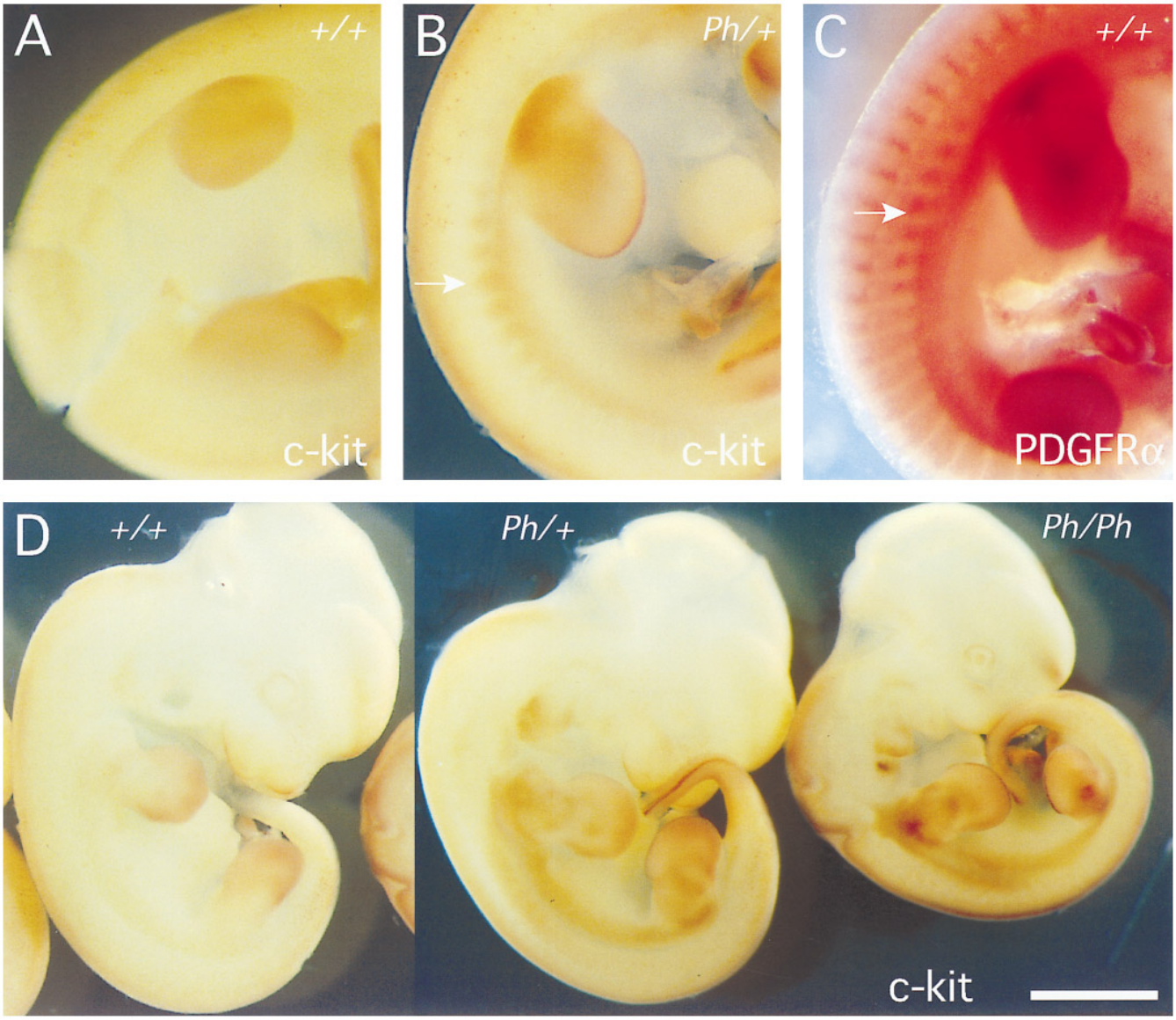

FIG. 6. c-kit mRNA expression pattern is altered in *Ph* mutant embryos. Lateral views of whole mount *in situ* hybridizations with c-kit and PDGFR*α* antisense riboprobe. Trunk of e10.5 embryos of +/+ (A) and *Ph*/+ (B) genotypes stained with c-kit riboprobe. Trunk of an e10.5 wildtype embryo stained with PDGFR*α* riboprobe (C). (D) c-kit mRNA localization in embryos of an e11.5 *Ph* litter, showing +/+ (left), *Ph*/+ (middle), and *Ph*/*Ph* (right). Arrows in B and C point to the newly transformed mesenchymal dermis expressing ectopic c-kit in *Ph* mutant and PDGFR*α* in wildtype embryos. All embryos stained for c-kit mRNA were treated identically to reveal differences in the staining pattern and intensities. Each photograph is representative of the reproducible staining pattern seen in multiple embryos, as follows: A, $n = 5$; B, $n = 7$; C, $n = 4$; D, (+/+) $n = 4$, (*Ph*/+) $n = 7$, (*Ph*/*Ph*) $n = 7$. Bar corresponds to 0.75 mm in A, B; to 0.8 mm in C; and to 2.2 mm in D.

sion is consistent with our inability to detect PDGFR*α* transcripts in migrating melanocytes *in vivo* and *in vitro* and the lack of PDGFR*α* expression by various melanoma cell lines (Halaban, 1994).

Since PDGFR*α* function is thought to be required in glial cells of the central and peripheral nervous systems (Barres *et al.*, 1992; Morrison-Graham *et al.*, 1992), it is interesting to note that PDGFR*α* appears to be absent in one of the lineages believed to segregate from a crest-derived glial/melanocyte precursor (Weston, 1991; Stocker *et al.*, 1991). This would suggest that the putative glial/melanocyte precursor lacks functional PDGFR*α*, but that this receptor and the

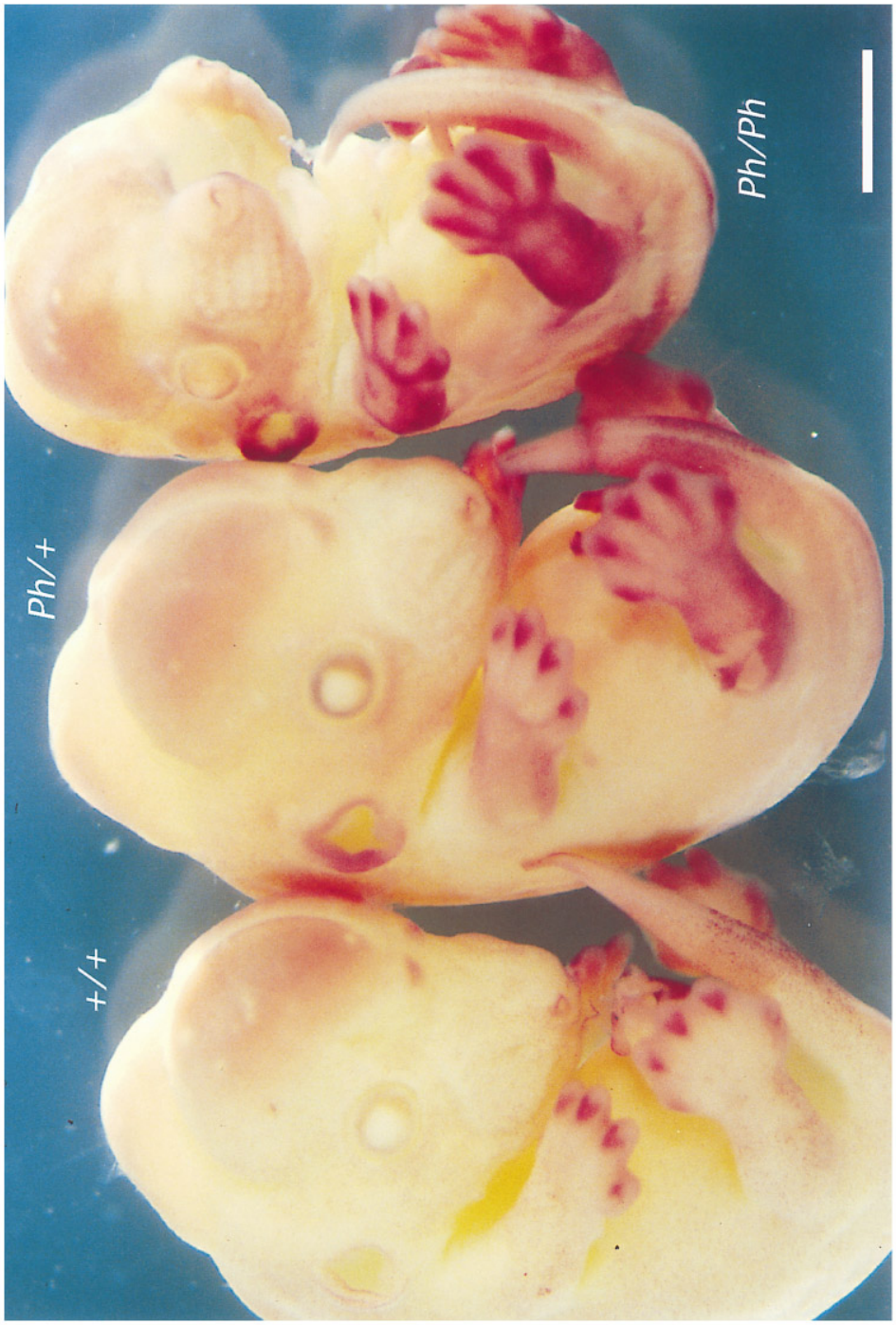

FIG. 7. c-kit mRNA expression pattern is also altered in older *Ph* mutant embryos. Lateral views of whole mount *in situ* hybridizations with c-kit antisense riboprobe of e13.5 +/+ (left), *Ph*/+ (middle), and *Ph*/*Ph* (right) embryos. All embryos were treated identically to reveal differences in the staining pattern and intensities. The photograph is representative of the reproducible staining pattern seen in multiple embryos, as follows: (+/+) $n = 3$, (*Ph*/+) $n = 5$, (*Ph*/*Ph*) $n = 3$. Bar, 2.4 mm.

requirement for its ligand arises later in the glial cell lineage, but not in the melanocyte. This notion remains to be tested using appropriate markers for the crest-derived glial lineage in older embryos.

SlF Localization, but Not Production, Is Altered in Patch Mutant Mice

Initial dispersal of MPs onto the lateral migration pathway and subsequent survival of melanocytes in the dermis both depend on SlF activity (Steel *et al.,* 1992; Wehrle-Haller and Weston, 1995). In the *Ph* mutant embryos, the initial SlF-dependent melanocyte precursor migration appears to be the same as that in wildtype embryos (see Wehrle-Haller and Weston, 1995). This supports our conclusion (above) that c-kit expression in melanocytes and SlF expression by target tissues are initially not affected in embryos homozygous for the *Ph* mutation. However, by e11.5, subsequent dispersal of MPs within the newly formed mesenchymal dermis of *Ph* embryos is dramatically different from that in wildtype embryos. This corresponds to a time when SlF is still required by migrating MPs (Nishikawa *et al.,* 1991; Morrison-Graham and Weston, 1993), but before SlF is expressed by the overlying epidermis, which is reported to occur at e12.5–e13.5 (Motro *et al.,* 1991; Bedell *et al.,* 1995). Interestingly, beginning at e10.5, wildtype embryos begin to express PDGFRα in the lateral dermatome as it starts to transform into dermal mesenchyme (Fig. 6C). In the absence of PDGFRα the newly transformed dermal fibroblasts fail to thrive (Morrison-Graham *et al.,* 1992; Schatteman *et al.,* 1992), which could possibly affect localization of SlF or other growth factors required for melanocyte development. It should be emphasized, however, that possible changes in the structure of the dermis are not sufficient to explain changes in pigment pattern since melanocytes are absent in the mid-trunk level of *Patch* heterozygotes where dermal mesenchyme appears to be normal.

Whether the absence of PDGFRα activity has an effect on the localization or presentation of SlF by the dermal mesenchyme can best be tested by immunohistochemical detection of SlF protein. In wildtype embryos, SlF-IR is detected in the dorsal aspect of the dermatome and ventrolaterally in the newly formed mesenchymal dermis. In contrast, SlF-IR in *Ph*/*Ph* embryos can be detected in the dorsal epithelial dermatome, but is absent from the newly formed ventrolateral mesenchymal dermis.

The loss of SlF-IR in the ventrolateral mesenchymal dermis might be related to our observation that c-kit is ectopically expressed by these cells in embryos carrying the *Patch* deletion. Thus, based on the appearance of the SlF-immunostained epithelial dermatome and the ventrolateral mesenchymal dermis (see Fig. 5), we suggest that some cell-bound SlF is retained by the dermatome and some is normally released by the epithelial dermatome and diffuses ventrolaterally. We further suggest that c-kit, which is ectopically expressed by dermal mesenchyme in *Patch* embryos, mediates internalization and degradation of the diffusible SlF initially expressed and released by the dermatome as it transforms into mesenchyme. As a consequence of ectopic c-kit expression, therefore, the limiting amounts of SlF activity provided by diffusible SlF protein normally present in the dermal mesenchyme would be reduced in the mutant tissue. The fate of MPs in mutant embryos is consistent with this interpretation, since they are seen to cluster (Fig. 3B) in the area of the dorsal epithelial dermatome, where SlF remains (see Fig. 5I), but do not disperse as in wildtype embryos (Fig. 3C) in ventrolateral mesenchyme, which lacks the SlF-IR that is present in wildtype embryos (compare Figs. 5E and 5J). It is presently not clear why the MPs also eventually disappear from these dorsal locations. We postulate, however, that after complete transformation of the epithelial dermatome into mesenchyme, the levels of SlF activity also decline in dorsal locations because of ectopic c-kit expression in mesenchymal cells (Fig. 7).

The Ph Deletion Might Interfere with Regulatory Elements of the c-kit Gene

Recently, two dominant pigmentation mutations, mapping to the *Patch* locus have been molecularly characterized. *Rump-white,* (*Rw*) and W^{sash}, characterized by a white sash/belt at mid-trunk level, have been shown to be large chromosomal inversions (Nagle *et al.,* 1994; Stephenson *et al.,* 1994; Bucan *et al.,* 1995; Duttlinger *et al.,* 1995). In both of these inversions, one of the breakpoints is located between the PDGFRα and the c-kit gene, apparently in the same genomic region that contains one end of the deletion in *Patch*. An analysis of the c-kit expression pattern has not been performed in the *Rw* embryo. However, in W^{sash}, c-kit mRNA and protein are ectopically expressed in somitic mesenchymal derivatives in a pattern that resembles that of *Patch* (Duttlinger *et al.,* 1993, 1995; Besmer *et al.,* 1993). In W^{sash}, where the heterozygous adult pigment pattern is similar to that of *Patch* heterozygotes, the phenotype might also be caused by a disruption of MP migration onto the lateral pathway as observed in *Patch*. Interestingly, in *Patch* as well as in W^{sash}, c-kit is ectopically expressed in locations that normally express PDGFRα (Duttlinger *et al.,* 1993, 1995; Besmer *et al.,* 1993).

Since *Ph* and W^{sash} pigment pattern phenotypes are almost identical *in vivo*, the behavior of MPs might also be similar *in vitro*. Indeed, it has been shown that neural crest explants from W^{sash} homozygous embryos can undergo pigmentation *in vitro* similar to that of *Ph*-derived neural crest cells (Huszar *et al.,* 1991). However, a possible non-cell-autonomous defect in W^{sash} is apparently not supported by a mosaic analysis of melanocyte development (Huszar *et al.,* 1991).

Taken together, these results suggest that the pigment defect in *Patch* mutants is likely to be caused by a competition for limited amounts of SlF on the lateral crest migration

pathway. This competition results from ectopic expression of c-kit by dermal mesenchyme, possibly caused by the removal of c-kit regulatory elements by the *Patch* genomic deletion. This inference is supported by the phenotype of mice carrying a targeted mutation in the PDGFRα gene, which, unlike the *Patch* deletion, do not exhibit a pigmentation phenotype as heterozygotes (P. Soriano, personal communication). This result suggests that the *Patch* mutation acts non-cell-autonomously to affect the development of MPs and further emphasizes the importance of characterizing the role of c-kit regulatory elements for c-kit expression *in vivo*.

ACKNOWLEDGMENTS

We thank Sheree Harrison for excellent technical assistance. We are grateful to Monique Wehrle-Haller and Dr. Stephen Johnson for their critical comments on the manuscript. We also thank Drs. John Flanagan, Ian Jackson, Robert Arceci, and Dan Bowen-Pope for generously providing cDNA plasmids and Dr. Peter Lonai for sharing primer sequences. We thank Drs. Shin-Ichi Nishikawa and Douglas Williams for generously providing ACK-2 anti-c-kit rat monoclonal antibody and recombinant SlF and antiserum to SlF, respectively. Special thanks to Drs. Deborah Nagle, Maja Bucan, and Peter Besmer for technical advice, discussions, and for sharing results in press, Phillipe Soriano for sharing unpublished results, and Yoshiko Takahashi and Yoshio Wakamatsu for advice on *in situ* and whole mount immunohistochemistry. Drs. Sherry Rogers and Carol Erickson provided helpful advice and criticisms. We are especially grateful to Rick Gosswiler for his careful animal husbandry and to Tom Maynard for advice concerning computer imaging methods. Our work has been supported by Grant DE-04316 from the USPHS. B.W.-H. has been supported by an EMBO postdoctoral fellowship (169-1993) and a grant from the Swiss Foundation for Medical and Biological Fellowships.

REFERENCES

Anderson, D., Lyman, S., Baird, A., Wignall, J., Eisenman, J., Rauch, C., March, C. J., Boswell, H., Gimpel, S., Cosman, D., and Williams, D. (1990). Molecular cloning of mast cell growth factor a hematopoietin that is active in both membrane bound and soluble forms. *Cell* 63, 235–243.

Barres, B. A., Hart, I. K., Coles, H. S. R., Burne, J. F., Voyvodic, J. T., Richardson, W. D., and Raff, M. C. (1992). Cell death and control of cell survival in the oligodendrocyte lineage. *Cell* 70, 31–46.

Bedell, M. A., Brannan, C. I., Evans, E. P., Copeland, N. G., Jenkins, N. A., and Donovan, P. J. (1995). DNA rearrangements located over 100 kb 5′ of the *Steel* (Sl)-coding region in *Steel-panda* and *Steel-contrasted* mice deregulate *Sl* expression and cause female sterility by disrupting ovarian follicle development. *Genes Dev.* 9, 455–470.

Besmer, P., Manova, K., Duttlinger, R., Huang, E. J., Packer, A., Gyssler, C., and Bachvarova, R. F. (1993). The *kit*-ligand (steel factor) and its receptor *c-kit*/*W:* pleiotropic roles in gametogenesis and melanogenesis. *Development Suppl.* 125–137.

Bucan, M., Nagle, D. L., Hough, R. B., Chapman, V. M., and Lo, C. W. (1995). Lethality of Rw/Rw mouse embryos during early postimplantation development. *Dev. Biol.* 168, 307–318.

Conlon, R. A., and Rossant, J. (1992). Exogenous retinoic acid rapidly induces anterior ectopic expression of murine Hox-2 genes in vivo. *Development* 116, 357–368.

Copeland, N., Gilbert, D., Cho, B., Donovan, P., Jenkins, N., Cosman, D., Anderson, D., Lyman, S., and Williams, D. (1990). Mast cell growth factor maps near the *Steel* locus on mouse chromosome 10 and is deleted in a number of *Steel* allels. *Cell* 63, 175–183.

Copeland, N. G., Gilbert, D. J., Jenkins, N. A., Nadeau, J. H., Eppig, J. T., Maltais, L. J., Miller, J. C., Dietrich, W. F., Steen, R. G., Lincoln, S. E., Weaver, A., Joyce, D. C., Merchant, M., Wessel, M., Katz, H., Stein, L. D., Reeve, M. P., Daly, M. J., Dredge, R. D., Marquis, A., Goodman, N., and Lander, E. S. (1993). Genome map IV. *Science* 262, 67–82.

Dietrich, W. F., Miller, J. C., Steen, R. G., Merchant, M., Damron, D., Nahf, R., Gross, A., Joyce, D. C., Wessel, M., Dredge, R. D., Marquis, A., Stein, L., Goodman, N., Page, D. C., and Lander, E. S. (1994). A genetic map of the mouse with 4006 simple sequence lenght polymorphisms. *Nature Genet.* 7, 220–245.

Duttlinger, R., Manova, K., Chu, T. Y., Gyssler, C., Zelenetz, A. D., Bachvarova, R. F., and Besmer, P. (1993). *W-sash* affects positive and negative elements controlling c-*kit* expression: Ectopic c-*kit* expression at sites of kit-ligand expression affects melanogenesis. *Development* 118, 707–717.

Duttlinger, R., Manova, K., Berrozpe, G., Chu, T.-Y., DeLeon, V., Timokhina, I., Chaganti, R. S. K., Zelenetz, A. D., Bachvarova, R. F., and Besmer, P. (1995). The W^{sh} and *Ph* mutations affect the c-*kit* expression profile: c-*kit* misexpression in embryogenesis impairs melanogenesis in W^{sh} and *Ph* mutant mice. *Proc. Natl. Acad. Sci. USA* 92, 3754–3758.

Erickson, C. A., and Weston, J. A. (1983). An SEM analysis of neural crest migration in the mouse. *J. Embryol. Exp. Morphol.* 74, 97–118.

Evans, G. I., Lewis, G. K., Ramsay, G., and Bishop, J. M. (1985). Isolation of monoclonal antibodies specific for human c-*myc* proto-oncogene product. *Mol. Cell. Biol.* 5, 3610–3616.

Flanagan, J., Chan, D., and Leder, P. (1991). Transmembrane form of the kit ligand growth factor is determined by alternative splicing and is missing in the Sl^{d} mutant. *Cell* 64, 1025–1035.

Geissler, E. N., Ryan, M. A., and Housman, D. E. (1988). The dominant-white spotting (*W*) locus of the mouse encodes the c-*kit* proto oncogene. *Cell* 55, 185–192.

Grüneberg, H., and Truslove, G. M. (1960). Two closely linked genes in the mouse. *Genet. Res.* 1, 69–90.

Halaban, R. (1994). Signal transduction in normal and malignant melanocytes. *Pigment Cell Res.* 7, 89–95.

Huang, E., Nocka, K., Beier, D. R., Chu, T., Buck, J., Lahm, H., Wellner, D., Leder, P., and Besmer, P. (1990). The hematopoetic growth factor KL is encoded by the *Sl* locus and is the ligand of the c-*kit* receptor, the gene product of the *W* locus. *Cell* 63, 225–233.

Huszar, D., Sharpe, A., and Jaenisch, R. (1991). Migration and proliferation of cultured neural crest cells in *W* mutant neural crest chimeras. *Development* 112, 131–141.

Lahav, R., Lecoin, L., Ziller, C., Nataf, V., Carnahan, J. F., Martin, F. H., and Le Douarin, N. M. (1994). Effect of the *Steel* gene product on melanogenesis in avian neural crest cell cultures. *Differentiation* 58, 133–139.

Marusich, M. F., and Weston, J. A. (1992). Identification of early neurogenic cells in the neural crest lineage. *Dev. Biol.* 149, 295–306.

Morrison-Graham, K., Schatteman, G. C., Bork, T., Bowen-Pope, D. F., and Weston, J. A. (1992). A PDGF receptor mutation in the mouse (*Patch*) perturbs the development of a non-neuronal subset of neural crest-derived cells. *Development* 115, 133–142.

Morrison-Graham, K., and Weston, J. A. (1993). Transient steel factor dependence by neural crest-derived melanocyte precursors. *Dev. Biol.* 159, 346–352.

Motro, B., Van der Kooy, D., Rossant, J., Reith, A., and Bernstein, A. (1991). Contiguous patterns of c-*kit* and *Steel* expression: Analysis of mutations at the *W* and *Sl* loci. *Development* 113, 1207–1221.

Mouse Genome Database (MGD), Mouse Genome Informatics Project, The Jackson Laboratory, Bar Harbor, Maine. World Wide Web (URL: http://www.informatics.jax.org). (July, 1995).

Murphy, M., Reid, K., Ford, M., Furness, J. B., and Bartlett, P. F. (1994). FGF2 regulates proliferation of neural crest cells, with subsequent neuronal differentiation regulated by LIF or related factors. *Development* 120, 3519–3528.

Nagle, D. L., Martin-DeLeon, P., Hough, R. B., and Bucan, M. (1994). Structural analysis of chromosomal rearrangements associated with the developmental mutations *Ph*, W^{19H} and *Rw* on mouse chromosome 5. *Proc. Natl. Acad. Sci. USA* 91, 7237–7241.

Nishikawa, S., Kusakabe, M., Yoshinaga, K., Ogawa, M., Hayashi, S., Kunisade, T., Era, T., Sakakura, T., and Nishikawa, S. (1991). *In utero* manipulation of coat color formation by a monoclonal anti-c-*kit* antibody: Two distict waves of c-*kit* dependency during melanocyte development. *EMBO J.* 10, 2111–2118.

Orr-Urtreger, A., Bedford, M. T., Do, M.-S., Eisenbach, L., and Lonai, P. (1992). Developmental expression of the α receptor for platelet-derived growth factor, which is deleted in the embryonic lethal *Patch* mutation. *Development* 115, 289–303.

Reid, K., Nishikawa, S., Bartlett, P. F., and Murphy, M. (1995). Steel factor directs melanocyte development *in vitro* through selective regulation of the number of c-kit$^+$ progenitors. *Dev. Biol.* 169, 568–579.

Schatteman, G. C., Morrison-Graham, K., Van Koppen, A., Weston, J. A., and Bowen-Pope, D. F. (1992). Regulation and role of PDGF receptor α-subunit expression during embryogenesis. *Development* 115, 123–131.

Smith, E. A., Seldin, M. F., Martinez, L., Watson, M. L., Choudhury, G. G., Lalley, P. A., Pierce, J., Aaronson, S., Barker, J., Naylor, S. L., and Sakaguchi, A. Y. (1991). Mouse platelet-derived growth factor receptor α gene is deleted in W^{19H} and *patch* mutations on chromosome 5. *Proc. Natl. Acad. Sci. USA* 88, 4811–4815.

Steel, K., Davidson, D., and Jackson, I. (1992). TRP-2/DT, a new early melanoblast marker, shows that Steel growth factor (c-kit ligand) is a survival factor. *Development* 115, 1111–1119.

Stephenson, D. A., Mercola, M., Anderson, E., Wang, C., Stiles, C. D., Bowen-Pope, D. F., and Chapman, V. M. (1991). Platelet-derived growth factor receptor α-subunit gene (*Pdgfr*α) is deleted in the mouse *patch* (*Ph*) mutation. *Proc. Natl. Acad. Sci. USA* 88, 6–10.

Stephenson, D. A., Lee, K.-H., Nagle, D. L., Yen, C.-H., Morrow, A., Miller, D., Chapman, V. M., and Bucan, M. (1994). Mouse rump-white mutation is associated with an inversion of chromosome 5. *Mamm. Genome* 5, 342–348.

Stocker, K. M., Sherman, L., Rees, S., and Ciment, G. (1991). Basic FGF and TGF-b1 influence commitment to melanogenesis in neural crest-derived cells of avian embryos. *Development* 111, 635–645.

Wang, C., Kelly, J., Bowen-Pope, D. F., and Stiles, C. D. (1990). Retinoic acid promotes transcription of the platelet-derived growth factor α-receptor gene. *Mol. Cell. Biol.* 10, 6781–6784.

Wehrle-Haller, B., and Weston, J. A. (1995). Soluble and cell-bound forms of steel factor activity play distinct roles in melanocyte precursor dispersal and survival on the lateral neural crest migration pathway. *Development* 121, 731–742.

Weston, J. A. (1991). Sequential segregation and fate of developmentally restricted intermediate cell populations in the neural crest lineage. *Curr. Top. Dev. Biol.* 25, 133–153.

Whitehead Institute/MIT Center for Genome Research, Genetic Map of the Mouse, Database Release 10, April 28, 1995.

Williams, D., Eisenman, J., Baird, A., Rauch, C., Van Ness, K., March, C., Park, L. S., Martin, U., Mochizuki, D., Boswell, H., Burgess, G., Cosman, D., and Lyman, S. D. (1990). Identification of a ligand for the c-kit proto-oncogene. *Cell* 63, 167–174.

Received for publication December 23, 1995
Accepted February 12, 1996

2.4. Stem Cell factor dependent migration and/or survival ?

Receptor tyrosine kinase-dependent neural crest migration in response to differentially localized growth factors

Bernhard Wehrle-Haller and James A. Weston

Summary

How different neural crest derivatives differentiate in distinct embryonic locations in the vertebrate embryo is an intriguing issue. Many attempts have been made to understand the underlying mechanism of specific pathway choices made by migrating neural crest cells. In this speculative review we suggest a new mechanism for the regulation of neural crest cell migration patterns in avian and mammalian embryos, based on recent progress in understanding the expression and activity of receptor tyrosine kinases during embryogenesis. Distinct subpopulations of crest-derived cells express specific receptor tyrosine kinases while residing in a migration staging area. We postulate that the differential expression of receptor tyrosine kinases by specific subpopulations of neural crest cells allows them to respond to localized growth factor ligand activity in the embryo. Thus, the migration pathway taken by neural crest subpopulations is determined by their receptor tyrosine kinase response to the differential localization of their cognate ligand.

Accepted
20 December 1996

Introduction

The neural crest is a transient embryonic structure which is formed by the epithelial to mesenchymal transformation of cells derived from the dorsal neural tube[1]. In the avian and mammalian embryonic trunk, after crest cells separate from the neural epithelium, they transiently reside in an extracellular matrix-rich space, the migration staging area (MSA†), bordered by the neural tube, somites and ectoderm[2,3]. In the cranial region, after separation from the neural tube and initial migration, crest cells reside transiently in a space underlying the ectoderm and extending laterally towards the level of the pharynx, an area functionally equivalent to the MSA in the trunk[4-6]. Neural crest cells disperse from the MSA along temporally and spatially distinct pathways and ultimately give rise to a variety of derivatives in specific embryonic locations, including neurons and glia of the peripheral nervous system, gland cells, connective tissue in branchial arch-derived craniofacial structures, and melanocytes (Fig. 1).

In the trunk, neural crest cells begin to migrate ventrally on an intersomitic and a medial pathway through the rostral part of the sclerotome[7], giving rise to both neuronal and nonneuronal derivatives. About a day later, a second wave of crest cells migrates on the lateral pathway, between the dermatome and the overlying epidermis[8], primarily giving rise to melanocytes. In the head, the MSA extends more laterally compared to the trunk[5] (Fig. 1A). From the MSA, an E/C8 immunoreactive cell population migrates on a dorsolateral pathway underlying the epidermis, ultimately forming the ectomesenchyme of the branchial arches and associating with the heart outflow tract. A medial population, immunoreactive to the HNK monoclonal antibody, migrates medioventrally to form the sympathetic ganglionic complex, and associates with pharynx and gut[6] (Fig. 1B). Significantly, as in the trunk, a small population of neural crest cells undergoes a delayed migration laterally underneath the epidermis; these cells will give rise to melanocytes in the skin and inner ear[9]. Various reviews further discuss the unique migration, proliferation and differentiation events of developing neural crest cells[3,4,10-15].

Different mechanisms might control the migration of neural crest cells along their specific pathways. For example, it has been suggested that extracellular matrix molecules favorable for adhesion and migration form a pathway for neural crest cell migration[12,16,17]. Recently, several members of the semaphorin family of inhibitory guidance proteins have been identified bordering the neural crest migration and peripheral nerve pathways[18,19], suggesting that neural crest cell guidance is regulated by restricting the random

†Abbreviations: MSA, migration staging area; RTK, receptor tyrosine kinase; NGF, nerve growth factor; SCF, stem cell or Steel factor; GDNF, glial cell line-derived neurotrophic factor; PDGF, platelet-derived growth factor.

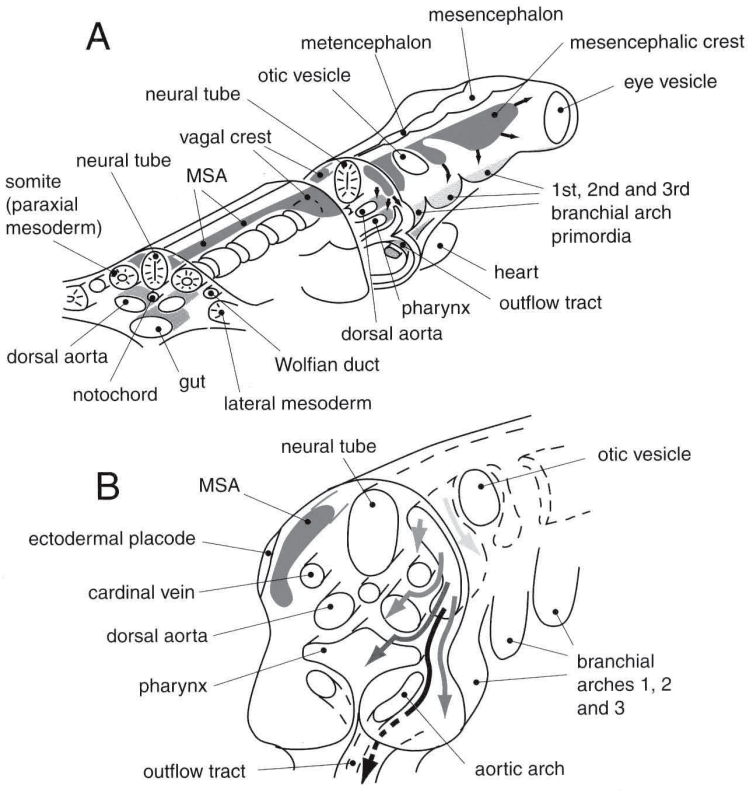

Fig. 1. Schematic representation of the neural crest 'migration staging area' and neural crest migration routes. (A) Suggested location for the cranial and trunk neural crest 'migration staging area' (MSA) (red area) in an approximately 2-day-old avian embryo. Neural crest cells have segregated from the neural epithelium and occupy a cell-free space lateral to the neural tube. In order to visualize the MSA at all axial levels in one drawing, the mesencephalic crest is shown at an earlier stage of its migration, compared to postotic neural crest. From the MSA, neural crest cells begin to migrate in directions indicated by the arrows. Mesencephalic crest cells migrate anteriorly over the eyes towards the nose and laterally to form the mandibular and maxillary arches. Preotic neural crest cells segregate from rhombomere 4 and migrate laterally into the hyoid arch, whereas postotic crest cells migrate both laterally and medioventrally. (B) Graphic representation of the MSA and subsequent migration pathways of the postotic (vagal) neural crest cells. On the left side, the approximate location of the MSA is indicated (red area). The right side shows the spatially and temporally distinct migration pathways of vagal neural crest cells leaving the MSA. Blue, lateral migration into branchial arches 3-6 (craniofacial ectomesenchymal precursor); purple, lateral pathway along aortic arches towards the heart outflow tract (smooth muscle and mesenchymal precursor); green, ventro-medial migration into the pharynx and gut (enteric ganglion precursors); pink, ventro-medial pathway towards dorsal aorta (sympathetic precursor); orange, dorso-medial pathway (neuronal and glial precursor of cranial ganglia); yellow, dorsolateral pathway (melanocyte precursors). For migration pathways in the trunk, refer to refs 3 and 7).

migration of neural crest cells onto specific pathways. Although these are probably important general mechanisms that influence neural crest cell migration, they do not provide sufficient specificity to account for the observed spatial and temporal complexity of neural crest migration, nor do they account for the stereotyped differentiation of specific neural crest derivatives in precise embryonic locations.

Advances in our understanding of receptor tyrosine kinase (RTK) expression and the activities of specifically localized growth factors such as sevenless and boss, respectively[20], however, suggest a new cellular mechanism to explain stereotyped patterns of neural crest migration and differentiation. The aims of this review are therefore firstly, to discuss recent data on the expression and activity of RTKs in neural crest subpopulations and secondly, to suggest a general mechanism for the patterning of neural crest migration, based on differential RTK expression by neural crest cells and the requirement for localized, pathway-specific activity of cognate ligands.

Neural crest-derived subpopulations express different receptor tyrosine kinases

Since the discovery of nerve growth factor (NGF)[21], it has been known that some neural crest derivatives require growth factor activity for survival[22]. RTKs have been identified in embryonic and adult neural crest derivatives. These include the neurotrophin (NGF, BDNF, NT-3, NT-4 and 5) receptors trkA, B and C[22], the neuregulin (glial growth factor, heregulin, ARIA) receptors erbB2, erbB3 and erbB4[23], the receptors for PDGF, PDGFR (α and β)[24], the receptor for Stem cell factor (SCF; also known as Steel factor, mast cell growth factor and kit-ligand)[25] and c-ret, which responds to GDNF[26] in the presence of GDNFRα[27,28].

Several mutations and gene knockouts in the mouse have demonstrated that RTK function is required for survival of subsets of neural crest derivatives, since the lack of growth factor activity or absence of growth factor receptors results in the failure of specific derivatives to persist[25,29-36]. This suggests that different neural crest-derived subpopulations develop distinct dependencies on growth factors. The presence of such distinct factor-dependent subpopulations suggests that acquiring RTK dependency is a critical step in the differentiation of multipotent neural crest precursor cells into specific neural crest derivatives.

Since the roles of RTK expression and activity in neural crest cells are largely unknown, the spatio-temporal identification of RTK activity may provide insights into the mechanism involved in early neural crest migration and segregation into various derivatives along their pathways of

migration. Accordingly, we will discuss recent discoveries concerning the role of RTK function and ligand localization in the morphogenetic behavior of several neural crest subpopulations.

Melanocyte precursors express c-kit, which is required for their initial dispersal on the lateral pathway and subsequent survival

Melanocyte precursors transiently depend on Steel factor (SCF), the kit-ligand, for survival of melanocytes *in vitro*[37,38]. *In vivo*, neural crest-derived melanocyte precursors express the RTK, c-kit, in the MSA, and appear to depend on SCF for migration and survival on the lateral pathway almost as soon as they start to express this RTK and other melanocyte-specific markers (e.g. tyrosinase related protein-2)[9,39,40] (summarized in Fig. 2).

SCF is transiently produced by the epithelial dermatome and localized on the lateral migration pathway in the trunk of the mouse[40-42] prior to the onset of melanocyte precursor dispersal. Subsequent expression of SCF in the overlying epidermis precedes the invasion of c-kit-expressing melanocyte precursors into the skin. Analysis of *Steel* mutations has shown that in the absence of SCF, melanocyte precursor cells appear in the MSA but fail to migrate. Mutant analysis has further revealed that a secreted form of SCF is

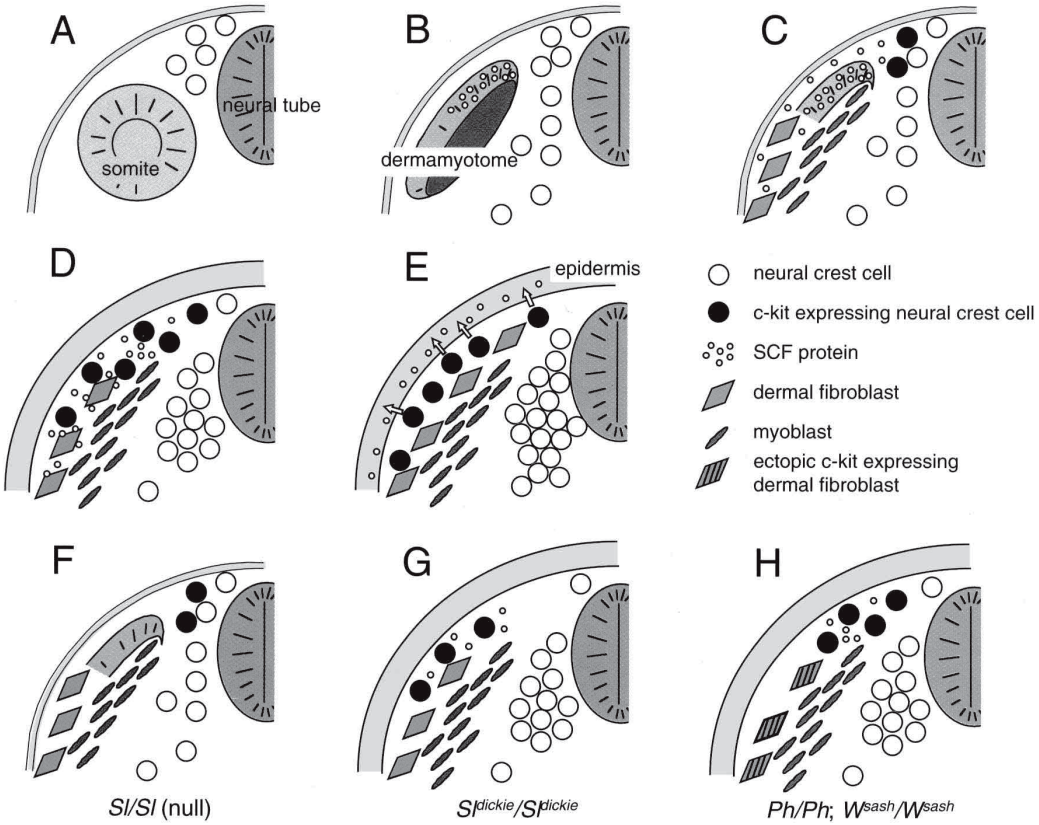

Fig. 2. Graphic representation of the stages of trunk melanocyte precursor migration on the lateral crest migration pathway and perturbations in mutant environments in the mouse. (A) Premigratory crest cells (open circles) accumulate in the MSA lateral to the dorsal neural tube. Neural crest cells begin to disperse on the medial pathway by e10.5, as soon as the epithelial somite transforms into the medial sclerotome. (B) At that time, crest cells have not begun to disperse on the lateral pathway, but the dorsal aspect of the dermatome begins to express SCF (small open circles). (C) Dermal mesenchyme forms by epithelial to mesenchymal transformation of the lateral aspects of the dermatome. SCF protein is secreted dorsally and ventrally, while a subpopulation of neural crest cells located in the MSA starts to express the receptor tyrosine kinase c-kit at e11 (filled circles). (D) As soon as c-kit is expressed in melanocyte precursors, these cells start to migrate on the lateral pathway, which has completely transformed into mesenchymal dermis, and no longer expresses SCF mRNA (e11.5). Note, however, that membrane bound SCF protein (small open circles) may still be attached to mesenchyme cell surfaces. (E) By e12.5, SCF is expressed in the overlying epidermis. Melanocyte precursors begin to enter the epidermis by e13.5. (F) In the absence of SCF, in *Steel* (*Sl*) mutant embryos, melanocyte precursors initially differentiate (filled circles) but fail to migrate and ultimately disappear[40]. (G) In the presence of secreted SCF only, as in Sl^{dickie} mutant embryos, melanocyte precursors begin to migrate on the lateral pathway but disappear subsequently[40]. (H) As a consequence of ectopic c-kit expression in dermal fibroblasts (but not dermatome), in *Patch* (*Ph*) and W^{sash} mutant embryos[40-42], SCF distribution and melanocyte precursor localization is altered[42,43].

Table I. *Growth factor ligands discussed in the text, and their receptor tyrosine kinases expressed in crest-derived subpopulations*

Growth factor ligand	Ligand source/location	Receptor	Migrating neural crest subpopulation
SCF (Steel factor)	Dermatome, epidermis/lateral pathway	c-kit	Melanocyte precursor
NT-3 (neurotrophin-3)*	Neural tube/medial pathway	trk C	Subset of medial migrating trunk neurogenic crest cells
GDNF	Gut mesenchyme	GDNFRα/c-ret	Subpopulation of cranial crest cells (enteric precursor)
Neuregulin	Motorneurons/ventral roots; rhombomeres 2, 4 and 6; migrating cranial crest and distinct branchial arch cells	erbB2/erbB3 erbB2/erbB4†	Schwann cell precursor; subpopulation of cranial and trunk neural crest cells
PDGF (AA, AB, BB)	Epidermis	PDGFRα	Subpopulation of cranial neural crest cells (ectomesenchymal)

*Other neurotrophins and their receptors are expressed later in neural crest derivatives[22, 29].
†erbB4 is not expressed in migrating neural crest cells[32].

sufficient to direct initial melanocyte precursor migration onto the lateral pathway, whereas a membrane-bound form of SCF is required for the survival of melanocyte precursors on that pathway[40] (Fig. 2A-E).

Essentially then, the localization of SCF on the lateral pathway forms a prepattern, which is reflected by the subsequent distribution of c-kit-expressing melanocyte precursors on that pathway. When the distribution of SCF activity (SCF protein) on the lateral pathway is perturbed either by ectopic expression of c-kit in dermal mesenchyme, as in the *W^sash*[43] and *Patch* mutations[42,44], or by altering SCF production, as in different *Steel* alleles, melanocyte migration pattern is changed and subsequent survival is affected[42-44] (Fig. 2F-H). This demonstrates that c-kit-expressing melanocyte precursors not only require SCF activity for survival, but also change their migration pattern in response to altered SCF availability in the tissue. This suggests that SCF exerts a chemotactic signal toward c-kit-expressing melanocyte precursors. This model is further supported by studies demonstrating that SCF can elicit chemotactic responses by c-kit expressing cells *in vitro*[45,46].

Thus, the control of pathway selection, migration and survival of melanocyte precursors by c-kit/SCF signaling, represents a clear example of RTK control of neural crest cell behavior. We suggest that the control of differential expression of RTKs in neural crest cells, combined with localized growth factor activity, may also provide the necessary specificity for the specific migration of other neural crest-derived subpopulations.

As implied above, differential expression of RTKs accompanies initial differentiation of specified cells, inducing partially restricted subpopulations. As these subpopulations arise, the ligands for their differentially expressed RTKs often appear concurrently in the embryonic environment. Several mechanisms may regulate ligand availability, including localized synthesis of ligand, dominant negative expression of receptors, differential expression of splice variants and presentation or sequestration by extracellular matrix. Below, we will suggest examples of such mechanisms as they affect development of other neural crest derivatives (Table 1).

trkC function is required for proliferation, migration and survival of some crest-derived neurogenic precursors

As early as e10.5 (embryonic day 10.5) of mouse development, embryos lacking NT-3, the ligand for trkC, exhibit an increase in cell death in the nascent sensory ganglia compared to wild type[47]. Consistent with this result, the application of neutralizing antibodies to NT-3 in avian embryos induces the loss of a subpopulation of neural crest cells in developing sensory ganglia as early as e3[48]. These results suggest that a subpopulation of neural crest-derived cells has acquired dependence on trkC function at the earliest stages of gangliogenesis and possibly even prior to gangliogenesis, while the crest-derived precursors are still dispersing on the medioventral pathway.

Consistent with that notion, trkC is expressed by subsets of premigratory and migratory neural crest cells[49,50]. Interestingly NT-3 has several different effects on neural crest cells including proliferation, survival and differentiation[50,51]. These pleiotropic effects might be explained by differential expression of trkC isoforms[29] with respect to developmental stages of the embryo and developmental state of neural crest derivatives. For example, different isoforms of trkC expressed in cultured neurons appear to mediate different responses to NT-3[52].

Alternatively, pleiotropic effects of NT-3 in trkC-dependent neural crest cells could also be mediated by different concentrations of NT-3. Consistent with this notion, application of pharmacological concentrations of NT-3 to e3 chick embryos during the formation of sensory and nodose ganglia, results in a severe reduction of ganglia size[53]. This might be explained by a premature differentiation of trkC-dependent neuronal precursors[53]. These results suggest that regulation of the levels of growth factor activity available to crest cells in precise embryonic locations is important for their normal behavior. That growth factor dosages influence cell

behavior in RTK-expressing cells has also been demonstrated in c-kit-expressing mast cells. Thus, low concentrations of SCF are sufficient for survival and induce spreading on extracellular matrix, whereas a 100-fold higher concentration of SCF is required for mast cell proliferation[54,55]. We suggest that low concentrations of NT-3 and other growth factors are sufficient to ensure initial dispersal and survival of neurogenic precursors, whereas higher local concentrations lead to overt neuronal differentiation and subsequent dependence on target-derived growth factor signaling. Elevated levels of NT-3 may therefore affect the normal differentiation program of neurogenic precursors[53]. It will be interesting to learn whether NT-3 application or overexpression before the start of neural crest cell migration influences the location and behavior of trkC-expressing neural crest cells *in vivo*.

Neurogenic neural crest-derived cells disperse primarily on the medial pathway. If neurotrophin activity plays a role in directing the choice of pathway by these cells, such activity would need to be localized to the medial and absent from the lateral pathway. It is not immediately clear, however, how local differences in NT-3 activity can be established and maintained when NT-3 appears to be diffusible and uniformly released from the neural tube[51]. Two possible mechanism are plausible. First, differential distribution of NT-3 binding extracellular matrix components[12] may create local differences in concentration and availability of NT-3. Second, it has recently been shown that besides a subpopulation of medial-migrating neural crest cells, trkC is also expressed in the dermatome, which borders the lateral crest migration pathway. At this time trkC-positive neural crest cells migrate solely on the medial pathway[49,56]. Based on our observation that ectopic c-kit expression reduces the levels of SCF-immunoreactivity and activity[42], we suggest that the expression of the trkC receptor on the lateral pathway reduces NT-3 availability to neural crest cells in that location, and thereby limits the location where NT-3-dependent (trkC-expressing) neural crest cells can migrate, survive and proliferate in response to NT-3.

c-ret function is required for colonization of the gut by crest-derived enteric ganglion precursors

Subpopulations of cranial neural crest cells begin to express c-ret between e9 and e10 of mouse development. Some of these cells make contributions to the enteric ganglia in the gut and ganglia in the head[57,58]. In the absence of a functional c-ret gene, the superior cervical ganglia is absent, and the enteric ganglia and myenteric plexus lack both neuronal and glial contributions at mid and hindgut levels[34,58]. Thus, although c-ret is expressed very early in different subsets of migrating neural crest cells, its activity appears to be required only by cells in the superior cervical ganglia, and by crest-derived cells that enter the gut and eventually give rise to neuronal and glial cells of enteric ganglia[58].

Disruption of GDNF expression yields the same developmental defects as seen in c-ret-deficient mice[33,35,36], suggesting that secreted GDNF could be a ligand of c-ret. It has recently been shown, however, that the functional ligand for c-ret is probably a complex of GDNF with a GPI-anchored receptor, GDNFRα[27,28]. This GDNF/GDNFRα complex can remain bound to the cell surface or be released[27]. In principle, therefore, the complex can activate c-ret expressed at the surface of the same cell or on adjacent cells[27,28]. Thus, neural crest cells that express c-ret will respond to GDNF only if GDNFRα is co-expressed in the same cell, or produced by other cells in the vicinity, which in the case of neural crest cells, is not yet known.

GDNF is normally expressed in the gut mesenchyme at high levels in close proximity to the enteric ganglia[28,36]. It has been reported that GDNFRα is expressed in the smooth and striated muscles, surrounding the enteric ganglia at e15.5 of mouse development[28]; however, the expression pattern of GDNFRα in enteric precursors themselves has not yet been clearly established. Thus, it is not known whether GDNFRα is co-expressed with c-ret in neural crest-derived cells or in surrounding tissue prior to the dependence of crest-derived cells on c-ret/GDNF signaling. Likewise, it is not known whether GDNF-dependence is acquired when GDNFRα is expressed in enteric precursors.

Based on our model that specific crest-derived subpopulations respond to differentially localized growth factor, we speculate that tissue expressing GDNFRα influences the local level of GDNF activity and thereby locally affects behavior of cells that depend on c-ret signaling. Thus, the fate of c-ret-expressing neural crest cells that do not coexpress GDNFRα may be influenced by released and membrane anchored GDNF/GDNFRα, reminiscent of c-kit-expressing melanocyte precursors, which normally encounter both secreted and membrane-bound SCF on the lateral pathway. Specifically, the migration and proliferation of c-ret expressing enteric precursors, which are known to depend on localized GDNF expression by the gut mesenchyme[33,35,36], may be influenced by GDNFRα expressing cells in the gut. Experimental manipulation of the localization of GDNF activity in the gut, either by changing GDNF levels or by ectopic expression of GDNFRα, has not yet been attempted. Nevertheless, GDNF expression in the target tissue of c-ret-expressing neural crest cells strongly suggests that both tropic and trophic roles of c-ret-mediated GDNF signaling might be regulated by localized GDNFRα expression during enteric ganglion precursor migration into the gut.

Subpopulations of cranial and trunk neural crest cells express erbB2/erbB3 and require localized neuregulin signaling for migration and survival

Neural crest-derived Schwann cell precursors respond to neuregulin signaling on ventral root nerve fibers

Neuregulin, also known as glial growth factor[22], is the ligand which activates the erbB family of receptor tyrosine

kinases[22]. ErbB4 binds neuregulin and induces tyrosine phosphorylation[22]. ErbB2 is necessary for tyrosine phosphorylation, but not sufficient for signal transduction[22]. It does not bind neuregulin; conversely, erbB3 binds neuregulin, but lacks a functional tyrosine kinase domain. Thus, a heterodimeric complex of erbB2/B3 or erbB2/B4, or a homodimeric complex of erbB4, is necessary for signal transduction of the cognate ligand neuregulin.

In the trunk, many neural crest cells migrating on the medial pathway express erbB3[32]. Subsequently, some of these cells are found in the sensory ganglia, and others associate as Schwann cell precursors with the ventral nerve root and the growing peripheral nerve. Mice carrying a deletion in the neuregulin[32] or the erbB2 gene[31] lack erbB3-expressing Schwann cell precursors associated with the ventral root and peripheral nerves in e10.5 motornerves[31,32], but still express erbB3 in the sensory ganglia. This suggests that the regulatory system involving erbB2/B3 is necessary to attract Schwann cell precursors to the peripheral nerves. At e10.5, erbB3-expressing cells in the sensory ganglia are not affected in embryos lacking erbB2 and neuregulin[31,32]. Therefore, these cells must either lack neuregulin signal transduction machinery (erbB2) or neuregulin dependence. Conversely, this result suggests that only the Schwann cell precursors coexpress erbB2 and erbB3 and are dependent on neuregulin signaling. We suggest, therefore, that localized neuregulin activity may be required for the initial association, proliferation and migration of neural crest cells along peripheral nerves.

Neuregulin is expressed in various differentially spliced forms, and is expressed both as a secreted and a membrane-bound growth factor[59,60]. In the trunk, migrating neural crest cells do not express neuregulin, nor is it expressed by tissues bordering their migration pathways[32]. In contrast, spinal motor neurons located in the ventral horn and forming axonal projections express neuregulin beginning at e10.5[59]. Later in development, neuregulin is also expressed in neurons of the sensory ganglia[59], where it might be involved in glial/neuron specification, as suggested by *in vitro* experiments[61]. It is likely, therefore, that neuregulin protein is localized to or secreted from the surfaces of growing motor and sensory nerves, where it regulates migration, survival and proliferation of a neural crest derived-subpopulation of neuregulin-dependent Schwann cell precursors[62].

A subpopulation of cranial crest cells requires differential erbB2 expression and localized neuregulin activity to promote its contribution to cranial ganglia

Cranial ganglia consist primarily of neurons of placodal origin and of neural crest-derived glial cells[63]. In the head, a subpopulation of cranial neural crest cells expressing erbB3 emerge from rhombomeres 2, 4 and postotic levels of the hindbrain at e9 of mouse development. At e10.5, erbB3-expressing cells are associated with the cranial ganglia and afferent nerves[32]. Mice that lack neuregulin or erbB2, lack the neural crest cell-derived neuronal and nonneuronal contributions to cranial ganglia at e10.5[31,32]. Defects are apparent as early as e9.5 of development[32], suggesting that neuregulin dependence (and, by inference, co-expression of erbB2) begins in erbB3-expressing neural crest cells as soon as they emerge from the neural tube. Other cranial neural crest cells which express a general neural crest marker, AP-2, and neurons of placodal origin, are not affected in mutant embryos[32].

Neuregulin is expressed by cells in rhombomeres 2, 4 and 6 and in a subpopulation of neural crest cells emanating from these levels[32]. In addition, neuregulin is expressed in a distinct subset of cells of the branchial arches in e9 mouse embryos[59] prior to emigration of erbB3-expressing crest cells. 1 day later (e10), neuregulin is strongly expressed in a subpopulation of cells in cranial ganglia[59]. Although neurons of placodal origin normally express neuregulin[32], they do not require it for survival, since they survive in neuregulin-negative embryos. Thus, the development of the distally located placode-derived neurons in the cranial ganglia[63] is not affected in neuregulin- or erbB2-deficient embryos[31,32]. We suggest, therefore, that placode-derived neurons support the development of erbB2/3-expressing *neurogenic* neural crest-derived cells in the proximal portion of the cranial ganglia, and the *non-neurogenic* crest-derived cells in the distal portion of the ganglia. This conclusion suggests an important role for localized paracrine neuregulin signaling between neuronal and glial precursors within a developing cranial ganglia.

Neural crest-derived cells do not migrate (or fail to survive) adjacent to rhombomeres 3 and 5[5]. Although neuregulin expression correlates well with cranial crest migration, it is not apparent whether or how the activity of secreted neuregulin can be restricted to the destination of these migrating cells. We suggest that due to their binding activity for neuregulin, either erbB3 or erbB4, can act as dominant negative regulators of neuregulin activity. Therefore, tissue or cells which express either erbB3 or erbB4 could negatively regulate the availability of neuregulin to dependent cells and thereby affect their dispersal and localization.

It is interesting, therefore, that erbB4 is expressed in rhombomeres 3 and 5, alternating with neuregulin expression in rhombomeres 2, 4 and 6. Due to the expression of erbB4 in rhombomeres 3 and 5, we suggest that neuregulin activity might be depleted adjacent to rhombomeres 3 and 5, resulting in the inability of erbB2/3-expressing, neuregulin-dependent neural crest cells to migrate in that region *in vivo*. According to this notion, removal of erbB4 from rhombomere 3 would result in a change of migration pattern of erbB2/3-expressing neural crest cells over rhombomere 3, reflecting the unrestricted availability of neuregulin protein released from the hind-

brain. Neural crest cells originating in rhombomeres 2 and 4 would spread over the area of rhombomere 3, effectively reducing the normal spatial separation between the trigeminal and facial/acoustic ganglia. In fact, fused trigeminal and facial/acoustic ganglia are exactly what has been observed by Gassmann and coworkers in mice deficient in erbB4[64]. A similar pattern of fused ganglia has been reported in mice lacking Krox-20, which is normally expressed in rhombomeres 3 and 5[65,66]. Although the early pattern of cranial neural crest cell migration has not been studied in either erbB4- or Krox-20-deficient embryos, we suggest that Krox-20 regulates the pattern of cranial ganglion distribution through the expression of erbB4 in rhombomeres 3 and 5.

PDGFRα function is required for the development of ectomesenchymal derivatives

Cells associated with the cranial crest express PDGFRα at e9 of mouse development[24,30] and give rise to branchial arch mesenchyme. However, in *Patch* mutants[30], which are deficient in PDGFRα[67], developmental defects are first manifested 2 days later when branchial arches fail to fuse. In addition, cells from the cardiac crest which normally migrate to the heart and form the septation of the outflow tract[5], fail to do so in *Patch* mutant embryos[30].

PDGFRα is able to bind to both forms of PDGF (A and B) expressed in the embryo[68]. During craniofacial development, PDGFA mRNA is expressed by the overlying epidermis, whereas PDGFRα is expressed in branchial arch mesenchyme[69]. PDGFA is produced as two splice variants with identical receptor binding domains but differential abilities to interact with cell surface or extracellular matrix heparan sulfate proteoglycan[70]. This suggests that one form of PDGFA protein is normally associated with epidermal basement membranes, and is contacted by migrating ectomesenchymal cells[16] that express PDGFRα. It is not known whether the cleft-face phenotype results from a failure of ectomesenchymal crest cells to reach the branchial arches during their early migration or their inability to proliferate in their appropriate locations. However, since PDGFRα has been shown to elicit tropic responses *in vitro*[71], it is tempting to speculate that such a mechanism directs ectomesenchymal neural crest precursor dispersal from the MSA into their target areas (Fig. 1B).

Discussion

In this review we suggest a new mechanism for regulating neural crest cell migration patterns. We postulate that developmentally distinct subpopulations of crest-derived cells arise after pluripotent crest cell precursors undergo epithelial-mesenchymal transformation and enter the MSA. Within the MSA, we suggest that crest-derived subpopulations begin to express specific RTKs, in response to presently unknown intrinsic or extrinsic cues, which thereby allow them to respond to differentially localized growth factor ligands in the embryo. Thus, the MSA would be the embryonic location where neural crest cells make their first specific pathway choices, informed by the presence of specific ligand activity on the different pathways, and the nature of the RTKs expressed by specific neural crest cells there.

During neural crest cell differentiation, migration represents one aspect of a complex web of developmental events. It is important to emphasize, however, that since the diversification of the crest cell population occurs soon after it segregates from the neuroepithelium, each subpopulation is likely to respond to unique environmental cues, and each has to be analyzed specifically. It is also likely, however, that irrespective of the differentiated state of a cell, the event of migration is linked to RTK expression and the consequent response to localized cognate ligand activity. For example, c-ret is expressed in enteric precursors before they undergo neuron/glia restriction[58,72]. Likewise, some multipotent cells appear to be transiently present at early stages of dispersal on the lateral pathway[14]. It is not known whether these multipotent cells express RTKs during migration, and if so, which ones. We do know, however, that although neurogenic cells appear very transiently on the lateral pathway (Y. Wakamatsu, M. Mochii, K. S. Vogel and J. A. Weston, unpublished; see also ref. 14), no neuronal crest derivatives persist there. This suggests that appropriate neuronal survival cues are absent or unavailable on this pathway[49].

Interestingly, the onset of migration of many precursor populations correlates very well with their dependence on RTK activity for survival. Thus, enteric ganglion precursors, cranial and trunk neuron and glial precursors, Schwann cell precursors, and melanocyte precursors all express and depend on specific RTKs and seem to rely on ligands uniquely active in specific embryonic locations. Since crest-derived cells, and especially melanocyte precursors, represent an unusually invasive cell type[73], the tight control of pathway choice and cell survival from the onset of migration from the MSA may therefore serve an important function to assure that derivatives of these invasive cells normally differentiate only in appropriate embryonic locations.

In summary, the neural crest cell distribution pattern established through RTK/ligand interaction could be exerted either by *trophic* or by *tropic* stimuli, or a combination of both. The persistent tight regulation of survival by the levels of available growth factors, however, makes it difficult to identify a *tropic* function in control of neural crest cell migration. Nevertheless, two models to explain differential migration and localization of subpopulations of neural crest cells in response to localized growth factors can be imagined (Fig. 3). First, neural crest cell subpopulations that acquire growth factor dependence migrate randomly through the embryo. Specific localization into the target area would be achieved by target-derived *trophic* support and apoptosis of

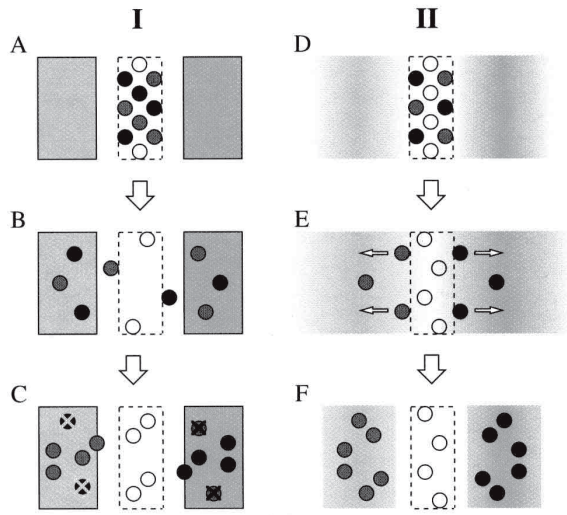

Fig. 3. Two different models explain growth factor-induced accumulation of RTK-expressing subpopulations of neural crest cells in ligand-expressing target areas. In model I (A-C), subpopulations of neural crest cells begin to express a specific RTK while residing in the MSA (A). From this location they disperse randomly within the adjacent tissue (B). Cells acquire growth factor dependence and undergo apoptosis when they are localized ectopically, but survive and proliferate when they are localized where their respective growth factor is expressed (C). In model II (D-F) growth factors released from the target areas form a gradient in the tissue while subpopulations of crest cells begin to express specific RTKs in the MSA (D). As soon as the growth factor gradient reaches the MSA, RTK-expressing cells will disperse up the gradient of their cognate ligand (E). Subsequently, the cells reach the source of their cognate ligand (target area) and begin to proliferate (F).

ectopically located cells outside of the target area (Fig. 3A-C). Alternatively, a gradient of growth factor might be released from the target tissue (Fig. 3D-F), which directs neural crest subpopulations towards their specific target organ. This could occur by some *tropic* mechanism, either chemotaxis or, if specific substrates are involved, some sort of haptotaxis[12,16]. The first model is based on classical evidence of cell death in peripheral ganglia associated with matching the number of neurons with the size of the target tissue and the amount of released growth factors. In contrast, the second model, which we suggest for consideration and further analysis, postulates that neural crest-derived cells migrate directly in response to a gradient of *tropic* signal provided by localized growth factor activity in the environment. Further tests of this hypothesis would be appropriate.

Acknowledgement

We thank Drs Paul Henion and Judith Eisen and Monique Wehrle-Haller for insightful discussions and for critical reading of the manuscript. We are also grateful to the anonymous reviewers who provided insightful and constructive criticisms. Our work has been supported by Grant DE-04316 from the USPHS. B. W.-H. has been supported by an EMBO postdoctoral fellowship (169-1993) and a grant from the Swiss Foundation for Medical and Biological Fellowships.

References

1 Duband, J.L., Monier, F., Delannet, M. and Newgreen, D. (1995). Epithelium-mesenchyme transition during neural crest development. *Acta Anat.* **154**, 63-78.

2 Derby, M. (1978). Analysis of glycosaminoglycans within the extracellular environments encountered by migrating neural crest cells. *Dev. Biol.* **66**, 321-336.

3 Weston, J.A. (1991). Sequential segregation and fate of developmentally restricted intermediate cell populations in the neural crest lineage. *Curr. Topics Dev. Biol.* **25**, 133-153.

4 Noden, D.M. (1988). Interactions and fates of avian craniofacial mesenchyme. *Development* **103 Suppl.**, 121-140.

5 Kuratani, S.C. and Kirby, M.L. (1991). Initial migration and distribution of the cardiac neural crest in the avian embryo: an introduction to the concept of the circumpharyngeal crest. *Am. J. Anat.* **191**, 215-227.

6 Kuratani, S.C. and Kirby, M.L. (1992). Migration and distribution of circumpharyngeal crest cells in the chick embryo. *Anat. Rec.* **234**, 263-280.

7 Erickson, C. and Loring, J. (1987). Neural crest cell migratory pathways in the trunk of the chick embryo. *Dev. Biol.* **121**, 220-236.

8 Erickson, C., Duong, T. and Tosney, K. (1992). Descriptive and experimental analysis of dispersion of neural crest cells along the dorsolateral path and their entry into ectoderm in the chick embryo. *Dev. Biol.* **151**, 251-271.

9 Steel, K., Davidson, D. and Jackson, I. (1992). TRP-2/DT, a new early melanoblast marker, shows that steel growth factor (c-kit ligand) is a survival factor. *Development* **115**, 111-1119.

10 LeDouarin, N.M., Ziller, C. and Couly, G. F. (1993). Patterning of neural crest derivatives in the avian embryo: in vivo and in vitro studies. *Dev. Biol.* **159**, 24-49.

11 Stemple, D.L. and Anderson, D.J. (1993). Lineage diversification of the neural crest: in vitro investigations. *Dev. Biol.* **159**, 12-23.

12 Erickson, C.A. and Perris, R. (1993). The role of cell-cell and cell-matrix interactions in the morphogenesis of the neural crest. *Dev. Biol.* **159**, 60-74.

13 Bronner-Fraser, M. (1994). Neural crest cell formation and migration in the developing embryo. *FASEB J.* **8**, 699-706.

14 Sieber-Blum, M., Ito, K., Richardson, M.K., Langtimm, C.J. and Duff, R.S. (1993). Distribution of pluripotent neural crest cells in the embryo and the role of brain-derived neurotrophic factor in the commitment to the primary sensory neuron lineage. *J. Neurobiol.* **24**, 173-184.

15 Gershon, M.D., Chalazonitis, A. and Rothman, T.P. (1993). From neural crest to bowel: development of the enteric nervous system. *J. Neurobiol.* **24**, 199-214.

16 Newgreen, D. and Thiery, J.-P. (1980). Fibronectin in early avian embryos: synthesis and distribution along the migration pathways of neural crest cells. *Cell Tissue Res.* **211**, 269-291.

17 Tosney, K. W., Dehnbostel, D. B. and Erickson, C. A. (1994). Neural crest cells prefer the myotome's basal lamina over the sclerotome as a substratum. *Dev. Biol.* **163**, 389-406.

18 Püschel, A.W., Adams, R.H. and Betz, H. (1995). Murine semaphorin D/collapsin is a member of a diverse gene family and creates domains inhibitory for axonal extension. *Neuron* **14**, 941-948.

19 Wright, D.E., White, F.A., Gerfen, R.W., Silos-Santiago, I. and Snider, W.D. (1995). The guidance molecule semaphorin III is expressed in regions of spinal cord and periphery avoided by growing sensory axons. *J. Comp. Neurol.* **361**, 321-333.

20 Hart, A.C., Krämer, H. and Zipursky, S.L. (1993). Extracellular domain of the boss transmembrane ligand acts as an antagonist of the sev receptor. *Nature* **361**, 732-736.

21 Levi-Montalcini, R. (1987). The nerve growth factor: thirty-five years later. *EMBO J.* **6**, 1145-1154.

22 Davies, A. M. (1994). The role of neurotrophins in the developing nervous system. *J. Neurobiol.* **25**, 1334-1348.

23 Carraway III, K.L. and Burden, S.J. (1995). Neuregulins and their receptors. *Curr. Opin. Neurobiol.* **5**, 606-612.

24 Schatteman, G.C., Morrison-Graham, K., Van Koppen, A., Weston, J.A. and Bowen-Pope, D.F. (1992). Regulation and role of PDGF receptor α-subunit expression during embryogenesis. *Development* **115**, 123-131.

25 Morrison-Graham, K. and Takahashi, Y. (1993). Steel factor and c-kit receptor: from mutants to a growth factor system. *BioEssays* **15**, 77-83.

26 Trupp, M. *et al.* (1996). Functional receptor for GDNF encoded by the c-ret proto-oncogene. *Nature* **381**, 785-789.

27 Jing, S. *et al.* (1996). GDNF-induced activation of the ret protein tyrosine kinase is mediated by GDNFR-α, a novel receptor for GDNF. *Cell* **85**, 1113-1124.

28 Treanor, J.J.S. *et al.* (1996). Characterization of a multicomponent receptor for GDNF. *Nature* **382**, 80-83.

29 Barbacid, M. (1994). The trk family of neurotrophin receptors. *J. Neurobiol.* **25**, 1386-1403.
30 Morrison-Graham, K., Schatteman, G.C., Bork, T., Bowen-Pope, D.F. and Weston, J.A. (1992). A PDGF receptor mutation in the mouse (*Patch*) pertubs the development of a non-neuronal subset of neural crest-derived cells. *Development* **115**, 133-142.
31 Lee, K., Simon, H., Chen, H., Bates, B., Hung, M. and Hauser, C. (1995). Requirement for neuregulin receptor erbB2 in neural and cardiac development. *Nature* **378**, 394-398.
32 Meyer, D. and Birchmeier, C. (1995). Multiple essential functions of neuregulin in development. *Nature* **378**, 386-390.
33 Sánchez, M.P., Silos-Santiago, I., Frisén J., He, B., Lira, S.A. and Barbacid, M. (1996). Renal agenesis and the absence of enteric neurons in mice lacking GDNF. *Nature* **382**, 70-73.
34 Schuchardt, A., D'Agati, V., Larsson-Blomberg, L., Costantini, F. and Pachnis, V. (1994). Defects in the kidney and enteric nervous system of mice lacking the tyrosine kinase receptor ret. *Nature* **367**, 380-383.
35 Pichel, J.G. *et al.* (1996). Defects in enteric innervation and kidney development in mice lacking GDNF. *Nature* **382**, 73-76.
36 Moore, M.W. *et al.* (1996). Renal and neuronal abnormalities in mice lacking GDNF. *Nature* **382**, 76-79.
37 Morrison-Graham, K. and Weston J. A. (1993). Transient steel factor dependence by neural crest-derived melanocyte precursors. *Dev. Biol.* **159**, 346-352.
38 Reid, K., Nishikawa, S., Bartlett, P.F. and Murphy, M. (1995). Steel factor directs melanocyte development *in vitro* through selective regulation of the number of c-kit$^+$ progenitors. *Dev. Biol.* **169**, 568-579.
39 Nishikawa, S. *et al.* (1991). *In utero* manipulation of coat color formation by a monoclonal anti-*c-kit* antibody: two distinct waves of *c-kit* dependency during melanocyte development. *EMBO J.* **10**, 2111-2118.
40 Wehrle-Haller, B. and Weston, J.A. (1995). Soluble and cell-bound forms of steel factor activity play distinct roles in melanocyte precursor dispersal and survival on the lateral neural crest migration pathway. *Development* **121**, 731-742.
41 Matsui, Y., Zsebo, K.M. and Hogan, B.L. (1990). Embryonic expression of a haematopoetic growth factor encoded by the *Sl* locus and the ligand for c-kit. *Nature* **347**, 667-669.
42 Wehrle-Haller, B., Morrison-Graham, K. and Weston, J.A. (1996). Ectopic c-kit expression affects the fate of melanocyte precursors in *Patch* mutant embryos. *Dev. Biol.* **177**, 463-474.
43 Duttlinger, R. *et al.* (1993). *W-sash* affects positive and negative elements controlling *c-kit* expression: ectopic *c-kit* expression at sites of kit-ligand expression affects melanogenesis. *Development* **118**, 705-717.
44 Duttlinger, R. *et al.* (1995). The W^{sh} and *Ph* mutations affect the c-*kit* expression profile: c-*kit* misexpression in embryogenesis impairs melanogenesis in W^{sh} and *Ph* mutant mice. *Proc. Natl Acad. Sci. USA* **92**, 3754-3758.
45 Blume-Jensen, P. *et al.* (1991). Activation of the human c-*kit* product by ligand-induced dimerization mediates circular actin reorganization and chemotaxis. *EMBO J.* **10**, 4121-4128.
46 Sekido, Y. *et al.* (1993). Recombinant human stem cell factor mediates chemotaxis of small-cell lung cancer cell lines aberrantly expressing the c-*kit* protooncogene. *Cancer Res.* **53**, 1709-1714.
47 ElShamy, W.M. and Ernfors, P. (1996). A local action of neurotrophin-3 prevents the death of proliferating sensory neuron precursor cells. *Neuron* **16**, 963-972.
48 Gaese, F., Kolbeck, R. and Barde, Y.-A. (1994). Sensory ganglia require neurotrophin-3 early in development. *Development* **120**, 1613-1619.
49 Henion, P.D., Garner, A.S., Large, T.H. and Weston, J.A. (1995). trkC-mediated NT-3 signaling is required for the early development of a subpopulation of neurogenic neural crest cells. *Dev. Biol.* **172**, 602-613.
50 Kalcheim, C., Carmeli, C. and Rosenthal, A. (1992). Neurotrophin-3 is a mitogen for cultured neural crest cells. *Proc. Natl Acad. Sci. USA* **89**, 1661-1665.
51 Pinco, O., Carmeli, C., Rosenthal, A. and Kalcheim, C. (1993). Neurotrophin-3 affects proliferation and differentiation of distinct neural crest cells and is present in the early neural tube of avian embryos. *J. Neurobiol.* **24**, 1626-1641.
52 Garner, A.S. and Large, T.H. (1994). Isoforms of the avian *trkC* receptor: a novel kinase insertion dissociates transformation and process outgrowth from survival. *Neuron* **13**, 457-472.
53 Ockel, M., Lewin, G.R. and Barde, Y.-A. (1996). *In vivo* effects of neurotrophin-3 during sensory neurogenesis. *Development* **122**, 301-307.
54 Kinashi, T. and Springer, T. A. (1994). Steel factor and *c-kit* regulate cell-matrix adhesion. *Blood* **83**, 1033-1038.
55 Dastych, J. and Metcalf, D. D. (1994). Stem cell factor induces mast cell adhesion to fibronectin. *J. Immunol.* **152**, 213-219.
56 Brill, G., Kahane, N., Carmeli, C., von Schack, D., Barde, Y. and Kalcheim, C. (1995). Epithelial-mesenchymal conversion of dermatome progenitors requires neural tube-derived signals: characterization of the role of neurotrophin-3. *Development* **121**, 2583-2594.
57 Pachnis, V., Mankoo, B. and Costantini, F. (1993). Expression of the c-ret proto-oncogene during mouse embryogenesis. *Development* **119**, 1005-1017.
58 Durbec, P.L., Larsson-Blomberg, L.B., Schuchardt, A., Costantini, F. and Pachnis, V. (1996). Common origin and developmental dependence on c-ret of subsets of enteric and sympathetic neuroblasts. *Development* **122**, 349-358.
59 Meyer, D. and Birchmeier, C. (1994). Distinct isoforms of neuregulin are expressed in mesenchymal and neuronal cells during mouse development. *Proc. Natl. Acad. Sci. USA* **91**, 1064-1068.
60 Marchionni, M.A. *et al.* (1993). Glial growth factors are alternatively spliced erbB2 ligands expressed in the nervous system. *Nature* **362**, 312-318.
61 Shah, N.M., Marchionni, M.A., Isaacs, I., Stroobant, P.W. and Anderson, D.J. (1994). Glial growth factor restricts mammalian neural crest stem cells to a glial fate. *Cell* **77**, 349-360.
62 Dong, Z., Brennan, A., Liu, N., Yarden, Y., Lefkowitz, G., Mirsky, R. and Jessen, K.R. (1995). Neu differentiation factor is a neuron-glial signal and regulates survival, proliferation and maturation of rat Schwann cell precursors. *Neuron* **15**, 585-596.
63 D'Amico-Martel, A. and Noden, D.M. (1983). Contributions of placodal and neural crest cells to avian cranial peripheral ganglia. *Amer. J. Anat.* **166**, 445-468.
64 Gassmann, M. *et al.* (1995). Aberrant neural and cardiac development in mice lacking the ErbB4 neuregulin receptor. *Nature* **378**, 390-394.
65 Schneider-Maunoury, S. *et al.* (1993). Disruption of *Krox-20* results in alteration of rhombomeres 3 and 5 in the developing hindbrain. *Cell* **75**, 1199-1214.
66 Swiatek, P.J. and Gridley, T. (1993). Perinatal lethality and defects in hindbrain development in mice homozygous for a targeted mutation of the zinc finger gene Krox-20. *Genes Dev.* **7**, 2071-2084.
67 Stephenson, D. A. *et al.* (1991). Platelet-derived growth factor receptor α-subunit gene (*Pdgfr*α) is deleted in the mouse *patch* (*Ph*) mutation. *Proc. Natl Acad. Sci.* **88**, 6-10.
68 Heldin, C.-H. (1992). Structural and functional studies on platelet-derived growth factor. *EMBO J.* **11**, 4251-4259.
69 Orr-Urtreger, A. and Lonai, P. (1992). Platelet-derived growth factor-A and its receptor are expressed in separate, but adjacent cell layers of the mouse embryo. *Development* **115**, 1045-1058.
70 Raines, E.W. and Ross, R. (1992). Compartmentalization of PDGF on extracellular binding sites dependent on exon-6-encoded sequences. *J. Cell Biol.* **116**, 533-543.
71 Vren, A., Yu, J.C., Gholami, N.S., Pierce, J.H. and Heidaran, M.A. (1994). The alpha PDGFR tyrosine kinase mediates locomotion of two different cell types through chemotaxis and chemokinesis. *Biochem. Biophys. Res. Commun.* **204**, 628-34.
72 Lo, L. and Anderson, D.J. (1995). Postmigratory neural crest cells expressing c-ret display restricted developmental and proliferative capacities. *Neuron* **15**, 527-539.
73 Erickson, C.A., Tosney, K.W. and Weston, J.A. (1980). Analysis of migratory behavior of neural crest and fibroblastic cells in embryonic tissues. *Dev. Biol.* **77**, 142-156.

Bernhard Wehrle-Haller* and **James A. Weston** are at the Institute of Neuroscience, 1254 University of Oregon, Eugene OR, 97403-1254, USA. E-mail: Bernhard.Wehrle-Haller@medecine.uniqe.ch; Weston@uoneuro.uoregon.edu
*Present address: Centre Médical Universitaire, Département de Pathologie, 1 rue Michel-Servel, 1211 Geneva 4, Switzerland.

2.5. Stem Cell factor induces chemotactic migration of melanocytes

Developmental Biology **232,** 471–483 (2001)
doi:10.1006/dbio.2001.0167, available online at http://www.idealibrary.com on

Analysis of Melanocyte Precursors in *Nf1* Mutants Reveals That MGF/KIT Signaling Promotes Directed Cell Migration Independent of Its Function in Cell Survival

Bernhard Wehrle-Haller,[1] Margaret Meller,[2] and James A. Weston[3]
Institute of Neuroscience, University of Oregon, Eugene, Oregon 97403-1254

Neural crest-derived melanocyte precursors (MPs) in avian and murine embryos emerge from the dorsal neural tube into a migration staging area (MSA). MPs subsequently migrate from the MSA on a dorsolateral pathway between the dermamyotome and the overlying epithelium. In mouse embryos, MPs express the receptor tyrosine kinase, KIT, and require its cognate ligand, Mast cell growth factor (MGF), for survival and differentiation. Prior to the onset of MP migration, MGF is expressed on the dorsolateral pathway at some distance from cells in the MSA and appears to be required for normal MP development. To learn if MGF is required solely for MP survival on this pathway, or if it also provides directional cues for migration, we uncoupled survival from chemoattractive or motogenic functions of this ligand using mice that carry a targeted mutation at the Neurofibromin (*Nf1*) locus and consequently lack RAS-GAP function. We show that *Nf1*-mutant MPs survive in the absence of MGF *in vitro* and *in vivo* and that *Nf1*-mutant MPs disperse normally on the lateral migration pathway in the presence of MGF. In contrast, *Nf1*-mutant MPs persist in the location of the MSA but are not observed on the lateral migration pathway in double-mutant mice that also lack MGF. We conclude that MGF/KIT function provides a signal required for directed migration of the MPs on the lateral pathway *in vivo*, independent of its function in survival. We further suggest that the MGF mediates MP migration through a signaling pathway that does not involve RAS.

Key Words: **neural crest; cell migration; chemoattraction; neurofibromin; RAS-GAP.**

INTRODUCTION

Cell migration is critically linked to morphogenesis and development of eukaryote embryos. During development, migrating cells often follow specific pathways to precise embryonic locations. Accordingly, migrating cells must be able to respond to cues on these pathways that promote migration or permit selective removal ("editing;" see Wakamatsu *et al.*, 1998) if they reach inappropriate locations. Genetic analysis in *Caenorhabditis elegans* and *Drosophila* has revealed critical genes involved in cell migration (for a review see Montell, 1999). Among them, receptor tyrosine kinases (RTK) and members of the RAS family of small GTPases play important roles. In vertebrates, however, it has been difficult to identify genes required for cell migration. One approach has relied on identifying gain-of-function mutations leading to tumor formation and metastasis. Other analyses of defects of the immune system (Ramesh *et al.*, 1999; Roberts *et al.*, 1999; Dekker and Segal, 2000) and of neural crest (NC) derivatives (Wehrle-Haller and Weston, 1997) have led to the identification of candidate genes involved in cell migration. Here, we use mutations affecting the NC-derived melanocyte lineage, *Steel* (Mgf^{Sl}) and *Nf-1*, to understand the role of the RAS signaling pathway in directed migration of melanocyte precursors.

Trunk NC cells segregate from the dorsal neural epithelium of vertebrate embryos and give rise to neurons and glia of the peripheral nervous system and to melanocytes in the skin (see Le Douarin and Kalcheim, 1999). As trunk NC cells emerge from the neural epithelium, they enter a

[1] Present address: Department of Pathology, University of Geneva, 1 Rue Michel-Servet, 1211 Geneva 4, Switzerland.
[2] Present address: Targeted Genetics, 1100 Olive Way, Suite 100, Seattle, WA 98101.
[3] To whom correspondence should be addressed at the Institute of Neuroscience, 1254 University of Oregon, Eugene, OR 97403-1254. Fax: (541) 346-4548. E-mail: weston@uoneuro.uoregon.edu.

0012-1606/01 $35.00

migration staging area (MSA), an extracellular matrix-rich space bounded by the dorsal neural tube, the dorsal somite, and the overlying surface epithelium (Weston, 1991). Crest cells in the MSA then enter and migrate on one of two temporally and spatially distinct pathways to precise locations in the embryo. Initially, crest cells in the MSA disperse into rostral sclerotome on a ventromedial migration pathway between the neural tube and the myotome of the somites, where they give rise primarily to cells of the peripheral nervous system. Later, crest cells leave the MSA and migrate on a dorsolateral pathway between the dermatome of the somite and the ectodermal epithelium. Most of these cells differentiate into melanocytes (Wehrle-Haller and Weston, 1995).

It is not yet known how the differential migration and localization of crest-derived cells is regulated, but recent results suggest that cell-type-specific RTK activity might play an important role in this process (Wehrle-Haller and Weston, 1997). For example, the RTK KIT and its ligand, Mast cell growth factor (MGF; also known as kit-ligand, KL, or stem cell factor, SCF), have been shown to function in normal migration and differentiation of melanocyte precursors (MPs) (Besmer, 1991; Besmer *et al.,* 1993). MGF, which is normally produced both as a cell-bound and as a proteolytically cleavable, potentially diffusible isoform, is expressed remotely on the lateral crest migration pathway just prior to the onset of MP migration. Interestingly, analysis of mice with mutations at the *Steel* locus, which encodes MGF, suggests that the two isoforms of MGF have different functions in MP development (Wehrle-Haller and Weston, 1995). MPs in *Steel* null mutant (Mgf^{Sl})embryos are not observed on the lateral pathway and ultimately disappear from the MSA. In contrast, MPs do leave the MSA and disperse on the lateral pathway in the *Steel-dickie* mutation ($Mgf^{Sl\text{-}d}$), which produces only a soluble form of MGF (Flanagan *et al.,* 1991; Wehrle-Haller and Weston, 1995). However, these MPs subsequently fail to survive and differentiate. MPs also survive only transiently after they disperse on the lateral pathway of mice homozygous for the $Mgf^{Sl\text{-}17H}$ mutation, which exhibits reduced cell surface expression of membrane-bound MGF (Wehrle-Haller and Weston, 1999). Thus, the diffusible isoform of MGF appears to be sufficient to permit MPs to enter the lateral pathway, whereas the cell-bound form of MGF is required for long-term survival and differentiation of melanocytes.

Diffusible MGF might function to permit dispersal of MPs on the lateral migration pathway in two ways. First, it might allow MGF-dependent cells to survive in the MSA and on the lateral migration pathway long enough for them to reach the remote source of cell-bound MGF in the dermal mesenchyme. Alternatively, soluble MGF originating from a remote source on the lateral migration pathway might stimulate cell locomotion, either as a motogenic cytokine (Dowrick and Warn, 1991; Gherardi and Coffer, 1991; Jordan and Jackson, 2000) or as a chemoattractive (tropic) cue for directional migration. To distinguish between these possibilities, the survival function of MGF (Besmer, 1991; Besmer *et al.,* 1993) must be uncoupled from possible migration function(s).

The possibility of uncoupling the survival and the migration functions of MGF was suggested by the report that cultured NC-derived sympathetic and dorsal root ganglion neurons from mice carrying a targeted mutation in the *Nf1* gene (Brannan *et al.,* 1994) survive in the absence of neurotrophins, whereas their wild-type counterparts die rapidly unless nerve growth factor or brain-derived neurotrophic factor is added to the culture medium (Vogel *et al.,* 1995). Mutations in the *Nf1* gene in humans cause the human disease neurofibromatosis, which is manifested by benign tumors of the peripheral nervous system and hyperpigmented lesions in the skin (café au lait spots; Rubenstein, 1986). *Nf1* encodes a protein, Neurofibromin, which contains a domain homologous to yeast Ras-GTPase-activating proteins (GAP) (Boguski and McCormick, 1993; Martin *et al.,* 1990; McCormick, 1995). Mutations in *Nf1* appear to sustain RAS activity, since conversion of the active form of RAS (RAS-GTP) to the inactive form (RAS-GDP) is impaired (Guha *et al.,* 1996; Henkemeyer *et al.,* 1995; McCormick, 1995; Rey *et al.,* 1994). Like the neurotrophin receptors (trkA, B, and C) and other RTKs, signaling by KIT is mediated, at least in part, through RAS (Duronio *et al.,* 1992; Serve *et al.,* 1995; Tauchi *et al.,* 1994). Accordingly, based on the hyperpigmented lesions observed in human neurofibromatosis patients, and the partial rescue of the coat color deficiency in a c-kit mutant (W^{41}) by *Nf1* haploinsufficiency (Ingram *et al.,* 2000), we reasoned that *Nf1*-mutant melanocytes, like *Nf1*-mutant peripheral neurons, might also persist in the absence of growth factor support. If this were true, *Nf1* mutants, in combination with the MGF-null mutation, would be useful to assess the migratory behavior of MPs in the absence of MGF activity.

We show here that *Nf1*-mutant melanocytes are independent of MGF for survival *in vitro* and *in vivo*. Additionally, we confirm that both MGF and Neurofibromin function in the RAS signal-transduction pathway for melanocyte survival. Finally, we have demonstrated that although MPs appear to migrate normally in *Nf1*-mutant mice, they remain in the region of the MSA of double-mutant embryos ($Mgf^{Sl^-};Nf1^-$) that lack both MGF and Neurofibromin function. We conclude, first, that MGF is required for directed migration of the MPs on the lateral pathway *in vivo;* second, that the role of MGF/KIT in cell migration is independent of its function in survival; and finally, that the tropic (chemoattractive) signal transduction pathway does not involve RAS-GAP activity.

MATERIALS AND METHODS

Embryos

An $Nf1^-$ heterozygous line (129/Sv $Nf1^-$), generously provided by Drs. Neal Copeland and Kristine Vogel (Brannan *et al.,* 1994), was crossed into a C57BL/6 background and then intercrossed to create homozygous $Nf1^{-/-}$ (referred to as *Nf1*-mutant) embryos,

which die *in utero* after embryonic day (e) 12.5, as well as $Nf1^{-/+}$ and $Nf1^{+/+}$ (wild-type) embryos. To identify the genotype of individual embryos, tail or limb bud tissue was digested in 55–60 μl of 10 mM Tris, pH 8, 2 mM EDTA, 0.2% Triton X-100, 200 mg/ml proteinase K at 55°C for 3 h. Samples were boiled for 10 min and 4 μl was amplified by PCR with primers and conditions as previously described (Brannan *et al.*, 1994). With these primers, template DNA from homozygous *Nf1*-mutant embryos produced a 340-bp fragment, wild-type embryos produced a 194-bp fragment, and both bands were present when template from heterozygous embryos was used.

WBReSl heterozygous lines from inbred colonies maintained in our laboratory were crossed to $Nf1^{-}$ heterozygotes. Resulting $Mgf^{Sl^{-}}/Nf1^{+}$; $Mgf^{Sl^{+}}/Nf1^{-}$ heterozygotes were intercrossed and genotyped by PCR as described (Wehrle-Haller and Weston, 1995). *Nf1*-mutant embryos were recognized as described above. Wild-type or Mgf^{Sl} heterozygous mice showed a PCR band at 700 bp, whereas homozygous Mgf^{Sl} embryos lacked the 700-bp band.

Neural Tube Cultures

Neural tubes from individual e9.5 embryos were cultured as previously described (Morrison-Graham and Weston, 1993). Cultures from homozygous *Nf1*-mutant embryos were compared with neural tubes explanted from heterozygous and wild-type littermates. Recombinant murine MGF (Pepro Tech) was added at a concentration of 100 ng/ml, and human (porcine sequence) Endothelin-3 (EDN3; Sigma) was added to the culture medium, when indicated, at a concentration of 100 nM. To eliminate endogenous MGF activity in control cultures or in cultures with EDN3 alone, MGF neutralizing antibody (R&D Systems) was added to the culture medium at a concentration of 10 μg/ml as described (Morrison-Graham and Weston, 1993). Based on the MEK inhibition studies of Zhang *et al.* (1998), 50 μM MEK inhibitor U0126 (Promega) in 0.5% DMSO was added on culture days 4 and 5. This inhibitor concentration corresponds to a thousandfold excess required for half-maximal inactivation of MEK1 and MEK2 but does not inactivate other MAP-related kinases (Favata *et al.*, 1998). Control cultures received 0.5% DMSO alone. On culture day 6, each culture was rinsed three or four times with half the volume of culture medium and given fresh culture medium containing only the original factors and/or antibodies. Melanocytes were visualized on culture day 10 by incubating fixed cultures with D,L-DOPA (Sigma) as previously described (Morrison-Graham and Weston, 1993).

Cryosectioning

Embryos were fixed in 4% paraformaldehyde (Sigma) in PBS at 4°C overnight, washed in PBS, and transferred through an alcohol series to 100% methanol. Embryos were bleached 4–5 h in 5:1 methanol:30% hydrogen peroxide (Fisher) at room temperature. Embryos were then rehydrated into PBS and embedded in agar-sucrose. Blocks were then equilibrated in 30% sucrose in PBS, frozen, and cryosectioned at 16 μm. Sections were stored at −20°C until use.

Whole-Mount and Histological in Situs

Mouse tyrosinase-related protein-2 (TRP2) digoxigenin-labeled riboprobes were synthesized from linear cDNAs kindly provided by Dr. Ian Jackson. Whole-mount *in situ* hybridization was performed as described (Wehrle-Haller and Weston, 1995). Embryos were dissected at the appropriate embryonic stage, fixed, bleached, and stored in methanol as above. *In situs* were performed on sectioned tissue as described (Strahle *et al.*, 1994), except for the following changes: 100 μl of diluted TRP2 probe was added to each slide and incubated overnight at 68°C. After hybridization, slides were washed in MABT (100 mM maleic acid, 150 mM NaCl, pH 7.5, 0.1% Tween 20) instead of PBS. Slides were blocked in MABT + 2% Boehringer blocking reagent (Roche) + 20% heat-inactivated goat serum (Sigma) for 1 h and incubated overnight at room temperature in anti-digoxigenin antibody conjugated to alkaline phosphatase (Roche) at 1:2000 in blocking solution. Four to five 20-min postantibody washes were done in MABT at room temperature. The alkaline phosphatase staining reaction was performed as outlined (Strahle *et al.*, 1994), except that 10% polyvinyl alcohol (low molecular weight; Aldrich) was added to the reaction mixture.

TUNEL Reactions

Whole-mount TUNEL reactions were performed on embryos after TRP2 RNA *in situ* as described (Gavrieli *et al.*, 1992; Gold *et al.*, 1993), with modifications as described (Wakamatsu *et al.*, 1998).

BrdU Labeling

Embryos were obtained from crosses as outlined in the RNA *in situ* section above. Embryos were dissected out of the mother at the appropriate embryonic stage in Hanks'/Hepes and the extraembryonic membranes were torn to expose the embryo. Embryos were incubated for 2 h in DMEM culture medium buffered with Hepes and containing 10% fetal bovine serum and 30 μg/ml BrdU. Embryos were then dissected away from extraembryonic tissues, fixed, bleached, and stored in methanol as outlined above. *In situs* for TRP2 were performed on BrdU-labeled embryos, which were then cryosectioned as specified above. BrdU labeling was immunohistochemically detected as previously described (Marusich *et al.*, 1994), except that preparations were labeled with mouse anti-BrdU Mab IgG (Roche) at 1:1000 and then incubated with Cy-3-conjugated goat anti-mouse IgG (Chemicon) at 1:300. Slides were then mounted in 50% glycerol, photographed, and processed as above.

Data Collection

Counts of melanocytes in crest cultures and of $TRP2^{+}$ cells in whole-mount *in situ* preparations were entered into an Excel database, where statistical analysis and graphing were performed. In some cases, counts were performed on scanned images of whole-mount *in situ* preparations. Embryos were photographed on a Leica Kombistereo microscope, and histological sections were photographed on a Zeiss Axiophot. Photos were scanned and converted to grayscale with PhotoShop (Adobe). All figures shown are representative of at least three embryos of each genotype and embryonic stage. Statistical comparisons of sample means were performed with Student's *t* test.

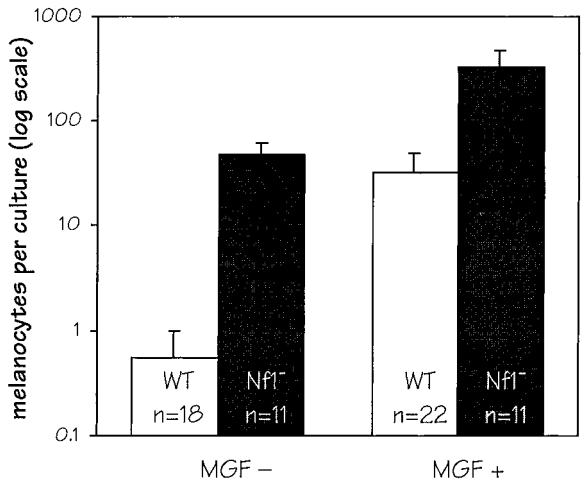

FIG. 1. Melanocytes in cultures of *Nf1*-mutant neural tubes survive in the absence of MGF and show increased sensitivity to the presence of MGF. Cultures of crest cells from *Nf1*-mutant mice contain the same number of melanocytes in the absence of MGF as wild-type cultures grown in the presence of MGF. Moreover, cultures of *Nf1*-mutant crest cells grown in the presence of MGF contain about an order of magnitude more melanocytes than wild-type cultures (note log scale), suggesting greater sensitivity to MGF signaling. Cultures designated MGF^- contained goat anti-MGF neutralizing antibody to block endogenous MGF activity (see Morrison-Graham and Weston, 1993). Bars represent SEM, n = number of cultures.

RESULTS

Nf1-Mutant Melanocytes Differentiate in the Absence of MGF in Vitro

Wild-type mouse MPs require the presence of MGF for survival/proliferation during a 4-day interval *in vitro* (Morrison-Graham and Weston, 1993), corresponding to the period of initial MP dispersal *in vivo* (Nishikawa *et al.*, 1991). If Neurofibromin functions as a RAS-GAP in the MGF/KIT signal transduction pathway, then loss of Neurofibromin activity in *Nf1*-mutant cells might cause this signaling pathway to remain continuously active. Accordingly, we reasoned that *Nf1*-mutant MPs might no longer require MGF for survival. To test this prediction, neural tubes from *Nf1*-mutant and wild-type embryos at e9.5 were cultured in the presence and absence of MGF. After 10 days in culture in the absence of MGF, few melanocytes are present in cultures of crest cells from wild-type mouse embryos. In contrast, cultures of *Nf1*-mutant crest cells contain approximately the same number of melanocytes in the absence of MGF as wild-type cultures in the presence of MGF (Fig. 1). We conclude, therefore, that *Nf1*-mutant melanocytes are independent of MGF for survival in culture. In addition, when cultured in the presence of MGF, the number of *Nf1*-mutant melanocytes was about an order of magnitude greater than in cultures of wild-type crest cells (note log scale in Fig. 1). This suggests that *Nf1*-mutant melanocytes are more sensitive to MGF stimulation than are wild-type cells, as has also been shown to be the case for hematopoietic stem cells derived from *Nf1*-mutant embryos (Zhang *et al.*, 1998).

MPs in Nf1-Mutant Embryos Disperse Normally on the Lateral Crest Migration Pathway

At e10.5, MPs are present in the trunk MSA of both mutant and wild-type embryos. Rostrally, at the level of the branchial arches, MPs of both mutant and wild-type embryos are present on the lateral pathway (see also Mackenzie *et al.*, 1997; Wehrle-Haller and Weston, 1995). At e11.5 (Fig. 2A), MPs are present on the lateral pathway in the trunk of both *Nf1*-mutant and wild-type embryos (Figs. 2B–2E). By e12.5 (Fig. 4A), MPs are widely dispersed on the lateral pathway at all axial levels (Figs. 4B and 4C). MPs were not observed in either wild-type or *Nf1*-mutant embryos on the medial migration pathway where spinal ganglia form from migrating crest-derived cells (Figs. 2D, 2E, 4F, and 4G). We conclude, therefore, that *Nf1*-mutant MPs migrate normally on the lateral pathway and that their dispersal on this pathway is not affected by loss of Neurofibromin function.

Some MPs Remain in the Region of the MSA of Mutant Embryos

MPs are transiently present in the MSA before entering the lateral migration pathway (Wehrle-Haller and Weston, 1995; Weston, 1991). At e11.5, some MPs are present in the original location of the MSA in the trunk of wild-type embryos (Figs. 2B and 2D), but the number of MPs in this location is greatly increased in *Nf1*-mutant embryos (Figs. 2C and 2E). Counts of $TRP2^+$ cells in e11.5 embryos reveal significantly more MPs on the lateral migration pathway of *Nf1*-mutant embryos (89.8 ± 10.4; $n = 5$) than at comparable axial levels of wild-type embryos (57.3 ± 5.9; $n = 7$; $P < 0.001$). By e12.5, no $TRP2^+$ cells are found in the original location of the MSA of wild-type embryos, whereas many $TRP2^+$ cells remain there in *Nf1*-mutant embryos (compare Figs. 4B and 4F with4C and 4G).

MP Survival in the MSA Is Increased in Nf1-Mutant Embryos

At e11.5 and later, significantly more $TRP2^+$ MPs are present in the region of the MSA in *Nf1*-mutant embryos than in wild-type embryos (see above). In wild-type embryos, some MGF-dependent cells might normally fail to leave the MSA in a timely way and, consequently, become vulnerable to editing by developmentally regulated cell death in this location (see Wakamatsu *et al.*, 1998; Maynard *et al.*, 2000). Accordingly, supernumerary MPs might be present in the location of the MSA in *Nf1*-mutant embryos because some cells, which do not disperse, are able to

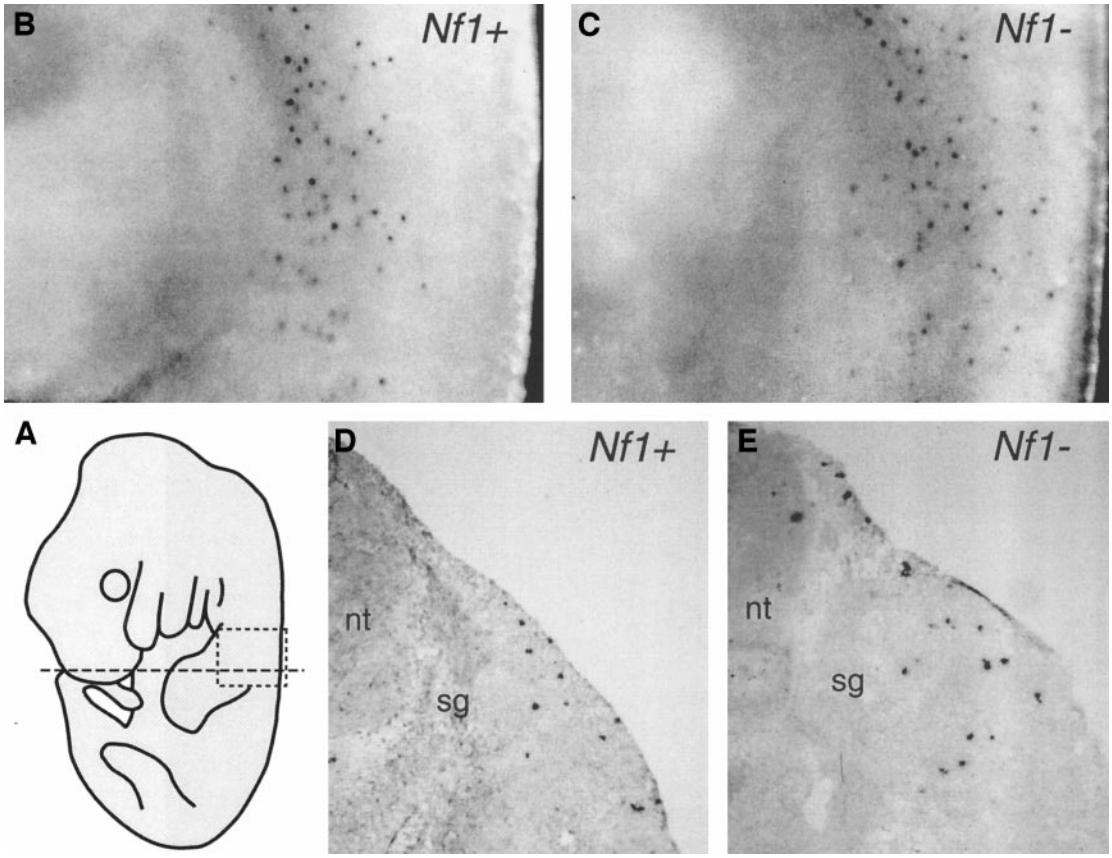

FIG. 2. Some melanocyte precursors remain in the MSA of *Nf1*-mutant embryos, but many migrate normally on the lateral pathway. TRP2 mRNA *in situs* on e11.5 embryos reveal location of MPs at the axial level designated in (A). (B, C) Photos of whole-mount preparations representing region outlined on diagram. (D, E) Photos of transverse sections at the axial level designated by the dotted line in the diagram. The neural tube (nt) and the location of nascent spinal ganglia (sg) on the medial migration pathway are noted. Wild-type embryos lack MPs in the original location of the MSA (B, D), whereas MPs remain in this location in *Nf1*-mutant embryos (C, E).

survive there. To test this inference, we compared the number of cells in the MSA of mutant and wild-type embryos that were undergoing developmental cell death at e10.5. At axial levels known to contain $TRP2^+$ cells in the MSA (Fig. 3B), fewer $TUNEL^+$ cells were present in *Nf1*-mutant embryos (Fig. 3D) than in comparable regions of wild-type embryos (Fig. 3C). Although it is unlikely that all dying cells in the MSA were MPs, it should be emphasized that, at these stages and axial levels, most neurogenic cells have already dispersed on the ventromedial crest-migration pathway, and therefore, most of the cells that remain in the MSA would be MPs. It is plausible, therefore, that prolonged survival of MPs accounts for the presence of many of the ectopic cells in the MSA of *Nf1*-mutant embryos.

In addition to reduced cell death in the MSA of *Nf1*-mutant embryos, a significant decrease in dying cells can be seen in the region of the lateral dermatome (compare Fig. 3C with 3D). In this region, apoptosis is normally associated with the epithelial-to-mesenchymal transformation of the epithelial dermatome. Since *Nf1*-mutant MPs disperse normally on the lateral pathway, however, reduced death of mesenchymal cells does not seem to impede their migration (Fig. 4C).

To address the possibility that there is also increased MP proliferation in mutant embryos, we compared the number of MPs that incorporate BrdU by double-labeling with the TRP2 probe in wild-type and *Nf1*-mutant embryos. Very few doubly labeled cells were observed in these preparations, but in any case, no significant differences could be detected in the proportion of $TRP2^+$ cells that incorporated BrdU at e10.5 and e11.5 (data not shown). Although we cannot exclude the possibility of increased proliferation of *Nf1*-mutant MPs on the lateral pathway, we suggest that increased survival is sufficient to account for the MPs observed in the region of the MSA in *Nf1*-mutant embryos (see Figs. 2C and 2E). This result appears paradoxical in light of the order of magnitude increase in the number of *Nf1*-mutant melanocytes in the presence of MGF *in vitro* (Fig. 1). However, the dramatic increase in the number of cultured MPs might reflect the difference between the

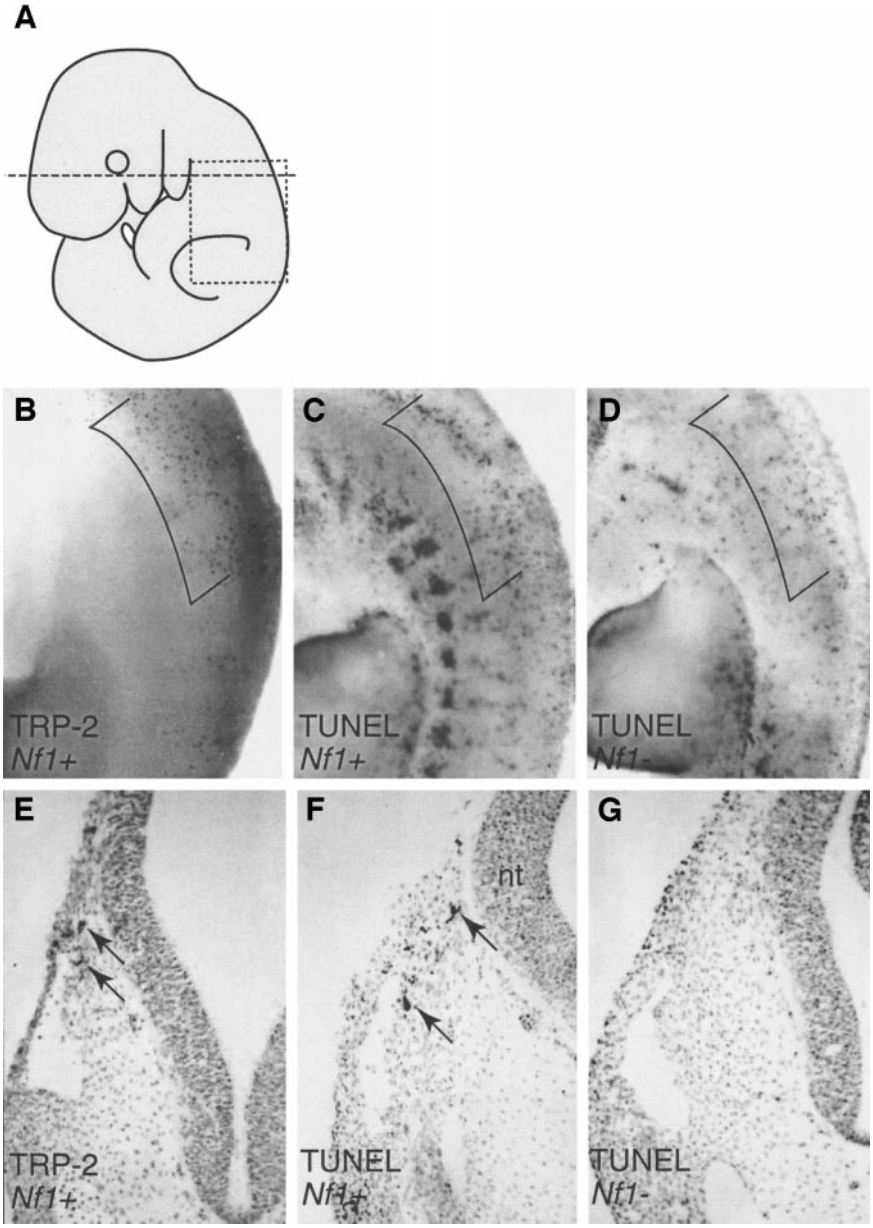

FIG. 3. Fewer TUNEL$^+$ cells are present in the MSA of *Nf1*-mutant embryos than in wild-type embryos. (A) Rectangle on schematic drawing of e10.5 embryo shows the location of photos of whole-mount embryos (B–D). Dotted line on schematic represents location of histological sections photographed in (E–G). (B, E) TRP2 *in situ* showing MPs in the MSA of wild-type embryo. (C, F) TUNEL staining in the MSA corresponding to that shown in (B) in wild-type embryos. (D, G) TUNEL staining in comparable locations of *Nf1*-mutant embryos.

limited amount of MGF normally present on the lateral migration pathway and the greater availability of exogenous MGF in culture.

MPs in Mgf^{Sl^-};$Nf1^-$ Double Mutant Embryos Do Not Leave the MSA

MPs are not seen on the lateral pathway of Mgf^{Sl} mutant embryos, which lack MGF (Wehrle-Haller and Weston, 1995). To determine if the absence of MPs is due to the failure of MPs to survive or their failure to migrate on the lateral pathway, we compared the presence of MPs on the lateral migration pathway of embryos that lack only endogenous MGF ($Mgf^{Sl^-};Nf1^+$) with embryos that lacked both MGF and Neurofibromin function ($Mgf^{Sl^-};Nf1^-$). As previously reported (Wehrle-Haller and Weston, 1995), few MPs remain in the region of the MSA of e11.5 Mgf^{Sl^-} mutant

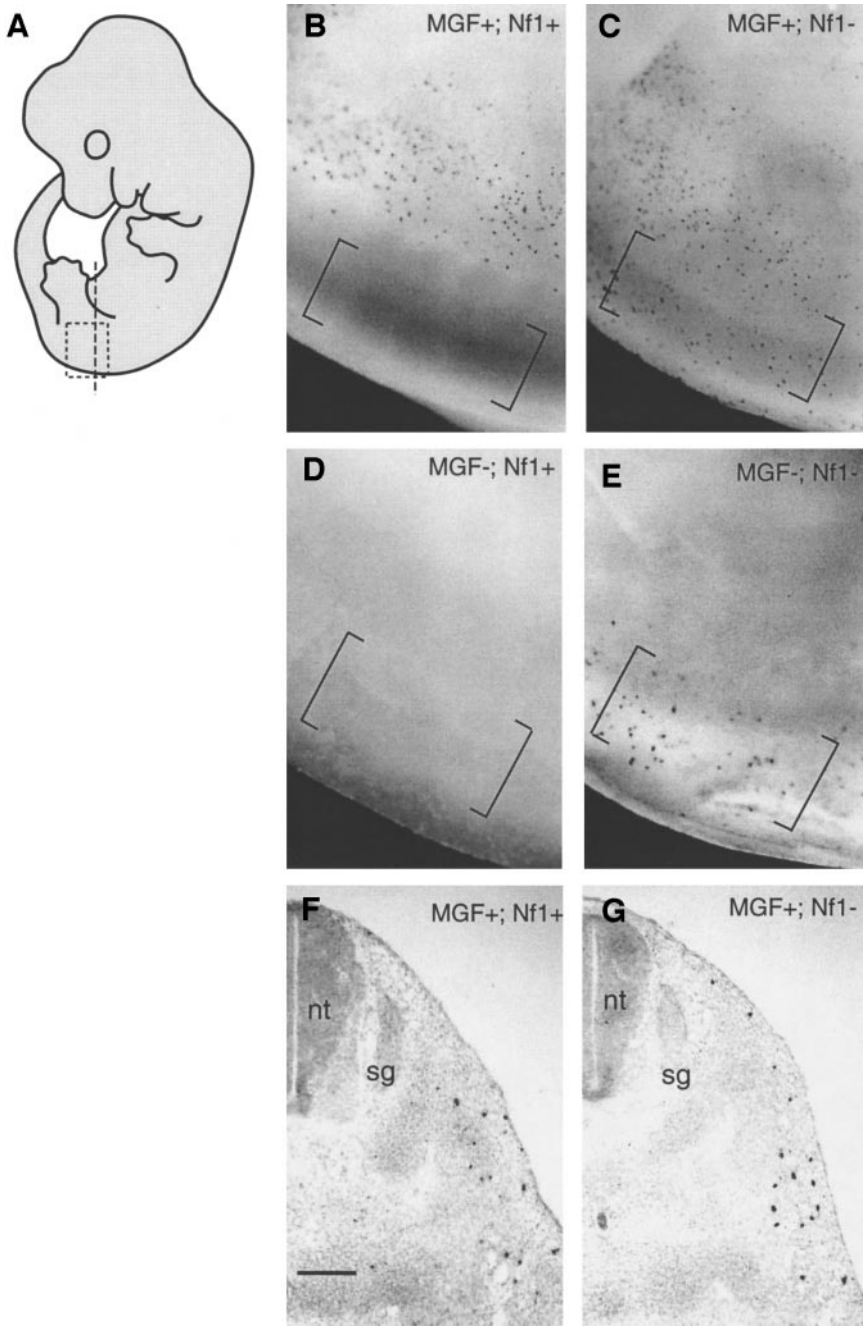

FIG. 4. Melanocyte precursor localization on the lateral migration pathway in whole-mount e12.5 embryos. (A) Schematic drawing of e12.5 mouse embryos shows location of photos (B–E). Brackets in (B–E) denote the original location of the MSA. Transverse sections of corresponding regions of (B and C) are represented in (F and G). The neural tube (nt) and the location of spinal ganglia (sg) on the medial pathway are noted. In the presence of MGF, MPs are observed on the lateral migration pathway, but not in the original location of the MSA in wild-type embryos (B, F). Likewise, in the presence of MGF, MPs are observed both on the lateral pathway and in the original location of the MSA in *Nf1*-mutant embryos (C, G). In the absence of MGF, MPs are observed in the original location of the MSA, but not on the lateral migration pathway of *Nf1*-mutant embryos (E), whereas MPs are absent in embryos that lack MGF but are wildtype for *Nf1* (D).

embryos, except at the most caudal axial levels, and MPs are completely absent by e12.5 (see above; Fig. 4D). In contrast, MPs persist in the MSA region of Mgf^{Sl^-};$Nf1^-$ double-mutant embryos, but are absent from the lateral pathway (Fig. 4E). TRP2 *in situs* performed on transverse sections of double-mutant embryos confirm that MPs are

TABLE 1
Effects of Growth Factors and MEK Inhibitor on Melanogenesis *in Vitro*

	Treatment			Genotype		
Expt	MGF[a]	EDN3[b]	MEK-I[c]	Wildtype	Nf1 mutant	*P*
1	—	—	—	5 ± 3 (8)	246 ± 109 (5)	<0.001
2	—	—	+	0.6 ± 0.6 (9)	23 ± 15 (6)	<0.1
3	+	—	—	217 ± 31 (23)	1169 ± 340 (5)	<0.001
4	+	—	+	42 ± 8 (20)	354 ± 84 (8)	<0.001
5	—	+	—	553 ± 162 (4)	340 ± 89 (3)	>0.4
6	—	+	+	303 ± 281 (9)	489 ± 163 (3)	>0.7

Note. The number of melanocytes/culture [mean ± SE (*n*)] is given.
[a] —, 10 μg/ml MGF blocking antibody (R&D Systems) present; +, 100 ng/ml MGF present.
[b] —, 10 μg/ml MGF blocking antibody present; +, EDN3 (100 nM) added to culture medium.
[c] —, 0.5% DMSO added; +, 50 μM MEK inhibitor U0126 (Promega) added to medium in 0.5% DMSO.

not present on the lateral pathway and remain in the region of the MSA (not shown).

MGF and Neurofibromin Signal through the RAS Pathway in Mouse Melanocytes

The signal-transduction cascade downstream of RAS is thought to involve activation of MAP kinase (ERK), which, in turn, is activated by MAP kinase kinase (MEK1 and 2 in mammals; see Widmann *et al.,* 1999). We reasoned that if Neurofibromin functions in the RAS pathway, then inhibition of MEK1 and 2 should abrogate rescue of MPs in cultures of *Nf1*-mutant crest cells. To test this prediction, a specific inhibitor of both MEK activities (U0126; Favata *et al.,* 1998) was added to cultures from day 4 to 6 when KIT signaling is known to be required for melanocyte survival in culture (Morrison-Graham and Weston, 1993). Treatment with MEK inhibitor (MEK-I) caused a significant (70–80%) decrease in the number of both *Nf1*-mutant and wild-type melanocytes present in cultures with MGF (Table 1, lines 3 and 4). These results suggest that MGF acts primarily through the signaling cascade that includes MEK and that Neurofibromin is the predominant GAP functioning within this pathway. Consistent with this conclusion, we observed that in cultures of *Nf1*-mutant cells treated with MEK-I, the number of MPs was also reduced significantly in the *absence* of MGF (>90%) compared to untreated controls (compare lines 1 and 2, Table 1).

Residual MPs, even in the presence of MEK-I, suggest that other survival pathways also operate in this system. To test this idea, we assessed the ability of EDN3, another trophic factor known to promote melanocyte development (Baynash *et al.,* 1994; Hosoda *et al.,* 1994; Reid *et al.,* 1996), to affect the number of MPs present *in vitro.* In the absence of MGF activity, EDN3 significantly increased the number of MPs in cultures of wild-type crest cells (compare lines 1 and 5, Table 1; $P < 0.001$). Moreover, although EDN3 treatment alone resulted in twice the number of melanocytes per culture compared to cultures treated with MGF (compare lines 3 and 5, Table 1; $P < 0.01$), EDN3 treatment of *Nf1*-mutant cultures did not significantly change the number of melanocytes compared to EDN3-treated cultures of wild-type cells (line 5, Table 1). Likewise, in the presence of EDN3, treatment with MEK-I did not significantly change the number of melanocytes produced by either mutant or wild-type cultures (compare lines 5 and 6, Table 1). We suggest, therefore, that other trophic factors, such as EDN3, whose signal is transduced by a G-protein-coupled receptor pathway (Baynash *et al.,* 1994; Imokawa *et al.,* 1996), can account for at least some of the residual survival of melanocytes in cultures of mutant cells and in wild-type cells cultured in the presence of MEK inhibitor.

DISCUSSION

Loss of Neurofibromin Activity Uncouples Melanocyte Survival from Migration

We have now demonstrated that *Nf1*-mutant melanocytes differentiate in culture in the absence of MGF. Likewise, the conclusion that mutant MPs have become independent of MGF signaling for survival *in vivo* is supported (1) by the decrease in the number of cells undergoing cell death in the MSA of *Nf1*-mutant embryos, in which melanocyte precursors are normally found in wild-type embryos at corresponding developmental stages and axial levels, and (2) by the significant increase in the number of MPs, compared to wild-type embryos, in the MSA and on the lateral migration pathway of *Nf1*-mutant embryos. It is also noteworthy that the extent of MP dispersal on the lateral pathway of *Nf1*-mutant embryos is comparable to that in wild-type embryos, suggesting that loss of Neurofibromin function does not impair the ability of mutant MPs to migrate. Thus, survival and migratory behavior of MPs can be uncoupled in *Nf1* mutants, which thereby permits the

consequences of the absence of MGF on the migration of MPs to be assessed *in vivo.*

MGF Promotes Migration of MPs on the Lateral Pathway

MPs disperse extensively on the lateral pathway in $Mgf^{Sl+};Nf1^{-}$ embryos, whereas they remain in the original location of the MSA and apparently do not enter the lateral migration pathway of $Mgf^{Sl-};Nf1^{-}$ double-mutant embryos. Although the double-mutant embryos do not survive beyond e12.5, it is unlikely that MP migration is merely delayed, since some MPs would then be expected to be present on the lateral pathway at developmentally older, rostral axial levels. However, few MPs were observed on the lateral pathway at any axial level. Moreover, based on tail size and limb bud phenotypes, the double-mutant embryos in our experiments appear to be at the same developmental stage as the controls. We conclude, therefore, that soluble MGF does not simply allow MPs to survive on the lateral migration pathway until they reach the remote source of cell-bound MGF in the dermatome. Alternatively, as suggested in the Introduction, diffusible MGF could normally promote dispersal of MPs by acting as a motogenic cytokine ("scatter factor"; Dowrick and Warn, 1991; Gherardi and Coffer, 1991; see also Jordan and Jackson, 2000) through the KIT receptor. If this were so, and if crest-derived cells were not inhibited from entering alternative pathways by other mechanisms (e.g., see Debby-Brafman, *et al.,* 1999; Eickholt *et al.,* 1999; Erickson *et al.,* 1992; Oakley *et al.,* 1994; Perris and Johansson, 1990; Perissinotto *et al.,* 2000; Smith *et al.,* 1997; Wahl *et al.,* 2000; Wehrle-Haller and Chiquet, 1993; Wenk *et al.,* 2000), *Nf1*-mutant crest-derived cells might be expected to migrate promiscuously. In *Nf1*-mutant embryos, such ectopically located MPs would be able to survive and, hence, would be detected in association with crest-derived structures on the medial migration pathway. It is noteworthy, however, that although pre- and paravertebral sympathetic ganglia, but not dorsal root ganglia, are enlarged in older *Nf1*-mutant mice (Brannan *et al.,* 1994), the size of ganglionic structures on the medial pathway is not initially affected (not shown), and MPs were not observed in association with these structures on the medial migration pathway in *Nf1*-mutant embryos. It seems unlikely, therefore, that the *Nf1* mutation, in which RAS-mediated signaling pathways are hyperactive, promotes cell-migratory activity on alternative pathways. Nevertheless, since other mechanisms might prevent entry or subsequent detection of crest-derived cells on particular migration pathways, we cannot eliminate the possibility that MGF signaling through the RAS pathway acts as a motogenic cytokine to promote MP motility, as recently suggested by Jordan and Jackson (2000). It should be emphasized, however, that (1) diffusible MGF is produced at a remote site on the lateral migration pathway relative to the initial location of MPs in the MSA (Wehrle-Haller and Weston, 1995), (2) MPs migrate from the region of the MSA toward the remote source of MGF, and (3) *Nf1*-mutant MPs are not found in ectopic locations (other than the original location of the MSA), in the presence of MGF. Taken together, these facts support the suggestion (see also Kunisada *et al.,* 1998) that MGF provides directional cues for MPs to migrate on the lateral pathway. Direct demonstration that identified MPs migrate up an MGF gradient *in vitro* will be required to confirm this inference, but such experiments are beyond the scope of the present work.

MGF Promotes MP Survival, but Not Migration, through the RAS Signaling Pathway

Both MGF and Neurofibromin function in the RAS signaling pathway in a variety of cell types (Boguski and McCormick, 1993; Lev *et al.,* 1994; McCormick, 1995). Our results are consistent with previous reports that Neurofibromin functions in the RAS pathway (Martin *et al.,* 1990). However, since some cells still survive in the presence of MEK inhibitors (see Table 1), it is important to note that some level of survival can also be mediated through other signaling pathways, as suggested by others (Blume-Jensen *et al.,* 1994, 1998; Serve *et al.,* 1995; Zhang *et al.,* 1998; possible alternative signaling pathways are indicated in Fig. 5). It is noteworthy that MGF activation of *Nf1*-mutant cultures results in a dramatic increase in MP survival that is not efficiently reversed by inhibiting MEK. This suggests that an alternative survival pathway exists. This pathway might also be activated during EDN3-stimulated MP survival (see Shin *et al.,* 1999), which is not affected by loss of Neurofibromin-GAP activity in cultures of *Nf1*-mutant cells (see Table 1). In this regard, it is interesting to note that Akt/protein kinase B, which plays an important role in cell survival, is normally activated by PI3 kinases and by G-protein-coupled receptors such as EndrB (see Fig. 5; Murga *et al.,* 1998; Blume-Jensen *et al.,* 1998). PI3 kinases, in turn, are known to be activated by oncogenic forms of RAS (Rodriguez-Viciana *et al.,* 1997). Accordingly, we suggest that hyperactivated RAS in *Nf1*-mutant cells might also result in "signal crosstalk" with other cellular signaling pathways that affect survival and proliferation, whereas rapid down-regulation of activated RAS by wild-type Neurofibromin-GAP might prevent such crosstalk.

Since *Nf1*-mutant melanocyte precursors are not found in ectopic areas in the embryo, such as in crest-derived structures on the medial pathway, our data do not support the idea that Neurofibromin-GAP, and hence the signaling pathway involving RAS, regulates the initial cell locomotory activity of crest-derived MPs (Dowrick and Warn, 1991; Gherardi and Coffer, 1991; Jordan and Jackson, 2000). In addition, several other developmental models for cell migration demonstrate that altering RAS activity (e.g., expressing oncogenic forms of RAS) either does not rescue or only partially rescues cell migration that otherwise depends on RTK signaling. This is the case for the sex myoblast migration in *C. elegans* and tracheal cell migration in *Drosophila* (Sundaram *et al.,* 1996; deVore *et al.,*

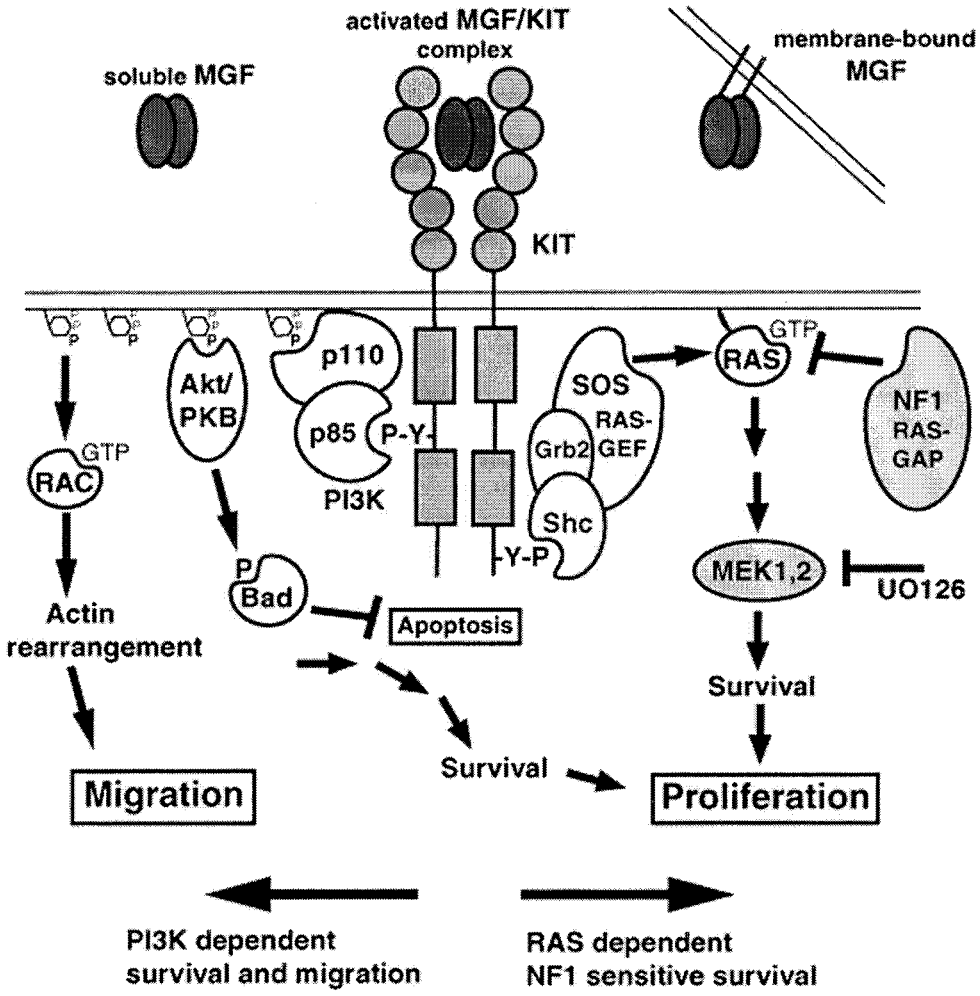

FIG. 5. Scheme of possible downstream signaling events induced by MGF/KIT interaction. The right side of the diagram shows that recruitment of Shc, Grb-2, and SOS by activated receptor results in activation of RAS and subsequent activation of the MAP kinase pathway involving MEK 1 and MEK 2. This pathway is required for survival, MITF activation (Hemesath *et al.,* 1998), and proliferation (Lennartsson *et al.,* 1999). In wild-type MPs, GAP activity of Neurofibromin (NF1) requires persistent MGF signaling to maintain survival mediated through this pathway. In contrast, inactivation of NF1 permits RAS signaling to persist after an initial RAS-GEF-mediated stimulation. Specific inhibition of MEK 1 and MEK 2 activity by U0126 selectively down-regulates the MAP kinase pathway even in the absence of NF1 function, consequently reducing survival-promoting activity of the RAS pathway. The left side of the diagram indicates binding of the regulatory subunit of PI3 kinase to KIT, which results in the production of PI3,4,5P, which serves to recruit and activate Akt/PKB serine–threonine kinase. Subsequent phosphorylation of Bad, a proapoptotic Bcl-2 family member, results in inactivation of apoptotic mechanisms and leads to survival of MGF-stimulated cells. Both PI3,4,5P by KIT-associated PI3 kinase and activated RAS (Denhardt, 1996) lead to the recruitment of RAC-GEFs and subsequent stimulation of RAC at the cell periphery. RAC activation results in rearrangements of the actin cytoskeleton required for cell migration. In melanoblasts from $Nf1^{-/-};MGF^{-/-}$ embryos, possible RAS activation of RAC appears to be insufficient to stimulate migration. In Mast cells and c-kit-transfected porcine aortic endothelial cells, efficient remodeling of the actin cytoskeleton induced by MGF also depends on protein kinase C activation (Blume-Jensen *et al.,* 1993; Vosseller *et al.,* 1997). This pathway is omitted for clarity, but might be essential for MP migration in homozygous mice expressing a mutant form of KIT deficient in PI3K recruitment (Blume-Jensen *et al.,* 2000). Furthermore, binding of Src to membrane-proximal phosphotyrosine residues is involved in the activation of the Shc/Grb-2/SOS complex and is required for RAS activation (pathway omitted for clarity; see Lennartsson *et al.,* 1999).

1995; Reichmann-Fried *et al.,* 1994). In contrast to these studies, in which oncogenic or dominant activated RAS proteins have been expressed, tissue-specific spatial and temporal signaling through RAS in *Nf1*-mutant MPs is not altered by misexpression of oncogenic forms of RAS. Instead, we describe a system in which RAS is activated by normal cellular signaling pathways, and its activity remains high due to the loss of Neurofibromin-GAP function. We

propose, therefore, that RAS signaling is normally required to maintain cell survival and regulate gene expression through the activation of the MEK pathway *in vivo*, but that MGF does not stimulate cell motility by signaling through the RAS pathway.

Since MGF is clearly required for MP dispersal on the lateral pathway, however, its ability to mediate cellular migration must be effected through other signaling pathways. In this regard, it is interesting that PI3K as well as protein kinase C have been shown to be required for KIT-dependent actin polymerization and membrane ruffling in Mast cells (Vosseller *et al.*, 1997) and for MGF-dependent migration of KIT-transfected porcine aortic endothelial cells (Blume-Jensen *et al.*, 1993). Downstream effectors of PI3K include the small GTPase RAC1 (see Fig. 5), which is crucial in inducing actin assembly and lamellipodia formation required for cell locomotion in general (for review see Lauffenburger and Horwitz, 1996; Hall, 1998) and melanogenic cells in particular (Ballestrem *et al.*, 2000). In *Drosophila*, RAC1 signaling is indispensable for border cell migration, while expression of a dominant-negative form of RHO-A does not affect this migration (Murphy and Montell, 1996). Similarly, although the signal required for RHO-A/B activation is not known, their activity is required for neural crest cell segregation from the neural tube, but does not appear to be needed for neural crest cell dispersal from the MSA (Liu and Jessell, 1998).

In summary, our results indicate that both MGF and EDN3 signals are required for MP survival, proliferation, and differentiation (see also Shin *et al.*, 1999). MGF-dependent MP survival is mediated through a pathway that includes both RAS and MEK. However, the facts (1) that some MPs remain when MEK is inhibited and (2) that EDN3 seems to promote MP survival independent of the ERK pathway suggest that other signaling pathways may be activated by MGF and EDN3 to promote survival. In any case, we suggest that MGF, possibly acting through a signal transduction pathway involving RAC GTPase (Fig. 5; Lauffenburger and Horwitz, 1996; Hall, 1998) and independent of RAS signaling, is uniquely required to provide cues for directed migration on the lateral pathway by MPs residing in the MSA.

ACKNOWLEDGMENTS

We thank Drs. Neal Copeland and Kristine Vogel for providing Nf1 mice and Dr. Ian Jackson for providing the TRP2 probe. We also thank Emma Kaichen for her histological expertise and Aaron Sundholm for his help with histological analysis. We are especially grateful to Rick Gosswiller for his devoted mouse husbandry, to Tom Maynard for advice and assistance with whole-mount preparations and graphics, and to Victoria Robinson for expert technical assistance. This work was supported in part by Grant DE04316 from the NIH, a grant from the National Neurofibromatosis Foundation, Inc., and a grant from the Swiss National Science Foundation (31-52727.97) to B.W.-H.

REFERENCES

Ballestrem, C., Wehrle-Haller, B., Hinz, B., and Imhof, B. A. (2000). Actin-dependent lamellipodia formation and microtubule-dependent tail retraction control directed cell migration. *Mol. Biol. Cell* **11,** 2999–3012.

Baynash, A. G., Hosoda, K., Giaid, A., Richardson, J. A., Emoto, N., Hammer, R. E., and Yanagisawa, M. (1994). Interaction of endothelin-3 with endothelin-B receptor is essential for development of epidermal melanocytes and enteric neurons. *Cell* **79,** 1277–1285.

Besmer, P. (1991). The kit ligand encoded at the murine Steel locus: A pleiotropic growth and differentiation factor. *Curr. Opin. Cell. Biol.* **3,** 939–946.

Besmer, P., Manova, K., Duttlinger, R., Huang, E. J., Packer, A., Gyssler, C., and Bachvarova, R. F. (1993). The kit-ligand (steel factor) and its receptor c-kit/W: Pleiotropic roles in gametogenesis and melanogenesis. *Development* **Suppl.,** 125–137.

Blume-Jensen, P., Siegbahn, A., Stabel, S., Heldin, C. H., and Ronnstrand, L. (1993). Increased Kit/SCF receptor induced mitogenicity but abolished cell motility after inhibition of protein kinase C. *EMBO J.* **12,** 4199–4209.

Blume-Jensen, P., Ronnstrand, L., Gout, I., Waterfield, M. D., and Heldin, C. H. (1994). Modulation of Kit/stem cell factor receptor-induced signaling by protein kinase C. *J. Biol. Chem.* **269,** 21793–21802.

Blume-Jensen, P., Janknecht, R., and Hunter, T. (1998). The c-kit receptor promotes cell survival via activation of PI3-kinase and subsequent akt-mediated phosphorylation of Bad on Ser136. *Curr. Biol.* **18,** 779–782.

Blume-Jensen, P., Jiang, G., Hyman, R., Lee, K. F., O'Gorman, S., and Hunter, T. (2000). Kit/stem cell factor receptor-induced activation of phosphatidylinositol 3′-kinase is essential for male fertility. *Nat. Genet.* **24,** 157–162.

Boguski, M. S., and McCormick, F. (1993). Proteins regulating Ras and its relatives. *Nature* **366,** 643–654.

Bollag, G., Clapp, D. W., Shih, S., Adler, F., Zhang, Y. Y., Thompson, P., Lange, B. J., Freedman, M. H., McCormick, F., Jacks, T., and Shannon, K. (1996). Loss of NF1 results in activation of the Ras signaling pathway and leads to aberrant growth in haematopoietic cells. *Nat. Genet.* **12,** 144–148.

Brannan, C. I., Perkins, A. S., Vogel, K. S., Ratner, N., Nordlund, M. L., Reid, S. W., Buchberg, A. M., Jenkins, N. A., Parada, L. F., and Copeland, N. G. (1994). Targeted disruption of the neurofibromatosis type-1 gene leads to developmental abnormalities in heart and various neural crest-derived tissues. *Genes Dev.* **8,** 1019–1029.

Debby-Brafman, A., Burstyn-Cohen, T., Klar, A., and Kalcheim, C. (1999). F-Spondin, expressed in somite regions avoided by neural crest cells, mediates inhibition of distinct somite domains to neural crest migration. *Neuron* **22,** 475–488.

Dekker, L. V., and Segal, A. W. (2000). Signals to move cells. *Science* **287,** 982–985.

Denhardt, D. T. (1996). Signal-transducing protein phosphorylation cascades mediated by Ras/Rho proteins in the mammalian cell: The potential for multiplex signaling. *Biochem. J.* **318,** 729–747.

DeVore, D. L., Horvitz, H. R., and Stern, M. J. (1995). An FGF receptor signaling pathway is required for the normal cell migrations of the sex myoblasts in C. elegans hermaphrodites. *Cell* **83,** 611–620.

Dowrick, P. G., and Warn, R. M. (1991). The cellular response to factors which induce motility in mammalian cells. *Exs* **59,** 89–108.

Duronio, V., Welham, M. J., Abraham, S., Dryden, P., and Schrader, J. W. (1992). p21ras activation via hemopoietin receptors and c-kit requires tyrosine kinase activity but not tyrosine phosphorylation of p21ras GTPase-activating protein. *Proc. Natl. Acad. Sci. USA* **89,** 1587–1591.

Eickholt, B. J., Mackenzie, S. L., Graham, A., Walsh, F. S., and Doherty, P. (1999). Evidence for collapsin-1 functioning in the control of neural crest migration in both trunk and hindbrain regions. *Development* **126,** 2181–2189.

Erickson, C. A., Duong, T. D., and Tosney, K. W. (1992). Descriptive and experimental analysis of the dispersion of neural crest cells. *Dev. Biol.* **151,** 251–272.

Favata, M. F., Horiuchi, K. Y., Manos, E. J., Daulerio, A. J., Stradley, D. A., Feeser, W. S., Van Dyk, D. E., Pitts, W. J., Earl, R. A., Hobbs, F., Copeland, R. A., Magolda, R. L., Scherle, P. A., and Trzaskos, J. M. (1998). Identification of a novel inhibitor of mitogen-activated protein kinase kinase. *J. Biol. Chem.* **273,** 18623–18632.

Flanagan, J. G., Chan, D. C., and Leder, P. (1991). Transmembrane form of the kit ligand growth factor is determined by alternative splicing and is missing in the Sld mutant. *Cell* **64,** 1025–1035.

Gavrieli, Y., Sherman, Y., and Ben-Sasson, S. A. (1992). Identification of programmed cell death in situ via specific labeling of nuclear DNA fragmentation. *J. Cell Biol.* **119,** 493–501.

Gherardi, E., and Coffer, A. (1991). Purification and characterization of scatter factor. *Exs* **59,** 53–62.

Gold, R., Schmied, M., Rothe, G., Zischler, H., Breitschopf, H., Wekerle, H., and Lassmann, H. (1993). Detection of DNA fragmentation in apoptosis: Application of in situ nick translation to cell culture systems and tissue sections. *J. Histochem. Cytochem.* **41,** 1023–1030.

Guha, A., Lau, N., Huvar, I., Gutmann, D., Provias, J., Pawson, T., and Boss, G. (1996). Ras-GTP levels are elevated in human NF1 peripheral nerve tumors. *Oncogene* **12,** 507–13.

Hall, A. (1998). Rho GTPases and the actin cytoskeleton. *Science* **279,** 509–514.

Hemesath, T. J., Price, E. R., Takemoto, C., Badalian, T., and Fisher, D. E. (1998). Map kinase links the transcription factor microphthalmia to c-kit signaling in melanocytes. *Nature* **391,** 298–301.

Henkemeyer, M., Rossi, D. J., Holmyard, D. P., Puri, M. C., Mbamalu, G., Harpal, K., Shih, T. S., Jacks, T., and Pawson, T. (1995). Vascular system defects and neuronal apoptosis in mice lacking ras GTPase-activating protein. *Nature* **377,** 695–701.

Hosoda, K., Hammer, R. E., Richardson, J. A., Baynash, A. G., Cheung, J. C., Giaid, A., and Yanagisawa, M. (1994). Targeted and natural (piebald-lethal) mutations of endothelin-B receptor gene produce megacolon associated with spotted coat color in mice. *Cell* **79,** 1267–1276.

Imokawa, G., Yada, Y., and Kimura, M. (1996). Signalling mechanisms of endothelin-induced mitogenesis and melanogenesis in human melanocytes. *Biochem. J.* **314,** 305–312.

Ingram, D. A., Yang, F.-C., Travers, J. B., Wenning, M. J., Hiatt, K., New, S., Hood, A., Shannon, K., Williams, D. A., and Clapp, D. W. (2000). Genetic and biochemical evidence that haploinsufficiency of the *Nf1* tumor suppressor gene modulates melanocyte and mast cell fates in vivo. *J. Exp. Med.* **191,** 181–187.

Jordan, S. A., and Jackson, I. J. (2000). MGF (KIT ligand) is a chemokinetic factor for melanoblast migration into hair follicles. *Dev. Biol.* **225,** 424–436.

Kunisada, T., Yoshida, H., Yamazaki, H., Miyamoto, A., Hemmi, H., Nishimura, E., Schultz, L., Nishikawa, S., and Hayashi, S. (1998). Transgene expression of steel factor in the basal layer of epidermis promotes survival, proliferation, differentiation and migration of melanocyte precursors. *Development* **125,** 2915–2923.

Lauffenburger, D. A., and Horwitz, A. F. (1996). Cell migration: A physically integrated molecular process. *Cell* **84,** 359–369.

Le Douarin, N., and Kalcheim, C. (1999). "The Neural Crest," 2nd ed. Cambridge Univ. Press, Cambridge, UK.

Lee, T., and Montell, D. J. (1997). Multiple ras signals pattern the *Drosophila* ovarian follicle cells. *Dev. Biol.* **185,** 25–33.

Lee, T., Feig, L., and Montell, D. J. (1996). Two distinct roles for ras in a developmentally regulated cell migration. *Development* **122,** 409–418.

Lennartsson, J., Blume-Jensen, P., Hermanson, M., Ponten, E., Carlberg, M., and Ronnstrand, L. (1999). Phosphorylation of Shc by Src family kinases is necessary for stem cell factor receptor/c-kit mediated activation of the Ras/MAP kinase pathway and c-fos induction. *Oncogene* **18,** 5546–5553.

Lev, S., Blechman, J. M., Givol, D., and Yarden, Y. (1994). Steel factor and c-kit protooncogene: Genetic lessons in signal transduction. *Crit. Rev. Oncog.* **5,** 141–168.

Liu, J. P., and Jessell, T. M. (1998). A role for rhoB in the delamination of neural crest cells from the dorsal neural tube. *Development* **125,** 5055–5067.

Mackenzie, M. A., Jordan, S. A., Budd, P. S., and Jackson, I. J. (1997). Activation of the receptor tyrosine kinase Kit is required for the proliferation of melanoblasts in the mouse embryo. *Dev. Biol.* **192,** 99–107.

Martin, G. A., Viskochil, D., Bollag, G., McCabe, P. C., Crosier, W. J., Haubruck, H., Conroy, L., Clark, R., O'Connell, P., Cawthon, R. M., Innis, M. A., and McCormick, F. (1990). The GAP-related domain of the neurofibromatosis type 1 gene product interacts with *ras* p21. *Cell* **63,** 843–849.

Marusich, M. F., Furneaux, H. M., Henion, P. D., and Weston, J. A. (1994). Hu neuronal proteins are expressed in proliferating neurogenic cells. *J. Neurobiol.* **25,** 143–155.

Maynard, T. M., Wakamatsu, Y., and Weston, J. A. (2000). Cell interactions within nascent neural crest cell populations transiently promote death of neurogenic precursors. *Development* **127,** 4461–4572.

McCormick, F. (1995). Ras signaling and NF1. *Curr. Opin. Genet. Dev.* **5,** 51–55.

Montell, D. J. (1999). The genetics of cell migration in Drosophila melanogaster and Caenorhabditis elegans development. *Development* **126,** 3035–3046.

Morrison-Graham, K., and Weston, J. A. (1993). Transient steel factor dependence by neural crest-derived melanocyte precursors. *Dev. Biol.* **159,** 346–352.

Murga, C., Laguinge, L., Wetzker, R., Cuadrado, A., and Gutkind, J. S. (1998). Activation of Akt/protein kinase B by G protein-coupled receptors. A role for the alpha and beta gamma subunits of heterotrimeric G proteins acting through phosphatidylinositol-OH kinasegamma. *J. Biol. Chem.* **273,** 19080–19085.

Murphy, A. M., and Montell, D. J. (1996). Cell-type specific roles for cdc42, rac and rhoL in Drosophila oogenesis. *J. Cell Biol.* **133,** 617–630.

Nishikawa, S., Kusakabe, M., Yoshinaga, K., Ogawa, M., Hayashi, S., Kunisada, T., Era, T., Sakakura, T., and Nishikawa, S. (1991). In utero manipulation of coat color formation by a monoclonal

anti-c-kit antibody: Two distinct waves of c-kit-dependency during melanocyte development. *EMBO J.* **10,** 2111–2118.

Oakley, R. A., Lasky, C. J., Erickson, C. A., and Tosney, K. W. (1994). Glycoconjugates mark a transient barrier to neural crest migration in the chick. *Development* **120,** 103–114.

Perissinotto, D., Iacopetti, P., Bellina, I., Doliana, R., Colombatti, A., Pettway, Z., Bronner-Fraser, M., Shinomura, T., Kimata, K., Morgelin, M., Lofberg, J., and Perris, R. (2000). Avian neural crest cell migration is diversely regulated by the two major hyaluronan-binding proteoglycans PG-M/versican and aggrecan. *Development* **127,** 2823–2842.

Perris, R., and Johansson, S. (1990). Inhibition of neural crest cell migration by aggregating chondroitin sulfate proteoglycan by their hyaluronan-binding region. *Dev. Biol.* **137,** 1–12.

Ramesh, N., Anton, I. M., Martinez-Quiles, N., and Geha, R. S. (1999). Waltzing with WASP. *Trends Cell Biol.* **9,** 15–19.

Reichman-Fried, M., Dickson, B., Hafen, E., and Shilo, B. Z. (1994). Elucidation of the role of breathless, Drosophila FGF receptor homolog, in tracheal cell migration. *Genes Dev.* **8,** 428–439.

Reid, K., Turnley, A. M., Maxwell, G. D., Kurihara, Y., Kurihara, H., Bartlett, P. F., and Murphy, M. (1996). Multiple roles for endothelin in melanocyte development: Regulation of progenitor number and stimulation of differentiation. *Development* **122,** 3911.

Rey, I., Taylor-Harris, P., van Erp, H., and Hall, A. (1994). R-ras interacts with rasGAP, Neurofibromin and c-raf but does not regulate cell growth or differentiation. *Oncogene* **9,** 685–692.

Roberts, A. W., Kim, C., Zhen, L., Lowe, J. B., Kapur, R., Petryniak, B., Spaetti, A., Pollock, J. D., Borneo, J. B., Bradford, G. B., Atkinson, S. J., Dinauer, M. C., and Williams, D. A. (1999). Deficiency of the hematopoietic cell-specific rho family GTPase rac2 is characterized by abnormalities in neutrophil function and host defense. *Immunity* **10,** 183–196.

Rodriguez-Viciana, P., Warne, P. H., Khwaja, A., Marte, B. M., Pappin, D., Das, P., Waterfield, M. D., Ridley, A., and Downward, J. (1997). Role of phosphoinositide 3-OH kinase in cell transformation and control of the actin cytoskeleton by Ras. *Cell* **89,** 457–467.

Rubenstein, A. E. (1986). Neurofibromatosis. A review of the clinical problem. *Ann. N.Y. Acad. Sci.* **486,** 1–13.

Scott, G., Ewing, J., Ryan, D., and Abboud, C. (1994). Stem cell factor regulates human melanocyte-matrix interactions. *Pigment Cell Res.* **7,** 44–51.

Scott, G., Liang, H., and Luthra, D. (1996). Stem cell factor regulates the melanocyte cytoskeleton. *Pigment Cell Res.* **9,** 134–141.

Serve, H., Yee, N. S., Stella, G., Sepp-Lorenzino, L., Tan, J. C., and Besmer, P. (1995). Differential roles of PI3-kinase and Kit tyrosine 821 in Kit receptor-mediated proliferation, survival and cell adhesion in mast cells. *EMBO J.* **14,** 473–483.

Shin, M. K., Levorse, J. M., Ingram, R. S., and Tilghman, S. M. (1999). The temporal requirement for endothelin receptor-B signaling during neural crest development. *Nature* **402,** 496–501.

Smith, A., Robinson, V., Patel, K., and Wilkinson, D. G. (1997). The EphA4 and EphB1 receptor tyrosine kinases and ephrin-B2 ligand regulate branchial neural crest cells. *Curr. Biol.* **7,** 651–570.

Strahle, U., Blader, P., Adam, J., and Ingham, P. W. (1994). A simple and efficient procedure for non-isotopic in situ hybridization to sectioned material. *Trends Genet.* **10,** 75–76.

Sundaram, M., Yochem, J., and Han, M. (1996). A ras-mediated signal transduction pathway is involved in the control of sex myoblast migration in Caenorhabditis elegans. *Development* **122,** 2823–2833.

Takahira, H., Gotoh, A., Ritchie, A., and Broxmeyer, H. E. (1997). Steel factor enhances integrin-mediated tyrosine phosphorylation of focal adhesion kinase (pp125FAK) and paxillin. *Blood* **89,** 1574–1584.

Tauchi, T., Feng, G. S., Marshall, M. S., Shen, R., Mantel, C., Pawson, T., and Broxmeyer, H. E. (1994). The ubiquitously expressed Syp phosphatase interacts with c-kit and Grb2 in hematopoietic cells. *J. Biol. Chem.* **269,** 25206–25211.

Vogel, K. S., Brannan, C. I., Jenkins, N. A., Copeland, N. G., and Parada, L. F. (1995). Loss of Neurofibromin results in neurotrophin-independent survival of embryonic sensory and sympathetic neurons. *Cell* **82,** 733–742.

Vosseller, K., Stella, G., Yee, N. S., and Besmer, P. (1997). C-kit receptor signaling through its phosphatidylinositide-3′-kinase-binding site and protein kinase C: Role in Mast cell enhancement of degranulation, adhesion and membrane ruffling. *Mol. Biol. Cell* **8,** 909–922.

Wahl, S., Barth, H., Ciossek, T., Aktories, K., and Mueller, B. K. (2000). Ephrin-A5 induces collapse of growth cones by activating Rho and Rho kinase. *J. Cell Biol.* **149,** 263–270.

Wakamatsu, Y., Mochii, M., Vogel, K. S., and Weston, J. A. (1998). Avian neural crest-derived neurogenic precursors undergo apoptosis on the lateral migration pathway. *Development* **125,** 4205–4213.

Wehrle-Haller, B., and Chiquet, M. (1993). Dual function of tenascin: Simultaneous promotion of neurite growth and inhibition of migration. *J. Cell Sci.* **106,** 597–610.

Wehrle-Haller, B., and Weston, J. A. (1995). Soluble and cell-bound forms of steel factor activity play distinct roles in melanocyte precursor dispersal and survival on the lateral neural crest migration pathway. *Development* **121,** 731–742.

Wehrle-Haller, B., and Weston, J. A. (1997). Receptor tyrosine kinase-dependent neural crest migration in response to differentially localized growth factors. *BioEssays* **19,** 337–345.

Wehrle-Haller, B., and Weston, J. A. (1999). Altered cell-surface targeting of stem cell factor causes loss of melanocyte precursors in *Steel*^{17H} mutant mice. *Dev. Biol.* **210,** 71–86.

Wenk, M. B., Midwood, K. S., and Schwarzbaurer, J. E. (2000). Tenascin-C suppresses Rho activation. *J. Cell Biol.* **150,** 913–920.

Weston, J. A. (1991). Sequential segregation and fate of developmentally restricted intermediate cell populations in the neural crest lineage. *Curr. Top. Dev. Biol.* **25,** 133–153.

Widmann, C., Gibson, S., Jarpe, M. B., and Johnson, G. L. (1999). Mitogen-activated protein kinase: Conservation of a three-kinase module from yeast to human. *Physiol. Rev.* **79,** 143–180.

Zhang, Y. Y., Vik, T. A., Ryder, J. W., Srour, E. F., Jacks, T., Shannon, K., and Clapp, D. W. (1998). Nf1 regulates hematopoietic progenitor cell growth and ras signaling in response to multiple cytokines. *J. Exp. Med.* **187,** 1893–1902.

Received for publication November 16, 2000
Revised December 18, 2000
Accepted December 18, 2000
Published online March 16, 2001

2.6. Intracellular targeting of Stem Cell factor: essential roles of the cytoplasmic tail

Developmental Biology **210,** 71–86 (1999)
Article ID dbio.1999.9260, available online at http://www.idealibrary.com on

Altered Cell-Surface Targeting of Stem Cell Factor Causes Loss of Melanocyte Precursors in *Steel*^{17H} Mutant Mice

Bernhard Wehrle-Haller*,[1] and James A. Weston†

**Department of Pathology, Centre Medical Universitaire, 1, Rue Michel-Servet, 1211 Geneva 4, Switzerland; and †Institute of Neuroscience, University of Oregon, Eugene, Oregon 97403*

The normal products of the murine *Steel (Sl)* and *Dominant white spotting (W)* genes are essential for the development of melanocyte precursors, germ cells, and hematopoietic cells. The *Sl* locus encodes stem cell factor (SCF), which is the ligand of c-kit, a receptor tyrosine kinase encoded by the *W* locus. One allele of the *Sl* mutation, *Sl*^{17H}, exhibits minor hematopoietic defects, sterility only in males, and a complete absence of coat pigmentation. The *Sl*^{17H} gene encodes SCF protein which exhibits an altered cytoplasmic domain due to a splicing defect. In this paper we analyzed the mechanism by which the pigmentation phenotype in *Sl*^{17H} mutant mice occurs. We show that in embryos homozygous for *Sl*^{17H} the number of melanocyte precursors is severely reduced on the lateral neural crest migration pathway by e11.5 and can no longer be detected by e13.5 when they would enter the epidermis in wildtype embryos. The reduced number of dispersing melanocyte precursors correlates with a reduction of SCF immunoreactivity in mutant embryos in all tissues examined. Regardless of the reduced amount, functional SCF is present at the cell surface of fibroblasts transfected with *Sl*^{17H} mutant SCF cDNA. Since SCF immunoreactivity normally accumulates in basolateral compartments of SCF-expressing embryonic epithelial tissues, we analyzed the localization of wildtype and *Sl*^{17H} mutant SCF protein in transfected epithelial (MDCK) cells *in vitro*. As expected, wildtype forms of SCF localize to and are secreted from the basolateral compartment. In contrast, mutant forms of SCF, which either lack a membrane anchor or exhibit the *Sl*^{17H} altered cytoplasmic tail, localize to and are secreted from the apical compartment of the cultured epithelium. We suggest, therefore, that the loss of melanocyte precursors prior to epidermal invasion, and the loss of germ cells from mature testis, can be explained by the inability of *Sl*^{17H} mutant SCF to be targeted to the basolateral compartment of polarized epithelial keratinocytes and Sertoli cells, respectively.

***Key Words: Sl*^{17H}*;* melanocyte precursors; stem cell factor; epithelia; MDCK cells.**

INTRODUCTION

Mutations at the *Steel (Sl)* and *Dominant white spotting (W)* loci in mice lead to absence of melanocyte populations in the skin and inner ear, sterility in both males and females, anemia, mast cell deficiencies, and other developmental defects (Williams *et al.*, 1992; Maeda *et al.*, 1992; Morrison-Graham and Takahashi, 1993; Galli *et al.*, 1994; Motro *et al.*, 1996). Mutations at the *W* and *Sl* loci affect the structure and function of the receptor tyrosine kinase, c-kit, and its ligand, Steel factor (a.k.a. stem cell factor (SCF), mast cell growth factor, and kit-ligand (KL)), respectively. As a receptor–ligand pair, phenotypic effects of the respective mutated genes are almost identical, except, of course, that *W* mutations are cell autonomous, whereas *Sl* mutations are not. A large number of alleles for both the *W* and the *Sl* loci have been identified and molecularly analyzed (Morrison-Graham and Takahashi, 1993; Bedell *et al.*, 1996). At the *Sl* locus, several alleles exhibit complete deletions of the *Sl* gene (Bedell *et al.*, 1996) or alterations in the enhancer regions of the *Sl* gene (*Steel-panda*, *Sl*^{pan}; *Steel-contrasted*, *Sl*^{con}), which affect mRNA levels of SCF in various tissues (Huang *et al.*, 1993; Bedell *et al.*, 1995). There is, however, a small class of *Sl* mutations affecting the coding sequence of SCF and therefore changing the structure of the expressed SCF protein. In these two mutations, *Steel-dickie (Sl*^{d}*)* and *Steel-17H (Sl*^{17H}*)*, the c-kit

[1] To whom correspondence should be addressed. Fax: (41 22) 702 57 46. E-mail: Bernhard.Wehrle-Haller@medecine.unige.ch.

0012-1606/99 $30.00

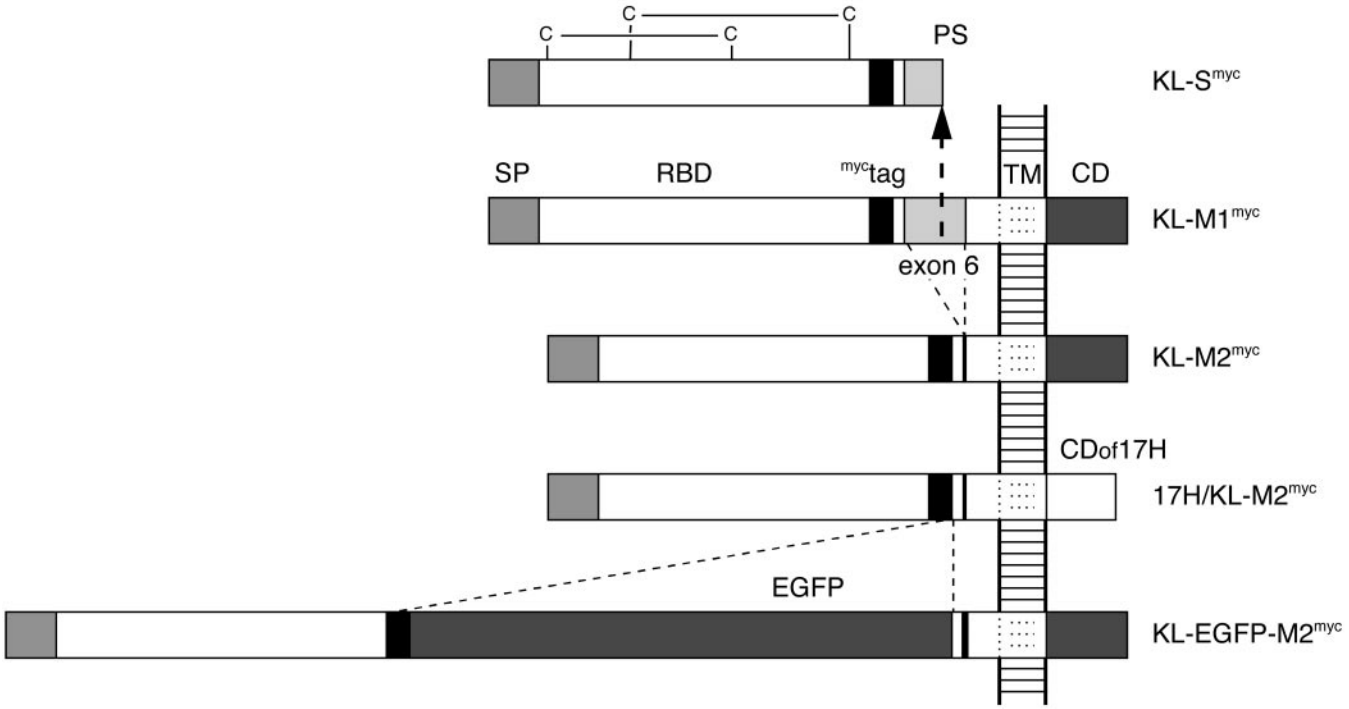

FIG. 1. Graphic representation of different wildtype and mutant forms of SCF used in the current study. Graphic representation of SCF cDNA constructs which produce wildtype, Sl^{17H} mutant, and EGFP-tagged SCF. Wildtype SCF exists in two alternative splice variants, which are both expressed as membrane-bound molecules. The small variant (KL-M2) remains membrane bound, while the larger variant (KL-M1) expresses exon 6 which exhibits a proteolytic site which leads to secreted SCF (KL-S). Sl^{17H} mutant forms of SCF (only the M2 variant is shown) display an altered cytoplasmic domain (17H/KL-M2). In order to visualize and trace various wildtype and mutant forms of SCF, we introduced a myc tag and the coding sequence for EGFP (enhanced green fluorescent protein) into the spacer region, which separates the receptor binding domain from the transmembrane domain (KL-EGFP-M2^{myc}). C–C, disulfide-linked extracellular cysteines; CD, cytoplasmic domain; ^{myc}tag, 9E-10 anti-human myc epitope; PS, proteolytic site; RBD; receptor binding domain; SP, signal peptide; TM, transmembrane domain.

binding domain of SCF remains functional (Brannan *et al.*, 1991, 1992; Flanagan *et al.*, 1991). Nevertheless, the phenotype of Sl^{d} is almost as severe as a *Sl* deletion, and Sl^{17H} exhibits complete absence of coat pigmentation. Interestingly, Sl^{17H} males are sterile, whereas females are fertile (Brannan *et al.*, 1992). Furthermore, although the Sl^{17H} mutation leads to altered homing behavior of hematopoietic precursors (Tajima *et al.*, 1998), it causes only minor effects in hemopoiesis.

Wildtype SCF is expressed in two alternatively spliced, initially membrane-bound forms. The alternatively spliced exon 6, which is present in the larger splice form of SCF (KL-M1; Fig. 1), codes for an extracellular site of proteolytic processing, so that an active form of SCF is released after a half-life of 15 to 30 min at the cell surface (Flanagan *et al.*, 1991; Huang *et al.*, 1992). The smaller splice form (KL-M2; Fig. 1) remains membrane bound, but can also be cleaved at alternative proteolytic sites, with a half-life of 3 to 5 h (Huang *et al.*, 1992). The Sl^{d} allele exhibits a deletion of the transmembrane and cytoplasmic domain of SCF yielding constitutively secreted SCF (Brannan *et al.*, 1991; Flanagan *et al.*, 1991). The strong phenotypes associated with this mutation show clearly that membrane-bound SCF is essential for the survival of SCF-dependent cell populations. Although secreted SCF is not sufficient to promote survival of c-kit-expressing melanocyte precursors it can transiently support their migration from the neural tube onto the lateral neural crest migration pathway (Wehrle-Haller and Weston, 1995). Therefore, secreted SCF either exerts a chemotactic response toward c-kit-expressing melanocyte precursors or provides long-range survival cues before melanocyte precursors reach the dermatome and remain associated with the dermatome-derived dermal fibroblasts expressing membrane-bound SCF (Wehrle-Haller and Weston, 1997).

Another mutant allele at the *Sl* locus, Sl^{17H}, exhibits a pronounced coat color phenotype similar to Sl^{d}. In contrast to Sl^{d}, however, Sl^{17H} is a point mutation that affects the splice acceptor for the exon encoding the cytoplasmic tail of SCF. Sl^{17H} mutant SCF exhibits a normal extracellular and transmembrane domain followed by a cytoplasmic tail, the deduced sequence of which is similar in length but com-

pletely changed in its amino acid composition (Fig. 1) (Brannan *et al.*, 1992). Functionally active SCF can be found in the supernatant of cultured fibroblasts transiently transfected with Sl^{17H} cDNA (Brannan *et al.*, 1992; Cheng and Flanagan, 1994). Because functional SCF appears to be secreted, and a membrane-bound form is made by mutants, the cause of the pigmentation defect in Sl^{17H} mutant animals is puzzling. It is possible, however, that Sl^{17H} mutant SCF exhibits a misfolded cytoplasmic tail that negatively affects the membrane insertion or protein stability of SCF and thereby reduces the amount of surface-expressed mutant protein. This hypothesis is consistent with the report (Cheng and Flanagan, 1994) that less Sl^{17H} mutant SCF can be detected by a c-kit alkaline phosphatase fusion protein on the surface of transiently transfected COS cells *in vitro*. The fact that only 10% of the total number of germ cells can be found in the genital ridges in Sl^{17H} homozygous embryos (Brannan *et al.*, 1992) would also be consistent with a reduced expression of SCF protein.

In order to gain further insight into the nature of the pigmentation defect in the Sl^{17H} mutation, we analyzed the melanocyte precursor migration pattern in homozygous Sl^{17H} mice using c-kit and tyrosinase-related protein-2 (TRP-2) mRNA as specific markers for premigratory and migratory melanocyte precursors in whole-mount *in situs* of mouse embryos (Steel *et al.*, 1992; Wehrle-Haller and Weston, 1995). In addition, we analyzed the SCF protein expression in wildtype embryos and compared it with the SCF protein distribution in Sl^{17H} mutant tissue. *In vitro*, we expressed wildtype and mutant forms of SCF in fibroblasts and analyzed cell surface expression and binding capabilities to c-kit-expressing melanocyte precursors. Furthermore, we analyzed the localization and secretion of wildtype and mutant SCF in polarized epithelial (MDCK) cells. We observed a severely reduced but persistent number of melanocyte precursors on the lateral neural crest migration pathway at e11.5 and e12.5. This correlates with reduced SCF immunoreactivity in the dermatome of Sl^{17H} mutant embryos at e10.5. We suggest that the reduction of functionally active Sl^{17H} mutant SCF protein on the surface of COS-7 cells reflects this finding. Subsequently, melanocyte precursors completely disappear prior to their epidermal invasion. We postulate, based on wildtype and Sl^{17H} mutant SCF immunoreactivity and evidence of localization and secretion of SCF in epithelial tissues, that both the complete loss of germ cells after sexual maturation in males and the disappearance of melanocyte precursors prior to invasion into the epidermis are caused by the failure to target Sl^{17H} mutant SCF to the basolateral compartment in polarized SCF-expressing epithelial Sertoli cells and keratinocytes.

MATERIAL AND METHODS

Mice and Embryonic Genotyping

Sl^{17H} mutant mice were obtained from Neal Copeland and were bred in a C3H background. Within the C3H background, homozygote Sl^{17H} mutant animals are white with black eyes; heterozygote animals exhibit white hairs on the forehead with otherwise normal pigmentation. Previous studies on the Sl^{17H} germ-cell phenotype by Brannan *et al.* (1992) were performed within a mixed C3H/C57Bl6 background, which is required to identify homozygous mutant embryos. Homozygous Sl^{17H} mutant embryos were obtained and genotyped as follows. Heterozygous Sl^{17H}/C3H animals were crossed with C57Bl6 wildtype mice. F1 heterozygous offspring, in contrast to the Sl^{17H}/C3H breeding stock, have normally pigmented heads, but exhibit a partially depigmented tail. This altered pigmentation phenotype of the heterozygous animals in a mixed C3H/C57Bl6 background was confirmed by test matings. All F1 mice with depigmented tails (putative heterozygotes) had offspring which contained Sl^{17H}/Sl^{17H} homozygous animals judged by their lack of coat pigmentation. Control matings of F1 mice with completely pigmented tails (wild type) never generated partially (tail) or completely depigmented offspring. However, in contrast to homozygous Sl^{17H} mice on the C3H background, homozygous Sl^{17H} F2 animals often displayed partially pigmented ears and a few pigmented hairs on the back at lumbar axial levels.

Heterozygous F1 animals which had been test mated were used to produce homozygous embryos. Embryos were dissected between e10.5 and e13.5 (e0.5 at the detection of the plug) and their genotypes were identified from limb bud tissue as described (Wehrle-Haller *et al.*, 1996). The genotypes of the embryos were determined with a primer pair corresponding to the D10Mit96 microsatellite marker (Research Genetics), which maps within 1 cM of the *Sl* locus (forward primer, CTTCTTTGAAGTTAGATGCAGCC, and reverse primer, TACGGAGAAGGGAACACCTG; Mouse Genome Database; Whitehead Institute/MIT Center for Genome Research; Copeland *et al.*, 1993; Dietrich *et al.*, 1994). PCR amplification with this primer pair yielded a 127-bp band from the mutant C3H chromosome and a 153-bp band from the wildtype C57Bl6 chromosome. To increase the size of the PCR products, which allowed better visibility on agarose gels, a new "forward" primer was designed based on the published sequence of the D10Mit96 marker (new forward primer, CTGGAGACACATGCGCAGAC). With the new primer pair, bands of 167 and 193 bp were obtained for the C3H Sl^{17H} mutant and the C57Bl6 wildtype chromosome, respectively. Previous genotype results with the D10Mit96 were confirmed with this new primer pair (not shown).

Whole-Mount in Situ Hybridization

Whole-mount *in situ* hybridization with the probes for TRP-2 (Steel *et al.*, 1992) and mouse c-kit was done with at least three embryos for each stage and genotype, as described in Wehrle-Haller *et al.* (1996). Detailed protocols will be provided on request.

Antibodies and Immunohistochemistry

A polyclonal rabbit anti-mouse SCF/GST antiserum was used for immunohistochemistry as well as Western blotting of SCF (Wehrle-Haller *et al.*, 1996). Anti-SCF/GST antibodies were affinity purified with recombinant double-tagged mouse SCF (N-terminal His tag (Invitrogen) and internal Myc tag (Fig. 1); Wehrle-Haller *et al.*, 1996). Double-tagged SCF was purified from bacterial lysates by affinity chromatography on a Ni^{2+} NTA-agarose column (Qiagen). Purified recombinant SCF was coupled to CNBr-activated Sepharose (Pharmacia) and polyclonal rabbit anti-mouse SCF/GST was adsorbed to the column. After extensive washing with PBS, anti-SCF antibodies were eluted with 0.1 M glycine, pH 2.5, and immediately neutralized with 1 M Tris, pH 8.0. Purified antibodies

were used in concentrations of 1/200 to 1/50 on sections depending on the amount of antibody recovered from the affinity column. Further adsorption of the affinity-purified antibodies with e15.5 embryo acetone powder obtained from *Sl/Sl* homozygous embryos did not further increase the specificity of the immunohistochemical staining (Wehrle-Haller *et al.*, 1996).

C57Bl6 wildtype embryos and homozygous and wildtype embryos from F1 Sl^{17H}/+ dated matings were used for immunohistochemistry. Embryos were fixed for 2 h or overnight in ice-cold 4% paraformaldehyde in PBS, washed with PBS, dehydrated, and stored in methanol at −20°C. For sectioning, embryos were gradually rehydrated in 20 mM Tris, pH 7.4; 150 mM NaCl (TBS) with 0.1% Tween 20 (TBST) and then heat treated for 30 min at 70°C in order to inactivate endogenous alkaline phosphatases. Embryos were subsequently submersed in 30% sucrose, embedded in OCT, frozen on dry ice, and sectioned at 16 μm. Sections were collected on gelatin/alum-coated slides, air dried, and stored at −20°C. To resume antibody staining, sections were briefly postfixed for 1 min, washed with TBST, and blocked with 2% heat-inactivated BSA (70°C for 15 min; hiBSA) in TBST for 30 min. Primary affinity-purified rabbit anti-mouse SCF antibodies were applied for 75 min, dissolved in blocking solution. Sections were washed 3 × 5 min each with blocking solution. Goat anti-rabbit alkaline phosphatase-conjugated secondary antibodies (Cappel) (diluted 1/500) were adsorbed with e13.5 heat-inactivated mouse acetone powder (70°C for 30 min) in 2% hiBSA in TBST for 1 h at 4°C with continuous rocking. Adsorbed secondary antibody was cleared by centrifugation and applied to the sections for 1 h. Sections were washed as above and subsequently incubated with adsorbed (see above) rabbit anti-goat alkaline phosphatase-conjugated antibody (Cappel) diluted at 1/1000 in blocking solution for 1 h.

For antigen detection, sections were washed 3 × 5 min with blocking solution, 1 × 5 min with TBST, and 1 × 5 min with color-developing buffer (100 mM Tris, pH 9.5; 100 mM NaCl; 50 mM $MgCl_2$, and 0.1% Tween 20). Staining was performed for 1 to 3 h in color-developing buffer containing 0.33 mg/ml nitroblue tetrazolium salt (NBT) and 0.166 mg/ml 5-bromo-4-chloro-3-indolyl phosphate (BCIP) in the dark. Stained sections were washed with TBST and embedded in glycerol. Sections were viewed under bright field on a Zeiss Axiovert 100 equipped with a digital camera (Hamamatsu). Adjustments of contrast and brightness were done in PhotoShop (Adobe) and performed identically between experimental and control sections. Mutant and wildtype sections were obtained from littermates treated identically and in parallel. Furthermore, staining, color reaction, and exposure times were identical between wildtype, mutant, or control sections, in order to reveal relative differences in intensity and staining patterns of SCF immunoreactivity.

SCF Constructs and Transient Transfection of COS-7 Cells

Mouse SCF cDNAs KL-S, KL-M1, and KL-M2 in pcDNAI (Invitrogen) were obtained from Dr. J. Flanagan, Boston (Flanagan *et al.*, 1991). These cDNAs code for the longer (KL-M1) and shorter (membrane bound, KL-M2) splice variants, whereas KL-S encodes only the proteolytically released form of SCF derived from the KL-M1 splice variant (Flanagan *et al.*, 1991). To allow immunohistochemical detection of expressed mouse SCF proteins, a 10-amino-acid epitope tag recognized by the 9E-10 mAb against human c-myc (Evans *et al.*, 1985) was introduced into the linker region following the growth factor domain and before the end of exon 5 (Fig. 1). Overlapping primers (forward primer, GTCCCGAGCAGAAGCTTATCTCCGAGGAGGACCTCG; reverse primer, GACCGAGGTCCTCCTCGGAGATAAGCTTCTGCTCGG) were synthesized, annealed, and ligated into the unique ppuMI site, creating a Gly-Pro duplication separated by the myc epitope tag. Secreted myc-tagged SCF was tested for its biological activity in mouse neural crest cultures in which it induced melanocyte proliferation and differentiation (Morrison-Graham and Weston, 1993). The large (KL-M1) and small (KL-M2) splice variants coding for the Sl^{17H} mutant version of SCF were constructed with overlap extension using PCR (Ho *et al.*, 1989). Two partially complementary primers which recreated the mutated splice site in Sl^{17H} mutant SCF were designed. The reverse primer at the mutated site (TTGCAACATACTTCCAGTATAAGGCTCC) was used together with a 5′-located T7 forward primer to amplify the N-terminal region of either myc-tagged KL-M1 or KL-M2 by PCR. The other primer amplified the C-terminal portion and 3′ untranslated region of mouse SCF from spleen reverse-transcribed mRNA by PCR (forward primer, ATACTGGAAGTATGTTGCAACAGAAAGAGA; reverse primer located in 3′ UTR, ATACTGCAGCAAACATGAACTGTTACCAGCC). Both PCR products which were partially overlapping at the Sl^{17H} mutant region, together with the T7 and reverse 3′ UTR primer, were included in a PCR yielding the Sl^{17H} mutant sequence for either the large (KL-M1) or the membrane-bound (KL-M2) splice variants. The mutant sequences in the vicinity of the Sl^{17H} mutant site were confirmed by dideoxy sequencing.

To visualize SCF localization in living cells, we incorporated the EGFP (enhanced green fluorescent protein; Clontech) gene in frame into the above-mentioned constructs (Fig. 1). EGFP was inserted 3′ of the myc tag using PCR overlap extension (see above). The N-terminal SCF sequence was amplified with a T7 forward and the reverse myc tag primer (see above). This product was partially overlapping to EGFP amplified with a forward primer, GGAGGACCTCGGTCAGGCCACCATGGTGAGCAAG, and reverse primer, TCGCTCGAGACCGGTCTTGTACAGCTCGTCC. The stop codon in EGFP was replaced with an *Age*I site followed by a *Xho*I site, which were used to insert the wildtype and mutant transmembrane and cytoplasmic sequences previously amplified with an *Age*I-containing forward primer (for KL-M1 sequences) AGAACCGGTCCCGAGAAAGATTCC or (for KL-M2 sequences) AGAACCGGTCCCGAGAAAGGGAAAG and a reverse SP6 primer located 3′ of the multiple cloning site in pcDNA3. Constructs were sequenced and judged functional due to their membrane staining and ability to immobilize melb-a cells when transiently expressed in COS-7 cells (see Results). Supercoiled plasmid DNA was purified by Qiagen plasmid maxipreps and CsCl banding. Concentrations were determined spectroscopically.

COS-7 cells were obtained from ATCC and cultured in 10% FCS in DMEM. Transient transfection was done with the LipofectAMINE reagent (Gibco) according to the manufacturer's recommendation. Briefly, cells were seeded at 250,000/well in a six-well plate (Falcon), the day before transfection. One microgram of plasmid DNA in 100 μl OptiMEM (Gibco) was mixed with 6 μl LipofectAMINE in 100 μl OptiMEM and incubated for 30 min at room temperature. Cells were washed with OptiMEM and incubated with the transfection mixture (volume adjusted to 1 ml with OptiMEM) for 6 h, after which the transfection solution was replaced with 10% FCS in DMEM. For coculture experiments with melb-a cells and expression of EGFP-tagged SCF, COS-7 cells were transiently transfected with Fugen 6 (Roche), according to the manufacturer's recommendations.

COS-7 Cell-Surface Biotinylation, Avidin Precipitation, Western Blotting, and Coculture Experiments

Forty-eight hours after transfection, cells were washed 3 × 5 min with prewarmed wash buffer (140 mM NaCl, 5 mM KCl, 0.5 mM $MgSO_4$, 1.5 mM $CaCl_2$, 0.05% $NaHC0_3$, and 0.1% glucose at pH 7.5). During washes a 0.5 mg/ml Sulfo-NHS–biotin (Pierce) solution was prepared in wash buffer by diluting a 100 mg/ml stock of Sulfo-NHS–biotin dissolved in DMSO (prepared immediately before the experiment). The cells were biotinylated for 15 min at 37°C with occasional rocking. After biotinylation, cells were chilled on ice and rinsed once with ice-cold wash buffer and subsequently blocked with DMEM containing 10% FCS. Biotinylated cells were washed with wash buffer and then extracted with 0.5 ml lysis buffer for 10 min on ice with occasional rocking (120 mM NaCl; 50 mM Tris–HCl, pH 8.0; 1% NP-40; 0.5% deoxycholate; 0.1% SDS; 1 mM PMSF; and 1 μg/ml chymostatin, leupeptin, antipain, and pepstatin, each). Biotinylated proteins were precipitated with 50 μl of a 50% suspension of avidin-agarose beads (Pierce) for 2 h at 4°C. Beads were washed once with 0.5 ml lysis buffer and twice with 1 ml TBST. Beads were boiled for 5 min in 50 μl 1× SDS–PAGE buffer containing β-mercaptoethanol. Proteins were separated on 12% SDS–PAGE and transferred to nitrocellulose according to standard protocols. Blots were blocked in 1% BSA in TBS and incubated with a rabbit anti-mouse SCF/GST polyclonal antiserum diluted 1/1000 in blocking buffer or 5 μg/ml anti-myc (9E-10) monoclonal antibody in blocking buffer. Nitrocellulose blots were washed with TBST and incubated with goat anti-rabbit antibodies conjugated either to alkaline phosphatase (Bio-Rad) or to peroxidase (Jackson ImmunoResearch) or with goat anti-mouse antibodies conjugated to peroxidase (Chemicon). Each secondary antibody was diluted 1/1000 in 1% BSA in TBS. Blots were developed with NBT/BCIP (see above) or with ECL reagents (Amersham).

As an internal control for transfection efficiency and respective synthesis of SCF proteins, we compared identical fractions of the total cell lysates for SCF immunoreactivity on Western blots. The obtained band represents the sum of transfection efficiency, protein synthesis, and half-life of the SCF protein under steady-state conditions. Only the surface biotinylations in which steady-state levels of SCF protein were comparable between wildtype and mutant proteins of a respective splice variant were analyzed (see Results). Furthermore, we used monoclonal antibody 9E-10 (Evans *et al.,* 1985) to reveal the myc-epitope-tagged wildtype and mutant SCF protein, in order to exclude possible changes in anti-SCF-antibody avidity toward mutant SCF protein.

The c-kit-expressing and SCF-dependent melanoblast cell line melb-a was obtained from Dr. Dot Benett (London) (Sviderskaya *et al.,* 1995) and cultured in RPMI medium with 10% FCS, 20 ng/ml SCF, and 40 pM bFGF. For coculture experiments, melb-a cells were washed, trypsinized, and blocked in RPMI containing 10% FCS and resuspended in RPMI without serum or growth factors. Melb-a cells were then added to previously transfected COS-7 cells and cultured in serum-free RPMI medium. Cultures were fixed after 24 h and fields were photographed randomly. Alternatively, COS-7 cells plated on glass coverslips were transfected with EGFP-tagged SCF constructs. After addition of melb-a cells, living cocultures were photographed on an inverted fluorescence microscope (Axiovert 100; Zeiss).

MDCK Cell Transfection with Normal and EGFP-Tagged Wildtype and Mutant SCF and Detection of Polarized Proteins

MDCK cells were obtained from ATCC and cultured in DMEM containing 10% FCS. Myc-epitope-tagged cDNAs encoding KL-S, KL-M1, KL-M2, and Sl^{17H}-mutated KL-M1 were subcloned into pcDNA3 (Invitrogen). MDCK cells were transfected at 30% confluency with LipofectAMINE reagent as described above. In order to increase the transfection efficiency, MDCK cells were transfected in the presence of 1000 U of hyaluronidase (Calbiochem) per 1 ml of transfection solution, which increased the number of transfected MDCK cells three- to fivefold (data not shown). Two days after transfection, cells were plated at different concentrations into 10-cm culture plates and selected in the presence of 500 μg/ml G418 (Gibco). After 2 weeks of selection, cells on plates containing multiple colonies (10–20) were trypsinized and cloned by serial dilutions in 96-well plates in the presence of G418. Individual clones were tested for anti-SCF immunoreactivity as described above. Positive clones were tested for their ability to form tight monolayers on high-density transwell filters (0.4 μm) (Becton–Dickinson). The confluency of the monolayers was confirmed visually and the integrity of tight junctions was tested overnight for their ability to prevent diffusion of phenol red from the lower to the upper compartment. Selected clones were grown to confluency on the transwell filters and were then incubated for 6 days in 10% FCS containing DMEM. An aliquot of medium from the upper and lower compartments was run on a 12% SDS gel, blotted, and analyzed for SCF immunoreactivity as described above.

To observe the distribution of wildtype and Sl^{17H} mutant EGFP-tagged SCF protein in polarized epithelial cells, we transfected MDCK cells using Fugen 6 (Roche) according to the manufacturer's recommendations. One day after transfection cells were plated at low density in the presence of 500 μg/ml G418. Fluorescent colonies were isolated and enriched for EGFP-expressing cells by fluorescent-activated cell sorting (FACStar Plus; Becton–Dickinson). Transfected cells were seeded onto glass coverslips and the EGFP tag was visualized on a Zeiss Axiovert 100 microscope equipped with a motorized stage and a digital camera (Hamamatsu). Image capture, stage movements, and three-dimensional reconstruction of SCF–EGFP-transfected MDCK cells were performed from optical slices taken every 0.2 μm using the Openlab software package (Improvision).

RESULTS

Reduced Numbers of Melanocyte Precursors Disperse in Sl^{17H} Homozygous Mutant Embryos

In the trunk of normal embryonic mice, melanocyte precursors begin to disperse on the lateral crest cell migration pathway from the migration staging area (MSA; Weston, 1991; Wehrle-Haller and Weston, 1997) at about e11–11.5. While still in the MSA, these melanocyte precursors begin to express c-kit and TRP-2, while mRNA encoding the c-kit ligand, SCF, is expressed in the dorsal aspect of the epithelial dermatome that borders the lateral migration pathway (Wehrle-Haller and Weston, 1995). In order to gain insight into the cause of the pigmentation defect in Sl^{17H} homozygous mice, we compared the initial dispersal of melanocyte precursors from the MSA (e11.5) onto the

lateral pathway and subsequent dispersal of these cells in the mesenchymal dermis (e12.5) in wildtype embryos and in Sl^{17H} mutant homozygotes.

In e11.5 homozygous Sl^{17H} mutant embryos, fewer TRP-2/c-kit mRNA-expressing cells were found in the MSA compared to wildtype littermates (arrows in Figs. 2A and 2B). Moreover, fewer cells were localized on the lateral pathway at hindlimb levels (Figs. 2A, 2B, 2C, and 2D). Interestingly, in mutant embryos (Figs. 2B and 2D), melanocyte precursors were found in a narrower band, in contrast to the broader distribution of cells in wildtype embryos (Figs. 2A and 2C). More anterior in the trunk, a few irregularly spaced melanocyte precursors could be detected on the lateral pathway in Sl^{17H} homozygous mutant embryos (not shown). In contrast to wild type, the head of mutant embryos contained only a small number of TRP-2/c-kit mRNA-expressing cells at the level of the second branchial arch, the precursor of the ear pinna (Figs. 2E and 2F).

At e12.5, a few TRP-2-positive cells were detected in Sl^{17H} homozygous embryos at the level of the ear pinna (not shown). Although cells could not be detected in the anterior trunk of mutant embryos, they were present on the lateral pathway at hindlimb levels (Fig. 2H). Some TRP-2-positive cells were also found entering the posterior portion of the hindlimb (a site of SCF mRNA and protein expression), comparable to wild type (Fig. 2G). Although melanocyte precursors occupied similar regions in Sl^{17H} and wildtype embryos, their number was dramatically reduced in Sl^{17H} mutant embryos compared to wild type.

By e13.5, TRP-2-positive cells could no longer be detected in mutant embryos at any location where they were normally observed in wildtype embryos (data not shown).

SCF Protein Expression Is Reduced, and Its Location Is Altered, in Sl^{17H} Mutant Embryos

Since the reduced number of melanocyte precursors in Sl^{17H} mutant embryos was already evident by e11.5, the cause of this phenotype seems likely to be associated with SCF expression normally seen in the dermatome by e10.5. Since SCF mRNA levels appear to be comparable in wildtype and Sl^{17H} homozygous mutant embryos (Brannan *et al.*, 1992), we analyzed SCF protein distribution in the dermatome of wildtype and Sl^{17H} mutant tissues in order to reveal possible differences. Compared to wild type, the amount of SCF immunoreactivity (SCF-IR) was dramatically reduced in all Sl^{17H} homozygous mutant embryos examined (e10.5, e11.5, e13.5; $n = 5$). At e10.5 in wildtype embryos, SCF protein was detected in the dermatome, pronephros, and genital ridges in the trunk and in the floorplate along the entire axis (Figs. 3A–3E). However, in Sl^{17H} homozygous mutant embryos, fainter SCF-IR was detected in the dermatome, pronephros, genital ridges, and floorplate (Figs. 3F–3J). Interestingly, in contrast to wildtype SCF-IR, which is found in luminal as well as in basolateral aspects of the dermatome, the pronephros, and the floorplate (Figs. 3A–3E), SCF-IR in Sl^{17H} mutant embryos is found only in the luminal aspect of the dermatome, pronephros, and floorplate (Figs. 3F–3J). Particularly, the accumulation of basal SCF-IR associated with neuronal fiber tracks crossing the floorplate is not observed in Sl^{17H} mutant embryos (brackets in Figs. 3E and 3J).

As with e10.5 embryos, the SCF-IR in e11.5 Sl^{17H} homozygous mutant embryos was severely reduced in the floorplate and genital ridges (not shown). At e13.5 SCF-IR in Sl^{17H} mutant embryos could not be detected in dermal mesenchymal regions in the dorsal aspect of the tail, a site of wildtype SCF-IR (not shown). In summary, SCF-IR in mesenchymal tissues is dramatically reduced in Sl^{17H} mutant embryos compared to wild type. In addition, in embryonic epithelial tissues, Sl^{17H} mutant SCF-IR is localized primarily to the apical compartment, whereas in wildtype embryos the majority of SCF-IR was found in basal compartments.

Sl^{17H} Mutant SCF Protein Is Expressed at Reduced Levels on the Surface of Transfected COS-7 Cells

From the immunohistochemical data presented above, it was clear that the level of SCF protein was reduced in Sl^{17H} mutant embryos. Similarly, Cheng and Flanagan (1994) found a reduced expression of Sl^{17H} mutant protein, by histochemical criteria, on the surface of transiently transfected COS-7 cells. Since quantitative determination and comparison of secreted and membrane-bound wildtype and mutant SCF protein levels was not performed (Brannan *et al.*, 1992; Cheng and Flanagan, 1994; Tajima *et al.*, 1998), however, we attempted to determine relative levels of wildtype and Sl^{17H} mutant SCF proteins expressed on cell surfaces. Accordingly, different forms of SCF, all tagged with the epitope of the anti-myc 9E-10 monoclonal antibody, were transiently expressed in cultured COS-7 cells (see Material and Methods).

In order to determine the relative amount of Sl^{17H} mutant SCF protein expressed on the surface of transfected cells, we biotinylated the surface of transiently transfected COS-7 cells for 15 min. After cell lysis, a fraction of the total amount of biotinylated surface proteins was precipitated with avidin beads and the relative amount of SCF precursors in this fraction was revealed on Western blots with a polyclonal SCF antibody directed against the extracellular SCF growth factor domain or the 9E-10 anti-myc tag monoclonal antibody (Evans *et al.*, 1985). Both the large splice variant and the membrane-bound form of SCF (KL-M1^{myc} and KL-M2^{myc}, respectively) were present in comparable amounts on the surface of COS-7 cells (Figs. 4A and 4C). Interestingly, however, biotinylation of the large splice variant of Sl^{17H} mutant SCF (17H/KL-M1^{myc}) was found to be significantly reduced, although it exhibits an identical extracellular domain, compared to wildtype SCF (KL-M1^{myc}) (Fig. 4A). Thus, although the amount of biotinylated mutant SCF expressed at the cell surface was significantly reduced compared with wildtype, the total amounts of

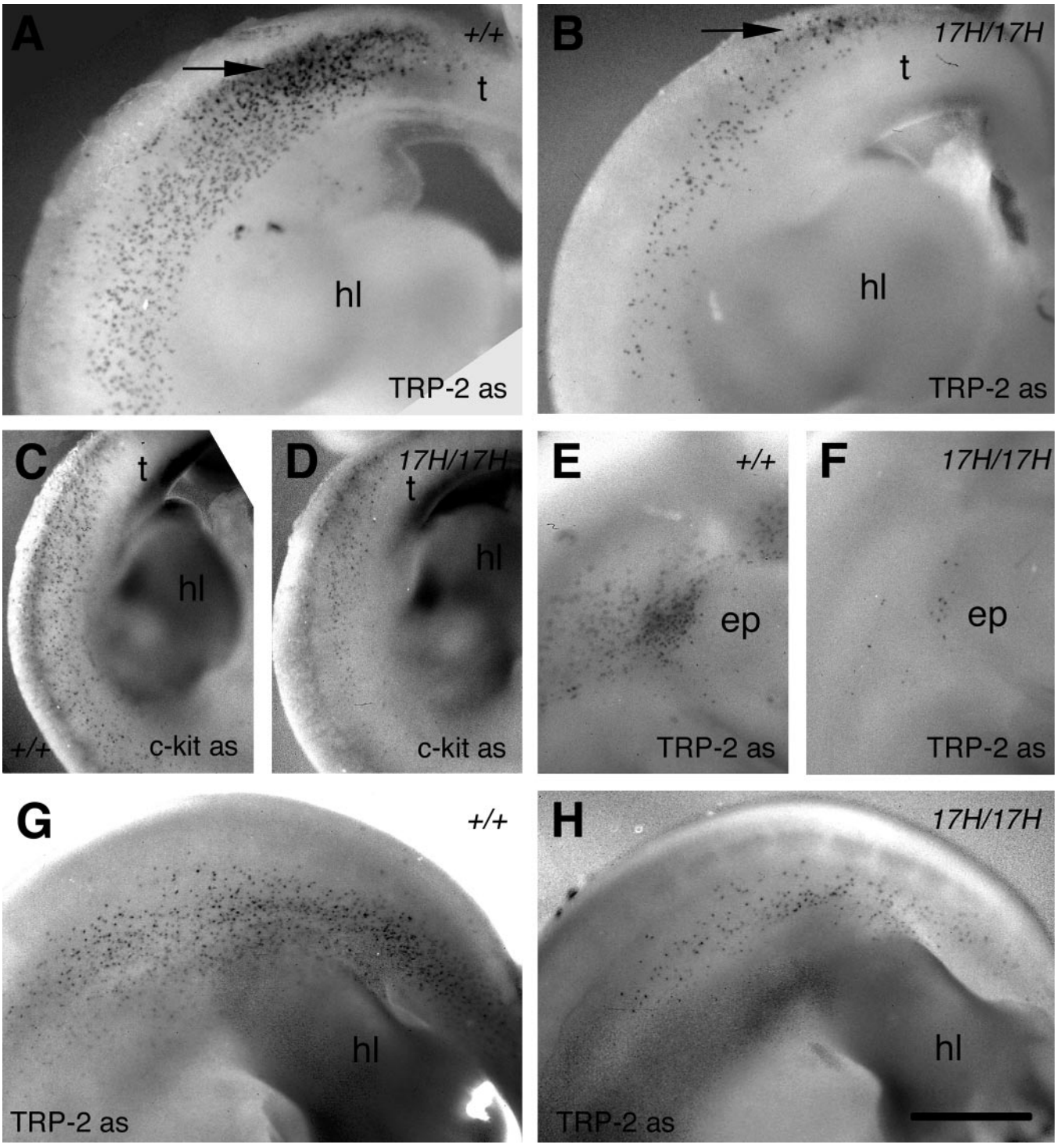

FIG. 2. Whole-mount *in situ* hybridization with TRP-2 and c-kit antisense probes of wildtype and *Sl*^{17H} homozygous mutant embryos. Whole-mount *in situ* hybridization of wildtype (A, C, E, and G) and *Sl*^{17H} homozygous mutant embryos (B, D, F, and H) with an antisense riboprobe against TRP-2 (A, B, and E–H) and c-kit (C and D). Embryos of e11.5 are shown in A–F and of e12.5 in G and H. Tail and hindlimb region of wildtype and *Sl*^{17H} homozygous mutant littermates exhibit TRP-2-positive cells in the MSA (arrows in A and B) and dispersed on the lateral neural crest migration pathway at hindlimb levels (A and B). Similar to A and B, a pair of wildtype (C) and *Sl*^{17H} homozygous (D) littermates were hybridized with a c-kit antisense riboprobe. A high concentration of TRP-2-positive cells can be detected at the primordia of the ear pinna in wildtype embryos (E). Only a few cells can be detected in that location in *Sl*^{17H} homozygous mutant embryos (F). E12.5 hindlimb region of wildtype (G) and *Sl*^{17H} homozygous mutant (H) littermates hybridized with a TRP-2 antisense riboprobe. Note the reduced number of TRP-2-positive cells on the lateral pathway. ep, primordia of ear pinna; hl, hindlimb; t, tail. Bar corresponds to 0.55 mm in A and B, to 0.9 mm in C and D, to 0.3 mm in E and F, and to 1 mm in G and H.

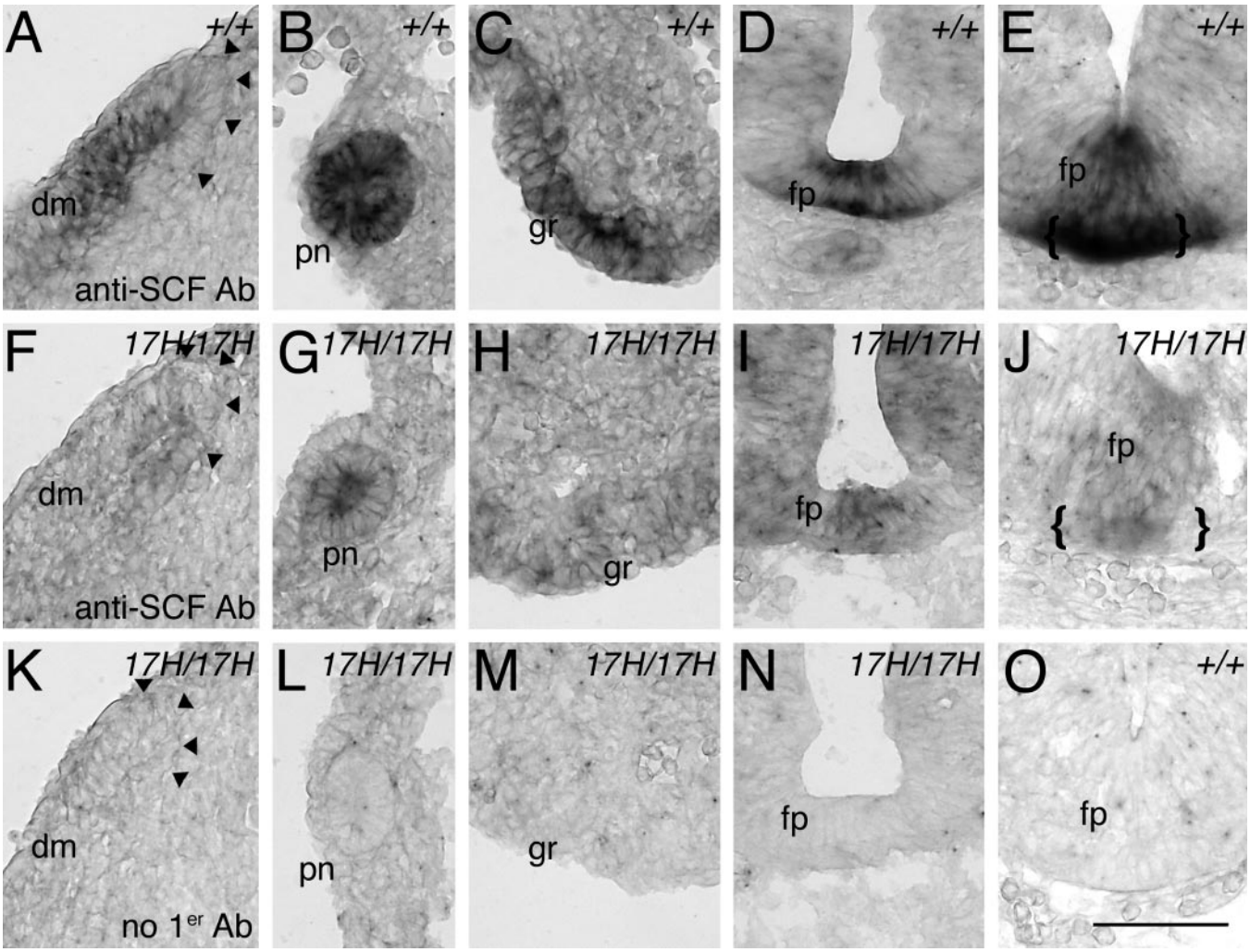

FIG. 3. SCF immunoreactivity (SCF-IR) in wildtype and Sl^{17H} homozygous mutant tissue. Cross sections of wildtype embryos (A–E) and Sl^{17H} homozygous littermates (F–J) at e10.5, stained in parallel with affinity-purified anti-SCF antiserum (A–J) or only secondary reagents (K–O). Sections stained with anti-SCF antibodies (anti-SCF Ab) or without primary antibody (no 1^{er} Ab) of the dermatome (A, F, and K), pronephros (B, G, and L), genital ridges (C, H, and M), and floorplate (D, I, and N) at posterior midtrunk levels of e10.5 embryos. The mediodorsal boundary of the dermatome is indicated by arrowheads. Note the reduced SCF-IR between wildtype and Sl^{17H} homozygous mutant sections in the dermatome and floorplate as well as pronephros and genital ridges (compare A–D with F–I). Note also the differential distribution of SCF-IR in the dermatome and pronephros between wildtype and Sl^{17H} homozygous embryos (compare A with F and B with G). Cross sections of the floorplate at midbrain levels of wildtype (E) and Sl^{17H} homozygous mutant embryos (J). The location of neuronal fiber tracks crossing the floorplate is indicated by brackets (in E and J). Note the absence of SCF-IR accumulation associated with these fibers in Sl^{17H} homozygous mutant embryos. dm, dermatome; fp, floorplate; gr, genital ridges; pn, pronephros. Bar corresponds to 63 μm in A–O.

SCF-immunoreactive proteins present in the lysates of wildtype and mutant SCF-transfected COS-7 cells were similar (Fig. 4B). Similar to the larger splice variant, biotinylation of the membrane-bound splice variant of Sl^{17H} mutant SCF (17H/KL-M2^{myc}) was found to be significantly less than the respective wildtype form (Fig. 4C).

Since we could not completely exclude possible changes of anti-SCF antibody avidity toward the extracellular domain of SCF due to the mutant cytoplasmic tail, we probed total cellular lysates and avidin-precipitated proteins with the 9E-10 antibody as well. Total COS-7 cell lysates of KL-M2^{myc}- and 17H/KL-M2^{myc}-transfected cells revealed bands of similar intensities when blotted with the 9E-10 antibody (Fig. 4D). Examination of cell surface biotinylated SCF from these two samples by the 9E-10 antibody illustrated a reduction of cell-surface-expressed Sl^{17H} mutant

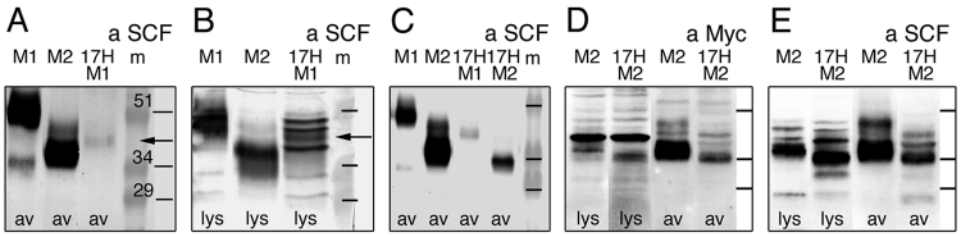

FIG. 4. Sl^{17H} mutant SCF is not efficiently cell surface biotinylated compared to wildtype forms of SCF. 48-h transiently transfected COS-7 cells were cell surface biotinylated for 15 min, washed, blocked in DMEM containing 10% FCS, and lysed with detergent. Total cell lysates (lys) or avidin-precipitated fractions (av) were analyzed on 12% SDS–PAGE minigels followed by Western blotting with polyclonal anti-SCF/GST antiserum (a SCF) or with 9E-10 (anti-myc; a Myc) monoclonal antibody as indicated. (A) Anti-SCF-reactive proteins precipitated with avidin beads from lysates of cells transfected with KL-M1^{myc} (M1), KL-M2^{myc} (M2), or 17H/KL-M1^{myc} (17HM1) cDNAs. (B) Total anti-SCF-reactive proteins present in lysates from A. (C) An experiment identical to A, in which, however, the membrane-bound version of the Sl^{17H} mutant SCF (17H/KL-M2^{myc}; 17HM2) was included. (D and E) The same blot of total cell lysates and avidin-precipitated proteins from either wildtype SCF- (KL-M2^{myc}; M2) or Sl^{17H} mutant SCF- (17H/KL-M2^{myc}; 17HM2) transfected cells. The blot was first developed with anti-myc monoclonal antibody (D) and subsequently with anti-SCF polyclonal antiserum (E). The arrows in A and B point to the biotinylated Sl^{17H} mutant SCF protein in A and its corresponding similar-sized band in the total cell lysate in B. Incubation with 9E-10 antibody revealed multiple non-SCF-related cytoplasmic proteins present equally in both lysates. The apparent molecular weights (in kDa) of the protein standards are indicated (m).

SCF (Fig. 4D). Incubation of the same blots with polyclonal anti-SCF antibodies revealed similar intensities of the bands as observed with the 9E-10 antibody (Fig. 4E).

Membrane-Associated Sl^{17H} Mutant SCF Protein Is Functional

The reduced numbers of melanocyte precursors seen in e11.5–12.5 mutant embryos might result from the inability of c-kit-expressing cells to recognize mutant SCF expressed on dermatome-derived dermal fibroblasts. In order to test whether Sl^{17H} mutant SCF expressed on dermal fibroblasts can be recognized by c-kit-containing cells, we developed a simple coculture assay: SCF-dependent melb-a cells (a melanoblast cell line; Sviderskaya *et al.*, 1995) were seeded in serum-free medium onto transiently transfected COS-7 cells (see Material and Methods). After 24 h, cultures were washed and assessed for the association of melanoblasts and transfected COS-7 cells. In four independent experiments, aggregates (asterisks in Fig. 5) of melanoblasts and COS-7 cells were found consistently in cultures in which COS-7 cells had been transfected with membrane-bound forms of SCF (KL-M1^{myc}, KL-M2^{myc}, Figs. 5A and 5B), but not in cultures transfected with secreted forms of SCF (KL-S^{myc}; Fig. 5C) or no DNA (Fig. 5F). Aggregates of melanoblasts and COS-7 cells transfected with 17H/KL-M1^{myc} and 17H/KL-M2^{myc} (Figs. 5D and 5F) were indistinguishable from cultures containing cells transfected with wildtype SCF cDNA. This indicates that the Sl^{17H} mutant forms of SCF, when expressed on the surface of fibroblasts, are active and accessible for binding by c-kit-expressing melanoblasts.

To further reveal details about the melb-a/COS-7 aggregates, we repeated the above experiment with COS-7 cells transfected with various EGFP-tagged SCF constructs. Aggregates which were formed were always associated with green fluorescent cells (Figs. 5G–5N). Two classes of attached melb-a cells were observed: (1) round cells which were detached from the substrate and only loosely connected to the surface of the COS-7 cells and (2) spread melb-a cells forming extensive areas of contacts which were often highlighted by EGFP fluorescence (Figs. 5G and 5H). Round pocket-like structures were formed within the surface of COS-7 cells (asterisk, Fig. 5H) only in cells transfected with the membrane-bound variant of wildtype SCF (KL-EGFP-M2^{myc}).

SCF Protein Accumulates in the Basolateral Compartment of Epithelia

Based on the foregoing results, it appears that membrane-associated Sl^{17H} mutant protein is recognized and bound by c-kit-expressing melanoblasts in culture, but a reduced amount of SCF expressed at the cell surface is responsible for the reduced number of melanocyte precursors on the lateral pathway by e11.5, as well as of primordial germ cells in the genital ridge (Brannan *et al.*, 1992) of Sl^{17H} homozygous mutant embryos. We were puzzled, however, by the apparent discrepancy between the ability of SCF-dependent hematopoietic cells and female germ cells to persist in Sl^{17H} mutants and the complete loss of melanocyte precursors prior to epidermal invasion and of male germ cells in the testis of mutant animals. In this regard, it is noteworthy that melanocyte precursors will migrate through the basement membrane into the basal portion of the SCF-expressing epidermal keratinocyte layer by e13.5. Similarly, male germ cells undergo SCF-dependent proliferation in the basal compartment of the Sertoli cell layer of the testis. Because of this association of SCF-dependent cell popula-

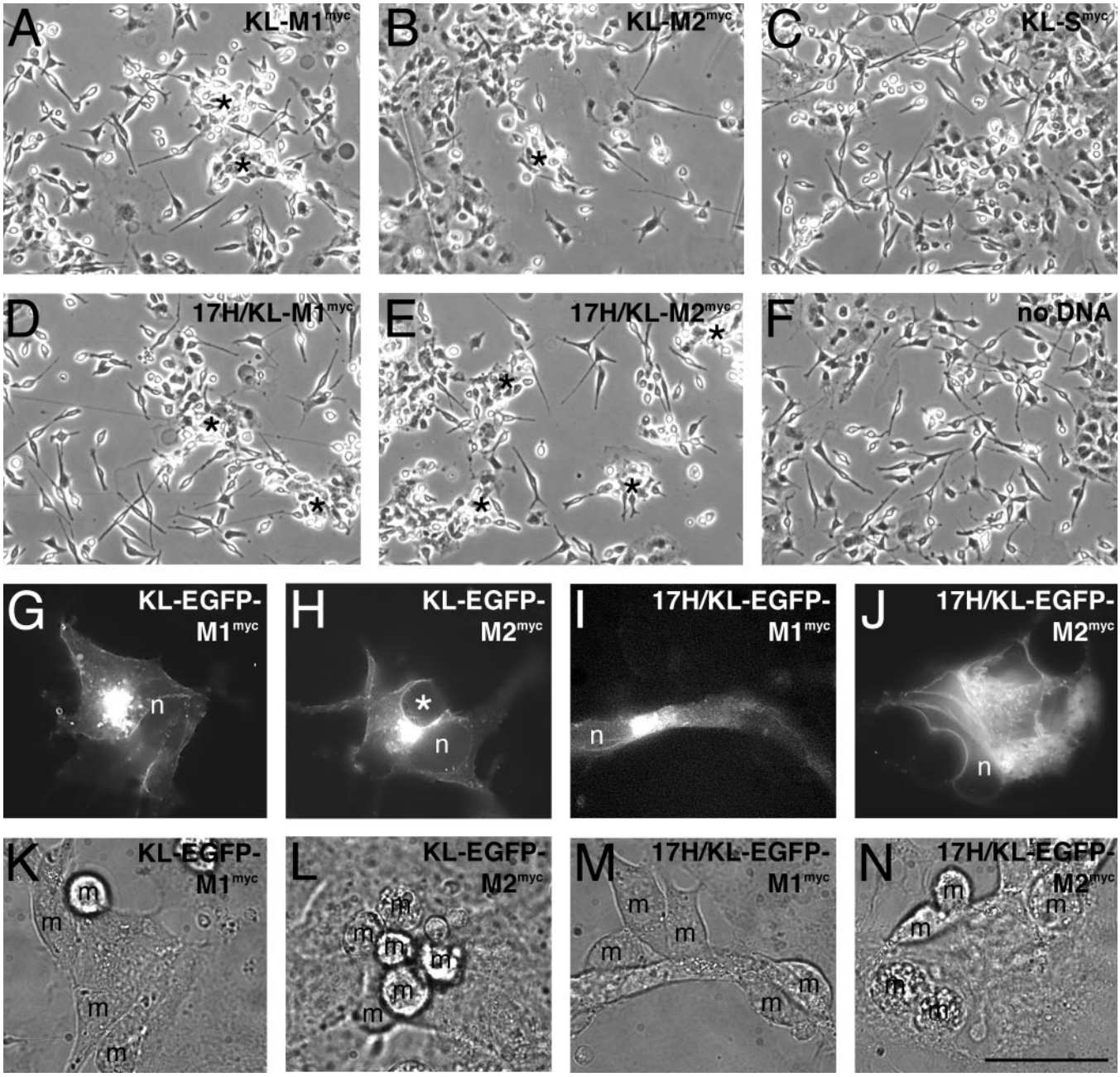

FIG. 5. Adhesion of melanoblasts to COS-7 cells transfected with cell-surface-associated wildtype and Sl^{17H} mutant SCF. COS-7 cells were transiently transfected with various forms of SCF (see Fig. 1). 24 h after transfection, COS-7 cells were washed and melb-a cells were plated in serum-free medium. After 24 h cultures were washed, fixed, and photographed (A–F) or they were cultured for 48 h and observed alive (G–N). Independent of the cDNA used to transfect the COS-7 cells, melb-a cells attached to the culture dish, displaying a characteristic spindle-like shape. When COS-7 cells were transfected with membrane-bound forms of wildtype SCF (A, KL-M1^{myc}; G, KL-EGFP-M1^{myc}; B, KL-M2^{myc}; and H, KL-EGFP-M2^{myc}), melb-a cells were observed to bind to COS-7 cells, forming aggregates of melb-a cells on COS-7 cells (asterisks). Similar aggregates were also observed when COS-7 cells were transfected with Sl^{17H} mutant forms of SCF (D, 17H/KL-M1^{myc}; I, 17H/KL-EGFP-M1^{myc}; E, 17H/KL-M2^{myc}; and J, 17H/KL-EGFP-M2^{myc}). No aggregates were observed in COS-7 cells transfected with cDNA coding for secreted SCF (C, KL-S^{myc}) or no DNA (F). (K–N) Bright-field views of the cells in G–J, respectively. Note the pocket-like structure formed by a KL-EGFP-M2^{myc}-transfected COS-7 cell (asterisk in H). The locations of the COS-7 cell nucleus (n) and melb-a cells (m) are indicated in G–J and K–N, respectively. Bar corresponds to 200 μm in A–F and 35 μm in G–N.

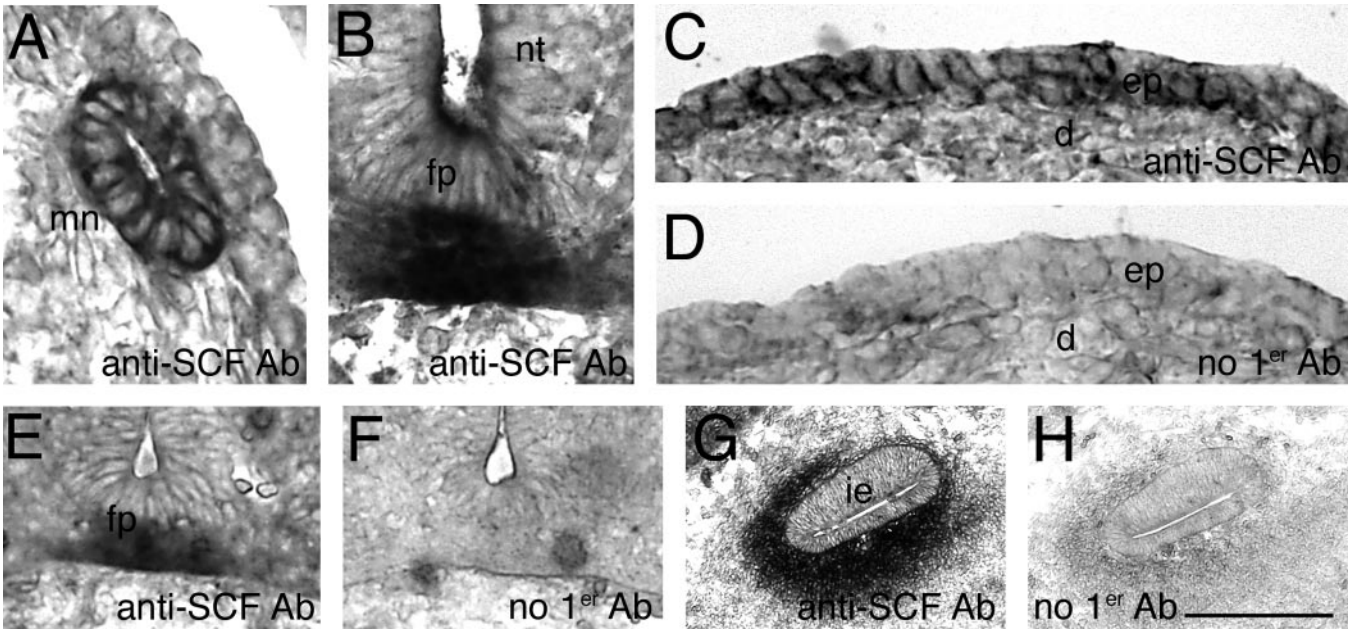

FIG. 6. Wildtype SCF-IR in embryonic epithelial and mesenchymal tissues. Sections from e11.5 (A and B) and e12.5 (C–H) wildtype embryos were stained with an affinity-purified anti-SCF polyclonal antisera (A–C, E, and G) or without primary antibody (D, F, and H). (A) Cross section at midtrunk level showing the mesonephros. (B) Cross section of the floorplate at midtrunk level. (C and D) Consecutive cross sections through the skin. Consecutive cross sections through the floorplate and the inner ear are shown in E, F and G, H, respectively. Note the SCF-IR associated with the basal compartment of the floorplate (B and E), mesonephros (A), and epidermal keratinocytes (C). Mesenchymal SCF-IR was detected in the condensed mesenchyme surrounding the epithelium of the inner ear (G). d, dermis; ep, epidermis; fp, floorplate; ie, inner ear; mn, mesonephros; nt, neural tube. Bar corresponds to 35 μm in A, C, and D; to 50 μm in B; to 80 μm in E and F; and to 210 μm in G and H.

tions with the basal compartment of epithelial tissues, it seemed possible that normal SCF function required appropriate asymmetric localization of SCF protein in embryonic epithelia.

To test this notion, we examined SCF protein localization in wildtype embryonic epithelial tissues. In general, SCF-IR was always detected in tissues previously reported to express SCF mRNA (Keshet *et al.,* 1991; Bedell *et al.,* 1995; Wehrle-Haller and Weston, 1995), as well as in some other locations like the optic stalk. Surprisingly, SCF protein expressed within epithelial tissues was predominantly accumulating within the basolateral compartment. Thus, at e10.5, SCF-IR can be detected in the apical and basolateral compartments of the dermatome, the floorplate, and the pronephros (Figs. 3A–3D). At e11.5 basolateral SCF-IR has increased in the mesonephros (Fig. 6A) and is almost exclusively localized to the basal aspect of the floorplate (populated by crossing axonal tracts) (Fig. 6B). At e12.5 SCF-IR can be detected in basolateral locations within the epidermal keratinocyte layer (Fig. 6C), the floorplate (Fig. 6E), and the mesonephros (not shown). At e13.5 SCF-IR is found in the basal aspect of the epidermis and nephritic tubules (not shown). It should be emphasized, however, that SCF-IR is also found uniformly distributed in many nonepithelial (mesenchymal) tissues such as the dermal mesenchyme formed from the epithelial dermatome, as well as the genital ridges, cartilage condensations in the head and ribs (not shown), and condensed mesenchyme surrounding the inner ear (Fig. 6G).

Differential Localization and Release of Wildtype and Sl^{17H} Mutant SCF from Polarized Epithelial Cells Might Explain the Paradoxical Survival of Some SCF-Dependent Cells

Melanocyte precursors and spermatogonia both depend on SCF support, while localized in the basal compartment of the epidermal keratinocytes (e13.5; Nishikawa, *et al.,* 1991) or the Sertoli cell layer (Yoshinaga *et al.,* 1991), respectively. We therefore tested the hypothesis that the cytoplasmic domain of wildtype SCF is required for polarized expression of SCF in the basal compartment of epithelial tissues. This hypothesis predicts that the lack of the membrane anchor in KL-S (Sl^{d} mutant) SCF, or the substitution of the cytoplasmic tail in Sl^{17H} mutant SCF, would lead to altered localization and subsequent secretion of SCF from epithelial tissues. To test this prediction, we stably transfected MDCK (epithelial) cells with plasmids containing myc epitope- or EGFP-tagged KL-S, KL-M1, KL-M2, and Sl^{17H} mutant SCF and observed the accumulation of SCF

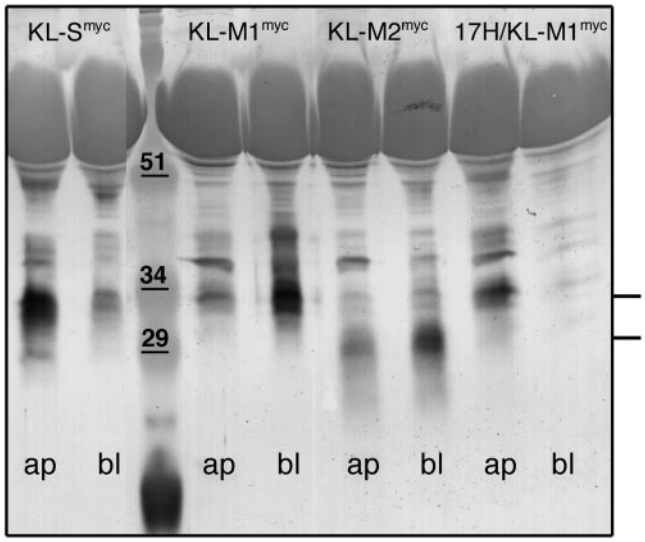

FIG. 7. Wildtype SCF is secreted from the basolateral compartment of polarized MDCK cells while mutant forms of SCF which either lack a transmembrane domain or display the Sl^{17H} mutant cytoplasmic tail are secreted from the apical compartment. Stably transfected MDCK cells were cultured on transwell filter inserts to confluency. Subsequently, 5-day-conditioned media which contacted either the apical (ap) or the basolateral (bl) surface of the monolayer were collected. A fraction of each sample was separated on a 12% SDS–PAGE minigel and analyzed with Western blotting with anti-SCF/GST antiserum for anti-SCF-IR. The cells were transfected with KL-S^{myc}, KL-M1^{myc}, KL-M2^{myc}, or 17H/KL-M1^{myc} as indicated. Markings to the right indicate the position of secreted SCF^{myc} derived from either the M1 splice variant (upper mark) or the M2 splice variant (lower mark). The apparent molecular weights (in kDa) of some of the protein standards are indicated.

released in a two-chamber culture system or expressed in confluent epithelial layers (see Material and Methods).

As seen in Fig. 7, secreted SCF derived from both wildtype forms of SCF (KL-M1^{myc} and KL-M2^{myc}) was found primarily in the lower culture chamber, which is in contact with the basolateral compartment of the MDCK monolayer. In contrast, SCF lacking a transmembrane and cytoplasmic tail (KL-S^{myc}), which is homologous to Sl^{d}, accumulated in the upper culture chamber, which is in contact with the apical surface of the MDCK monolayer. Similarly, secreted SCF derived from Sl^{17H} mutant SCF (17H/KL-M1^{myc}) also accumulated in the upper culture chamber.

Furthermore, the expression of EGFP-tagged SCF in mesenchymal-like COS-7 cells (Figs. 8A–8D) or subconfluent MDCK cells (not shown) revealed uniform cell surface expression with both Sl^{17H} mutant (17H/KL-EGFP-M1(M2)^{myc}) and wildtype membrane-bound forms of SCF (KL-EGFP-M1(M2)^{myc}). However, when transfected MDCK cells reached confluency, EGFP-tagged wildtype SCF was relocalized to intercellular and basal regions of positive cells (Figs. 8E and 8G). In contrast, EGFP-tagged Sl^{17H} mutant forms of SCF remained expressed on the apical (medium-facing) membrane and were never found in intercellular regions (basolateral localization) (Figs. 8F and 8H). We conclude, therefore, that the cytoplasmic domain of wildtype SCF plays a role in targeting SCF to the basolateral compartment in MDCK cells, while SCF with a truncated or mutant cytoplasmic domain is relocalized to the apical compartment.

DISCUSSION

Altered Melanocyte Precursor Distribution in Sl^{17H} Homozygous Mutant Embryos Correlates with Reduced SCF Immunoreactivity on the Lateral Migration Pathway

In order to understand the pigmentation defect in the Sl^{17H} mutant animals we followed the dispersal of melanocyte precursors on the lateral crest migration pathway of mutant homozygous embryos. We found that the number of melanocyte precursors is dramatically reduced very soon after they first appear in the neural crest migration staging area (Wehrle-Haller and Weston, 1995, 1997). Specifically, in Sl^{17H} mutant tissue, melanocyte precursors can be detected only in regions, such as the ear pinna and the hindlimb and tail regions (Wehrle-Haller and Weston, 1995), where the density of melanocyte precursors in wildtype embryos is very high.

To account for this reduced number of migrating melanocyte precursors between e11.5 and e12.5, we hypothesize that an overall reduction in the amounts of SCF protein in dermatome-derived mesenchymal dermis leads to the loss of SCF-dependent cells. This is supported by the very faint staining of SCF protein in the dermatome in Sl^{17H} homozygous mutant embryos. The low density of melanocyte precursors in the Sl^{17H} mutants would indicate a reduced amount of SCF protein in almost all areas of the embryo, allowing survival of melanocyte precursors only in regions where SCF protein concentration is above some critical threshold. Similar to the situation of melanocyte precursors, the number of germ cells present in the genital ridge, between e10.5 and e12.5, is reduced to 10% of its original level in Sl^{17H} mutant tissue (Brannan *et al.*, 1992). This reduction in germ-cell number correlates well with the reduced levels of SCF-IR in the genital ridges at e10.5 and therefore a lack of proliferation of germ-cell precursors in this area.

Reduced Surface Expression of Sl^{17H} Mutant SCF Is Due to the Altered Cytoplasmic Tail

It is possible that the reduced SCF-IR in Sl^{17H} mutant embryo is due to a low expression of mutant SCF on the surface of cells. This low cell-surface expression is inferred from our inability to biotinylate Sl^{17H} mutant SCF expressed on the surface of COS-7 cells, a difference which was not noted previously when SCF proteins were immunoprecipi-

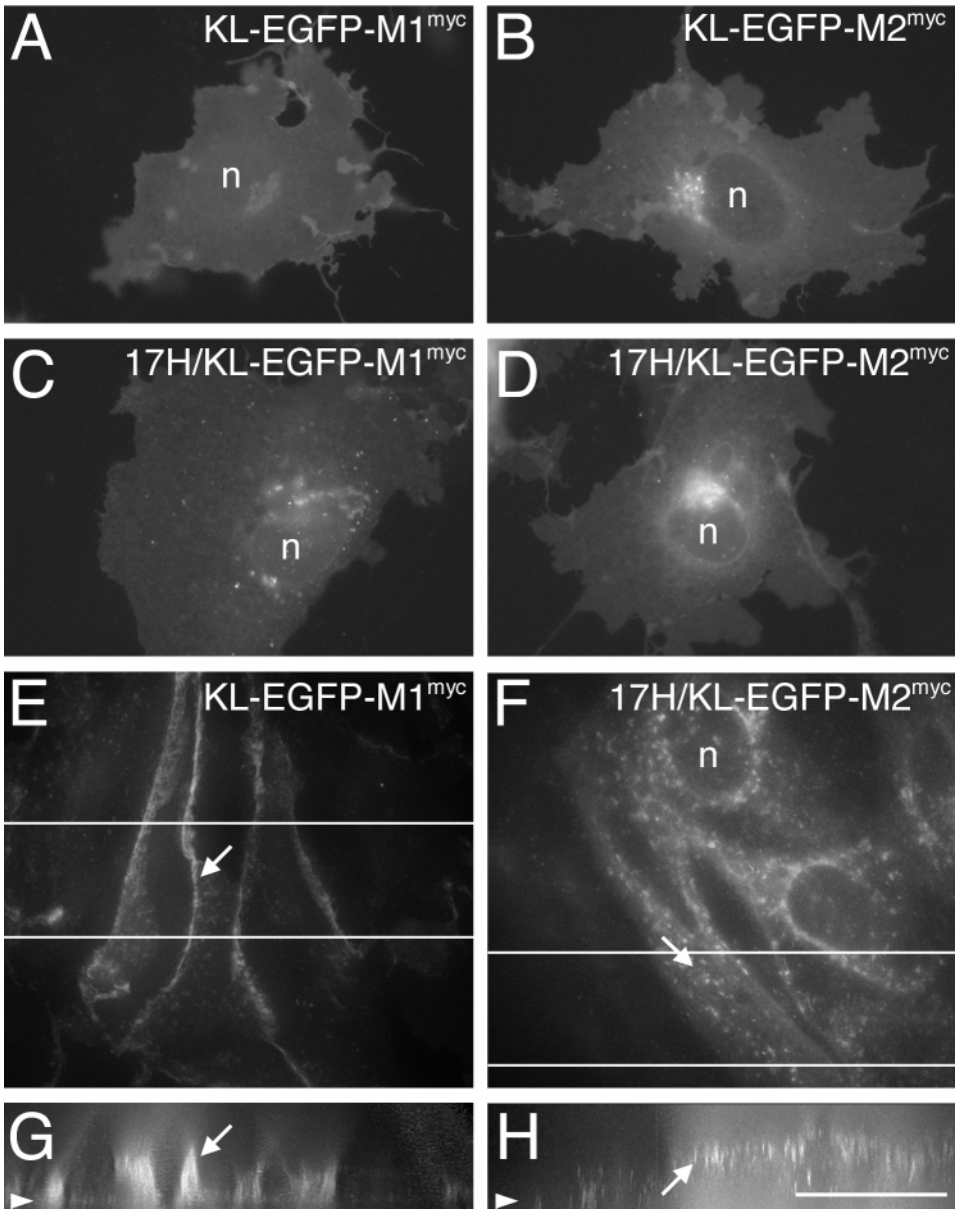

FIG. 8. Differential localization of wildtype versus Sl^{17H} mutant EGFP-tagged SCF in epithelial but not mesenchymal cells. Fluorographs of living COS-7 cells (mesenchymal cells) transiently transfected with EGFP-tagged forms of wildtype and mutant forms of SCF after 24 h (A–D). Fluorograph of confluent MDCK cells (epithelial cells) stable transfected with either EGFP-tagged KL-M1 (E, KL-EGFP-M1^{myc}) or EGFP-tagged Sl^{17H} mutant form of KL-M2 (F, 17H/KL-EGFP-M2^{myc}). The region between the two white bars shown in E and F was optically sectioned every 0.2 μm and reconstructed in three dimensions. In G and H the reconstructions from E and F, respectively, are viewed from the side. Note the basolateral localization of wildtype SCF versus the apical localization (upper surface) observed in mutant SCF (arrows in E, G and F, H, respectively, point to corresponding EGFP-labeled structures). The location of the nucleus (n) is indicated in A–D and F and the level of the coverslip by white arrowheads in G and H. Bar corresponds to 34 μm in A–H and to 17 μm along the *z* axis in G and H.

tated from cell lysates (Cheng and Flanagan, 1994; Tajima *et al.*, 1998). Our results, however, are consistent with those of Cheng and Flanagan (1994), who reported a 10-fold reduction in the amount of surface Sl^{17H} mutant SCF detected by binding and subsequent detection of alkaline phosphatase coupled to the extracellular portion of c-kit. Furthermore, Briley and colleagues (1997) have recently shown that mutations in the cytoplasmic tail of TGFα,

which is very similar to that of SCF, lead to reduced cell-surface expression of TGFα and an accumulation of mutated proteins in the ER. Accordingly, our results support their hypothesis that the Sl^{17H} mutation leads to a general reduction of cell-surface-expressed Sl^{17H} mutant SCF protein, possibly by retaining mutant SCF protein in the ER. Therefore, the reduced amount of cell-surface SCF observed *in vitro* could account for the lower numbers of melanocyte precursors and germ cells present *in vivo*.

Functional Membrane-Bound Sl^{17H} Mutant SCF Promotes Cell Adhesion and Survival of c-kit$^+$ Cells

It has been previously noted that membrane-bound SCF could serve as an adhesion receptor for c-kit-expressing cells (e.g., mast cells) (Flanagan *et al.*, 1991). The consequences of the Sl^d mutation, in which only soluble SCF is produced, suggest that membrane-bound SCF is also required for survival of melanocyte precursors in the dermis (e12.5) (Wehrle-Haller and Weston, 1995). Because of the survival of melanocyte precursors in Sl^{17H} mutant dermis and binding of melb-a cells to Sl^{17H} SCF-transfected fibroblasts, the presence of membrane-bound SCF even at lower levels appears to be sufficient to allow attachment to dermal fibroblasts as well as survival of melanocyte precursors in the dermis at e12.5. Therefore, the phenotype of the Sl^{17H} mutation suggests that membrane-bound SCF provides cell attachment and survival irrespective of its cytoplasmic tail. In contrast, morphogenetic functions like melanocyte precursor homing into the epidermis or homing of hematopoietic stem cells to the spleen (Tajima *et al.*, 1998) require the correct cytoplasmic tail of SCF to be present.

The Cytoplasmic Tail of SCF Is Required for Basolateral Targeting and Polarized Secretion of SCF in Epithelial Tissues

We have established that the amounts of SCF protein encountered by migrating melanocyte precursors are reduced in Sl^{17H} embryos. It is important to emphasize, however, that there is yet another mechanism, in addition to reduced surface expression, that could limit the amount of SCF activity that dispersing cells encounter and that could account for the paradoxical survival of some SCF-dependent cells in Sl^{17H} embryos. Specifically, a mechanism that causes mislocalization of SCF activity in embryonic tissues would result in the same phenotype. Thus, several different observations led us to investigate the possibility that polarized expression of SCF is altered in mutant epithelia. First, several tissues that express SCF during embryogenesis and in the adult, including the dermatome, the epidermal keratinocyte layer, the floorplate, the pronephros, and the Sertoli cell layer in the testis, are epithelial tissues. Second, melanocyte precursors and spermatogonia ultimately reside and differentiate in the basolateral portion of the keratinocyte and Sertoli cell layers, respectively. Third, the SCF protein accumulates predominantly in the basolateral aspect of many of these epithelial tissues (see Results). In the adult testis, although SCF-IR can be found throughout the Sertoli cell layer, SCF seems to be increased in the basal compartment at stages of spermatogonia proliferation during the spermatocyte maturation cycle (Manova *et al.*, 1993). In apparent contrast, however, SCF-IR in dermal capillary endothelial cells is predominantly found on the luminal (apical) side of the endothelial cells (Weiss *et al.*, 1995), and the earliest SCF-IR in the floorplate is detected in the apical compartment (Fig. 3D). As soon as axonal tracts begin to cross the floorplate basal compartment, however, SCF protein predominantly accumulates in this basal compartment colocalizing with the crossing axonal fiber tracts (Campbell and Peterson, 1993). In this case, SCF localization to the basal compartment of the floorplate may be in response to floorplate differentiation or axonal contact.

Many proteins have been studied for their polarized expression in a model epithelial system (i.e., a monolayer culture of MDCK cells). Within this system, secreted glycoproteins which do not exhibit a membrane anchor are released into the apical compartment (Fiedler and Simons, 1995). Similarly, GPI-anchored proteins localize to the apical compartment. Therefore, the default pathway for protein transport in MDCK cells appears to be directed toward the apical domain (Matter and Mellman, 1994; Fiedler and Simons, 1995; Weimbs *et al.*, 1997). Only proteins that contain a specific basolateral targeting signal are found in the basolateral compartment of MDCK cells (Matter and Mellman, 1994). TGFα, the cytoplasmic tail of which is similar in length to that of SCF, has been shown to be associated with the basolateral surface of MDCK cells (Dempsey and Coffey, 1994). However, a fraction of wild-type SCF-IR is also localized to the apical domain (e.g., dermatome and floorplate), which could represent the pool of intracellular, unsorted SCF. Alternatively, SCF may localize initially to the apical compartment from which it is then specifically transported to the basolateral compartment. The mechanism, as well as the peptide sequences responsible for the basolateral targeting of SCF seen in MDCK cells, remains to be identified, but this system promises to be informative in this regard.

Because we find that secreted SCF (KL-S) as well as Sl^{17H} mutant SCF accumulates in the medium in contact with the apical compartment, we suggest that these mutant forms of SCF use the default pathway of protein transport in MDCK cells. The fact that we see a pattern of SCF-IR within the apical compartment of the dermatome, pronephros, and floorplate in e10.5 Sl^{17H} mutant embryos suggests that other epithelial tissues may also aberrantly express Sl^{17H} mutant SCF in the apical compartment. However, it is important to acknowledge that we do not know to what extent SCF is targeted in other epithelial cell types or whether a kidney-derived epithelial cell line (MDCK) can be compared with either keratinocytes or Sertoli cells.

Basolateral Localization of SCF Provides Ligand to Responsive Cells Located at the Basal Aspect of Epithelia

Regardless of the mechanism of localization, we suggest that altered localization of SCF mutant protein negatively affects the survival of melanocyte precursors during the stages at which they require SCF protein released from the epidermal layer. The basolateral secretion of SCF by epidermal keratinocyte may serve both as a survival and as an invasion signal for c-kit-dependent melanocyte precursors prior to their migration into the epidermis. Similarly, male germ cells require SCF during the proliferation and differentiation of spermatogonia while they reside in the basolateral compartment of the Sertoli cell layer (Yoshinaga *et al.*, 1991; Manova *et al.*, 1993; for review see Morrison-Graham and Takahashi, 1993). A lack of delivery of SCF to the basolateral compartment in Sertoli cells could be responsible for the absence of spermatogonial proliferation during the time of testicular maturation of Sl^{17H} mutant males (Brannan *et al.*, 1992). During sexual maturation (about the third and fourth postnatal weeks), the blood–testis barrier, which prevents diffusion of proteins across the tight junctions within the Sertoli cell layer is established (Vitale *et al.*, 1973). This barrier would prevent the diffusion of apical Sl^{17H} mutant membrane-bound SCF to the spermatogonia located in the basolateral compartment.

In both males and females, the numbers of spermatogonia and oogonia, respectively, are equally reduced due to the lack of primordial germ-cell proliferation in the genital ridges (Brannan *et al.*, 1992). In females, oocytes that arise from persistent oogonia can undergo successful maturation stimulated by granulosa cell-derived Sl^{17H} mutant SCF. In contrast, continuously proliferating spermatogonia appear to be more sensitive to reduced levels of SCF activity (Yoshinaga *et al.*, 1991). Moreover, since oocytes associate with the apical aspect of the SCF-producing granulosa cells (Manova *et al.*, 1993; Packer *et al.*, 1994), the targeting defect in Sl^{17H} mutant SCF does not further reduce access of oocytes to SCF and therefore would be expected to allow maturation of oocytes and hence fertility in females.

In conclusion, we propose that a general reduction of SCF mutant protein expressed on the cell surface accounts for the reduced number of melanocyte precursors and primordial germ cells on the lateral pathway and genital ridges, respectively. However, the main cause for the loss of melanocyte precursors, hence the Sl^{17H} pigmentation defect, as well as the sterility in males appears to be the inability of Sl^{17H} mutant SCF to be targeted to the basolateral compartment in SCF-producing epidermal keratinocytes and Sertoli cells. As a consequence, SCF-dependent cell types do not encounter the appropriately localized SCF signals for epidermal invasion and proliferation. We propose, therefore, that not only the amount of growth factor expression is critical for development, but also its appropriate presentation toward responsive cells.

ACKNOWLEDGMENTS

We are grateful to Monique Wehrle-Haller and Dr. Beat Imhof for their critical comments on the manuscript. We also thank Drs. John Flanagan and Carolyn Brannan for generously providing cDNA plasmids. Special thanks to Marie-Claude Jacquier, Sheree Harrison, Adam Hadley, Zigmus Kingis, Victoria Robinson, Dominique Wohlwend, and Dr. Kathleen- Morrison-Graham for technical assistance and Drs. Yoshiko Takahashi, Yoshio Wakamatsu, Linda Hansen, and Ruth Bremiller for advice on *in situ* hybridization and immunohistochemistry. We thank Drs. Mary Bedell and Shin-Ishi Nishikawa for insightful discussions and for sharing unpublished results. We are especially grateful to Rick Gosswiler for his careful animal husbandry. Our work has been supported by Grant DE-04316 from the USPHS to J.A.W. B.W.-H. has been supported by a grant from the Swiss Foundation for Medical and Biological Fellowships and from the Swiss National Science Foundation (31-52727.97).

REFERENCES

Bedell, M. A., Brannan, C. I., Evans, E. P., Copeland, N. G., Jenkins, N. A., and Donovan, P. J. (1995). DNA rearrangement located 100 kb 5′ of the Steel (Sl)-coding region in Steel-panda and Steel-contrasted mice deregulate Sl expression and cause female sterility by disrupting ovarian follicle development. *Genes. Dev.* **9,** 455–470.

Bedell, M. A., Cleveland, L. S., O'Sullivan, N., Copeland, N. G., and Jenkins, N. A. (1996). Deletion and interallelic complementation analysis of Steel mutant mice. *Genetics* **142,** 935–944.

Brannan, C. I., Lyman, S. D., Williams, D. E., Eisenman, J., Anderson, D. M., Cosman, D., Bedell, M. A., Jenkins, N. A., and Copeland, N. G. (1991). Steel-dickie mutation encodes a c-kit ligand lacking transmembrane and cytoplasmic domains. *Proc. Natl. Acad. Sci. USA* **88,** 4671–4674.

Brannan, C., Bedell, M. A., Resnick, J. L., Eppig, J. J., Handel, M. A., Williams, D. E., Lyman, S. W., Donovan, P. J., Jenkins, N. A., and Copeland, N. G. (1992). Developmental abnormalities in Steel-17H mice results from a splice defect in the steel factor cytoplasmic tail. *Genes Dev.* **6,** 1832–1842.

Briley, G. P., Hissong. M. A., Chiu, M. L., and Lee, D. C. (1997). The carboxyl-terminal valine residues of proTGFα are required for its efficient maturation and intracellular routing. *Mol. Biol. Cell* **8,** 1619–1631.

Campbell, R. M., and Peterson, A. C. (1993). Expression of a lacZ transgene reveals floor plate cell morphology and macromolecular transfer to commissural axons. *Development* **119,** 1217–1228.

Cheng, H.-J., and Flanagan, J. G. (1994). Transmembrane kit ligand cleavage does not require a signal in the cytoplasmic domain and occurs at a site dependent on spacing from the membrane. *Mol. Biol. Cell* **5,** 943–953.

Copeland, N. G., Gilbert, D. J., Jenkins, N. A., Nadeau, J. H., Eppig, J. T., Maltais, L. J., Miller, J. C., Dietrich, W. F., Steen, R. G., Lincoln, S. E., Weaver, A., Joyce, D. C., Merchant, M., Wessel, M., Katz, H., Stein, L. D., Reeve, M. P., Daly, M. J., Dredge, R. D., Marquis, A., Goodman, N., and Lander, E. S. (1993). Genome map IV. *Science* **262,** 67–82.

Dempsey, P. J., and Coffey, R. J. (1994). Basolateral targeting and efficient consumption of transforming growth factor-α when expressed in Madin–Darby canine kidney cells. *J. Biol. Chem.* **269,** 16878–16889.

Dietrich, W. F., Miller, J. C., Steen, R. G., Merchant, M., Damron, D., Nahf, R., Gross, A., Joyce, D. C., Wessel, M., Dredge, R. D., Marquis, A., Stein, L., Goodman, N., Page, D. C., and Lander, E. S. (1994). A genetic map of the mouse with 4006 simple sequence length polymorphisms. *Nature Genet.* **7,** 220–245.

Evans, G. I., Lewis, G. K., Ramsey, G., and Bishop, M. J. (1985). Isolation of monoclonal antibodies specific for human c-myc proto-oncogene product. *Mol. Cell. Biol.* **5,** 3610–3616.

Fiedler, K., and Simons, K. (1995). The role of N-glycans in the secretory pathway. *Cell* **81,** 309–312.

Flanagan, J. G., Chan, D. C., and Leder, P. (1991). Transmembrane form of the kit ligand growth factor is determined by alternative splicing and is missing in the sl^d mutant. *Cell* **64,** 1025–1035.

Galli, S. J., Zsebo, K. M., and Geissler, E. N. (1994). The kit ligand, stem cell factor. *Adv. Immunol.* **55,** 1–96.

Ho, S. N., Hunt, H. D., Horton, R. M., Pullen, J. K., and Pease, L. R. (1989). Site-directed mutagenesis by overlap extension using polymerase chain reaction. *Gene* **77,** 51–59.

Huang, E. J., Nocka, K. H., Buck, J., and Besmer, P. (1992). Differential expression and processing of two cell associated forms of the kit-ligand: Kl-1 and Kl-2. *Mol. Biol. Cell* **3,** 349–362.

Huang, E. J., Manova, K., Packer, A. I., Sanchez, S., Bachvarova, R. F., and Besmer, P. (1993). The murine Steel panda mutation affects kit ligand expression and growth of early ovarian follicles. *Dev. Biol.* **157,** 100–109.

Keshet, E., Lyman, S. D., Williams, D. E., Anderson, D. E., Jenkins, N. A., Copeland, N. G., and Parada, L. F. (1991). Embryonic RNA expression patterns of the c-kit receptor and its cognate ligand suggest multiple functional roles in mouse development. *EMBO J.* **10,** 2425–2435.

Maeda, H., Yamagata, A., Nishikawa, S., Yoshinaga, K., Kobayashi, S., Nishi, K., and Nishikawa, S. (1992). Requirement of c-kit for development of intestinal pacemaker system. *Development* **116,** 369–375.

Manova, K., Huang, E. J., Angeles, M., De Leon, V., Sanchez, S., Pronovost, S. M., Besmer, P., and Bachvarova, R. F. (1993). The expression pattern of the c-kit ligand in gonads of mice supports a role for the c-kit receptor in oocyte growth and in proliferation of spermatogonia. *Dev. Biol.* **157,** 85–99.

Matter, K., and Mellman, I. (1994). Mechanisms of cell polarity: Sorting and transport in epithelial cells. *Curr. Opin. Cell Biol.* **6,** 545–554.

Morrison-Graham, K., and Takahashi, Y. (1993). Steel factor and c-kit receptor: From mutants to a growth factor system. *BioEssays* **15,** 77–83.

Morrison-Graham, K., and Weston, J. A. (1993). Transient steel factor dependence by neural crest-derived melanocyte precursors. *Dev. Biol.* **159,** 346–352.

Motro, B., Wojtowicz, J. M., Bernstein, A., and van der Kooy, D. (1996). Steel mutant mice are deficient in hippocampal learning but not long-term potention. *Proc. Natl. Acad. Sci. USA* **93,** 1808–1813.

Nishikawa, S., Kusakabe, M., Yoshinaga, K., Ogawa, M., Hayashi, S., Kunisada, T., Era, T., Sakakura, T., and Nishikawa, S. (1991). In utero manipulation of coat color formation by a monoclonal anti-c-kit antibody: Two distinct waves of c-kit-dependency during melanocyte development. *EMBO J.* **10,** 2111–2118.

Packer, A. I., Hsu, Y. C., Besmer, P., and Bachvarova, R. F. (1994). The ligand of the c-kit receptor promotes oocyte growth. *Dev. Biol.* **161,** 194–205.

Steel, K., Davidson, D., and Jackson, I. (1992). TRP-2/DT, a new early melanoblast marker, shows that Steel growth factor (c-kit ligand) is a survival factor. *Development* **115,** 1111–1119.

Sviderskaya, E. V., Wakeling, W. F., and Bennett, D. C. (1995). A cloned, immortal line of murine melanoblasts inducible to differentiate to melanocytes. *Development* **121,** 1547–1557.

Tajima, Y., Huang, E. J., Vosseller, K., Ono, M., Moore, M. A. S., and Besmer, P. (1998). Role of dimerization of the membrane-associated growth factor kit ligand in juxtacrine signaling: The Sl^{17H} mutation affects dimerization and stability phenotypes in hematopoiesis. *J. Exp. Med.* **187,** 1451–1461.

Vitale, R., Fawcett, D. W., and Dym, M. (1973). The normal development of the blood–testis barrier and the effects of clomiphene and estrogen treatment. *Anat. Rec.* **176,** 333–344.

Wehrle-Haller, B., and Weston, J. A. (1995). Soluble and cell-bound forms of steel factor activity play distinct roles in melanocyte precursor dispersal and survival on the lateral neural crest migration pathway. *Development* **121,** 731–742.

Wehrle-Haller, B., Morrison-Graham, K., and Weston, J. A. (1996). Ectopic c-kit expression affects the fate of melanocyte precursors in *Patch* mutant embryos. *Dev. Biol.* **177,** 463–474.

Wehrle-Haller, B., and Weston, J. A. (1997). Receptor tyrosine kinase dependent neural crest migration in response to differentially localized growth factor. *BioEssays* **19,** 337–345.

Weimbs, T., Low, S. H., Chapin, S. J., and Mostov, K. E. (1997). Apical targeting in polarized epithelial cells: There's more afloat than rafts. *Trends Cell Biol.* **7,** 393–399.

Weiss, R. R., Whitaker-Menezes, D., Longley, J., Bender, J., and Murphy, G. F. (1995). Human dermal endothelial cells express membrane-associated mast cell growth factor. *J. Invest. Dermatol.* **104,** 101–106.

Weston, J. A. (1991). Sequential segregation and fate of developmentally restricted intermediate cell populations in the neural crest lineage. *Curr. Top. Dev. Biol.* **25,** 133–153.

Williams, D. E., De Vries, P., Namen, A. E., Widmer, M. B., and Lyman, S. D. (1992). The *Steel* factor. *Dev. Biol.* **151,** 368–376.

Yoshinaga, K., Nishikawa, S., Ogawa, M., Hayashi, S., Kunisada, T., Fujimoto, T., and Nishikawa, S. (1991). Role of c-kit in mouse spermatogenesis: Identification of spermatogonia as a specific site of c-kit expression and function. *Development* **113,** 689–699.

Received for publication October 13, 1998
Revised March 1, 1999
Accepted March 2, 1999

2.7. A mono-leucine, acidic cluster associated basolateral targeting domain

THE JOURNAL OF BIOLOGICAL CHEMISTRY
Vol. 276, No. 16, Issue of April 20, pp. 12667–12674, 2001
Printed in U.S.A.

Stem Cell Factor Presentation to c-Kit

IDENTIFICATION OF A BASOLATERAL TARGETING DOMAIN*

Received for publication, September 12, 2000, and in revised form, December 28, 2000
Published, JBC Papers in Press, January 10, 2001, DOI 10.1074/jbc.M008357200

Bernhard Wehrle-Haller‡ and Beat A. Imhof

From the Department of Pathology, Centre Medical Universitaire, 1 Rue Michel-Servet, 1211 Geneva 4, Switzerland

Stem cell factor (also known as mast cell growth factor and kit-ligand) is a transmembrane growth factor with a highly conserved cytoplasmic domain. Basolateral membrane expression in epithelia and persistent cell surface exposure of stem cell factor are required for complete biological activity in pigmentation, fertility, learning, and hematopoiesis. Here we show by site-directed mutagenesis that the cytoplasmic domain of stem cell factor contains a monomeric leucine-dependent basolateral targeting signal. N-terminal to this motif, a cluster of acidic amino acids serves to increase the efficiency of basolateral sorting mediated by the leucine residue. Hence, basolateral targeting of stem cell factor requires a mono-leucine determinant assisted by a cluster of acidic amino acids. This mono-leucine determinant is functionally conserved in colony-stimulating factor-1, a transmembrane growth factor related to stem cell factor. Furthermore, this leucine motif is not capable of inducing endocytosis, allowing for persistent cell surface expression of stem cell factor. In contrast, the mutated cytoplasmic tail found in the stem cell factor mutant *Mgf*^{Sl17H} induces constitutive endocytosis by a motif that is related to signals for endocytosis and lysosomal targeting. Our findings therefore present mono-leucines as a novel type of protein sorting motif for transmembrane growth factors.

Stem cell factor (SCF)[1] belongs to the family of cell surface-anchored growth factors with highly conserved cytoplasmic domains, which includes the related colony-stimulating factor-1 (CSF-1) (1). SCF is expressed as two alternatively spliced membrane-bound forms (M1 and M2), distinguished by an exon containing a proteolytic cleavage site in the M1 form. This site is used to generate soluble growth factor from the M1 membrane-bound precursor. The membrane anchor of SCF is required for its biological activity *in vivo* because the expression of only the extracellular receptor binding domain leads to the loss of SCF-dependent cells affecting skin pigmentation, sterility, hematopoiesis, and learning (2–4). Furthermore, a point mutation, which results in the skipping of the exon coding for the cytoplasmic tail of mouse SCF (*Mgf*^{Sl17H}), leads to an altered cytoplasmic sequence that abrogates coat pigmentation and male fertility and reduces hematopoiesis (5–7). In this mouse mutant, cell surface expression of SCF is reduced, and basolateral sorting in epithelial tissues is lost (8). Hence, the cytoplasmic tail of SCF harbors information required for efficient cell surface presentation and basolateral targeting of SCF, functions that are absolutely required to fulfill its function *in vivo*.

Polarized epithelial cells exhibit an apical and basolateral surface with distinct protein compositions. Basolateral sorting of transmembrane proteins takes place in the *trans*-Golgi network (TGN) or endosomal compartments and is mediated by clathrin-coated vesicles (9). Selective incorporation of proteins into these transport vesicles is accomplished by adaptor complexes (10). Short cytoplasmic targeting sequences frequently containing either a tyrosine or di-leucine motif have been identified in the sorted proteins and are required for the interaction with adaptor complexes and for basolateral transport of the proteins (11). Recently a tyrosine-based targeting motif has been shown to bind to an epithelial specific AP1 subunit that is required for basolateral transport (12). When the tyrosine or the di-leucine sorting domains are removed from the proteins, apical instead of basolateral sorting occurs, mediated by *N*-linked carbohydrates or by association with lipid rafts (13–15). Some basolateral sorting signals resemble endocytic signals used to incorporate membrane proteins into clathrin-coated pits at the plasma membrane, suggesting that basolateral sorting and endocytosis are regulated by similar mechanisms. For example, the macrophage Fc receptor and the invariant chain of the class II major histocompatibility complex contain a di-leucine-based determinant that is used for basolateral sorting as well as endocytosis (16, 17). Furthermore, many membrane proteins carry several different targeting determinants, which enables them to shuttle between the basolateral plasma membrane and endosomes (18, 19).

Although SCF does not have typical tyrosine or di-leucine sorting sequences in its cytoplasmic tail, it is delivered directly to the basolateral cell surface in epithelial cells and does not accumulate in an intracellular compartment (8). Consequently, SCF remains at the cell surface until the extracellular domain is proteolytically shed within 0.5 (M1) to 5 (M2) h depending on the respective splice form (20). Because basolateral sorting is critical for the proper biological function of SCF, we tried to identify the possibly novel basolateral targeting determinant in the cytoplasmic tail of SCF. To do so, we used reporter constructs consisting of extracellular green fluorescent protein (GFP)-tagged SCF or chimeras of the extracellular domain of the interleukin-2 receptor α-chain (Tac) fused to the transmembrane and cytoplasmic sequences of SCF. In these chimeras the normal intracellular domain of SCF is left intact, allowing optimal interaction of the latter with the sorting machinery of

* This work was supported by the Swiss National Science Foundation Grants 31-52727-97 (to B. W.-H.) and 31-49241-96 (to B. A. I.). The costs of publication of this article were defrayed in part by the payment of page charges. This article must therefore be hereby marked "*advertisement*" in accordance with 18 U.S.C. Section 1734 solely to indicate this fact.

‡ To whom correspondence should be addressed. Tel.: 41-22-702-5735; Fax: 41-22-702-5746; E-mail: Bernhard.Wehrle-Haller@medecine.unige.ch.

[1] The abbreviations used are: SCF, stem cell factor; CSF-1, colony-stimulating factor-1; TGN, *trans*-Golgi network; GFP, green fluorescent protein; EGFP, enhanced green fluorescent protein; Tac, interleukin-2 receptor α-chain; MDCK, Madin-Darby canine kidney; PACS, phosphofurin acidic cluster-sorting.

polarized cells and the identification of critical targeting domains by mutagenesis.

EXPERIMENTAL PROCEDURES

SCF Chimeras and Site-directed Mutagenesis—cDNA for SCF and Tac were kindly provided by Drs. John Flanagan (Harvard Medical School, Boston) and Pierre Cosson (University of Geneva, Switzerland), respectively. Mouse CSF-1 and mouse tyrosinase cDNAs were kindly provided by Drs. Willy Hofstetter (MMI, Bern, Switzerland) and Friedrich Beermann (ISREC, Lausanne, Switzerland), respectively. SCF-GFP chimeras were constructed in pcDNA3 (Invitrogen, Groningen, The Netherlands) by inserting the enhanced GFP sequence (CLONTECH Laboratories, Palo Alto, CA) together with a Myc tag 5′ into the exon 5/6 junction of SCF (SSTLGPEK/DSRV), which resulted in the following sequence: SSTLGPEQKLISEEDLGQS··IV . . . (enhanced GFP) . . . YK··TGPEK/DSRV (single letter amino acid code; the sequence of the Myc tag is underlined). To prevent translation at internal start sites producing cytoplasmic GFP, we replaced the start codon of GFP with nucleotides coding for a *Cla*I site. A unique *Pin*AI site was introduced C-terminal to the GFP sequence to swap wild-type and mutant cytoplasmic tail sequences at this site.

To generate the Tac-SCF chimera (all in pcDNA3), the transmembrane and cytoplasmic domains of SCF were swapped at a unique *Bgl*II site in Tac located at a homologous leucine (L) and glutamine (Q) residue upstream of the transmembrane sequences of SCF and Tac. This resulted in the sequence: . . . SIFTTD**LQ**WTAMALP . . . at this position (conserved LQ is bold and transmembrane residues of SCF are underlined).

The Tac-CSF-1 and Tac-tyrosinase (Tac-tyr) chimeras were constructed in a similar way. CSF-1 and tyrosinase transmembrane and cytoplasmic sequences were polymerase chain reaction amplified with a *Bgl*II site containing the forward primers (CSF-1: AACAGATCTCCAGATCCCTGAGTCTG; tyrosinase: AACAGATCTCCAAGCCAGTCGTATCTGG) at a common glutamine residue (Q) and swapped with the Tac sequence of this region creating the respective junctional sequences: Tac-CSF-1: . . . SIFTDL**Q**IPESVFHLLV . . . and Tac-tyr: . . . bold, and the respective transmembrane region is underlined). Tac-EGFP was cloned by polymerase chain reaction amplification of EGFP with a *Hin*dIII-containing primer and inserted at a unique *Hin*dIII site at the extreme C terminus of Tac (TIQASSstop) resulting in the new junctional sequence (TIQASTMV . . . (EGFP)).

Site-specific mutagenesis of the cytoplasmic tail of SCF was performed using polymerase chain reaction overlap extension. Two overlapping polymerase chain reaction fragments containing a specific mutation were amplified with external primers (containing either the *Pin*AI or *Bgl*II site for SCF-GFP or Tac-SCF chimeras, respectively) and swapped with the wild-type sequence of the cytoplasmic tail. All constructs were verified by dideoxy sequencing. A list of primers used to generate the different constructs listed in Fig. 2 can be provided upon request.

Cell Culture, Live Fluorescence Microscopy, and Immunocytochemistry—MDCK II cells were kindly provided by Dr. Karl Matter (University of Geneva, Switzerland) and cultured in Dulbecco's modified Eagle's medium (Life Technologies, Paisley, Scotland) supplemented with 10% fetal calf serum (Inotech, Dottikon, Switzerland). Cells at 60% confluence were transfected using calcium phosphate as described (21), and stable clones were selected with 0.6 mg ml^{-1} G418 (Life Technologies). For each construct, at least two different clones were analyzed for the steady-state distribution of SCF-GFP fluorescence or anti-Tac immunohistochemistry. To visualize the GFP fluorescence, cells were grown to confluence on glass coverslips. Prior to observation, the culture medium was exchanged with F-12 medium (Life Technologies) supplemented with 10% fetal calf serum to reduce autofluorescence, which is higher in Dulbecco's modified Eagle's medium. Cells were mounted on an inverted confocal microscope (LSM-410, Zeiss, Oberkochen, Germany) and visualized with standard fluorescein isothiocyanate optics. To reveal the localization of transfected Tac-SCF chimeras or endogenous E-cadherin in SCF-GFP-transfected MDCK II cells, monolayers of stable transfected clones grown on glass coverslips were fixed with 4% paraformaldehyde in phosphate-buffered saline for 5 min. Cells were washed with phosphate-buffered saline, permeabilized with 1% Triton X-100 (Sigma Chemical Co., St. Louis, MO) in phosphate-buffered saline and blocked with 1% bovine serum albumin (Sigma) in phosphate-buffered saline. Cells were then stained as indicated with either anti-Tac monoclonal antibody 7G7 (22) or with anti-Arc-1 monoclonal antibody (23), which is directed against canine E-cadherin. After washing, bound antibodies were revealed with Texas Red-coupled anti-mouse antibodies (Southern Biotechnoloy Associates Inc., Birmingham, AL). Fluorescence was subsequently analyzed on a confocal microscope as indicated above. Contrast enhancement was performed in Photoshop (Adobe Systems Inc., San Jose, CA).

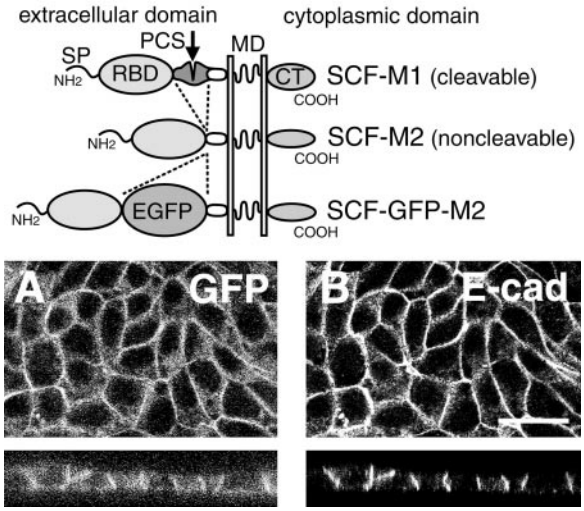

FIG. 1. **SCF-GFP chimeras localize to the basolateral aspect of polarized MDCK II cells.** Confocal microscopy of wild-type membrane-bound (M2) SCF-GFP proteins (*A*, fluorescein isothiocyanate channel) and anti-E-cadherin staining (*B*, Texas Red channel) of fixed MDCK II is shown. A corresponding Z-scan of the monolayer is shown below. Note the overlap of staining in lateral regions of individual cells. Above the *panels*, a schematic view of the two differentially spliced wild-type forms of SCF (SCF-M1, cleavable and SCF-M2, noncleavable) and the chimera of SCF with GFP (SCF-GFP) is shown. *SP*, signal peptide; *RBD*, SCF receptor binding domain; *PCS* (*arrow*), proteolytic cleavage site; *MD*, membrane domain; *CT* cytoplasmic tail. The *bar* in *B* corresponds to 24 μm.

Endocytosis Assay—Wild-type and mutant Tac-SCF constructs were transfected into SV40-transformed African green monkey kidney cells (COS-7) using Fugen 6 according to the manufacturer's recommendation (Roche, Basel, Switzerland). 2 days after transfection, cells were cooled on ice, and anti-Tac antibodies were added for 1 h at 1 $\mu g\ ml^{-1}$. Prior to warming, unbound antibodies were washed away, and internalization was allowed for 30 min at 37 °C in Dulbecco's modified Eagle's medium supplemented with 10% fetal calf serum. Antibodies that remained cell surface-bound were subsequently removed with ice-cold acidic glycine buffer (0.1 M, pH 2.5). Cells were then fixed with 4% paraformaldehyde for 5 min, washed, permeabilized, blocked, and stained with Texas Red-conjugated anti-mouse antibodies (Southern Biotech) to reveal internalized anti-Tac·Tac-SCF complexes (see above). Cells were viewed on an Axiovert 100 microscope (Zeiss) equipped with a digital camera (C4742-95, Hamamatsu Photonics, Shizuoka, Japan) and the Openlab software (Improvision, Oxford, UK). Contrast enhancement was done in Photoshop (Adobe). The experiment was performed three times with qualitatively similar results, and representative examples of cells from one experiment were chosen for Fig. 7.

RESULTS

Leucine 26 Is Required for Basolateral Targeting of SCF—GFP was inserted into the alternatively spliced extracellular domains of both membrane-bound variants of SCF and transfected into polarized epithelial MDCK II cells (Fig. 1). Confocal microscopy revealed that both wild-type constructs accumulated in basal and lateral membranes where they colocalized with E-cadherin, a marker for the lateral membrane compartment in polarized epithelial cells (shown for M2 variant; Fig. 1).

To identify the motif in the cytoplasmic tail of SCF responsible for basolateral sorting, we created various cytoplasmic SCF mutants of the membrane-bound (M2) form of GFP-tagged SCF (SCF-GFP) (Fig. 2*A*). Mutants lacking the last eight C-terminal amino acids (d36, d29) still localized to the basolateral membrane. However, when 15 or more amino acids were deleted (d22, d12), SCF-GFP was located on the apical membrane

A

1 10 20 30 36	Construct 1	Polarity 2
KKKQSSLTRAVENIQINEEDNEISMLQQKEREFQEV	wt	BL
KKKQSSLTRAVENIQINEEDNEISMLQQKEREFQE.	d36	BL
KKKQSSLTRAVENIQINEEDNEISMLQQ.....	d29	BL
KKKQSSLTRAVENIQINEEDN.....	d22	AP
KKKQSSLTRAV.....	d12	AP
KKKQSSLTRAVENIQINEED.....KEREFQEV	d21-28	AP
KKKQSSLTRAV.....KEREFQEV	d12-28	AP
KKKQ.....NEISMLQQKEREFQEV	d5-20	AP
KKKQSSLTRAV.....NEISMLQQKEREFQEV	d12-20	BL/AP
KKKQSSLTRAVENIQINEEDNEI**A**MLQQKEREFQEV	S24A	BL
KKKQSSLTRAVENIQINEEDNEI**D**MLQQKEREFQEV	S24D	BL
KKKQSSLTRAVENIQINEEDNEISM**A**QQKEREFQEV	L26A	AP
KKKQSSLTRAVENIQINEEDNEIS**AA**QQKEREFQEV	M25A/L26A	AP
KKKQSSLTRAVENIQINEEDNEIS**A**LQQKEREFQEV	M25A	BL
KKKQSSLTRAVENIQIN**E**KDNEISMLQQKEREFQEV	E19K	BL
KKKQSSLTRAVENIQINEEDN**A**ISMLQQKEREFQEV	E22A	BL
KKKQSSLTRAVENIQIN**AAA**NEISMLQQKEREFQEV	E-D18A-A	BL/AP

B

```
Human SCF:        KKRQP.SLTRAVENIQI..NEEDNEISMLQEKEREFQEV
Mouse SCF:        KKKQS.SLTRAVENIQI..NEEDNEISMLQQKEREFQEV
Chicken SCF:      KKTHPKSRPESNETIQCHGCQEENEISMLQQKEKEHLQV
Salamander SCF:   KMKHRESGSGCEPTAPCPVRKEAEQASMLNQTGKAVHLV

Consensus:        K-----S--------------E----SML---------V
```

FIG. 2. **Cytoplasmic tail sequences of wild-type and mutant SCF.** *A*, alignment of sequences of wild-type and cytoplasmic tail mutants of mouse SCF and their respective steady-state distribution in MDCK II cells. *Construct 1*, the name of the constructs represents the site of amino acid deletions (marked with a *dotted line*) or point mutations (*bold* and *underlined*). *Polarity 2*, steady-state localization of GFP and Tac SCF chimeric proteins in polarized MDCK II cells (*wt*, wild-type; *BL*, basolateral; *AP*, apical). *B*, Clustal W alignment of different SCF cytoplasmic tail sequences. GenBank accession numbers are M59964 (human), M57647 (mouse), D13516 (chicken), and AF119044 (salamander).

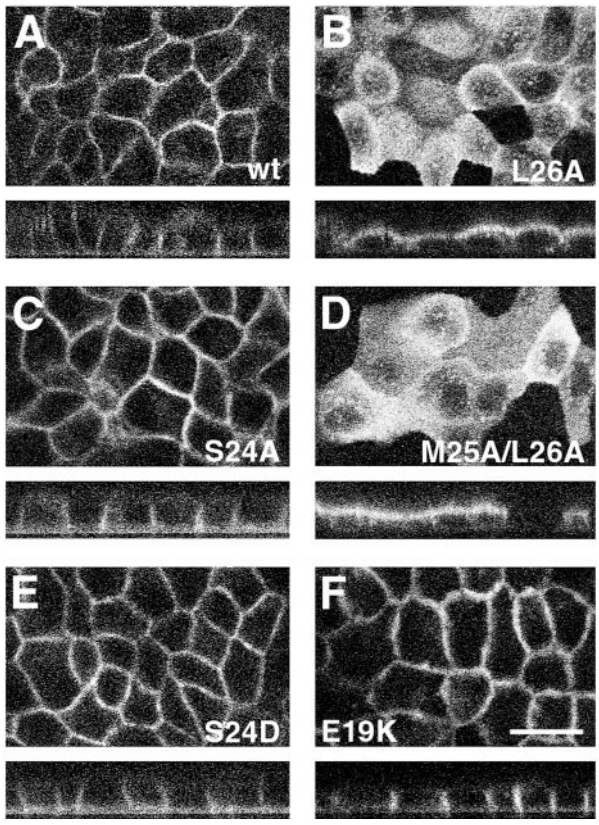

FIG. 3. **Leucine 26 is required for basolateral targeting of SCF-GFP constructs in polarized MDCK II cells.** Confocal microscopy (fluorescein isothiocyanate channel) of live wild-type (*A*) and mutant SCF-GFP-M2 (*B–F*) expressing confluent MDCK II cells. Basolateral staining is lost upon mutation of leucine 26 to alanine (*B*), or methionine 25 and leucine 26 to a double alanine (*D*). Replacement of serine 24 by alanine (*C*) or aspartic acid (*E*), as well as the change of glutamic acid 19 to lysine (*F*), did not alter basolateral localization of the constructs. Below each *panel* a corresponding Z-scan is shown. The *bar* in *F* corresponds to 24 μm.

and showed no basolateral expression. The critical region for basolateral sorting was demonstrated to reside within the sequence ^{21}NEISMLQQ^{28} because an internal deletion mutant (d21–28) also localized to the apical membrane. Interestingly, to be functional, it appeared that this sequence must be considerably separated from the membrane; deletion of intervening amino acids proximal to the membrane (d5–20) interfered with basolateral sorting. Increasing the distance of the ^{21}NEISMLQQ^{28} motif from the membrane by reinserting amino acids 5–11 (d12–20) only partially rescued basolateral targeting, suggesting that other amino acids important for basolateral targeting are present N-terminal to the ^{21}NEISMLQQ^{28} motif (see below).

Sequence comparison among human, mouse, chicken, and salamander SCF (24) revealed the residues ^{24}SML^{26} as being completely conserved within the ^{21}NEISMLQQ^{28} motif (Fig. 2*B*). This sequence encompasses a serine at position 24 as well as a di-hydrophobic methionine-leucine at positions 25 and 26, respectively (see above). To test whether a portion of this motif was required for basolateral sorting of SCF, we created various point mutations encompassing these conserved residues (Fig. 2*B* and Fig. 3). The modification of serine 24 to either an alanine (S24A) or to an aspartic acid (S24D) resembling a phosphoserine, as well as the replacement of the conserved glutamic acid 19 by lysine (E19K) had no effect on basolateral targeting (Fig. 3, *C, E, F*). In contrast, the modification of leucine 26 to either alanine (L26A) or the replacement of methionine 25 and leucine 26 by a double-alanine (M25A/L26A) led to apical accumulation of the mutant SCF-GFP constructs (Fig. 3, *B* and *D*). The analysis of the SCF-GFP chimeric mutant proteins thus suggests that the leucine at position 26 of the cytoplasmic tail of SCF is critical for basolateral sorting of SCF. However, it is not known whether this putative basolateral signal requires the context of dimerized SCF molecules or whether it can provide intracellular targeting information independently.

Extracellular SCF Sequences Are Not Required for Basolateral Targeting—Dimer formation involving the extracellular domain of SCF or lateral association of the extracellular and/or intracellular portions of SCF with other proteins that contain targeting information may in fact be responsible for the polarized expression of SCF. Therefore, to test the ability of the cytoplasmic targeting sequence of SCF to mediate polarized expression independently of the extracellular domain, we replaced the latter with the extracellular domain of Tac (Fig. 4) (22). Wild-type Tac as well as Tac with a C-terminally fused EGFP accumulated apically when expressed in MDCK II cells (Fig. 4*A*). In contrast, Tac-SCF chimeras expressing the wild-type cytoplasmic domain of SCF localized to basolateral membranes in a manner identical to the SCF-GFP wild-type constructs (Fig. 4*B*). Likewise, constructs involving extracellular Tac with deletion mutations of the cytoplasmic tail of SCF (d29, basolateral, Fig. 4*C*; d22, apical, Fig. 4*D*; d21–28, apical, Fig. 4*E*; d5–20, apical (not shown); and d12–20, basolateral/apical, Fig. 4*F*), showed identical basolateral sorting behaviors compared with the mutant SCF-GFP constructs. This indicates that the extracellular domain of SCF is not required for basolateral targeting and that the basolateral targeting motif of SCF contained within its cytoplasmic portion is sufficient to direct the Tac extracellular domain basolaterally. Moreover, sequences N-terminal to methionine 25 and leucine 26 removed in the d12–20 mutation influence the efficiency of basolateral

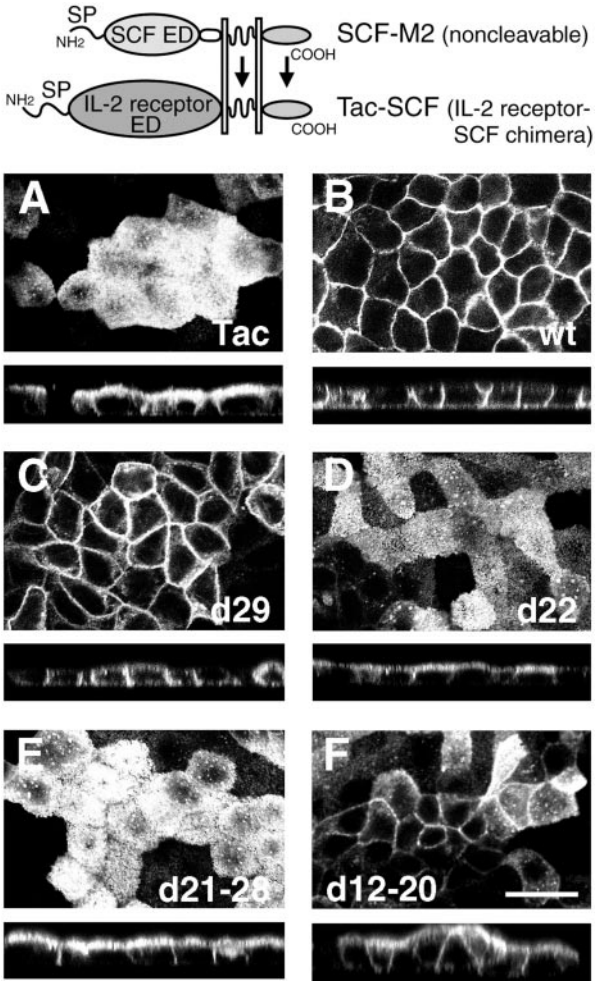

FIG. 4. **The basolateral targeting determinant in SCF acts independently of the extracellular domain.** Confocal microscopy of anti-Tac antibody stained and fixed MDCK II cells stable transfected with Tac-EGFP (*A*) and wild-type (*B*) or mutant (*C–F*) Tac-SCF chimeric constructs is shown. A scheme representing the Tac-SCF chimera is shown above the *panels*. The fusion protein consists of the extracellular domain of Tac and the transmembrane and cytoplasmic sequence of SCF. *A*, unmodified Tac with C-terminal EGFP fusion of which the anti-Tac is antibody-stained. *B*, Tac-SCF chimera with wild-type SCF sequences. *C*, deletion of the last 8 amino acids from the cytoplasmic tail of SCF does not alter basolateral targeting of the Tac hybrid (d29). However, removal of the last 15 amino acids (d22) (*D*) or amino acids 21–28 (*E*) resulted in an apical localization of Tac-SCF. The deletion of amino acids N-terminal to the leucine 26-containing region (d12–20) resulted in basolateral as well as apical localization of the chimeric proteins (*F*). Below each *panel*, a corresponding Z-scan is shown. *SP*, signal peptide of SCF and Tac, respectively; *ED*, extracellular domain. The *bar* in *F* corresponds to 24 μm.

targeting (Fig. 4*F*).

Efficient Basolateral Targeting Is Mediated by an Acidic Cluster N-terminal to the Monomeric Leucine Determinant—Although it is evident that the leucine residue at position 26 is critical for basolateral targeting it is not known whether a second hydrophobic residue (methionine 25) as found in all di-leucine-like determinants is equally required for basolateral sorting of SCF. Moreover, the region N-terminal to the ML motif which is also required for efficient basolateral targeting (^{12}ENIQINEED^{20}) bears a domain important for SCF sorting as well.

To address the first question, we replaced methionine 25 with an alanine residue and analyzed the distribution of the Tac-SCF construct at steady-state conditions. In contrast to the leucine 26 to alanine mutation, the change of methionine 25 to alanine did not affect basolateral targeting of Tac-SCF (Fig. 5, *A* and *B*). Moreover, replacement of methionine by leucine in an attempt to create a classical di-leucine determinant led to intracellular and apical localization of Tac-SCF (not shown). Therefore, this finding revealed the existence of a novel type of leucine-based basolateral targeting signal in SCF, which does not require a second hydrophobic amino acid to be functional.

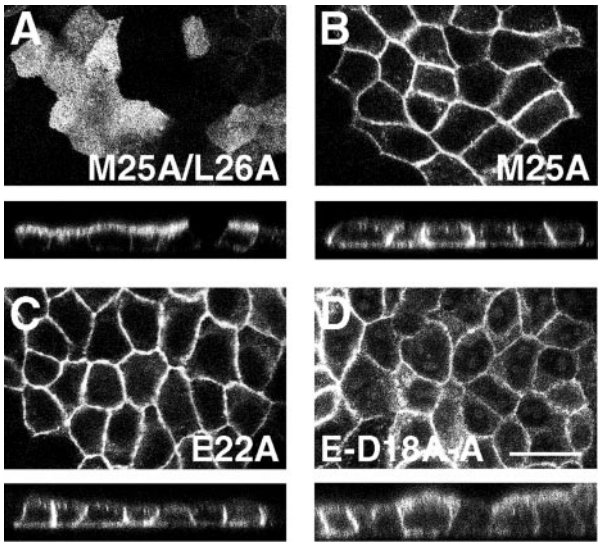

FIG. 5. **An acidic cluster-assisted monomeric leucine-dependent basolateral targeting determinant.** Confocal microscopy of anti-Tac antibody-stained fixed MDCK II cells stable transfected with Tac-SCF point mutations of hydrophobic and acidic amino acids is shown. *A*, apical localization of the Tac-SCF chimera carrying a double alanine substitution of methionine 25 and leucine 26 (M25A/L26A). *B*, the single point mutation at methionine 25 to alanine did not alter basolateral targeting. Similarly, the point mutation of glutamic acid 22 to alanine (E22A) did not influence basolateral targeting (*C*). Alanine substitution of the acidic cluster ^{18}EED^{20} (E-D18A-A) resulted in basolateral as well as apical accumulation of Tac chimeric proteins (*D*). Below each *panel*, a corresponding Z-scan is shown. The *bar* in *D* corresponds to 24 μm.

Analysis of sequences N-terminal to leucine 26 which are absent in the d12–20 mutation reveal an unusually high concentration of acidic amino acids. An acidic cluster N-terminal to an FI motif has recently been identified as a basolateral targeting signal in the furin protease (25). To test whether the acidic cluster in SCF contributes to basolateral sorting or whether other acidic amino acid residues localized closely to the leucine residue are critical, we mutated glutamic acid 22 (^{22}E*XX*ML^{26}) to alanine (Fig. 5C). In addition, we replaced glutamic acid 19 with a lysine to destroy the acidic cluster formed by residues ^{18}EED^{20} (Fig. 3*F*). Neither modification had any effect on basolateral targeting of Tac or of the GFP chimeric SCF constructs. However, the replacement of all three acidic residues 18, 19, and 20, with alanine residues (E-D18A-A) did alter basolateral sorting of the Tac-SCF chimeras. In clones expressing relatively low amounts of the Tac-E-D18A-A chimera, basolateral targeting was still efficient; however, in clones expressing higher amounts of mutant Tac-SCF, both basolateral and apical surface staining was detected (Fig. 5*D*). Anti-Tac staining of these clones strongly resembled the phenotype already seen with the d12–20 mutation (Fig. 4*F*). These data suggest that the removal of the acidic cluster (^{18}EED^{20}) is the cause of the phenotype of the d12–20 mutation which results in a reduced efficiency of basolateral transport mediated by the monomeric leucine determinant.

Comparison of the Basolateral Targeting Domain of SCF with That of CSF-1—SCF belongs to a large family of transmembrane growth factors that play important roles during development, tissue homeostasis, and hematopoiesis. Based on

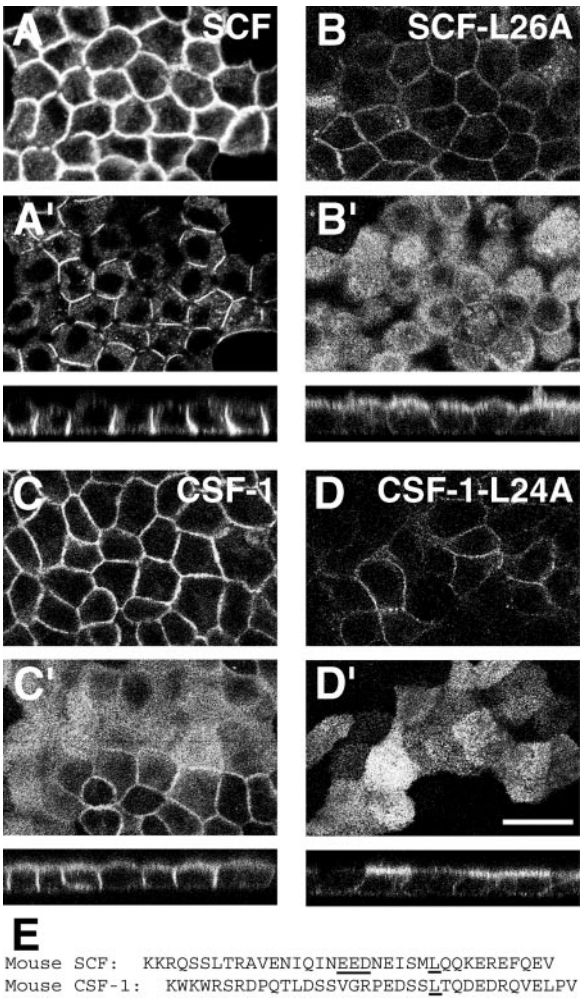

FIG. 6. **Functional conservation of the leucine determinant in CSF-1.** Confocal microscopy of anti-Tac antibody-stained, fixed MDCK II cells stable transfected with wild-type and leucine to alanine (L26A, SCF; L24A, CSF-1) mutation of Tac-SCF (*A* and *B*) and Tac-CSF-1 (*C* and *D*) chimeras is shown. A confocal section at the level of the nucleus (*A–D*) and the apical cell surface (*A′–D′*) is shown to appreciate the differences between basolateral and apical expression of wild-type *versus* mutant chimeric constructs at steady-state levels. Below each *panel*, a corresponding Z-scan is shown. The *bar* in *D′* corresponds to 24 μm. *E*, comparison of the cytoplasmic tail sequences of mouse SCF with mouse CSF-1. The basolateral targeting sequences for SCF identified in this study (acidic cluster and leucine 26) and the functionally conserved leucine 24 in CSF-1 are *underlined*.

sequence and functional homologies, SCF is most closely related to CSF-1 (26). The similarities between the two factors extend to their respective receptor tyrosine kinases, c-Fms, the receptor for CSF-1, and c-Kit, the receptor for SCF, which are structurally conserved and which have evolved by chromosomal duplication (27). Sequence comparison (Fig. 6*E*) of the cytoplasmic domain of CSF-1 with that of SCF reveals in addition to the most C-terminal valine residue, a leucine-containing motif at a position comparable to the basolateral targeting domain of SCF. However, the cluster of acidic amino acids N-terminal to this leucine motif is not conserved in CSF-1. To determine the basolateral sorting activities of CSF-1, we expressed the transmembrane and the cytoplasmic tail domains fused to the extracellular domain of Tac and studied its steady-state distribution in confluent monolayers of MDCK II cells (Fig. 6). The wild-type Tac-CSF-1 chimeric construct was expressed on the basolateral surface of MDCK II cells (Fig. 6*C*). However, a considerable amount of Tac-CSF-1 was also detected on the apical surface of confluent MDCK II cells (Fig. 6*C′*), a situation unlike the one observed with wild-type Tac-SCF chimeras (Fig. 6*A* and *A′*). The distribution of Tac-CSF-1 on basolateral as well as apical surfaces gave the impression that this construct is not sorted. To determine whether the homologous leucine in CSF-1 can interact with the sorting machinery of the cell, we mutated leucine 24 of CSF-1 to alanine. The respective Tac chimera (Tac-CSF-L24A) accumulated apically (Fig. 6*D′*), similar to Tac-SCF-L26A (Fig. 6*D′*), suggesting that the leucine at the respective position in CSF-1 is nevertheless recognized as a basolateral sorting signal but that the efficiency of basolateral transport is lower compared with that of wild-type SCF. This difference may depend on the presence of the acidic cluster in SCF which is absent from CSF-1.

In Contrast to Wild-type, the Mutant Cytoplasmic Tail of Mgf^{Sl17H} SCF Induces Constitutive Endocytosis—Many basolateral sorting determinants have been shown to induce endocytosis, for example the basolateral targeting motif (ML) in the invariant chain of the major histocompatibility complex II also mediates endocytosis of the respective proteins (11, 28). Therefore, we tested whether the wild-type cytoplasmic tails of SCF, expressed as a Tac chimera (Tac-SCF), are able to internalize Tac-SCF·anti-Tac complexes in nonpolarized COS-7 cells. Anti-Tac antibodies were bound to transfected cells in the cold. Subsequently, Tac-SCF·anti-Tac antibody complexes were allowed to internalize at 37 °C and visualized after acid removal of cell surface remaining anti-Tac antibodies. Wild-type Tac-SCF-expressing cells (Fig. 7*B*) as well as cells expressing various C-terminal deletions encompassing the basolateral sorting signal showed a similar low amount of internalized anti-Tac antibodies (not shown). This suggests that the mono-leucine determinant in SCF does not induce endocytosis, a finding that is consistent with the persistent cell surface expression of membrane-bound SCF.

In contrast to wild-type SCF, GFP and Tac-SCF chimeras containing the cytoplasmic tail of the *Mgf*^{Sl17H} mutation accumulated in intracellular vesicular structures (Tac-SCF-17H, Fig. 7*D*; see also Ref. 8). This intracellular accumulation of the mutant constructs could be the result of retention of newly synthesized chimeric proteins in the endoplasmic reticulum as suggested by Briley and colleagues (29) or of endocytosis of cell surface SCF. To determine, whether the intracellular steady-state localization of Tac-SCF-17H in polarized MDCK II was the result of endocytosis (Fig. 7*D*), we compared the localization with that of Tac-tyr. Tyrosinase is a protein that carries an established signal for endocytosis and lysosomal/melanosomal targeting and is therefore constitutively internalized from the cell surface (30). Interestingly, in polarized MDCK II cells, Tac-tyr localized to intracellular vesicular structures (Fig. 7*G*), resembling the staining seen for the Tac-SCF-17H construct (Fig. 7*D*). Sequence analysis of the cytoplasmic domain of *Mgf*^{Sl17H} (KYAATERERISRGVIVDVSTLLPSHSGW; Ref. 5) revealed a sequence homologous to the signal for endocytosis and lysosomal/melanosomal targeting, identified in tyrosinase, LIMP II and CD3γ (D^{17}*XXX*LL^{22}) (30–32). Furthermore, mutation of the leucine residues (Leu^{21}-Leu^{22}), which are part of this putative motif in *Mgf*^{Sl17H} to alanines, resulted in the loss of intracellular but led to apical accumulation of Tac-17H-LLAA in polarized MDCK cells (Fig. 7*J*). In addition, using the anti-Tac internalization assay in COS-7 cells, we tested whether the intracellular localization of the *Mgf*^{Sl17H} mutant was caused by increased endocytosis of surface-expressed *Mgf*^{Sl17H} Tac chimeras. Indeed, compared with wild-type Tac-SCF, significantly more Tac-SCF-17H·anti-Tac complexes were internalized (Fig. 7*E*), and a similar intracellular staining pattern was observed as for the Tac-tyr construct (Fig. 7*H*). Fur-

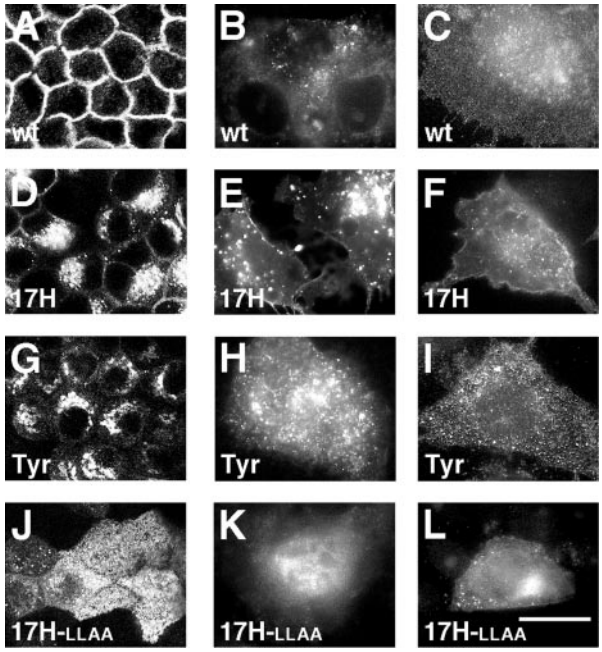

FIG. 7. **Endocytosis of Mgf^{Sl17H} mutant Tac-SCF by a lysosomal targeting signal.** Confocal microscopic sections at the level of the nucleus or apical surface of anti-Tac antibody-labeled confluent MDCK II stable transfected with different Tac-SCF constructs (*A*, *D*, *J*) and Tac-tyrosinase (Tac-tyr, *G*) are shown. Only a weak staining of intracellular Tac chimeras is detected in wild-type Tac-SCF-expressing cells (*A*). In cells transfected with the Tac-SCF-17H (*D*) construct, extensive intracellular vesicular anti-Tac staining can be observed, which resembled cells transfected with the Tac-tyr chimera (*G*). Mutation of the di-leucine of the putative internalization motif of Tac-SCF-17H to a di-alanine (17H-LLAA) resulted in a loss of intracellular but led to apical localization (*J*). Standard fluorescence microscopy of endocytosed anti-Tac antibody bound to wild-type and mutant Tac-SCF or Tac-tyr constructs transiently transfected into COS-7 cells is also shown. After 30 min at 37 °C, internalized Tac-SCF (or tyr)/anti-Tac antibodies complexes were visualized with (*B*, *E*, *H*, *K*) or without (*C*, *F*, *I*, *L*) acid removal of cell surface-bound noninternalized antibodies. Wild-type Tac-SCF proteins were not internalized during the 30-min incubation period (*B*). In contrast, Tac-SCF-17H mutant proteins accumulated in large intracellular vesicles (*E*). Likewise, Tac-tyr constructs were internalized efficiently (*H*). However, the di-leucine mutation in Tac-SCF-17H (17H-LLAA) abolished the capacity to internalize cell surface-bound anti-Tac antibodies (*K*). Comparable levels of the different Tac-SCF constructs were initially expressed on the COS-7 cell surfaces as illustrated by staining of parallel cultures from which the anti-Tac antibody was not removed from the cell surface (*C*, *F*, *I*, *L*). The *bar* in *L* corresponds to 24 μm.

thermore, internalization of the Tac-SCF-17H chimera was blocked by the di-leucine mutation (17H-LLAA; Fig. 7*K*). This suggests that the reduced amount of cell surface SCF observed in the *Mgf*^{Sl17H} mutation (8, 33) is caused by constitutive removal of the *Mgf*^{Sl17H} mutant SCF from the cell surface by endocytosis. Therefore, the *Mgf*^{Sl17H} mutation represents a molecular gain of function mutation with respect to the endocytosis of SCF.

DISCUSSION

An Acidic Cluster Assists the Leucine-dependent Basolateral Targeting Signal in SCF—We identified here a novel motif in a transmembrane growth factor that is used for basolateral targeting but not for endocytosis. Both an acidic cluster and a critical leucine residue are required for efficient basolateral targeting of SCF. Although the leucine is indispensable for basolateral transport, the presence of the acidic cluster enhances the efficiency of basolateral sorting. Because the acidic cluster is not absolutely required for basolateral targeting, it is unlikely that the two motifs form a single sorting determinant. Interestingly, a basolateral targeting motif has been described

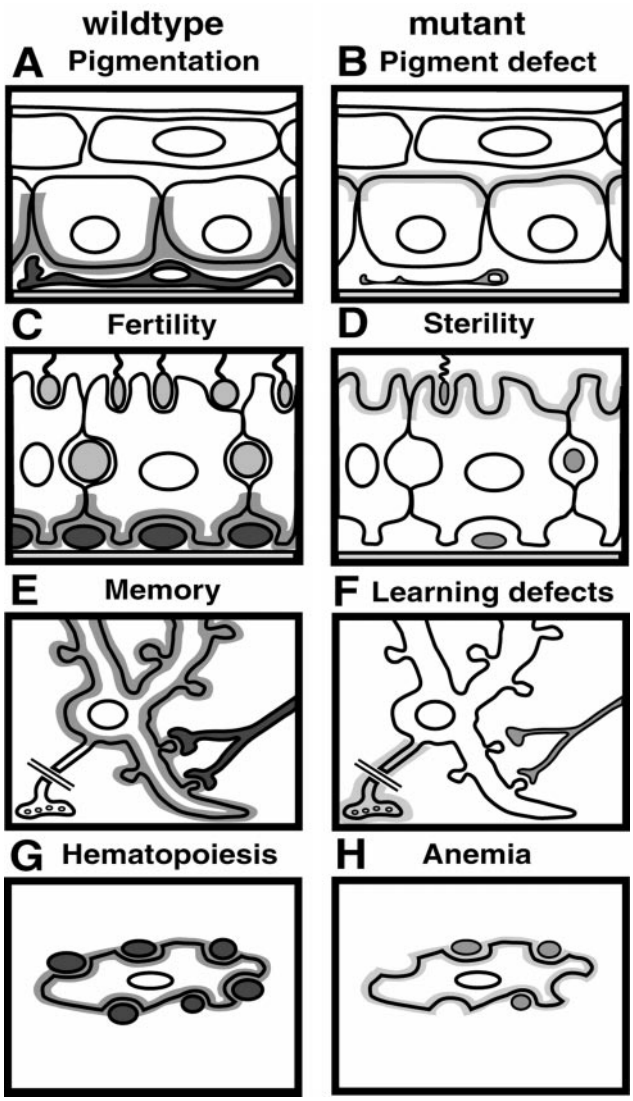

FIG. 8. **Multiple biological effects of cytoplasmic mutations in SCF.** Illustration of the polarized expression of SCF in basolateral and dendritic aspects of basal keratinocytes (*A*), Sertoli cells (*C*), and neurons (*E*), respectively. Cell surface expression of SCF is also found in nonpolarized stromal cells of the bone marrow or dermal fibroblasts in the skin (*G*). Cell surface SCF protein is represented by *gray* shading and c-Kit-expressing (SCF-dependent) cells by *dark* shading (*A*, *C*, *E*, and *G*). The mutation of the cytoplasmic targeting determinants of SCF leads to apical or axonal accumulation as well as reduced cell surface expression (*light* shading in *B*, *D*, *F*, and *H*). Consequently, pigmentation defects (*B*), sterility in males (*D*), and learning (*F*) and hematopoietic defects are observed in the respective tissues (*H*) (affected cells are indicated by reduced size, numbers, and *gray* shading; *B*, *D*, *F*, and *H*). Note, dendritic and axonal localization of wild-type and cytoplasmic mutant SCF protein in neurons is extrapolated from the polarized expression patterns in epithelial cells reported in this paper. The loss of spatial learning has so far only been demonstrated in mice lacking transmembrane and cytoplasmic sequences of SCF (*Mgf*^{Sld}) (4), a mutant form of SCF which is secreted from apical aspects of polarized epithelia (8). *wt*, wild-type tissue; *mutant*, tissue expressing cytoplasmic tail mutants of SCF.

for the polymeric Ig receptor, which does not belong to the family of tyrosine or di-leucine determinants and which does not mediate endocytosis. This critical targeting domain consists of a single valine located in a β-turn and two critical residues 3 and 4 amino acids N-terminal to it. Mutation of valine to alanine reduces basolateral targeting and destabilizes the β-turn (34). In addition, the amino acids N-terminal to the valine which do not participate in the β-turn are also required for efficient basolateral sorting and form a second, valine-

independent, functional targeting domain (35). Based on these similarities, it is possible that leucine 26 of SCF is part of a β-turn or loop, exposing its hydrophobic side chain in such a way that it could bind to the adaptor complex of clathrin-coated vesicles. In addition, many di-leucine sorting motifs have been described which require critical N- or C-terminally located acidic residues as described for the furin protease (25), the low density lipoprotein receptor (16) and the invariant chain of major histocompatibility complex class II (17). In contrast to these determinants, in which the acidic amino acids are essential for basolateral targeting, the acidic cluster in SCF is partially dispensable serving however to increase the fidelity of the basolateral sorting process. Members of the recently identified phosphofurin acidic cluster-sorting (PACS) family of adaptor proteins, which bind to clusters of acidic amino acids, are involved in directing TGN localization and plasma membrane sorting (18, 19). Interestingly, intracellular sorting of the furin protease by PACS is regulated by the phosphorylation of critical serine residues adjacent to a cluster of acidic amino acids. The same PACS binding, acidic cluster which directs TGN localization, is also required for basolateral sorting of furin (25). Although PACS may bind to the acidic amino acid cluster in SCF and thereby increasing the fidelity of the basolateral sorting process in the TGN, there is no indication that this is a phosphorylation-dependent interaction involving the conserved serine residue at position 24. However, in the absence of such acidic clusters as in the cytoplasmic tail of CSF-1, reduced protein recognition at the level of the TGN could affect the fidelity of basolateral targeting compared with SCF. Consequently this inefficiency of basolateral sorting might lead to the apical accumulation of CSF-1 by an *N*-glycan-dependent apical targeting pathway (13).

Mgf^{Sl17H}, a Gain of Function Mutation Leading to Constitutive Endocytosis of Mutant SCF—Many basolateral targeting signals resemble those for coated pit localization and endocytosis. In contrast to the protease furin or the invariant chain, wild-type SCF is expressed at the cell surface and is not endocytosed. Interestingly, the cytoplasmic tail of SCF found in the Mgf^{Sl17H} mutation has a high capacity for inducing endocytosis when expressed as a Tac chimera. Analysis of the cytoplasmic tail of the Mgf^{Sl17H} mutant reveal a match of sequence between KYAATERERISRGVIVDVSTLLPSHSGW (5), and the signal for endocytosis or lysosomal/melanosomal/vacuolar targeting (D*XXX*LL). This sequence was found in CD3γ (D*XXX*LL) (31) and in related form in the invariant chain (DDQ*XX*LI; E*XXX*ML) (17, 28, 36), Vam3p (E*XXX*LL) (37), LIMP II (EE-*XXX*LL) (32), and tyrosinase (D/EE*XXX*LL) (30). In all these proteins, the endocytotic activity is critically dependent on the presence of the di-leucine motif and is lost after alanine mutagenesis similar to our observations for the Mgf^{Sl17H} mutation. Therefore the Mgf^{Sl17H} mutation may represent a gain of function in respect to endocytosis and lysosomal targeting of SCF. As a consequence, only a limited amount of mutant SCF would be available on the cell surface to stimulate responsive, c-Kit-expressing neighboring cells. This could be the cause for the reduced amount of peripheral SCF-dependent mast cells and a limited capacity to support hematopoiesis as observed in Mgf^{Sl17H} mutant animals (6, 7). In contrast, based on our results, wild-type SCF lacks a signal for endocytosis, and this is consistent with the role of the cytoplasmic tail of SCF for continuous presentation and signaling of the noncleavable form of SCF toward responsive cells.

The Biological Role of Intracellular Targeting of SCF and Related Transmembrane Growth Factors—Our results suggest multiple roles for the cytoplasmic tail of SCF. First, SCF is targeted to the cell surface in a polarized fashion, being expressed basolaterally and not at the apical surface. Second, after reaching the surface, SCF is retained at the plasma membrane. The first function of the cytoplasmic tail would be important in cells within polarized tissues, such as keratinocytes, Sertoli cells, and neurons, whereas the second function would be relevant to all SCF-expressing cells (Fig. 8). We suggest that the absence of basolateral delivery of SCF leads to the death of melanocytes and male germ cells, which normally require basal delivery of SCF from polarized keratinocytes and Sertoli cells, respectively, as illustrated by the Mgf^{Sl17H} mutation (8). In addition to the loss of pigmentation and fertility, the absence of spatial learning has been demonstrated in a mouse mutant of SCF (Mgf^{Sld}), which lacks the transmembrane and cytoplasmic domain (4). In contrast to wild-type SCF, such mutant forms of SCF are secreted from the apical surfaces of polarized epithelia (8). Cell surface expression of SCF in unpolarized stromal cells of the bone marrow is required for hematopoiesis (8). Consequently, constitutive endocytosis resulting in reduced cell surface expression of SCF would lead to a hematopoietic defect comparable to that of the Mgf^{Sl17H} mutant mice (6, 7).

Based on functional similarities and sequence comparison with other transmembrane growth factors such as CSF-1, we propose that the basolateral determinant and associated functions are not unique to SCF. Because of the absence of mouse mutations affecting the cytoplasmic tail of CSF-1 it is not known whether the role of its cytoplasmic tail is equally important as that of SCF. In op/op mice that lack CSF-1, CSF-1-dependent macrophages are absent from epithelial as well as mesenchymal tissues. Intravenous injection of soluble CSF-1 rescues only mesenchymal macrophages, suggesting a specific requirement for epithelial derived CSF-1 in promoting the survival of epithelial macrophages *in vivo* (38). Moreover, neurological defects have been reported in op/op mice (39), and accumulation of microglia in the brain is induced by amyloid-β peptide-stimulated neuronal release of CSF-1 in Alzheimer's disease (40).

Clearly defined targeting determinants in SCF and other transmembrane growth factors may offer possibilities for altering polarized presentation and cell surface expression of these factors. This may lead to new therapeutic approaches for treatment of pathological conditions such as allergies, chronic inflammation, osteoporosis, or hyperpigmented lesions caused by overexpression or mutations of these factors.

Acknowledgments—We thank Marie-Claude Jacquier for excellent technical assistance and Caroline Johnson-Léger, Monique Wehrle-Haller, Claes Wollheim, Pierre Cosson, and James Weston for discussions and critical reading of the manuscript. We give special thanks to Robert Kelsh for suggesting a gain of function mutation as the cause of the Mgf^{Sl17H} phenotype. We thank Willy Hofstetter, Friedrich Beermann, and Karl Matter for providing cDNAs for CSF-1, tyrosinase, and MDCK II cells.

REFERENCES

1. Massague, J., and Pandiella, A. (1993) *Annu. Rev. Biochem.* **62,** 515-541
2. Brannan, C. I., Lyman, S. D., Williams, D. E., Eisenman, J., Anderson, D. M., Cosman, D., Bedell, M. A., Jenkins, N. A., and Copeland, N. G. (1991) *Proc. Natl. Acad. Sci. U. S. A.* **88,** 4671–4674
3. Flanagan, J. G., Chan, D. C., and Leder, P. (1991) *Cell* **64,** 1025–1035
4. Motro, B., Wojtowicz, J. M., Bernstein, A., and van der Kooy, D. (1996) *Proc. Natl. Acad. Sci. U. S. A.* **93,** 1808–1813
5. Brannan, C. I., Bedell, M. A., Resnick, J. L., Eppig, J. J., Handel, M. A., Williams, D. E., Lyman, S. D., Donovan, P. J., Jenkins, N. A., and Copeland, N. G. (1992) *Genes Dev.* **6,** 1832–1842
6. Kapur, R., Cooper, R., Xiao, X., Weiss, M. J., Donovan, P., and Williams, D. A. (1999) *Blood* **94,** 1915–1925
7. Tajima, Y., Huang, E. J., Vosseller, K., Ono, M., Moore, M. A., and Besmer, P. (1998) *J. Exp. Med.* **187,** 1451–1461
8. Wehrle-Haller, B., and Weston, J. A. (1999) *Dev. Biol.* **210,** 71–86
9. Traub, L. M., and Kornfeld, S. (1997) *Curr. Opin. Cell Biol.* **9,** 527–533
10. Hirst, J., and Robinson, M. S. (1998) *Biochim. Biophys. Acta* **1404,** 173–193
11. Heilker, R., Spiess, M., and Crottet, P. (1999) *Bioessays* **21,** 558–567
12. Folsch, H., Ohno, H., Bonifacino, J. S., and Mellman, I. (1999) *Cell* **99,** 189–198
13. Benting, J. H., Rietveld, A. G., and Simons, K. (1999) *J. Cell Biol.* **146,** 313–320
14. Gut, A., Kappeler, F., Hyka, N., Balda, M. S., Hauri, H. P., and Matter, K.

(1998) *EMBO J.* **17,** 1919–1929
15. Weimbs, T., Low, S. H., Chapin, S. J., and Mostov, K. E. (1997) *Trends Cell Biol.* **7,** 393–399
16. Matter, K., Yamamoto, E. M., and Mellman, I. (1994) *J. Cell Biol.* **126,** 991–1004
17. Simonsen, A., Bremnes, B., Nordeng, T. W., and Bakke, O. (1998) *Eur. J. Cell Biol.* **76,** 25–32
18. Molloy, S. S., Thomas, L., Kamibayashi, C., Mumby, M. C., and Thomas, G. (1998) *J. Cell Biol.* **142,** 1399–1411
19. Wan, L., Molloy, S. S., Thomas, L., Liu, G., Xiang, Y., Rybak, S. L., and Thomas, G. (1998) *Cell* **94,** 205–216
20. Huang, E. J., Nocka, K. H., Buck, J., and Besmer, P. (1992) *Mol. Biol. Cell* **3,** 349–362
21. Matter, K., Hunziker, W., and Mellman, I. (1992) *Cell* **71,** 741–753
22. Rubin, L. A., Kurman, C. C., Biddison, W. E., Goldman, N. D., and Nelson, D. L. (1985) *Hybridoma* **4,** 91–102
23. Imhof, B. A., Vollmers, H. P., Goodman, S. L., and Birchmeier, W. (1983) *Cell* **35,** 667–675
24. Parichy, D. M., Stigson, M., and Voss, S. R. (1999) *Dev. Genes Evol.* **209,** 349–356
25. Simmen, T., Nobile, M., Bonifacino, J. S., and Hunziker, W. (1999) *Mol. Cell. Biol.* **19,** 3136–3144
26. Bazan, J. F. (1991) *Cell* **65,** 9–10
27. Pawson, T., and Bernstein, A. (1990) *Trends Genet.* **6,** 350–356
28. Simonsen, A., Stang, E., Bremnes, B., Roe, M., Prydz, K., and Bakke, O. (1997) *J. Cell Sci.* **110,** 597–609
29. Briley, G. P., Hissong, M. A., Chiu, M. L., and Lee, D. C. (1997) *Mol. Biol. Cell* **8,** 1619–1631
30. Simmen, T., Schmidt, A., Hunziker, W., and Beermann, F. (1999) *J. Cell Sci.* **112,** 45–53
31. Dietrich, J., Kastrup, J., Nielsen, B. L., Odum, N., and Geisler, C. (1997) *J. Cell Biol.* **138,** 271–281
32. Honing, S., Sandoval, I. V., and von Figura, K. (1998) *EMBO J.* **17,** 1304–1314
33. Cheng, H. J., and Flanagan, J. G. (1994) *Mol. Biol. Cell* **5,** 943–953
34. Aroeti, B., Kosen, P. A., Kuntz, I. D., Cohen, F. E., and Mostov, K. E. (1993) *J. Cell Biol.* **123,** 1149–1160
35. Reich, V., Mostov, K., and Aroeti, B. (1996) *J. Cell Sci.* **109,** 2133–2139
36. Pond, L., Kuhn, L. A., Teyton, L., Schutze, M. P., Tainer, J. A., Jackson, M. R., and Peterson, P. A. (1995) *J. Biol. Chem.* **270,** 19989–19997
37. Darsow, T., Burd, C. G., and Emr, S. D. (1998) *J. Cell Biol.* **142,** 913–922
38. Cecchini, M. G., Dominguez, M. G., Mocci, S., Wetterwald, A., Felix, R., Fleisch, H., Chisholm, O., Hofstetter, W., Pollard, J. W., and Stanley, E. R. (1994) *Development* **120,** 1357–1372
39. Michaelson, M. D., Bieri, P. L., Mehler, M. F., Xu, H., Arezzo, J. C., Pollard, J. W., and Kessler, J. A. (1996) *Development* **122,** 2661–2672
40. Du Yan, S., Zhu, H., Fu, J., Yan, S. F., Roher, A., Tourtellotte, W. W., Rajavashisth, T., Chen, X., Godman, G. C., Stern, D., and Schmidt, A. M. (1997) *Proc. Natl. Acad. Sci. U. S. A.* **94,** 5296–5301

2.8. Cytoplasmic domain of SCF: a new therapeutic target?

In the previous chapters, we have learned the existence of critical expression and splicing patterns of SCF mRNA along the migration pathway of melanocyte precursors. In addition to the transcriptional and splicing level, SCF protein, in order to be successively presented to c-Kit expressing cells requires intracellular sorting signals to deliver SCF efficiently to basolateral domains of epithelial tissues. Due to these multiple levels of control, it is also likely to find pathological conditions of SCF/c-Kit dependent cells that are caused by mis-expression, mis-processing or mis-targeting of SCF. In 1993 the laboratory of Ruth Halaban published an article in which they demonstrated that during mastocytosis, the proteolytically cleavable splice variant of SCF was over-expressed (Longley et al., 1993). In 1998 it was demonstrated that the inhibition of SCF/c-kit signaling by antibody treatment or injection of soluble SCF led to the respective loss or hyperproliferation of melanocytes in human skin explants (Grichnik et al., 1998). Moreover, the transgenic expression of SCF by the keratin14 promoter in basal keratinocytes increased the amount of melanocytes in the epidermis but led also to cutaneous mastocytosis (Kunisada et al., 1998a; Kunisada et al., 1998b). In addition, UV-light exposed human skin reacted with the production of SCF and c-Kit. In turn, the UV induced tanning process could be blocked with anti-c-Kit antibodies in brown guinea pig skin (Hachiya et al., 2001). Besides the SCF dependent control of melanocytes and mastocytes of the skin, it has recently been suggested that the c-Kit receptor is also expressed on eosinophiles. Since eosinophiles are responsible for acute or chronic allergic reactions, SCF expression in the nasal epithelium has been examined. Otsuka and coworkers reported an increase in SCF immunoreactivity with inflamed nasal epithelia (Otsuka et al., 1998). In addition, the application of SCF antisense oligonucleotides to the bronchial epithelium reduced asthma symptoms in the mouse ovalbumin model (Finotto et al., 2001). It remains open whether pathological SCF modulations are also associated with dermatological lesions such as congenital nevus syndrome or vitelligo.

The above mentioned examples suggest that controlling SCF expression in epithelial cell layers would be a possible therapeutic strategy, in order to reduce hyperpigmented lesions associated with, for example cutaneous mastocytosis. However, inhibitors to the SCF/c-kit system need to be highly specific as well as topically applied. It would not be advisable to administer c-kit blocking

antibodies to large areas of the skin, since they might be carried to the reproductive organs or the bone marrow where they could affect vital cellular systems. Therefore, the cytoplasmic targeting domains of SCF, required for basolateral transport and efficient cell surface expression, offer a therapeutic target for locally applied drugs. The cytoplasmic tail sequence of SCF is unique in amino acid sequence and the local deposition of inhibitors within the epidermal cells of the skin could prevent diffusion of the pharmacological compound throughout the body. Currently we are studying the design of potential inhibitory peptides and of protein domains that could serve to specifically reduce SCF surface expression and basolateral targeting by interfering with the normal function of the cytoplasmic tail of SCF.

3. Melanocyte Migration *in vitro*: The Role of the Cytoskeleton

3.1. Growth factor mediated changes in the actin cytoskeleton

Stem cell factor is produced by keratinocytes and is expressed in two alternatively- spliced forms resulting in a proteolytically released form (soluble) and a membrane bound form with increased proteolytic stability (cell-bound) (Huang et al., 1992). The in vitro activation of c-Kit using soluble SCF has been shown to result in the activation of the small GTPase Rac1 which controls the polymerization of actin and the formation of membrane ruffles and lamellipodia (Hall, 1998; Ridley et al., 1992; Timokhina et al., 1998; Vosseller et al., 1997) and this signal transduction pathway may be responsible for cell migration and chemotaxis (Allen et al., 1997; Blume-Jensen et al., 1991; Sekido et al., 1993; Ueda et al., 2002). An example of such a directed melanoblast migration is illustrated in Fig. 5. and can also be seen in chapter 6 as a quicktime movie. In addition to chemotaxis and migration, c-Kit signaling leads to cell survival and proliferation, and it has been suggested that the signaling pathways involved are partially overlapping to those leading to cell migration (Timokhina et al., 1998). However *in vivo* and *in vitro*, the cellular response upon c-Kit signaling may depend whether stimulation occurs via soluble SCF or cell-bound SCF. Indeed, presentation of membrane bound SCF might be expected to increase the duration of c-Kit activation at the plasma membrane, resulting in a robust survival signal (Miyazawa et al., 1995). In contrast, soluble SCF induces rapid internalization of the SCF/c-Kit complex that led to an intracellular signaling cascade resulting in cell motility. The exact differences in cellular responses towards soluble or membrane-bound SCF are still a matter of intense research.

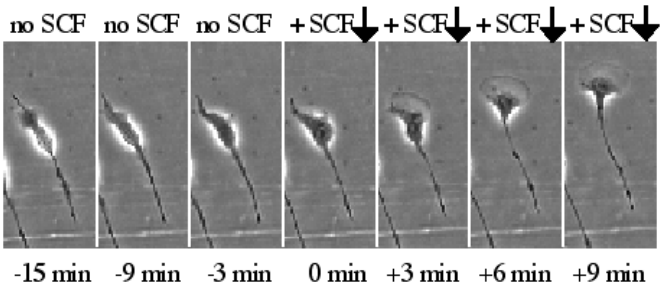

Fig. 5. *Directed migration of melanoblasts towards a gradient of SCF*. Melanoblasts starved for 4 hrs were exposed to a diffusion gradient of SCF in a Zigmund chamber: Frames 1-3 show the cell before SCF addition. SCF was added at time 0 from the top (arrows). Soon after SCF addition, cells responded by lamellipodia formation and directed migration.

In addition to c-Kit, many other RTK's induce the reorganization of the actin cytoskeleton into lamellipodial structures consisting of a criss-cross pattern of actin filament (Small et al., 2002). Although of paramount importance, I will not further discuss the complex intracellular signaling

pathways that emanate from c-Kit activation and internalization to the actin polymerization at the leading edge.

In order for the entire cell to move forward, the cell body has to follow the leading edge and the cell rear has to retract and detach from the substrate. It is therefore clear that the respective signals, which induce cell migration have to organize the actin cytoskeleton in respect to its particular function in the cell. For example, actin filaments are polymerized in the advancing lamellipodia and filopodia at the cell front, while myosin activity in the main cell body controls the forward pull of the nucleus. At the cell rear, the actin cytoskeleton has to detach from the substrate and de-polymerize the retraction trailing portions of the cell. It is still an open question how the cell is able to specifically induce and maintain these different levels of actin organization in migrating cells. Apparently, the microtubule network is playing a pivotal role in maintaining cellular polarity and keeping apart the cellular regions that are organized by different actin cytoskeletal structures (see chapter 3.3). In addition microtubules are required for the polarization of the actin cytoskeleton into protruding actin networks at the cell front and retracting actin structures at the cell rear.

Although the paraformaldehyde-fixed actin cytoskeleton can be easily visualized by fluorescent phallodin labeling, this represents only a snapshot of the otherwise dynamic actin cytoskeleton. In order to gain further insight into the dynamic remodelling of the actin cytoskeleton in migrating cells we constructed a fusion protein between β-actin and the green fluorescent protein (GFP) from Aquoria victoria (a jellyfish from the pacific ocean) (Chalfie and Kain, 1998). This construct transfected into migrating melanoma cells allowed us to understand the different dynamic organizations assumed by the actin cytoskeleton during cell migration (see chapter 3.2).

3.2. Actin dynamics during cell migration

Journal of Cell Science 111, 1649-1658 (1998)
Printed in Great Britain © The Company of Biologists Limited 1998
JCS4557

Actin dynamics in living mammalian cells

Christoph Ballestrem, Bernhard Wehrle-Haller and Beat A. Imhof*

Department of Pathology, Centre Medical Universitaire, Geneva, Switzerland
*Author for correspondence

Accepted 20 April; published on WWW 27 May 1998

SUMMARY

The actin cytoskeleton maintains the cellular architecture and mediates cell movements. To explore actin cytoskeletal dynamics, the enhanced green fluorescent protein (EGFP) was fused to human β-actin. The fusion protein was incorporated into actin fibers which became depolymerized upon cytochalasin B treatment. This functional EGFP-actin construct enabled observation of the actin cytoskeleton in living cells by time lapse fluorescence microscopy. Stable expression of the construct was obtained in mammalian cell lines of different tissue origins. In stationary cells, actin rich, ring-like structured 'actin clouds' were observed in addition to stress fibers. These ruffle-like structures were found to be involved in the reorganization of the actin cytoskeleton. In migratory cells, EGFP-actin was found in the advancing lamellipodium. Immobile actin spots developed in the lamellipodium and thin actin fibers formed parallel to the leading edge. Thus EGFP-actin expressed in living cells unveiled structures involved in the dynamics of the actin cytoskeleton.

Key words: EGFP-actin, Cell migration, Cell adhesion, Actin filament

INTRODUCTION

Actin is a highly conserved and abundant cytoskeletal protein in eukaryotic cells. It is implicated in a number of cellular activities, including reorganization of cell shape and cell motility (Stossel, 1993; Small, 1994a,b; Lauffenburger and Horwitz, 1996; Mitchison and Cramer, 1996). Many of these processes require the dynamic behavior of the actin cytoskeleton which involves the polymerization and depolymerization of actin filaments (Welch et al., 1997). Monomeric actin (G-actin) polymerizes in a head to tail fashion to form helical actin filaments (F-actin) (Wegner, 1976; Pollard and Mooseker, 1981; Holmes et al., 1990). Most cells keep a large pool of G-actin to maintain the ability to quickly reorganize the cytoskeleton when subjected to environmental changes. The G-actin pool and the stability of F-actin is controlled by a large number of actin binding proteins. The amount of G-actin available for polymerization is controlled by proteins selectively binding to monomeric actin (Carlier and Pantaloni, 1994; Sun et al., 1995). Another class of G-actin binding proteins modulate the rate of assembly and disassembly of G-actin into F-actin, hence increasing the rate of actin polymerization and treadmilling significantly (Carlier et al., 1997; Theriot, 1997). Furthermore, certain actin binding proteins have actin filament severing activity allowing the creation of new nucleation sites for actin polymerization (Cunningham et al., 1991; Witke et al., 1995). Finally, existing F-actin can be bundled by bivalent F-actin binding proteins leading to the formation of thick actin cables (stress fibers) (Matsudaira, 1994).

Although many studies of actin behavior in vitro exist, the complex dynamics of the actin cytoskeleton which is required for maintaining cell shape or cellular locomotion are not well understood. Reagents such as cytochalasins or phalloidin have been widely used to perturb actin dynamics. The former inhibits actin polymerization by blocking the barbed end of actin filaments, while the latter binds selectively along the sides of actin filaments and inhibits their depolymerization (Dancker et al., 1975; MacLean-Fletcher and Pollard, 1980; Cooper, 1987; Forscher and Smith, 1988). An alternative method to study the dynamics of the actin cytoskeleton in living cells is to microinject fluorescently labeled actin, anti-actin antibodies or caged resorufin (CR)-actin (Wang, 1984; Symons and Mitchison, 1991; Theriot and Mitchison, 1991; Cao et al., 1993).

When transfected into recipient cells, green fluorescent protein (GFP)-tagged proteins can be visualized in living cells using fluorescence microscopy (Gerdes and Kaether, 1996; Ludin and Matus, 1998). In yeast cells, an actin-GFP fusion protein was used to study the movement of cortical actin patches (Doyle and Botstein, 1996). In *Dictyostelium discoideum*, GFP-actin fusion proteins were integrated into actin filaments which allowed the observation of microfilament dynamics during *Dictyostelium* movement and chemotaxis (Westphal et al., 1997). So far studies in mammalian cells were hampered due to the lack of corresponding functional GFP-actin construct.

The aim of this investigation was to study cellular processes which lead to actin reorganization in immobile and migrating mammalian cells. In order to visualize the actin cytoskeleton during these complex morphological changes, we constructed an EGFP human β-actin fusion protein which was expressed

in mammalian cells of different tissue origins. Among the EGFP β-actin transfected cells we focused on B16F1 melanoma. These cells can either assume a very well spread, stationary morphology similar to fibroblasts, or develop a lamellipodium and undergo extensive migration similar to fish keratocytes (Wang, 1984; Theriot and Mitchison, 1991; Dunlevy and Couchman, 1993; Lee et al., 1993; Small, 1994a; Small et al., 1995; Cramer et al., 1997). Therefore a possible bias of EGFP β-actin towards the formation of a particular actin structure was excluded.

In stationary spread cells we found EGFP β-actin incorporated into stress fibers. In these cells, expanding circular F-actin containing structures were found to be associated with cell shape changes and reorganization of the actin cytoskeleton. Migrating cells showed a prominent actin rich lamellipodium, followed by the lamella, a transition zone with low actin content and the cell body with the nucleus. These cells did not contain stress fibers but close inspection revealed that long thin actin fibers existed. The reorientation of those were associated with the directional change in migration. Furthermore, 'actin spots' were formed within the lamellipodium of migrating cells and remained immobile with respect to the substrate. The data presented here suggest further roles for different entities in the actin cytoskeleton which may be important for the maintenance of cell shape and the onset of cellular locomotion.

MATERIALS AND METHODS

Cell lines, plasmids and reagents

Mouse melanoma cells (B16F1) were kindly provided by G. Nicholson (Houston, TX, USA). Swiss 3T3 fibroblasts and Chinese hamster ovary cells (CHO) were from the American Type Tissue Culture Collection (ATCC). Mouse thymic endothelioma cells (t.End3) were obtained from Dr Werner Risau (Max Planck Institute, Bad Nauheim, Germany). B16F1, 3T3 fibroblasts, and t.End cells were grown in DMEM and CHO cells in F12 medium (Gibco BRL, Paisley, Scotland), each supplemented with 10% FCS (PAA Laboratories, Linz, Austria), 2 mM glutamine, 100 i.u./ml penicillin and 100 μg/ml streptomycin (all Gibco BRL).

The mammalian expression vector for enhanced green fluorescent protein (pEGFP-1) and polyclonal anti-EGFP antibodies were obtained from Clontech (Basel, Switzerland) and pcDNA3 expression vector was from Invitrogen (Leek, Netherlands). The human β-actin promotor was amplified from the pHβ Apr-1-neo plasmid (Ng et al., 1989). Human β-actin cDNA was obtained from Dr Perriard (Zürich, Switzerland). A polyclonal anti-β-actin antibody specifically reacting with the acetylated N terminus of β-actin was kindly provided by Dr Gabbiani (Geneva, Switzerland) (Yao et al., 1995). Human fibronectin (FN) was purchased from Collaborative Biomedical Products (Bedford, MA, USA), mouse EHS-laminin (LN) was a gift from M. Chiquet (Bern, Switzerland).

Construction of EGFP β-actin fusion protein

Human β-actin promoter, EGFP and human β-actin sequences were amplified by PCR with primers containing restriction sites for cloning into pcDNA3. The cytomegalovirus (CMV) promoter of pcDNA3 was excised with *Bgl*II and *Hin*dIII and replaced by a 3 kb or 1.2 kb fragment of the human β-actin promoter (Ng et al., 1989) which were amplified using *Pfu* polymerase (Stratagen, Basel, Switzerland). The amplification of the 3 kb promoter was carried out with the following primers: forward primer (GGAAGATCTTGGCCAGCTGAATGGAG) and reverse primer (CCCAAGCTTGAGCTGCGAGAATAGCCG). The 1.2 kb human β-actin promoter was amplified with the same reverse primer and the following forward primer (GGAAGATCTGAAGTCGGCAAGGGG).

Subsequently, the EGFP sequence was amplified with *Pfu* polymerase utilizing a forward primer with a *Hin*dIII and reverse primer with *Bam*HI restriction site: forward primer (TGGAAGCTTCCACCATGGTGAGCAAGGGC) and reverse primer (CCGGATCCCTTGTACAGCTCGTCCATGC). Finally, human β-actin was amplified with *Pfu* polymerase using primers containing a *Bam*HI and *Eco*RI site respectively, and cloned into the EGFP containing pcDNA3 vector; forward primer (CCGGATCCACTAGTGGCATGGATGATGATATCGC), and reverse primer (CCGAATTCCTAGAAGCATTTGCGGTGG). The constructs were subsequently sequenced, in order to verify the integrity of the fusion protein. Final constructs were: (1) pcDNA3 with CMV promoter plus EGFP and β-actin, (2) pcDNA3 with a long version of the β-actin promoter followed by EGFP and β-actin, and (3) pcDNA3 containing the short version of the β-actin promoter followed by EGFP and β-actin.

Transient and stable protein expression

Plasmids containing the EGFP β-actin fusion construct were transfected with Lipofectamine according to the manufacturer's recommendation (Gibco BRL). Briefly, 1.5 μg of plasmid DNA and 6 μl Lipofectamine solution was incubated for 15 minutes in 200 μl of OPTIMEM (Gibco BRL) then diluted with 800 μl OPTIMEM. This solution was added to cells at 30-60% confluence in a 35 mm tissue culture plate (Falcon, Becton Dickinson, Basel, Switzerland). After 10 hours incubation at 37°C without serum, 2 ml of 10% FCS medium was added to the cells, and was changed fourteen hours later to the culture medium described for the corresponding cell lines. Two days after transfection, expression of the fusion construct was evaluated by fluorescence microscopy using a FITC filter set (Carl Zeiss, Jena, Germany). Stable expressing clones were obtained by sorting of EGFP fluorescent cells into 96-well plates using a Fluorescence Activating Cell Sorter (FACStar; Becton Dickinson, San Jose, CA, USA) and cultured in G418 (1.5 mg/ml; Geneticin, Gibco BRL) supplemented media. Colonies expressing EGFP-actin were expanded for further analysis.

Fluorescence microscopy of living cells and image analysis

Cells transfected with EGFP β-actin, were detached from plastic tissue culture plates by EDTA treatment for 5 minutes, washed 2 times in Ham's F12 medium, and plated in presence of Ham's F12 containing 10% FCS on glass coverslips coated with 5 μg/ml fibronectin or laminin. Living cells were observed under an inverted fluorescent microscope (Zeiss-Axiovert 100) equipped with Plan-Neofluar ×40, ×100 Fluar oil immersion objectives (Zeiss), and an incubation chamber for constant temperature and CO_2 regulation. EGFP fluorescence was visualized using a FITC filter set (450-490, FT 510, LP 520). Single or time lapse pictures were acquired with a Hamamatsu C4742-95-10 digital CCD camera (Hamamatsu Photonics, Japan) controlled by the Openlab software (Improvision, Oxford, UK). For time-lapse recordings, cells expressing EGFP-constructs were kept constantly at 37°C and 5% CO_2. To obtain low background fluorescence from the culture medium, we used Ham's F12 medium which has a low concentration of fluorescent media components, such as Phenol Red and riboflavin. Since prolonged exposure to intense light led to deterioration and bleaching of the observed cells, light intensity was controlled using neutral density filters, and exposure times never exceeded 600 milliseconds per 20 second interval during time lapse recording.

Fluorescence microscopy of fixed cells

Stable EGFP β-actin transfected cells were cultured on FN (5 μg/ml) coated glass coverslips at 37°C and 5% CO_2 for 12 hours. Cells were

then fixed with 2% paraformaldehyde for 30 minutes at room temperature (RT). After rinsing 3 times with PBS cells were permeabilized with 0.5% Triton X-100 in PBS for 5 minutes at RT. Samples were rinsed again with PBS containing 0.5% BSA followed by a 30 minute incubation at RT with 100 nM rhodamine-phalloidin (Fluka, Buchs, Switzerland). After final washing (3 times) with PBS, cells were embedded in 1% *N*-propyl-gallate, 80% glycerol in PBS, and analyzed using a Zeiss-Axiovert 100 microscope.

Western blotting

Western blot analysis was performed after SDS-PAGE (10% gel) according to established procedures (Winston and Fuller, 1991). EGFP β-actin expressing B16F1 cells (10^7) were washed in PBS and lysed in 0.5% Triton X-100 in PBS containing protease inhibitors (inhibitor cocktail from Boehringer Mannheim, Mannheim, Germany). The cell lysate was then mixed with an equal volume of 2× SDS-PAGE sample buffer and boiled for 5 minutes. Proteins separated by SDS-PAGE were transferred to nitrocellulose membranes and non-specific binding sites were blocked with TBS containing 1% BSA and 0.1% Tween-20. After incubation with primary polyclonal anti-β-actin or anti-EGFP antibody followed by secondary peroxidase-conjugated anti-rabbit antibodies (Sigma, Basel, Switzerland), peroxidase activity was visualized by chemiluminescence (ECL, Amersham, Buckinghamshire, UK).

RESULTS

Expression of EGFP β-actin in mammalian cells

In order to visualize the actin cytoskeleton in stationary and migrating mammalian cells, the enhanced green fluorescent protein (EGFP) was fused to the amino-terminal end of the human β-actin (Fig. 1). EGFP and β-actin sequences were separated by a flexible, hydrophilic 5 amino acid spacer. This hinge region should reduce steric hindrance by EGFP, in order to allow interaction of actin with actin binding proteins.

Since overexpression of β-actin cDNA in mammalian cells has been shown to have a severe impact on cell morphology (Mounier et al., 1997) three plasmids encoding EGFP β-actin were constructed with promoters of different strength; the CMV promoter, a long and short version of the human β-actin promoter (see Materials and Methods). Transient expression of EGFP β-actin in COS-7 cells was strong under the control of the CMV and readily detectable with the long actin promoter. Expression under the short actin promoter was barely visible. The strong expression of EGFP β-actin under the CMV promoter affected the cellular morphology of COS-7 cells. Many of these cells were round shaped, unable to spread, and green fluorescence was observed in clusters along the cell periphery or in vesicular structures within the cell (data not shown). In contrast, cell morphology of COS-7 cells expressing EGFP β-actin under the long actin promoter appeared normal, therefore this promoter was chosen for subsequent studies.

This EGFP β-actin construct was then tested for expression in cells of different tissue origins. Transfection was performed with B16 F1 melanoma cells, mouse 3T3 fibroblasts, Chinese hamster ovary cells (CHO), and thymic endothelial cells (t.End 3). All four cell lines expressed EGFP β-actin (Fig. 2). This suggests that expression and function of this construct is not cell lineage restricted. After two weeks of G418 selection, stable expression was obtained in B16, 3T3, and CHO cells demonstrating that cell proliferation was not blocked by EGFP β-actin fusion protein. Expression of EGFP β-actin was also analyzed by western blotting using stable transfected B16 cell lines (Fig. 3). Anti-GFP specific antibodies detected a single band with an apparent molecular mass of 70 kDa using cell lysate of EGFP β-actin transfected cells; non-transfected cells were negative. Normal β-actin appeared at 43 kDa and was detected with a polyclonal monospecific antibody recognizing the acetylated N terminus of β-actin (Yao et al., 1995). Apparently the epitopes of this antiserum were lost by generating the EGFP β-actin fusion protein. Both, transfected and non-transfected cells showed the 43 kDa wild-type actin band at the same level of expression. Thus coexpression of EGFP β-actin did not influence the expression level of wild-type actin. The band detected with the anti-GFP antibody at 70 kDa corresponds to the calculated molecular mass of the EGFP β-actin fusion protein (69, 45 kDa).

EGFP β-actin fusion protein integrates into actin filaments

The fiber-like structures seen in EGFP β-actin expressing cells were strongly reminiscent of stress fiber bundles in adherent cells. In order to test whether EGFP β-actin was incorporated into actin filaments, cells were fixed and then filamentous actin (F-actin) was counter-stained with rhodamine-phalloidin (Rh-Ph). All Rh-Ph labeled fibers were also positive for EGFP β-actin, indicating that the fusion protein is incorporated into actin stress fibers in living cells (Fig. 4A,B). In addition to stress fibers EGFP β-actin was also found in non-filamentous structures surrounding the nucleus. This staining disappeared after detergent treatment suggesting that it consisted of monomeric G-actin (data not shown). Thus EGFP β-actin can be visualized as monomeric G-actin and as polymerized F-actin.

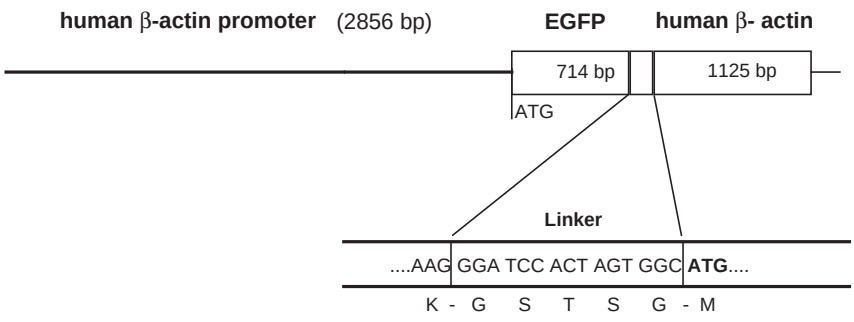

Fig. 1. Scheme of the EGFP-human β-actin DNA construct. A 2,856 bp long version of the human β-actin promoter was linked to the coding sequence of enhanced green fluorescent protein (EGFP) followed by human β-actin. A flexible linker encoding five amino acids was introduced between the EGFP and actin genes.

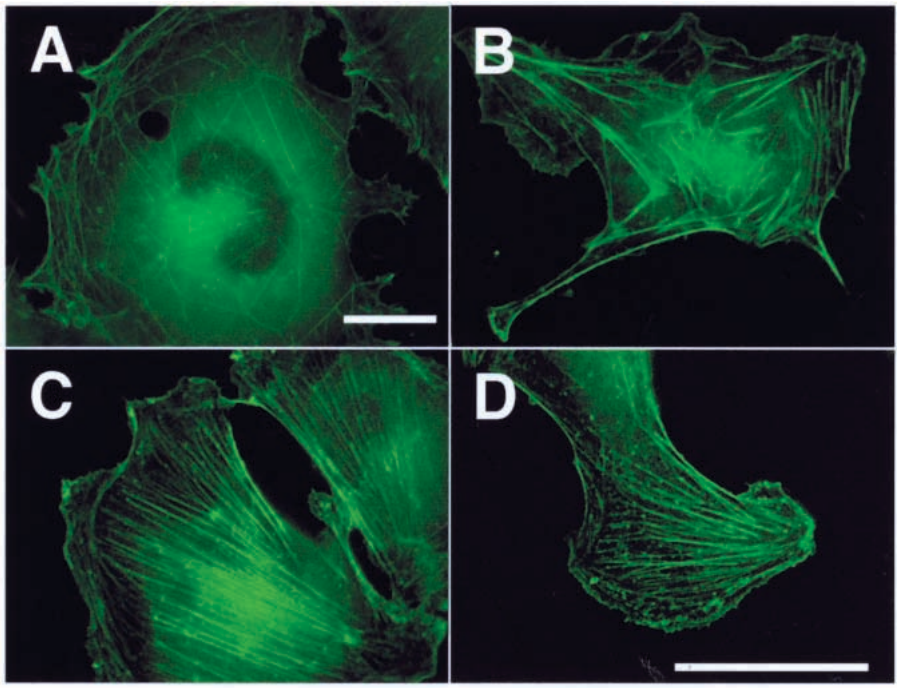

Fig. 2. Expression of EGFP β-actin in cell lines of different tissue origin. The EGFP β-actin construct driven by the long actin promoter was transfected into adherent cell lines. The EGFP β-actin expression was observed by fluorescence microscopy. (A) B16F1 mouse melanoma cells; (B) 3T3 mouse fibroblasts; (C) Chinese hamster ovary (CHO) cells; (D) thymus derived endothelioma (t-End). (A-C) Cell lines expressed the fusion protein stably; (D) transient expression. Bar, 20 μM.

Polymerization and depolymerization of EGFP β-actin in living cells

Actin depolymerization and polymerization are required for cell locomotion and reorganization of the actin cytoskeleton. To test whether these processes were altered by the presence of the EGFP-tag, EGFP β-actin depolymerization and polymerization were recorded by time lapse video fluorescence microscopy. Actin depolymerization was obtained with cytochalasin B which prevents association and dissociation of G-actin at the barbed end of actin filaments, without affecting the depolymerization at the pointed end of actin filaments. B16 cells were cultured for 24 hours on fibronectin (FN) coated glass coverslips to obtain stress fiber containing spread cells. Cells were then treated with 2 μM cytochalasin B, which resulted in rapid rupturing of fibers at the cell periphery. Subsequently, the ruptured fibers were shortened by depolymerization (Fig. 5A-C), and F-actin was lost within 10 minutes of cytochalasin B application.

Further evidence that the EGFP β-actin fusion protein did not disturb actin function was shown by recording the video images of spreading cells. As shown in Fig. 5D-F, actin polymerization readily occurred in spreading B16 cells plated on FN coated glass coverslips. Growing actin filaments showed intense fluorescence at the tip and advanced towards the cell border (arrow in Fig. 5G), indicating accumulation of G-actin at actin polymerization sites. Subsequently, these filaments were further bundled to stress fibers which appeared as thicker fluorescent lines than the de novo formed filaments (data not shown). Spreading and adhesion occurred within 15 minutes, which is the same time scale as for non-transfected B16 cells, indicating that the EGFP-actin fusion protein is a valuable tool to study the actin cytoskeleton dynamics in living mammalian cells.

These results show that the EGFP β-actin fusion protein has no severe impact upon function of the actin cytoskeleton with respect to actin-polymerization, depolymerization, and cell adhesion.

Actin dynamics in stationary cells

B16 cells were stationary when plated on FN coated at 5 μg/ml. Twelve hours after plating, immobile cells were observed using time lapse fluorescence microscopy. The cells exhibited many stress fibers and intense ruffling at the cell edges (Fig. 6A-F). Furthermore, in the presence of serum, ring-shaped actin structures with intense green fluorescence appeared spontaneously within the cell (arrow in Fig. 6A). As shown in Fig. 6A-D, these ring-like actin structures, which most likely represent actin ruffles, expanded concentrically (Ruusala et al., 1998). Because of their appearance we will refer to these structures from now on as ‘actin clouds’. When associated with

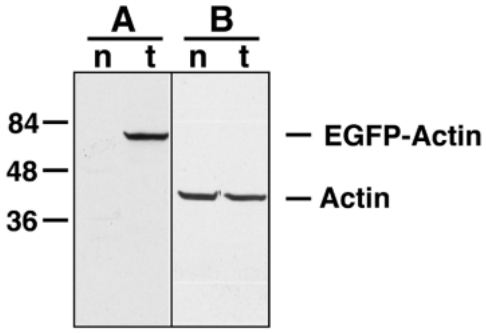

Fig. 3. Western blot of EGFP β-actin fusion protein. Whole cell lysates of nontransfected control B16 (n) and EGFP β-actin expressing B16 cells (t) were separated on 10% SDS-PAGE and transferred to nitrocellulose membrane. (A) Polyclonal anti-EGFP antibody detected a single band with an apparent molecular mass of 70 kDa in transfected but not in nontransfected control cells. (B) A polyclonal anti-actin antibody recognizing the N terminus of β-actin detected a single band with an apparent molecular mass of 43 kDa in both transfected and nontransfected cells. The 70 kDa EGFP β-actin was not detectable with this antibody, since the N terminus of β-actin was modified by the fusion to EGFP.

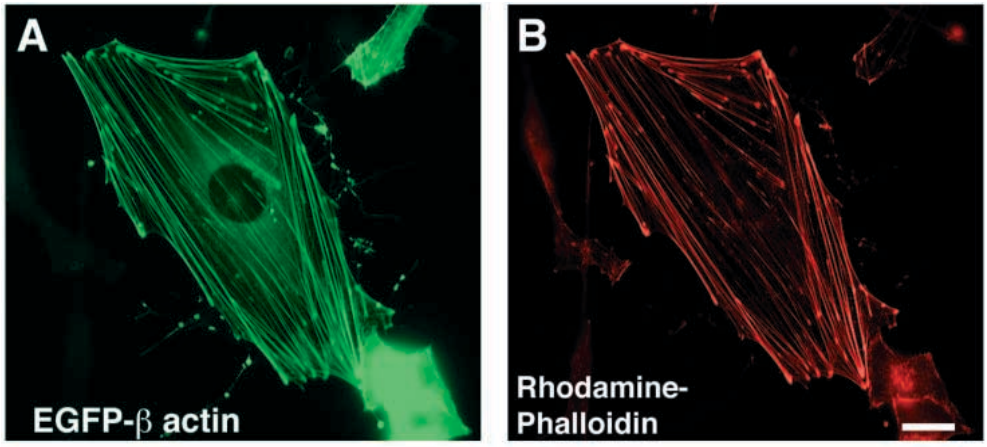

Fig. 4. Overlapping staining of EGFP β-actin organized in stress fibers with rhodamine-phalloidin. EGFP β-actin expressing B16 cells were allowed to spread on culture dishes for 14 hours. (A) The image of living cells was taken by fluorescence microscopy. (B) The cells were then fixed, lysed and stained with rhodamine-phalloidin. Note the identical pattern of F-actin in the two images. Bar, 10 μm.

the cell periphery these expanding actin clouds lead to the local protrusion of the plasma membrane with subsequent formation of new stress fibers. The actin in clouds is in its polymerized form as phalloidin binds to these structures (Fig. 6G). The clouds were stained with the anti-β-actin antibody which exclusively recognizes endogenous β-actin and can not bind to the EGFP β-actin (Fig. 6H, compare with Fig. 3). This assured that the clouds were not an artifact of the EGFP β-actin expression in B16 cells. Artifacts due to EGFP β-actin expression can be excluded by visualization of clouds by phalloidin in nontransfected B16 cells (Fig. 6I). Interestingly these clouds were always associated with the lower side of the cells (data not shown), in contrast to dorsal ruffles observed in MDCK cells (Dowrick et al., 1993).

Actin dynamics in migrating cells

Next we studied actin dynamics in migrating EGFP β-actin expressing B16 cells by time lapse microscopy. These cells moved with a velocity of 3 to 5 μm/minute on laminin (LN) coated at 5 μg/ml. Cells migrated by forming a large lamellipodium and retracting the rear part of the cell (Fig. 7). The lamellipodium was formed by an EGFP β-actin containing

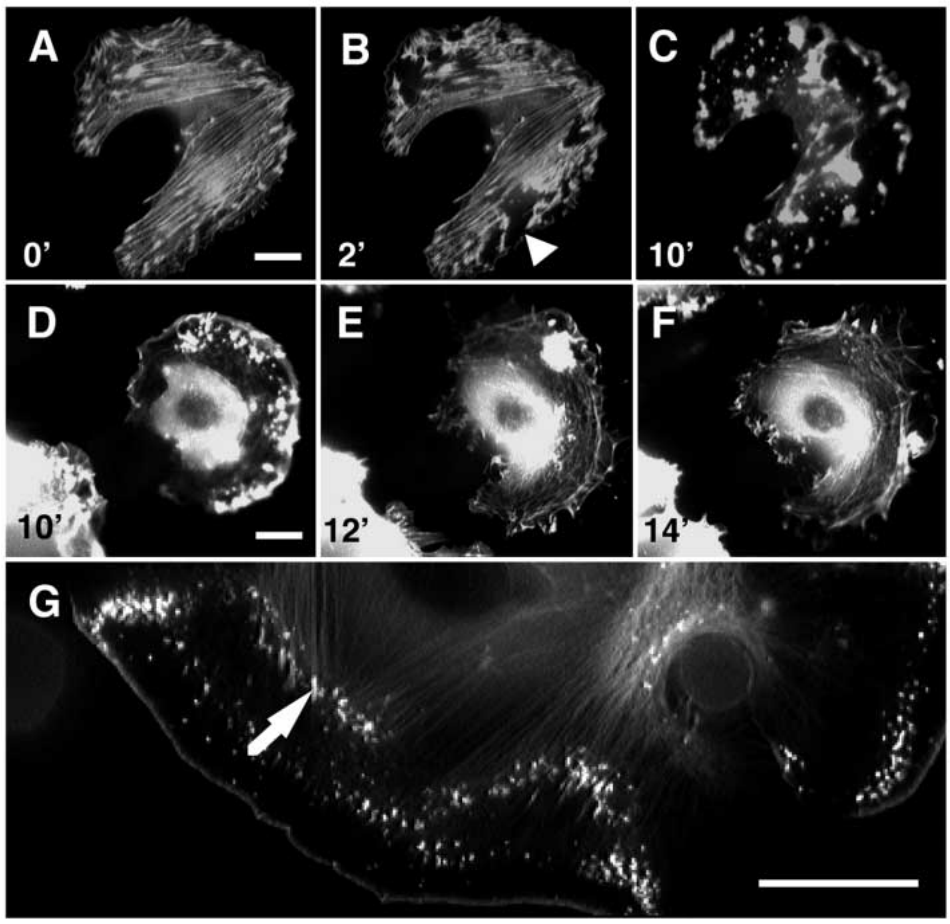

Fig. 5. EGFP β-actin does not interfere with depolymerization and polymerization of F-actin. (A-C) Spreaded, EGFP β-actin expressing B16 cells on FN were treated with 2 μM cytochalasin B at time point 0' (A), the depolymerizing actin stress fibers were then observed for 10 minutes (A-C). Note that 2 minutes after cytochalasin B treatment large zones were already free of stress fibers (arrowhead in B); depolymerization was complete after 10 minutes (C). (D-F) The formation of the actin filament network was observed in spreading B16 cells on FN. Already within 10 minutes the cell was well spread (D). Filaments were formed by 12 minutes (E), reaching a complete level at 14 minutes (F). High magnification of growing actin filaments in a different spreading cell on FN (arrow in G). Bars, 20 μm.

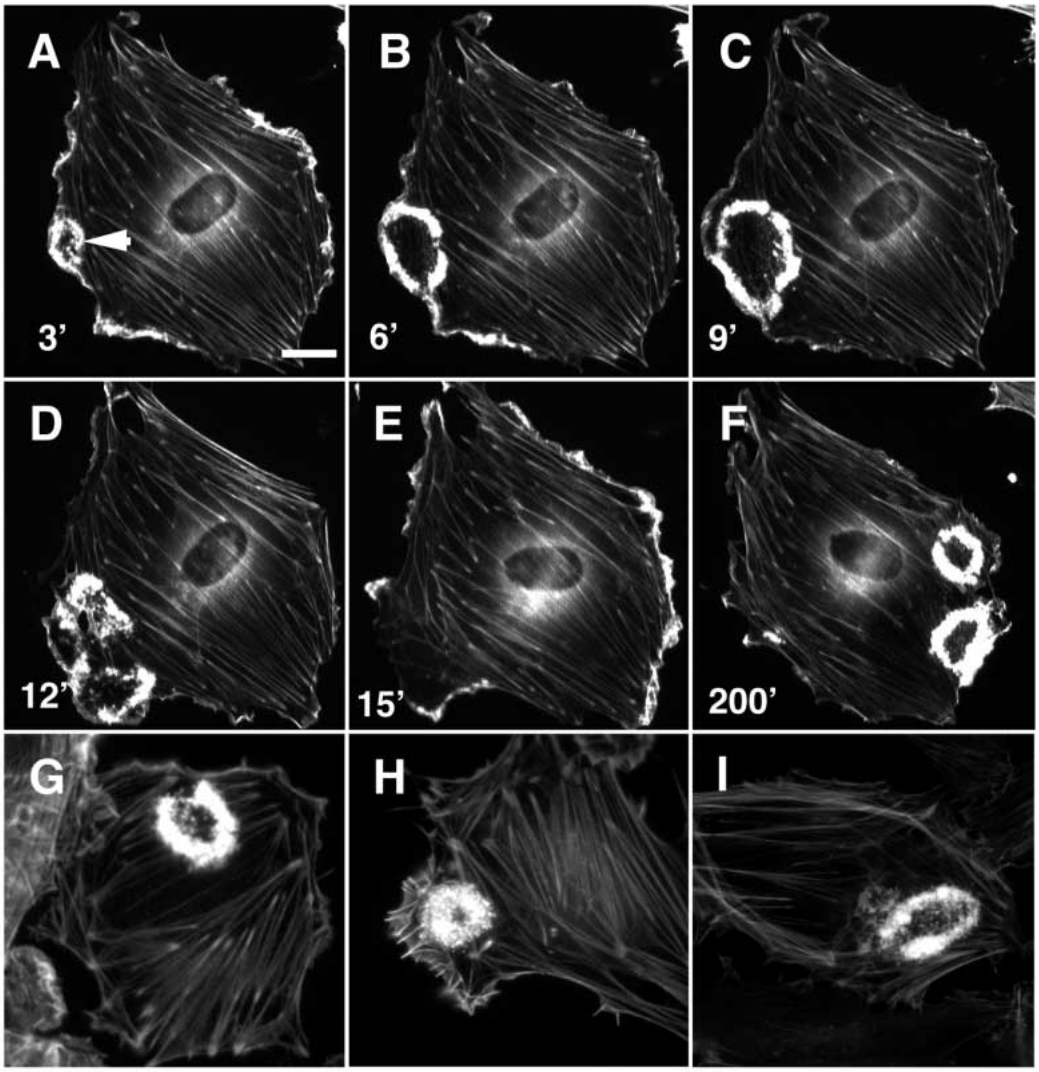

Fig. 6. Reorganization of the actin cytoskeleton in stationary cells. B16 cells were allowed to adhere for 24 hours on glass coverslips coated with 5 μg/ml of FN. (A-F) Actin stress fibers are clearly visible. (A-E) A series of images with 3 minutes intervals showed the appearance and disappearance of 'actin clouds' (arrow in A). (F) The same cell developed new 'actin clouds' at a different location by 200 minutes. (G) RH-phallodin staining of an 'actin cloud' in EGFP β-actin transfected B16 cells. (H) Visualization of an 'actin cloud' in an EGFP β-actin transfected B16 cell with an anti-β-actin specific antibody. Note that this antibody recognizes only endogenous β-actin (Fig. 3). (I) RH-phalloidin staining of an 'actin cloud' in nontransfected B16 cells. Bar, 20 μm.

rim with a constant diameter of 4-5 μm. The lamellipodium contained a ribbed pattern of intense fluorescent actin bundles (Figs 7, 8). These bundles remained associated with the protruding leading edge of the migrating cell and their length was constant while approaching a given reference point (arrowhead in Fig. 8A'-C'). Similar to the lamellipodium, the EGFP β-actin fluorescent intensity in these bundles was maximal at the cell margin and declined towards the interior of the cell (Fig. 8). In the moving lamellipodium, distinct fluorescent spots of actin were observed, which at first glance seemed to migrate against the motion of the advancing cell. Closer inspection, however, proved that they were immobile in respect to the substrate (compare circles in Fig. 8A'-C'), suggesting that they could represent anchoring points of the cell.

Within the cell body, EGFP β-actin was organized in fibers perpendicular to the direction of cell migration, parallel to the leading edge (Fig. 9A). Similar to the fluorescent actin spots most fibers were static. In all observed migrating cells the nucleus moved over this network in direction of migration (data not shown). All migrating cells changed the direction of locomotion during the time of observation. This occurred in a very characteristic way and is exemplified on the cell shown in Fig. 7 and 9. The leading edge started to split into two parts after six minutes of observation. Both fronts then migrated in different directions until the smaller edge collapsed and was retracted towards the main part of the cell body. After 27 minutes of observation the remaining leading edge divided again into two fronts and the cell movement proceeded as described before. During this change of direction the actin fibers were reorganized parallel to the leading edge. Fig. 9 shows a schematic outline of the actin fibers; the direction of the migrating cell is indicated by arrows.

DISCUSSION

EGFP β-actin integrates into actin filaments

Expression of β- and γ-actin isoforms was shown to have different impact on myoblasts morphology. Beta isoform transfectants displayed well defined filamentous organization, whereas gamma isoforms showed a more diffuse organization of actin cables (Schevzov et al., 1992). This result prompted us to choose the β-actin isoform for fusion to EGFP. Transfection experiments with the EGFP β-actin fusion protein under the strong CMV promoter showed accumulation of green

fluorescent proteins at the cell periphery and morphological changes of transfected COS-7 cells. These changes could be due to a cytotoxic effect of overexpressed EGFP alone, but this is unlikely since transfection of EGFP under the CMV promoter had no effect on the cell shape of COS cells (data not shown).

Morphological changes may be affected by altering the proportion of actin isoforms. Recent work has shown that overexpression of β-actin influences the function of cardiomyocytes (von Arx et al., 1995). Cellular malfunctions could also result from steric hindrance due to the linkage of the 26 kDa EGFP to the 43 kDa actin, as shown by in vitro experiments with *Dictyostelium* GFP-actin (Westphal et al., 1997). It was found that GFP-actin was fully functional in in vitro motility experiments when the fusion protein did not exceed 30% of native actin. In order to be within these limits the control of the transcription rate was achieved by the long form of the β-actin promoter. By testing the different constructs in mammalian cells, a correlation between increased changes in cell morphology and increased expression levels of EGFP β-actin fusion protein was observed. Therefore the selection of the appropriate promoter is crucial for successful use of the EGFP-tagged β-actin.

Polymerization and depolymerization of actin filaments

Counter-staining of actin filaments with Rh-Ph in cells expressing EGFP β-actin showed the successful incorporation of the fluorescent fusion protein into actin filaments. The time course of changes observed in cytochalasin treated cells was similar to that in control cells, indicating that actin polymerization and the binding of capping proteins to actin is not disturbed by the fusion of EGFP to actin.

The mechanism of cytochalasin B is not yet entirely clear. Besides the fact that this drug inhibits polymerization by binding to the barbed end, in vitro studies have shown that it severs F-actin (Hartwig and Stossel, 1979; Theodoropoulos et al., 1994). Fragmentation of large actin stress fibers in living cells within seconds after addition of cytochalasin B was indeed observed in the experimental setup used. After the severing of actin filaments depolymerization of the fragments followed, and within ten minutes most F-actin was

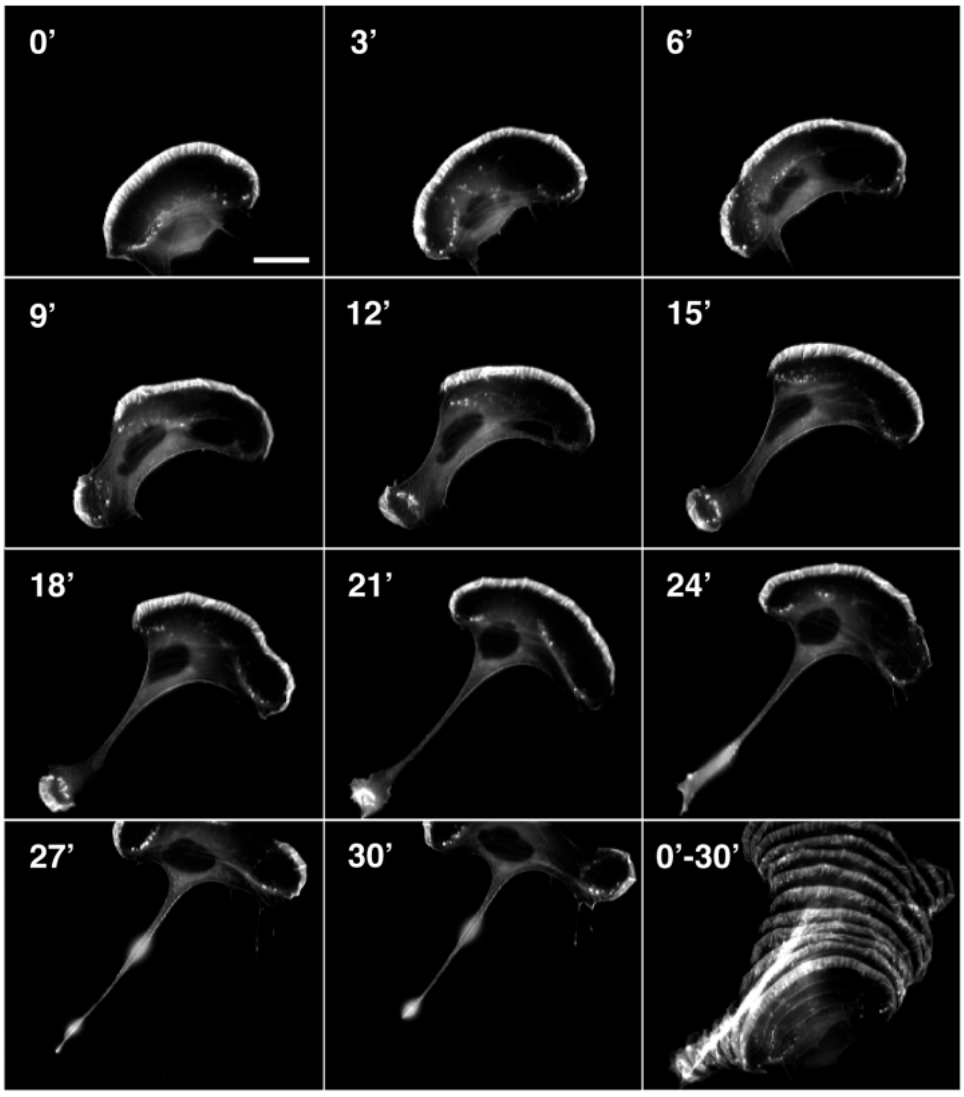

Fig. 7. EGFP β-actin in a migrating cell. EGFP β-actin transfected B16 cells were allowed to adhere for 12 hours to glass coverslips coated with 5 μg/ml of LN. The illustrated images correspond to three minute time intervals of a migrating cell. The composite at the lower right represents an overlay of images taken during the 30 minute period of migration. Bar, 20 μm.

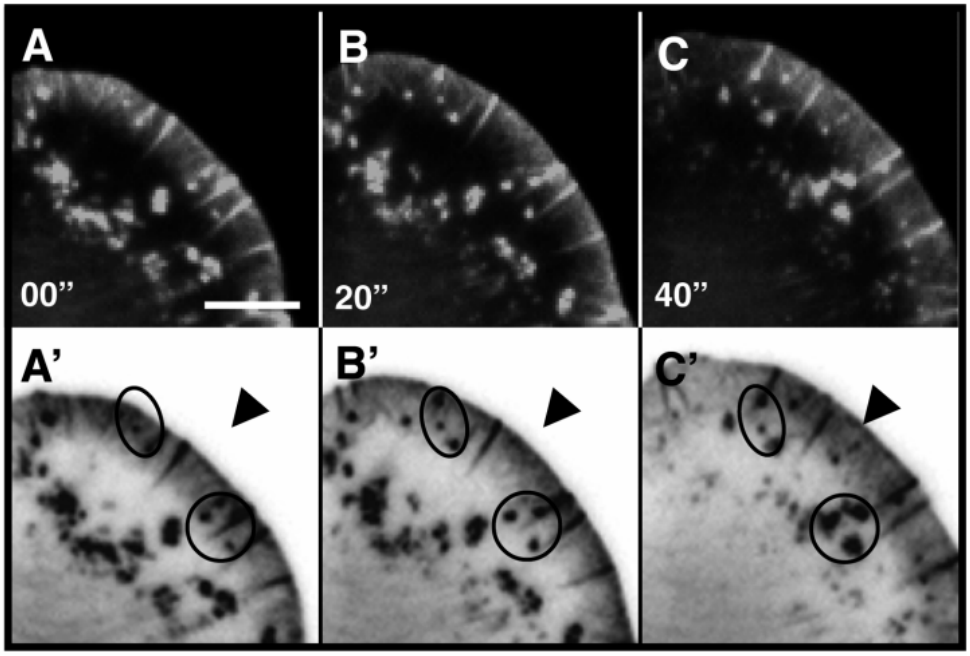

Fig. 8. Immobile actin spots in a migrating B16F1 cell. Cells were plated on LN as described in Fig. 7. Fluorescent β-actin was observed at high magnification in a migrating cell. (A-C) Images taken at intervals of 20 seconds. (A’-C’) Image colors were inverted in order to obtain better visibility of EGFP β-actin structures. Migration is illustrated by a static arrowhead given as reference point. Immobile actin spots are marked by circles at identical coordinates. Bar, 10 μm.

depolymerized. In general, peripheral stress fibers in stationary cells depolymerized more rapidly than stress fibers in the center of the cell. This indicates that the turnover of actin filaments is more rapid at the periphery of the cell and demonstrates that two mechanisms are involved in the decay of F-actin by cytochalasin B; severing and depolymerization.

Dynamics of actin clouds

Observed stationary cells displayed actin stress fibers and showed prominent ruffling of the plasma membrane. These cells spontaneously formed ‘actin clouds’, actin rich ring-like structures most likely represent actin ruffles (Boschek et al., 1981; Mellström et al., 1988; Dowrick et al., 1993; Ruusala et al., 1998). The clouds emerged irrespective of the cell region and their ring-shaped extension coincided with local protrusions of the cell membrane. When the actin rich ring developed close to the edge of the cell a local lamellipodium was formed. The structure of this lamellipodium resembles the lamellipodium found in migrating cells. Therefore the generation of ‘actin clouds’ may be a ubiquitous mechanism essential for the building of lamellipodia by the actin cytoskeleton (Ruusala et al., 1998). In stationary and migrating cells the outer semicircle of the actin cloud forms an organized lamellipodium, whereas the inner semicircle persists as a diffuse actin rich area. While the leading edge in a migrating cell is constitutive, the actin cloud in a stationary cell is a temporary structure which is replaced by polymerizing fibers. A further function of actin clouds may be the reorientation of stress fibers within the stationary cell. This function may be prevalent in ‘actin clouds’ appearing in the center of the cell, away from the plasma membrane, possibly allowing the cell to adapt to changes of the extracellular microenvironment.

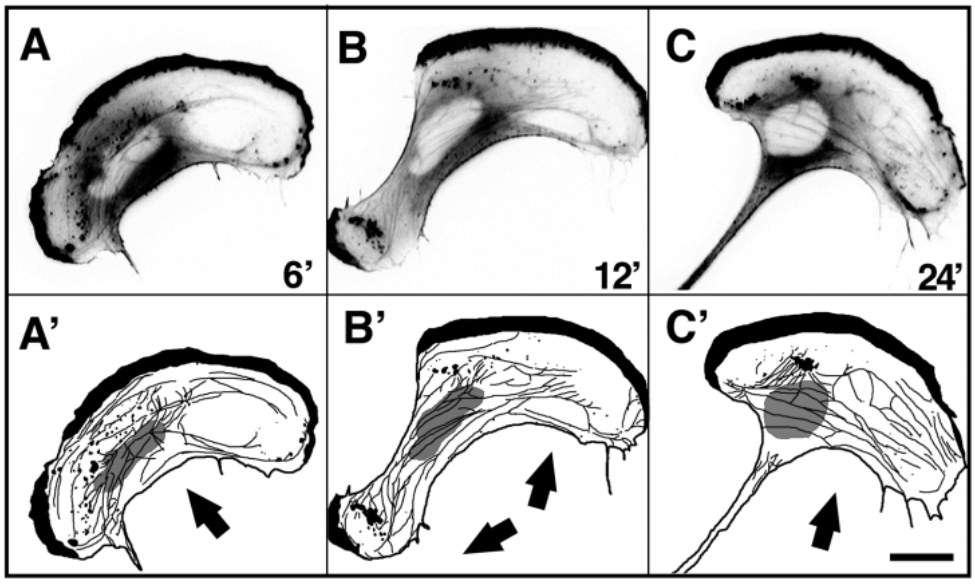

Fig. 9. Behavior of the actin cytoskeleton in cells changing the direction of migration. (A-C) Color inverted illustration of the migrating cell shown in Fig. 7 at time point 6’, 12’, and 24’, respectively. (A’-C’) The actin filaments (black lines), the lamellipodium (black) and the nucleus (gray) are outlined in the drawings derived from image overlays with A,B,C, respectively. The direction of migration is indicated by arrows. Bar, 20 μm.

Actin cytoskeleton remodeling in migrating cells

Migrating B16 cells showed an actin rich, arc-shaped lamellipodium containing microspikes, which was followed by the lamella, a zone low of actin content, and the cell body containing the nucleus. The direction of cell migration was imposed by the progression of the lamellipodium.

Studies with fish keratocytes proposed two hypothesis for the advancement of the lamellipodium. In the nucleation release model, short actin filaments are created at the cell front and then subsequently released into the cell body (Theriot and Mitchison, 1991, 1992). A particular orientation of actin filaments is not required in this model. In the treadmilling model, actin filaments are oriented with their barbed ends towards the cell margin; polymerization is expected to occur at the front of the cell edge and depolymerization towards the rear of the lamellipodium (Wang, 1985; Small, 1994b). Studies with fixed cells demonstrated that the highest density of actin filaments in the lamellipodium is at the cell edge and that the barbed ends of these filaments point towards the cell margin, thus forming an actin density gradient within the lamellipodium (Small et al., 1995; Cramer et al., 1997; Svitkina et al., 1997). In the present study, actin rich lamellipodia were observed to remain constant in width during cell migration and displayed an actin concentration gradient. This finding seemed to be more consistent with the treadmilling model. We postulate that treadmilling also occurs at the edge of spreading cells and in local lamellipodia of stationary cells. Since we also observed an actin concentration gradient in microspikes embedded in the lamellipodium, their forward movement may also be achieved by treadmilling.

Several actin structures in moving cells were reported to be stationary or follow a retrograde movement with respect to the substrate (Symons and Mitchison, 1991; Theriot and Mitchison, 1991; Cramer et al., 1997). One study with fish keratocytes suggested that myosin II is involved in the compression of actin filaments in the lamellipodium leading to arc-shaped actin bundles parallel to the leading edge. Compression of the actin network was thought to result in the forward translocation of the cell body (Svitkina et al., 1997). In B16 cells actin fibers were observed to evolve out of the lamellipodium and then oriented parallel to the leading edge. These actin fibers remained fixed relative to the substrate, suggesting that they were linked to anchoring points and participated in the forward translocation of the cell.

In migrating cells, Cao et al. (1993) observed rearward moving punctuate structures which were formed behind the lamellipodium. It is likely that these spots consist of G-actin since they were not detectable by phalloidin. The authors suggested that such spots may represent an actin reservoir from which G-actin can be released and then reincorporated into filaments of the lamellipodium. We found actin spots evolving at the cell margin which remained fixed in respect to the substrate and increased in diameter during forward movement of the cell. In our opinion these spots resembled anchoring points of the cell, which have the capacity to immobilize G-actin. Treatment of cells with phorbol esters, which increases the adhesion strength of cells by activation of integrins (Shaw et al., 1990; Gismondi et al., 1992), enhanced the appearance of actin spots. A recent study reported that actin spots which developed in the lamellipodium of fish keratocytes contained β1 integrin, and several other molecules which are normally found to be in focal adhesion contacts (Lee and Jacobson, 1997). We are currently investigating whether the actin rich spots correspond to nascent focal adhesion sites.

In summary, the EGFP β-actin fusion protein proved to be a valuable tool to study the dynamic changes of the different components of the actin cytoskeleton. Since the actin cytoskeleton is involved in a vast number of cellular functions, the EGFP β-actin fusion protein will help to provide further insights into actin function in living cells.

We are grateful to Dr Gabbiani for his gifts of antibodies, Dr Perriard for cDNA of human β-actin, M. Zonta for technical support, J. C. Rumbeli for photography, D. Wohlwend for FACS operation and J. Ntah for secretarial assistance. We thank Dr C. Chaponnier and C. Wong for critical reading of the manuscript. This work has been supported by the 'Schweizerische Krebsliga' grant No. KFS 412-1-1997 and grants from the Swiss National Science Foundation 31-49241-96 and 31-052727.97.

REFERENCES

Boschek, C. B., Jockush, B. M., Friis, R. R., Back, R., Grundmann, E. and Bauer, H. (1981). Early changes in the distribution and organization of microfilament proteins during cell transformation. *Cell* **24**, 175-184.

Cao, L., Fishkind, D. J. and Wang, Y. (1993). Localization and dynamics of nonfilamentous actin in cultured cells. *J. Cell Biol.* **123**, 173-181.

Carlier, M. F. and Pantaloni, D. (1994). Actin assembly in response to extracellular signals: role of capping proteins, thymosin β2 and profilin. *Semin. Cell Biol.* **5**, 183-191.

Carlier, M. F., Laurent, V., Santolini, J., Melki, R., Didry, D., Xia, G. X., Hong, Y., Chua, N. H. and Pantaloni, D. (1997). Actin depolymerizing factor (ADF/cofilin) enhances the rate of filament turnover: implication in actin-based motility. *J. Cell Biol.* **136**, 1306-1323.

Cooper, J. A. (1987). Effects of cytochalasin and phalloidin on actin. *J. Cell Biol.* **105**, 1473-1478.

Cramer, L. P., Siebert, M. and Mitchison, T. J. (1997). Identification of novel graded polarity actin filament bundles in locomoting heart fibroblasts: implications for the generation of motile force. *J. Cell Biol.* **136**, 1287-1305.

Cunningham, C. C., Stossel, T. P. and Kwiatkowski, D. J. (1991). Enhanced motility in NIH 3T3 fibroblasts that overexpress gelsolin. *Science* **251**, 1233-1236.

Dancker, P., Low, I., Hasselbach, W. and Wieland, T. (1975). Interaction of actin with phalloidin: polymerization and stabilization of F-actin. *Biochim. Biophys. Acta* **400**, 407-414.

Dowrick, P., Kenworthy, P., McCann, B. and Warn, R. (1993). Circular ruffle formation and closure lead to macropinocytosis in hepatocyte growth factor/scatter factor-treated cells. *Eur. J. Cell Biol.* **61**, 44-53.

Doyle, T. and Botstein, D. (1996). Movement of yeast cortical actin cytoskeleton visualized *in vivo*. *Proc. Nat. Acad. Sci. USA* **93**, 3886-3891.

Dunlevy, J. R. and Couchman, J. R. (1993). Controlled induction of focal adhesion disassembly and migration in primary fibroblasts. *J. Cell Sci.* **105**, 489-500.

Forscher, P. and Smith, S. J. (1988). Actions of cytochalasins on the organization of actin filaments and microtubules in a neuronal growth cone. *J. Cell Biol.* **107**, 1505-1516.

Gerdes, H. H. and Kaether, C. (1996). Green fluorescent protein: applications in cell biology. *FEBS Lett.* **389**, 44-47.

Gismondi, A., Mainiero, F., Morrone, S., Palmieri, G., Piccoli, M., Frati, L. and Santoni, A. (1992). Triggering through CD16 or phorbol esters enhances adhesion of NK cells to laminin via very late antigen 6. *J. Exp. Med.* **176**, 1251-1257.

Hartwig, J. H. and Stossel, T. P. (1979). Cytochalasin B and the structure of actin gels. *J. Mol. Biol.* **134**, 539-553.

Holmes, K. C., Popp, D., Gebhard, W. and Kabsch, W. (1990). Atomic model of the actin filament. *Nature* **347**, 44-49.

Lauffenburger, D. A. and Horwitz, A. F. (1996). Cell migration: a physically integrated molecular process. *Cell* **84**, 359-369.

Lee, J., Ishihara, A., Theriot, J. A. and Jacobson, K. (1993). Principles of locomotion for simple-shaped cells. *Nature* **362**, 167-171.

Lee, J. and Jacobson, K. (1997). The composition and dynamics of cell-substratum adhesions in locomoting fish keratocytes. *J. Cell Sci.* **110**, 2833-2844.

Ludin, B. and Matus, A. (1998). GFP illuminates the cytoskeleton. *Trends Cell Biol.* **8**, 72-77.

MacLean-Fletcher, S. and Pollard, T. D. (1980). Mechanism of action of cytochalasin B on actin. *Cell* **20**, 329-341.

Matsudaira, P. (1994). Actin crosslinking proteins at the leading edge. *Semin. Cell Biol.* **5**, 165-174.

Mellström, K., Heldin, C. H. and Westermark, B. (1988). Induction of circular membrane ruffling on human fibroblasts by platelet-derived growth factor. *Exp. Cell Res.* **177**, 347-359.

Mitchison, T. J. and Cramer, L. P. (1996). Actin-based cell motility and cell locomotion. *Cell* **84**, 371-379.

Mounier, N., Perriard, J. C., Gabbiani, G. and Chaponnier, C. (1997). Transfected muscle and non-muscle actins are differentially sorted by cultured smooth muscle and non-muscle cells. *J. Cell Sci.* **110**, 839-846.

Ng, S. Y., Gunning, P., Liu, S. H., Leavitt, J. and Kedes, L. (1989). Regulation of the human β-actin promoter by upstream and intron domains. *Nucl. Acids Res.* **17**, 601-615.

Pollard, T. D. and Mooseker, M. S. (1981). Direct measurement of actin polymerization rate constants by electron microscopy of actin filaments nucleated by isolated microvillus cores. *J. Cell Biol.* **88**, 654-659.

Ruusala, A., Sundberg, C., Arvidsson, A. K., Rupp-Thuresson, E., Heldin, C. H. and Claesson-Welsh, L. (1998). Platelet-derived growth factor (PDGF)-induced actin rearrangement is deregulated in cells expressing a mutant Y778F PDGF β-receptor. *J. Cell Sci.* **111**, 111-120.

Schevzov, G., Lloyd, C. and Gunning, P. (1992). High level expression of transfected β- and γ-actin genes differentially impacts on myoblast cytoarchitecture. *J. Cell Biol.* **117**, 775-785.

Shaw, L. M., Messier, J. M. and Mercurio, A. M. (1990). The activation dependent adhesion of macrophages to laminin involves cytoskeletal anchoring and phosphorylation of the alpha 6 beta 1 integrin. *J. Cell Biol.* **110**, 2167-2174.

Small, J. V. (1994a). Introduction: actin and cell crawling. *Semin. Cell Biol.* **5**, 137-138.

Small, J. V. (1994b). Lamellipodia architecture: actin filament turnover and the lateral flow of actin filaments during motility. *Semin. Cell Biol.* **5**, 157-163.

Small, J. V., Herzog, M. and Anderson, K. (1995). Actin filament organization in the fish keratocyte lamellipodium. *J. Cell Biol.* **129**, 1275-1286.

Stossel, T. P. (1993). On the crawling of animal cells. *Science* **260**, 1086-1094.

Sun, H. Q., Kwiatkowska, K. and Yin, H. L. (1995). Actin monomer binding proteins. *Curr. Opin. Cell Biol.* **7**, 102-110.

Svitkina, T. M., Verkhovsky, A. B., McQuade, K. M. and Borisy, G. G. (1997). Analysis of the actin-myosin II system in fish epidermal keratocytes: mechanism of cell body translocation. *J. Cell Biol.* **139**, 397-415.

Symons, M. H. and Mitchison, T. J. (1991). Control of actin polymerization in live and permeabilized fibroblasts. *J. Cell Biol.* **114**, 503-513.

Theodoropoulos, P. A., Gravanis, A., Tsapara, A., Margioris, A. N., Papadogiorgaki, E., Galanopoulos, V. and Stournaras, C. (1994). Cytochalasin B may shorten actin filaments by a mechanism independent of barbed end capping. *Biochem. Pharmacol.* **47**, 1875-1881.

Theriot, J. A. and Mitchison, T. J. (1991). Actin microfilament dynamics in locomoting cells. *Nature* **352**, 126-131.

Theriot, J. A. and Mitchison, T. J. (1992). The nucleation-release model of actin filament dynamics in cell motility. *Trends Cell Biol.* **2**, 219-222.

Theriot, J. A. (1997). Acceleration on a treadmill: ADF/cofilin promotes rapid actin filament turnover inthe dynamic cytoskeleton. *J. Cell Biol.* **136**, 1165-1168.

von Arx, P., Bantle, S., Soldati, T. and Perriard, J. C. (1995). Dominant negative effect of cytoplasmic actin isoproteins on cardiomyocyte cytoarchitecture and function. *J. Cell Biol.* **131**, 1759-1773.

Wang, Y. L. (1984). Reorganization of actin filament bundles in living fibroblasts. *J. Cell Biol.* **99**, 1478-1485.

Wang, Y. L. (1985). Exchange of actin subunits at the leading edge of living fibroblasts: possible role of treadmilling. *J. Cell Biol.* **101**, 597-602.

Wegner, A. (1976). Head to tail polymerization of actin. *J. Mol. Biol.* **108**, 139-150.

Welch, M. D., Mallavarapu, A., Rosenblatt, J. and Mitchison, T. J. (1997). Actin dynamics *in vivo*. *Curr. Opin. Cell Biol.* **9**, 54-61.

Westphal, M., Jungbluth, A., Heidecker, M., Mühlbauer, B., Heizer, C., Schwartz, J. M., Marriot, G. and Gerisch, G. (1997). Microfilament dynamics during cell movement and chemotaxis monitored using a GFP-actin fusion protein. *Curr. Biol.* **7**, 176-183.

Winston, S. E. and Fuller, S. A. (1991). Isolation and analysis of proteins. In *Current Protocols in Immunology* (ed. J. E. Coligan et al.), section 8.10. pp. 11-171. Greene Publishing Associates & Wiley-Interscience, New York.

Witke, W., Sharpe, A. H., Hartwig, J. H., Azuma, T., Stossel, T. P. and Kwiatkowski, D. J. (1995). Hemostatic, inflammatory, and fibroblast responses are blunted in mice lacking gelsolin. *Cell* **81**, 41-51.

Yao, X., Chaponnier, C., Gabbiani, G. and Forte, J. G. (1995). Polarized distribution of actin isoforms in gastric parietal cells. *Mol. Biol. Cell* **6**, 541-557.

3.3. Microtubule dependent rear retraction is required for directed cell migration

Molecular Biology of the Cell
Vol. 11, 2999–3012, September 2000

Actin-dependent Lamellipodia Formation and Microtubule-dependent Tail Retraction Control-directed Cell Migration

Christoph Ballestrem,† Bernhard Wehrle-Haller,* Boris Hinz,* and Beat A. Imhof†

Department of Pathology, Centre Médical Universitaire, Geneva, Switzerland

Submitted February 17, 2000; Revised June 21, 2000; Accepted June 27, 2000
Monitoring Editor: Ted Salmon

Migrating cells are polarized with a protrusive lamella at the cell front followed by the main cell body and a retractable tail at the rear of the cell. The lamella terminates in ruffling lamellipodia that face the direction of migration. Although the role of actin in the formation of lamellipodia is well established, it remains unclear to what degree microtubules contribute to this process. Herein, we have studied the contribution of microtubules to cell motility by time-lapse video microscopy on green flourescence protein-actin- and tubulin-green fluorescence protein–transfected melanoma cells. Treatment of cells with either the microtubule-disrupting agent nocodazole or with the stabilizing agent taxol showed decreased ruffling and lamellipodium formation. However, this was not due to an intrinsic inability to form ruffles and lamellipodia because both were restored by stimulation of cells with phorbol 12-myristate 13-acetate in a Rac-dependent manner, and by stem cell factor in melanoblasts expressing the receptor tyrosine kinase c-kit. Although ruffling and lamellipodia were formed without microtubules, the microtubular network was needed for advancement of the cell body and the subsequent retraction of the tail. In conclusion, we demonstrate that the formation of lamellipodia can occur via actin polymerization independently of microtubules, but that microtubules are required for cell migration, tail retraction, and modulation of cell adhesion.

INTRODUCTION

Cell motility plays a central role in a variety of biological processes, including embryonic development, wound healing, and tumor cell metastasis (Lauffenburger and Horwitz, 1996; Hangan *et al.*, 1997; Shattil and Ginsberg, 1997; Montell, 1999). The driving force for cell migration is directed by the reorganization of the actin cytoskeleton, which includes the protrusion of the lamellipodium at the cell front and the retraction of the cell rear. The protrusion of the lamellipodium is provided by continuous growth of actin filaments toward the leading edge of the lamellipodium, the retraction of the rear is regulated by the release of adhesive contacts from extracellular matrix proteins (Lauffenburger and Horwitz, 1996).

Microtubules have been suggested to play a role in regulating cell migration because destruction of microtubules in fibroblasts resulted in inhibition of protrusive lamellipodial activity (Vasiliev and Gelfand, 1976; Bershadsky *et al.*, 1991). More recently there has been evidence to suggest that microtubules regulate adhesive or protrusive events through pathways involving the small GTPases Rho and Rac (Nobes and Hall, 1999; Waterman-Storer and Salmon, 1999). Rho induces assembly of stress fibers and focal contacts, and Rac activates actin-dependent lamellipodium formation and ruffling (Ridley and Hall, 1992b; Ridley *et al.*, 1992). It has been shown that disrupting microtubules led to Rho activation, which resulted in an increased size of focal contacts and enhanced phosphorylation of paxillin and focal adhesion kinase (Bershadsky *et al.*, 1996; Enomoto, 1996). Direct targeting of microtubules to focal contacts followed by their dissociation from the substrate has recently been demonstrated in fibroblasts, and it was hypothesized that microtubules deliver a relaxing impulse to substrate contacts, thus facilitating the turnover of adhesive contact sites (Kaverina *et al.*, 1999).

Other studies indicate that microtubules exert their control on the reorganization of the actin cytoskeleton via a Rac-dependent pathway at the cell front. Rac1-guanosine 5′-triphosphate (GTP) has been shown to bind to tubulin dimers (Best *et al.*, 1996), and hence it was proposed that the polymerization of microtubules at the cell front liberates Rac1-GTP, thereby inducing actin polymerization (Water-

* These authors contributed equally to this study.
† Corresponding authors. E-mail address: ballestr@cmu.unige.ch. or Beat.Imhof@medecine.unige.ch
FN, fibronectin; GFP, green fluorescence protein; PMA, phorbol 12-myristate 13-acetate; SACED, stroboscopic analysis of cell dynamics; SCF, stem cell factor.

man-Storer *et al.*, 1999). Furthermore, it has been shown that the growth of microtubules induced in fibroblasts after the removal of the microtubule disrupter nocodazole activates Rac1 GTPase. Waterman-Storer and Salmon (1999) suggested a model of positive feedback interactions between microtubules and actin. In this model the authors propose that microtubule disassembly in the main cell body activates RhoA, which is responsible for stress fiber and focal contact formation and contraction of the cell. In contrast, microtubule assembly at the leading edge results in Rac1 activation and lamellipodium formation (Waterman-Storer and Salmon, 1999; Waterman-Storer *et al.*, 1999).

However, this model does not address the following questions: Can microtubules regulate the activation of Rac1 induced by external signals such as growth factors? Do microtubules influence cell migration by regulation of cell adhesion? Are microtubules implicated in mechanisms of tail retraction? To address these issues, we used B16 melanoma cells and Melb-a melanoblasts. In contrast to fibroblasts these cells are highly motile with a high frequency of lamellipodia formation. Green fluorescence protein (GFP)-actin- or tubulin-GFP–transfected cells were used for time lapse experiments to visualize cytoskeletal reorganization. Lamellipodial and ruffling events were quantified by kymograph analysis. Phorbol 12-myristate 13-acetate (PMA) was used to induce cell motility in B16 cells, and stem cell factor (SCF) was used for melanoblasts.

MATERIALS AND METHODS

Cell Lines, Plasmids, and Reagents

Mouse melanoma cells (B16F1) were kindly provided by G. Nicholson (M.D. Anderson Cancer Center, Houston, TX); melb-a melanoblasts were from Dr. Dot Bennett (St. George Hospital, London, UK) (Sviderskaya *et al.*, 1995). B16 cells were grown in DMEM (Life Technologies, Paisley, Scotland) supplemented with 10% fetal calf serum (FCS) (PAA Laboratories, Linz, Austria), 2 mM glutamine, 100 international units/ml penicillin, and 100 μg/ml streptomycin (= complete medium; all Life Technologies). Melb-a cells were grown in complete RPMI additionally supplemented with stem cell factor (SCF; 20 ng/ml) and basic fibroblast growth factor (20 ng/ml).

The construction of the GFP-actin plasmid has been described elsewhere (Ballestrem *et al.*, 1998). The original β5 tubulin-GFP plasmid was kindly provided by Dr. Matus (FMI, Basel, Switzerland) and was modified as follows: to enhance tubulin-GFP expression, the promoter region was replaced by a longer form of the β-actin promoter containing serum response elements as described for the GFP-actin construct (Ballestrem *et al.*, 1998). Plasmids containing myc-tagged Rac1 were kindly provided by Dr. Ballmer-Hofer (Paul Scherrer Institute, Villigen, Switzerland).

Human fibronectin (FN) was purchased from collaborative Biomedical Products (Bedford, MA). Taxol (paclitaxel) and nocodazole were purchased from Sigma (Sigma Chemical Co., St. Louis, MO). Rhodamine-phalloidin was obtained by Fluka (Buchs, Switzerland); antibodies against vinculin (clone V-9131) or tubulin (clone T-5168) were obtained from Sigma; 9E-10 antihuman myc hybridoma was from American Type Culture Collection.

Transfections

Transient and stable protein expression was obtained by transfection of cells with Fugene 6 (Roche, Basel, Switzerland) according to the manufacturer's recommendation. Briefly, 2.5 μg of plasmid DNA and 3 μl of Fugene 6 were incubated for 15 min in 100 μl of OPTIMEM (Life Technologies). This solution was added to cells at 30–60% confluence cultured in complete DMEM in a 35-mm tissue culture plate (Falcon, Becton Dickinson, Basel, Switzerland). After 10 h cells were detached by trypsinizing, washed with phosphate-buffered saline (PBS), and transferred to a 10-cm culture dish. Stable clones were obtained by treatment of cells with 1.5 mg/ml G418 (Geneticin; Life Technologies). For experiments with rac1, transiently transfected cells were plated onto FN (5 μg/ml)-coated glass coverslips. Two days after transfection, expression of the construct was evaluated by fluorescence microscopy by using an anti-myc antibody.

Time-Lapse Studies

Time-lapse studies were preformed as described previously (Ballestrem *et al.*, 1998). B16 cells were detached from plastic tissue culture plates by trypsin/EDTA treatment for 5 min, washed twice in complete DMEM, and plated in Ham's F12 containing 10% FCS on glass coverslips previously coated with 5 μg/ml FN. After a 4- to 12-h incubation cells were treated as indicated with nocodazole (10 μg/ml final), taxol (10 μM final), PMA (100 ng/ml final), or the combination of taxol/PMA, nocodazole/PMA.

SCF-induced lamellipodium formation was analyzed in c-kit expressing melb-a cells plated on serum-coated glass coverslips. After overnight culture in complete medium supplemented with 20 ng/ml SCF, cells were serum and SCF starved for 4 h prior to treatment with nocodazole (10 μg/ml) or taxol (10 μM). One hour later SCF (final concentration of 50 ng/ml) was added to induce lamellipodium formation and images were recorded at 1-min intervals.

Living cells were observed under an inverted fluorescent microscope (Zeiss-Axiovert 100) equipped with Plan-Neofluar 40×, 63×, 100× fluar oil immersion objectives (Zeiss, Oberkochen, Germany), and an incubation chamber for constant temperature and CO_2 regulation. GFP fluorescence was visualized by using a fluorescein isothiocyante filter set (450-490, FT 510, LP 520). Single or time-lapse pictures were acquired with a Hamamatsu C4742-95-10 digital charge-coupled device camera (Hamamatsu Photonics, Shizuoka, Japan) controlled by the Openlab software (Improvision, Oxford, UK). For time-lapse recordings, cells expressing GFP-constructs were kept at constant temperature of 37°C and 10% CO_2.

Fluorescence Microscopy

B16 cells were cultured on FN (5 μg/ml)-coated glass coverslips at 37°C and 10% CO_2 for indicated periods of time. Cells were then fixed with 4% paraformaldehyde for 10 min at room temperature. After 3 washes with PBS cells were permeabilized with 0.5% Triton X-100 in PBS for 5 min and washed again. For actin staining, cells were subsequently incubated with 100 nM Rhodamine-Phalloidin (Fluka) at room temperature; for tubulin staining and myc staining, cells were incubated with primary antibody dilutions of 1/400 in PBS/1% BSA for 30 min. Samples were then washed three times with PBS followed by staining with the secondary fluorescein isothiocyante- or Texas-Red–linked antibody diluted in PBS/1% BSA. For two-color staining with rhodamine-phalloidin and anti-myc antibody, the cells were always stained first with the phalloidine-coupled dye. After three final washes with PBS, cells were analyzed by using a Zeiss-Axiovert 100 microscope.

Quantification of Lamella Dynamics by Kymograph Analysis

B16 cells were seeded at 20,000 cells/ml in glass chambers coated with 5 μg/ml FN. Cells were grown for 18 h in DMEM/10% FCS and shifted to carbonate-free complete F12 medium 2 h prior to commencement of experiments. Cells were then observed under an inverted microscope (Zeiss, Jena, Germany), equipped with a 63× 1.4 NA Ph3 plan apochromat objective. Cell movements were monitored with a low-light video camera (AVT Horn BC-5, Aalen, Germany). Taxol (10 μM final concentration) and nocodazole (10

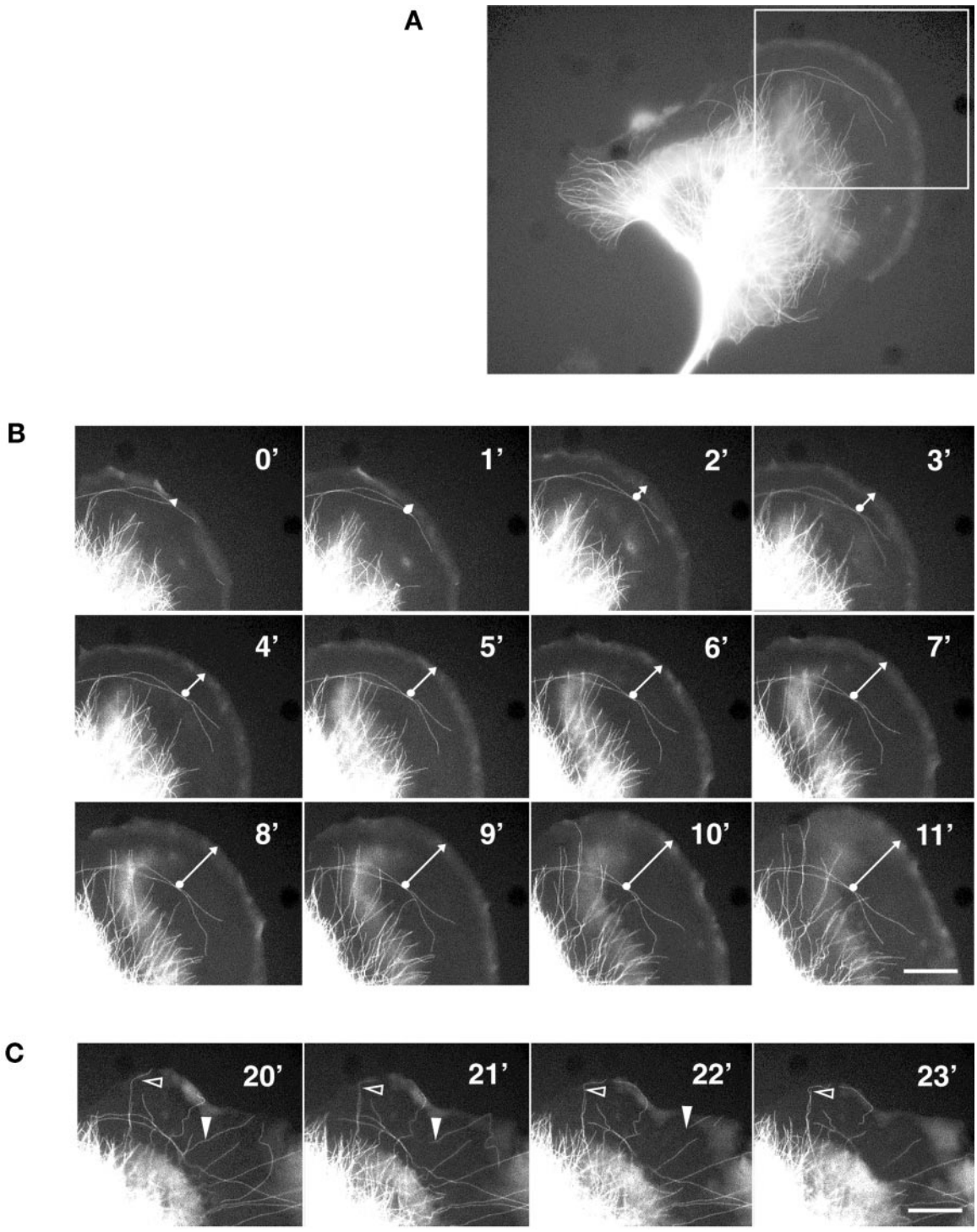

Figure 1. Dynamics of microtubules in a migrating melanoma cell. (A) Distribution of microtubules in a migrating B16 melanoma cell transfected with β5-tubulin-GFP. Note that the lamella is almost devoid of microtubules. (B) Consecutive fluorescence micrographs of the protruding lamella and lamellipodium were taken at 1-min intervals and show the dynamics of microtubules in the advancing lamella. Microtubules perpendicular to the leading edge barely enter the lamella, whereas microtubules growing parallel to the lamellipodium remain fixed with respect to the substrate. The arrow indicates the increasing distance between microtubules oriented parallel to the lamellipodium and the protruding leading edge. (C) As in B after stop of lamellipodium protrusion. Many microtubules reach the leading edge where they become stabilized (empty arrowhead) and eventually depolymerize from the minus end in the perinuclear region (filled arrowhead). Bar, 15 μm.

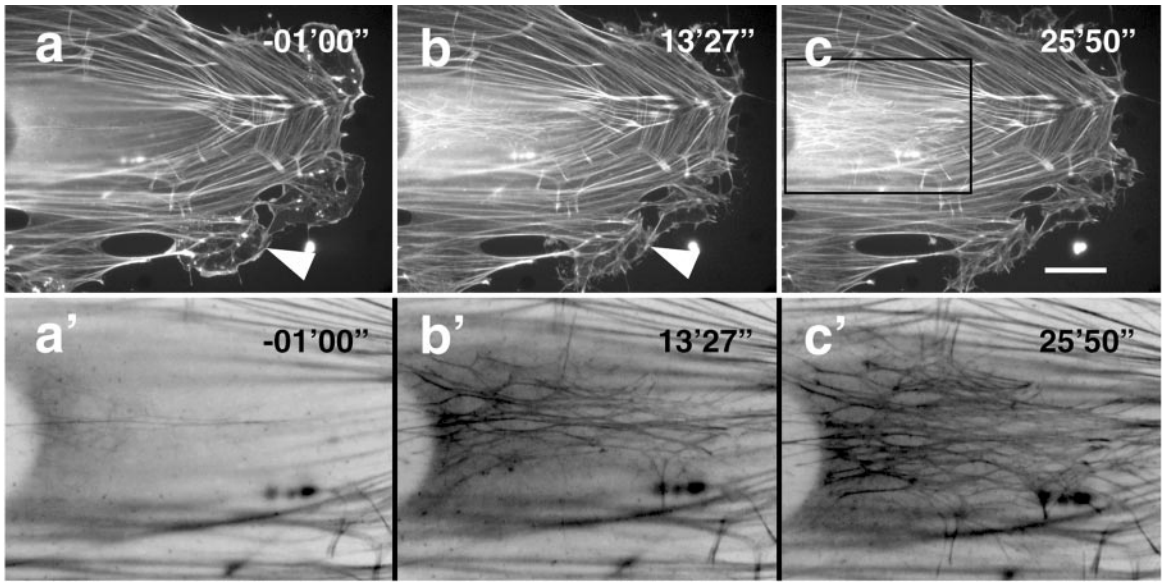

Figure 2. Actin dynamics in B16 cells during disruption of microtubules. GFP-actin–transfected cells were plated on FN and treated with 10 μg/ml nocodazole at time 00′00″. Images at time 13′27″ and 25′50″ demonstrate the inhibition of cell edge ruffling, (filled arrowheads) and the formation of new stress fibers and focal contacts (inserts). A′–c′) are high-power images of a–c, respectively, the depicted region is indicated in c. Improved visibility of the newly formed dense actin network was achieved by inverting colors. Bar, 10 μm.

μg/ml final concentration) were added 60 min, and PMA (100 ng/ml final concentration) 15 min prior to the start of recording.

To quantify lamella dynamics, phase contrast images of living B16 cells were digitized by using a video frame grabber card and analyzed by computer-assisted stroboscopic analysis (SACED) as recently described (Hinz *et al.*, 1999).

To monitor dynamics of isolated regions of the cell, the area of interest was selected on the phase contrast image. This area was digitally recorded, producing a gray value image with the width of one pixel encompassing structures along a single line drawn transversally over the cell edge. Dynamics of this selected cell region was studied at intervals of 1 s over the course of 5 min. The digital snapshots were lined up on a time scale in order of their acquisition. The resulting composite phase contrast picture allowed us to continuously follow the translocation of recorded structures over time. In total 11 lines/cell was created, resulting in stroboscopic images randomly distributed across the entire cell perimeter (Figure 6A). The described process was automated by KS 400 software (Zeiss). Ruffles were identified by their dark gray appearance and characteristic centripetal movement, beginning at the lamella edge; protruding cell edges and retracting ruffles were marked (Figure 6A). The main parameters characterizing cell motility were the velocity of lamellipodium protrusions, ruffle retraction rate (μm/min), and the frequency of these events (min^{-1}). Mean values were calculated from 15 cells/condition and analyzed by SACED on 11 lamella regions/cell. At least five independent experiments were performed to calculate mean values ($\pm$ SD). To determine significant differences between averages, unpaired *t* tests assuming equal variance were performed, and differences were considered as significant when $p < 0.01$.

Cell Migration Assay

B16 melanoma cells were plated at a density of 5000 cells/well (20% confluency) on serum-coated 24-well culture dishes and incubated overnight in complete medium at 37°C. Cells were placed under an Axiovert 100TV (Zeiss) inverted microscope equipped with an incubation chamber and a 10× objective (CP-Achromat 10×/0.25 Ph1 Var1). The distance of cell migration was measured from recordings over 2 h by using Openlab software. From measurements of all cells ($n > 50$) in the field covered by the objective, the average speed of migration per cell per hour was calculated for each indicated condition. The average speed from one representative experiment ($n = 5$) is shown in Figure 9A.

Adhesion Assays

Cell adhesion assays on FN were performed as described previously (von Ballestrem *et al.*, 1996) with slight modifications. Briefly, cells were trypsinized, washed once in complete DMEM, and stained with calcein according to manufacturer's recommendations (Molecular Probes, Eugene, OR). After two washes with RPMI/1% BSA, 5×10^4 cells were added to each well coated with the indicated concentrations of matrix proteins. Cells were allowed to spread for 1 h prior to treatment with taxol, nocodazole, PMA, or combinations of taxol/PMA, nocodazole/PMA at the indicated final concentrations. After 1 h incubation for taxol- and nocodazole-treated cells, 30 min for PMA treatment (combination taxol/PMA, nocodazole/PMA: 1 h taxol or nocodazole followed by 30 min taxol/PMA or nocodazole/PMA) the plate was washed a minimum of three times with 200 μl of prewarmed RPMI/1% BSA. Adherent fluorescent cells were measured by using a Cytofluor fluorescence reader (Stehlin, Basel, Switzerland). Cell adhesion was enumerated as cells bound per unit area based on the fluorescence measured for the total input (50,000 cells/well) of calcein-labeled cells. Adhesion to BSA-coated wells was used as control to provide the background fluorescence, which was subtracted from both, the bound and total input fluorescence.

RESULTS

Microtubule Dynamics in Migrating Melanoma Cells

Migrating cells show a large protruding lamellipodium followed by the lamella and the main cell body. To investigate

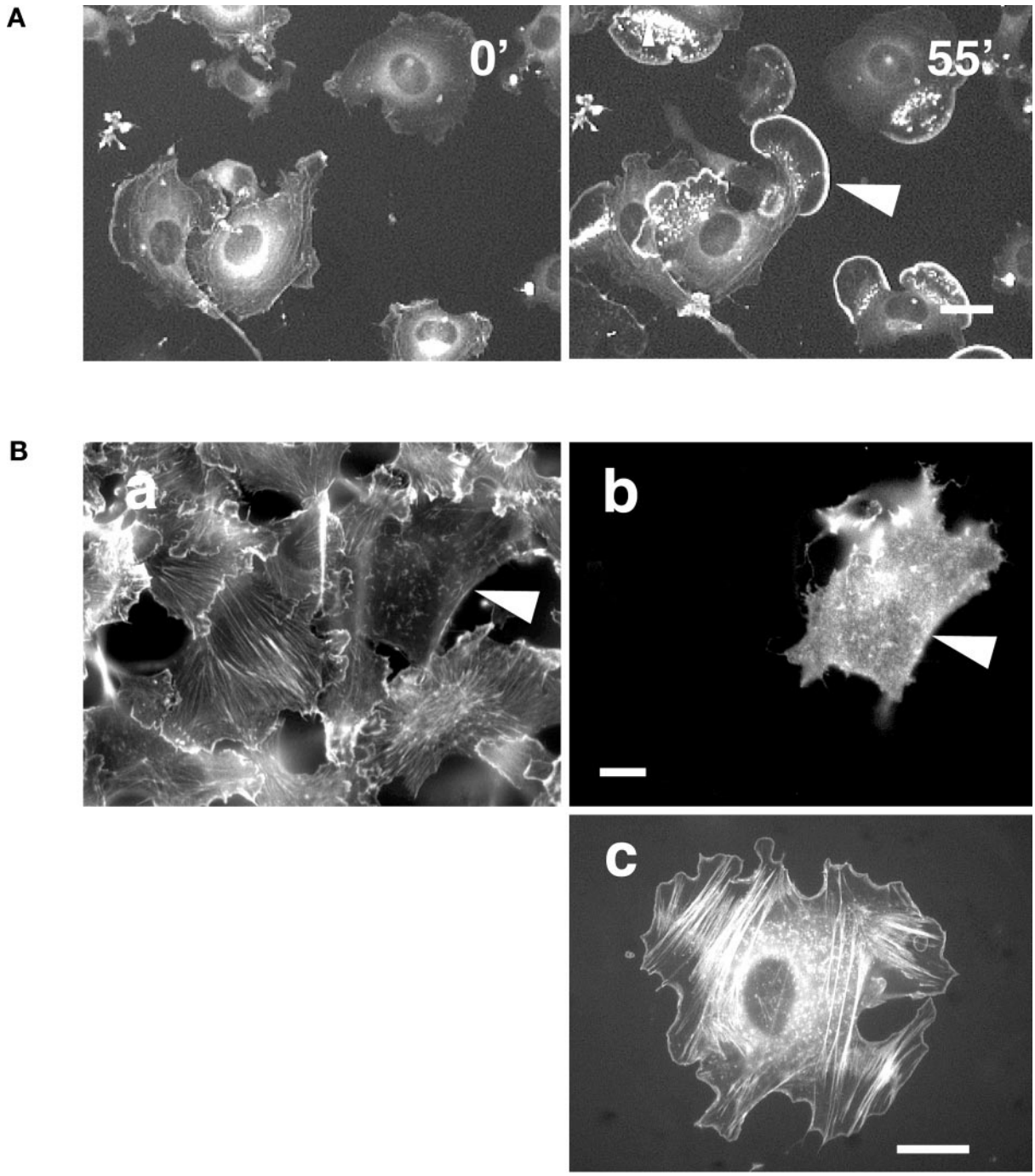

Figure 3. Lamellipodium formation after stimulation with PMA is Rac1 dependent. (A) GFP-actin–transfected B16 cells were plated on FN and treated with 100 ng/ml PMA at time 0′. Cells show intense ruffling and lamellipodium formation 55′ after addition of PMA (arrowheads). Bar, 40 μm. (B) B16 melanoma cells transiently transfected with N17Rac (dominant negative) were plated on FN and stimulated with 100 ng/ml PMA for 30 min. Fixed cells were stained for actin (a) and double labeled for N17Rac expression (b). In contrast to nontransfected cells, the N17Rac-transfected cell does not show stress fibers and lamellipodia (a, b). Bar, 20 μm. B16 cell cotransfected with GFP-actin and L61Rac (constitutively active) plated on FN (c) exhibits stress fibers and a smooth rim around the cell edge. Bar, 20 μm.

the contribution of microtubules to lamellipodia formation during migration, melanoma cells were stably transfected with β5-tubulin-GFP and plated on FN. B16 melanoma cells were used for our studies because of their high motility in comparison to the slowly migrating fibroblasts or epithelial cells. Using time-lapse fluorescence microscopy we show

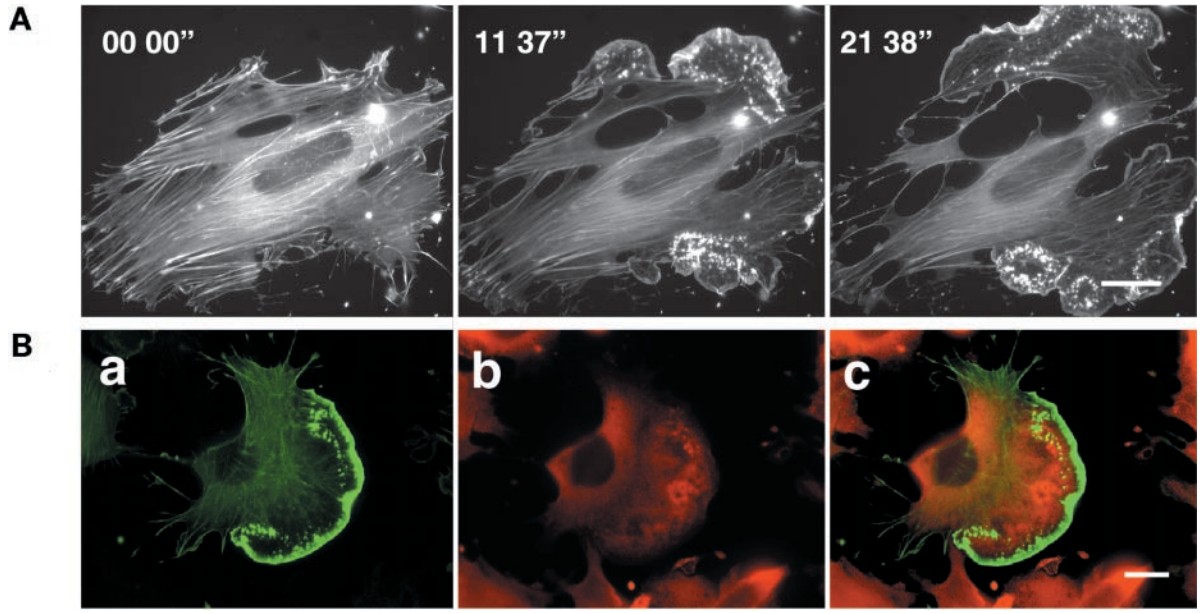

Figure 4. PMA-induced lamellipodium formation in cells pretreated with nocodazole. (A) GFP-actin–transfected cells were plated on FN and treated with 10 μg/ml nocodazole for 1 h prior to stimulation with 100 ng/ml PMA (time 00′00″). Time-lapse images show lamellipodia formation resulting in disruption of the cell after PMA stimulation (time 05′00″-21′38″). Bar, 20 μm. (B) Tubulin and actin distribution in cells treated with nocodazole and PMA. GFP-actin–expressing cells were plated on FN and treated subsequently with nocodazole and PMA. Cells were then fixed and stained for tubulin. a, actin distribution; b, tubulin distribution; and c, overlay of tubulin (red) and actin (green) within the cell. Note the cells show lamella and actin-rich lamellipodium (a, c) without any filamentous tubular structures (b, c). The red staining in lamella and lamellipodium of the cell in b and c represents unpolymerized tubulin. Bar, 20 μm

that the dynamic behavior of microtubules in the lamella of migrating B16 cells was similar to that observed by other studies with epithelial cells (Waterman-Storer and Salmon, 1997; Wadsworth, 1999).

A typical illustration of the distribution of microtubules in a lamella of a migrating melanoma cell is shown in Figure 1. The main cell body contains a dense network of microtubules, whereas the lamella is almost devoid of filamentous tubulin (Figure 1A). The protruding leading edge can be identified by the presence of unpolymerized tubulin-GFP versus the polymerized form. Time-lapse fluorescence microscope images of this cell were taken at 1-min intervals (Figure 1, B and C). A few rare microtubules are visible along the rear of the lamellipodium (Figure 1B, 0′-3′). These tubules become stabilized and stationary while the lamellipodium continues to advance; hence the lamellipodium and part of the lamella advance although they contain no microtubules (Figure 1B, 3′-11′). The tubules of the cell body grow perpendicular to the lamellipodium but remain at a constant distance of ~10 to 15 μm from the protruding leading edge (Figure 1B, 0′-11′). Generally, we observe that the distance between the perpendicular growing microtubules and the leading edge becomes larger at higher speed of cell migration. When the speed of lamellipodium protrusion slows down, many microtubules grow until they reach the edge of the cell (Figure 1C, open arrowhead). They then become stabilized and eventually depolymerize from the rear end of the microtubule (Figure 1B, filled arrowhead).

Are Microtubules Involved in Regulation of Ruffling and Formation of Lamellipodia?

Several studies have proposed a role for microtubules in mediating signals, which control cell migration. Because it became evident that part of the lamella in migrating cells was devoid of microtubules, we wished to investigate whether microtubule assembly would be necessary for actin-dependent ruffling and lamellipodium formation.

Treatment of cells with 10 μg/ml of the microtubule-disrupting reagent nocodazole resulted in a loss of essentially all polymerized tubulin filaments within 30 min (our unpublished results). To examine the effect of microtubule disruption on the dynamics of the actin cytoskeleton, GFP-actin–transfected cells were plated on coverslips and time-lapse images were recorded after the addition of nocodazole at time 00′00″. Prior to microtubule disruption the stationary cell exhibited prominent stress fibers and some lamellipodial extensions (Figure 2, arrows in –01′00″). At time point 13′27″ these extensions were retracted and new actin stress fibers and focal contacts were formed in the middle of the cell (Figure 2, bottom time frame 13′27″ and 25′50″). These results are similar to those obtained by other groups by using fibroblasts (Danowski, 1989; Bershadsky *et al.*, 1991), and clearly suggest that microtubules are involved in the regulation of ruffling and the formation of lamellipodia.

PMA-induced Ruffling Is Rac-dependent

Our findings thus far confer with those obtained in fibroblasts demonstrating that disruption of microtubules leads

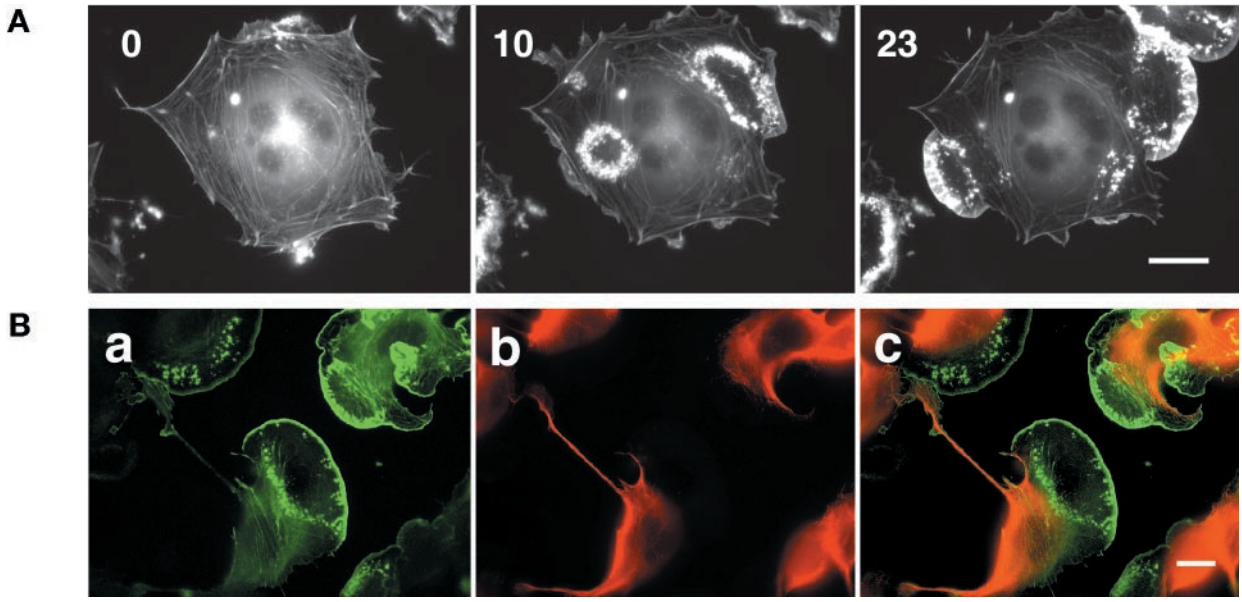

Figure 5. PMA-induced lamellipodium formation in B16 cells pretreated with taxol. (A) Melanoma cells transfected with GFP-actin were plated on FN and treated with 10 μM taxol for 1 h prior to 100 ng/ml PMA at time 0′. Subsequent images show circular actin ruffles and lamellipodium formation after addition of PMA (time 10′ and 23′). Bar, 20 μm. (B) Tubulin and actin distribution in cells treated with taxol and PMA. GFP-actin–expressing cells were plated on FN and treated subsequently with taxol and PMA. Cells were then fixed and stained for tubulin. a, actin distribution; b, tubulin distribution; and c, overlay of tubulin (red) and actin (green) within the cell. Note the cells show lamella and actin-rich lamellipodium (a, c) without any tubular structures (b, c). Bar, 20 μm.

to inhibition of spontaneous ruffling and lamellipodium formation. It was therefore interesting to investigate whether this disruption also would inhibit stimulation-induced ruffling and lamellipodium formation. Because PMA has been shown to induce the reorganization of the actin cytoskeleton (Schliwa *et al.*, 1984; Bershadsky *et al.*, 1990; Downey *et al.*, 1992), we used this agent to study ruffle and lamellipodium formation in the presence or absence of microtubules. Upon PMA treatment of GFP-actin–transfected cells, it was possible to induce extensive ruffling and lamellipodium formation (Figure 3A). One hour after addition of PMA all cells showed ruffling or lamellipodia (Figure 3A, 55′).

Because the small GTPase Rac is reportedly responsible for ruffling and lamellipodium formation in cells (Hall, 1998), we examined whether our PMA-induced ruffling is Rac dependent. Therefore, B16 cells were transiently transfected with a dominant-negative form of Rac (N17Rac). Cells were plated 5 h after transfection on FN-coated coverslips and treated 42 h later with PMA to induce ruffling. Thirty minutes after treatment, cells were fixed and stained for actin, and N17Rac expression. As shown in Figure 3B (a, b), N17Rac-transfected cells had no lamellipodia. In contrast, nontransfected cells showed an actin-rich rim, indicating active wild-type Rac in these cells. As a further control B16 cells were doubly transfected with a constitutively active form of Rac (L61Rac) and GFP-actin. These cells also showed an actin-rich rim similar to those treated with PMA (Figure 3B, c). The cells transfected with a constitutively active form of Rac no longer responded to PMA treatment, confirming that signals mediated by PMA are upstream of Rac.

Are Microtubules "Essential" for Ruffling and Formation of a Lamellipodium?

To investigate whether PMA treatment is still able to induce ruffle formation in cells devoid of microtubules, cells pretreated with 10 μg/ml nocodazole, were stimulated with 100 ng/ml PMA and time lapse images were recorded. Nocodazole-treated cells contained prominent stress fibers and showed no ruffles and lamellipodia (Figure 4A, time 00′00″). Within 5 min of application of PMA, however, ruffles began to develop, which extended in the direction of their leading edges to form large lamellipodia (Figure 4A, time 05′00″-21′38″). Despite extensive actin polymerization at the cell periphery, focal contacts and stress fibers remained stable. Consequently, the cell edges advanced tearing the cell apart. PMA stimulation in the absence of nocodazole lead to the expected lamellipodium formation and subsequent displacement of the cell (our unpublished results). At the completion of experiments conducted in presence of nocodazole and PMA, GFP-actin cells were fixed and stained for tubulin, revealing the absence of microtubules throughout the entire cell (Figure 4B).

Stimulation of taxol-pretreated cells with PMA resulted in enhancement of ruffling (Figure 5A). Ruffles often appeared as circular structures, which eventually extended toward the cell edge to form lamellipodia (Figure 5A, 10′ and 23′). Interestingly, similar to induction of lamellipodia after exchange from nocodazole-to-taxol–containing medium (Waterman-Storer *et al.*, 1999), taxol-stabilized microtubules did not enter the newly formed lamella (Figure 5B). Lamellipodium formation also was observed in nocodazole- and taxol-

treated cells in the absence of PMA although with a lower frequency, suggesting that spontaneous lamellipodia formation, as well as PMA-induced lamellipodia formation can occur in these cells. These results indicate that microtubules do not appear to be essential for actin-dependent ruffling and lamellipodium formation.

To quantify the ruffling events we analyzed kymographs obtained by SACED (Hinz *et al.*, 1999). This method allows recording of areas of interest along a line with the width of one pixel (Figure 6A). Individual line scans were assembled in sequence of their acquisition, resulting in a composite phase contrast picture (Figure 6, A and B). The activity of cell motion was measured for a period of 5 min and subdivided into lamellipodium protrusion velocity, lamellipodium frequency, ruffle retraction rate, and ruffle frequency. Lamellipodium protrusion velocity in nontreated cells was ~4.3 μm/min, and was significantly inhibited by taxol (20%) and by nocodazole (50%; Figure 6, B and C). Similarly, the ruffle retraction rate was significantly inhibited by taxol (25%) and by nocodazole (50%) (Figure 6, B and C). Both, ruffle retraction rate and lamellipodium protrusion velocity were fully restored by PMA treatment of the cells (Figure 6, B and C). Frequency of lamellipodium protrusion and ruffle formation remained almost constant after taxol but was significantly inhibited by nocodazole treatment. Lamellipodium and ruffling frequency were fully restored after addition of PMA. These results indicate that it is possible to induce cell motility events despite the disturbance of the microtubule dynamics.

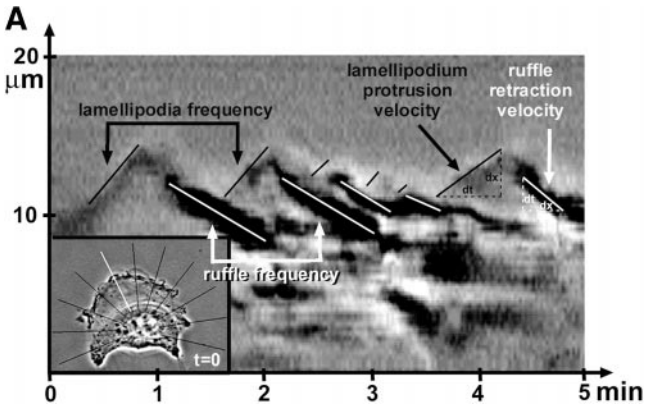

Figure 6. Kymograph analysis. (A) Motility of B16 melanoma cells was analyzed by measuring cell edge movements along regions of interest (insert, white line). Movements at these regions (20-μm line) were recorded in 1-s intervals for a period of 5 min. Pictures were assembled resulting in a stroboscopic image, which displays lamellipodia protrusion (black lines) and ruffle retraction (white lines). Lamellipodia protrusion velocity and ruffle retraction rate in these time/space images are indicated by the ascent (dx/dt, μm/min) of protrusive or retracted structures with notable gray values; frequencies are measured counting the number of lamellipodia or ruffles per minute (1/period, min^{-1}). (B) Stroboscopic images under different conditions. Taxol (+tax) and nocodazole (+noc) treatment for 60 min reduced velocity and frequency of lamellipodia protrusions and ruffle retractions. Protrusions and retractions are indicated by white arrows. Cell edge motility was enhance by PMA (+PMA); stimulation with PMA restored the motility of cells that were pretreated with taxol (+tax +PMA), or nocodazole (+noc +PMA). (C) Quantification of B16 cell motility by kymograph analysis. B16 melanoma cells were left untreated (nt) or were treated with taxol (tax), nocodazole (noc), or/and stimulated with PMA. Cell motility was recorded by SACED. The following cell motility parameters were quantified from stroboscopic images: 1) lamellipodia protrusion velocity, 2) ruffle retraction velocity (retraction rate), 3) lamellipodia frequency, and 4) ruffle frequency. Compared with nt cells, noc and tax decreased cell motility. Stimulation by PMA restored lamellipodia and ruffle velocity and frequency of cells pretreated with taxol (tax +PMA) or nocodazole (noc +PMA). At least 15 cells were analyzed per experimental condition. Error bars indicate SD of mean values, calculated from five independent experiments. $p \leq 0.01$, $p \leq 0.001$ compared with untreated control B16 cells.

SCF Induces Ruffling in Melanoblasts Pretreated with Nocodazole or Taxol

Although we demonstrated clearly that PMA induces Rac-dependent ruffling in the absence of microtubules, this does not represent a physiological situation. Therefore, we wanted to investigate whether it was possible to reproduce these findings after stimulation of cells via a surface receptor tyrosine kinase.

Melb-a is a melanoblast cell line expressing the receptor tyrosine kinase c-kit. Serum starved-melb-a cells do not show any ruffling and lamellipodia. Upon addition of the c-kit ligand SCF these cells immediately form lamellipodia and begin to migrate. In our experiments we plated melb-a cells on serum-coated glass coverslips, serum starved the cells for 4 h, and incubated them for 1 h in presence of 10 μg/ml nocodazole or 10 μM taxol prior to adding 50 ng/ml SCF (final concentration). Nocodazole- and taxol-pretreated cells began to form large lamellipodia within 10 min of SCF treatment (Figure 7, A and B). These observations confirm results obtained with PMA-stimulated melanoma cells, showing that microtubules are not essential for the activation of the actin machinery to form lamellipodia.

Microtubules Regulate Adhesion and Tail Retraction in Migrating Cells

In contrast to cells treated with SCF alone (example in Figure 8A) most of the melb-a cells (90%) treated with nocodazole prior to SCF addition displayed virtually no cell migration, despite the formation of lamellipodia (our unpublished results; Figure 8B). The remaining 10% that were able to advance moved with ~10 times slower kinetics compared with cells stimulated with SCF alone. Perhaps even more strikingly, these cells were unable to retract their tail (example in Figure 8B).

Similarly, B16 cells treated with nocodazole in combination with PMA were inhibited in cell migration (Figure 9A). However, probably because of the driving force created by polymerizing actin at the leading edge and the stable focal contact in the main cell body, cells were sometimes torn apart, resulting in fragments separated from the main cell body. These "breakaway" fragments continued to migrate autonomously leaving a trace of actin-containing membrane behind (Figure 9B). These observations and the finding that focal contacts in the main cell body remain stable (cf. Figure 4A) suggest that microtubules might regulate the strength of cell adhesion to extracellular matrix.

To verify this hypothesis we tested adhesion of B16 cells to FN under the different conditions. As shown in Figure 9C, adhesion of cells increased little when stimulated with PMA.

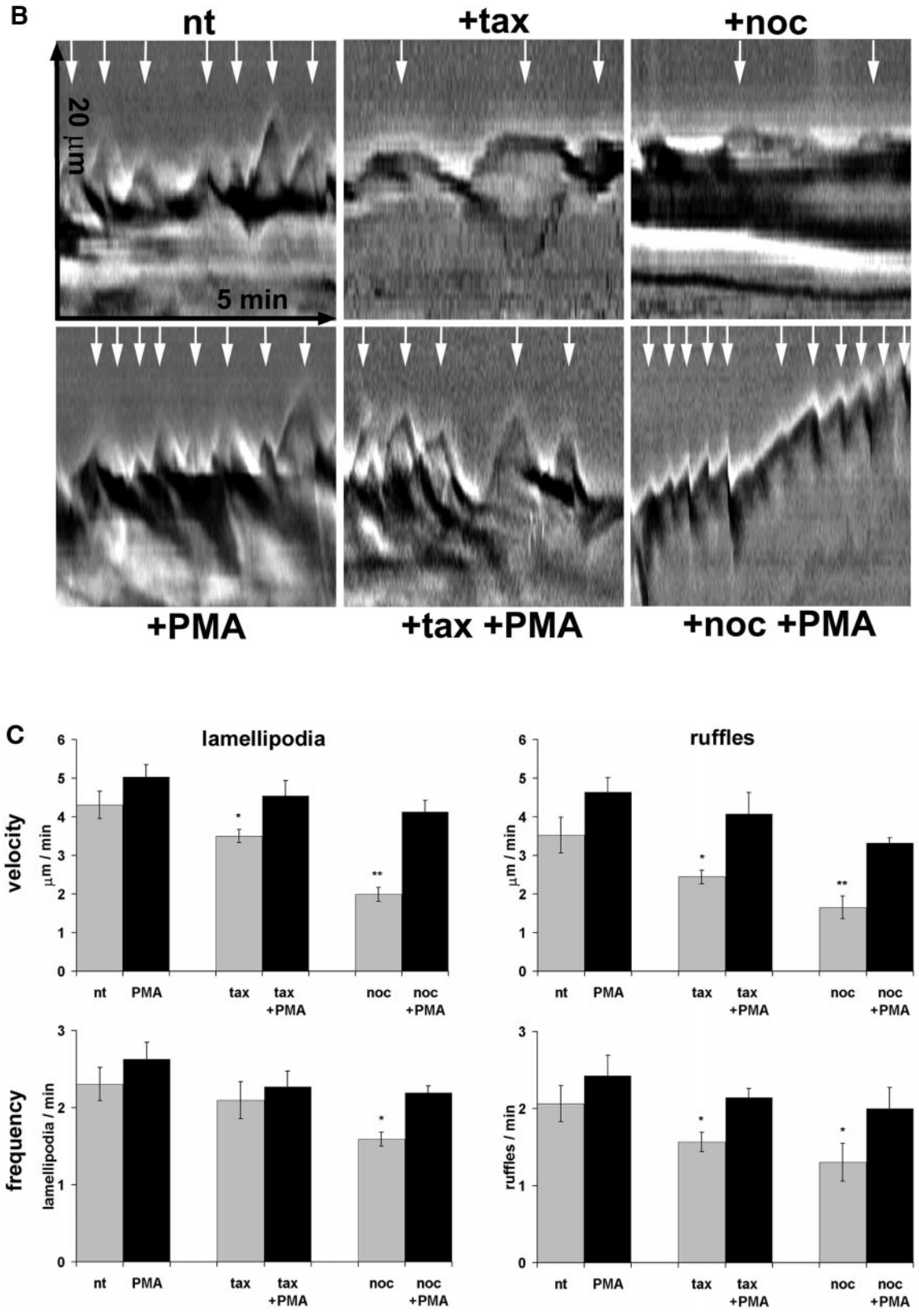

Figure 6 (legend on facing page).

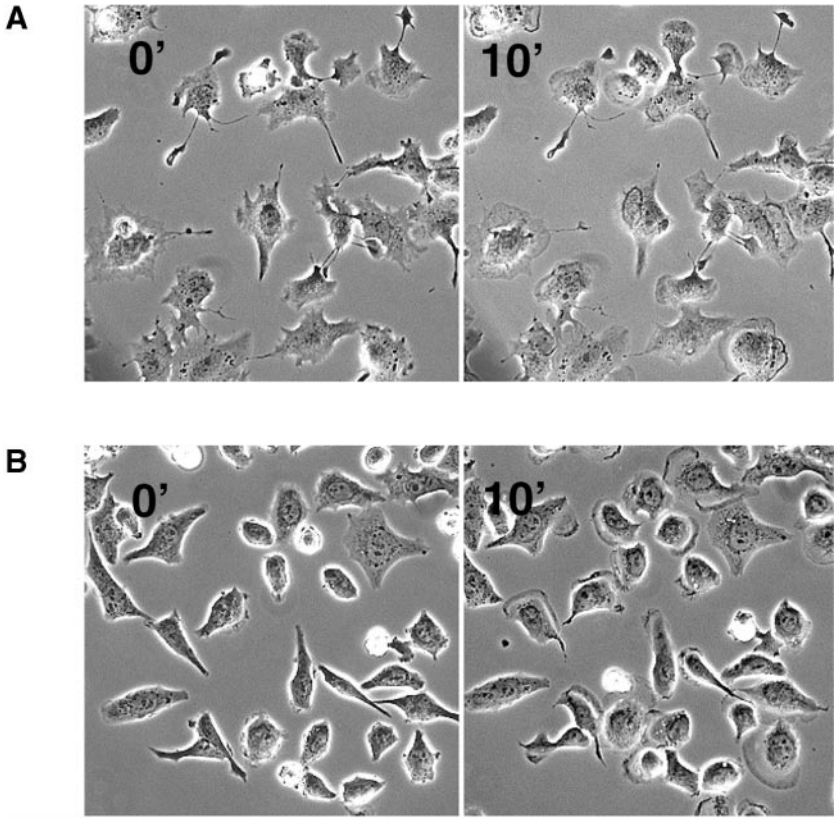

Figure 7. Lamellipodium formation in melanoblasts (melb-a) after c-kit stimulation with SCF. Starved melanoblasts pretreated with nocodazole (A) or taxol (B) were stimulated with 50 ng/ml SCF. Both taxol- and nocodazole-pretreated cells show lamellipodium formation 10 min after addition of SCF (10′).

However, an increase of cell adhesion (45%) was observed upon treatment of cells with nocodazole alone or with nocodacole and PMA. Thus, these results indicate that microtubules regulate cell-substrate adhesion, which is required for tail retraction of advancing cells.

DISCUSSION

The cytoskeleton is the key modulator of cell motility. The organization of the actin cytoskeleton determines whether a cell moves or remains stationary. It has been shown that disruption of microtubules in fibroblasts leads to the loss of lamellipodium protrusions, cell ruffling, and cell migration, thus indicating a functional link between the actin and the microtubular cytoskeleton (Vasiliev *et al.*, 1970; Liao *et al.*, 1995; Bershadsky *et al.*, 1996; Waterman-Storer *et al.*, 1999). In contrast, other studies demonstrated that microtubules were not required for actin-based cell movements (Zigmond *et al.*, 1981; Euteneuer and Schliwa, 1984). These observations led us to investigate more closely the contribution of microtubular dynamics to cell movements. Using GFP constructs and video microscopy we confirmed that destruction or stabilization of the microtubular network blocked the formation of lamellipodia and inhibited cell migration. However, protrusion of lamellipodia was recovered upon stimulation of the cells with PMA or SCF.

Recent publications have proposed an involvement of microtubules in activation of the small GTPase Rac1 (Best *et al.*, 1996; Waterman-Storer *et al.*, 1999). This has led to the hypothesis that microtubules are directly involved in the polymerization of actin at the cell periphery inducing lamellipodial protrusions. It was shown that Rac1-GTP directly binds to tubulin dimers (Best *et al.*, 1996), and it was hypothesized that tubulin polymerization liberates activated Rac1, which can then result in lamellipodium formation (Waterman-Storer and Salmon, 1999). Furthermore, it was demonstrated that destruction of microtubules results in activation of RhoA, a small GTPase involved in stress fiber formation (Ridley and Hall, 1992a; Nobes and Hall, 1995). These observations led to a model of positive feedback interactions between microtubule and actin dynamics in cell motility (Waterman-Storer and Salmon, 1999). This model proposes that microtubule disassembly in the perinuclear region activates RhoA, leading to a contractile network of actin fibers in the main cell body, thereby regulating contraction of the cell. Simultaneously, microtubule growth at the cell periphery activates Rac1, promoting lamellipodium formation and subsequent advancement of the leading edge. These concerted events, Rho and Rac activation, finally regulate cell migration. In this model, microtubules feature as key players in Rac1-mediated lamellipodia formation. However, our results indicate that although they may play a role (and indeed we see less ruffling and lamellipodium formation in the presence of nocodacole or taxol) they are not essential: First, protruding cell edges in rapidly locomoting cells have only few associated microtubules and the distance between tips of growing microtubules to the leading edge increases with augmented speed of cell migration (our observations;

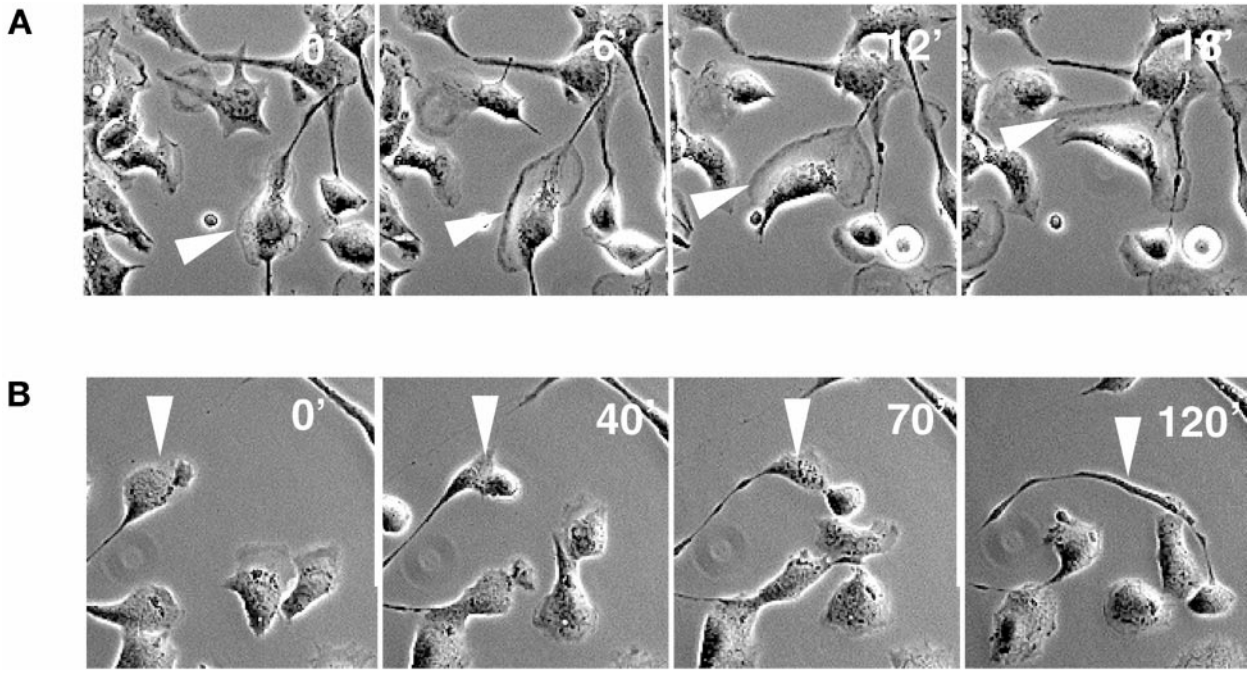

Figure 8. Tail retraction is inhibited in cells devoid of microtubules. (A) Migration of a melb-a melanoblast after stimulation with SCF. Cell form lamellipodia and advance quickly (arrowhead). (B) In contrast cells treated with nocodazole prior to SCF form lamellipodia but are inhibited in cell migration. The depicted cell advances very slowly and leaves a trace of membrane behind, indicating inhibition of tail retraction (arrowhead).

Euteneuer and Schliwa, 1984; Wadsworth, 1999). Second, spontaneous ruffle and lamellipodium formation was still observed in nocodazole- and taxol-treated cells. However, this did not address the issue of whether microtubules may be essential in stimulated ruffle formation. PMA and growth factors are known to be potent stimulators for actin reorganization (Schliwa *et al.*, 1984; Blume-Jensen *et al.*, 1991; Nobes *et al.*, 1995; Vosseller *et al.*, 1997; Timokhina *et al.*, 1998). Melanoma cells treated with PMA showed ruffling and lamellipodium formation in a Rac-dependent manner because ruffling was not observed in cells expressing the dominant-negative form of Rac. In our experiments it was possible to stimulate actin-dependent ruffling and lamellipodium formation in taxol- and nocodazole-pretreated cells to levels comparable with that obtained in untreated cells. Interestingly, lamella of taxol-pretreated cells were devoid of microtubules. Growth factor stimulation of the actin machinery provided physiological evidence that microtubules are not necessary for the transduction of signals leading to Rac1-dependent lamellipodium protrusion. Neither disruption nor stabilization of microtubules resulted in inhibition of SCF-induced lamellipodium formation.

Vasiliev *et al.* (1970) suggested that microtubules might be required for proper placement of ruffles. In B16 cells circular ruffle emergence was irrespective of the region, but formed lamellipodia when localized close to the cell edge (Ballestrem *et al.*, 1998). No differences in ruffle localization were apparent in cells treated with the combination of nocodacole/taxol and PMA with respect to cells stimulated with PMA only. In both cases big ruffles were formed, often starting as circular structures in the cell body extending toward the cell edges forming lamellipodia. Thus, microtubules seem not to play a role in localization of ruffle formation in PMA-stimulated melanoma cells in contrast to findings in nonstimulated fibroblasts (Vasiliev *et al.*, 1970).

One current hypothesis for lamellipodium formation is that endocytosed membrane vesicles in the cell center are transported via microtubules to the front of the cell were they reinsert, thereby enlarging the leading edge (Rodionov *et al.*, 1993; Bretscher, 1996a,b; Bretscher and Aguado-Velasco, 1998b). There are several aspects that suggest that this may be the case. Because both the actin and the microtubule network are involved in axonal vesicle transport they may have overlapping roles. Interestingly, it has been shown that either destruction of actin filaments or microtubules leads to partial inhibition of neurite outgrowth (Marsh and Letourneau, 1984; Lamoureux *et al.*, 1990). Similarly, in our present study, kymograph analysis demonstrated only partial inhibition of ruffling and lamellipodium formation after disruption or stabilization of microtubules in B16 cells. That microtubules were not essential for ruffling and lamellipodium formation could therefore be explained by an actin-dependent transport of vesicles that is up-regulated upon PMA stimulation. Indeed actin-dependent transport of endocytotic vesicles in mast cells was recently reported by Merrifield *et al.* (1999). Enhanced transport of melanophore-containing vesicles to the membrane has been shown after addition of PMA in melanoma cells (Reilein *et al.*, 1998). Furthermore, Bretscher and Aguado-Velasco (1988a) demonstrated that epidermal growth factor-induced ruffles arise by exocytosis of internal membrane from the endocytotic cycle in a Rac-dependent manner. It may be possible that

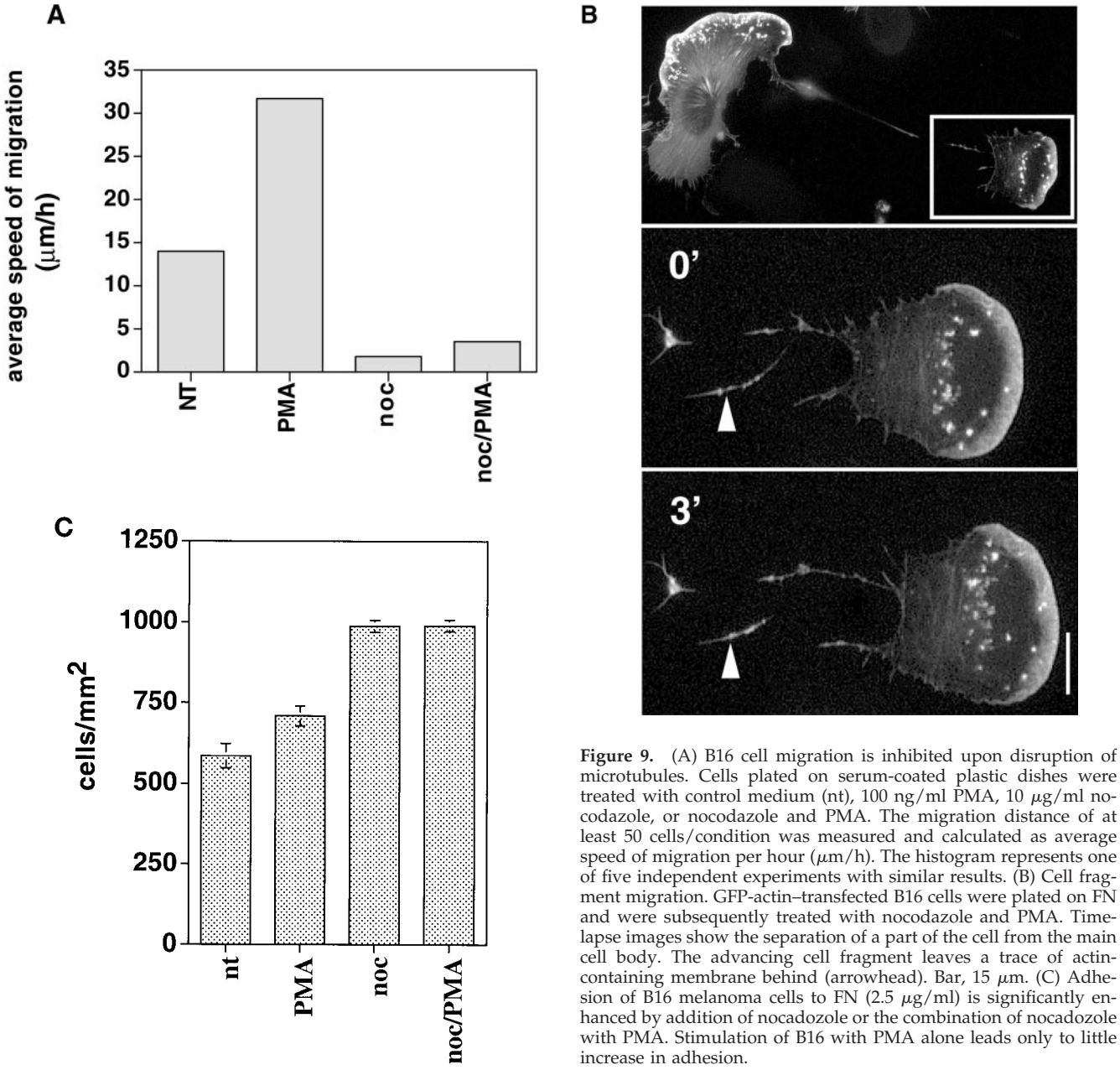

Figure 9. (A) B16 cell migration is inhibited upon disruption of microtubules. Cells plated on serum-coated plastic dishes were treated with control medium (nt), 100 ng/ml PMA, 10 μg/ml nocodazole, or nocodazole and PMA. The migration distance of at least 50 cells/condition was measured and calculated as average speed of migration per hour (μm/h). The histogram represents one of five independent experiments with similar results. (B) Cell fragment migration. GFP-actin–transfected B16 cells were plated on FN and were subsequently treated with nocodazole and PMA. Time-lapse images show the separation of a part of the cell from the main cell body. The advancing cell fragment leaves a trace of actin-containing membrane behind (arrowhead). Bar, 15 μm. (C) Adhesion of B16 melanoma cells to FN (2.5 μg/ml) is significantly enhanced by addition of nocadozole or the combination of nocadozole with PMA. Stimulation of B16 with PMA alone leads only to little increase in adhesion.

lamellipodium formation after PMA or SCF stimulation is based upon a similar mechanism.

Although microtubules were clearly not necessary for ruffling and lamellipodia formation, nocodazole-treated cells did not migrate even after PMA or SCF stimulation. Therefore, they evidently play a role in cell translocation. A recent publication demonstrated that focal contacts were released after multiple targeting by microtubules (Kaverina *et al.*, 1999). It has been proposed that microtubules may deliver relaxing signals to focal contacts, resulting in the release of focal adhesion sites that would enable the cell to move forward, rather than remaining anchored to one spot (Kaverina *et al.*, 1999; Small *et al.*, 1999). Our observations are consistent with these findings in that migration is inhibited in cells devoid of microtubules. Even stimulation with PMA or SCF, although leading to lamellipodium formation and surface actin-dependent ruffling, did not result in cell migration. In PMA-treated cells, focal adhesion contacts remained stable in the main cell body, whereas fragments of cells separated away from the main cell body, apparently under the driving force created by actin polymerization in the continuously protruding lamellipodium. Furthermore, we demonstrate that treatment of cells with nocodazole leads to an increase in cell adhesion to extracellular matrix. Thus, one task of microtubules may be to regulate the turnover of focal contacts and modulate the adhesive strength to extracellular matrix.

In conclusion, we have shown herein that microtubules influence cell motility events, such as stress fiber formation, ruffling, and lamellipodium formation in nonstimulated cells. We demonstrated that microtubules are not essential for actin-dependent lamellipodium formation upon activation of Rac through stimulation with PMA or growth factors such as SCF. In addition we showed that the formation of lamellipodia is actin dependent but microtubules are essential for tail retraction, the release of focal contacts, and hence regulation of coordinated cell migration.

ACKNOWLEDGMENTS

We thank Dr. C. Johnson-Léger and Prof. Dr. G. Gabbiani for critical reading of this article. We are grateful to M.C. Jacquier for excellent technical support, and J. Ntah for secretarial assistance. This work has been supported by the Schweizerische Krebsliga grant KFS 412-1-1997; grants from the Swiss National Science Foundation 31-49241-96, 31-052727.97, 31-50568.97; and grants from the Fondation Gabrielle Giorgi-Cavaglieri and Helmut Horten Stiftung.

REFERENCES

Ballestrem, C., Wehrle-Haller, B., and Imhof, B.A. (1998). Actin dynamics in living mammalian cells. J. Cell Sci. *111*, 1649–1658.

Bershadsky, A., Chausovsky, A., Becker, E., Lyubimova, A., and Geiger, B. (1996). Involvement of microtubules in the control of adhesion-dependent signal transduction. Curr. Biol. *6*, 1279–1289.

Bershadsky, A.D., Ivanova, O.Y., Lyass, L.A., Pletyushkina, O.Y., Vasiliev, J.M., and Gelfand, I.M. 1990. Cytoskeletal reorganizations responsible for the phorbol ester-induced formation of cytoplasmic processes: possible involvement of intermediate filaments. Proc. Natl. Acad. Sci. USA *87*, 1884–1888.

Bershadsky, A.D., Vaisberg, E.A., and Vasiliev, J.M. (1991). Pseudopodial activity at the active edge of migrating fibroblast is decreased after drug-induced microtubule depolymerization. *Cell Motil Cytoskeleton 19,* 152–158.

Best, A., Ahmed, S., Kozma, R., and Lim, L. (1996). The Ras-related GTPase Rac1 binds tubulin. J. Biol. Chem. *271*, 3756–3762.

Blume-Jensen, P., Claesson-Welsh, L., Siegbahn, A., Zsebo, K.M., Westermark, B., and Heldin, C.H. (1991). Activation of the human c-kit product by ligand-induced dimerization mediates circular actin reorganization and chemotaxis. EMBO J. *10*, 4121–4128.

Bretscher, M.S. (1996a). Getting membrane flow and the cytoskeleton to cooperate in moving cells. Cell *87*, 601–606.

Bretscher, M.S. (1996b). Moving membrane up to the front of migrating cells. Cell *85*, 465–467.

Bretscher, M.S., and Aguado-Velasco, C. (1998a). EGF induces recycling membrane to form ruffles. Curr. Biol. *8*, 721–724.

Bretscher, M.S., and Aguado-Velasco, C. (1998b). Membrane traffic during cell locomotion. Curr. Opin. Cell Biol. *10*, 537–541.

Danowski, B.A. (1989). Fibroblast contractility and actin organization are stimulated by microtubule inhibitors. J. Cell Sci. *93*, 255–266.

Downey, G.P., Chan, C.K., Lea, P., Takai, A., and Grinstein, S. (1992). Phorbol ester-induced actin assembly in neutrophils: role of protein kinase C. J. Cell Biol. *116*, 695–706.

Enomoto, T. (1996). Microtubule disruption induces the formation of actin stress fibers and focal adhesions in cultured cells: possible involvement of the rho signal cascade. Cell Struct. Funct. *21*, 317–326.

Euteneuer, U., and Schliwa, M. (1984). Persistent, directional motility of cells and cytoplasmic fragments in the absence of microtubules. Nature *310*, 58–61.

Hangan, D., Morris, V.L. Boeters, L., von Ballestrem, C., Uniyal, S., and Chan, B.M. (1997). An epitope on VLA-6 ($\alpha 6\beta 1$) integrin involved in migration but not adhesion is required for extravasation of murine melanoma B16F1 cells in liver. Cancer Res. *57*, 3812–3817.

Hinz, B., Alt, W., Johnen, C., Herzog, V., and Kaiser, H.W. (1999). Quantifying lamella dynamics of cultured cells by SACED, a new computer-assisted motion analysis. Exp. Cell Res. *251*, 234–243.

Kaverina, I., Krylyshkina, O., and Small, J.V. (1999). Microtubule targeting of substrate contacts promotes their relaxation and dissociation. J. Cell Biol. *146*, 1033–1044.

Lamoureux, P., Steel, V.L., Regal, C., Adgate, L., Buxbaum, R.E., and Heidemann, S.R. (1990). Extracellular matrix allows PC12 neurite elongation in the absence of microtubules. J. Cell Biol. *110*, 71–79.

Lauffenburger, D.A., and Horwitz, A.F. (1996). Cell migration: a physically integrated molecular process. Cell *84*, 359–369.

Liao, G., T. Nagasaki, and G.G. Gundersen. 1995. Low concentrations of nocodazole interfere with fibroblast locomotion without significantly affecting microtubule level: implications for the role of dynamic microtubules in cell locomotion. J. Cell Sci. *108*, 3473–3483.

Marsh, L., and Letourneau, P.C. (1984). Growth of neurites without filopodial or lamellipodial activity in the presence of cytochalasin B. J. Cell Biol. *99*, 2041–2047.

Merrifield, C.J., Moss, S.E., Ballestrem, C., Imhof, B.A., Giese, G., Wunderlich, I., and Almers, W. (1999). Endocytic vesicles move at the tips of actin tails in cultured mast cells [In Process Citation]. Nat. Cell Biol.*1,* 72–74.

Montell, D.J. (1999). The genetics of cell migration in *Drosophila melanogaster* and *Caenorhabditis elegans* development. Development *126*, 3035–3046.

Nobes, C.D., and Hall, A. (1995). Rho, rac, and cdc42 GTPases regulate the assembly of multimolecular focal complexes associated with actin stress fibers, lamellipodia, and filopodia. Cell *81*, 53–62.

Nobes, C.D., and Hall, A. (1999). Rho GTPases control polarity, protrusion, and adhesion during cell movement. J. Cell Biol. *144*, 1235–1244.

Nobes, C.D., Hawkins, P., Stephens, L., and Hall, A. (1995). Activation of the small GTP-binding proteins rho and rac by growth factor receptors. J. Cell Sci. *108*, 225–233.

Reilein, A.R., Tint, I.S., Peunova, N.I., Enikolopov, G.N., and Gelfand, V.I. (1998). Regulation of organelle movement in melanophores by protein kinase A (PKA), protein kinase C (PKC), and protein phosphatase 2A (PP2A). J. Cell Biol. *142*, 803–813.

Ridley, A.J., and Hall, A. (1992a). The small GTP-binding protein rho regulates the assembly of focal adhesions and actin stress fibers in response to growth factors. Cell *70*, 389–399.

Ridley, A.J., and Hall, A. (1992b). The small GTP-binding protein rho regulates the assembly of focal adhesions and actin stress fibers in response to growth factors. Cell *70*, 389–399.

Ridley, A.J., Paterson, H.F., Johnston, C.L., Diekmann, D., and Hall, A. (1992). The small GTP-binding protein rac regulates growth factor-induced membrane ruffling. Cell *70*, 401–410.

Rodionov, V.I., Gyoeva, F.K., Tanaka, E., Bershadsky, A.D., Vasiliev, J.M., and Gelfand, V.I. (1993). Microtubule-dependent control of cell shape and pseudopodial activity is inhibited by the antibody to kinesin motor domain. J. Cell Biol. *123*, 1811–1820.

Schliwa, M., Nakamura, T., Porter, K.R., and Euteneuer, U. (1984). A tumor promoter induces rapid and coordinated reorganization of actin and vinculin in cultured cells. J. Cell Biol. *99*, 1045–1059.

Shattil, S.J., and Ginsberg, M.H. (1997). Integrin signaling in vascular biology. J. Clin. Invest. *100*, S91–S95.

Small, J.V., Rottner, K., and Kaverina, I. (1999). Functional design in the actin cytoskeleton. Curr. Opin. Cell Biol. *11*, 54–60.

Sviderskaya, E.V., Wakeling, W.F., and Bennett, D.C. (1995). A cloned, immortal line of murine melanoblasts inducible to differentiate to melanocytes. Development *121*, 1547–1557.

Timokhina, I., Kissel, H., Stella, G., and Besmer, P. (1998). Kit signaling through PI 3-kinase and Src kinase pathways: an essential role for Rac1 and JNK activation in mast cell proliferation. EMBO J. *17*, 6250–6262.

Vasiliev, J.M., and Gelfand, I.M. (1976). Morphogenetic reactions and locomotory behavior of transformed cells in culture. In: Fundamental Aspects of Metastasis, ed. L. Weiss, Amsterdam: North-Holland, 71–98.

Vasiliev, J.M., Gelfand, I.M., Domnina, L.V., Ivanova, O.Y., Komm, S.G., and Olshevskaja, L.V. (1970). Effect of colcemid on the locomotory behavior of fibroblasts. J. Embryol. Exp. Morphol. *24*, 625–640.

von Ballestrem, C.G., Uniyal, S., McCormick, J.I., Chau, T., Singh, B., and Chan, B.M. (1996). VLA-β1 integrin subunit-specific monoclonal antibodies MB1.1 and MB1.2: binding to epitopes not dependent on thymocyte development or regulated by phorbol ester and divalent cations. Hybridoma *15*, 125–132.

Vosseller, K., Stella, G., Yee, N.S., and Besmer, P. (1997). c-kit receptor signaling through its phosphatidylinositide-3′-kinase-binding site and protein kinase C: role in mast cell enhancement of degranulation, adhesion, and membrane ruffling. Mol. Biol. Cell *8*, 909–922.

Wadsworth, P. (1999). Regional regulation of microtubule dynamics in polarized, motile cells. Cell Motil. Cytoskeleton *42*, 48–59.

Waterman-Storer, C.M., and Salmon, E. (1999). Positive feedback interactions between microtubule and actin dynamics during cell motility. Curr. Opin. Cell Biol. *11*, 61–67.

Waterman-Storer, C.M., and Salmon, E.D. (1997). Actomyosin-based retrograde flow of microtubules in the lamella of migrating epithelial cells influences microtubule dynamic instability and turnover and is associated with microtubule breakage and treadmilling. J. Cell Biol. *139*, 417–434.

Waterman-Storer, C.M., Worthylake, R.A., Liu, B.P., Burridge, K., and Salmon, E.D. (1999). Microtubule growth activates Rac1 to promote lamellipodial protrusion in fibroblasts [In Process Citation]. Nat. Cell. Biol. *1*, 45–50.

Zigmond, S.H., Levitsky, H.I., and Kreel, B.J. (1981). Cell polarity: an examination of its behavioral expression and its consequences for polymorphonuclear leukocyte chemotaxis. J. Cell Biol. *89*, 585–592.

4. Melanocyte Migration *in vitro*: Cell-Substrate Interactions

4.1. Cell migration requires dynamic remodeling of cell-substrate interactions

Integrins are a large family of heterodimeric transmembrane receptors mediating cell-cell and cell-extracellular matrix adhesion (Hynes, 1992). Growth factor signaling leads to the recruitment of integrins from intracellular stores to the cell surface (Fabbri et al., 1999). During cell migration, integrins establish the essential link to the extracellular matrix substrate and are recycled from the back of the cell to the front (Pierini et al., 2000). Integrin β-chains combine with various α-chains to generate integrins with different ligand specificity (Critchley et al., 1999; Hynes, 1992). The spreading and adhesion of mast cells onto fibronectin via α5β1 is induced by SCF dependent c-Kit activation (Kinashi and Springer, 1994). Important for melanocyte migration is the integrin αvβ3 which is involved in neural crest cell migration and stimulates metastasis formation of melanoma cells (Albelda et al., 1990; Delannet et al., 1994; Filardo et al., 1995; Scott et al., 1994).

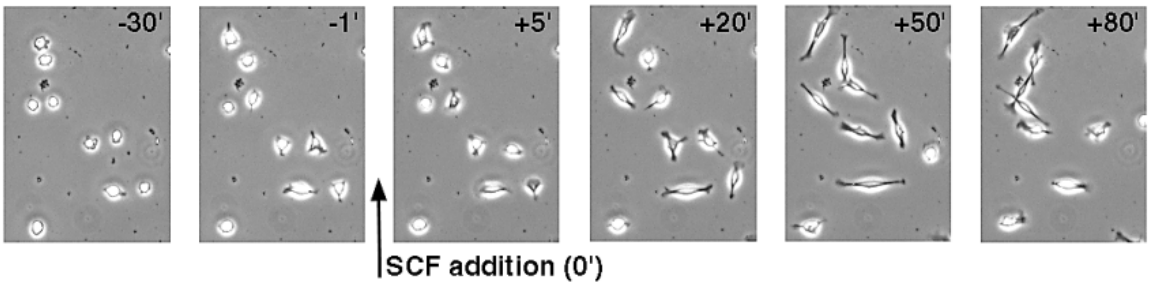

Fig. 6. *SCF induced spreading and migration on low concentrations of laminin-1*. Melb-a cells were plated for 4 hrs in the absence of SCF onto glass coverslip previousely coated with laminin-1 at 2 μg/ml. On this low concentration of laminin-1 only about 10-20% of melb-a cells are able to spread. Cells adhere but fail to spread under these conditions (-30',-1'). After addition of SCF at 50 ng/ml to the culture medium (0'), melb-a cells begin to develop lamellipodia and spread and migrate onto a laminin-1 substrate that otherwise does not support cell spreading (5'-80').

Melb-a melanoblasts express αVβ3, α5β1, and α6β1 and they adhere and spread on high concentrations of fibronectin and laminin-1 substrates in the absence of SCF. However, while melb-a cells are still able to adhere to low concentrations of extracellular matrix proteins, they loose the ability to spread. Interestingly, the addition of SCF to the medium induces rapid spreading on substrate concentrations which otherwise do not provide sufficient signals for spreading (Fig. 6 see also video chapter 6). This suggests that soluble SCF signaling provides a synergistic signal for

integrin dependent cell spreading on ECM substrates. The underlying molecular mechanism of this effect however remains elusive.

This *in vitro* experiment however demonstrates that growth factor signals can control cell-substrate interactions, in addition to their role in modifying the actin cytoskeleton. Since integrins are anchored within the actin cytoskeleton, it is tempting to speculate that the same intracellular signaling pathways that control the remodeling of the actin cytoskeleton control also integrin adhesion (see chapter 4.3).

A further aspect of this *in vitro* experiment is the similarity to the melanocyte behavior observed *in vivo* (described in chapter 2.5). In the *in vivo* situation, $Nf1^-$ (immortal) melanocyte precursors persist in the MSA (lateral to the neural tube) but do not migrate on the lateral pathway in the absence of SCF signal. Although these cells are immortalized, they do not acquire the capacity to randomly migrate away from the neural tube. It is not clear whether this is due to repulsive cues in the surrounding tissue represented by ephrins (Santiago and Erickson, 2002) or due to a limitation or balancing of adhesive extracellular matrix proteins such as fibronectin and laminin by proteoglycans or tenascins (Wehrle and Chiquet, 1990; Wehrle-Haller and Chiquet, 1993). It appears logical however, that a healthy tissue restricts cellular movements in order to maintain its integrity. I therefore propose, that any cellular migration within our organism is tightly controlled by signals that affect cell movement and cell-substrate interactions (Figure 6).

4.2. The role of the αvβ3-integrin in cell migration

Integrins belong to a family of heterodimeric cell-substrate receptors (Hynes, 1992). Since the β1 subunit can pair with at least nine different alpha subunits, it is difficult to classify the different heterodimers into physiologically interesting classes. One obvious class is formed by the β2 containing integrins that are only found on cells of hematopoietic origin and have cell surface glycoproteins as ligands. Another potential subclass could be defined by the αv containing integrins. αv can associate with several different beta subunits.

An alternative way to classify integrins is according to cellular function and association with pathological conditions such as cancer. In this respect, the αvβ3 heterodimer turned out to be an interesting integrin, since its expression correlated with the ability of increased cellular mobility such as in the case of tumor cells (Felding-Habermann et al., 1992; Felding-Habermann et al., 2001; Filardo et al., 1995). In addition, αvβ3 integrin plays an essential role in osteoclast function (McHugh et al., 2000). The β3 subunit is of special interest to pathologists, since Glanzmann thrombasthenia, one of three integrin based syndromes, is caused by defects in this integrin chain (Hogg and Bates, 2000). The importance of the β3 subunit in platelet function has been confirmed in the mouse (Hodivala-Dilke et al., 1999). The αvβ3 integrin has also been found to be important for angiogenesis in relation to development and tumor vascularization. The inhibition of this integrin did interfere with neovascularization and endothelial function (Brooks et al., 1994a; Brooks et al., 1994b; Dormond et al., 2001; Eliceiri and Cheresh, 1999; Storgard et al., 1999). The importance for αvβ3 integrin for neovascularization, however, has been recently challenged by the inability to block tumor vascularization by the deletion of β3 and β5 integrins in double knockout mice (Reynolds et al., 2002). Although this result seems a paradox, it underscores the importance for RTK signaling during cell migration. Reynolds et al. (2002) found an increase in the expression of Flk1 (the VEGF receptor) in endothelial cells of the knockout animals. It is tempting to speculate that the reduced ability to migrate caused by the absence of αvβ3 integrins has been compensated by a more efficient signaling system to overcome differences in the dynamic potentials of the various classes of integrin receptors.

In chapter 4.3 we present data how the αvβ3 integrin dynamics can be measured with the help of the GFP technology. This chapter clearly demonstrates the need for a rigorous quantitative analysis of integrin and focal adhesion dynamics, in order to fully understand the functional consequences upon pharmacological or genetic interference with integrin function.

4.3. Marching at the front dragging behind: differential αvβ3-integrin dynamics during cell migration

JCB Article

Marching at the front and dragging behind: differential αVβ3-integrin turnover regulates focal adhesion behavior

Christoph Ballestrem, Boris Hinz, Beat A. Imhof, and Bernhard Wehrle-Haller

Department of Pathology, Centre Médical Universitaire, Geneva, Switzerland

Integrins are cell–substrate adhesion molecules that provide the essential link between the actin cytoskeleton and the extracellular matrix during cell migration. We have analyzed αVβ3-integrin dynamics in migrating cells using a green fluorescent protein–tagged β3-integrin chain. At the cell front, adhesion sites containing αVβ3-integrin remain stationary, whereas at the rear of the cell they slide inward. The integrin fluorescence intensity within these different focal adhesions, and hence the relative integrin density, is directly related to their mobility. Integrin density is as much as threefold higher in sliding compared with stationary focal adhesions. High intracellular tension under the control of RhoA induced the formation of high-density contacts. Low-density adhesion sites were induced by Rac1 and low intracellular tension. Photobleaching experiments demonstrated a slow turnover of β3-integrins in low-density contacts, which may account for their stationary nature. In contrast, the fast β3-integrin turnover observed in high-density contacts suggests that their apparent sliding may be caused by a polarized renewal of focal contacts. Therefore, differential acto-myosin–dependent integrin turnover and focal adhesion densities may explain the mechanical and behavioral differences between cell adhesion sites formed at the front, and those that move in the retracting rear of migrating cells.

Introduction

Modulation of cell–substrate adhesion plays a crucial role in cellular processes such as migration, spreading, or contraction. These morphological changes result from the coordinated reorganization of the actin cytoskeleton induced by intra- or extracellular stimuli (Lauffenburger and Horwitz, 1996). Cell migration is sustained by the continuous growth of actin filaments at the leading edge, and the controlled retraction of adhesive contacts at the rear of the cell (Palecek et al., 1998; Horwitz and Parsons, 1999; Ballestrem et al., 2000). Integrin αβ heterodimers provide the physical link between the continuously reorganizing actin cytoskeleton and components of the extracellular matrix (ECM)* during cell migration (Hynes, 1992). Different types of integrin-containing cell–substrate contacts have been described, of which focal complexes and contacts are the best studied. These two types of contacts have been distinguished according to several features including size, the site where they are formed in the cell, their age, their appearance in interference reflection microscopy, and their regulation by small GTPases (Geiger and Bershadsky, 2001). In fibroblasts, small point-like focal complexes form at sites of Rac1-dependent lamellipodia induction (Ridley et al., 1992; Nobes and Hall, 1995; Rottner et al., 1999), whereas large and elongated focal contacts localize to the ends of actin stress fibers upon RhoA activation (Ridley and Hall, 1992; Nobes and Hall, 1995; Amano et al., 1997; Rottner et al., 1999). The mechanical influence of acto-myosin–induced intracellular contractility and extracellular tension was suggested as a major factor converting focal complexes into focal contacts (Chrzanowska-Wodnicka and Burridge, 1996; Pelham and Wang, 1997; Riveline et al., 2001). In this study, we will use the general term focal adhesion, and will classify them according to their different behavior and localization in migrating cells as well as their integrin dynamics.

Although the pathways leading to the changes in the actin cytoskeleton are well understood, it is not known how the

The online version of this article contains supplemental material.

Address correspondence to Bernhard Wehrle-Haller, Dept. of Pathology, Centre Médical Universitaire, 1, Rue Michel-Servet, 1211 Geneva 4, Switzerland. Tel.: 0041-22-702-57-35. Fax: 0041-22-702-57-46. E-mail: Bernhard.Wehrle-Haller@medecine.unige.ch

C. Ballestrem's current address is Dept. of Molecular Cell Biology, The Weizmann Institute of Science, Rehovot 76100 Israel.

*Abbreviations used in this paper: EGFP, enhanced GFP; GFP, green fluorescent protein; LPA, lysophosphatidic acid, MF, mobile fraction, ECM, extracellular matrix

Key words: cell migration; cell adhesion; green fluorescent protein; Rho GTPases; integrin density

The Journal of Cell Biology, Volume 155, Number 7, December 24, 2001 1319–1332
http://www.jcb.org/cgi/doi/10.1083/jcb.200107107

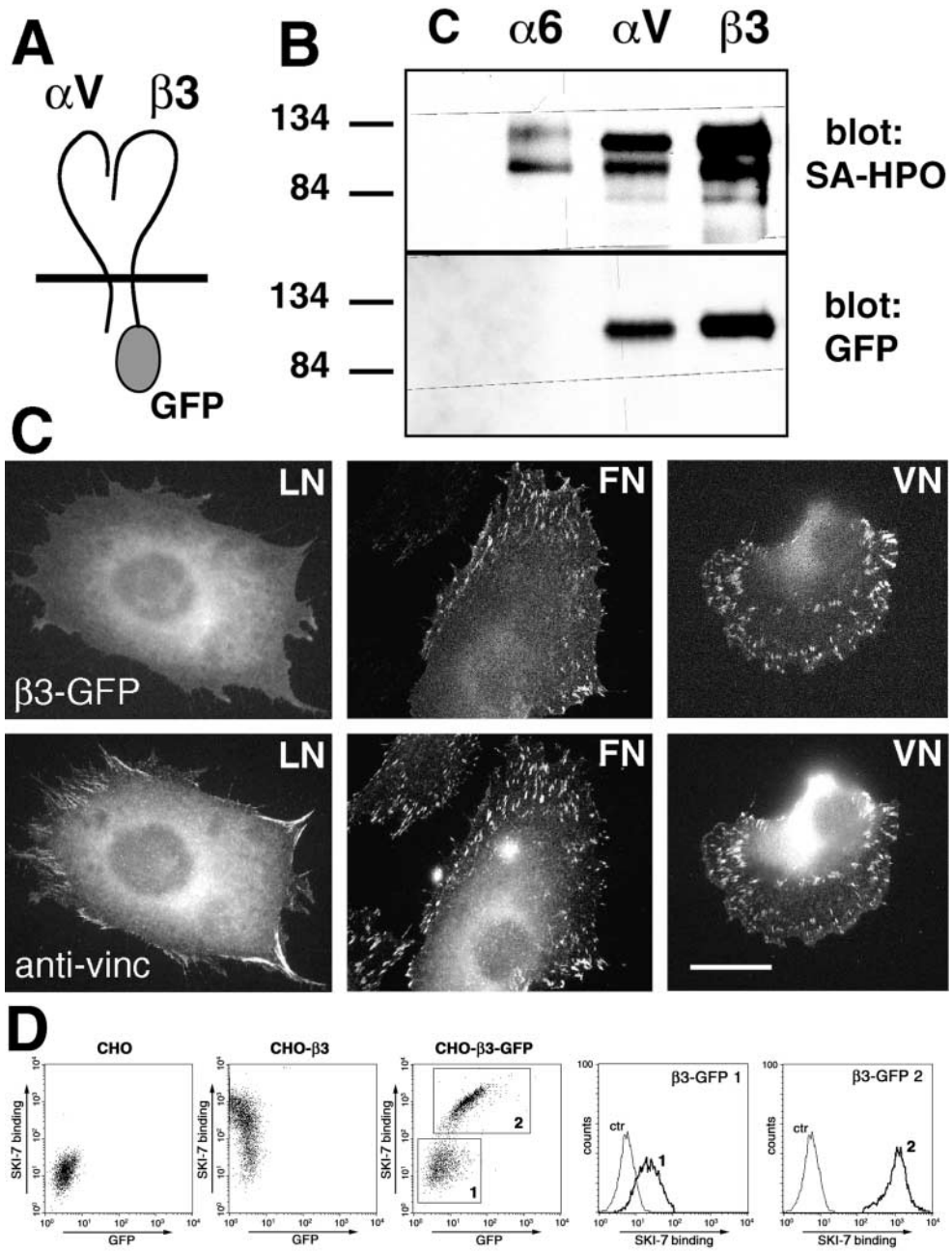

Figure 1. **The GFP-tagged β3-integrin chain forms functional heterodimers with endogenous αV.** (A) Scheme of the αVβ3–GFP-integrin heterodimer. The GFP protein is tagged COOH-terminally to the cytoplasmic domain of the β3 subunit. (B) Immunoprecipitations of cell extracts from surface biotinylated B16 β3–GFP cells. Extracts were precipitated with the indicated antibodies (c, control) and separated under reducing conditions by PAGE followed by transfer onto nitrocellulose membranes. Revelation with either streptavidin coupled horseradish peroxidase (SA-HPO, top) or anti-GFP antibodies (GFP, bottom) demonstrated the typical double-band pattern for integrin heterodimers and the coprecipitated GFP-tagged β3-integrin subunit, respectively. The position of the molecular mass markers is indicated to the left of the blots. (C) Substrate-specific clustering of the αVβ3–GFP-integrin into adhesions sites. B16 β3–GFP cells were plated overnight on glass coverslips, previously coated with 5 μg ml^{-1} laminin-1 (LN), 5 μg ml^{-1} fibronectin (FN), or 1 μg ml^{-1} vitronectin (VN). Cells were subsequently fixed and substrate adhesion sites were revealed by immunohistochemical detection of vinculin. Note that β3–GFP-integrin–positive adhesion sites were only found on fibronectin and vitronectin, which are ligands for αVβ3-integrin. In contrast, β3–GFP-integrin did not cluster on laminin-1, for which it is not a ligand. Because B16 cells use a different type of integrin receptor (α6β1) to adhere to LN than to FN or VN (α5β1, αVβ3), their morphology and migration behavior is different between these substrates (Ballestrem et al., 1998). (D) FACS analysis of nontransfected, β3-, and β3–GFP-transfected CHO cells with a Kistrin–CD31 fusion construct (SKI-7) (Legler et al., 2001). Note that the β3–GFP-transfected CHO clone is not homogeneous, exhibiting cells that lost β3-GFP expression, which reduces their SKI-7 reactivity to endogenous αVβ3-integrin levels (gate 1) (ctr; SKI-7, unpublished data). Bar, 20 μm.

strength of the integrin-mediated link between the actin cytoskeleton and the ECM is controlled to promote either firm adhesion or detachment. Nonaggregated integrins exhibit a high lateral diffusion within the plasma membrane (Duband et al., 1988). However, upon extracellular ligand binding, integrins become anchored to the actin cytoskele-

ton by a large set of structural and regulatory proteins (Miyamoto et al., 1995), thereby forming cell–ECM adhesion sites. A "sliding" of β1-integrin–containing focal contacts has recently been demonstrated, and was suggested to represent weak attachment of stationary cells (Smilenov et al., 1999). In addition, the movement of α5β1-integrins on the ventral side of fibroblasts has been related to ECM reorganization by fibrillar adhesions (Katz et al., 2000; Pankov et al., 2000; Zamir et al., 2000).

To analyze the dynamics of individual integrin heterodimers within adhesion sites of migrating cells, we focused on the integrin αVβ3. Integrin αVβ3 is expressed on various motile cells such as neural crest cells (Delannet et al., 1994) and plays an important role in tumor metastasis (Albelda et al., 1990; Felding-Habermann et al., 2001), angiogenesis (Brooks et al., 1994), leukocyte transmigration (Weerasinghe et al., 1998), and osteoclast function (McHugh et al., 2000). Its ECM ligands include fibronectin, vitronectin, and fibrinogen (Cheresh and Spiro, 1987).

The use of a directly green fluorescent protein (GFP)-labeled β3-integrin chain that was coexpressed with the endogenous αV-integrin subunit on the cell surface allowed us to follow clustering and dispersal, and to perform quantitative analysis of αVβ3-integrins within adhesion sites of living cells. We specifically asked whether the organization of β3-integrins in focal adhesions differed according to their subcellular localization, and whether distinct organization patterns could be attributed to the activities of members of the Rho family of small GTPases. In particular, we studied the influence of intracellular tension, analyzed with the help of elastic silicon substrata, on the organization of β3-integrins within focal adhesion sites. Moreover, using FRAP, we analyzed the turnover rates of β3-integrins within different focal adhesions, in order to understand whether the motile behavior and function of a given focal adhesion site could be correlated to the temporal stability of the embedded integrins. We found differential densities of integrins within focal adhesion sites that correlated with the degree of actomyosin–dependent intracellular contraction, and an inverse correlation to the temporal stability of integrins within these sites. Our data reveal casual connections between the behavior of integrins and the state of the actin cytoskeleton that provides the base for a detailed mechanical model of cell migration.

Results

Dimerization of β3–GFP-integrin chain with αV

To study and quantify αVβ3-integrin dynamics in living cells, we generated a fusion protein of the β3 integrin subunit with GFP (Fig. 1 A). To determine whether this β3–GFP-integrin chain formed heterodimers with the endogenous αV subunit, we surface biotinylated stable β3–GFP-integrin–transfected cells (B16 F1 melanoma and 3T3 fibroblasts), and performed immunoprecipitations with antibodies against either the αV- or the β3-integrin subunits (Fig. 1 B). After precipitation of the integrin and subsequent Western blotting, both α- and β-integrin subunits could be detected with avidin-peroxidase (Fig. 1 B). Bands for the β3–GFP-integrin fusion protein were only detected in precipitations with anti–αV- or –β3-integrin subunits, but not with control rat serum nor with anti–α6-integrin subunit which forms heterodimers with the β1 and β4 chains (Fig. 1 B, bottom). These experiments clearly demonstrated that β3–GFP-integrin was expressed on the cell surface as a heterodimeric complex in association with the endogenous αV chain.

Ligand-specific clustering of αVβ3–GFP-integrin

To further test whether the αVβ3–GFP-integrin heterodimer was functional and did not unspecifically associate with cytoskeletal elements of focal adhesions, we plated β3–GFP-transfected cells on the αVβ3 ligands fibronectin and vitronectin, and on laminin-1, which is not a ligand for αVβ3. Clustering of GFP was observed on fibronectin and vitronectin, but not on laminin-1 (Fig. 1 C). Vinculin and paxillin are present in, and used as markers for, cell–substrate adhesion sites. Both localized to focal adhesion sites on all three substrates (Fig. 1 C, paxillin, unpublished data). In contrast, αVβ3-integrin–containing focal adhesions were only detected in cells cultured on fibronectin or vitronectin substrata (Fig. 1 C). To demonstrate that the transfected β3–GFP-integrin engaged in ECM binding was comparable to wild-type β3 chains, we analyzed stable β3–GFP- and β3-transfected CHO cells for their binding to a αVβ3-integrin–specific snake venom disintegrin (Kistrin). A FACS profile using a Kistrin–CD31 fusion protein (SKI-7) revealed only low levels of endogenous αVβ3-integrin in nontransfected CHO cells (Legler et al., 2001). In contrast, both β3- and β3–GFP-transfected cells displayed extensive SKI-7 reactivity (Fig. 1 D). These results demonstrate that αVβ3–GFP-integrin behaves like endogenous αVβ3, indicating that ligand binding, integrin signaling, and substrate specificity are not perturbed by the fusion of GFP to the β3-integrin chain. Moreover, these data suggest that the associated αV-integrin integrin chain specifically protects the cytoplasmic domain of β3–GFP from matrix-independent engagement with cytoskeletal elements of focal adhesions (Yauch et al., 1997). Therefore, direct labeling of the β3-integrin with GFP allowed us to follow and quantify β3-containing integrins in living cells.

Dynamics of β3-integrin

This αVβ3–GFP tool permitted now the direct observation of integrin clustering and turnover in adhesion sites of migrating or stationary cells. Therefore, we performed time-lapse experiments with stably β3–GFP-transfected, fast-migrating B16 F1 melanoma cells, or stationary 3T3 fibroblasts (B16 β3–GFP or 3T3 β3–GFP, respectively). In B16 β3–GFP cells, we observed the formation of small integrin clusters just behind the leading edge of the advancing lamellipodia (Fig. 2, A and B). These clusters remained stationary with respect to the substratum, whereas the cell moved forward. When GFP-containing focal adhesions reached a distance of 10 μm from the leading edge, they began to shrink and finally disappeared (Fig. 2, A, circled, and B, boxed; Video1, available at http://www.jcb.org/cgi/content/full/jcb.200107107/DC1). We noted that some of the focal adhesions in the smoothly protruding lamellipodia assumed an elongated shape. Although we never observed actin stress

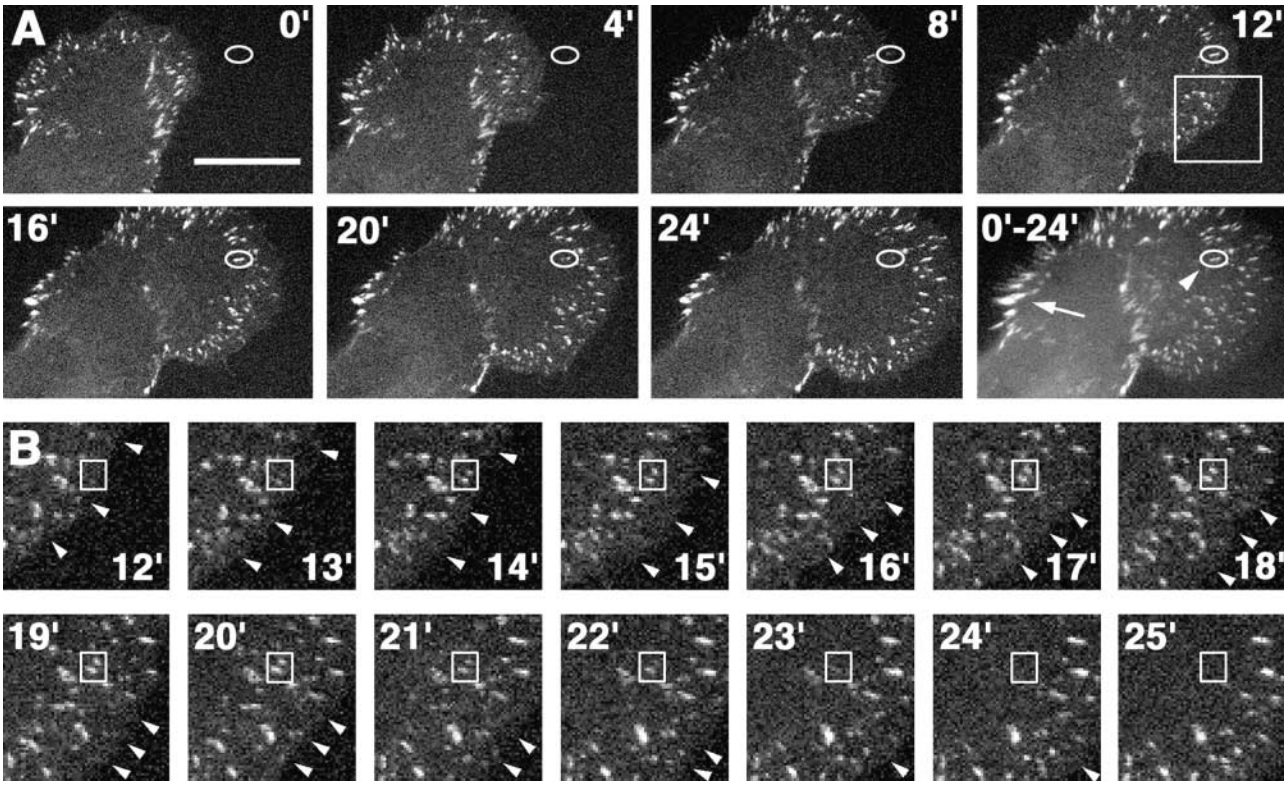

Figure 2. **Dynamics of β3–GFP-integrin in stable transfected B16 F1 cells.** Time-lapse analysis of a B16 β3–GFP cell plated overnight on vitronectin (1 μg ml^{-1}) revealed the transient β3–GFP-integrin clustering and subsequent dispersal in the advancing lamellipodium. A typical β3-integrin cluster (A, circled) appeared close to the leading edge (8′) and remained stationary (12′) until it began to gradually disappear (16′–24′). In retracting parts of the cells, integrin clusters began to slide inward (arrow). To appreciate the relative movement of the different integrin clusters during this time-lapse, an overlay revealed the stationary nature of focal adhesions in the lamellipodia (arrowhead) and the streak-like pattern of sliding focal adhesions in retracting parts of the cell (arrow). In B, a higher temporal and spatial resolution of the boxed area in A (12′) revealed the polymorphic appearance of the stationary integrin clusters (small box as reverence). Although shapes were variable, the fate of the clusters were identical. Arrowheads in B mark the smoothly advancing leading edge of the lamellipodium. Bar, 18 μm.

fibers in actively protruding lamellipodia, the presence of radially oriented actin ribs within the lamellipodia was frequent (Ballestrem et al., 1998). Continuous appearance and disappearance of stationary β3-integrin focal adhesions occurred within a restricted area in the advancing lamella. We refer to this area as the zone of transient integrin clustering. In posterior regions of the cell, integrin-containing focal adhesions moved in relation to the substratum during retraction (Fig. 2 A, arrow; Video2, available at http://www.jcb.org/cgi/content/full/jcb.200107107/DC1). To examine the possibility that integrin contacts in highly migratory melanoma cells might behave differently from stationary or slow moving fibroblasts (3T3 β3–GFP cells), we compared the appearance of GFP fluorescence in transfected B16 and 3T3 cells. 3T3 cells displayed continuous cycles of lamellipodia formation followed by retraction, and they showed comparable integrin cluster dynamics to what had been seen in B16 β3–GFP cells (Fig. 3; Video3, available at http://www.jcb.org/cgi/content/full/jcb.200107107/DC1). However, during collapse of lamellipodia, small focal adhesions in 3T3 cells transformed into larger, fluorescently brighter focal adhesions (Fig. 3 B). During retraction, these focal adhesions began to move in relation to the substratum (Fig. 3, B and C). In conclusion, our data show that αVβ3-integrins aggregate into stationary focal adhesions within the zone of transient integrin clustering during the protrusion of lamellipodia. After the collapse of lamellipodia and subsequent retraction, small stationary focal adhesions transform into inwards sliding larger focal adhesions.

Induction of differential β3-integrin cluster densities upon transfection with dominant Rac1, Cdc42, and RhoA

Lamellipodia formation, as well as the retraction of cell edges, depends on the reorganization of the actin cytoskeleton. In addition, the transition from small and stationary to larger, retracting focal adhesions was associated with an increase in fluorescence intensity, and hence increased integrin density (Fig. 3). Because signaling through members of the Rho family of small GTPases is known to cause changes in the actin cytoskeleton (Ridley and Hall, 1992; Ridley et al., 1992; Nobes and Hall, 1995), we asked if changes in activation of these GTPases would influence the organization and density of αVβ3-integrin in focal adhesion sites. To answer this question, we transfected dominant active forms of Rac1, Cdc42, and RhoA into B16 β3–GFP cells, and quantified integrin fluorescence and focal adhesion morphology (Fig. 4). Control cells typically displayed a leading lamella with small β3-integrin– positive focal adhesions and larger, fluorescently brighter β3-integrin focal adhesions at the side and

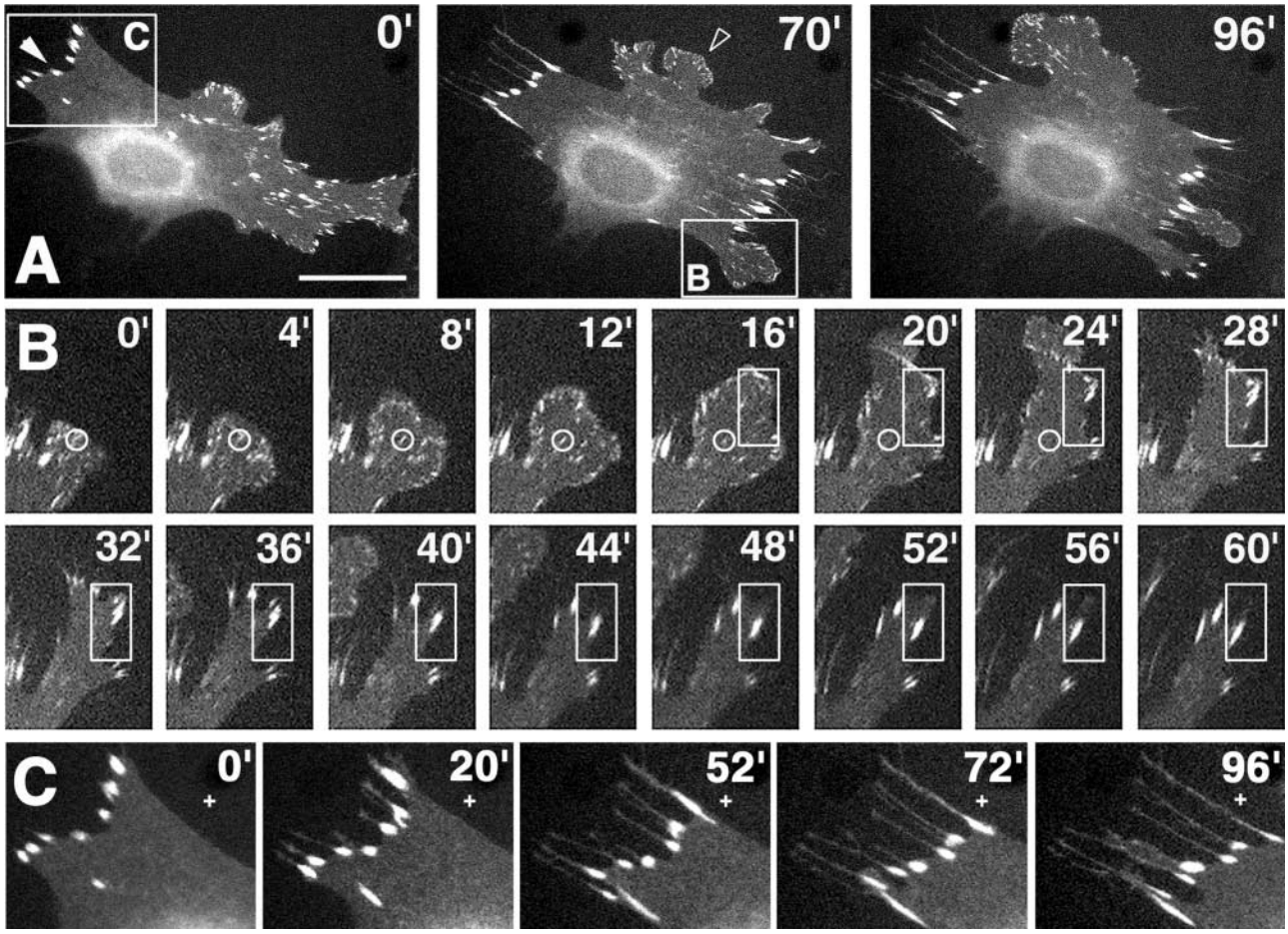

Figure 3. **Dynamics of β3–GFP-integrin in stable transfected 3T3 cells.** Time-lapse analysis of a 3T3 β3–GFP cell plated overnight on vitronectin (1 μg ml^{-1}), exhibiting cycles of lamellipodia extension (B) followed by cell edge retraction (B and C). During lamellipodia extension, transient stationary small focal adhesions formed behind the leading edge (B, circled focal adhesion). During cessation of the extension phase, small peripheral focal adhesions grew in size and were transformed into inward sliding focal adhesions (B, boxed area). Note that the start of the time lapse in B corresponds to 54′ in A. Continuous inward sliding of large focal adhesions occurred in parallel with cell edge retraction (C). A fiduciary mark on the substrate (C, white crosses) can be used to gauge the speed and position of retracting focal adhesions. Bar, 24 μm.

rear of the cell (Fig. 4 A). Expression of dominant active Cdc42 (V12) and Rac1 (L61) that are known to induce filopodia and lamellipodia, respectively (Ridley et al., 1992; Nobes and Hall, 1995), led to the appearance of flat and well-spread B16 β3–GFP cells. Compared with control cells the surface area increased by 188 and 248%, respectively (see Materials and methods), and cells exhibited actin-rich filopodia and lamellipodia and many small caliber actin filaments (unpublished data). This phenotype is apparent only after prolonged exposure to dominant active Rac1, and is associated with the formation of many small caliber actin filaments as previously reported (Ridley et al., 1992). In these cells, β3–GFP fluorescence resulted in a streak-like pattern of integrin clusters associated with filopodia (cdc42) or lamellipodia (Rac1) covering large areas of the substratum. These extensive clusters exhibited a granular pattern that resembled assemblies of numerous small focal adhesions (Fig. 4, B and C). The fluorescence intensity profiles indicated in Fig. 4, A–C, revealed that the density of β3-integrin in small focal adhesions in control cells (Fig. 4 E, profile a) corresponded to the densities measured across the integrin clusters of dominant Cdc42- and Rac1-transfected cells (Fig. 4 E, profile da-Cdc42 and da-Rac1). In contrast, measurements of GFP intensity (and hence, integrin densities) in focal adhesions that were localized in retracting cell edges at the rear of control cells were consistently higher (Fig. 4 E, profile b). Moreover, expression of dominant active RhoA (V14) induced robust stress fiber formation and the cells appeared contracted (64% of control cell surface area) with large, even brighter fluorescent β3-integrin focal adhesions (Fig. 4, D and E, profile da-RhoA). From these data we calculated (see Materials and methods) that the relative αVβ3-integrin densities compared with nonclustered integrin in the plasma membrane increased by three- to fivefold in lamellipodial and Rac1- or Cdc42-induced low-density focal adhesions, by five- to eightfold in lateral and rear high-density focal adhesions of control cells, and by 9–14-fold in focal adhesions of dominant RhoA-stimulated cells (Fig. 4 F). Similar to the raise in integrin densities, we also observed a RhoA-dependent increase in anti-vinculin labeling of focal adhesions (unpublished data). These results demonstrate that the Rac1- and RhoA-induced changes in the bundling

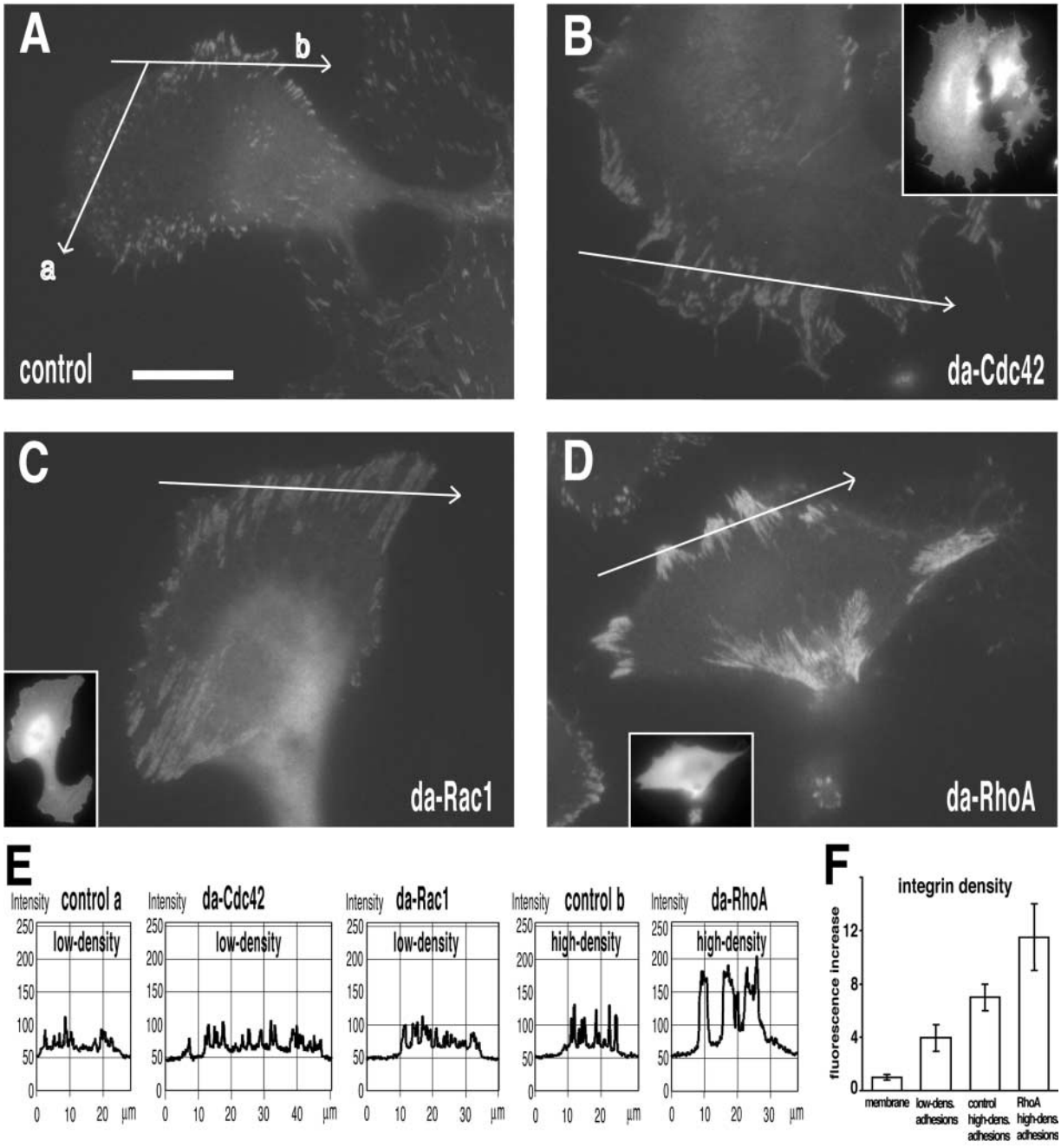

Figure 4. **Members of the Rho family of small GTPases regulate β3-integrin clustering differentially.** B16 β3–GFP cells transfected with myc-epitope–tagged dominant active forms of Cdc42, Rac1, and RhoA were plated overnight on vitronectin (1 μg ml^{-1})-coated glass coverslips. Cells were fixed and stained for the expression of the myc-epitope (inserts), and GFP fluorescence images were recorded with identical camera settings in order to appreciate qualitative as well as quantitative differences in the integrin localization pattern. (A) Nontransfected control cells displayed the typical pattern of small low-fluorescent focal adhesions in the lamellipodium (profile a) and larger high-fluorescent focal adhesions at lateral borders and rear of the cell (profile b). (B) Dominant active Cdc42 (da-Cdc42) induced the formation of long, streak-like arrays of low-fluorescent β3 integrin focal adhesions mainly localized in the lamella or periphery of the cell. Similarly, dominant active Rac1 (da-Rac1) induced extensive β3-integrin clustering into low-fluorescent adhesion sites at the periphery of the cell (C). In contrast, dominant active RhoA (da-RhoA) induced a retracted cellular morphology with intensively fluorescent β3-integrin focal adhesions at the cell periphery (D). Fluorescence intensity profiles of the indicated traces in A–D are shown in E. Note that the intensity profiles are similar between focal adhesions in the lamellipodium of control cells and cells transfected with dominant active Cdc42 and Rac1. Peak fluorescent intensities of lateral and rear focal adhesions in control cells are consistently higher compared with lamellipodial focal adhesions, but can increase even more after dominant active RhoA induction. A quantification of the β3-integrin density (fluorescence intensity increase over membrane) is shown in F. Bar, 15 μm.

state of the actin filament network led to changes in the clustering behavior of β3 integrin, i.e., the generation of integrin low- and high-density focal adhesions, respectively.

Intracellular tension controls integrin density transition within focal adhesions

What causes this RhoA-induced increase in integrin density?

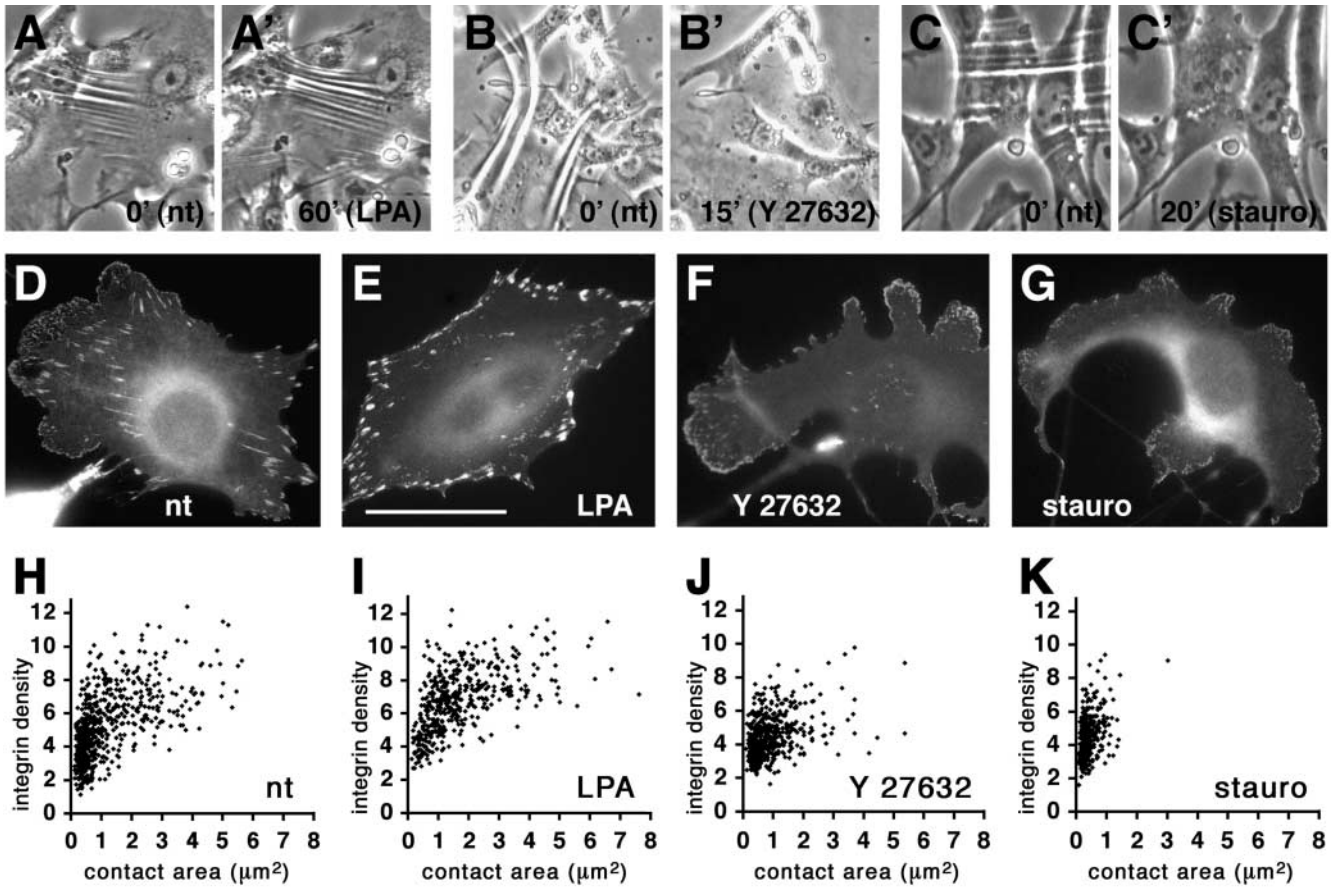

Figure 5. **Intracellular tension correlates with integrin density in focal adhesion sites.** 3T3 β3–GFP cells were grown on flexible silicone rubber substrates in order to visualize intracellular contractile forces by the appearance of substrate wrinkles. (A–C) Cells were recorded for 1 h under control conditions to confirm stability of the wrinkles (nt). After addition of drugs, the increase in substrate wrinkles (LPA, 10 μM) or their disappearance (Y 27632, 10 μM, or staurosporine, 50 nM) were recorded for the indicated times (A′–C′) (Videos 4–6). In a parallel experiment, 3T3 β3–GFP cells were grown overnight on serum-coated glass coverslips (D, nt), and changes in β3–GFP-integrin localization in response to the above mentioned drugs was determined after 60 min of treatment (E, LPA; F, Y27632; G, staurosporine). The peak β3-integrin density/focal adhesion area relationship was plotted for untreated (H), LPA- (I), Y 27632- (J), and staurosporine- (K)treated cells. Note the shift in the focal adhesion population after addition of agonist. Bar: (A–C), 80 μm; (D–G), 40 μm.

Previously it has been shown that activated RhoA increases myosin-dependent contraction of the actin cytoskeleton, leading to intracellular tension (Chrzanowska-Wodnicka and Burridge, 1996; Amano et al., 1997). Integrins in focal adhesion sites are anchored within the actin cytoskeleton, such that contraction of this actin filament backbone induced by myosin activity may lead to increased integrin density, i.e., the transition of lamellipodial to lateral focal adhesions. To test this, we determined whether intracellular tension induced by RhoA was correlated with this transition. Intracellular tension was measured by plating 3T3 fibroblasts on flexible silicone rubber that formed wrinkles in response to cellular contraction (Harris et al., 1980). Activation of RhoA by lysophosphatidic acid (LPA) (10 μM) within these cells increased the number of wrinkles (Fig. 5 A; Video4, available at http://www.jcb.org/cgi/content/full/jcb.200107107/DC1) (Amano et al., 1997). RhoA activates Rho-kinase, which blocks myosin light chain phosphatase, resulting in myosin-dependent actin contraction (Kimura et al., 1996). Treatment of cells with the Rho-kinase inhibitor Y-27632 (10 μM) removed the wrinkles (Fig. 5 B; Video5, available at http://www.jcb.org/cgi/content/full/jcb.200107107/DC1) (Uehata et al., 1997). Similarly, blocking of myosin light chain kinase with the wide-spectrum protein kinase inhibitor staurosporine (50 nM) resulted also in the disappearance of wrinkles (Fig. 5 C; Video6, available at http://www.jcb.org/cgi/content/full/jcb.200107107/DC1). Using these modulators of intracellular tension, the formation of high- and low-density focal adhesions was analyzed. Treatment of 3T3 fibroblasts with LPA increased β3-integrin compaction and formed high-density focal adhesions (Fig. 5 E). In contrast, cells treated with Y-27632 or staurosporine displayed the disappearance of high-density focal adhesions, whereas low-density focal adhesions remained in the periphery of the cells in the lamellipodia (Fig. 5, F and G). To correlate the changes in intracellular tension with that of the integrin density and focal adhesion size, we displayed the relative peak integrin density (compared with the integrin density in the membrane) and the respective area of focal adhesions (see Materials and methods). For each experimental condition, we analyzed ~500 focal adhesions from different cells. Control cells displayed a significant number of small-sized, low-density focal adhesions that were mainly associated with protruding lamellipodia (Fig. 5 H). In addition, a considerable

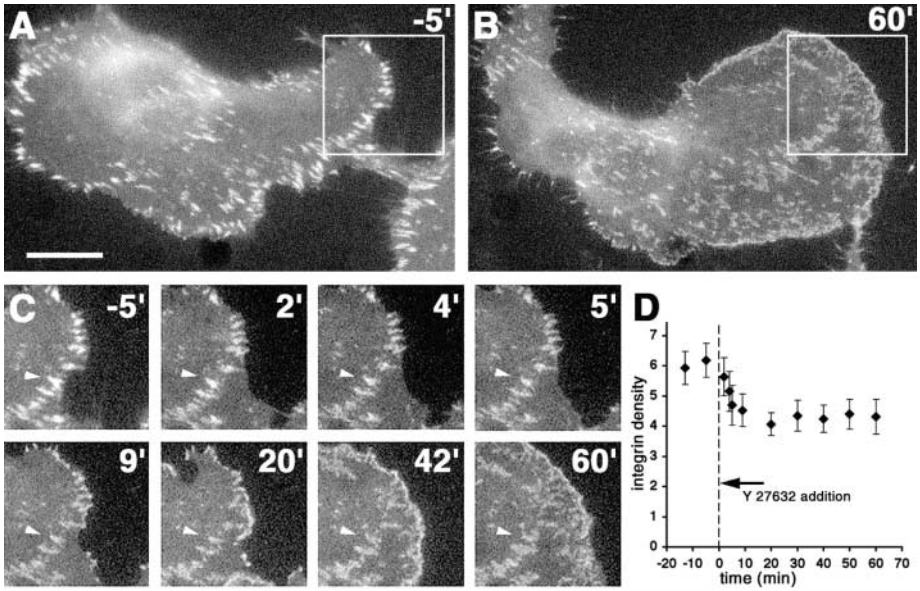

Figure 6. **Block of intracellular tension reduces focal adhesion density.** Time-lapse analysis of β3-integrin fluorescence of focal adhesions in B16 β3–GFP cells after addition of Y-27632 (20 μM) (A, 5′ before addition; B, 60′ after addition). (C) Higher magnification of the boxed area in A demonstrates (a) the reduction in β3-integrin density (fluorescence intensity) during the first 10 min of treatment and (b) the further dispersal of compact β3-integrin focal adhesions into irregularly shaped β3- integrin clusters (arrowhead). (D) The average peak β3-integrin integrin density in the peripheral focal adhesions was measured before and after the addition of the inhibitor. The indicated time refers to the addition of inhibitor. Bar, 20 μm.

number of large-sized, generally high-density focal adhesions were found (Fig. 5 H) (average relative integrin density and size: 5.14-fold, 1.15 μm^2). The stimulation of the RhoA pathway with LPA led to a shift to denser and generally larger focal adhesions (Fig. 5 I) (average relative integrin density and size: 6.77-fold, 1.69 μm^2). In contrast, treatment with either Y-27632 or staurosporine resulted in a drop in integrin densities (Fig. 5, J and K). Interestingly, the average size of the contacts in Y-27632–treated cells was only slightly lower compared with control cells, whereas the average size of staurosporine treated contacts was dramatically reduced (average relative integrin density and size: Y-27632, 4.39-fold, 0.87 μm^2; staurosporine, 4.49-fold, 0.43 μm^2). Furthermore, the dynamic transition of high- to low-density focal adhesions was analyzed in living B16 F1 cells by time-lapse microscopy (Fig. 6; Video7, available at http://www.jcb.org/cgi/content/full/jcb.200107107/DC1). Release of intracellular tension by Y-27632 induced the rapid decrease in integrin densities in peripheral focal adhesions (Fig. 6, B and C, arrowhead). During the first 10 min of treatment, neither the shape of the contacts nor that of the cell did change. With time, the cell developed large lamellipodia that contained numerous dot-like tension-independent focal adhesions. In addition, the Y-27632–induced low-density focal adhesions began to change shape but remained undispersed during the entire time of observation (up to 90 min) (Video7, available at http://www.jcb.org/cgi/content/full/jcb.200107107/DC1). These observations suggest that high intracellular tension correlates with the formation and maintenance of high-density αVβ3-integrin focal adhesions. The formation of low-density αVβ3-integrin focal adhesions is favored under conditions of low intracellular tension.

Exchange rates of integrins differ between low- and high-density focal adhesions

In the previous experiments, we determined that the density of αVβ3-integrin and the apparent sliding of focal adhesions are critically linked to the tension created by the actin cytoskeleton in a Rac1/RhoA-dependent fashion. During cell migration, newly formed, small, stationary, low-density focal adhesions firmly anchor the cell to the substratum. At the cell rear, retraction and apparent sliding of high-density focal adhesions require a more flexible interaction with the substrate. To understand the mechanical differences between these two types of adhesion sites, it is necessary to determine the dynamics of integrins within these substrate contacts. Therefore, we performed FRAP of β3–GFP-integrins within high-density focal adhesions and compared it with the recovery of integrins in low-density focal adhesions. FRAP measurements of β3–GFP-integrins in high-density focal contacts revealed a fast exchange (Fig. 7 A). Within 120 s, 50% of the integrin fluorescence recovered in the bleached contacts, whereas the exchange of all the β3-integrins was completed within 5–10 min (mobile fraction [MF] = 80–100%) (Fig. 7 B). This exchange was independent whether a high-density focal adhesion was stationary or sliding (Fig. 7 A). Due to the transient nature of low-density focal adhesions within an advancing lamellipodia, it was impossible to measure FRAP (Fig. 2). Therefore, we analyzed low-density focal adhesions formed upon transfection with dominant active Rac1 (Fig. 4). These low-density focal adhesions revealed a 2.5× slower recovery of integrins than high-density focal adhesions (Fig. 7 B). In addition, during the time of observation recovery reached only 50% (MF), suggesting that half the integrins in low-density focal adhesions are immobilized. Our experiments showed that although the integrin density in Rac1-induced focal adhesions was lower (see above), the retention time of integrins was dramatically increased compared with high-density focal adhesions. These data also suggest that an increase in intracellular tension, and hence the activation of RhoA, increases the turnover rate of integrins in focal adhesions.

Discussion

Migration is a complex cellular behavior that involves protrusion and adhesion at the cell front, and contraction and detachment at the rear. During these processes, members

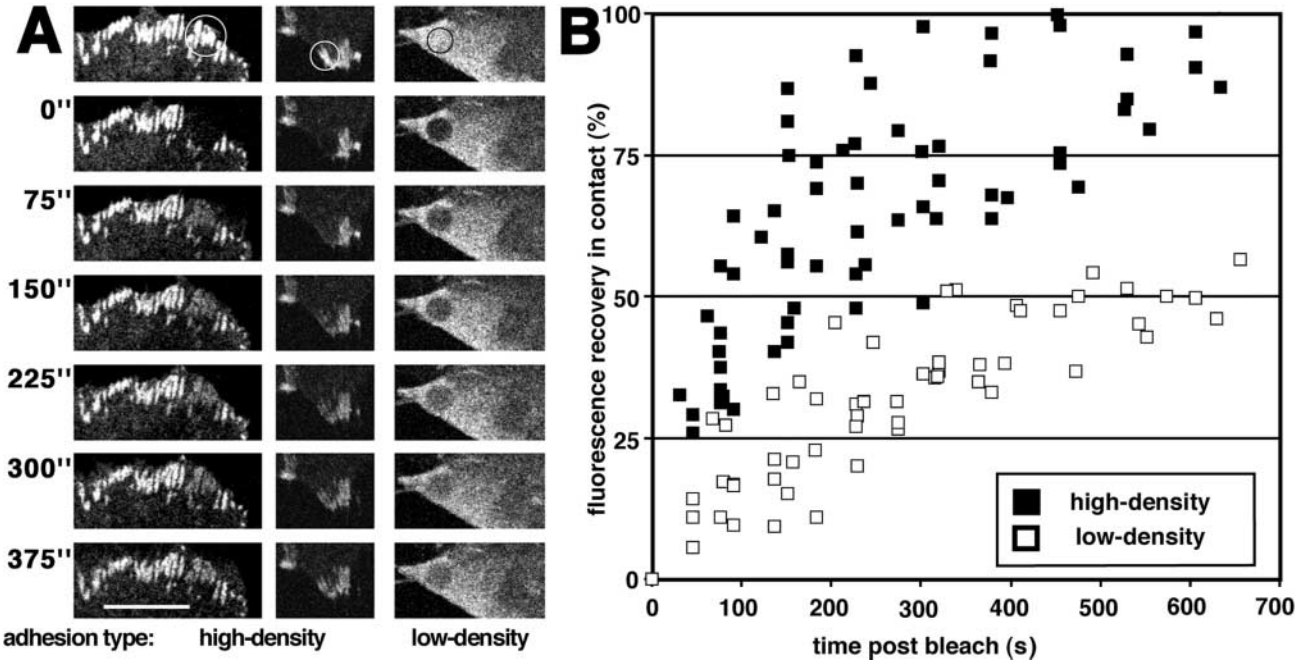

Figure 7. **FRAP reveals different β3-integrin exchange rates in high- versus low-density focal adhesions.** (A) Nontransfected or dominant active Rac1 transfected B16 β3–GFP cells were cultured overnight on serum-coated glass coverslips and FRAP was performed on focal adhesions localized to the edge of cells. The bleached area of each series is circled in the first frame and the recovery time (seconds after completion of bleach) indicated to the left. In control cells, immobile (first series) and inward sliding (second series) high-density focal adhesions show almost complete recovery (MF >80%). In cells transfected with dominant active Rac1 (third series) in which low-density focal adhesions were formed, fluorescence recovery was only partial (50% MF), reaching fluorescent levels just slightly above fluorescence intensities of nonclustered β3–GFP-integrin present in the plasma membrane (visible on the right hand side of the frame). Qualitative FRAP curves from several cells (5–8) are displayed in B. Each data point is the median of three to five individual focal adhesions. Bar, 10 μm.

of the integrin family provide the physical link between the actin cytoskeleton and the extracellular environment (Hynes, 1992). Here, we developed a new tool to follow and quantify αVβ3-integrins within focal adhesions formed in living cells by GFP labeling of the β3-integrin subunit (Plancon et al., 2001) for a similar construct). We have chosen the β3-integrin subunit for GFP tagging, as it forms heterodimers uniquely with the V and the platelet-specific IIb α chains. Therefore, GFP–β3-integrin transfected into cells (except platelets), will pair exclusively with αV to create a single species of labeled integrins. Most importantly, for quantitative studies of integrins, the amount of GFP fluorescence correlates directly with the number of αVβ3 heterodimers, and represents a direct measure of the relative integrin density within the two-dimensional plasma membrane and focal adhesion sites. In addition, the β3–GFP-integrin subunit, like normal β-integrin chains, requires heterodimerization with the αV chain for ER export and for an ECM-dependent engagement into focal adhesions (Heino et al., 1989; Lenter and Vestweber, 1994; Yauch et al., 1997). This is in contrast to monomeric chimeric β-integrin constructs that associate with focal adhesions in an ECM-independent manner, and therefore are not suited for quantitative measurements of integrin behavior (LaFlamme et al., 1994; Smilenov et al., 1999). Our analysis of αVβ3-integrin–containing contacts in migrating and stationary cells revealed two differently behaving types of cell adhesion sites. At the cell front, stationary focal adhesions formed within a zone of transient integrin clustering, whereas focal adhesions in retracting cell processes moved in relation to the substratum. The relative abundance of these two types of contacts may determine the migratory behavior of a cell. In the short-lived lamellipodia of slow-migrating fibroblasts, the zone of transient integrin clustering was difficult to define. In contrast, extremely fast-moving cells such as fish keratocytes exhibit stationary focal adhesions throughout the entire width of the lamellipodium that represent a major part of their total cell area (Lee and Jacobson, 1997; Anderson and Cross, 2000). Thus, the size of the area occupied by stationary focal adhesions, in respect to the total cell area, may determine the stability and persistence of lamellipodial protrusion and hence the overall speed of cell locomotion. In these different cell types, the zone of transient integrin clustering is equivalent to the area that is occupied by actin filaments originating at the edge of the lamellipodium (Svitkina et al., 1997; Ballestrem et al., 1998). It is conceivable that the actin filament turnover within the lamellipodium determines the half-lives of these stationary focal adhesions. In contrast to the stationary focal adhesions at the front of migrating cells, focal adhesions in retracting cell edges move relative to the substratum. This mobility of focal adhesions, previously described as sliding, has been suggested important for cell edge retraction and migration (Smilenov et al., 1999; Anderson and Cross, 2000; Zamir et al., 2000). Because the efficiency of cell migration is determined by the speed and ability of rear retraction (Palecek et al., 1998; Ballestrem et al., 2000), the

degree of focal adhesion sliding may limit the maximal speed of cell migration.

The quantitative analysis of GFP-labeled αVβ3-integrin allowed us to determine the changes in integrin densities within different types of focal adhesions. Hence, we observed a low αVβ3-integrin density in small, stationary focal adhesions, and a high αVβ3-integrin density in large, sliding focal adhesions. The formation of small dot-like focal adhesions (named focal complexes) in response to Rac1 and Cdc42 activation was first described by Nobes and Hall (1995) in fibroblasts, and they were distinguished from larger RhoA induced focal adhesions (named focal contacts) by their size (Nobes and Hall, 1995; Rottner et al., 1999). It is likely that these focal complexes and focal contacts are homologous to the low-density, respectively high-density focal adhesions observed by us. However, in contrast to focal adhesion size, integrin density represents a parameter that enables one to distinguish focal complexes from focal contacts in many different cell types, where the size differences are less accentuated as in fibroblasts, and is more specific than the recently questioned interference reflection microscopy (Iwanaga et al., 2001). Because activation of RhoA induces the bundling of actin filaments into stress fibers (Chrzanowska-Wodnicka and Burridge, 1996; Machesky and Hall, 1997), we suggest that the acto-myosin–dependent contraction of the actin scaffold increases integrin density in focal adhesions. This idea is supported by the observation that the gradual raise in acto-myosin–dependent intracellular tension strictly correlates with the amount of stress fiber formation and the increase in size of focal adhesions (Balaban et al., 2001). The increase in focal adhesion size has been recently attributed to RhoA activated mDia1, resulting in de novo actin polymerization at sites of focal complexes (Riveline et al., 2001). In contrast to RhoA, Rac1 or Cdc42 induces the formation of a looser actin filament lattice (Machesky and Hall, 1997) that could form the initial scaffold for low-density focal adhesions. The fate of these low-density focal adhesions, and hence their respective size and density, is then independently controlled by mDia1-stimulated actin polymerization and RhoA/Rac1-regulated acto-myosin contraction, respectively (Ridley et al., 1992; Sanders et al., 1999; van Leeuwen et al., 1999; Riveline et al., 2001). The importance of mechanical tension for focal adhesion compaction was corroborated by studies analyzing fields of intracellular tension during cell migration (Dembo and Wang, 1999; Oliver et al., 1999). In the lamellipodia of fish keratocytes, tension was low and isometric, predicting stationary low-density focal adhesions, whereas tension was high and vectorial at the lateral edges of the cell consistent with the formation of sliding high-density focal adhesions (Oliver et al., 1999; Anderson and Cross, 2000).

We have concluded that the integrin density within focal adhesion sites is determined by the degree of intracellular tension. Accordingly, changes in the elasticity of the ECM must similarly influence integrin density. We propose the following model. During cell migration, newly formed adhesion sites at the cell front are always in a low-density configuration. Subsequently, these sites mature into high-density contacts upon acto-myosin–dependent contraction. A rigid substratum such as glass resists the intracellular contraction resulting in a distortion of the actin integrin linkage. This mechanical stress within the focal adhesion site generates a signal for actin polymerization and growth of the focal adhesion. In contrast, an elastic ECM substratum will not resist the acto-myosin–dependent focal adhesion contraction failing to generate a distortion signal that would enforce the focal adhesion. Therefore, cells will favor a rigid over an elastic substrate for adhesion, a behavior consistent with the observed increase in cell motility and reduced spreading of fibroblasts on elastic substrates (Pelham and Wang, 1997). Furthermore, we propose that integrin density within a focal adhesion may act as a relay to exchange information about the degree of intracellular tension and extracellular elasticity, hence allowing cells to respond to gradients of extracellular elasticity and to adapt to mechanical distortions of the extracellular environment (Lo et al., 2000; Jalali et al., 2001; Riveline et al., 2001).

Induction of intracellular tension leads to the apparent sliding of focal adhesions in the rear of the cells. What is the mechanism of contacts sliding and how is αVβ3-integrin involved in this process? Focal adhesion have been considered as stable anchor points of the cell, supported by the observation that integrin containing fragments are left on the tracks of migrating cells (Chen, 1981). However, more recently it has become clear that fast-migrating cells recover integrins from the retracting, trailing portion of their body (Palecek et al., 1998; Pierini et al., 2000). Our FRAP analysis demonstrated a complete exchange of αVβ3-integrins in high-density focal adhesions within 5–10 min. This fast integrin turnover may provide a mechanistic explanation for focal adhesion sliding, resulting from a polarized renewal of integrins. We propose that the continuous loss of integrins from the distal edge, and recruitment of new integrins at the proximal edge of focal contacts, creates the illusion of sliding. In addition, high integrin turnover would increase the plasticity of focal adhesions, permitting rapid responses to local changes in intra- or extracellular tension. Because integrin turnover requires the loss of intracellular as well as extracellular links, the apparent turnover rates of integrins depend on the respective rate-limiting binding reaction. Measurement of fibrinogen to αIIb/β3 integrin affinity revealed a dissociation constant in the mM range (Rivas et al., 1996). Due to this low binding affinity, the rate-limiting step for integrin turnover is likely to be determined by the interaction of the integrin with the actin cytoskeleton.

Focal adhesions that are formed at sites of Rac1 activity at the cell front exhibit a surprisingly slow turnover and high temporal stability. Recently, it has been reported that Rac1 activation induces the high-affinity state of αVβ3-integrins, preferentially located within the leading edge of the cell (Kiosses et al., 2001). We propose that the slow and fast turnover rates of αVβ3-integrin in different focal adhesions directly represent its respective high- and low-affinity state. Hence, the high-affinity state of αVβ3-integrin in low-density focal adhesions may result in their stationary nature, whereas the low-affinity state in high-density focal adhesions may lead to their sliding. The RhoA signaling pathway leads to accumulation of phosphorylated myosin light chains, which in turn results in focal adhesions exhibiting high αVβ3-integrin turnover rates. Activation of the RAS/MAPK/

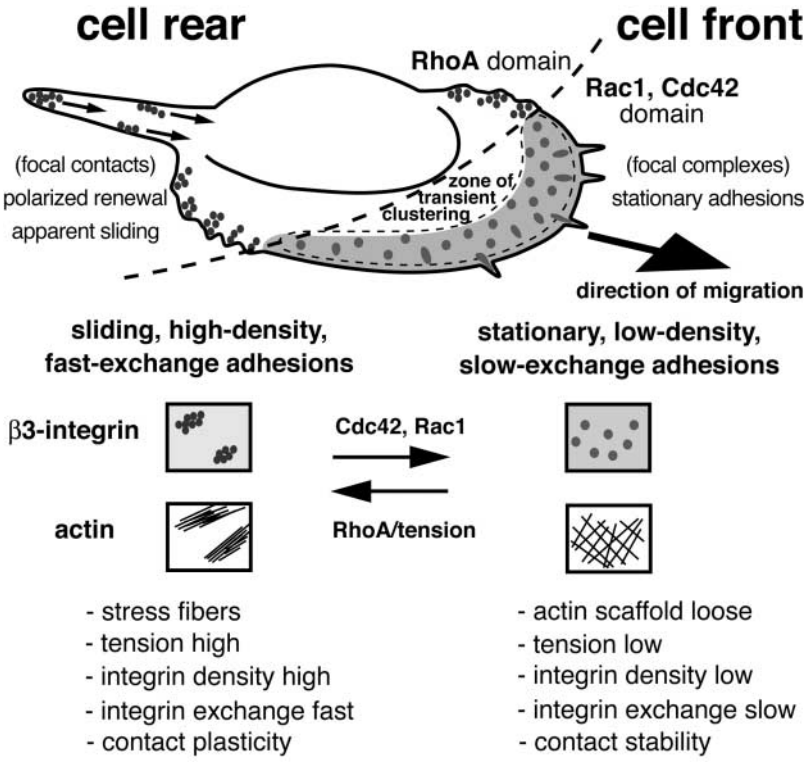

Figure 8. **Model of cell migration based on differential integrin turnover.** Cell migration is driven by Rac1- and Cdc42-dependent actin polymerization in the advancing lamellipodium. Integrin αVβ3 is incorporated in the lamellipodial actin filament lattice (gray shading) to form low-density integrin focal adhesions (focal complexes) (large and irregular shaped dots). These low-density focal adhesions remain stationary in respect to the substrate, firmly anchored in the cytoskeletal scaffold due to their slow turnover rate. These stabilized focal adhesions support the advancing lamellipodium. At the rear of the zone of transient clustering (circumferenced by dotted line), stationary focal adhesions rapidly disperse due to the depolymerization of the lamellipodial actin filament lattice (gray shading). While the cell moves forward, low-density focal adhesions at the lateral edges of the lamellipodium transform into high-density integrin focal adhesions (focal contacts) (accumulation of small dots). This transformation is directed by the acto-myosin–driven local collapse of the lamellipodial actin filaments into stress fibers and provides a means to sense the rigidity of the substrate. Integrins localized in high-density focal adhesions loose their firm cytoskeletal anchor and begin to show fast turnover, creating a great degree of plasticity for modulation of the contact. This plasticity can lead to polarized renewal of focal adhesions, the loss of integrins from the distal edge and their addition at the proximal edge of the contact, giving the illusion of sliding (small arrows).

ERK signaling pathway also results in myosin light chain phosphorylation. This pathway induces the low-affinity states of integrins and enhances rear retraction (Hughes et al., 1997; Klemke et al., 1997; Nobes and Hall, 1999; Fincham et al., 2000). These data suggest that myosin light chain phosphorylation might be the key step to the generation of low-affinity integrins in high-density focal adhesions that results in fast integrin turnover and is required to generate the sliding phenotype of these focal adhesions. Consistent with this hypothesis, it has recently been demonstrated that the RhoA signaling pathway, involving Rho-kinase and acto-myosin contraction, is required for integrin recycling and tail retracting of migrating leukocytes (Niggli, 1999; Pierini et al., 2000; Worthylake et al., 2001). Moreover, it has been demonstrated that nascent focal adhesions at the front of migrating fibroblasts generate the strongest propulsive forces (Beningo et al., 2001). These contacts display the typical phenotype of low-density and slow-turnover integrin contacts defined by this study.

To conclude, we propose a model of dynamic integrin clustering and dispersal in motile cells (Fig. 8). Rac1 and Cdc42 become activated and induce filopodia and lamellipoda that exhibit many stationary, low-density focal adhesions. Maximal cell motility is maintained by their ability to form firm adhesions due to slow integrin turnover and rapid dispersal at the rear of the zone of "transient integrin clustering," possibly caused by the depolymerization of lamellipodial actin filaments. Low-density focal adhesions form independent of intracellular tension, but transform into integrin dense focal adhesions at the lateral edge of the lamellipodium in response to RhoA induced acto-myosin–dependent intracellular tension. During this contraction, the actin integrin linkage senses the mechanical condition of the contacted ECM substrate resulting in the enforcement of focal adhesions on rigid substrates. High-density focal adhesions maintained by high traction forces at the lateral borders, begin to slide and subsequently detach due to their fast integrin turnover, a prerequisite for cell migration. Therefore, acto-myosin induced integrin turnover would offer a crucial therapeutic target to control migratory behavior of many cell types and might be relevant for pathological situations involving excessive migration of cells.

Materials and methods

β3–GFP-integrin fusion protein

Full-length mouse β3-integrin cDNA was provided by Dr. Patrick Ross (Washington University School of Medicine, St. Louis, MO) (Weerasinghe et al., 1998; Legler et al., 2001). Fusion of the enhanced GFP (EGFP) coding sequence (CLONTECH Laboratories, Inc.) with β3-integrin cDNA was performed in two steps. First, a COOH-terminal fragment of β3-integrin, containing a unique EcoRV site (underlined), was amplified with a 5′-ATGGATCCAAGGGTCCTGATATCCTG-3′ forward and 5′-AATACCGGTGAAGTCCCCCGGTAGGTGATA-3′ reverse primer pair, in order to remove the stop codon. The amplified sequence was digested with BamHI (5′) and AgeI (3′) restriction enzymes and cloned into pcDNA3/EGFP, containing the EGFP cDNA sequence 3′ to an AgeI site. pcDNA3/EGFP was prepared by insertion of the HindIII/NotI EGFP containing fragment from pEGFP-N1 (CLONTECH Laboratories, Inc.) into pcDNA3 at these sites (Invitrogen). The remaining NH_2-terminal part of the β3-integrin cDNA sequence (5′ to the EcoRV site) was cut out of the original vector with BamHI and EcoRV, and inserted at the respective sites into pcDNA3/EGFP, resulting in full-length β3–GFP-integrin joined by a short spacer (SerProValAlaThr).

Cells and transfections

NIH 3T3 fibroblasts and mouse B16F1 melanoma cells were cultured in DME and CHO cells in F12 medium, both supplemented with antibiotics and 10% FCS as described (Ballestrem et al., 1998). Superfect (QIAGEN)

or Fugen 6 (Roche) were used according to the manufacturers' recommendation for stable and transient transfections. Cells were cultured in the presence of 1 mg ml^{-1} G418 (GIBCO BRL) to select for stable β3–GFP-integrin–expressing clones (B16 β3–GFP; 3T3 β3–GFP).

NH_2 terminally myc-tagged (9E-10 epitope) (Evans et al., 1985) cDNA's for dominant active (L61) Rac, dominant active (V12) Cdc42, and dominant active (V14) RhoA, all in pRK5, were provided by Dr. Kurt Ballmer-Hofer (Paul Scherrer Institute, Villigen, Switzerland). The DS Red expression vector was obtained from CLONTECH Laboratories, Inc.

Antibodies and immunofluorescence

Anti–human vinculin were obtained from Sigma-Aldrich (Cat # V-9131). Mouse anti–chicken paxillin (clone 349) was from Transduction Laboratories, and mouse anti-myc (9E-10) was from American Type Culture Collection. The Kistrin–CD31 fusion protein (SKI-7) and the rat anti-CD31 monoclonal antibody (CG51) were used for FACS analysis as described (Legler et al., 2001).

B16 β3–GFP and 3T3 β3–GFP cells were cultured overnight in complete culture medium on Lab-Tek chambers (Nunc), previously coated with 5 μg ml^{-1} laminin-1, a gift from M. Chiquet (Morris Mueller Institute, Bern, Switzerland), 5 μg ml^{-1} fibronectin (Biomedical Products), or vitronectin 1 μg ml^{-1} (Sigma-Aldrich). Cells were fixed for 10 min with 4% paraformaldehyde in PBS and permeabilized with 0.5% Triton X-100 in PBS, washed, and blocked with PBS supplemented with 1% BSA. Cells were incubated 1 h with the respective monoclonal antibody diluted in PBS supplemented with 1% BSA. After rinsing twice with PBS, cells were incubated in the presence of goat anti–mouse antibodies conjugated to Texas red diluted in PBS supplemented with 1% BSA (Jackson Laboratories Inc.) and washed three times with PBS. Stained cells were examined and photographed using a Zeiss Axiovert 100 TV microscope equipped with a digital CCD camera (Hamamatsu Photonics) controlled by the Openlab software (Improvisions).

Immunoprecipitations

B16 β3–GFP were harvested by trypsinization and washed twice in ice-cold PBS before surface biotinylation with 0.5 mg ml^{-1} sulfo NHS-biotin (Pierce Chemical Co.) in PBS. Biotinylation was stopped by washing the cells in 2 ml ice-cold FCS. After three more washes in ice-cold PBS, cells were lysed in extraction buffer (1% Triton X-100, 0.5% deoxycholate, 0.1% SDS, 120 mM NaCl, and protease inhibitors) for 20 min at 4°C. Cell lysates were centrifuged at maximal speed for 15 min in a precooled microfuge. Supernatants were precleared with protein G beads (Amersham Pharmacia Biotech), and subsequently incubated overnight at 4°C with rat serum as control, a rat monoclonal against the integrin α6 subunit (EA-1) (Ruiz et al., 1993), a rat monoclonal against the αV subunit (RMV-7) (Takahashi et al., 1990), and a hamster anti-β3 subunit (anti-αVβ3, Cat # 01522D; PharMingen), coupled to protein G beads. Beads were washed four times in extraction buffer and then boiled in SDS sample buffer. An equivalent of 10^6 cells per lane was run under reducing conditions on 7% SDS PAGE gel. Proteins were transferred to nitrocellulose membranes and nonspecific binding sites were blocked with TBS containing 1% BSA and 0.1% Tween-20. After incubation with streptavidin–horse radish peroxidase or polyclonal rabbit anti-GFP antibodies (CLONTECH Laboratories, Inc.) followed by peroxidase-conjugated anti–rabbit immunglobulin antibodies (Sigma-Aldrich), peroxidase activity was visualized by chemiluminescence (ECL; Amersham).

Flexible silicone rubber contraction assay

Flexible rubber silicone substrata were prepared as described previously (Harris et al., 1980) with some modifications in order to obtain even and thin substrata. 5 μl of silicone fluid (poly dimethyl siloxane; 30,000 centistokes; Dow Corning) were deposited onto glass coverslips and centrifuged at 1,000 rpm for 1 min. The silicone surface was then crosslinked by passing the coverslip through a very low Bunsen flame for ~0.5 s. An incubation chamber was created by placing a silicone ring onto the coverslip. Silicone substrates were equilibrated with 0.1% gelatin in Tris-HCl buffer, pH 8.4 to facilitate cell adhesion, sterilized by UV light exposure for 3 h and left overnight in the incubator at 37°C. 3T3 fibroblasts were then seeded in DME/10%FCS and allowed to spread and to deform the silicone substratum for 2 d. Live cells were observed at 37°C on a Zeiss Axiovert microscope using a 32× Ph2 objective. Cells were recorded (KS400, 1 frame/15 s) for 60 min under control conditions before agonists were added to the culture medium. Three experiments were performed per experimental condition.

Time-lapse and inhibitor studies

Time-lapse studies were performed as described (Ballestrem et al., 1998, 2000). Briefly, B16 β3–GFP and 3T3 β3–GFP were cultured overnight on Lab-Tek chambers previously coated overnight at 4°C with indicated concentrations of ECM proteins. Cells were visualized on an Axiovert 100 TV inverted microscope (Zeiss), equipped with an incubation chamber, a standard GFP filter set (Omega), and a Hamamatsu C4742–95–10 digital charge coupled device camera. Images were recorded in intervals of 1 or 2 min and processed using Openlab software (Improvision).

LPA and staurosporine were obtained from Sigma-Aldrich and used at 10 μM and 50 nM, respectively. Rho kinase inhibitor Y-27632 (Uehata et al., 1997) was obtained from Yoshitomi Pharmaceutical Industries and used at 10 μM for 3T3 β3–GFP cells, and at 20 μM for B16 β3–GFP cells.

Measurement of fluorescence intensities of integrin clusters and cell surface areas

Stable and homogeneously β3-integrin–expressing B16 β3–GFP and 3T3 β3–GFP cells derived from clonal selection were either transiently transfected with dominant active Rac1, Cdc42, and RhoA or treated with various drugs (see above). 24 h after transfection, or 1 h after the addition of drugs, cells were fixed and, where appropriate, were counterstained with anti-myc (9E-10) anti–mouse Texas red, in order to detect the transfected GTPases. GFP fluorescence images were recorded with identical exposure settings for all different experimental conditions on an Axiovert 100TV equipped with a CCD-camera (see above). Cell surface and focal adhesion areas and their respective mean and peak fluorescence were measured using the Openlab software (Improvision). For the GTPase transfection experiments, 20 or more cells were measured per experimental condition, and mean surface areas were calculated (nontransfected, 1127 ± 283 μm^2; da-Rac1, 2800 ± 1072 μm^2; da-Cdc42, 2117 ± 500 μm^2; da-RhoA, 724 ± 315 μm^2; data from one out of three qualitatively similar experiments). Fluorescence intensity profiles were obtained with the software of the LSM510 confocal microscope (Zeiss). The range of fluorescence values (expressed in 8-bit gray levels) were derived from several intensity profiles (three to five profiles per cell, from three to five different cells per condition) by determining the local minima and maxima: 48–52 (background fluorescence outside of cells), 65–75 (nonclustered integrin fluorescence in the cell periphery corresponding to two sheets of plasma membrane), 90–110 (peak fluorescence intensities of focal complexes in control, da-Rac1-, or da-Cdc42-transfected cells), 110–140 (peak fluorescence intensities of focal contacts in control cells) and 150–200 (peak fluorescence intensities of focal contacts in RhoA transfected cells). To calculate the relative increase in integrin densities in respect to the density of nonclustered integrins in one sheet of plasma membrane, we subtracted the background fluorescence (50) and the fluorescence of one of the plasma membrane sheets (10) from each value and divided it by the fluorescence of one plasma membrane sheet (10).

The same type of calculation was used to determine the x-fold fluorescence increase between the relative integrin density of membranes and that of individual focal adhesions in normal and drug treated cells. To develop an integrin density/contact area profile, we analyzed between 400–600 contacts from four to six cells from one out of three similar experiments. To follow the integrin densities in Y-27632–treated cells (see Fig. 6), the average peak fluorescence intensities of 40–60 peripheral focal adhesions were measured.

FRAP

Control or dominant active Rac1/Ds red–transfected B16 β3–GFP cells were plated and grown on serum-coated glass coverslips in DMM/10%FCS for 24 h. For photo-bleaching and fluorescence recovery, the culture medium was changed to F12/10%FCS medium and cells were mounted on an inverted confocal microscope equipped with an incubation chamber (LSM510; Zeiss). Confocal images of focal adhesion sites were recorded with 2–3% of the intensity of the 488-nm line from living Mock and Rac1/Ds red–transfected cells. GFP fluorescence was eliminated using five bleach cycles at 100% intensity of the 488 line. Control bleach experiments performed over the entire cell surface demonstrated that the GFP chromophore was completely inactivated by this treatment and that recovery of fluorescence due to newly synthesized GFP proteins was not detectable during the period of recovery (15–20 min). Qualitative recovery curves (R[t]) were obtained per cell, by comparing fluorescence intensities of three to five bleached contacts ($I_{bleached\ contact}[t]$) with neighboring unbleached ($I_{unbleached\ contacts}[t]$) contacts after background ($I_{background}[t]$) subtraction: $R(t) = (I_{bleached\ contact}[t] - I_{background}[t])/(I_{unbleached\ contacts}[t] - I_{background}[t])$; t, time of recovery (White and Stelzer, 1999). This internal calibration compensated for intrinsic changes in fluorescence due to small focus changes and or the gradual loss of cellular GFP fluorescence during the observation period due to fluorophore inactivation by the laser. For comparison of several recovery curves, the fractional recovery ($R_{frac}[t]$) of each curve was

plotted against time. The analysis of the fractional recovery corrected for differences between cells due to incomplete inactivation of the chromophores during bleaching. Typically, the fluorescence intensity just after bleaching (I_{bleach}) was between 5 and 20% of the prebleach fluorescence (100%). The fractional recovery ($R_{frac}[t]$) (all curves start at 0) was therefore $R_{frac}(t) = (R[t] - I_{bleach})/(1 - I_{bleach})$ (Axelrod et al., 1976). A single logarithmic regression curve was calculated from the datapoints (Excel; Microsoft), in order to determine the half-maximal recovery time ($T_{1/2}$) and the MF ($MF = R_{frac}[t_{end}]$); t_{end} corresponds to the endpoint of the recovery period (10–15 min). Due to the variable size of the focal contacts analyzed, and a likely second order logarithmic recovery of integrins in focal contacts, a diffusion coefficient was not calculated. In addition, we did not correct the error that is due to the integrin fluorescence of the contact-overlaying membrane sheet in which the recovery is much faster (unpublished data). This error is more important for low- than high-density contacts, as the differences in the fluorescence between the membrane and high-density contacts is bigger than that for low-density contacts.

Online supplemental material

Video sequences of untreated and Rho-kinase inhibitor–treated β3–GFP-integrin–transfected cells reveal the dynamics of β3–GFP-containing adhesion sites. In addition, video sequences of cells cultured on elastic silicon substrata reveal the change in intracellular tension caused by the application of drugs. Video 1 demonstrates the stationary and transient nature of focal complexes appearing within an advancing lamellipodium. Video 2 reveals the apparent sliding of focal contacts localized within the rear of a migrating cell. Video 3 illustrates lamellipodia extension, collapse, and retraction in a nonmigratory cell, and follows the cycling of integrin fluorescence intensity as well as mobility between small and large focal adhesions. Video 4 demonstrates the increase in intracellular tension manifested by an increase in wrinkling of the flexible silicon substrate after LPA addition. Videos 5 and 6 illustrate the respective loss of intracellular tension after addition of Rho-kinase inhibitor (Y 27632 or staurosporine, respectively. Video 7 shows the behavioral and structural changes of β3–GFP-containing focal adhesion sites upon release of intracellular tension after inhibition of Rho-kinase. All videos are available at http://www.jcb.org/cgi/content/full/jcb.200107107/DC1.

We thank Dr. Caroline Johnson-Léger and Michel Aurrands-Lions for critical reading and discussion of this manuscript. We are grateful to Marie-Claude Jacquier for excellent technical support, and to Jacqueline Ntah for secretarial assistance. We would like to thank Drs. Giulio Gabbiani (Centre Médical Universitaire, Geneva, Switzerland), Matthias Chiquet, Kurt Ballmer-Hofer, and Patrick Ross for providing us with reagents.

This work has been supported by grants from the Schweizerischen Krebsliga (KFS 412-1-1997), the Swiss National Science Foundation (31-49241-96, 31-052727.97, 31.059173.99, and 31-64000.00), the Fondation Gabrielle Giorgi-Cavaglieri, and Helmut Horten Stiftung.

Submitted: 25 July 2001
Revised: 14 November 2001
Accepted: 14 November 2001

References

Albelda, S.M., S.A. Mette, D.E. Elder, R. Stewart, L. Damjanovich, M. Herlyn, and C.A. Buck. 1990. Integrin distribution in malignant melanoma: association of the beta 3 subunit with tumor progression. *Cancer Res.* 50:6757–6764.

Amano, M., K. Chihara, K. Kimura, Y. Fukata, N. Nakamura, Y. Matsuura, and K. Kaibuchi. 1997. Formation of actin stress fibers and focal adhesions enhanced by Rho-kinase. *Science.* 275:1308–1311.

Anderson, K.I., and R. Cross. 2000. Contact dynamics during keratocyte motility. *Curr. Biol.* 10:253–260.

Axelrod, D., D.E. Koppel, J. Schlessinger, E. Elson, and W.W. Webb. 1976. Mobility measurement by analysis of fluorescence photobleaching recovery kinetics. *Biophys. J.* 16:1055–1069.

Balaban, N.Q., U.S. Schwarz, D. Riveline, P. Goichberg, G. Tzur, I. Sabanay, D. Mahalu, S. Safran, A. Bershadsky, L. Addadi, and B. Geiger. 2001. Force and focal adhesion assembly: a close relationship studied using elastic micropatterned substrates. *Nat. Cell Biol.* 3:466–472.

Ballestrem, C., B. Wehrle-Haller, and B.A. Imhof. 1998. Actin dynamics in living mammalian cells. *J. Cell Sci.* 111:1649–1658.

Ballestrem, C., B. Wehrle-Haller, B. Hinz, and B.A. Imhof. 2000. Actin-dependent lamellipodia formation and microtubule-dependent tail retraction control-directed cell migration. *Mol. Biol. Cell.* 11:2999–3012.

Beningo, K.A., M. Dembo, I. Kaverina, J.V. Small, and Y.L. Wang. 2001. Nascent focal adhesions are responsible for the generation of strong propulsive forces in migrating fibroblasts. *J. Cell Biol.* 153:881–888.

Brooks, P.C., R.A. Clark, and D.A. Cheresh. 1994. Requirement of vascular integrin alpha v beta 3 for angiogenesis. *Science.* 264:569–571.

Chen, W.T. 1981. Mechanism of retraction of the trailing edge during fibroblast movement. *J. Cell Biol.* 90:187–200.

Cheresh, D.A., and R.C. Spiro. 1987. Biosynthetic and functional properties of an Arg-Gly-Asp-directed receptor involved in human melanoma cell attachment to vitronectin, fibrinogen, and von Willebrand factor. *J. Biol. Chem.* 262:17703–17711.

Chrzanowska-Wodnicka, M., and K. Burridge. 1996. Rho-stimulated contractility drives the formation of stress fibers and focal adhesions. *J. Cell Biol.* 133:1403–1415.

Delannet, M., F. Martin, B. Bossy, D.A. Cheresh, L.F. Reichardt, and J.L. Duband. 1994. Specific roles of the alpha V beta 1, alpha V beta 3 and alpha V beta 5 integrins in avian neural crest cell adhesion and migration on vitronectin. *Development.* 120:2687–2702.

Dembo, M., and Y.L. Wang. 1999. Stresses at the cell-to-substrate interface during locomotion of fibroblasts. *Biophys. J.* 76:2307–2316.

Duband, J.L., G.H. Nuckolls, A. Ishihara, T. Hasegawa, K.M. Yamada, J.P. Thiery, and K. Jacobson. 1988. Fibronectin receptor exhibits high lateral mobility in embryonic locomoting cells but is immobile in focal contacts and fibrillar streaks in stationary cells. *J. Cell Biol.* 107:1385–1396.

Evans, G.I., G.K. Lewis, G. Ramsey, and M.J. Bishop. 1985. Isolation of monoclonal antibodies specific for human c-myc proto-oncogene product. *Mol. Cell Biol.* 5:3610–3616.

Felding-Habermann, B., T.E. O'Toole, J.W. Smith, E. Fransvea, Z.M. Ruggeri, M.H. Ginsberg, P.E. Hughes, N. Pampori, S.J. Shattil, A. Saven, and B.M. Mueller. 2001. Integrin activation controls metastasis in human breast cancer. *Proc. Natl. Acad. Sci. USA.* 98:1853–1858.

Fincham, V.J., M. James, M.C. Frame, and S.J. Winder. 2000. Active ERK/MAP kinase is targeted to newly forming cell-matrix adhesions by integrin engagement and v-Src. *EMBO J.* 19:2911–2923.

Geiger, B., and A. Bershadsky. 2001. Assembly and mechanosensory function of focal contacts. *Curr. Opin. Cell Biol.* 13:584–592.

Harris, A.K., P. Wild, and D. Stopak. 1980. Silicone rubber substrata: a new wrinkle in the study of cell locomotion. *Science.* 208:177–179.

Heino, J., R.A. Ignotz, M.E. Hemler, C. Crouse, and J. Massague. 1989. Regulation of cell adhesion receptors by transforming growth factor-beta. Concomitant regulation of integrins that share a common beta 1 subunit. *J. Biol. Chem.* 264:380–388.

Horwitz, A.R., and J.T. Parsons. 1999. Cell migration—movin' on. *Science.* 286:1102–1103.

Hughes, P.E., M.W. Renshaw, M. Pfaff, J. Forsyth, V.M. Keivens, M.A. Schwartz, and M.H. Ginsberg. 1997. Suppression of integrin activation: a novel function of a Ras/Raf-initiated MAP kinase pathway. *Cell.* 88:521–530.

Hynes, R.O. 1992. Integrins: versatility, modulation, and signaling in cell adhesion. *Cell.* 69:11–25.

Iwanaga, Y., D. Braun, and P. Fromherz. 2001. No correlation of focal contacts and close adhesion by comparing GFP-vinculin and fluorescence interference of Dil. *Eur. Biophys. J.* 30:17–26.

Jalali, S., M.A. del Pozo, K. Chen, H. Miao, Y. Li, M.A. Schwartz, J.Y. Shyy, and S. Chien. 2001. Integrin-mediated mechanotransduction requires its dynamic interaction with specific extracellular matrix (ECM) ligands. *Proc. Natl. Acad. Sci. USA.* 98:1042–1046.

Katz, B.Z., E. Zamir, A. Bershadsky, Z. Kam, K.M. Yamada, and B. Geiger. 2000. Physical state of the extracellular matrix regulates the structure and molecular composition of cell-matrix adhesions. *Mol. Biol. Cell.* 11:1047–1060.

Kimura, K., M. Ito, M. Amano, K. Chihara, Y. Fukata, M. Nakafuku, B. Yamamori, J. Feng, T. Nakano, K. Okawa, et al. 1996. Regulation of myosin phosphatase by Rho and Rho-associated kinase (Rho-kinase). *Science.* 273:245–248.

Kiosses, W.B., S.J. Shattil, N. Pampori, and M.A. Schwartz. 2001. Rac recruits high-affinity integrin alphavbeta3 to lamellipodia in endothelial cell migration. *Nat. Cell. Biol.* 3:316–320.

Klemke, R.L., S. Cai, A.L. Giannini, P.J. Gallagher, P. de Lanerolle, and D.A. Cheresh. 1997. Regulation of cell motility by mitogen-activated protein kinase. *J. Cell Biol.* 137:481–492.

LaFlamme, S.E., L.A. Thomas, S.S. Yamada, and K.M. Yamada. 1994. Single subunit chimeric integrins as mimics and inhibitors of endogenous integrin

functions in receptor localization, cell spreading and migration, and matrix assembly. *J. Cell Biol.* 126:1287–1298.

Lauffenburger, D.A., and A.F. Horwitz. 1996. Cell migration: a physically integrated molecular process. *Cell.* 84:359–369.

Lee, J., and K. Jacobson. 1997. The composition and dynamics of cell-substratum adhesions in locomoting fish keratocytes. *J. Cell Sci.* 110:2833–2844.

Legler, D.F., G. Wiedle, F.P. Ross, and B.A. Imhof. 2001. Superactivation of integrin alphavbeta3 by low antagonist concentrations. *J. Cell Sci.* 114:1545–1553.

Lenter, M., and D. Vestweber. 1994. The integrin chains beta 1 and alpha 6 associate with the chaperone calnexin prior to integrin assembly. *J. Biol. Chem.* 269:12263–12268.

Lo, C.M., H.B. Wang, M. Dembo, and Y.L. Wang. 2000. Cell movement is guided by the rigidity of the substrate. *Biophys. J.* 79:144–152.

Machesky, L.M., and A. Hall. 1997. Role of actin polymerization and adhesion to extracellular matrix in Rac- and Rho-induced cytoskeletal reorganization. *J. Cell Biol.* 138:913–926.

McHugh, K.P., K. Hodivala-Dilke, M.H. Zheng, N. Namba, J. Lam, D. Novack, X. Feng, F.P. Ross, R.O. Hynes, and S.L. Teitelbaum. 2000. Mice lacking beta3 integrins are osteosclerotic because of dysfunctional osteoclasts. *J. Clin. Invest.* 105:433–440.

Miyamoto, S., H. Teramoto, O.A. Coso, J.S. Gutkind, P.D. Burbelo, S.K. Akiyama, and K.M. Yamada. 1995. Integrin function: molecular hierarchies of cytoskeletal and signaling molecules. *J. Cell Biol.* 131:791–805.

Niggli, V. 1999. Rho-kinase in human neutrophils: a role in signalling for myosin light chain phosphorylation and cell migration. *FEBS Lett.* 445:69–72.

Nobes, C.D., and A. Hall. 1995. Rho, rac, and cdc42 GTPases regulate the assembly of multimolecular focal complexes associated with actin stress fibers, lamellipodia, and filopodia. *Cell.* 81:53–62.

Nobes, C.D., and A. Hall. 1999. Rho GTPases control polarity, protrusion, and adhesion during cell movement. *J. Cell Biol.* 144:1235–1244.

Oliver, T., M. Dembo, and K. Jacobson. 1999. Separation of propulsive and adhesive traction stresses in locomoting keratocytes. *J. Cell Biol.* 145:589–604.

Palecek, S.P., A. Huttenlocher, A.F. Horwitz, and D.A. Lauffenburger. 1998. Physical and biochemical regulation of integrin release during rear detachment of migrating cells. *J. Cell Sci.* 111:929–940.

Pankov, R., E. Cukierman, B.Z. Katz, K. Matsumoto, D.C. Lin, S. Lin, C. Hahn, and K.M. Yamada. 2000. Integrin dynamics and matrix assembly: tensin-dependent translocation of alpha(5)beta(1) integrins promotes early fibronectin fibrillogenesis. *J. Cell Biol.* 148:1075–1090.

Pelham, R.J., Jr., and Y. Wang. 1997. Cell locomotion and focal adhesions are regulated by substrate flexibility. *Proc. Natl. Acad. Sci. USA.* 94:13661–13665.

Pierini, L.M., M.A. Lawson, R.J. Eddy, B. Hendey, and F.R. Maxfield. 2000. Oriented endocytic recycling of alpha5beta1 in motile neutrophils. *Blood.* 95: 2471–2480.

Plancon, S., M.C. Morel-Kopp, E. Schaffner-Reckinger, P. Chen, and N. Kieffer. 2001. Green fluorescent protein (GFP) tagged to the cytoplasmic tail of alphaIIb or beta3 allows the expression of a fully functional integrin alphaIIb(beta3): effect of beta3GFP on alphaIIb(beta3) ligand binding. *Biochem. J.* 357:529–536.

Ridley, A.J., and A. Hall. 1992. The small GTP-binding protein rho regulates the assembly of focal adhesions and actin stress fibers in response to growth factors. *Cell.* 70:389–399.

Ridley, A.J., H.F. Paterson, C.L. Johnston, D. Diekmann, and A. Hall. 1992. The small GTP-binding protein rac regulates growth factor-induced membrane ruffling. *Cell.* 70:401–410.

Rivas, G., K. Tangemann, A.P. Minton, and J. Engel. 1996. Binding of fibrinogen to platelet integrin alpha IIb beta 3 in solution as monitored by tracer sedimentation equilibrium. *J. Mol. Recognit.* 9:31–38.

Riveline, D., E. Zamir, N.Q. Balaban, U.S. Schwarz, T. Ishizaki, S. Narumiya, Z. Kam, B. Geiger, and A.D. Bershadsky. 2001. Focal contacts as mechanosensors: externally applied local mechanical force induces growth of focal contacts by an mDia1-dependent and ROCK-independent mechanism. *J. Cell Biol*. 153:1175-86.

Rottner, K., A. Hall, and J.V. Small. 1999. Interplay between Rac and Rho in the control of substrate contact dynamics. *Curr. Biol.* 9:640–648.

Ruiz, P., D. Dunon, A. Sonnenberg, and B.A. Imhof. 1993. Suppression of mouse melanoma metastasis by EA-1, a monoclonal antibody specific for alpha 6 integrins. *Cell. Adhes. Commun.* 1:67–81 (published erratum appears in *Cell. Adhes. Commun.* 1993. 2:190).

Sanders, L.C., F. Matsumura, G.M. Bokoch, and P. de Lanerolle. 1999. Inhibition of myosin light chain kinase by p21-activated kinase. *Science.* 283:2083–2085.

Smilenov, L.B., A. Mikhailov, R.J. Pelham, E.E. Marcantonio, and G.G. Gundersen. 1999. Focal adhesion motility revealed in stationary fibroblasts. *Science.* 286:1172–1174.

Svitkina, T.M., A.B. Verkhovsky, K.M. McQuade, and G.G. Borisy. 1997. Analysis of the actin-myosin II system in fish epidermal keratocytes: mechanism of cell body translocation. *J. Cell Biol.* 139:397–415.

Takahashi, K., T. Nakamura, M. Koyanagi, K. Kato, Y. Hashimoto, H. Yagita, and K. Okumura. 1990. A murine very late activation antigen-like extracellular matrix receptor involved in CD2- and lymphocyte function-associated antigen-1-independent killer-target cell interaction. *J. Immunol.* 145:4371–4379.

Uehata, M., T. Ishizaki, H. Satoh, T. Ono, T. Kawahara, T. Morishita, H. Tamakawa, K. Yamagami, J. Inui, M. Maekawa, and S. Narumiya. 1997. Calcium sensitization of smooth muscle mediated by a Rho-associated protein kinase in hypertension. *Nature.* 389:990–994.

van Leeuwen, F.N., S. van Delft, H.E. Kain, R.A. van der Kammen, and J.G. Collard. 1999. Rac regulates phosphorylation of the myosin-II heavy chain, actinomyosin disassembly and cell spreading. *Nat. Cell Biol.* 1:242–248.

Weerasinghe, D., K.P. McHugh, F.P. Ross, E.J. Brown, R.H. Gisler, and B.A. Imhof. 1998. A role for the alphavbeta3 integrin in the transmigration of monocytes. *J. Cell Biol.* 142:595–607.

White, J., and E. Stelzer. 1999. Photobleaching GFP reveals protein dynamics inside live cells. *Trends Cell Biol.* 9:61–65.

Worthylake, R.A., S. Lemoine, J.M. Watson, and K. Burridge. 2001. RhoA is required for monocyte tail retraction during transendothelial migration. *J. Cell Biol.* 154:147–160.

Yauch, R.L., D.P. Felsenfeld, S.K. Kraeft, L.B. Chen, M.P. Sheetz, and M.E. Hemler. 1997. Mutational evidence for control of cell adhesion through integrin diffusion/clustering, independent of ligand binding. *J. Exp. Med.* 186: 1347–1355.

Zamir, E., M. Katz, Y. Posen, N. Erez, K.M. Yamada, B.Z. Katz, S. Lin, D.C. Lin, A. Bershadsky, Z. Kam, and B. Geiger. 2000. Dynamics and segregation of cell-matrix adhesions in cultured fibroblasts. *Nat. Cell. Biol.* 2:191–196.

5. Conclusions

5.1. Cross-talk between integrin, actin and microtubule cytoskeleton regulate cell adhesion

PERGAMON

The International Journal of Biochemistry & Cell Biology 1324 (2002) 1–12

IJBCB

www.elsevier.com/locate/ijbcb

Actin, microtubules and focal adhesion dynamics during cell migration

Bernhard Wehrle-Haller*, Beat A. Imhof

Department of Pathology, Centre Médical Universitaire, 1 Rue Michel-Servet, 1211 Geneva 4, Switzerland

Received 12 November 2001; received in revised form 10 May 2002; accepted 14 May 2002

Keywords: Green fluorescent protein; Cytoskeleton; Actin; Tubulin; Focal adhesion; Migration

1. Introduction

Within the last few years the dynamic analysis of the major cytoskeletal elements has gained new impetus due to the application of the GFP technology. The stable or transient transfection of GFP-labeled cytoskeletal components ranging from actin, tubulin and a number of accessory proteins has allowed analysis of cytoskeletal dynamics in living cells (Fig. 1, Video 1) [1]. The dynamic remodeling of the actin cytoskeleton as well as the microtubule network has been studied in great detail [2,3]. The reciprocal cross-talk between these important cytoskeletal systems and their dynamic link to the substrate in focal adhesions has helped to unravel the critical regulatory pathways essential for cell motility. Here, we review the recent progress in understanding the function of cytoskeletal structures formed by the actin and microtubule network. In addition, we discuss the importance of the actin and the microtubule system in the regulation of focal adhesion dynamics, required for cell adhesion and migration.

2. Different actin dynamics in stationary and motile cells

During the development of multicellular organisms different cell types work together to perpetuate growth and tissue homeostasis, mechanisms that require cell migration. A cell can change from a stationary to a mobile status depending on the microenvironment that provides signals, such as extracellular matrix molecules, growth factors or chemokines. In response to these signals, cell movement is propelled by the cytoskeleton. More precisely, the actin cytoskeleton is associated with protruding cellular structures that form at the front of migrating cells such as filopodia and lamellipodia [4]. These structures are composed of numerous actin filaments (F-actin) that are polymerized at their barbed;[1] end from monomeric actin

Abbreviations: APC, adenomatous polyposis coli; CSF-1, colony stimulating factor-1; EGF, epidermal growth factor; ER, endoplasmic reticulum; GEF, GTPase exchange factor; GFP, green fluorescent protein; MTOC, microtubule-organizing center; PDGF, platelet-derived growth factor; PMA, phorbol 12-myristate 13-acetate; SCF, stem cell factor

* Corresponding author. Tel.: +41-22-702-57-35; fax: +41-22-702-57-46.

E-mail address: bernhard.wehrle-haller@medecine.unige.ch (B. Wehrle-Haller).

[1] The orientation of actin polymerization can be detected by addition of cleaved myosin heads. These bind laterally to the actin filaments giving the impression of a barb at one end (barbed end) and an arrow at the other end (pointed end).

1357-2725/02/$ – see front matter
PII: S1357-2725(02)00071-7

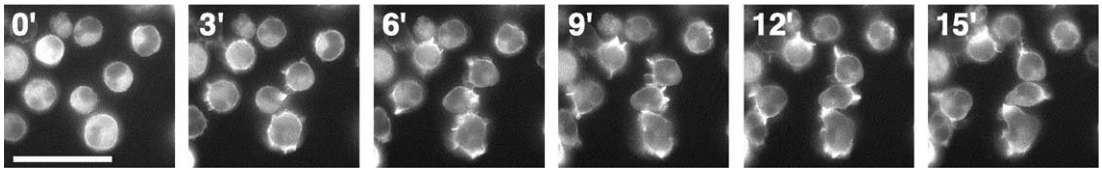

Fig. 1. Visualization of actin dynamics in lymphocytes. Time-lapse analysis of L1–2 lymphocytes double transfected with GFP–β-actin and fMLP peptide receptor. At the beginning of the sequence fMLP peptide was added to activate actin remodeling and migration. Note the appearance of GFP–β-actin containing filopodia and lamellipodia and the time indicated. Bar corresponds to 25 μm. *Video 1:* In the first part of the sequence non-stimulated cells were recorded. A white frame indicates the addition of the fMLP peptide to the medium that is followed by actin remodeling and migration. The width of the frame corresponds to 45 μm and the sequence is accelerated 300-fold (1 frame/min to 5 frames/s).

(G-actin). At the pointed end of these filaments, G-actin is liberated by de-polymerization [3,5–7]. This process is referred to as treadmilling and in a lamellipodium, it operates towards the interior of the cell, i.e. actin molecules are added to filaments at the periphery and they are released towards the cell center. In general, the orientation of treadmilling indicates the polarity of each actin filament. One might consider a cell as stationary as long as the sum of the vectors defined by treadmilling equals zero. The sum of the treadmilling vectors in a migrating keratinocyte may therefore define the direction of migration [8]. In order to transform the treadmilling, for example within a lamellipodium, into forward movement, the actin filaments have to be anchored to the substrate at sites known as focal complexes [9,10]. Once treadmilling actin filaments are anchored to the substrate, the continuous addition of G-actin at their barbed ends will push the lamellipodia and the plasma membrane forward [11].

In contrast to fast migrating cells, such as keratinocytes, leukocytes or melanoma cells, slow migrating cells, such as fibroblasts, exhibit actin filaments that are bundled into stress fibers anchored within focal contacts located at the cell periphery. These stress fibers are often found oriented along

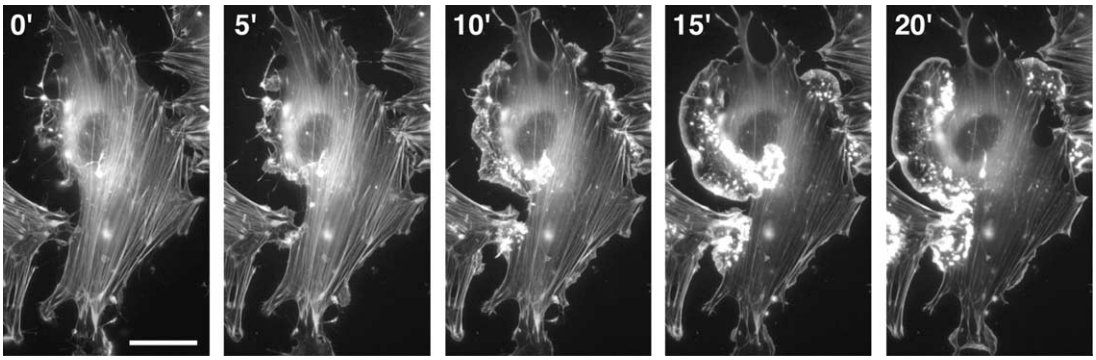

Fig. 2. Reshuffling of the actin-pool during the onset of cell migration. Stable GFP–β-actin transfected B16 F1 mouse melanoma cells were plated onto serum coated glass cover slips. After overnight culture, a stationary cell exhibiting a well established stress fiber network was stimulated with 100 nM PMA at −5 min. After treatment for 10 min the cell began to develop lamellipodia that grew into large lamella. Associated with the formation of this lamella, the number and caliber of stress fibers reduced simultaneously. Note the indicated time in minutes and the bar representing 30 μm. *Video 2:* Microtubules lag behind rapidly advancing lamellipodial edges. Stable β5-tubulin–GFP transfected mouse B16 F1 melanoma cell that undergo lamellipodial extension and retraction [31]. During the rapid advance of a lamellipodium (visible by the increased fluorescence of non-polymerized GFP–tubulin), microtubules do not polymerize at the same rate and stay behind. After the arrest or the collapse of the lamellipodium, microtubules catch up with the cell edge. Note that the collapse of the lateral edge of the lamellipodium correlates with the arrival of new microtubules. The frame width corresponds to 60 μm and the sequence is accelerated 300-fold (1 frame/min to 5 frames/s).

lines of tension strapping the cell to the substrate. In comparison to the lamellipodia of migrating cells, actin stress fibers are anchored with their barbed ends to these focal contacts. Thus, the orientation of the actin filaments is reversed in respect to the different adhesion sites, meaning that G-actin incorporation occurs within focal contacts in stationary cells and distal to focal complexes in the lamellipodium of migratory cells [12,13]. This fundamental difference in orientation, anchorage and polymerization of actin filaments in stationary and migrating cells is key to understanding cell migration.

In order to switch from a stationary (stress fiber rich), into a migratory state (lamellipodium rich), the actin cytoskeleton has to be reorganized from G-actin molecules of which a considerable amount may still be trapped as F-actin in stress fibers. Monomeric actin can be recruited from existing actin filaments by severing and de-polymerization [3,14,15] (see Fig. 2, Video 2). Due to the limited size of the actin-pool, the F- to G-actin ratio may have considerable influence on cellular motility. Recently it has been demonstrated that increased levels of thymosin-β4, a G-actin binding protein, is associated with a change in cell migration [16–19]. This behavior could be attributed to an increase in the G-actin pool that reduces the threshold for de novo actin polymerization. Similarly, by over-expression of β-actin the dynamic equilibrium between G- and F-actin may be affected [20]. Therefore, the comprehension of the regulatory mechanisms leading to local actin polymerization is crucial for understanding cell migration [3,4].

3. Microtubule dynamics in stationary and motile cells

In contrast to the actin cytoskeleton that is polarized in the direction of migration, the microtubule network is polarized from the center to the periphery of the cell. Microtubules emanate from the MTOC regardless whether a cell is stationary or motile. The MTOC is located close to the nucleus, and it can undergo reorientation towards the side facing the direction of migration [21]. This migration-induced reorientation of the MTOC can be disturbed by dominant negative Cdc42, a member of the Rho family of GTPases [21,22]. Since Cdc42 is also involved in the reorganization of the actin cytoskeleton, it is conceivable that the MTOC position is determined by the interaction of the actin cytoskeleton with the microtubule network. Dynamic analysis of proteins that associate with the tip of polymerizing microtubules such as CLIP-170, EB1 or APC have revealed a continuous outward polymerization of microtubules from the MTOC towards the cell periphery (Fig. 3, Video 3) [23–25]. We might wonder whether growing microtubules interact with the plasma membrane when they reach the cell periphery? In yeast, microtubules are captured by cortical actin patches, a process required for proper cell division involving proteins such as Kar9, Bim1/Yeb1, Bud6 and Kip3 [26–28]. Although mammalian orthologues have only been found for Bim1 (EB1), a related mechanism involving the contact between the tips of the microtubules and the cortical actin cytoskeleton could be responsible for positioning of polarity cues such as the recently described Par3–Par6–atypical PKC com-

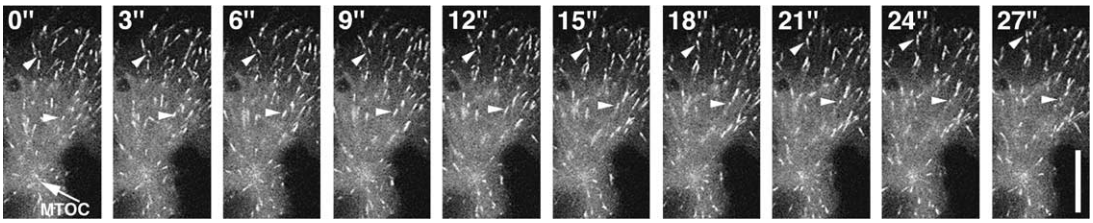

Fig. 3. GFP–CLIP-170 fusion protein reveals microtubule tip dynamics. GFP–CLIP-170 [23] was transiently transfected into mouse B16 F1 melanoma cells. Forty-eight hours after transfection, tips of growing microtubules to which GFP–CLIP-170 associates were recorded. From the MTOC (arrow), microtubules constantly polymerized towards the periphery of the cell. Note that the tips of two growing microtubules are marked with arrowheads and that the indicated time is in seconds. Bar represents 12 μm. *Video 3:* Originating at the MTOC, microtubules constantly polymerized towards the periphery of the cell. The width of the frame corresponds to 85 μm and the sequence is accelerated by a factor of 15 (1 frame/3 s to 5 frames/s).

plex [29]. This interaction of microtubules with the cortical actin network may represent an important aspect of the cross-talk between these cytoskeletal structures and as such be decisive in determining whether a cell is stationary or migratory. In this respect it is interesting to note that in stationary cells, the tips of microtubules extend to the cell edge around the entire periphery, whereas the advancing lamellipodium of migrating epithelial and melanoma cells is only occasionally penetrated by microtubules [30,31] (Video 2). Therefore, it is likely that the cross-talk between the actin and microtubule network is qualitatively different in the lamellipodium at the cell front compared to the retracting rear of migrating cells.

4. Potential mechanisms of cross-talk between the actin cytoskeleton and the microtubule network

From the above-mentioned observations, it is suggested that a cross-talk exists between the actin cytoskeleton and the microtubule network. From studies of the dynamic microtubule growth and collapse in stationary cells, Kaverina et al. have observed that microtubules can repetitively target the end points of actin stress fibers, the focal contacts. In fact, focal contacts targeted in this manner frequently disappeared [32,33]. We also observed that trailing and retracting portions of migrating cells are extremely rich in microtubule projections [31], which situates the site of cross-talk most likely to rear portions of migrating cells.

A possible cross-talk between microtubules and actin cytoskeleton could be mediated through the Rho family of small GTPases well known for their ability to modify the actin cytoskeleton [34–36]. Notably it has been demonstrated that activated forms of Cdc42, Rac1 and RhoA induce the polymerization of filopodia, lamellipodia and stress fibers, respectively. It has also been demonstrated recently that activated Rac1 is localized to membrane ruffles [37]. It is not known where activated RhoA is localized; nevertheless, downstream effectors such as mDia1 required for stress fiber polymerization localize partly to microtubules [13,38,39] and can bind to RhoA and taxol stabilized microtubules [40]. In addition to downstream effectors such as mDia1, a RhoA–C and Rac1 activating GTP exchange factor (GEF) has been localized to the surface of microtubules (GEF-H1) [41]. Moreover, a Rac1 specific GEF (Asef) is activated and bound to APC that can associate with the tips of growing microtubules [42]. Over-expression of both these GEFs resulted in membrane ruffling. Therefore, modification of the polymerized state of microtubules may change intracellular localization of Rho family GEFs and downstream effectors and hence modify actin polymerization and cell migration.

5. Actin dynamics in response to modulation of microtubules

5.1. At the front of the cell

Microtubules have been suggested to play a role in regulating cell migration and actin dynamics, since destruction of microtubules in fibroblasts resulted in inhibition of protrusive lamellipodial activity [43–45]. More recently there has been evidence to suggest that microtubules regulate adhesive and protrusive events through pathways involving the small GTPases Rho and Rac [2,46] (see Section 4). Furthermore, it has been shown that the disruption of microtubules led to RhoA activation, which resulted in stress fiber formation, an increased size of focal contacts and enhanced phosphorylation of paxillin and focal adhesion kinase [47,48]. Other studies indicated that microtubules exerted their control on the reorganization of the actin cytoskeleton via a Rac1-dependent pathway at the cell front. Rac1–GTP has been shown to bind to tubulin dimers [49], and hence it was proposed that the polymerization of microtubules at the cell front liberated Rac1–GTP thereby inducing actin polymerization [50]. In addition, it has been shown that the induced growth of microtubules in fibroblasts following the removal of the microtubule disrupter nocodazole activated Rac1–GTPase [46]. This effect could be mediated through the microtubule tip associated transport of the Rac1-specific GEF (Asef) to the cell periphery [42].

In contrast, other studies demonstrated that microtubules were not required for actin-based cell movements [51,52]. Furthermore, it has recently been demonstrated that activated Rac1 blocked intracellular RhoA activity while activated RhoA blocked Rac1 activity [53]. Therefore, it cannot be excluded that the observed microtubule polymerization dependent

activation of either RhoA or Rac1 is caused by the inactivation of either one of the counter players. These observations led us to investigate more closely the contribution of microtubule dynamics to cell movements. Using GFP constructs and video microscopy we confirmed that destruction or stabilization of the microtubule network reduced actin dynamics in the lamellipodia and inhibited cell migration [31]. However, spontaneous ruffle and lamellipodium formation was still observed in nocodazole and taxol treated cells, suggesting that Rac1 activity cannot be completely blocked by microtubule de-polymerization. In addition, protruding cell edges in rapidly locomoting cells have only few associated microtubules and the distance between tips of growing microtubules to the leading edge increases with augmented speed of cell migration (our observations; [8,54,55]).

Furthermore, in cells of the melanocyte lineage the external stimulation of nocodazole or taxol treated cells with either growth factors (SCF) or PMA induced potent reorganization of the actin cytoskeleton in a Rac1 dependent manner and reinstalled actin-dependent ruffling and lamellipodium formation to levels comparable with that of untreated cells [31]. Moreover, growth factor stimulation of the actin machinery provided physiological evidence that microtubules are not necessary for the transduction of signals leading to Rac1-dependent lamellipodium protrusion. These data suggest that the microtubule network plays a modulatory rather than an instructive role regarding the control of the actin cytoskeleton in the front of fast migrating cells.

5.2. Actin dynamics at the rear of the cell

Although microtubules were clearly not necessary for ruffling and lamellipodia formation at the front of fast migrating cells, nocodazole treated cells were unable to migrate following PMA stimulation [31]. Nocodazole treated cells remained glued to the substrate and were unable to retract their rear portions, a requirement for successful migration. In normal cells, PMA stimulation led to de-polymerization of actin stress fibers (Fig. 2). However, in PMA and nocodazole co-treated cells, stress fibers did not de-polymerize nor did focal contacts detach after initiation of lamellipodia formation [31]. Therefore, PMA derived signals require the microtubule network to achieve stress fiber de-polymerization. Hence, the presence of microtubules is necessary in order to weaken stress fibers and to reduce focal contact adhesion in response to migratory signals. Interestingly, Kaverina et al. have observed the release of focal contacts after multiple targeting by microtubules in fibroblasts [33]. The authors of this study suggested that microtubules deliver a relaxing signal that destabilizes the focal contacts. The nature of this signal is unknown. Moreover, we cannot exclude the possibility, that stress fibers are the targets of this signal, and that their de-polymerization is the cause for the disintegration of focal contacts. Possible mechanisms that could account for the release of focal contacts in the rear part of cells are discussed further.

Based on these data it is apparent that microtubules modify the state of the actin cytoskeleton at the rear, contracting end of migrating cells. However, it might also be possible that microtubules control cell migration by influencing other intracellular processes. Such a mechanism could involve microtubule dependent membrane traffic required for cell migration.

6. Membrane traffic in migrating cells

Recently the requirements for growth factor dependent ruffling or lamellipodia formation have included intracellular membrane recruitment to the cell surface. Bretscher and Aguado-Velasco demonstrated that EGF-induced ruffles arise by exocytosis of internal membrane from the endocytotic cycle in a Rac-dependent manner [56]. Furthermore, the signaling through CSF-1 in macrophages, PDGF in fibroblasts or PMA treatment, resulted in the activation of the ARF6 small GTPase [57–59]. ARF6 is involved in the export of lipid membranes from the endosomal compartment to the cell surface [60,61] and ARF6 dependent membrane ruffling can be inhibited by over expression of a negative regulator of ARF6/ARF1, ASAP1 [59]. This suggests that ARF6 activation is similarly important for actin dependent lamellipodia formation, as is Rac1 [62]. Moreover, since activated ARF6 and Rac1 bind both to a common adaptor protein Por1/arfaptin-2, that is required for lamellipodia formation, it is likely that their concomitant activation determines actin polymerization and lamellipodium extension [63–65].

At the rear end of migrating cells, membranes as well as membrane proteins that are involved in cell adhesion such as integrins (see Section 7) are internalized and delivered to the front of the cell by vesicular transport [66–69]. Based on these data, the role of plasma membrane internalization at the rear and membrane export at the front of migrating cells is again highlighted [70]. Since, an important part of the intracellular membrane transport depends on an intact microtubules network, its de-polymerization may slow down membrane dependent lamellipodium formation at the cell front and membrane recycling from the rear, effectively obstructing cell migration [31,71–73].

While we have reviewed the essential cytoskeletal and membrane components important for cell migration, we have so far ignored a third requirement. In fact, in order for a cell to move, the intracellular cytoskeletal changes have to be transduced into motility by coupling the cytoskeleton to the extracellular matrix at sites of cell–substrate adhesion. The formation and controlled release of these adhesion sites are crucial for coordinated cell migration.

7. Differential behavior of focal adhesion at the front and the rear of migrating cells

7.1. At the cell front, stationary focal complexes form in the advancing lamellipodium

The appearance of small dot like cell–substrate adhesions have been noted within Rac1 induced lamellipodia of fibroblasts. These structures are highlighted by the presence of cytoskeletal linker proteins such as vinculin and have been referred to as focal complexes [9,74]. In fast migrating cells such as fish keratinocytes, small dot-like focal adhesions are found throughout the leading lamella where they anchor actin filaments emanating from the lamellipodial edge to the substrate [12,75,76]. These focal adhesions remain stationary in respect to the substrate while the lamella advances [76]. Similarly, focal complexes in lamellipodia of fibroblasts and small focal adhesions in the lamella of migrating melanoma cells remain stationary in respect to the substrate [77]. In fibroblasts and melanoma cells these small focal adhesions disappear at positions that correlate with the rear of the protruding lamellipodial actin filament lattice [77], while they remain throughout the actin filament filled lamella of fish keratinocytes [76]. This suggests that focal complexes directly depend on the presence of the lamellipodial actin filament network, which in turn is pinned down to the substrate by these stationary adhesion sites. Although the morphology and distribution pattern of these small focal adhesions vary between these different cell types, they have several points in common. First, they remain stationary in respect to the substrate, second they are associated with an actin filament lattice that forms in a Rac1-dependent manner and third they appear in cellular locations that are free of intracellular or extracellular tension [9,12,74,77,78]. Furthermore, their structural and functional similarity is also underlined by the fact that the αvβ3 integrin aggregation density is similarly low in these focal adhesion sites (Fig. 4) [77].

Due to the stationary behavior of αvβ3 integrin low-density focal complexes and the simultaneous forward movement of the cell body, low-density focal complexes located at the lateral edges of Rac1 induced lamellipodia transit into the cellular domain that is under the influence of RhoA activity (see Fig. 6). In fibroblasts, focal complexes undergo dramatic RhoA induced remodeling that is associated with an increase in size, leading to large focal contacts [9]. In addition, RhoA induced intracellular acto-myosin contraction increases the αvβ3 integrin density in focal adhesions, resulting in the formation of high-density focal contacts (Fig. 4) [77].

Therefore, in the advancing lamellipodia of migrating cells, stationary low-density focal complexes either form and disappear in an actin cytoskeleton dependent but microtubule independent manner or transform into high-density focal contacts located at the cell rear that can be modulated by the microtubule network (see Section 7.2).

7.2. Focal contacts are sliding cell–substrate contacts at the cell rear

In fast migrating, polarized cells the actin rich lamellipodium covers the front of the cell like a crescent, which continuously advances due to polymerization of actin at the leading edge [4]. While the cell moves forward, actin filaments emerging from this lamellipodium remain fixed to the substrate by

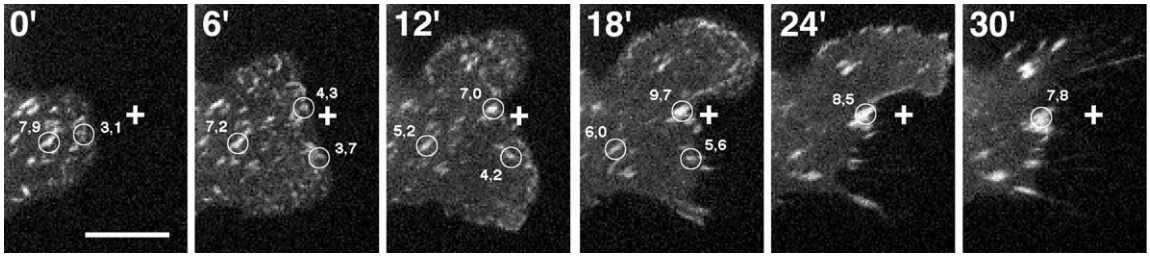

Fig. 4. Different GFP–β3 integrin aggregation densities in focal complexes and focal contacts. Stable GFP–β3 integrin transfected 3T3 mouse fibroblasts were plated overnight on serum coated glass cover slips [77]. GFP fluorescence signals were recorded during extension and retraction of a lamellipodium. Since the GFP–β3 integrin is incorporated into the plasma membrane, the increase in the fluorescence signal reflects the lateral aggregation, hence the relative density of integrins in focal complexes and focal contacts. Low-density GFP–β3 integrin adhesions or focal complexes are associated with the protruding lamellipodium, while high-density GFP–β3 integrin adhesions or focal contacts form during cell edge retraction. The number next to the circled focal adhesions represent the relative increase of the GFP–β3 integrin fluorescence intensity (local maximum) over that of the plasma membrane (density of focal adhesion) (for methods see [77]). Note the inward sliding of the circled high-density focal adhesion located next to the judiciary mark (+). Bar represents 9 μm. *Video 4:* GFP–β3 integrin dynamics in focal complexes and focal contacts. The sequence shows the extension and retraction of a lamellipodium in a stationary cell. Stationary, low-density GFP–β3 integrin adhesions or focal complexes are associated with the protruding lamellipodium, while sliding, high-density GFP–β3 integrin adhesions or focal contacts form during cell edge retraction. Note the continuous inward sliding (or flow) of focal contacts during the second phase of the video. The width of the frame corresponds to 31 μm and the sequence is accelerated by a factor of 600 (1 frame/2 min to 5 frames/s).

focal complexes (Figs. 4 and 5, Videos 4 and 5). At the lateral edge of the lamellipodial crescent, the fine actin network collapses into stress fibers ending in focal adhesions (Fig. 5) [75,76,79]. Subsequently the actin fibers anchored at these lateral contact sites, begin to retract and slide towards the cell center (Fig. 5). Similarly, sliding focal contacts visualized by GFP–vinculin, GFP–β1 and GFP–β3 integrins have been observed at the lateral edges of migrating and stationary cells (Fig. 4) [76,77,80]. The sliding of focal contacts and the associated retraction is exclusively found at the rear of migrating cells [77], suggesting that effector proteins responsible for this behavior are distributed in a polarized way (Fig. 6).

Several laboratories have proposed different mechanism to explain the phenomenon of rear retraction,

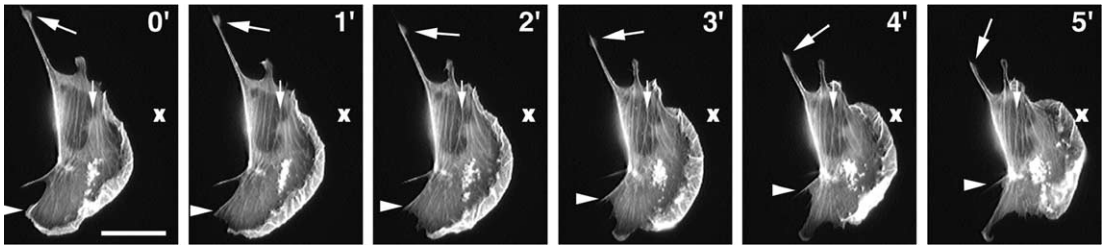

Fig. 5. Inward retracting stress fibers appear at the rear of migrating cells. Stable GFP–β-actin expressing mouse B16 F1 melanoma cell were plated overnight on laminin-1 (10 μg/ml) coated glass cover slips. The cell advanced employing an actin rich lamellipodium. At the lateral edges of the lamellipodium, actin filaments split off, that span the width of the lamella. These actin fibers remained stationary in respect to the substrate (small arrow). In contrast, actin stress fibers located at the rear of the cell probably linked to focal adhesions, began to retract inwards (large arrow and arrowhead). A judiciary mark was introduced (×) to judge the movement of the cell. Bar corresponds to 20 μm. *Video 5:* Actin dynamics at the rear of migrating cells. The cell advanced employing an actin rich lamellipodium in the front. At the rear of the cell, actin stress fibers retracted continuously to allow the advance of the cell. In the middle of the sequence, the cell gets immobilized due to the equal pull of two opposing lamellipodia. Note that one of the lamellipodia had to collapse in order for the cell to resume migration. The width of the frame corresponds to 120 μm and the sequence is accelerated by a factor of 300 (1 frame/min to 5 frames/s).

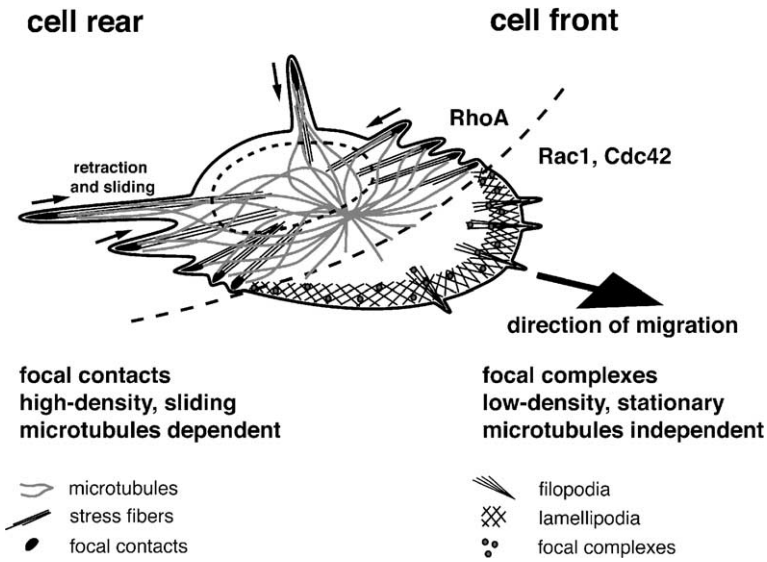

Fig. 6. Actin driven cell migration in the front and microtubule controlled retraction in the rear. A schematic view of a migrating cell is shown that illustrates the main features of the actin and microtubule cytoskeleton. At the cell front, Cdc42/Rac1 induced actin polymerization results in the formation of filopodia and lamellipodia that drive the cell edge forward. The advancing lamellipodia is anchored to the substrate by stationary focal complexes (see text). While the cell moves forward, low-density focal complexes located at the lateral edges of the lamellipodium transform into high-density focal contacts that are linked to actin stress fibers in a RhoA dependent manner. When the focal contacts localize to the rear of the cell, a microtubule controlled inward sliding, release and retraction takes place (arrows), which allows the cell to move forward.

consisting of: (i) actin cytoskeleton contraction; (ii) focal contact sliding and subsequent; (iii) focal contact disassembly. It has been demonstrated that extracellular calcium influx mediated by stretch sensitive calcium channels is responsible for detachment of focal adhesions and retraction of the cell rear [81]. Mobilization of calcium from intracellular stores such as ER might be sensitive to the presence of microtubules, since their de-polymerization leads to a collapse of the ER network in the cell periphery [82]. Therefore, microtubules could regulate calcium release from intracellular stores; modifying the activity of calcium regulated calmodulin associated myosins [83]. Myosin-IXb is of particular interest since it inactivates Rho. When over-expressed it leads to loss of actin filaments and rounding up of cells [84,85]. In addition to myosins, calcium targets involved in cell motility include the calcium activated phosphatase calcineurin [67]; calcium activated intracellular proteases calpain [68,86] as well as acto-myosin-dependent intracellular contraction [87]. Another microtubule sensitive focal contact and stress fiber controlling pathway could involve the activity and localization of a class of Rho-effectors known as diaphanous-related formins (mDia1 and mDia2) [38]. RhoA activated mDias mediate stress fiber and focal contact formation and they stabilize microtubules [13,40,88]. In turn, mDias also bind to stabilized microtubules leading to the sequestration of part of the cytoplasmic mDia pool [40]. Therefore, the de-polymerization of microtubules in the rear of migrating cells could increase the concentration of cytoplasmic free mDia that leads to actin stress fiber formation and the polymerization of focal contacts. Furthermore, since de novo actin polymerization within focal adhesions, thus their increase in size, depends on mDia activation [12], it is plausible that polarized, microtubule-dependent mDia delivery to focal adhesions could lead to unilateral actin polymerization and focal contact growth at the proximal aspect of focal contacts. This model would predict that the observed focal contact “sliding” is due to a polarized remodeling of focal contacts. The recent obser-

vation, that RhoA dependent high-density focal adhesions undergo complete renewal of their β3 integrin pool within 10 min is in favor of such a hypothesis of "polarized remodeling" of focal contacts [77]. Hence, changes in the microtubule network, by means of differential localization and delivery of actin cytoskeletal effectors, may control cell migration by influencing focal contact formation, stability and remodeling [10,77].

The question arises how cells with low numbers of microtubules are able to release their rear focal contacts. One example are migrating fish keratocytes that release their focal contacts by the acto-myosin system that might be under the control of localized calcium influx [8,81,89]. Similarly, other studies have indicated a role for RhoA and Rho kinase in focal adhesion release at the rear of migrating leukocytes [69,90,91]. In addition, Ras and or v-src activation leads to release of focal contacts at the rear of migrating cells through the MAP kinase pathway [21,92–96]. It has been suggested that v-src induced recruitment of p190 Rho–GAP to focal contacts may be involved in focal contact disassembly [97]. Furthermore, the src pathway has been demonstrated to be a downstream target of mDia, suggesting that microtubule-dependent and independent focal adhesion sliding and release are not so different after all [98]. It will be important to determine the potential interactions and hierarchies of these different focal adhesion regulating mechanisms in order to understand the modulation of cell migration through differential substrate binding at the rear.

8. Conclusion

Migration is a complex cellular behavior that is controlled by extracellular as well as intracellular processes. The proper regulation of migration within an organism is a challenging task requiring the control at the level of the cytoskeleton as well as at the sites where cells adhere to the extracellular matrix or neighboring cells. While the actin cytoskeleton is the actor, microtubules have assumed the role of the conductor. Dynamic analysis of adaptor proteins with the help of in vivo labeling tools such as GFP will eventually allow us to study not only the qualitative but also the quantitative aspects of cell migration.

Acknowledgements

We thank Dr. Caroline Johnson-Léger for critical reading and discussion of this manuscript. We are grateful to Marie-Claude Jacquier for excellent technical support and Jacqueline Ntah for secretarial assistance. We would like to thank Drs. Andrew Matus, Stefanie Kaech and Thomas Kreis for the tubulin–GFP and CLIP170–GFP constructs, respectively. A special thank to Dr. Christoph Ballestrem who was involved in the initial phases of cytoskeletal analysis in our laboratory and who contributed some of the movies. This work has been supported by grants from the Schweizerischen Krebsliga (KFS 412-1-1997), the Swiss National Science Foundation (31-059173.99 and 31-64000.00), the Foundation Gabrielle Giorgi-Cavaglieri and Helmut Horten Stiftung.

References

[1] B. Ludin, A. Matus, GFP illuminates the cytoskeleton, Trends Cell Biol. 8 (1998) 72–77.
[2] T. Wittmann, C.M. Waterman-Storer, Cell motility: can Rho GTPases and microtubules point the way? J. Cell Sci. 114 (2001) 3795–3803.
[3] D. Pantaloni, C. Le Clainche, M.F. Carlier, Mechanism of actin-based motility, Science 292 (2001) 1502–1506.
[4] J.V. Small, T. Stradal, E. Vignal, K. Rottner, The lamellipodium: where motility begins, Trends Cell Biol. 12 (2002) 112–120.
[5] K.C. Holmes, D. Popp, W. Gebhard, W. Kabsch, Atomic model of the actin filament, Nature 347 (1990) 44–49.
[6] A. Wegner, Head to tail polymerization of actin, J. Mol. Biol. 108 (1976) 139–150.
[7] T.D. Pollard, M.S. Mooseker, Direct measurement of actin polymerization rate constants by electron microscopy of actin filaments nucleated by isolated microvillus cores, J. Cell Biol. 88 (1981) 654–659.
[8] A.B. Verkhovsky, T.M. Svitkina, G.G. Borisy, Self-polarization and directional motility of cytoplasm, Curr. Biol. 9 (1999) 11–20.
[9] K. Rottner, A. Hall, J.V. Small, Interplay between Rac and Rho in the control of substrate contact dynamics, Curr. Biol. 9 (1999) 640–648.
[10] B. Geiger, A. Bershadsky, Assembly and mechanosensory function of focal contacts, Curr. Opin. Cell Biol. 13 (2001) 584–592.
[11] G.G. Borisy, T.M. Svitkina, Actin machinery: pushing the envelope, Curr. Opin. Cell Biol. 12 (2000) 104–112.
[12] D. Riveline, E. Zamir, N.Q. Balaban, U.S. Schwarz, T. Ishizaki, S. Narumiya, Z. Kam, B. Geiger, A.D. Bershadsky,

Focal contacts as mechanosensors: externally applied local mechanical force induces growth of focal contacts by an mDia1-dependent and ROCK-independent mechanism, J. Cell Biol. 153 (2001) 1175–1186.
[13] N. Watanabe, T. Kato, A. Fujita, T. Ishizaki, S. Narumiya, Cooperation between mDia1 and ROCK in Rho-induced actin reorganization, Nat. Cell Biol. 1 (1999) 136–143.
[14] M.F. Carlier, V. Laurent, J. Santolini, R. Melki, D. Didry, G.X. Xia, Y. Hong, N.H. Chua, D. Pantaloni, Actin de-polymerizing factor (ADF/cofilin) enhances the rate of filament turnover: implication in actin-based motility, J. Cell Biol. 136 (1997) 1306–1323.
[15] M.F. Carlier, F. Ressad, D. Pantaloni, Control of actin dynamics in cell motility: role of ADF/cofilin, J. Biol. Chem. 274 (1999) 33827–33830.
[16] D. Pantaloni, M.F. Carlier, How profilin promotes actin filament assembly in the presence of thymosin-β4, Cell 75 (1993) 1007–1014.
[17] E.A. Clark, T.R. Golub, E.S. Lander, R.O. Hynes, Genomic analysis of metastasis reveals an essential role for RhoC, Nature 406 (2000) 532–535.
[18] L.W. Roth, P. Bormann, C. Wiederkehr, E. Reinhard, β-Thymosin, a modulator of the actin cytoskeleton is increased in regenerating retinal ganglion cells, Eur. J. Neurosci. 11 (1999) 3488–3498.
[19] P. Roy, Z. Rajfur, D. Jones, G. Marriott, L. Loew, K. Jacobson, Local photorelease of caged thymosin-β4 in locomoting keratocytes causes cell turning, J. Cell Biol. 153 (2001) 1035–1048.
[20] M. Peckham, G. Miller, C. Wells, D. Zicha, G.A. Dunn, Specific changes to the mechanism of cell locomotion induced by over-expression of β-actin, J. Cell Sci. 114 (2001) 1367–1377.
[21] C.D. Nobes, A. Hall, Rho GTPases control polarity, protrusion, and adhesion during cell movement, J. Cell Biol. 144 (1999) 1235–1244.
[22] A.F. Palazzo, H.L. Joseph, Y. Chen, D.L. Dujardin, A.S. Alberts, K.K. Pfister, R.B. Vallee, G.G. Gundersen, Cdc42, dynein, and dynactin regulate MTOC reorientation independent of Rho-regulated microtubule stabilization, Curr. Biol. 11 (2001) 1536–1541.
[23] F. Perez, G.S. Diamantopoulos, R. Stalder, T.E. Kreis, CLIP-170 highlights growing microtubule ends in vivo, Cell 96 (1999) 517–527.
[24] Y. Mimori-Kiyosue, N. Shiina, S. Tsukita, The dynamic behavior of the APC-binding protein EB1 on the distal ends of microtubules, Curr. Biol. 10 (2000) 865–868.
[25] Y. Mimori-Kiyosue, N. Shiina, S. Tsukita, Adenomatous polyposis coli (APC) protein moves along microtubules and concentrates at their growing ends in epithelial cells, J. Cell Biol. 148 (2000) 505–518.
[26] W.S. Korinek, M.J. Copeland, A. Chaudhuri, J. Chant, Molecular linkage underlying microtubule orientation toward cortical sites in yeast, Science 287 (2000) 2257–2259.
[27] L. Lee, J.S. Tirnauer, J. Li, S.C. Schuyler, J.Y. Liu, D. Pellman, Positioning of the mitotic spindle by a cortical-microtubule capture mechanism, Science 287 (2000) 2260–2262.
[28] R.K. Miller, S.C. Cheng, M.D. Rose, Bim1p/Yeb1p mediates the Kar9p-dependent cortical attachment of cytoplasmic microtubules, Mol. Biol. Cell 11 (2000) 2949–2959.
[29] C.Q. Doe, Cell polarity: the PARty expands, Nat. Cell Biol. 3 (2001) E7–9.
[30] C.M. Waterman-Storer, E.D. Salmon, Actomyosin-based retrograde flow of microtubules in the lamella of migrating epithelial cells influences microtubule dynamic instability and turnover and is associated with microtubule breakage and treadmilling, J. Cell Biol. 139 (1997) 417–434.
[31] C. Ballestrem, B. Wehrle-Haller, B. Hinz, B.A. Imhof, Actin-dependent lamellipodia formation and microtubule-dependent tail retraction control-directed cell migration, Mol. Biol. Cell 11 (2000) 2999–3012.
[32] I. Kaverina, K. Rottner, J.V. Small, Targeting, capture, and stabilization of microtubules at early focal adhesions, J. Cell Biol. 142 (1998) 181–190.
[33] I. Kaverina, O. Krylyshkina, J.V. Small, Microtubule targeting of substrate contacts promotes their relaxation and dissociation, J. Cell Biol. 146 (1999) 1033–1044.
[34] A.J. Ridley, H.F. Paterson, C.L. Johnston, D. Diekmann, A. Hall, The small GTP-binding protein Rac regulates growth factor-induced membrane ruffling, Cell 70 (1992) 401–410.
[35] A.J. Ridley, A. Hall, The small GTP-binding protein Rho regulates the assembly of focal adhesions and actin stress fibers in response to growth factors, Cell 70 (1992) 389–399.
[36] A.J. Ridley, Rho GTPases and cell migration, J. Cell Sci. 114 (2001) 2713–2722.
[37] V.S. Kraynov, C. Chamberlain, G.M. Bokoch, M.A. Schwartz, S. Slabaugh, K.M. Hahn, Localized Rac activation dynamics visualized in living cells, Science 290 (2000) 333–337.
[38] N. Watanabe, P. Madaule, T. Reid, T. Ishizaki, G. Watanabe, A. Kakizuka, Y. Saito, K. Nakao, B.M. Jockusch, S. Narumiya, p140mDia, a mammalian homolog of *Drosophila* diaphanous, is a target protein for Rho small GTPase and is a ligand for profilin, EMBO J. 16 (1997) 3044–3056.
[39] T. Ishizaki, Y. Morishima, M. Okamoto, T. Furuyashiki, T. Kato, S. Narumiya, Coordination of microtubules and the actin cytoskeleton by the Rho effector mDia1, Nat. Cell Biol. 3 (2001) 8–14.
[40] A.F. Palazzo, T.A. Cook, A.S. Alberts, G.G. Gundersen, mDia mediates Rho-regulated formation and orientation of stable microtubules, Nat. Cell Biol. 3 (2001) 723–729.
[41] Y. Ren, R. Li, Y. Zheng, H. Busch, Cloning and characterization of GEF-H1, a microtubule-associated guanine nucleotide exchange factor for Rac and Rho GTPases, J. Biol. Chem. 273 (1998) 34954–34960.
[42] Y. Kawasaki, T. Senda, T. Ishidate, R. Koyama, T. Morishita, Y. Iwayama, O. Higuchi, T. Akiyama, Asef, a link between the tumor suppressor APC and G-protein signaling, Science 289 (2000) 1194–1197.
[43] A.D. Bershadsky, E.A. Vaisberg, J.M. Vasiliev, Pseudopodial activity at the active edge of migrating fibroblast is decreased after drug-induced microtubule de-polymerization, Cell Motil. Cytoskeleton 19 (1991) 152–158.
[44] J.M. Vasiliev, I.M. Gelfand, L.V. Domnina, O.Y. Ivanova, S.G. Komm, L.V. Olshevskaja, Effect of colcemid on the

locomotory behavior of fibroblasts, J. Embryol. Exp. Morphol. 24 (1970) 625–640.
[45] G. Liao, T. Nagasaki, G.G. Gundersen, Low concentrations of nocodazole interfere with fibroblast locomotion without significantly affecting microtubule level: implications for the role of dynamic microtubules in cell locomotion, J. Cell Sci. 108 (1995) 3473–3483.
[46] C.M. Waterman-Storer, R.A. Worthylake, B.P. Liu, K. Burridge, E.D. Salmon, Microtubule growth activates Rac1 to promote lamellipodial protrusion in fibroblasts, Nat. Cell Biol. 1 (1999) 45–50.
[47] A. Bershadsky, A. Chausovsky, E. Becker, A. Lyubimova, B. Geiger, Involvement of microtubules in the control of adhesion-dependent signal transduction, Curr. Biol. 6 (1996) 1279–1289.
[48] T. Enomoto, Microtubule disruption induces the formation of actin stress fibers and focal adhesions in cultured cells: possible involvement of the Rho signal cascade, Cell Struct. Funct. 21 (1996) 317–326.
[49] A. Best, S. Ahmed, R. Kozma, L. Lim, The Ras-related GTPase Rac1 binds tubulin, J. Biol. Chem. 271 (1996) 3756–3762.
[50] C.M. Waterman-Storer, E. Salmon, Positive feedback interactions between microtubule and actin dynamics during cell motility, Curr. Opin. Cell Biol. 11 (1999) 61–67.
[51] S.H. Zigmond, H.I. Levitsky, B.J. Kreel, Cell polarity: an examination of its behavioral expression and its consequences for polymorphonuclear leukocyte chemotaxis, J. Cell Biol. 89 (1981) 585–592.
[52] U. Euteneuer, M. Schliwa, The function of microtubules in directional cell movement, Ann. N. Y. Acad. Sci. 466 (1986) 867–886.
[53] E.E. Sander, J.P. ten Klooster, S. van Delft, R.A. van der Kammen, J.G. Collard, Rac downregulates Rho activity: reciprocal balance between both GTPases determines cellular morphology and migratory behavior, J. Cell Biol. 147 (1999) 1009–1022.
[54] P. Wadsworth, Regional regulation of microtubule dynamics in polarized, motile cells, Cell Motil. Cytoskeleton 42 (1999) 48–59.
[55] U. Euteneuer, M. Schliwa, Persistent, directional motility of cells and cytoplasmic fragments in the absence of microtubules, Nature 310 (1984) 58–61.
[56] M.S. Bretscher, C. Aguado-Velasco, EGF induces recycling membrane to form ruffles, Curr. Biol. 8 (1998) 721–724.
[57] S.R. Frank, J.C. Hatfield, J.E. Casanova, Remodeling of the actin cytoskeleton is coordinately regulated by protein kinase C and the ADP-ribosylation factor nucleotide exchange factor ARNO, Mol. Biol. Cell 9 (1998) 3133–3146.
[58] Q. Zhang, J. Calafat, H. Janssen, S. Greenberg, ARF6 is required for growth factor- and Rac-mediated membrane ruffling in macrophages at a stage distal to Rac membrane targeting, Mol. Cell. Biol. 19 (1999) 8158–8168.
[59] P.A. Randazzo, J. Andrade, K. Miura, M.T. Brown, Y.Q. Long, S. Stauffer, P. Roller, J.A. Cooper, The Arf GTPase-activating protein ASAP1 regulates the actin cytoskeleton, Proc. Natl. Acad. Sci. U.S.A. 97 (2000) 4011–4016.
[60] H. Radhakrishna, J.G. Donaldson, ADP-ribosylation factor 6 regulates a novel plasma membrane recycling pathway, J. Cell Biol. 139 (1997) 49–61.
[61] H. Radhakrishna, O. Al-Awar, Z. Khachikian, J.G. Donaldson, ARF6 requirement for Rac ruffling suggests a role for membrane trafficking in cortical actin rearrangements, J. Cell Sci. 112 (1999) 855–866.
[62] J. Song, Z. Khachikian, H. Radhakrishna, J.G. Donaldson, Localization of endogenous ARF6 to sites of cortical actin rearrangement and involvement of ARF6 in cell spreading, J. Cell Sci. 111 (1998) 2257–2267.
[63] C. D'Souza-Schorey, R.L. Boshans, M. McDonough, P.D. Stahl, L. Van Aelst, A role for POR1, a Rac1-interacting protein, in ARF6-mediated cytoskeletal rearrangements, EMBO J. 16 (1997) 5445–5454.
[64] O.H. Shin, J.H. Exton, Differential binding of arfaptin 2/POR1 to ADP-ribosylation factors and Rac1, Biochem. Biophys. Res. Commun. 285 (2001) 1267–1273.
[65] T. Joneson, M. McDonough, D. Bar-Sagi, L. Van Aelst, RAC regulation of actin polymerization and proliferation by a pathway distinct from Jun kinase, Science 274 (1996) 1374–1376.
[66] C.M. Laukaitis, D.J. Webb, K. Donais, A.F. Horwitz, Differential dynamics of α5 integrin, paxillin, and α-actinin during formation and disassembly of adhesions in migrating cells, J. Cell Biol. 153 (2001) 1427–1440.
[67] M.A. Lawson, F.R. Maxfield, Ca^{2+}- and calcineurin-dependent recycling of an integrin to the front of migrating neutrophils, Nature 377 (1995) 75–79.
[68] S.P. Palecek, A. Huttenlocher, A.F. Horwitz, D.A. Lauffenburger, Physical and biochemical regulation of integrin release during rear detachment of migrating cells, J. Cell Sci. 111 (1998) 929–940.
[69] L.M. Pierini, M.A. Lawson, R.J. Eddy, B. Hendey, F.R. Maxfield, Oriented endocytic recycling of α5β1 in motile neutrophils, Blood 95 (2000) 2471–2480.
[70] M.S. Bretscher, C. Aguado-Velasco, Membrane traffic during cell locomotion, Curr. Opin. Cell Biol. 10 (1998) 537–541.
[71] M.S. Bretscher, Getting membrane flow and the cytoskeleton to cooperate in moving cells, Cell 87 (1996) 601–606.
[72] M.S. Bretscher, Moving membrane up to the front of migrating cells, Cell 85 (1996) 465–467.
[73] V.I. Rodionov, F.K. Gyoeva, E. Tanaka, A.D. Bershadsky, J.M. Vasiliev, V.I. Gelfand, Microtubule-dependent control of cell shape and pseudopodial activity is inhibited by the antibody to kinesin motor domain, J. Cell Biol. 123 (1993) 1811–1820.
[74] C.D. Nobes, A. Hall, Rho, Rac, and Cdc42 GTPases regulate the assembly of multimolecular focal complexes associated with actin stress fibers, lamellipodia, and filopodia, Cell 81 (1995) 53–62.
[75] J. Lee, K. Jacobson, The composition and dynamics of cell–substratum adhesions in locomoting fish keratocytes, J. Cell Sci. 110 (1997) 2833–2844.
[76] K.I. Anderson, R. Cross, Contact dynamics during keratocyte motility, Curr. Biol. 10 (2000) 253–260.
[77] C. Ballestrem, B. Hinz, B.A. Imhof, B. Wehrle-Haller, Marching at the front and dragging behind: differential αvβ3

integrin turnover regulates focal adhesion behavior, J. Cell Biol. 155 (2001) 1319–1332.
[78] T. Oliver, M. Dembo, K. Jacobson, Separation of propulsive and adhesive traction stresses in locomoting keratocytes, J. Cell Biol. 145 (1999) 589–604.
[79] C. Ballestrem, B. Wehrle-Haller, B.A. Imhof, Actin dynamics in living mammalian cells, J. Cell Sci. 111 (1998) 1649–1658.
[80] L.B. Smilenov, A. Mikhailov, R.J. Pelham, E.E. Marcantonio, G.G. Gundersen, Focal adhesion motility revealed in stationary fibroblasts, Science 286 (1999) 1172–1174.
[81] J. Lee, A. Ishihara, G. Oxford, B. Johnson, K. Jacobson, Regulation of cell movement is mediated by stretch-activated calcium channels, Nature 400 (1999) 382–386.
[82] C.M. Waterman-Storer, E.D. Salmon, Endoplasmic reticulum membrane tubules are distributed by microtubules in living cells using three distinct mechanisms, Curr. Biol. 8 (1998) 798–806.
[83] V. Mermall, P.L. Post, M.S. Mooseker, Unconventional myosins in cell movement, membrane traffic, and signal transduction, Science 279 (1998) 527–533.
[84] R.T. Muller, U. Honnert, J. Reinhard, M. Bahler, The rat myosin myr 5 is a GTPase-activating protein for Rho in vivo: essential role of arginine 1695, Mol. Biol. Cell 8 (1997) 2039–2053.
[85] P.L. Post, G.M. Bokoch, M.S. Mooseker, Human myosin-IXb is a mechanochemically active motor and a GAP for Rho, J. Cell Sci. 111 (1998) 941–950.
[86] A. Huttenlocher, S.P. Palecek, Q. Lu, W. Zhang, R.L. Mellgren, D.A. Lauffenburger, M.H. Ginsberg, A.F. Horwitz, Regulation of cell migration by the calcium-dependent protease calpain, J. Biol. Chem. 272 (1997) 32719–32722.
[87] W.T. Chen, Mechanism of retraction of the trailing edge during fibroblast movement, J. Cell Biol. 90 (1981) 187–200.
[88] T.A. Cook, T. Nagasaki, G.G. Gundersen, Rho guanosine triphosphatase mediates the selective stabilization of microtubules induced by lysophosphatidic acid, J. Cell Biol. 141 (1998) 175–185.
[89] T.M. Svitkina, A.B. Verkhovsky, K.M. McQuade, G.G. Borisy, Analysis of the actin–myosin II system in fish epidermal keratocytes: mechanism of cell body translocation, J. Cell Biol. 139 (1997) 397–415.
[90] R.A. Worthylake, S. Lemoine, J.M. Watson, K. Burridge, RhoA is required for monocyte tail retraction during transendothelial migration, J. Cell Biol. 154 (2001) 147–160.
[91] V. Niggli, Rho kinase in human neutrophils: a role in signaling for myosin light chain phosphorylation and cell migration, FEBS Lett. 445 (1999) 69–72.
[92] D.A. Cheresh, J. Leng, R.L. Klemke, Regulation of cell contraction and membrane ruffling by distinct signals in migratory cells, J. Cell Biol. 146 (1999) 1107–1116.
[93] V.J. Fincham, M.C. Frame, The catalytic activity of src is dispensable for translocation to focal adhesions but controls the turnover of these structures during cell motility, EMBO J. 17 (1998) 81–92.
[94] V.J. Fincham, M. James, M.C. Frame, S.J. Winder, Active ERK/MAP kinase is targeted to newly forming cell–matrix adhesions by integrin engagement and v-src, EMBO J. 19 (2000) 2911–2923.
[95] R.L. Klemke, S. Cai, A.L. Giannini, P.J. Gallagher, P. de Lanerolle, D.A. Cheresh, Regulation of cell motility by mitogen-activated protein kinase, J. Cell Biol. 137 (1997) 481–492.
[96] P.E. Hughes, M.W. Renshaw, M. Pfaff, J. Forsyth, V.M. Keivens, M.A. Schwartz, M.H. Ginsberg, Suppression of integrin activation: a novel function of a Ras/Raf-initiated MAP kinase pathway, Cell 88 (1997) 521–530.
[97] V.J. Fincham, A. Chudleigh, M.C. Frame, Regulation of p190 Rho–GAP by v-src is linked to cytoskeletal disruption during transformation, J. Cell Sci. 112 (1999) 947–956.
[98] S. Satoh, T. Tominaga, mDia-interacting protein acts downstream of Rho–mDia and modifies src activation and stress fiber formation, J. Biol. Chem. 276 (2001) 39290–39294.

5.2. The inner lives of focal adhesions

The inner lives of focal adhesions

Bernhard Wehrle-Haller and Beat A. Imhof

In focal adhesions of eukaryotic cells, transmembrane receptors of the integrin family and a large set of adaptor proteins form the physical link between the extracellular substrate and the actin cytoskeleton. During cell migration, nascent focal adhesions within filopodia and lamellipodia make the initial exploratory contacts with the cellular environment, whereas maturing focal adhesions pull the cell forward against the resistance of 'sliding' focal adhesions at the cell rear. Experimental approaches are now available for analysing the dynamics and interior structure of these different focal adhesions. Analysing focal-adhesion dynamics using green-fluorescent-protein-linked integrin leads us to propose that the acto-myosin-controlled density and turnover of integrins in focal adhesions is used to sense the elasticity and spacing of extracellular ligands, regulating cell migration by mechanically transduced signaling.

A supplementary movie is available at: http://archive.bmn.com/supp/tcb/imhof.mov

Bernhard Wehrle-Haller*
Beat A. Imhof
Dept of Pathology, Centre Médical Universitaire, 1 Rue Michel-Servet, 1211 Genève 4, Switzerland.
*e-mail: Bernhard.Wehrle-Haller@medecine.unige.ch

During recent years our knowledge about focal adhesions and their role in cell spreading, migration and survival has increased vastly. The ever-increasing number of proteins being found to participate in focal adhesions makes them one of the most complex protein aggregates formed in a cell [1]. Focal adhesions fulfil mechanical and sensing functions that involve reversible anchorage of the actin cytoskeleton to the extracellular matrix during migration and monitoring intracellular or extracellular tension. Understanding the molecular mechanisms that account for these distinct functions of focal adhesions is a major challenge.

Eukaryotic cells have differently sized and shaped cell–substrate adhesion sites, which we here generally refer to as 'focal adhesions'. In fibroblasts, these different focal adhesions are commonly referred to as focal complexes, focal contacts and fibrillar adhesions [2]. Many attempts have been made to classify focal adhesions using descriptive features such as shape, size, cellular location, GTPase dependency and protein composition [3–7]. Unfortunately, some of these characteristics vary depending on the environment of the cells [8]. Here, we propose the use of functional criteria to classify focal adhesions according to their physiological role, such as sensing the environment or providing mechanical support, and give new definitions to distinguish focal complexes from focal contacts.

The recent use of chimeras comprising green fluorescent protein (GFP) attached to various focal adhesion proteins has made important contributions to our understanding of focal adhesions. Owing to the stoichiometric fusion of GFP to focal adhesion proteins, such GFP chimeras can be used not only as markers for cellular attachment sites but also to provide dynamic and quantitative information about the composition of focal adhesions [6,9–13]. In parallel, progress has been made in measuring the mechanical traction forces exerted by cells when they interact with elastic surfaces [9,10,14–16]. One of the emerging ideas from these studies is that focal adhesions are mechanical transducing devices with a mechanical sensor function. Hence, they relay changes of intra- and extracellular tension into signaling pathways that, in turn, modify the composition and behaviour of focal adhesion, directly influencing the migratory and contractile state of the cell [17,18].

Although this model provides a major breakthrough and contributes significantly to the understanding of focal adhesion and cellular behaviour, the underlying molecular mechanism and the concept behind mechanically transduced signaling remains obscure. Here, we review the topology of focal adhesions and propose that they are sensors for the elasticity and spacing of extracellular ligands. Our model is based on the quantitative analysis of GFP-tagged focal adhesion proteins associated with the two-dimensional (2D) plane of the plasma membrane that give dynamic insight into the interior structure of focal adhesions.

The second dimension of focal adhesions

In focal adhesions, the actin cytoskeleton is linked through various adaptor proteins to heterodimeric receptors of the integrin family (Fig. 1a) [19]. Integrin receptors bind to extracellular matrix proteins organized in either basement membranes (Fig. 1a) or connective tissues (Fig. 1b). Importantly, whether a focal adhesion is formed on a flat surface (e.g. glass coverslip) or within a network of extracellular-matrix proteins, the integrin receptors are confined to the 2D plane of the plasma membrane, in which they can diffuse laterally [20]. By contrast, the actin cytoskeleton and adaptor proteins are recruited from a cytoplasmic pool and aggregate in complex ways to form ~60-nm-thick focal contacts [21]. Therefore, one can classify focal adhesion components that are confined to or entrapped within the 2D plasma membrane, such as integrins, as 2D focal adhesion markers. By contrast, adaptor proteins that are stacked on top of each other within the actin backbone of focal adhesions, such as vinculin and paxillin, represent markers of the focal adhesion volume.

This observation is important when the fluorescence intensity of such GFP chimeras is measured by light microscopy, which is unable to resolve the depth of focal adhesions (Fig. 1c) [22]. For example, if one observes an increase in the fluorescence intensity of a given GFP marker within a focal adhesion, the following conclusions can be

http://tcb.trends.com 0962-8924/02/$ – see front matter PII: S0962-8924(02)02321-8

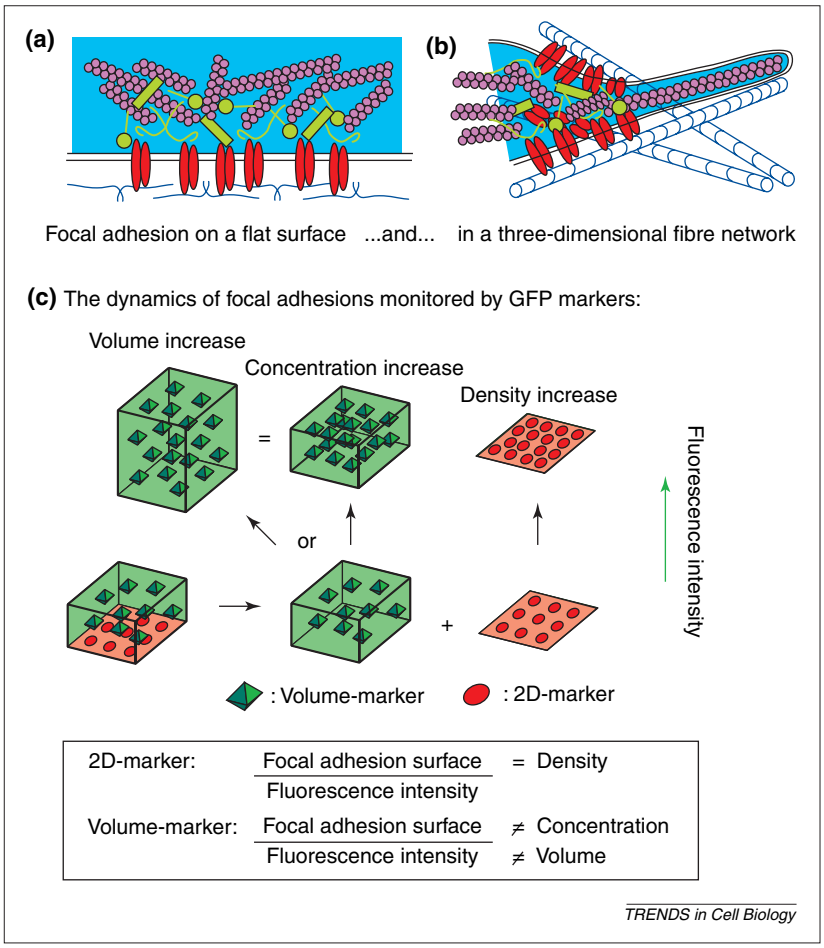

Fig. 1. The topology of focal adhesions and their components on a flat surface such as a fibronectin-coated glass coverslip (a) or formed within a three-dimensional network of collagen fibres (b). The topology of focal adhesion is identical in (a) and (b), linking the extracellular substrate (blue) via integrin heterodimers (red) embedded in the plasma membrane (thin lines) and various adaptor proteins (green) to the actin cytoskeleton (purple). Although focal adhesions are very flat structures, they nevertheless have a certain volume occupied by many adaptor proteins stacked on top of each other. This volume can be considered as a box (c) in which the adaptor proteins appear as volume markers that fill the inside of the focal adhesion. By contrast, transmembrane constituents of focal adhesions such as integrins will behave as two-dimensional (2D) markers labelling just the lower surface of the box. The increase in the fluorescent intensity of the 2D marker indicates a higher packing density within the focal adhesion. By contrast, owing to the missing resolution along the *z* axis, an increase in fluorescence intensity of the volume marker does not allow us to distinguish between an increase in packing density (concentration) or an increase in focal adhesion volume. This makes a 2D marker a better diagnostic instrument to analyse the interior physical structure of focal adhesions.

drawn (Fig. 1c). For a 2D marker, the equation is simple: an increase in fluorescence intensity indicates a higher packing density in the focal adhesion. For a volume marker, the situation is more complex: higher fluorescence intensity indicates more GFP molecules, but this yields no structural information about the organization of the extra molecules recruited to the focal adhesion. The issue is further complicated by the fact that certain focal adhesion adaptor proteins can, owing to their multiple protein–protein interactions [1], behave as 2D or volume markers depending whether they interact with plasma-membrane- or actin-backbone-associated focal adhesion components. In general, however, a 2D marker has a higher diagnostic potential than a volume marker for interpreting changes in fluorescence intensity.

This problem with quantifying GFP marker proteins that do not exclusively associate with the plasma membrane of focal adhesions is highlighted in the following two examples. In human foreskin fibroblasts, it has been demonstrated that the amount of tension generated by a focal adhesion correlates directly with focal adhesion size and with the amount of fluorescence of the focal adhesion adaptor protein GFP–vinculin in it [9]. In another study, the fluorescence intensity of GFP–zyxin, another focal adhesion adaptor protein, has been compared with the traction forces exerted by focal adhesions in migrating fish fibroblasts. In contrast to the analysis with vinculin, the fluorescence intensity of GFP–zyxin in focal adhesions demonstrated an inverse correlation with the generated traction stress in the respective focal adhesions [10]. We are led to conclude that the different focal adhesion markers used in these studies have distinct functions and are being recruited by signals that might not be generated by the mechanical forces applied to focal adhesions. Moreover, bearing in mind the complexity and multiple functions of focal adhesions, it is very difficult to assign a specific cause to changes in the fluorescence intensities of any particular GFP marker. Hence, we propose the use of a 2D GFP marker for the quantitative analysis of tension-dependent changes in focal adhesion structure. Preferably, this 2D marker should also serve a mechanical function, for example by being part of the physical link between the extracellular matrix and the actin cytoskeleton.

Using a 2D GFP–β3-integrin marker

The two examples of changing intensities of the focal adhesion markers GFP–vinculin and GFP–zyxin show dramatically that focal adhesions are complex structures that require multiple functional parameters to describe their behaviour, such as fluorescence intensity, traction forces and focal adhesion mobility (also termed 'sliding' [13]). When a 2D GFP–β3-integrin marker is used to study focal adhesions, the respective fluorescence intensity correlates directly with the packing 'density' of this particular integrin in each focal adhesion. The analysis of GFP–β3-integrin in five different focal adhesions in a migrating melanoblast revealed several important features (Fig. 2). First, focal adhesion can be classified into low-density and high-density forms. Second, focal adhesion density can change dramatically with time. Third, high- and low-density contacts are located in different cellular compartments. Fourth, only high-density focal adhesions show mobility ('sliding') [11]. The value of this complex information can be further extrapolated taking into account the fact that low-density focal adhesions form in response to the activity of the GTPases Rac1 and Cdc42, and high-density focal adhesions form in a manner dependent on the GTPase RhoA and acto-myosin contraction [11]. This implies that, at least for

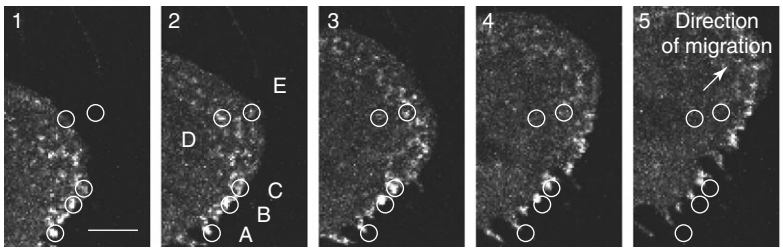

Fig. 2. The two-dimensional (2D) marker green-fluorescent-protein (GFP)–β3-integrin reveals the multidimensionality of focal adhesions. A melanoblast (melb-a [50]) stably transfected with GFP–β3-integrin was stimulated with a growth factor to induce migration. The migration is characterized by the formation of an actin-filament-rich lamellipodium at the cell front and a subsequent coalescence of these actin filaments into actin bundles at the lateral edges of the lamellipodium [41,51]. Focal adhesions A, B and C are located along this lateral edge, whereas focal adhesions D and E are positioned within the advancing lamellipodium. The circles mark the positions of the focal adhesions in the first frame (A, B and C) or where they first appear (D, E) and are kept in a constant position throughout the different frames (1–5). Focal adhesions D and E remain stationary, whereas focal adhesions A, B and C show inward 'sliding'. In addition, notice the differences between the focal adhesion fluorescence intensities of low-density focal adhesions (D, E) within the lamellipodium and high-density focal adhesions (A, B and C) located along the lateral edge of the lamellipodium [11]. Bar, 4.5 μm.

β3-integrins, myosin-dependent actin-cytoskeleton contraction is at the origin of the formation of high-density focal adhesions.

Importantly, the notion that focal adhesions can exhibit different densities would not have been anticipated by the use of GFP markers that are not confined to the 2D plane of the plasma membrane. The observation that the packing densities of β3-integrins can increase two- to threefold [11] has important consequences, bearing in mind that integrins are anchored simultaneously via adaptor proteins to the actin cytoskeleton and their extracellular ligands. Owing to this mechanical link, either density changes in the actin backbone of focal adhesions or changes in the spacing of extracellular ligands (e.g. induced by extracellular tension) will mechanically distort the link between integrins and actin-bound adaptor proteins. Furthermore, the induction of acto-myosin contraction of low-density focal adhesions, as observed in migrating cells (Fig. 2) [11], might have different behavioural consequences depending on whether the bound extracellular ligands form a rigid or elastic surface or whether they exhibit dense or widely spaced integrin binding sites. Some of these theoretical concepts are outlined below with the relevant cellular responses.

Elasticity and spacing of extracellular-matrix ligands

Anybody who has cultured cells on a plastic dish will have realized that, although cells spread, adhere and divide, they will, in living tissues, encounter non-homogeneous microenvironments consisting of rigid as well as flexible domains. Therefore, experiments in which cells have been cultured on elastic substrates have provided interesting information about the cellular responses within a flexible environment. Fibroblasts plated on a flexible substrate were unable to adhere tightly and migrated much faster than on a rigid substrate [23]. Furthermore, when cells were plated on a gradient of different elasticities, they migrated from the flexible towards the more rigid surface [24]; the term 'durotaxis' is used for this movement towards a more rigid surface. Therefore, cells must be able to measure extracellular resistance by physical contact with their environment.

How do cells measure or sense the physical constraints of their environment? It is plausible that mechanical sensing occurs inside focal adhesions, considering that the sensing organelles of cells – the filopodia and lamellipodia – have low-density focal adhesions (also called focal complexes in fibroblasts) that form in a Rac1- or Cdc42-dependent manner [5,11]. When the cell moves forward (Fig. 2), the low-density adhesions transform into high-density adhesions (also called focal contacts in fibroblasts) in response to RhoA activation and myosin-dependent actin-filament contraction [5,11]. The combination of an increase in focal adhesion density and centripetal acto-myosin contraction is sufficient to probe the resistance of the extracellular environment (Fig. 3). It has been observed that, on elastic substrates, focal adhesions retract, whereas they are reinforced and maintained on a rigid surface, anchoring the cell for forward motion [24].

The mechanism of focal adhesion reinforcement and maintenance on a rigid surface is not well understood but can be observed under different experimental conditions. Fibronectin-coated beads that attach to the dorsal surface of cells show retrograde motion and can be easily removed with optical tweezers. However, holding the bead on the cell surface for only a short period of time is sufficient to reinforce cellular binding to the bead, a process that can be blocked by the tyrosine phosphatase inhibitor phenylarsine oxide (PAO) [25]. Furthermore, it has been demonstrated that focal adhesion loss or reinforcement in response to a local reduction or increase in substrate tension, respectively, requires the presence of focal adhesion kinase (FAK) [26]. In addition, brushing against a moving lamellipodium with a microneedle induces the maturation of lamellipodial focal complexes (low-density focal adhesions) into focal contacts (high-density focal adhesions) [27]. This maturation of focal adhesions in response to extracellularly applied tension depends on RhoA activation and its downstream target Diaphanous (mDia) [18,27,28]. Because mDia acts as an actin polymerization factor, the observed increase in size and density of focal adhesions could be linked to increased amounts of polymerized actin [28,29]. Similarly, in undisturbed cells, the molecular signals involved in transforming low-density into high-density focal adhesions and the synthesis of associated actin stress fibres involves RhoA activation and its downstream targets Rho kinase and mDia [3,5,29,30]. Whereas Rho kinase inhibits the myosin light chain phosphatase, which results in continuous acto-myosin

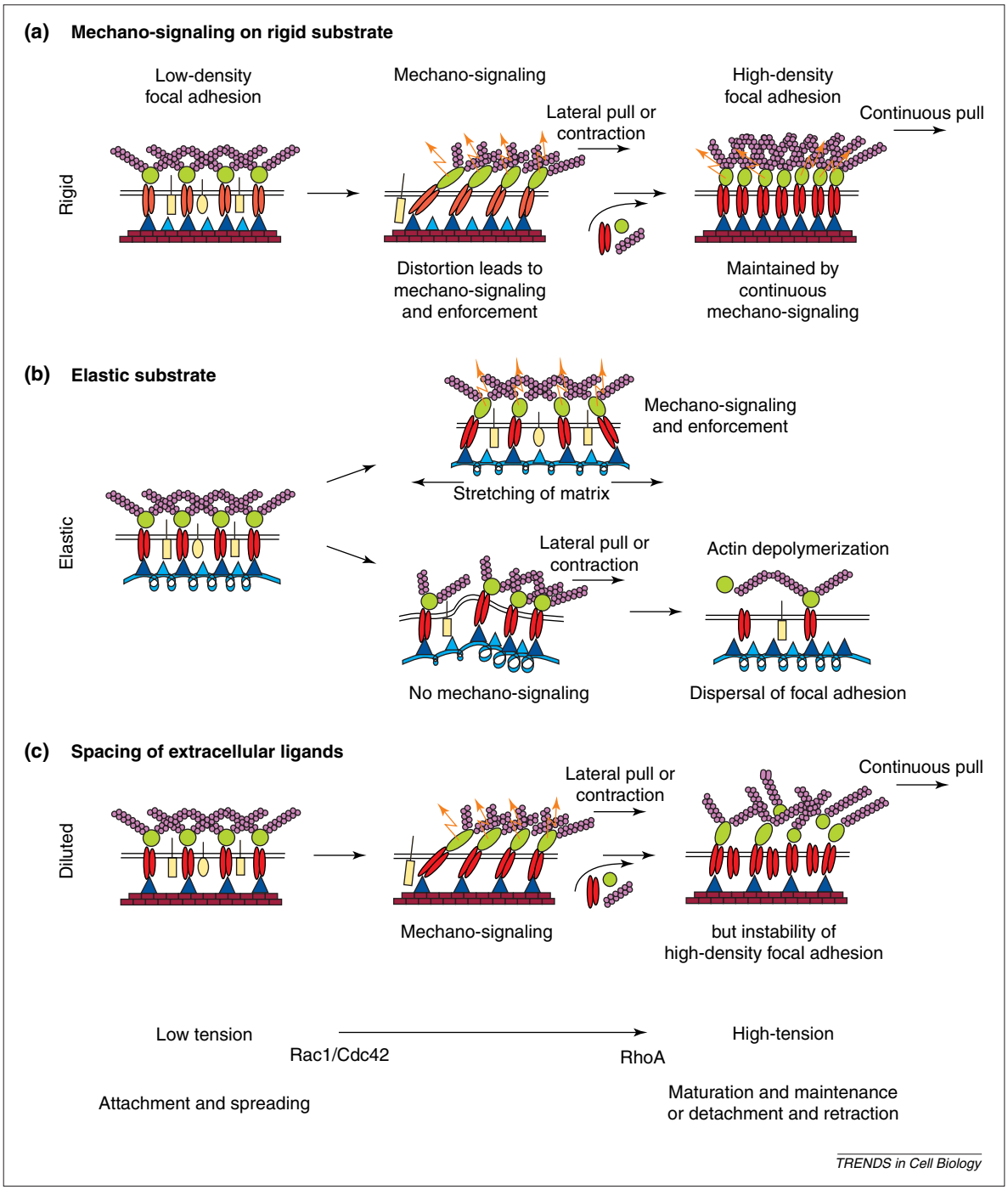

Fig. 3. The influence of substrate elasticity and spacing on focal adhesions formed on rigid [brick wall; (a, c)] and elastic [blue ribbon (b)] substrates. The integrin-binding sites are represented by blue triangles in a dense (a, b) or wider-spaced (c) configuration. When focal adhesions are formed within filopodia or lamellipodia, they assume a low-density configuration that does not necessarily occupy all available extracellular-matrix-binding sites (left-hand side). In addition, the loose integrin spacing might leave space for additional non-integrin transmembrane receptors within the adhesion site (yellow). Owing to the absence of acto-myosin contraction, adaptor proteins are in a relaxed configuration (green circles). In response to RhoA activity and increased tension, the actin cytoskeleton will contract, generating a lateral pull. We propose that the distortions created in integrins (red) and adaptor proteins (green ovals) between the rigid extracellular binding sites and the contracting actin cytoskeleton induces mechanical signaling ('zigzag' orange arrows) by exposing so-far-unidentified stress-sensitive binding sites for adaptor or signaling proteins [31]. The subsequent recruitment of new integrins and adaptor proteins together with actin polymerization will lead to high-density focal adhesions that, however, need to be continuously pulled to maintain mechanical signaling. When the cell establishes a low-density focal adhesion on an elastic substrate, the subsequent acto-myosin-dependent contraction will not be able to create a distortion within the condensing focal adhesion because of the lack of resistance of the substrate (b). In the absence of a mechanical distortion, no mechanical signaling will occur. The lack of focal adhesion reinforcement will result in the dispersal of the focal adhesion site. By contrast, when an elastic substrate is locally pulled or stretched, mechanical signaling is initiated by the distortion of the focal adhesion site, resulting in a high-density adhesion (b). When low-density focal adhesions on widely spaced extracellular-matrix ligands are contracted by RhoA-induced acto-myosin activity, mechanical signaling will be initiated, leading to the formation of high-density adhesions (c). However, when the spacing of extracellular ligands is too wide, only a suboptimal amount of integrins will be engaged in substrate adhesion, insufficient for the formation of stress fibres and resistance to a further increase in tension (c).

contraction, mDia acts as an actin polymerization factor within focal adhesion sites.

Most importantly, however, it has recently been demonstrated that the mechanically stretched, Triton-resistant cytoskeleton of fibroblasts recruits signaling molecules such as paxillin and FAK to stretched focal adhesions [31]. These signaling molecules are recruited to the focal adhesions and not to the actin cytoskeleton extended between them. This is of particular importance because it suggests that the mechanical distortion of focal adhesions itself is at the origin of mechanical signaling. However, it has to be demonstrated whether the mechanical distortion of integrin receptors or the specific adaptor proteins such as FAK [26] or paxillin, which extend between integrins and the actin cytoskeleton, is involved in mechanical sensing. Interestingly, when the extracellular tension is reduced, focal adhesion sites loose the ability to recruit paxillin [31] and will detach from the relaxed substrate [26], suggesting that continuous generation of intracellular tension (and hence high-density focal adhesions) is required to maintain mechanical signaling. Figure 3b demonstrates the different fates of low- and high-density focal adhesions with respect to the elasticity of the substrates. The absence of mechanical signaling on an elastic substrate is proposed to be because of the lack of physical distortion during the contraction of focal adhesions.

A second model based on the different densities of focal adhesions can be extrapolated from the spacing of extracellular ligands. RGD peptides represent the integrin recognition sequence of the major cell binding site of fibronectin [2]. Differently spaced RGD peptides have been used to study the minimal RGD densities required for cell spreading and adhesion [32]. Whereas cells readily spread and attached to an RGD density of 1 fmol cm^{-2}, cells were unable to form focal contacts (high-density focal adhesions) and stress fibres on this substrate. Only at RGD densities of 10 fmol cm^{-2} or above were high-density adhesions and stress fibres formed. This suggests that, beyond a crucial density of integrin ligands (e.g. RGD), cells can only use low-density focal adhesions for attachment, which form in spreading lamellipodia and filopodia, exhibiting wider integrin spacing to establish a stable contact to the substrate.

These data have recently been complemented by an elegant study analysing cell adhesion in a centrifugal force field on a substrate coated either with small clusters of RGD peptides or with monomeric RGD peptides [33]. Interestingly, when pulled by a centrifugal force field, cells plated on the clustered RGD substrate showed reinforcement of cell adhesion, suggesting the formation of high-density focal adhesions. Cells plated on an equimolar amount of monomeric RGD peptides, however, could not resist the centrifugal force and detached. These data suggest that, on the evenly spaced, monomeric RGD substrate, the high-density focal adhesions (which formed in response to mechanical forces) could not be stabilized because of the absence of the appropriate high-density spacing of RGD ligands found only in the clusters.

Based on these data, it is therefore possible (Fig. 3c) that low-density focal adhesions within filopodia or lamellipodia can bind to surfaces with widely spaced extracellular matrix ligands. As soon as a cell generates RhoA-induced acto-myosin contraction of focal adhesion, these sites will only resist if the spacing of the extracellular-matrix ligands matches that of the packing density of the integrins within the high-density focal adhesion. An important prediction of this model is that Rac1- or Cdc42-induced cellular processes such as neuronal growth cones, which move forward by the force generated by actin polymerization in lamellipodia and filopodia, can adhere to and explore substrates that have only widely spaced extracellular ligands. These processes, however, will retract on these substrates when RhoA activity leads to acto-myosin contraction [34,35].

FRAP analysis reveals the dynamic interior of focal adhesions

The model of focal adhesion behaviour and mechanical signaling presented here is based on the notion that the initial stress-induced physical distortion of focal adhesions causes changes in their densities and subsequent recruitment of signaling and structural focal adhesion proteins. Although this model explains many of the experimental findings, it does not explain the observed mobility ('sliding') of focal adhesions [11,13]. One of the best techniques for measuring the internal dynamics of complex structures is fluorescence recovery after photobleaching (FRAP) [36]. This technique can be used to analyse many cellular structures and is particularly suited for use with GFP chimeras. During FRAP, the chromophore in the GFP protein is irreversibly inactivated and the generated radicals are efficiently scavenged by the GFP protein cage, reducing the phototoxicity of the laser pulse. The time and degree of fluorescence recovery within the bleached spot give information about the reorganization and renewal of the analysed structure. When this technique is applied to focal adhesions, each focal adhesion marker will have its own characteristic FRAP 'value' that depends on its intracellular concentration (availability) as well as the number and strength of binding sites to other focal adhesion components. Because integrins are a structural component of the link between the cytoskeleton and the extracellular matrix, FRAP can give information about the dynamic state of the focal-adhesion–substrate interface.

Analysing GFP–β3-integrins by FRAP revealed that high-density focal adhesions undergo renewal that results in the complete exchange of integrins within 5–10 min. Interestingly, low-density focal adhesions that do not exhibit acto-myosin

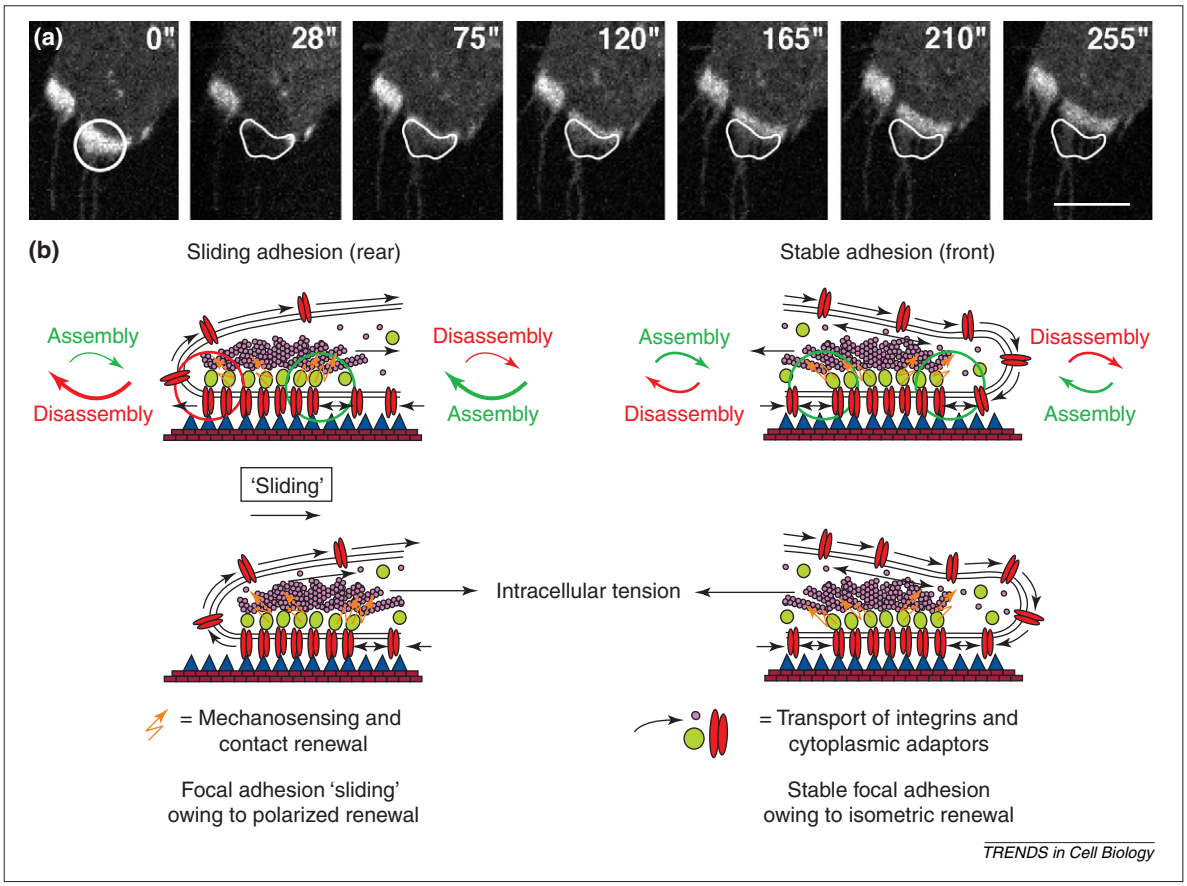

Fig. 4. Fluorescence recovery after photobleaching (FRAP) reveals the dynamic remodelling of high-density focal adhesions. An inwardly 'sliding' high-density focal adhesion of a green-fluorescent-protein (GFP)–β3-integrin-transfected melanoblast (melb-a) was analysed by FRAP [11] (a). Between 0 and 25 sec, the fluorescence has been inactivated within the circled region. In all subsequent frames, the initial outline (at 0″) of the focal adhesion has been traced to show the relative locations of the reappearance of the GFP fluorescence. Some fluorescence recovers within the former location of the focal adhesion, but most GFP–β3-integrin accumulates at the edge of the bleached focal adhesion facing the interior of the cell. (See also the accompanying supplementary video at: http://archive.bmn.com/supp/tcb/imhof.mov. In the video, the bleached region is indicated by a circle in frame 1. After the fluorescence inactivation (0′), each subsequent frame is labeled with the respective time after bleach. The width of field is 27 μm.) A schematic view of the proposed mechanism of sliding caused by a polarized renewal of high-density focal adhesion is shown (b). High-density focal contacts demonstrate continuous dispersal of old (Disassembly, red) and polymerization and aggregation of new (Assembly, green) focal adhesion components. Local differences in the cellular traffic of these building blocks along the polarized microtubule network creates an imbalance between disassembly and assembly in focal adhesion localized to the retracting rear of migrating cells. This imbalance results in a polarized renewal of focal adhesions, giving the impression of 'sliding' (left-hand side). At the cell front, however, defined by the presence of an advancing lamellipodium, integrins and adaptor proteins ready to become incorporated into the renewing focal adhesion have similar access to all sides to induce a nonpolarized renewal that does not result in sliding (right-hand side). Bar, 5.5 μm.

contraction show a reduced turnover [11]. Focal complexes formed at the cell front do not 'slide' or demonstrate integrin turnover; by contrast, focal contacts at the cell rear slide and renew their integrins at a high rate [11,13]. This suggests that sliding of focal contacts might be a consequence of integrin renewal.

In Figure 4a, a rapidly sliding focal adhesion has been bleached by a laser pulse (see also the supplementary video at: http://archive.bmn.com/supp/tcb/imhof.mov). Although there is some renewal of the focal adhesion within the bleached region, a much faster *de novo* recruitment of integrins can be observed at the side of the focal adhesion facing the cell centre. This suggests that sliding focal adhesions demonstrate a polarized renewal leading to their displacement (Fig. 4b). The renewal of focal adhesions requires the delivery of new building blocks. The disassembly, at the side of the focal adhesion facing the cell periphery, could therefore be caused by the absence of delivery of new focal adhesion components. In this respect, it is interesting that integrins, like many other membrane components, are transported away from the cell rear towards the front by vesicular transport [12,37–39]. By contrast, when the building blocks required for focal adhesion renewal are transported towards pre-existing focal adhesion sites, for example to form a local lamellipodium (Fig. 4b), focal adhesions can renew at their distal as well as their proximal end. This isometric renewal could explain why retracting focal adhesions temporarily halt their inward sliding at sites of local lamellipodium formation [11] and why maturing focal adhesions that are formed behind the cell front in migrating fibroblasts do not demonstrate sliding [13]. This model is also in agreement with the observation that high-affinity αvβ3 integrins are generated by Rac1 activity, associated with the formation of lamellipodia [40]. To conclude, the

continual renewal of high-density focal adhesions gives the cell the necessary plasticity to continuously adapt pre-existing focal adhesions to modify cellular shape and function.

Concluding remarks

We have proposed here that new models to explain focal adhesion structure, function and regulation require the analysis of functional criteria such as focal adhesion density, renewal and the amount of traction force. Nevertheless, much work remains to be done to identify the regulatory pathways involved in focal adhesion dynamics and mechanical signaling. Although it is plausible that the physical distortion of focal adhesions is at the root of mechanical signaling, it is not known which protein domains can fold in a tension-dependent manner to expose binding sites for signaling proteins.

A second crucial task involves the elucidation of the signals that lead to and control focal adhesion turnover. This is especially important for migrating cells, because the efficient release of focal adhesions at the cell rear allows fast migration [41,42]. It has been demonstrated that stretch-activated calcium channels play an important role in rear detachment [43]. Calcium influx might stimulate RhoA and subsequent Rho-kinase activation, which is required for rear detachment of cells of haematopoietic origin [44,45]. This suggests, however, that acto-myosin contraction within focal adhesions is part of the signaling pathway that leads to focal adhesion disassembly. It remains a paradox that the same signaling pathway is also involved in focal adhesion enforcement. Finding the molecular switch remains a crucial task.

Although the model presented here is mainly based on data generated with the αvβ3 integrin, which is involved in cell migration, the integrin family comprises more than 20 different members with potentially different functions [19]. One remarkable example is the α5β1 integrin, which initially localizes with αvβ3 in focal contacts of fibroblasts but subsequently segregates into fibrillar adhesions involved in fibronectin matrix assembly [6,46]. It has been suggested that this difference is due to the constitutive high-affinity state of α5β1 integrins required to bind to fibronectin, whereas the high-affinity (or ligand-bound) state of αvβ3 integrins is less stable [47]. Alternatively, it has been demonstrated that the non-receptor tyrosine kinase Src selectively suppresses the reinforcement of substrate binding (the high-affinity state) of αvβ3 integrins but not of α5β1 integrins [48]. Whether the high- to low-affinity switch of αvβ3 or other integrins is correlated with focal adhesion turnover and cell migration remains to be shown [49].

What is most pertinent, however, is that volume and 2D focal adhesion markers have to be analysed in parallel, to calibrate focal adhesion density changes with the recruitment or loss of focal adhesion components. For example, RhoA-induced high-density GFP–β3-integrin contacts have much more vinculin (as determined by conventional immunofluorescence) than control focal adhesions (B. Wehrle-Haller, unpublished). This suggests that vinculin is recruited to high-density focal adhesions in response to RhoA signaling and/or tension [9]. However, vinculin is not recruited to stretched and Triton-extracted focal adhesions [31], suggesting that it plays a structural role by supporting the increased tension within focal adhesion but is not directly involved in mechanical sensing.

A careful analysis of the functional role and the topology of several GFP markers is required in order to correctly interpret qualitative changes in fluorescence intensities and FRAP behaviour. This will allow the construction of a structural, dynamic model of focal adhesion. Revealing the regulatory circuits involved in focal adhesion dynamics should facilitate the discovery of new therapeutic approaches for wound healing or to prevent metastasis.

Acknowledgements
We thank Caroline Johnson-Léger, Caroline Cluzel, Michel Aurrand-Lions and Boris Hinz for stimulating discussions. Special thanks to Christoph Ballestrem for his tenacity in developing the GFP–β3-integrin construct. This study was supported by grants from the Swiss National Science Foundation.

References

1 Zamir, E. and Geiger, B. (2001) Molecular complexity and dynamics of cell–matrix adhesions. *J. Cell Sci.* 114, 3583–3590
2 Geiger, B. *et al.* (2001) Transmembrane crosstalk between the extracellular matrix–cytoskeleton crosstalk. *Nat. Rev. Mol. Cell Biol.* 2, 793–805
3 Chrzanowska-Wodnicka, M. and Burridge, K. (1996) Rho-stimulated contractility drives the formation of stress fibers and focal adhesions. *J. Cell Biol.* 133, 1403–1415
4 Nobes, C.D. and Hall, A. (1995) Rho, Rac, and Cdc42 GTPases regulate the assembly of multimolecular focal complexes associated with actin stress fibers, lamellipodia, and filopodia. *Cell* 81, 53–62
5 Rottner, K. *et al.* (1999) Interplay between Rac and Rho in the control of substrate contact dynamics. *Curr. Biol.* 9, 640–648
6 Zamir, E. *et al.* (2000) Dynamics and segregation of cell–matrix adhesions in cultured fibroblasts. *Nat. Cell Biol.* 2, 191–196
7 Adams, J.C. (2002) Regulation of protrusive and contractile cell–matrix contacts. *J. Cell Sci.* 115, 257–265
8 Cukierman, E. *et al.* (2001) Taking cell–matrix adhesions to the third dimension. *Science* 294, 1708–1712
9 Balaban, N.Q. *et al.* (2001) Force and focal adhesion assembly: a close relationship studied using elastic micropatterned substrates. *Nat. Cell Biol.* 3, 466–472
10 Beningo, K.A. *et al.* (2001) Nascent focal adhesions are responsible for the generation of strong propulsive forces in migrating fibroblasts. *J. Cell Biol.* 153, 881–888
11 Ballestrem, C. *et al.* (2001) Marching at the front and dragging behind: differential αVβ3-integrin turnover regulates focal adhesion behavior. *J. Cell Biol.* 155, 1319–1332
12 Laukaitis, C.M. *et al.* (2001) Differential dynamics of alpha 5 integrin, paxillin, and α-actinin during formation and disassembly of adhesions in migrating cells. *J. Cell Biol.* 153, 1427–1440
13 Smilenov, L.B. *et al.* (1999) Focal adhesion motility revealed in stationary fibroblasts. *Science* 286, 1172–1174
14 Dembo, M. *et al.* (1996) Imaging the traction stresses exerted by locomoting cells with the elastic substratum method. *Biophys. J.* 70, 2008–2022
15 Dembo, M. and Wang, Y.L. (1999) Stresses at the cell-to-substrate interface during locomotion of fibroblasts. *Biophys. J.* 76, 2307–2316
16 Oliver, T. *et al.* (1999) Separation of propulsive and adhesive traction stresses in locomoting keratocytes. *J. Cell Biol.* 145, 589–604
17 Beningo, K.A. and Wang, Y.L. (2002) Flexible substrata for the detection of cellular traction forces. *Trends Cell Biol.* 12, 79–84
18 Geiger, B. and Bershadsky, A. (2001) Assembly and mechanosensory function of focal contacts. *Curr. Opin. Cell Biol.* 13, 584–592
19 Hynes, R.O. (1992) Integrins: versatility, modulation, and signaling in cell adhesion. *Cell* 69, 11–25

20 Duband, J.L. *et al.* (1988) Fibronectin receptor exhibits high lateral mobility in embryonic locomoting cells but is immobile in focal contacts and fibrillar streaks in stationary cells. *J. Cell Biol.* 107, 1385–1396
21 Chen, W.T. and Singer, S.J. (1982) Immunoelectron microscopic studies of the sites of cell–substratum and cell–cell contacts in cultured fibroblasts. *J. Cell Biol.* 95, 205–222
22 Kam, Z. *et al.* (2001) Probing molecular processes in live cells by quantitative multidimensional microscopy. *Trends Cell Biol.* 11, 329–334
23 Pelham, R.J., Jr and Wang, Y. (1997) Cell locomotion and focal adhesions are regulated by substrate flexibility. *Proc. Natl. Acad. Sci. U. S. A.* 94, 13661–13665
24 Lo, C.M. *et al.* (2000) Cell movement is guided by the rigidity of the substrate. *Biophys. J.* 79, 144–152
25 Choquet, D. *et al.* (1997) Extracellular matrix rigidity causes strengthening of integrin–cytoskeleton linkages. *Cell* 88, 39–48
26 Wang, H.B. *et al.* (2001) Focal adhesion kinase is involved in mechanosensing during fibroblast migration. *Proc. Natl. Acad. Sci. U. S. A.* 98, 11295–11300
27 Riveline, D. *et al.* (2001) Focal contacts as mechanosensors: externally applied local mechanical force induces growth of focal contacts by an mDia1-dependent and ROCK-independent mechanism. *J. Cell Biol.* 153, 1175–1186
28 Watanabe, N. *et al.* (1997) p140mDia, a mammalian homolog of *Drosophila* diaphanous, is a target protein for Rho small GTPase and is a ligand for profilin. *EMBO J.* 16, 3044–3056
29 Watanabe, N. *et al.* (1999) Cooperation between mDia1 and ROCK in Rho-induced actin reorganization. *Nat. Cell Biol.* 1, 136–143
30 Kimura, K. *et al.* (1996) Regulation of myosin phosphatase by Rho and Rho-associated kinase (Rho-kinase). *Science* 273, 245–248
31 Sawada, Y. and Sheetz, M.P. (2002) Force transduction by Triton cytoskeletons. *J. Cell Biol.* 156, 609–615
32 Massia, S.P. and Hubbell, J.A. (1991) An RGD spacing of 440 nm is sufficient for integrin αVβ3-mediated fibroblast spreading and 140 nm for focal contact and stress fiber formation. *J. Cell Biol.* 114, 1089–1100
33 Koo, L.Y. *et al.* (2002) Co-regulation of cell adhesion by nanoscale RGD organization and mechanical stimulus. *J. Cell Sci.* 115, 1423–1433
34 Shamah, S.M. *et al.* (2001) EphA receptors regulate growth cone dynamics through the novel guanine nucleotide exchange factor ephexin. *Cell* 105, 233–244
35 Wahl, S. *et al.* (2000) Ephrin-A5 induces collapse of growth cones by activating Rho and Rho kinase. *J. Cell Biol.* 149, 263–270
36 White, J. and Stelzer, E. (1999) Photobleaching GFP reveals protein dynamics inside live cells. *Trends Cell Biol.* 9, 61–65
37 Lawson, M.A. and Maxfield, F.R. (1995) Ca^{2+}- and calcineurin-dependent recycling of an integrin to the front of migrating neutrophils. *Nature* 377, 75–79
38 Palecek, S.P. *et al.* (1998) Physical and biochemical regulation of integrin release during rear detachment of migrating cells. *J. Cell Sci.* 111, 929–940
39 Bretscher, M.S. and Aguado-Velasco, C. (1998) Membrane traffic during cell locomotion. *Curr. Opin. Cell Biol.* 10, 537–541
40 Kiosses, W.B. *et al.* (2001) Rac recruits high-affinity integrin alphavbeta3 to lamellipodia in endothelial cell migration. *Nat. Cell Biol.* 3, 316–320
41 Ballestrem, C. *et al.* (2000) Actin-dependent lamellipodia formation and microtubule-dependent tail retraction control-directed cell migration. *Mol. Biol. Cell* 11, 2999–3012
42 Palecek, S.P. *et al.* (1997) Integrin-ligand binding properties govern cell migration speed through cell–substratum adhesiveness. *Nature* 385, 537–540
43 Lee, J. *et al.* (1999) Regulation of cell movement is mediated by stretch-activated calcium channels. *Nature* 400, 382–386
44 Niggli, V. (1999) Rho-kinase in human neutrophils: a role in signalling for myosin light chain phosphorylation and cell migration. *FEBS Lett.* 445, 69–72
45 Worthylake, R.A. *et al.* (2001) RhoA is required for monocyte tail retraction during transendothelial migration. *J. Cell Biol.* 154, 147–160
46 Pankov, R. *et al.* (2000) Integrin dynamics and matrix assembly: tensin-dependent translocation of α(5)β(1) integrins promotes early fibronectin fibrillogenesis. *J. Cell Biol.* 148, 1075–1090
47 Hughes, P.E. *et al.* (1996) Breaking the integrin hinge. A defined structural constraint regulates integrin signaling. *J. Biol. Chem.* 271, 6571–6574
48 Felsenfeld, D.P. *et al.* (1999) Selective regulation of integrin–cytoskeleton interactions by the tyrosine kinase Src. *Nat. Cell Biol.* 1, 200–206
49 Shimaoka, M. *et al.* (2002) Conformational regulation of integrin structure and function. *Annu. Rev. Biophys. Biomol. Struct.* 31, 485–516
50 Sviderskaya, E.V. *et al.* (1995) A cloned, immortal line of murine melanoblasts inducible to differentiate to melanocytes. *Development* 121, 1547–1557
51 Ballestrem, C. *et al.* (1998) Actin dynamics in living mammalian cells. *J. Cell Sci.* 111, 1649–1658

5.3. Outlook

Although progress in understanding cell motility has been substantial, cell migration remains a fascinating but still pristine aspect of cellular physiology. Significant work has to be done in order to understand the interactions between chemotactic signals and the actin cytoskeleton. It has become apparent that cell migration requires efficient mechanisms to establish and maintain cell polarity, which involves recycling, sorting and rear to front transport of membranes and proteins across the cell. It will be particularly challenging to functionally connect cytoskeletal and membrane remodeling that are both stimulated by RTKs or chemokine receptors. In addition, the detailed analysis of integrin and focal adhesion dynamics with the help of the GFP technology will be paramount to develop focal adhesion specific tools that can fine-tune intracellular tension and focal adhesion remodeling, involved in pathological situations associated with excessive cell migration. The task will be to turn a cell into a reaction tube in which each protein component can be quantitatively analyzed in its physiological environment. This has now become possible to various spectral and functional GFP variants that allow distance and dynamic measurements of protein-protein and protein-membrane interactions. Combining theses experimental approaches will lead to a further understanding of normal or pathological migratory events. With this knowledge it will be possible to create new therapeutic tools to stabilize or revert pathological situations associated with excessive cell migration.

6. Supplementary Material and Acknowledgement

6.1. Video sequences

For technical reasons, the printed version of this thesis does not include video sequences. Please refer to the PDF version of this thesis.

6.2. Acknowledgement

I would like to thank Professors Beat A. Imhof, James A. Weston, Matthias Chiquet, Jürgen Engel, Kurt Ballmer-Hofer and Max. M. Burger for their guidance and continuous support during my time as a student and postdoctoral fellow.

A special thank to all the granting organizations that believed in me and supported my education and research, notably the European Molecular Biology Organization (EMBO) and the Stiftung für Medizinisch-Biologische Stipendien providing me with a two, respectively one year postdoctoral fellowship and the Swiss National Science Foundation for grants: 31-52727.97 and 31-64000.00.

A special thank to all the members of the Friedrich Miescher Institute and the Biocenter in Basel, the Institute of Neuroscience in Eugene and the Centre Médical Universitaire that I had the pleasure to work with. I would specifically thank Carlo Bernasconi, Sheree Harrison, Victoria Robinson, Victoria Larson, Rick Gosswiler, Ruth Brewmiller, Claude Magnin, Susanne Bissat, Phillipe Hammel, Jean-Claude Rumbeli and especially Marie-Claude Jacquier for their patience and excellent technical support. Many thanks to Stephanie Käch, Dorothee Brubacher, Claudia Bagutti, Susanne Schenk, Beate Müller, Manuel Koch, Ralf Brandenberger, Ruth Chiquet, Gertraud Ohrend, Steve Johnson, Paul Henion, Yoshiko Takahashi, Yoshio Wakamatsu, Linda Hanson, Mike Marusich, Kathie Morrison-Graham, Gretchen Meller, Michel Aurrons-Lyons, Caroline Johnson-Léger, Lydia Duncan, Guido Wiedle, Caroline Cluzel, Frédérique Paulhe, Christoph Ballestrem, Cindy Wong, Christelle Lamagne and Christiane Ody for the hours of stimulating discussions and sharing of their know-how with me. A special thank to Jacqueline Ntah for her secretarial assistance and all the pre- and graduate students that endured me while developing my teaching skills such as Adam Hadley, Aaron Sundholm, Christoph Ballestrem, Cindy Wong, Roland Püttman and Christine Rossier. Many thanks to David Raible and Christiane Ody for introducing and sharing their preferred sport with me. I am grateful to Profs. Shin-ichi Nishikawa, Judith Eisen, Chuck Kimmel, Monte Westerfield, Sherry Rogers, Dot Bennett, Peter Besmer, Giulio Gabbiani, Patrick Ross, Neal Copeland, Kris Vogel for stimulating discussions, support and sharing of reagents.

However, I will not end this thesis without thanking Monique, Noëlle and Cédric Wehrle-Haller for their patience and forgiving when I was just too far away for a good-night kiss or fighting with another deadline.

7. References

Albelda, S.M., S.A. Mette, D.E. Elder, R. Stewart, L. Damjanovich, M. Herlyn, and C.A. Buck. 1990. Integrin distribution in malignant melanoma: association of the beta 3 subunit with tumor progression. *Cancer Res*. 50:6757-64.

Allen, W.E., G.E. Jones, J.W. Pollard, and A.J. Ridley. 1997. Rho, Rac and Cdc42 regulate actin organization and cell adhesion in macrophages. *J Cell Sci*. 110:707-20.

Anderson, D.M., S.D. Lyman, A. Baird, J.M. Wignall, J. Eisenman, C. Rauch, C.J. March, H.S. Boswell, S.D. Gimpel, D. Cosman, and et al. 1990. Molecular cloning of mast cell growth factor, a hematopoietin that is active in both membrane bound and soluble forms. *Cell*. 63:235-43.

Badolato, R., S. Sozzani, F. Malacarne, S. Bresciani, M. Fiorini, A. Borsatti, A. Albertini, A. Mantovani, A.G. Ugazio, and L.D. Notarangelo. 1998. Monocytes from Wiskott-Aldrich patients display reduced chemotaxis and lack of cell polarization in response to monocyte chemoattractant protein-1 and formyl-methionyl-leucyl-phenylalanine. *J Immunol*. 161:1026-33.

Baggiolini, M. 2001. Chemokines in pathology and medicine. *J Intern Med*. 250:91-104.

Ballestrem, C., B. Wehrle-Haller, B. Hinz, and B.A. Imhof. 2000. Actin-dependent lamellipodia formation and microtubule-dependent tail retraction control-directed cell migration. *Mol Biol Cell*. 11:2999-3012.

Baynash, A.G., K. Hosoda, A. Giaid, J.A. Richardson, N. Emoto, R.E. Hammer, and M. Yanagisawa. 1994. Interaction of endothelin-3 with endothelin-B receptor is essential for development of epidermal melanocytes and enteric neurons. *Cell*. 79:1277-85.

Bazan, J.F. 1991. Genetic and structural homology of stem cell factor and macrophage colony-stimulating factor [letter]. *Cell*. 65:9-10.

Berrozpe, G., I. Timokhina, S. Yukl, Y. Tajima, M. Ono, A.D. Zelenetz, and P. Besmer. 1999. The W(sh), W(57), and Ph Kit expression mutations define tissue- specific control elements located between -23 and -154 kb upstream of Kit. *Blood*. 94:2658-66.

Blume-Jensen, P., L. Claesson-Welsh, A. Siegbahn, K.M. Zsebo, B. Westermark, and C.H. Heldin. 1991. Activation of the human c-kit product by ligand-induced dimerization mediates circular actin reorganization and chemotaxis. *Embo J*. 10:4121-8.

Brannan, C.I., S.D. Lyman, D.E. Williams, J. Eisenman, D.M. Anderson, D. Cosman, M.A. Bedell, N.A. Jenkins, and N.G. Copeland. 1991. Steel-Dickie mutation encodes a c-kit ligand lacking transmembrane and cytoplasmic domains. *Proc Natl Acad Sci U S A*. 88:4671-4.

Brooks, P.C., R.A. Clark, and D.A. Cheresh. 1994a. Requirement of vascular integrin alpha v beta 3 for angiogenesis. *Science*. 264:569-71.

Brooks, P.C., A.M. Montgomery, M. Rosenfeld, R.A. Reisfeld, T. Hu, G. Klier, and D.A. Cheresh. 1994b. Integrin alpha v beta 3 antagonists promote tumor regression by inducing apoptosis of angiogenic blood vessels. *Cell*. 79:1157-64.

Chalfie, M., and S. Kain. 1998. Green Fluorescent Protein: Properties, Applications, and Protocols. Wiley & Sons, New York.

Chen, Y.P., I. Djaffar, D. Pidard, B. Steiner, A.M. Cieutat, J.P. Caen, and J.P. Rosa. 1992. Ser-752-->Pro mutation in the cytoplasmic domain of integrin beta 3 subunit and defective activation of platelet integrin alpha IIb beta 3 (glycoprotein IIb-IIIa) in a variant of Glanzmann thrombasthenia. *Proc Natl Acad Sci U S A*. 89:10169-73.

Conway, S.J., D.J. Henderson, and A.J. Copp. 1997. Pax3 is required for cardiac neural crest migration in the mouse: evidence from the splotch (Sp2H) mutant. *Development*. 124:505-14.

Copeland, N.G., D.J. Gilbert, B.C. Cho, P.J. Donovan, N.A. Jenkins, D. Cosman, D. Anderson, S.D. Lyman, and D.E. Williams. 1990. Mast cell growth factor maps near the steel locus on mouse chromosome 10 and is deleted in a number of steel alleles. *Cell*. 63:175-83.

Critchley, D.R., M.R. Holt, S.T. Barry, H. Priddle, L. Hemmings, and J. Norman. 1999. Integrin-mediated cell adhesion: the cytoskeletal connection. *Biochem Soc Symp*. 65:79-99.

Dastych, J., and D.D. Metcalfe. 1994. Stem cell factor induces mast cell adhesion to fibronectin. *J Immunol*. 152:213-9.

Debard, N., F. Sierro, and J.P. Kraehenbuhl. 1999. Development of Peyer's patches, follicle-associated epithelium and M cell: lessons from immunodeficient and knockout mice. *Semin Immunol*. 11:183-91.

Delannet, M., F. Martin, B. Bossy, D.A. Cheresh, L.F. Reichardt, and J.L. Duband. 1994. Specific roles of the alpha V beta 1, alpha V beta 3 and alpha V beta 5 integrins in avian neural crest cell adhesion and migration on vitronectin. *Development*. 120:2687-702.

Derby, M.A. 1978. Analysis of glycosaminoglycans within the extracellular environments encountered by migrating neural crest cells. *Dev Biol*. 66:321-36.

Dietrich, S., F. Abou-Rebyeh, H. Brohmann, F. Bladt, E. Sonnenberg-Riethmacher, T. Yamaai, A. Lumsden, B. Brand-Saberi, and C. Birchmeier. 1999. The role of SF/HGF and c-Met in the development of skeletal muscle. *Development*. 126:1621-9.

Dormond, O., A. Foletti, C. Paroz, and C. Ruegg. 2001. NSAIDs inhibit alpha V beta 3 integrin-mediated and Cdc42/Rac-dependent endothelial-cell spreading, migration and angiogenesis. *Nat Med*. 7:1041-7.

Duband, J.L., F. Monier, M. Delannet, and D. Newgreen. 1995. Epithelium-mesenchyme transition during neural crest development. *Acta Anat*. 154:63-78.

Duttlinger, R., K. Manova, G. Berrozpe, T.Y. Chu, V. DeLeon, I. Timokhina, R.S. Chaganti, A.D. Zelenetz, R.F. Bachvarova, and P. Besmer. 1995. The Wsh and Ph mutations affect the c-kit expression profile: c-kit misexpression in embryogenesis impairs melanogenesis in Wsh and Ph mutant mice. *Proc Natl Acad Sci U S A*. 92:3754-8.

Duttlinger, R., K. Manova, T.Y. Chu, C. Gyssler, A.D. Zelenetz, R.F. Bachvarova, and P. Besmer. 1993. W-sash affects positive and negative elements controlling c-kit expression: ectopic c-kit expression at sites of kit-ligand expression affects melanogenesis. *Development*. 118:705-17.

Eliceiri, B.P., and D.A. Cheresh. 1999. The role of alphav integrins during angiogenesis: insights into potential mechanisms of action and clinical development. *J Clin Invest*. 103:1227-30.

Erickson, C.A., T.D. Duong, and K.W. Tosney. 1992. Descriptive and experimental analysis of the dispersion of neural crest cells along the dorsolateral path and their entry into ectoderm in the chick embryo. *Dev Biol*. 151:251-72.

Fabbri, M., L. Fumagalli, G. Bossi, E. Bianchi, J.R. Bender, and R. Pardi. 1999. A tyrosine-based sorting signal in the beta2 integrin cytoplasmic domain mediates its recycling to the plasma membrane and is required for ligand-supported migration. *Embo J*. 18:4915-25.

Felding-Habermann, B., B.M. Mueller, C.A. Romerdahl, and D.A. Cheresh. 1992. Involvement of integrin alpha V gene expression in human melanoma tumorigenicity. *J Clin Invest*. 89:2018-22.

Felding-Habermann, B., T.E. O'Toole, J.W. Smith, E. Fransvea, Z.M. Ruggeri, M.H. Ginsberg, P.E. Hughes, N. Pampori, S.J. Shattil, A. Saven, and B.M. Mueller. 2001. Integrin activation controls metastasis in human breast cancer. *Proc Natl Acad Sci U S A*. 98:1853-8.

Filardo, E.J., P.C. Brooks, S.L. Deming, C. Damsky, and D.A. Cheresh. 1995. Requirement of the NPXY motif in the integrin beta 3 subunit cytoplasmic tail for melanoma cell migration in vitro and in vivo. *J Cell Biol*. 130:441-50.

Finotto, S., M. Buerke, K. Lingnau, E. Schmitt, P.R. Galle, and M.F. Neurath. 2001. Local administration of antisense phosphorothioate oligonucleotides to the c-kit ligand, stem cell factor, suppresses airway inflammation and IL-4 production in a murine model of asthma. *J Allergy Clin Immunol*. 107:279-86.

Flanagan, J.G., D.C. Chan, and P. Leder. 1991. Transmembrane form of the kit ligand growth factor is determined by alternative splicing and is missing in the Sld mutant. *Cell*. 64:1025-35.

Flanagan, J.G., and P. Leder. 1990. The kit ligand: a cell surface molecule altered in steel mutant fibroblasts. *Cell*. 63:185-94.

Forster, R., A.E. Mattis, E. Kremmer, E. Wolf, G. Brem, and M. Lipp. 1996. A putative chemokine receptor, BLR1, directs B cell migration to defined lymphoid organs and specific anatomic compartments of the spleen. *Cell*. 87:1037-47.

Grichnik, J.M., J.A. Burch, J. Burchette, and C.R. Shea. 1998. The SCF/KIT pathway plays a critical role in the control of normal human melanocyte homeostasis. *J Invest Dermatol*. 111:233-8.

Hachiya, A., A. Kobayashi, A. Ohuchi, Y. Takema, and G. Imokawa. 2001. The paracrine role of stem cell factor/c-kit signaling in the activation of human melanocytes in ultraviolet-B-induced pigmentation. *J Invest Dermatol*. 116:578-86.

Hall, A. 1998. Rho GTPases and the actin cytoskeleton. *Science*. 279:509-14.

Hay, E.D. 1995. An overview of epithelio-mesenchymal transformation. *Acta Anat*. 154:8-20.

Hodivala-Dilke, K.M., K.P. McHugh, D.A. Tsakiris, H. Rayburn, D. Crowley, M. Ullman-Cullere, F.P. Ross, B.S. Coller, S. Teitelbaum, and R.O. Hynes. 1999. Beta3-integrin-deficient mice are a model for Glanzmann thrombasthenia showing placental defects and reduced survival. *J Clin Invest*. 103:229-38.

Hogg, N., and P.A. Bates. 2000. Genetic analysis of integrin function in man: LAD-1 and other syndromes. *Matrix Biol*. 19:211-22.
Hosoda, K., R.E. Hammer, J.A. Richardson, A.G. Baynash, J.C. Cheung, A. Giaid, and M. Yanagisawa. 1994. Targeted and natural (piebald-lethal) mutations of endothelin-B receptor gene produce megacolon associated with spotted coat color in mice. *Cell*. 79:1267-76.
Huang, E., K. Nocka, D.R. Beier, T.Y. Chu, J. Buck, H.W. Lahm, D. Wellner, P. Leder, and P. Besmer. 1990. The hematopoietic growth factor KL is encoded by the Sl locus and is the ligand of the c-kit receptor, the gene product of the W locus. *Cell*. 63:225-33.
Huang, E.J., K.H. Nocka, J. Buck, and P. Besmer. 1992. Differential expression and processing of two cell associated forms of the kit-ligand: KL-1 and KL-2. *Mol Biol Cell*. 3:349-62.
Hynes, R.O. 1992. Integrins: versatility, modulation, and signaling in cell adhesion. *Cell*. 69:11-25.
Jiang, X., O. Gurel, E.A. Mendiaz, G.W. Stearns, C.L. Clogston, H.S. Lu, T.D. Osslund, R.S. Syed, K.E. Langley, and W.A. Hendrickson. 2000. Structure of the active core of human stem cell factor and analysis of binding to its receptor kit. *Embo J*. 19:3192-203.
Jones, G.E. 2000. Cellular signaling in macrophage migration and chemotaxis. *J Leukoc Biol*. 68:593-602.
Jordan, S., and F. Beermann. 2000. Nomenclature for identified pigmentation genes in the mouse. *Pigment Cell Res*. 13:70-1.
Jordan, S.A., and I.J. Jackson. 2000a. A late wave of melanoblast differentiation and rostrocaudal migration revealed in patch and rump-white embryos. *Mech Dev*. 92:135-43.
Jordan, S.A., and I.J. Jackson. 2000b. MGF (KIT ligand) is a chemokinetic factor for melanoblast migration into hair follicles. *Dev Biol*. 225:424-36.
Kapur, R.P. 1999. Early death of neural crest cells is responsible for total enteric aganglionosis in Sox10(Dom)/Sox10(Dom) mouse embryos. *Pediatr Dev Pathol*. 2:559-69.
Kataoka, H., N. Takakura, S. Nishikawa, K. Tsuchida, H. Kodama, T. Kunisada, W. Risau, T. Kita, and S.I. Nishikawa. 1997. Expressions of PDGF receptor alpha, c-Kit and Flk1 genes clustering in mouse chromosome 5 define distinct subsets of nascent mesodermal cells. *Dev Growth Differ*. 39:729-40.
Kinashi, T., and T.A. Springer. 1994. Steel factor and c-kit regulate cell-matrix adhesion. *Blood*. 83:1033-8.
Krull, C.E., R. Lansford, N.W. Gale, A. Collazo, C. Marcelle, G.D. Yancopoulos, S.E. Fraser, and M. Bronner-Fraser. 1997. Interactions of Eph-related receptors and ligands confer rostrocaudal pattern to trunk neural crest migration. *Curr Biol*. 7:571-80.
Kundra, V., B. Anand-Apte, L.A. Feig, and B.R. Zetter. 1995. The chemotactic response to PDGF-BB: evidence of a role for Ras. *J Cell Biol*. 130:725-31.
Kunisada, T., S.Z. Lu, H. Yoshida, S. Nishikawa, M. Mizoguchi, S. Hayashi, L. Tyrrell, D.A. Williams, X. Wang, and B.J. Longley. 1998a. Murine cutaneous mastocytosis and epidermal melanocytosis induced by keratinocyte expression of transgenic stem cell factor. *J Exp Med*. 187:1565-73.
Kunisada, T., H. Yoshida, H. Yamazaki, A. Miyamoto, H. Hemmi, E. Nishimura, L.D. Shultz, S. Nishikawa, and S. Hayashi. 1998b. Transgene expression of steel factor in the basal layer of epidermis promotes survival, proliferation, differentiation and migration of melanocyte precursors. *Development*. 125:2915-23.
Lauffenburger, D.A., and A.F. Horwitz. 1996. Cell migration: a physically integrated molecular process. *Cell*. 84:359-369.
Le Douarin, N., and C. Kalcheim. 1999. The Neural Crest. Cambridge University Press, Cambridge, UK.
Lee, J., and K. Jacobson. 1997. The composition and dynamics of cell-substratum adhesions in locomoting fish keratocytes. *J Cell Sci*. 110:2833-2844.
Lee, J., M. Leonard, T. Oliver, A. Ishihara, and K. Jacobson. 1994. Traction forces generated by locomoting keratinocytes. *J Cell Biol*. 127:1957-1964.
Longley, B.J., Jr., G.S. Morganroth, L. Tyrrell, T.G. Ding, D.M. Anderson, D.E. Williams, and R. Halaban. 1993. Altered metabolism of mast-cell growth factor (c-kit ligand) in cutaneous mastocytosis. *N Engl J Med*. 328:1302-7.
Loring, J.F., and C.A. Erickson. 1987. Neural crest cell migratory pathways in the trunk of the chick embryo. *Dev Biol*. 121:220-36.
Mackenzie, M.A., S.A. Jordan, P.S. Budd, and I.J. Jackson. 1997. Activation of the receptor tyrosine kinase Kit is required for the proliferation of melanoblasts in the mouse embryo. *Dev Biol*. 192:99-107.
Martin, F.H., S.V. Suggs, K.E. Langley, H.S. Lu, J. Ting, K.H. Okino, C.F. Morris, I.K. McNiece, F.W. Jacobsen, E.A. Mendiaz, and et al. 1990. Primary structure and functional expression of rat and human stem cell factor DNAs. *Cell*. 63:203-11.

McHugh, K.P., K. Hodivala-Dilke, M.H. Zheng, N. Namba, J. Lam, D. Novack, X. Feng, F.P. Ross, R.O. Hynes, and S.L. Teitelbaum. 2000. Mice lacking beta3 integrins are osteosclerotic because of dysfunctional osteoclasts. *J Clin Invest*. 105:433-40.

Miyazawa, K., D.A. Williams, A. Gotoh, J. Nishimaki, H.E. Broxmeyer, and K. Toyama. 1995. Membrane-bound Steel factor induces more persistent tyrosine kinase activation and longer life span of c-kit gene-encoded protein than its soluble form. *Blood*. 85:641-9.

Morrison-Graham, K., G.C. Schatteman, T. Bork, D.F. Bowen-Pope, and J.A. Weston. 1992. A PDGF receptor mutation in the mouse (Patch) perturbs the development of a non-neuronal subset of neural crest-derived cells. *Development*. 115:133-42.

Morrison-Graham, K., and Y. Takahashi. 1993. Steel factor and c-kit receptor: from mutants to a growth factor system. *Bioessays*. 15:77-83.

Nagle, D.L., C.A. Kozak, H. Mano, V.M. Chapman, and M. Bucan. 1995. Physical mapping of the Tec and Gabrb1 loci reveals that the Wsh mutation on mouse chromosome 5 is associated with an inversion. *Hum Mol Genet*. 4:2073-9.

Nagle, D.L., P. Martin-DeLeon, R.B. Hough, and M. Bucan. 1994. Structural analysis of chromosomal rearrangements associated with the developmental mutations Ph, W19H, and Rw on mouse chromosome 5. *Proc Natl Acad Sci U S A*. 91:7237-41.

Niggli, V. 1999. Rho-kinase in human neutrophils: a role in signalling for myosin light chain phosphorylation and cell migration. *FEBS Lett*. 445:69-72.

Nishikawa, S., M. Kusakabe, K. Yoshinaga, M. Ogawa, S. Hayashi, T. Kunisada, T. Era, and T. Sakakura. 1991. In utero manipulation of coat color formation by a monoclonal anti-c- kit antibody: two distinct waves of c-kit-dependency during melanocyte development. *Embo J*. 10:2111-8.

Nurden, A.T., and P. Nurden. 2001. Inherited defects of platelet function. *Rev Clin Exp Hematol*. 5:314-34; quiz following 431.

Otsuka, H., T. Kusumi, S. Kanai, M. Koyama, Y. Kuno, and R. Takizawa. 1998. Stem cell factor mRNA expression and production in human nasal epithelial cells: contribution to the accumulation of mast cells in the nasal epithelium of allergy. *J Allergy Clin Immunol*. 102:757-64.

Pierini, L.M., M.A. Lawson, R.J. Eddy, B. Hendey, and F.R. Maxfield. 2000. Oriented endocytic recycling of alpha5beta1 in motile neutrophils [see comments]. *Blood*. 95:2471-80.

Qiu, F.H., P. Ray, K. Brown, P.E. Barker, S. Jhanwar, F.H. Ruddle, and P. Besmer. 1988. Primary structure of c-kit: relationship with the CSF-1/PDGF receptor kinase family--oncogenic activation of v-kit involves deletion of extracellular domain and C terminus. *Embo J*. 7:1003-11.

Reynolds, L.E., L. Wyder, J.C. Lively, D. Taverna, S.D. Robinson, X. Huang, D. Sheppard, R.O. Hynes, and K.M. Hodivala-Dilke. 2002. Enhanced pathological angiogenesis in mice lacking beta3 integrin or beta3 and beta5 integrins. *Nat Med*. 8:27-34.

Ridley, A.J., and A. Hall. 1992. The small GTP-binding protein rho regulates the assembly of focal adhesions and actin stress fibers in response to growth factors. *Cell*. 70:389-399.

Ridley, A.J., H.F. Paterson, C.L. Johnston, D. Diekmann, and A. Hall. 1992. The small GTP-binding protein rac regulates growth factor-induced membrane ruffling. *Cell*. 70:401-410.

Russell, E.S. 1979. Hereditary anemias of the mouse: a review for geneticists. *Adv Genet*. 20:357-459.

Santiago, A., and C.A. Erickson. 2002. Ephrin-B ligands play a dual role in the control of neural crest cell migration. *Development*. 129:3621-32.

Schuchardt, A., V. D'Agati, L. Larsson-Blomberg, F. Costantini, and V. Pachnis. 1994. Defects in the kidney and enteric nervous system of mice lacking the tyrosine kinase receptor Ret. *Nature*. 367:380-3.

Scott, G., J. Ewing, D. Ryan, and C. Abboud. 1994. Stem cell factor regulates human melanocyte-matrix interactions. *Pigment Cell Res*. 7:44-51.

Sekido, Y., T. Takahashi, R. Ueda, M. Takahashi, H. Suzuki, K. Nishida, T. Tsukamoto, T. Hida, K. Shimokata, K.M. Zsebo, and et al. 1993. Recombinant human stem cell factor mediates chemotaxis of small-cell lung cancer cell lines aberrantly expressing the c-kit protooncogene. *Cancer Res*. 53:1709-14.

Selleck, M.A., T.Y. Scherson, and M. Bronner-Fraser. 1993. Origins of neural crest cell diversity. *Dev Biol*. 159:1-11.

Silvers, W.K. 1979. The Coat Colors of Mice: A Model for Mammalian Gene Action and Interaction. Springer, New York.

Small, J.V., T. Stradal, E. Vignal, and K. Rottner. 2002. The lamellipodium: where motility begins. *Trends Cell Biol*. 12:112-20.

Southard-Smith, E.M., L. Kos, and W.J. Pavan. 1998. Sox10 mutation disrupts neural crest development in Dom Hirschsprung mouse model. *Nat Genet*. 18:60-4.
Stemple, D.L., and D.J. Anderson. 1993. Lineage diversification of the neural crest: in vitro investigations. *Dev Biol*. 159:12-23.
Stephenson, D.A., K.H. Lee, D.L. Nagle, C.H. Yen, A. Morrow, D. Miller, V.M. Chapman, and M. Bucan. 1994. Mouse rump-white mutation associated with an inversion of chromosome 5. *Mamm Genome*. 5:342-8.
Stephenson, D.A., M. Mercola, E. Anderson, C.Y. Wang, C.D. Stiles, D.F. Bowen-Pope, and V.M. Chapman. 1991. Platelet-derived growth factor receptor alpha-subunit gene (Pdgfra) is deleted in the mouse patch (Ph) mutation. *Proc Natl Acad Sci U S A*. 88:6-10.
Storgard, C.M., D.G. Stupack, A. Jonczyk, S.L. Goodman, R.I. Fox, and D.A. Cheresh. 1999. Decreased angiogenesis and arthritic disease in rabbits treated with an alphavbeta3 antagonist. *J Clin Invest*. 103:47-54.
Sviderskaya, E.V., W.F. Wakeling, and D.C. Bennett. 1995. A cloned, immortal line of murine melanoblasts inducible to differentiate to melanocytes. *Development*. 121:1547-57.
Tassabehji, M., V.E. Newton, K. Leverton, K. Turnbull, E. Seemanova, J. Kunze, K. Sperling, T. Strachan, and A.P. Read. 1994. PAX3 gene structure and mutations: close analogies between Waardenburg syndrome and the Splotch mouse. *Hum Mol Genet*. 3:1069-74.
Timokhina, I., H. Kissel, G. Stella, and P. Besmer. 1998. Kit signaling through PI 3-kinase and Src kinase pathways: an essential role for Rac1 and JNK activation in mast cell proliferation. *Embo J*. 17:6250-62.
Ueda, S., M. Mizuki, H. Ikeda, T. Tsujimura, I. Matsumura, K. Nakano, H. Daino, Z. Honda Zi, J. Sonoyama, H. Shibayama, H. Sugahara, T. Machii, and Y. Kanakura. 2002. Critical roles of c-Kit tyrosine residues 567 and 719 in stem cell factor-induced chemotaxis: contribution of src family kinase and PI3- kinase on calcium mobilization and cell migration. *Blood*. 99:3342-9.
Verkhovsky, A.B., T.M. Svitkina, and G.G. Borisy. 1999. Self-polarization and directional motility of cytoplasm. *Curr Biol*. 9:11-20.
Vosseller, K., G. Stella, N.S. Yee, and P. Besmer. 1997. c-kit receptor signaling through its phosphatidylinositide-3'-kinase- binding site and protein kinase C: role in mast cell enhancement of degranulation, adhesion, and membrane ruffling. *Mol Biol Cell*. 8:909-22.
Wahl, S., H. Barth, T. Ciossek, K. Aktories, and B.K. Mueller. 2000. Ephrin-A5 induces collapse of growth cones by activating Rho and Rho kinase. *J Cell Biol*. 149:263-70.
Wang, H.U., and D.J. Anderson. 1997. Eph family transmembrane ligands can mediate repulsive guidance of trunk neural crest migration and motor axon outgrowth. *Neuron*. 18:383-96.
Wehrle, B., and M. Chiquet. 1990. Tenascin is accumulated along developing peripheral nerves and allows neurite outgrowth in vitro. *Development*. 110:401-15.
Wehrle-Haller, B., and M. Chiquet. 1993. Dual function of tenascin: simultaneous promotion of neurite growth and inhibition of glial migration. *J Cell Sci*. 106:597-610.
Wehrle-Haller, B., and J.A. Weston. 1995. Soluble and cell-bound forms of steel factor activity play distinct roles in melanocyte precursor dispersal and survival on the lateral neural crest migration pathway. *Development*. 121:731-42.
Wehrle-Haller, B., and J.A. Weston. 1997. Receptor tyrosine kinase-dependent neural crest migration in response to differentially localized growth factors. *Bioessays*. 19:337-45.
Weston, J.A. 1991. Sequential segregation and fate of developmentally restricted intermediate cell populations in the neural crest lineage. *Curr Top Dev Biol*. 25:133-53.
Wilkinson, D.G. 2000. Eph receptors and ephrins: regulators of guidance and assembly. *Int Rev Cytol*. 196:177-244.
Williams, D.E., P. de Vries, A.E. Namen, M.B. Widmer, and S.D. Lyman. 1992. The Steel factor. *Dev Biol*. 151:368-76.
Williams, D.E., J. Eisenman, A. Baird, C. Rauch, K. Van Ness, C.J. March, L.S. Park, U. Martin, D.Y. Mochizuki, H.S. Boswell, and et al. 1990. Identification of a ligand for the c-kit proto-oncogene. *Cell*. 63:167-74.
Yarden, Y., J.A. Escobedo, W.J. Kuang, T.L. Yang-Feng, T.O. Daniel, P.M. Tremble, E.Y. Chen, M.E. Ando, R.N. Harkins, U. Francke, and et al. 1986. Structure of the receptor for platelet-derived growth factor helps define a family of closely related growth factor receptors. *Nature*. 323:226-32.
Yarden, Y., W.J. Kuang, T. Yang-Feng, L. Coussens, S. Munemitsu, T.J. Dull, E. Chen, J. Schlessinger, U. Francke, and A. Ullrich. 1987. Human proto-oncogene c-kit: a new cell surface receptor tyrosine kinase for an unidentified ligand. *Embo J*. 6:3341-51.

Zhang, Z., R. Zhang, A. Joachimiak, J. Schlessinger, and X.P. Kong. 2000. Crystal structure of human stem cell factor: implication for stem cell factor receptor dimerization and activation. *Proc Natl Acad Sci U S A*. 97:7732-7.

Zsebo, K.M., D.A. Williams, E.N. Geissler, V.C. Broudy, F.H. Martin, H.L. Atkins, R.Y. Hsu, N.C. Birkett, K.H. Okino, D.C. Murdock, and et al. 1990a. Stem cell factor is encoded at the Sl locus of the mouse and is the ligand for the c-kit tyrosine kinase receptor. *Cell*. 63:213-24.

Zsebo, K.M., J. Wypych, I.K. McNiece, H.S. Lu, K.A. Smith, S.B. Karkare, R.K. Sachdev, V.N. Yuschenkoff, N.C. Birkett, L.R. Williams, and et al. 1990b. Identification, purification, and biological characterization of hematopoietic stem cell factor from buffalo rat liver--conditioned medium. *Cell*. 63:195-201.